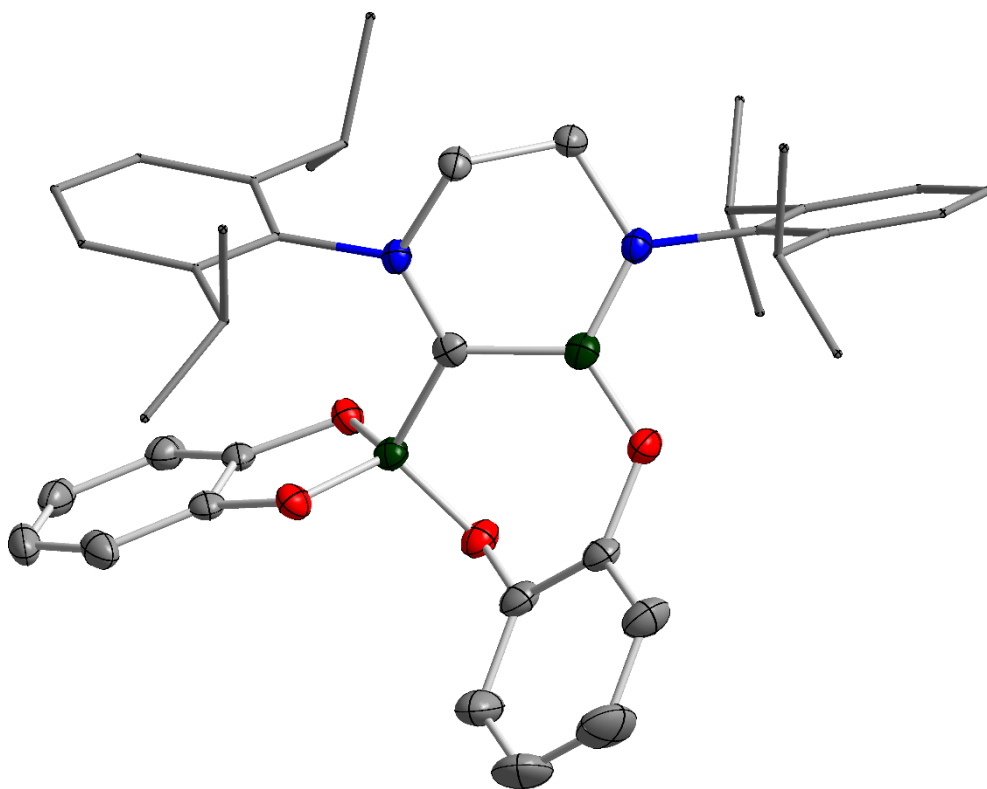


Anionic and Neutral Lewis-Base Adducts of Diboron(4) Compounds



Dissertation zur Erlangung des naturwissenschaftlichen Doktorgrades
der Julius-Maximilians-Universität Würzburg

vorgelegt von

Sabrina Würtemberger-Pietsch

aus Birkenfeld

Würzburg 2016

Eingereicht bei der Fakultät für Chemie und Pharmazie

am: _____

Gutachter der schriftlichen Arbeit

1. Gutachter: Prof. Dr. Todd B. Marder

2. Gutachter: Prof. Dr. Udo Radius

Prüfer des öffentlichen Promotionskolloquiums

1. Prüfer: Prof. Dr. Todd B. Marder

2. Prüfer: Prof. Dr. Udo Radius

3. Prüfer: _____

Datum des öffentlichen Promotionskolloquiums

am: _____

Doktorurkunde ausgehändigt

am: _____

Meiner Familie gewidmet

Die Experimente zur vorliegenden Arbeit wurden in der Zeit von Oktober 2012 bis Mai 2016 am Institut für Anorganische Chemie der Julius-Maximilians-Universität Würzburg in Kooperation von Prof. Dr. Todd B. Marder und Prof. Dr. Udo Radius durchgeführt.

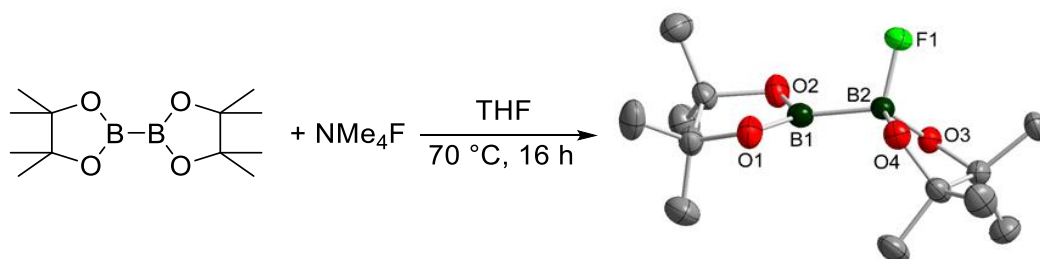
Content

1. Chapter One: Anionic Adducts	1
1.1. Introduction	1
1.1.1. 1,2-Diborylation of α,β -unsaturated compounds with diboron(4) reagents	1
1.1.2. β -Borylation reaction of α,β -unsaturated carbonyl compounds with diboron(4) reagents	4
1.1.3. Metal-free β -borylation reactions	7
1.1.4. Metal-free β -borylation reactions promoted by NHCs	8
1.1.5. Metal-free β -borylation reactions promoted by other bases	10
1.1.6. sp^2 - sp^3 and sp^3 - sp^3 diboron adducts	14
1.2. Results and Discussion	23
1.2.1. Studies on formation and reactivity of anionic sp^2 - sp^3 diboron adducts of the type $[B_2pin_2(OR)][M]$ and $[B_2pin_2F][nBu_4N]$	23
1.2.2. Synthesis of the fluoride adducts of the type $[B_2(OR)_4F][NMe_4]$	24
1.2.3. Reactivity of the anionic sp^2 - sp^3 diboron adducts	34
1.2.4. Experiments to obtain sp^3 - sp^3 diboron adducts	53
2. Chapter Two: Neutral Adducts	60
2.1. Introduction	60
2.1.1. Decomposition pathways of NHCs	60
2.1.2. Metal-containing ring expansion reactions	63
2.1.3. Main-group element-containing ring expansion reactions	68
2.1.4. Limitation of ring expansion reactions	75
2.2. Results and Discussion	77
2.2.1. Mono- and bis-NHC adducts of diboron(4) compounds	77
2.2.2. Ring expansion reactions	96
2.2.3. Reaction of $HB(OR)_2$ with saturated and unsaturated NHCs as well as $CAAC^{Me}$	128
2.2.4. Synthesis of mono-NHC adducts of the type $R_3B \cdot NHC$	150
2.2.5. Synthesis of the backbone-activated compounds of the type R_3B-tBu_2Im-H	159
3. Experimental Section	164
3.1. General procedures	164
3.2. Analytical methods	164
3.3. Spectroscopic methods	165
3.4. Synthesis of the starting material	166
3.5. Synthesis of novel compounds	168

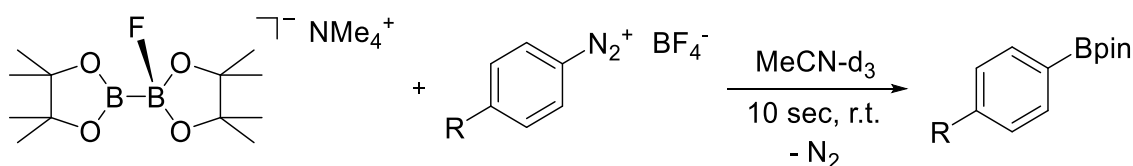
3.5.1. Synthesis of anionic sp^2 - sp^3 diboron adducts of the type $[B_2(OR)_4F][NMe_4]$	168
3.5.2. Reactivity of adduct 4 and the <i>in situ</i> formed adducts 7 and 9 with different diazonium $[BF_4]^-$ salts	170
3.5.3. Synthesis of the mono-NHC adducts of the type FBpin•NHC	177
3.5.4. Synthesis of the mono-NHC diboron adducts of the type $B_2(OR)_4$ •NHC	179
3.5.5. Synthesis of the ring expanded products (RER)	183
3.5.6. Reactions of HBcat with different unsaturated NHCs and CAAC ^{Me}	190
3.5.7. Synthesis of the mono-NHC adducts of the type HBpin•NHC	195
3.5.8. Synthesis of the mono-NHC adducts of the type Ph_3B •NHC	196
3.5.9. Synthesis of the mono-NHC adducts of the type Et_3B •NHC	199
3.5.10. Synthesis of the backbone-activated products of the type R_3B - <i>t</i> Bu ₂ Im-H	202
4. Crystallographic data	203
4.1. Crystallographic data collection parameters	203
4.2. CCDC-numbers of published compounds	204
4.3. Crystallographic data collection parameters	205
5. Summary	229
5.1. Chapter One: Anionic Adducts	229
5.2. Chapter Two: Neutral Adducts	231
6. Zusammenfassung	236
6.1. Kapitel Eins: Anionische Addukte	236
6.2. Kapitel Zwei: Neutrale Addukte	238
7. Appendix	244
7.1. Abbreviations	244
7.2. Symbols and non-SI units	246
7.3. List of compounds	247
7.4. Additional NMR spectra	250
7.4.1. Compound 29 : RER- B_2 neop ₂ •(<i>n</i> Pr ₂ Im) ₂ •toluene	250
8. References	253
9. Acknowledgment	261
10. Affidavit	263
11. Eidesstaatliche Erklärung	263
12. Publications	264
12.1. List of publications	264

Anionic Adducts

Sp²-sp³ tetraalkoxy diboron compounds have gained attention due to the development of new, synthetically useful catalytic reactions either with or without transition-metals. Lewis-base adducts of the diboron(4) compounds were suggested as possible intermediates in Cu-catalyzed borylation reactions some time ago. However, intermolecular adducts of tetraalkoxy diboron compounds have not been studied yet in great detail. In preliminary studies, we have synthesized a series of anionic sp²-sp³ adducts of B₂pin₂ with alkoxy-groups (L = [OMe]⁻, [OtBu]⁻), a phenoxy-group (L = [4-tBuC₆H₄O]⁻) and fluoride (L = [F]⁻, with [nBu₄N]⁺ as the counter ion) as Lewis-bases.



Herein, we present the synthesis and characterization of a further fluoride anionic sp²-sp³ diboron compound with [NMe₄]⁺ as the counter ion. Detailed NMR spectroscopic studies of all of these adducts revealed the sp²-sp³ diboron structure of these compounds both in solution and in the solid state, in agreement with structures established by X-ray crystallography. Moreover, selected adducts transfer a nucleophilic pinB-moiety to organic electrophiles, hence acting as formal source of boryl anions. Experimental studies on the structure and reactivity of the [B₂pin₂F][NMe₄] adduct as well as of the “*in situ* formed” [B₂neop₂F][NMe₄] and [B₂cat₂F][NMe₄] are presented.

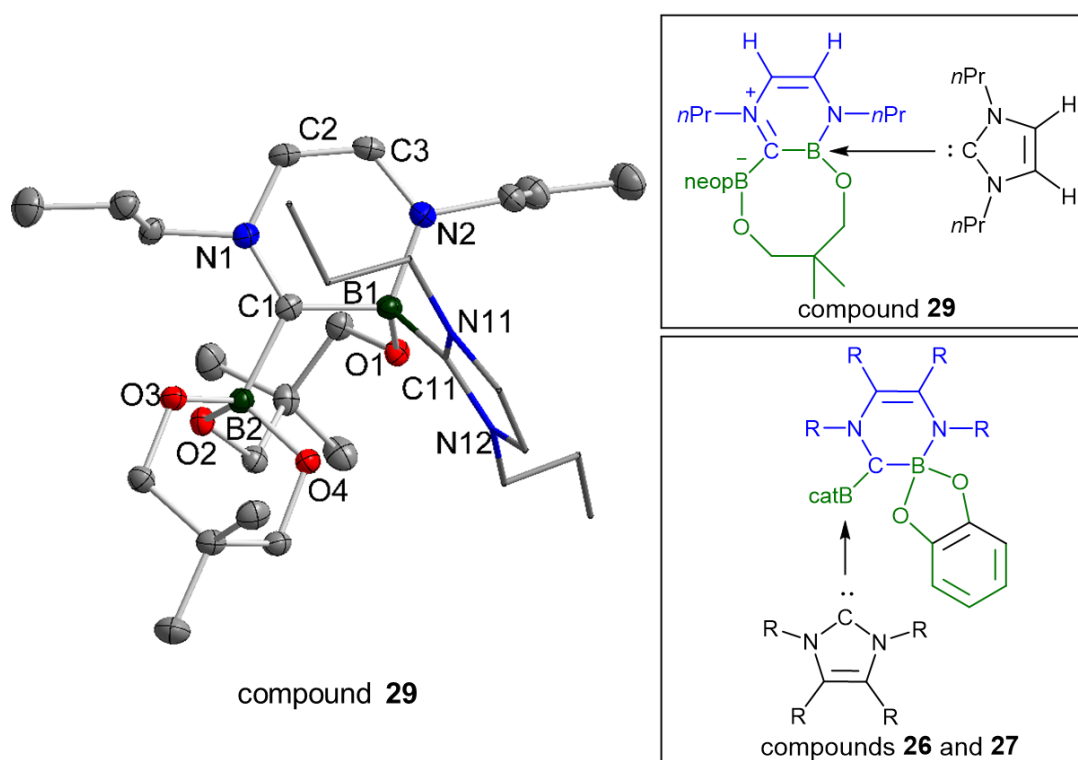


Neutral Adducts

Since their isolation and characterization, applications of *N*-heterocyclic carbenes (NHCs) and related molecules, e.g., cyclic alkylaminocarbenes (CAACs) and acyclic diaminocarbenes (aDCs), have grown rapidly. Their use as ligands in homogeneous catalysis and directly in organocatalysis, including recently developed borylation reactions, is now well established. Recently, several examples of ring expansion reactions (RER) involving NHCs were reported to take place at elevated temperatures, involving Be, B, and Si.

Furthermore, preliminary studies in the group of Marder *et al.* showed the presence of neutral sp^2 - sp^3 diboron compounds with B_2pin_2 and the NHC Cy_2Im . In this work, we focused on the synthesis and characterization of further neutral sp^2 - sp^3 as well as sp^3 - sp^3 diboron adducts with B_2cat_2 and B_2neop_2 and different NHCs.

Whereas the mono-NHC adduct is stable for several hours at temperatures up to 60 °C, the bis-NHC adducts undergo thermally induced rearrangement to form the ring expanded products compound **26** and **27**. B_2neop_2 is much more reactive than B_2cat_2 giving ring expanded product **29** at room temperature in quantitative yields, demonstrating that NHC ring expansion and B–B bond cleavage can be very facile processes.



Additionally, the reaction of B_2cat_2 with the saturated NHC $Dipp_2Slm$ showed that even the mono-NHC adduct rearranges at higher temperatures to the ring expanded product **33**. Related observations were made using $HBcat$ as the boron reagent. The reaction with the unsaturated NHCs formed the expected mono-NHC adducts; however, using $CAAC^{Me}$ led to the formation of the B–H activation product $CAAC^{Me}(H)Bcat$ **40**. In addition, a further ring expanded product $RER-Dipp_2Slm(H_2)B-cat-Bcat \cdot Dipp_2Slm$ **41** was obtained by reaction of $HBcat$ with the saturated NHC $Dipp_2Slm$.

To examine the limitations of ring expansion reactions, in further studies we tried to synthesize different kinds of ring expanded products with NHCs including alkylboranes, such as BPh_3 and BEt_3 ; however, all of these reactions led to the expected adduct formation, but these adducts are stable at higher temperatures.

Since the first reports on metal-free catalysis and the interesting role of the base in borylation reactions, the synthesis and characterization of these intermediates gained more and more attention in our group.

One aim of this thesis was the synthesis of anionic sp^2 - sp^3 diboron compounds of the type $[B_2pin_2(OR)]K$ and the fluoride adduct $[B_2pin_2F][NMe_4]$. Additionally, these adducts were to be tested in further reactivity studies as reagents in borylation reactions. Additionally, the diboron reagents B_2neop_2 and B_2cat_2 were also to be reacted with NMe_4F to form further anionic adducts of the type $[B_2(OR)_4F][NMe_4]$. These *in situ* formed adducts were to be examined for their abilities to transfer a nucleophilic $(OR)_2B$ -moiety to organic electrophiles.

Besides the anionic sp^2 - sp^3 adducts, further investigations on the synthesis and characterization of neutral sp^2 - sp^3 and sp^3 - sp^3 diboron adducts of the type $B_2(OR)_4 \cdot NHC$ and $B_2(OR)_4 \cdot (NHC)_2$ were to be performed, their stability at elevated temperatures was to be examined. Furthermore, the reactions of unsaturated and saturated NHCs with diboron reagents was to be investigated, to determine whether the reaction products are similar or slightly different.

A further focus of this thesis was an exploration of the reactions of $HBcat$ as the boron source with unsaturated and saturated NHCs as well as $CAAC^{Me}$; to see whether the obtained products are mono-NHC adducts or if there are some differences in the reactivity and the resulting products.

Final investigations were to be undertaken to confirm an early literature report of initial ring expansion of an NHC and further ring contraction to form five-membered boron-containing heterocyclic rings. Therefore, the synthesis of the adducts of the form $R_3B \cdot NHC$ ($R = Ph$ and Et) and their behavior at elevated temperatures was to be examined.

Chapter One

Borylation reactions of anionic sp^2 - sp^3
diboron(4) compounds

“Isn’t it anionic?”

1. CHAPTER ONE: ANIONIC ADDUCTS

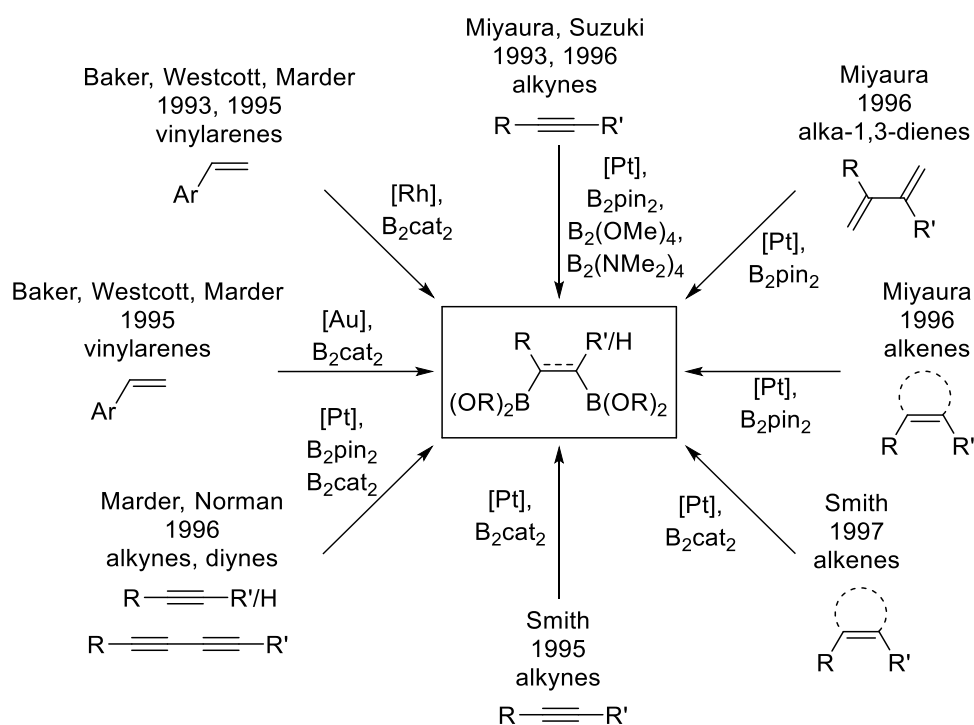
In 1959, Schlesinger *et al.* reported the first addition of diboron tetrahalide compounds of the type X_2B-BX_2 ($X = Cl, F$) to alkenes and alkynes;^[1] however, the use of their ester and amide analogues, as the boron source, did not lead to any borylation reactions.

Albeit, since the synthesis of the ester derivatives, such as B_2pin_2 (bis(pinacolato)diboron)^[2-4], B_2cat_2 (bis(catecholato)diboron)^[5] as well as B_2neop_2 (bis(neopentylglycolato)diboron),^[6] which are relatively stable towards moisture and air, and demonstrations of their activation by both metals^[7-17] and Lewis-bases.^[18-23] The applications of these diboron compounds in borylation reactions have become more and more of interest to many working groups.

1.1. Introduction

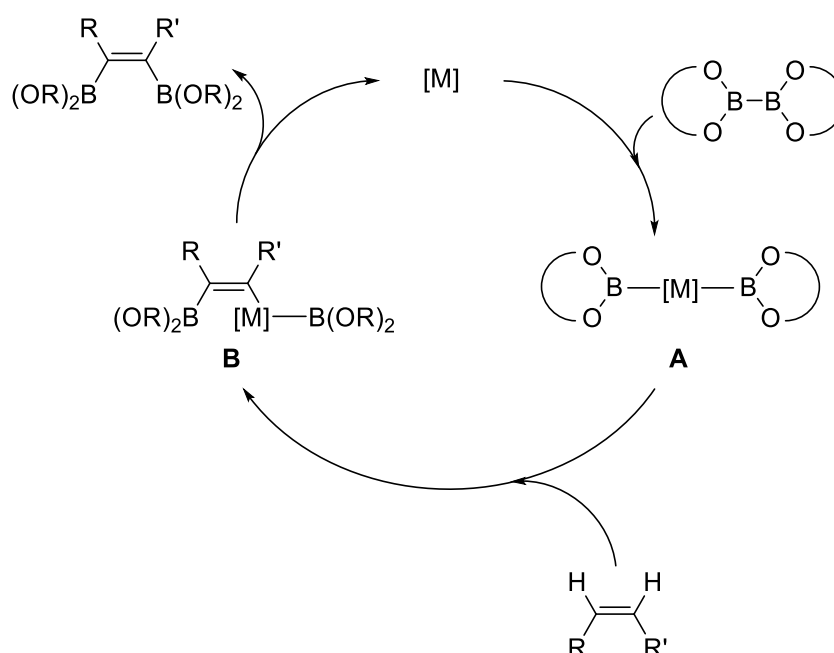
1.1.1. 1,2-Diborylation of α,β -unsaturated compounds with diboron(4) reagents

In the early to the mid 1990's, several groups were interested in the metal-catalyzed β -borylation of α,β -unsaturated compounds with diboron(4) reagents, such as B_2pin_2 , B_2cat_2 , $B_2(NMe_2)_4$ (tetra(dimethylamino)diboron) and $B_2(OMe)_4$ ((tetramethoxy)diboron).^[7-16] These borylation reactions primarily used $[Pt]$ ^[7-10, 13-16], $[Rh]$ ^[11-12] and $[Au]$ ^[12] complexes for the activation of the diboron reagent, and were mainly reported by the groups of Miyaura and Suzuki, Baker, Marder and Westcott as well as Iverson and Smith (Scheme 1).



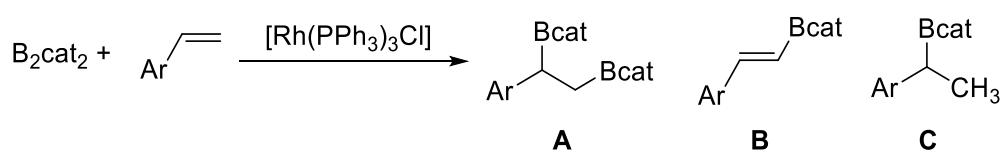
Scheme 1: Overview of the first reported metal-mediated 1,2-diborylation reactions of α,β -unsaturated compounds with diboron(4) reagents.

In 1993, Miyaura, Suzuki *et al.* reported the first 1,2-diborylation of alkynes, using $[\text{Pt}(\text{PPh}_3)_4]$ as the catalyst precursor and B_2pin_2 as the boron source.^[7] However, the application of $[\text{Pd}(\text{PPh}_3)_4]$ or $[\text{Pd}(\text{OAc})_2]$ as the pre-catalyst did not lead to any conversion of the starting material. Additionally, they proposed a mechanism for the diborylation reaction of the alkynes; i) the first step is the oxidative addition of the diboron compound to the transition-metal (**A**); ii) the next step is the insertion of the substrate to form intermediate **B**; iii) finally, the desired product will be obtained *via* reductive elimination (Scheme 2). This depicted catalytic cycle is generally valid for most borylation reactions. In addition to the reported 1,2-diborylation of alkynes, Miyaura and co-workers published further 1,2-diborylation reactions of alka-1,3-dienes^[9] as well as alkenes^[10] in the late 1990s.



Scheme 2: Proposed mechanism of the 1,2-diborylation reaction of α,β -unsaturated compounds.

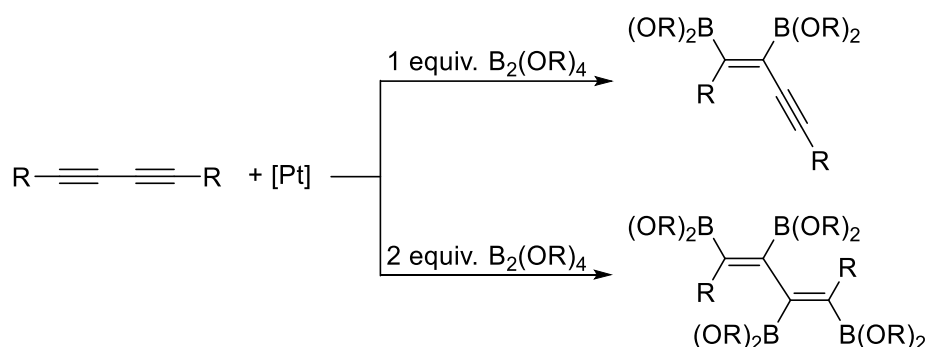
In 1993, Baker, Marder *et al.* mentioned, for the first time, the rhodium-catalyzed 1,2-diborylation of alkenes with B_2cat_2 as the boron source.^[11] During their study of alkene insertion into the $\text{Rh}-\text{B}$ bond, they reported the reaction of two equivalents of 4-vinylanisole with the complex $[\text{Rh}(\text{PPh}_3)_2(\text{Bcat})_2\text{Cl}]$, whereby three different kinds of borylated products could be obtained, namely the bis-boronate ester $\text{CH}_2(\text{Bcat})-\text{CHAr}(\text{Bcat})$ (**A**), vinyl-boronate ester (*E*)- $\text{CH}(\text{Bcat})=\text{CHAr}$ (**B**) and an internal hydroboration product $\text{CH}_3\text{CHAr}(\text{Bcat})$ (**C**) (Scheme 3).



Scheme 3: Rhodium-catalyzed 1,2-diborylation reaction of vinylarenes with B_2cat_2 .

Furthermore, Baker, Marder, Westcott *et al.* reported related diboration reactions, using gold-complexes of the type $[\text{Au}(\text{PR}_3)_n\text{Cl}]$ for the 1,2-diborylation reaction of vinylarenes.^[12] The big advantage of the gold-mediated borylation reaction was the exclusive formation of the 1,2-diborylated product, without any β -elimination products.

In 1996, Marder, Norman and co-workers published the diboration of alkynes and diynes with B_2cat_2 and B_2pin_2 , as well as the molecular structures of the intermediates of the borylation mechanism.^[13] The reaction of one equivalent of the diboron source with diynes yielded the 1,2-diborylated product; however, increasing the amount of the $\text{B}_2(\text{OR})_4$ up to two equivalents led to the formation of the 1,2-3,4-tetraborylated products.



Scheme 4: Platinum-mediated di- and tetraborylation of diynes.

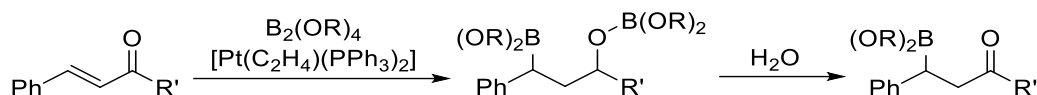
Iverson and Smith investigated several reaction pathways to synthesize and characterize the borylated-Pt-complexes $[\text{Pt}(\text{PPh}_3)(\text{Bcat})_2]$ in 1995 (Scheme 4).^[14] They found that the alkyne complex $[\text{Pt}(\text{PPh}_3)_2(\eta^2\text{-4-octyne})]$ reacts with B_2cat_2 to give the desired diborylated Pt-complex; however, thermolyses of the [Pt]-complex and 4-octyne in the absence of additional B_2cat_2 yielded a mixture of compounds. Furthermore, to examine the obtained mixture of compounds, they reacted the complex $[\text{Pt}(\text{PPh}_3)(\text{Bcat})_2]$ with 4-octyne in the presence of an excess of B_2cat_2 , which led to the formation of the 4,5-bis(boryl)octene. Smith and Iverson also reported mechanistic investigations of the alkyne insertion into the Pt–B bonds and further diborylation reactions of alkynes.^[15]

In addition, Iverson and Smith published the platinum-mediated diborylation reactions of alkenes, using $[\text{Pt}(\text{COD})_2]$ as the catalyst and B_2cat_2 as the boron source.^[16] All of these mentioned diborylation reactions presumably follow the same catalytic cycle, although the Au-catalysis may have a different mechanism.

1.1.2. β -Borylation reaction of α,β -unsaturated carbonyl compounds with diboron(4) reagents

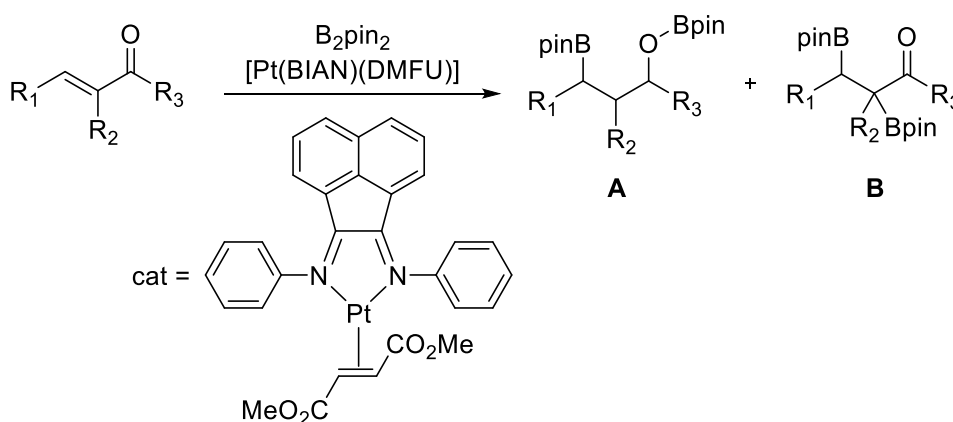
In the early 1990s, the metal-mediated 1,2- or 1,4-diborylation reactions of alkenes, alkynes, diynes as well as vinylarenes were successful using different diboron reagents of the type $B_2(OR)_4$. Several working groups began to explore the borylation reactions of α,β -unsaturated carbonyl compounds, to obtain a novel class of boronate esters, which are useful substrates for further reactions, e.g. Suzuki-Miyaura cross-coupling.^[17]

In 1997, Marder, Norman and co-workers investigated the first diborylation reaction of α,β -unsaturated carbonyl compounds with diboron(4) reagents to obtain synthetically useful intermediates.^[24] The reaction of the α,β -unsaturated ketones with the platinum-complex $[Pt(C_2H_4)(PPh_3)_2]$ as the catalyst precursor, and B_2pin_2 as well as B_2cat_2 as the boron source, yielded the desired 1,4-bis-boronate ester and, after aqueous work-up, the β -borylated product (Scheme 5).



Scheme 5: Platinum-mediated β -borylation of α,β -unsaturated ketones with diboron(4) reagents.

Additionally, Marder *et al.* reported the platinum-catalyzed 1,4- and 3,4-diborylation of α,β -unsaturated carbonyl compounds with B_2pin_2 as the diboron reagent, using the literature known platinum-complex $[Pt(BIAN)(DMFU)]$ ^[25] (BIAN = bis(phenylimino)acenaphthene, DMFU = dimethyl fumarate). Of interest is the observation of the expected 1,4-diborylated products (**A**) as well as the rare formation of the 3,4-diborylated bis-boronate ester (**B**) (Scheme 6) with some substrates.



Scheme 6: Platinum-catalyzed 1,4- and 3,4-diborylation of α,β -unsaturated carbonyl compounds.

The bis-boronate ester **B** was only observed, when the starting material contains an alkoxy-group as R_3 . In the case of $R_3 = OEt$ 9% of the bis-boronate ester **A** was obtained in

the *in situ* ^1H NMR spectrum. This is interesting in so far, as the reported mechanism of the 1,4-borylation reaction does not agree with the obtained results and can not explain the formation of the 3,4-diborylated product.

Recently, Zhao, Marder, Lin and co-workers reported DFT studies to explain the platinum-mediated diborylation reaction,^[26] in which, they used acrolein and methyl acrylate as the model substrates. In the case of acrolein, the calculations showed that the formation of the 3,4-diborylated product has a barrier of 33.7 kcal/mol which is not favorable, in comparison to the formation of the 1,4-diborylated ester (18.6 kcal/mol); however, the application of methyl acrylate instead of acrolein gives rise to the same results, which means that the formation of 1,4-diborylated product is also favored. Nevertheless, additional DFT calculations showed that the expected product **A** isomerizes to the 3,4-diborylated product *via* a 1,3-shift of the oxygen-bonded boryl-group, which is kinetically and thermodynamically favored (Figure 1).^[26]

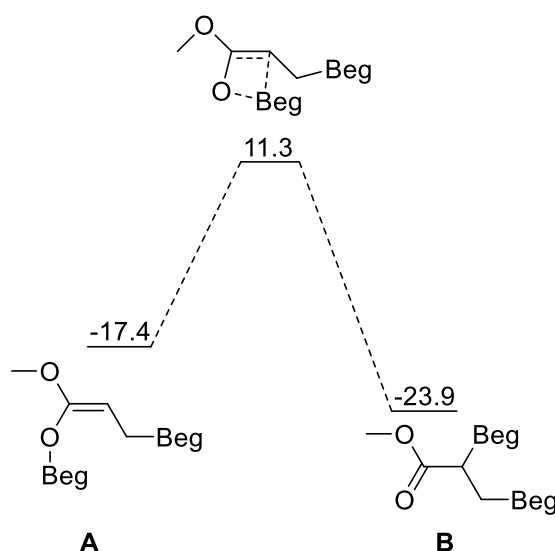
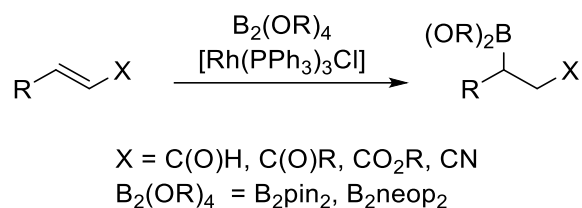


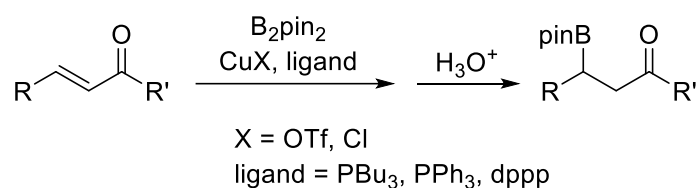
Figure 1: Energy profiles calculated for the isomerization of the 1,4-diborylated product **A** to the 3,4-diborylated product **B** (eg = ethylenglykol).

A further example of a platinum-mediated diborylation reaction was reported by Srebnik *et al.*, using $[\text{Pt}(\text{PPh}_3)_4]$ as the precursor catalyst.^[27]

In 2002, Kabalka and co-workers published the first rhodium-catalyzed borylation reaction of α,β -unsaturated compounds, such as ketones, aldehydes as well as nitriles, using B_2pin_2 and B_2neop_2 as the boron source.^[28] They used the “Wilkinson-catalyst” $[\text{Rh}(\text{PPh}_3)_3\text{Cl}]$ as the pre-catalyst and obtained the desired boronate esters in up to 78% yield (Scheme 7), although Marder *et al.* have not been able to reproduce these findings.

Scheme 7: Rhodium-mediated β -borylation of α,β -unsaturated compounds.

The first reports of the copper-promoted borylation reaction of α,β -unsaturated carbonyl compounds were published by the groups of Hosomi *et al.*^[29] and Miyaura *et al.*^[30] in 2000 and 2001. Hosomi and co-workers investigated the borylation reaction at room temperature by using different CuX salts (X = OTf, Cl) as the pre-catalyst, phosphines (PBU₃, PPh₃ and dppp) (dppp = 1,3-bis(diphenylphosphino)propane) as ligands and B₂pin₂ as the boron source. After aqueous work-up, the boronate ester was isolated in very good yield (up to 96%) (Scheme 8).^[29] Of interest was the observation that the borylation reaction even took place without any CuX salts, by using only 11 mol% of PBU₃; however, the yields were very low (7%) (*vide infra*).

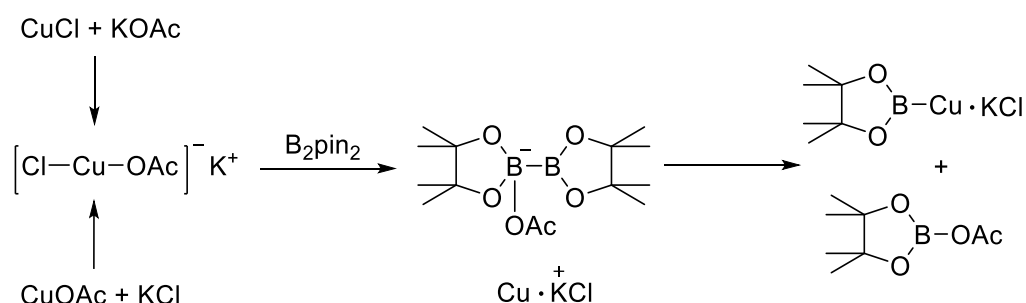
Scheme 8: Copper-mediated borylation reaction of α,β -unsaturated carbonyl compounds.

Another possibility to generate β -boryl carbonyl compounds and alkenyl boronates was reported by Miyaura *et al.* in 2001, based on the reaction of α,β -unsaturated compounds with B₂pin₂, copper(I) halide and base. The best results were obtained using CuCl as the copper salt and potassium acetate (KOAc) as the base. The first step during the reaction was proposed to be the transmetalation of B₂pin₂ with CuCl in the presence of KOAc, forming the copper-boryl species pinB-Cu•KCl (Scheme 9).^[30]

Scheme 9: Formation of the copper-boryl species pinB-Cu•KCl via reaction of B₂pin₂ with CuCl in the presence of KOAc.

Furthermore, Miyaura and co-workers proposed a possible intermediate for the borylation. The first step is the reaction of CuCl with KOAc to form [Cl-Cu-OAc]K or via reaction of Cu(OAc) with KCl. This intermediate reacts with B₂pin₂ to form the active copper-boryl species pinB-Cu•KCl. Further investigations claimed that this reaction took place *via* formation of an *in situ*

formed anionic sp^2 - sp^3 diboron adduct $[B_2pin_2OAc][Cu \cdot KCl]$, which then decomposes to pinB-OAc and the catalytic active species pinB-Cu·KCl (Scheme 10).^[30] At that time, copper boryl-complexes obtained more and more attention and application in the so called, “copper-mediated β -borylation of α,β -unsaturated compounds”.^[31-35]



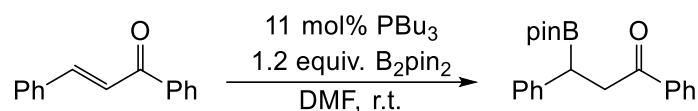
Scheme 10: Formation of a sp^2 - sp^3 diboron adduct *via* reaction of $[Cl-Cu-OAc]K$ with B_2pin_2 and further reaction to pinB-OAc and the catalytic active species pinB-Cu·KCl.

The proposed but not observed anionic sp^2 - sp^3 diboron adduct $[B_2pin_2OAc][Cu \cdot KCl]$ is the first example of an *in situ* formed adduct during the borylation of α,β -unsaturated compounds.

These two reactions were the starting point of the copper-catalyzed borylation reaction, which since then has been very well investigated,^[36-42] using symmetric as well as unsymmetric diboron reagents.^[43-47] Furthermore, several more metal-mediated β -borylation reactions were reported.^[33-35, 48-49]

1.1.3. Metal-free β -borylation reactions

Since Norman, Marder *et al.* reported the first so called “ β -borylation of α,β -unsaturated compounds” catalyzed by a platinum-complex,^[24, 26, 50] this borylation reaction became the starting point for a number of investigations on metal-promoted as well as metal-free β -borylation reactions. Due to the fact that the role of the base was still not very well understood at this time, several working groups assumed that the base, such as alkoxides, phosphines or NHCs, can activate the B–B bond, and metal-free β -borylation reactions were developed.^[18-23] Furthermore, the use of various phosphines in the catalytic process is known. In 2000, as an early example, Hosomi *et al.* published the reaction of benzylideneacetophenone with B_2pin_2 and 11 mol% of PBu_3 , which gave the corresponding borylated product in very low yield (7%); however, this reaction showed that the role of the base should not be undervalued (Scheme 11).^[29]

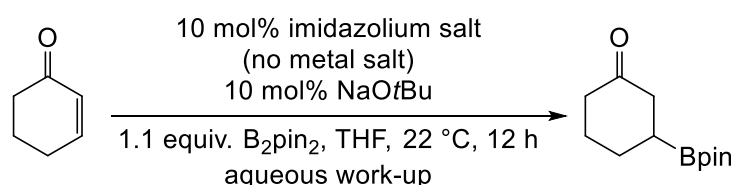


Scheme 11: PBU₃-promoted β -borylation of benzylideneacetophenone with B₂pin₂.

In the following chapter several examples of borylation reactions are summarized, including the metal-free β -borylation reactions using alkoxide bases as well as NHCs and phosphines as activators of the B–B bond.

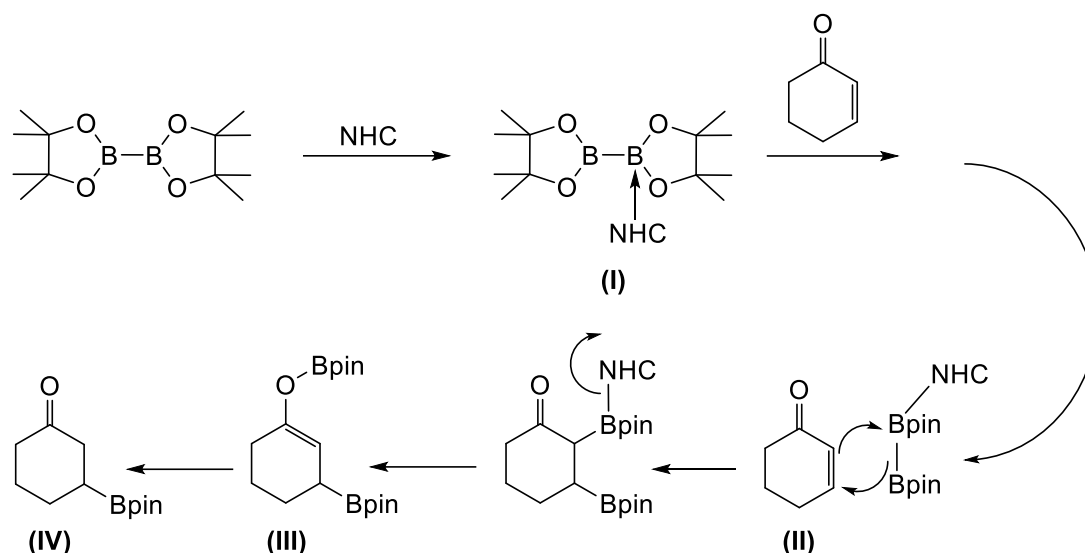
1.1.4. Metal-free β -borylation reactions promoted by NHCs

The first metal-free β -borylation reaction of α,β -unsaturated compounds, promoted by NHCs, was reported by Hoveyda *et al.* in 2009, by activating the B–B bond of the diboron compound B₂pin₂.^[18, 23] The catalytically active NHC, which was generated *in situ via* reaction of NHC•HCl with 10 mol% NaOtBu, activates the B–B bond of the B₂pin₂ and which reacts with the substrate, to form the desired boronate ester in 66% yield (Scheme 12). The best results were obtained using Cy₂Im (1,3-bis(cyclohexyl)imidazol-2-ylidene) as the catalytically active species; however, the use of PPh₃ or PCy₃ as the catalyst, without any base, led to the conversion to the expected product of less than 2%.^[18, 23]



Scheme 12: NHC-promoted borylation reaction of cyclohexanone with B₂pin₂.

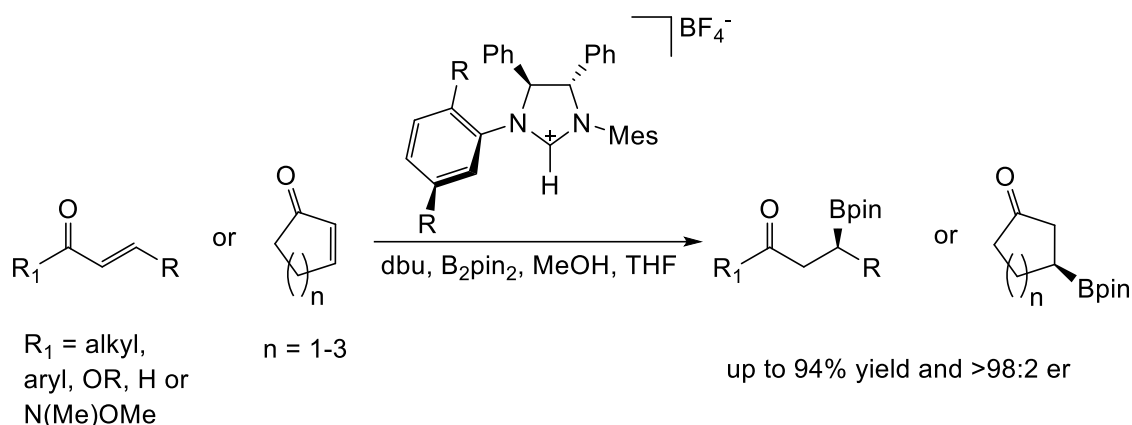
The group proposed a mechanism for the B₂pin₂ activation and conjugate addition to an enone. The first step is the reaction of B₂pin₂ and the NHC to form the neutral B₂pin₂•Cy₂Im adduct, which features a polarized B–B bond. In the next step, the C=C double bond of the enone reacts with the NHC-diboron adduct (**I**), which led to the formation of the intermediate (**II**). After rearrangement and aqueous work-up the corresponding boronate ester (**IV**) could be isolated; however, the 1,4-diborylated intermediate (**III**) was not observed (Scheme 13).



Scheme 13: Proposed mechanism for the NHC-promoted borylation reaction of cyclohexanone with B_2pin_2 .

Furthermore, Hoveyda *et al.* investigated the synthesis and characterization of the expected adduct $B_2pin_2 \cdot Cy_2Im$.^[18, 23] The coordination of the NHC to the diboron compound led to one sp^2 and one sp^3 hybridized boron atom, weakening the B–B bond; however, the initial NMR spectroscopic investigations by Hoveyda and co-workers were incorrect (corrections^[23]) and the system was reinvestigated in detail by Marder *et al.* in 2012.^[51] The reported ^{11}B NMR shifts at 4.5 and 6.3 ppm did not fit to the expected shifts of a sp^2 - sp^3 diboron adduct (sp^2 -B \geq 20 ppm, sp^3 -B \leq 20 ppm); Marder and co-workers reported the synthesis and full characterization of the adduct $B_2pin_2 \cdot Cy_2Im$ *via* single crystal X-ray diffraction, solid state as well as temperature dependent NMR spectroscopy, and showed that the signals for the two boron atoms are shifted to 2.4 (sp^3 -B) and 37.2 ppm (sp^2 -B) at 5 °C.^[51]

Recent reports by Hoveyda *et al.* present the metal-free enantioselective borylation reaction of α,β -unsaturated compounds, such as ketones and esters^[22] and enones.^[52] The reaction of the imidazolium salt with 1,8-diazabicyclo[5.4.0]undec-7-ene (dbu) yielded the deprotonated NHC which then can activate the B–B bond of the diboron reagent (Scheme 14). The use of MeOH as an additive, did not lead to the formation of the expected $B_2pin_2 \cdot NHC$ adduct; however, Hoveyda *et al.* proposed that one Bpin-moiety is exchanged by two $[MeO]^-$ -groups. The second step is the addition of the corresponding substrate to form the intermediate which reacts then with a further equivalent of MeOH to form the desired product *via* elimination of $B(OMe)_3$ and the free NHC.^[22]



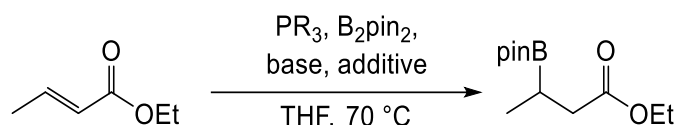
Scheme 14: Boron conjugated addition to α,β -unsaturated carbonyl compounds *via* metal-free catalytic enantioselective C–B bond formation.

Hoveyda *et al.* also published several copper-mediated borylation reactions.^[53-65] Furthermore, they reported the use of borosilane compounds, such as pinB–SiMe₂Ph, in similar silylation reactions.^[66-69]

In summary, all these mentioned borylation reactions have in common that the *in situ* formed “free” NHC can activate the B–B bond of the diboron reagent to form a formal “B(OR)₂”-species which can be used as a boryl anion source.

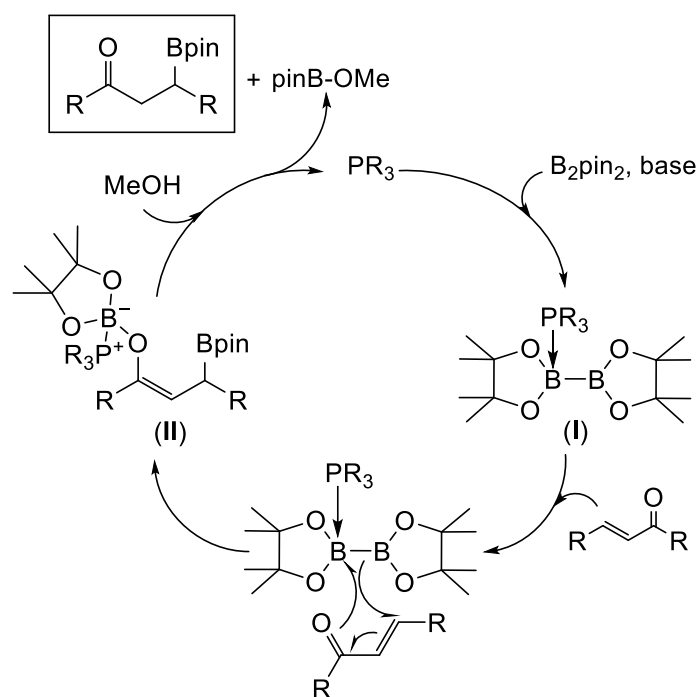
1.1.5. Metal-free β -borylation reactions promoted by other bases

In 2010, Fernández *et al.* reported the metal-free β -borylation of α,β -unsaturated compounds, using B₂pin₂ as the boron source, triphenylphosphine (PPh₃) as the catalyst, MeOH and a base as additives (Scheme 15).^[19] The best results (99% conversion *via* GC analysis) were obtained using Cs₂CO₃ as the base and 20 mol% of PPh₃ in THF at 70 °C; however, the role of the base and, indeed, the phosphine, is still not well understood.^[41-42, 70]



Scheme 15: Phosphine-mediated β -borylation of ethyl crotonate with B₂pin₂.

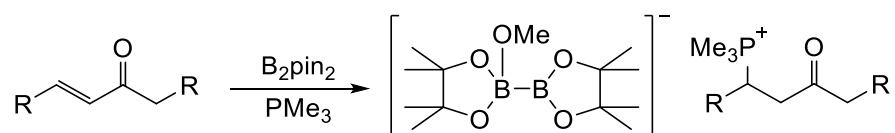
Fernández and co-workers also postulated a mechanism for the phosphine-catalyzed β -borylation reaction. In their initial report, they proposed that the first step is the addition of the “free” phosphine and the base to B₂pin₂, leading to a phosphine-adduct (I), although the role of the base was not addressed. In the second step, the intermediate reacts with the substrate, forming the β -borylated intermediate with another Bpin-species at the oxygen atom (II). After work-up with methanol, the desired product and pinB–OMe are formed (Scheme 16).^[19]



Scheme 16: Initially postulated mechanism for the phosphine-catalyzed β -borylation of α,β -unsaturated carbonyl compounds.

Based on NMR studies, the group of Fernández also suggested a possible neutral $\text{sp}^2\text{-sp}^3$ diboron adduct of B_2pin_2 and PMe_3 . Therefore, they reacted a mixture of PMe_3 and B_2pin_2 in the presence of base and methanol in an NMR tube. The result was that the resonance of the “free” phosphine at -61.9 ppm shifted to -10.5 ppm and the original boron atom signal at 31.6 ppm was transformed into two signals at 39.4 and -9.2 ppm, which may belong to a possible $\text{sp}^2\text{-sp}^3$ diboron adduct; however, they did not succeed in the isolation of the possible $\text{B}_2\text{pin}_2\cdot\text{PMe}_3$ adduct.

Later on, Fernández *et al.* revised their proposal and described that deprotonated MeOH activates the B-B bond of the diboron reagent and the phosphine interacts with the substrate to form zwitterionic phosphonium enolates (Scheme 17).^[71] However, Marder *et al.* presented structures of this adduct $[\text{B}_2\text{pin}_2(\text{OMe})]\text{K}^{[72-73]}$ and the $[\text{B}_2\text{pin}_2(\text{OtBu})]\text{K}$ at two conferences before the publication by Fernández and co-workers.^[74]



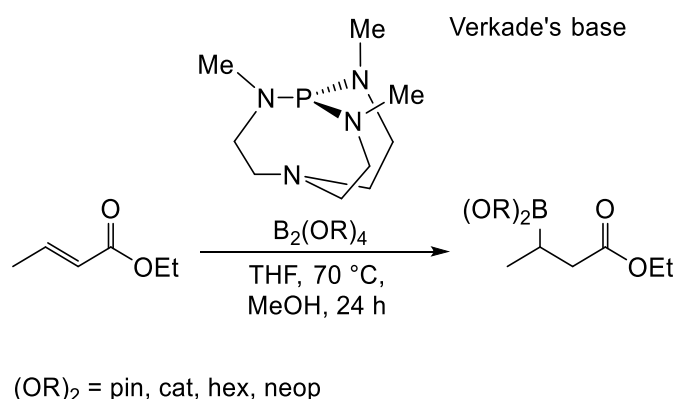
Scheme 17: Possible intermediate during the β -borylation of α,β -unsaturated compounds.

The reaction of B_2pin_2 with PR_3 ($\text{R} = \text{Me}, \text{Cy}, \text{Ph}$) was monitored *via* $^{11}\text{B}\{^1\text{H}\}$ NMR spectroscopy, and they could not observe any difference in the NMR spectra; even theoretical investigations did not give evidence for any adduct formation between B_2pin_2 and the different phosphines. These latter results were consistent with the reported results by Marder, Norman *et al.* in 1997,

when they synthesized several Lewis-base adducts of diborane(4) compounds, such as B_2cat_2 and $B_2(1,2-S_2C_8H_4)_2$, with 4-methylpyridine (mpy; 4-picoline). PMe_2Ph as well as PEt_3 only bound to the dithiocatecholato compound and not to B_2cat_2 .^[75] Marder, Norman and co-workers also reported that 4-picoline did not bind, to a measureable extent, to B_2pin_2 .^[76]

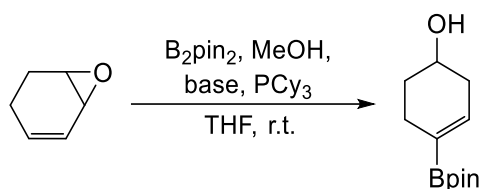
In 2011, Fernández and co-workers described the transition-metal-free diborylation reaction *via* B–B bond activation of the diboron compound with simple Lewis-bases.^[20] They pointed out that using B_2pin_2 is more reactive than B_2cat_2 or B_2neop_2 as well as other diboron reagents in these borylation reactions. They also suggested a mechanism in which $[MeO]^-$, which is *in situ* formed, generates an anionic sp^2 - sp^3 diboron adduct $[B_2pin_2 \cdot OMe]^-$ as the catalytic intermediate.^[77-79] From DFT calculations, Fernández *et al.* thus postulated a possible catalytic cycle wherein the *in situ* formed $[MeO]^-$ activates the B–B bond. The sp^2 -hybridized boron atom attacks the substrate and after work-up, the desired product could be isolated.^[20, 77] Marder *et al.* already mentioned a similar potassium *tert*-butoxide ($KOtBu$) adduct $[B_2pin_2(OtBu)]K$ during their copper-catalyzed borylation of aryl halides in 2009.^[80]

Further investigations by Fernández *et al.* highlighted the importance of the alcohol, especially MeOH. Furthermore, they screened several bases to optimize the reaction conditions. The best results were observed, using Verkade's base^[81-84] (69% conversion *via* GC analysis). With the application of NaOMe or NaOtBu, conversions between 27 and 40% were achieved. They also mentioned that the use of primary alcohols, such as MeOH and *n*BuOH as additives, led to higher conversion than secondary (*i*PrOH) and tertiary (*t*BuOH) alcohols. Another point of the publication was the application of different diboron reagents as the boron source, such as B_2pin_2 , B_2cat_2 , B_2hex_2 (bis(hexenylenglycolato)diboron) and B_2neop_2 , which gave very high conversion up to 99%; only the reaction with B_2neop_2 achieved moderate conversion (78%) (Scheme 18).^[19, 78]



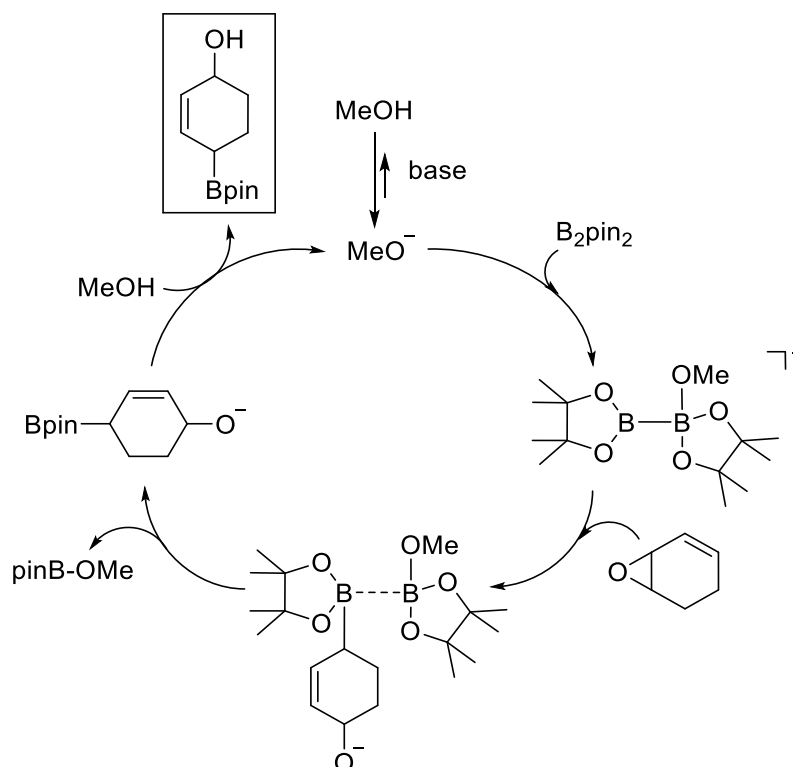
Scheme 18: Verkade's base-mediated β -borylation of ethyl crotonate with different diboron reagents.

Recent publications of Fernández *et al.* report the metal-free borylative ring-opening of vinyl epoxides and aziridines. As an example, they react methanol, base, B_2pin_2 and 3,4-epoxy-1-cyclohexene as the substrate to obtain the corresponding borylated product (Scheme 19).^[85]



Scheme 19: Organocatalytic borylative ring-opening of 3,4-epoxy-1-cyclohexene.

Scheme 20 shows the proposed reaction pathway for the borylative ring-opening of 3,4-epoxy-1-cyclohexene. In 2012, Fernández *et al.* already published the calculated reaction mechanism for the β -borylation of α,β -unsaturated carbonyl compounds, which is comparable to the ring-opening mechanism.^[78] The first step is the deprotonation of methanol followed by the reaction with B_2pin_2 . After adding the substrate to the reaction, the corresponding intermediate was formed. The next step is the elimination of pinB-OMe, and after adding another equivalent of methanol to the reaction mixture, the borylated product is formed and $[OMe]^-$ is regenerated.



Scheme 20: Proposed reaction pathway for the borylative ring-opening of 3,4-epoxy-1-cyclohexene.

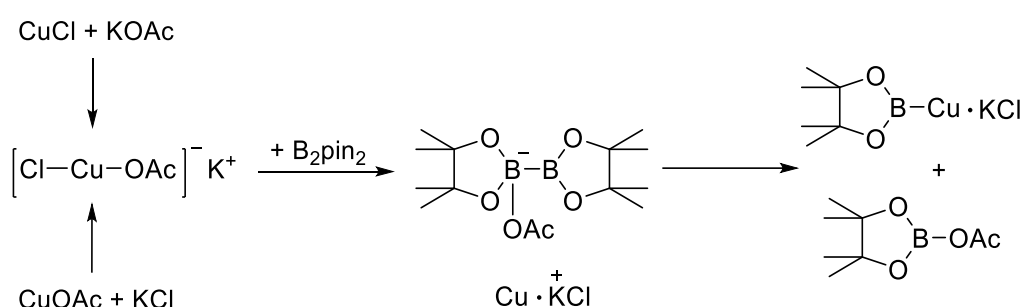
Recently, Fernández *et al.* described a series of different borylation reactions^[35, 77, 86-90] with several compounds, including boryl addition to tosylaldimines,^[91] asymmetric diborylation of alkenes,^[92] borylative ring-opening reactions of vinyl epoxides and aziridines^[85] as well as borylation reaction using mixed diboron reagents, such as pinB-Bdan (dan = $(NH)_2$ -1,8- $C_{10}H_6$),^[93] to transfer a Bdan-moiety to α,β -unsaturated compounds.

1.1.6. sp^2 - sp^3 and sp^3 - sp^3 diboron adducts

1.1.6.1. sp^2 - sp^3 diboron adducts observed in metal-catalyzed borylation reactions

Boronic acids and boronate esters are in widespread use as reagents for organic synthesis, as they are important substrates, for example, in Suzuki-Miyaura cross-coupling reactions.

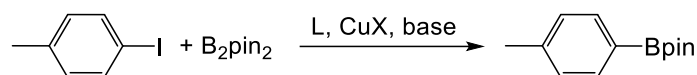
Miyaura and co-workers reported possible intermediates for the copper-catalyzed borylation, the first step is the reaction of CuCl with KOAc to form [Cl-Cu-OAc]K, this intermediate reacts with B_2pin_2 to the active copper-boryl species pinB-Cu·KCl. Further investigations claimed that this reaction took place *via* formation of an *in situ* formed anionic sp^2 - sp^3 diboron adduct “[B_2pin_2OAc][Cu·KCl]”, which then forms pinB-OAc and the catalytic active species pinB-Cu·KCl (Scheme 21).^[30] However, this compound was only identified by a singlet in the 1H NMR spectrum which could be any Bpin-species.^[31-35]



Scheme 21: Formation of a sp^2 - sp^3 diboron adduct *via* reaction of [Cl-Cu-OAc]K with B_2pin_2 and further reaction to pinB-OAc and the catalytic active species pinB-Cu·KCl.^[30]

The proposed, but not yet observed, anionic sp^2 - sp^3 diboron adduct [B_2pin_2OAc][Cu·KCl] is the first example mentioned of an *in situ* formed adduct during the borylation of α,β -unsaturated compounds; however, in the following paragraph, the metal-free borylation reaction is discussed, wherein anionic sp^2 - sp^3 diboron adducts as well as neutral sp^2 - sp^3 diboron adducts play an important role during the catalysis.

Another possibility to generate aryl boronates is the copper-catalyzed borylation of arylhalides with alkoxy diboron reagents $B_2(OR)_4$, which was reported by Marder and co-workers in 2009. Based on the well-characterized boryl-complex [(Dipp₂Im)CuBpin]^[94-96] (Dipp₂Im = 1,3-bis(2,6-di-*iso*-propylphenyl)imidazolin-2-ylidene), which was prepared *in situ* from [(Dipp₂Im)CuOtBu] and B_2pin_2 , the reaction with 4-Me-C₆H₄I leads to the formation of 4-Me-C₆H₄-Bpin.^[80] Marder *et al.* examined the reaction of B_2pin_2 with 4-Me-C₆H₄I using different ligands, bases and CuX sources (Scheme 22).



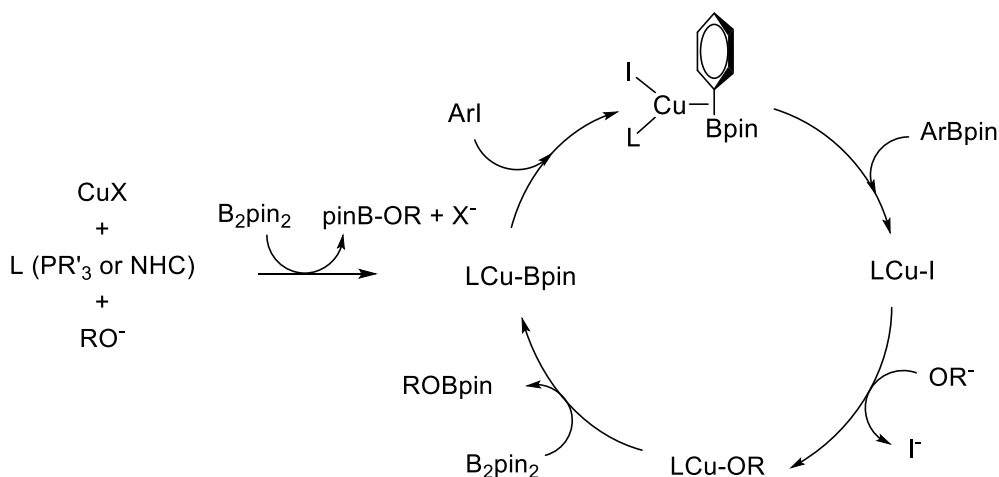
L = PBU₃, PPh₃, dtbpe, pyridine, Me₂bipy
 X = Cl, OAc, I, Cu₂O
 base = KOtBu, KOAc, K₂CO₃

Scheme 22: Reaction of B₂pin₂ with 4-MeC₅H₄I using different ligands, bases and CuX sources.

For example, the reaction of copper(I) iodide, PBU₃ (13 mol%) as the ligand and KOtBu as the base led to a conversion of 100% after 17 hours at room temperature and the isolated yield was 92%. When they used PBU₃ as well as CuX in 3 mol% instead of 13 mol% the conversion was not complete after 17 hours, but when the reaction mixture was heated to 60 °C the conversion was complete after 2.5 hours.

Marder and co-workers also screened different aryl halides and used B₂neop₂ (neop = OCH₂CMe₂CH₂O) instead of B₂pin₂. The fact that the reaction with 4-bromophenyl iodide only led to the 4-bromophenyl boronate shows that the reaction is faster with aryl iodides. The use of B₂neop₂ instead of B₂pin₂ was successful. It gives the corresponding aryl-Bneop compounds in slightly lower yields to those observed with B₂pin₂.^[80]

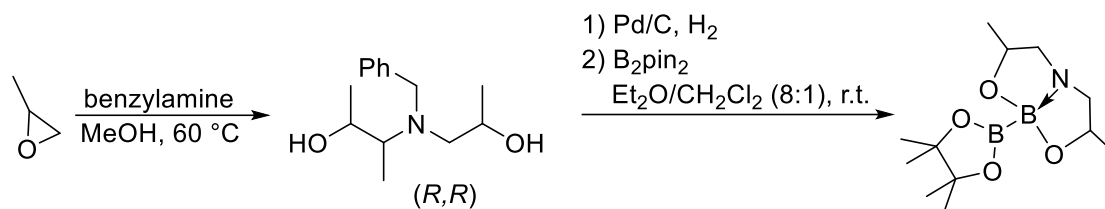
Marder *et al.* also published a possible and simple catalytic cycle for the copper-catalyzed borylation of aryl halides (Scheme 23).



Scheme 23: Possible catalytic cycle for the copper-catalyzed borylation of aryl halides.

Furthermore, Marder *et al.* mentioned, for the first time, the presence of a possible anionic sp²-sp³ diboron adduct, namely [B₂pin₂OtBu]K, which is a potential reason for the observation of traces of products in the absence of copper. Nonetheless, this observation was the beginning of a series of metal-free borylation reactions, using only alkoxide bases, such as KOtBu and MeOH, in catalytic borylation reactions.

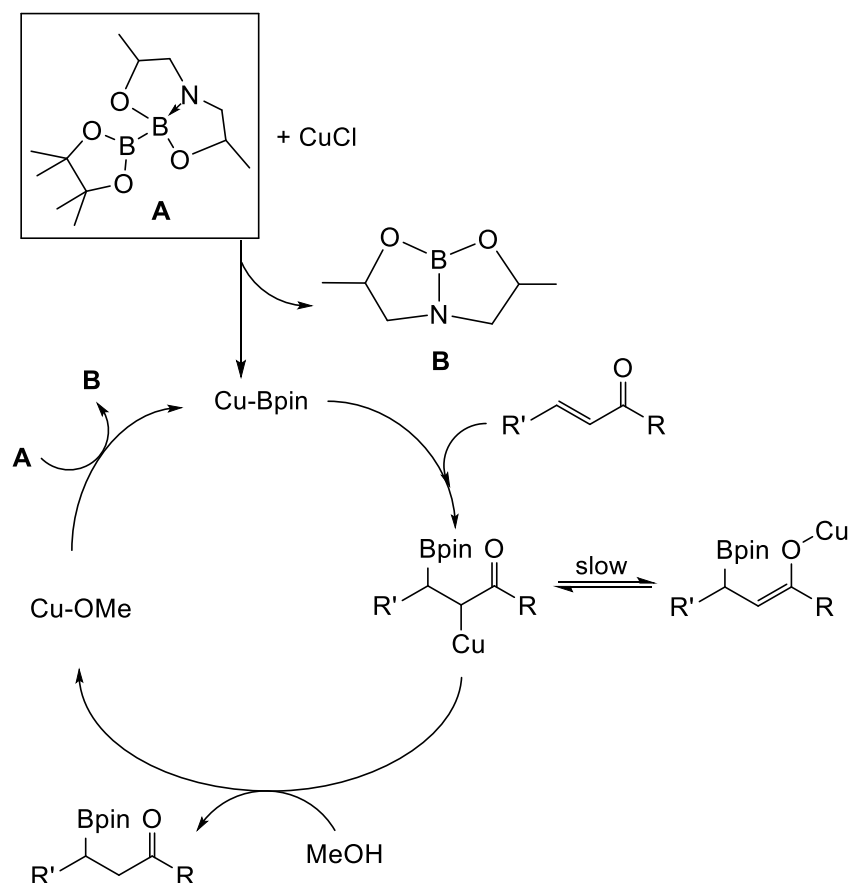
In 2011 Santos and co-workers reported the reaction and full characterization of enantiomerically pure pinacolato di-*iso*-propanol-aminato diboron (PDIPA diboron) to determine the unambiguously coordination at the boron atoms (Scheme 24).^[44]



Scheme 24: Synthesis of enantiomerically pure PDIPA diboron (*R,R*).

Santos *et al.* were able to synthesize large amounts of different borylation products with the application of the “pre-activated” pinacolato di-*iso*-propanol-aminato diboron (PDIPA diboron) and the addition of the Bpin-moiety to the β -carbon atom of the α,β -unsaturated conjugated compounds.

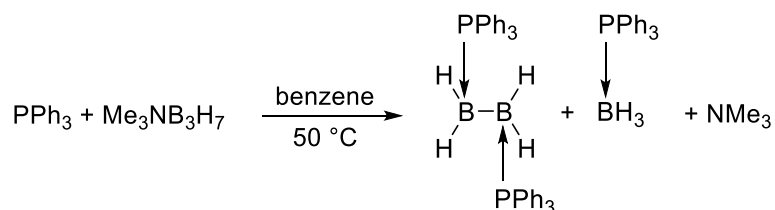
Scheme 25 shows a possible catalytic cycle for the copper-catalyzed borylation. The first step is the reaction of the “pre-activated” PDIPA diboron reagent with CuCl to form a Cu-Bpin species. Afterwards, the α,β -unsaturated conjugated compound is added and the corresponding organo cuprate is generated. The next step is the reaction of methanol with the intermediate to form the desired product and Cu-OMe. With the addition of more PDIPA diboron the catalytic cycle starts again.



Scheme 25: Proposed catalytic cycle for the copper-catalyzed borylation.

1.1.6.2. sp^2 - sp^3 and sp^3 - sp^3 diboron adducts of the type $B_2X_4 \cdot L$ and $B_2X_4 \cdot (L)_2$

The first neutral diboron adducts of the type $B_2X_4 \cdot L$ ($X = Cl$ or F , $L = Et_2O$) were reported by Schlesinger *et al.* in 1949^[97] and 1958^[98] and by Wartik and Apple^[99] ($L = NC(4-C_6H_4F)$). Furthermore, VanDoorne *et al.* published the first structurally characterized diboron adduct of the generally type $B_2X_4 \cdot L$ ($X = H$, $L = PCy_3$) in 1973;^[100] however, this bis-diboron adduct was first mentioned by Graybill and Ruff in 1962.^[101] The bis- PR_3 diboron adduct was synthesized *via* reaction of PPh_3 with the borane $Me_3NB_3H_7$ by cleavage of the B_3H_7 -group (Scheme 26).

Scheme 26: Synthesis of the first reported bis- PR_3 diboron adduct $B_2H_4 \cdot (PPh_3)_2$.

Additional structurally characterized diboron adducts are summarized in Figure 2. In 1970, Schaeffer *et al.* published the structure of the earlier reported $B_2Cl_4 \cdot (NMe_3)_2$ diboron adduct **(I)**.^[102-103] Niedenzu and co-workers synthesized and characterized the bis-diboron adduct $B_2pz_2 \cdot (Hpz)_2$ ($Hpz = \text{pyrazole}$) **(II)** *via* reaction of tetrakis(dimethylamino)diborane $B_2(NMe_2)_4$ with an excess of pyrazole in 1988.^[104] Haubold *et al.* reported the mono-diboron adduct $BCl_2BCl(MeN-CH_2-CH_2-NMe_2)$ **(III)**.^[105] In 1988, the mono-diboron adducts $B_2F_4 \cdot Me_nN(SiMe_3)_{3-n}$ **(IV-VII)** were observed at lower temperature *via* distinct signals in the ^{11}B NMR spectra, which are significantly different from the signal for the starting material; thus, two signals were obtained in the ^{11}B NMR spectra.^[106] Other early examples of mono- and bis-diboron adducts were published by Keller *et al.* in 1992. They isolated and characterized three types of diboron adducts, namely bis-diboron adduct $B_2Br_4 \cdot (PBr_3)_2$ **(VIII)**, mono-diboron adduct $B_2Cl_4 \cdot P(SiMe_3)_3$ **(IX)** and the chelated bis-boron adduct $B_2Cl_4 \cdot (Cl_2P-CH_2-CH_2-PCl_2)$ **(X)**.^[107]

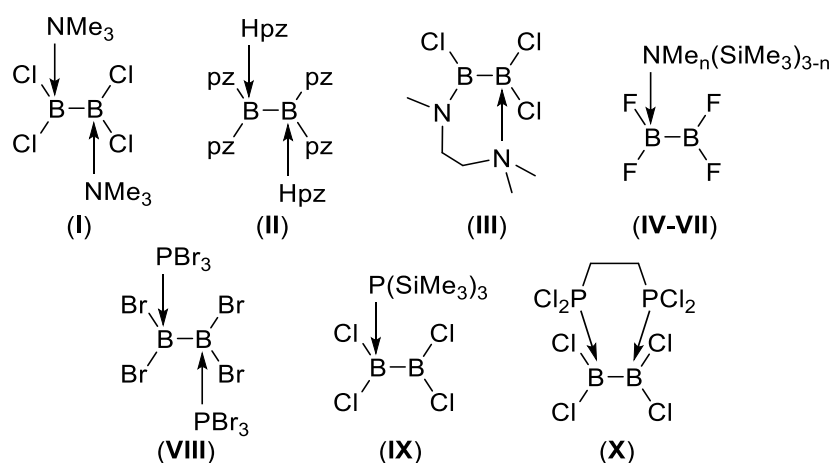


Figure 2: Structurally characterized mono- and bis-diboron adducts $B_2X_4 \cdot L$ and $B_2X_4 \cdot (L)_2$.

Recently, Braunschweig *et al.* reported several examples of diboron adducts with phosphines and NHCs as well as amines, with diboron reagents of the type $B_2X_2R_2$ ($X = Cl, Br, R = Mes$). The reaction of $(Cl)(Mes)B-B(Mes)(Cl)$ with Mes_2Im ($Mes_2Im = 1,3\text{-bis}(2,4,6\text{-trimethylphenyl})\text{imidazolin-2-ylidene}$) yielded a neutral $sp^2\text{-}sp^3$ diboron adduct $Mes_2B-BCl_2 \cdot Mes_2Im$ **(XI)** with an unexpected exchange of one mesityl-group and a chloride (Figure 3).^[108]

In 2012, similar results were published using phosphines (PEt_3 and $PMeCy_2$) instead of an NHC; however, only in the case of the sterically less demanding PEt_3 , the major product was the expected $(Br)(Mes)B-B(Mes)(Br) \cdot PEt_3$ diboron adduct **(XII)** with a rare $B-Br-B$ bridge. Albeit, the reaction of the sterically more demanding phosphine $PMeCy_2$ provided the similar exchanged mono phosphine-diboron adduct **(XIII)** as reported one year before (Figure 3).^[109] A further example is the reaction of $(I)(Mes)B-B(Mes)(I)$ ($I = \text{iodide}$) with two equivalents of NEt_3 in pentane at room temperature; the products are a racemic mixture of two boracycles **(XIV and XV)** and $[Et_3NH][I]$ as the by-product.^[110]

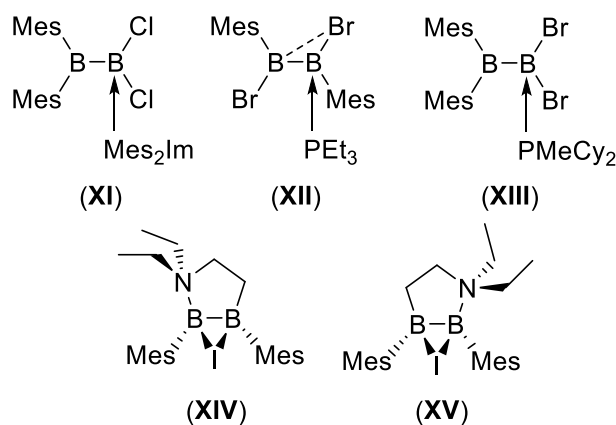


Figure 3: Several reported examples of adduct formations of diboron reagents of the type $B_2X_2R_2$ ($X = Cl, Br, R = Mes$).

In summary, all these mentioned sp^2 - sp^3 and sp^3 - sp^3 diboron adducts of the type $B_2X_4 \cdot L$ and $B_2X_4 \cdot (L)_2$ have in common that first substitution of the ligand (L) takes place at the boron atom with the higher Lewis-acidity of the substituents. Furthermore, the coordination at the second boron atom is possible; however, it is dependent on the steric hindrance and the size of the substituents at the sp^2 -hybridized boron atom. Furthermore, some examples showed that the substituents at the boron atoms can exchange and migrate to the other boron atom to minimize the steric hindrance, so that the sp^3 - sp^3 adducts can be formed (Figure 4).

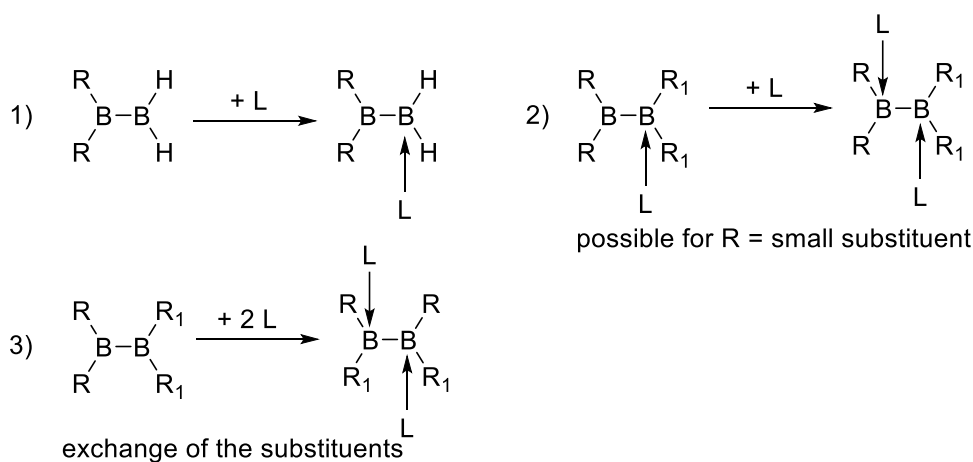
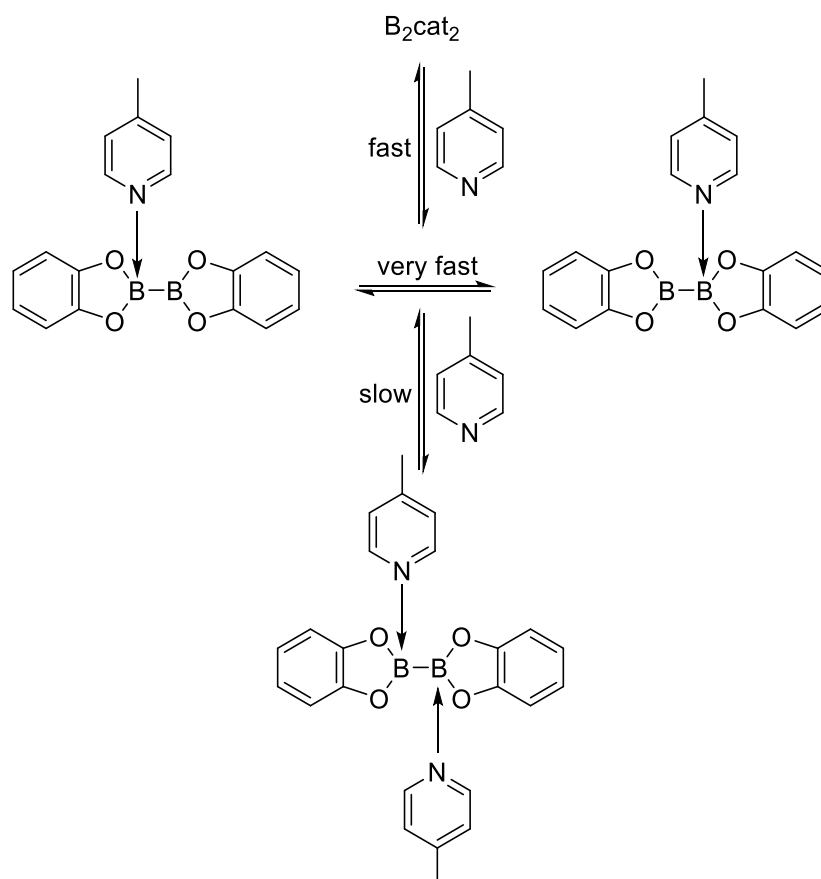


Figure 4: Overview of the coordination of the ligands to the boron reagent, dependent on the size of the ligand and the Lewis-acidity of the substituents at the boron atom.

1.1.6.3. sp^2 - sp^3 and sp^3 - sp^3 diboron adducts of the type $B_2(OR)_4 \cdot L$ and $B_2(OR)_4 \cdot (L)_2$

In the literature, anionic sp^2 - sp^3 diboron compounds are often proposed as intermediates in the catalytic cycle of metal-promoted as well as metal-free borylation reactions. Recent reports proposed that B_2pin_2 reacts with different bases, such as $KOMe$ ^[20] or $KOtBu$ ^[80] as well as $KOAc$ ^[111] to form anionic sp^2 - sp^3 diboron adducts, likely activating the B–B-bond; however, there are only a few examples of isolated neutral and anionic adducts known in the literature.^[77, 112]

In 1995, Marder, Norman and co-workers reported the reaction of B_2cat_2 and one or two equivalents of 4-methylpyridine (mpy), which led to the formation of the mono- and bis-adducts $B_2cat_2 \cdot (mpy)$ and $B_2cat_2 \cdot (mpy)_2$. These were the first structurally characterized diboron adducts of the type $B_2(OR)_4$ (Scheme 27).^[76]



Scheme 27: Mono- and bis-adducts $B_2cat_2 \cdot (mpy)$ and $B_2cat_2 \cdot (mpy)_2$.

Furthermore, in 1997, Marder, Norman *et al.* reported further mono- and bis-diboron adducts of $B_2(1,2-S_2C_6H_4)_2$ with 4-methylpyridine as well as phosphines (PMe_2Ph and PEt_3) *via* reaction of the thioborane with one or two equivalents of Lewis-base.^[75] So far, no further phosphine adducts of the type $B_2(OR)_4 \cdot PR_3$ or $B_2(OR)_4 \cdot (PR_3)_2$ were characterized or even isolated;

however, Norman, Orpen *et al.* claimed the formation of the mono- and bis-phosphine diboron adducts $B_2cat_2 \cdot PMe_3$ and $B_2cat_2 \cdot (PMe_3)_2$ during their study on platinum-boryl-complexes.^[113] At this time, the phosphine mediated mono- and bis-diboron adducts could only be observed using the corresponding thioboranes ($B_2(1,2-S_2C_6H_4)_2$) which are more Lewis-acidic than the analogous oxygen-containing compounds.

Recently, Ingleson *et al.* reported similar results on the synthesis of sp^2-sp^3 as well as sp^3-sp^3 diboron adducts as Marder, Norman and co-workers; however, they observed a rare rearrangement of B_2cat_2 .^[114] The reaction of B_2cat_2 with one or two equivalents of 1,5-diazabicyclo[4.3.0]non-5-ene (DBN) yielded the desired mono- and bis-diboron adducts $B_2cat_2 \cdot (DBN)$ and $B_2cat_2 \cdot (DBN)_2$. The ^{11}B NMR spectrum of the bis-diboron adduct displayed two signals instead of the expected single signal; however, through recrystallization of the compounds, they could identify the second peak as the bis-adduct of the 1,2 isomeric form of B_2cat_2 (Figure 5).

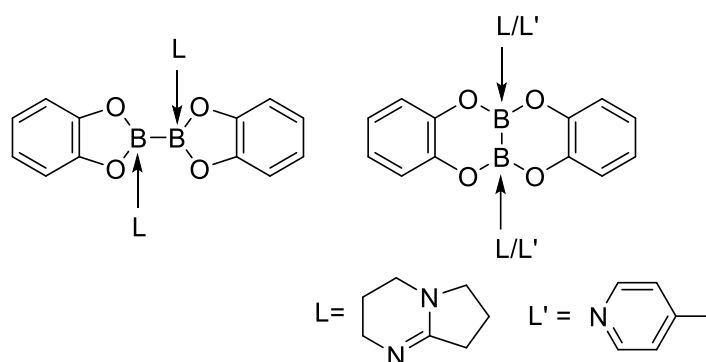


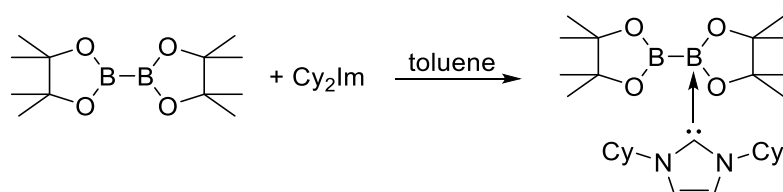
Figure 5: Structures of the two isomers of $B_2cat_2 \cdot (DBN)_2$; left 1,1- $B_2cat_2 \cdot (DBN)_2$ and right 1,2- $B_2cat_2 \cdot (DBN)_2$.

In addition, this report by Ingleson *et al.* confirmed earlier results that the substituents on the boron atoms can migrate or rearrange. This kind of rearrangement of B_2cat_2 (common one: 1,1- B_2cat_2) to the uncommon 1,2- B_2cat_2 (and its similar boron compounds)^[5, 115] was not often reported in the literature, however, similar observations were reported in the case of $B_2(BINOL)$ ^[116] (BINOL = binaphthalenolate or binolate) and $B_2cat(NMe_2)_2$.^[117]

In 2009, Santos and co-workers published a novel sp^2-sp^3 diboron reagent, which can be used for catalytic regioselective borylation of α,β -unsaturated conjugated compounds.^[43-45] This sp^2-sp^3 diboron adduct can be regarded as an intramolecular variety of these diboron adducts (Scheme 24).

Marder *et al.* published the isolation and full characterization of the neutral sp^2-sp^3 diboron adduct $B_2pin_2 \cdot Cy_2Im$ ^[51], which was incorrectly characterized by Hoveyda and co-workers.^[18, 23]

Based on the stoichiometric reaction of B_2pin_2 with Cy_2Im in toluene, they were able to obtain the corresponding neutral diboron adduct *via* crystallization from toluene (Scheme 28).



Scheme 28: Synthesis of the neutral sp^2 - sp^3 diboron adduct $B_2pin_2 \cdot Cy_2Im$.

^{11}B NMR spectra at different temperatures gave evidence for a dynamic behavior of the neutral adduct in solution. At 50 °C, one signal at 20.4 ppm is detected. No signal is obtained at 20 °C due to the broadening of the signal close to the coalescence temperature. However, at 5 °C, two signals at 2.4 and 37.2 ppm are detected, consistent with the existence of one sp^2 and one sp^3 -hybridized boron atom.^[23] These results are in good agreement with the solid state NMR of the neutral adduct. Additionally, the recorded ^{11}B NMR spectra confirmed the evidence that the ligands, in this case the NHC, could exchange between the two boron atoms of the B_2pin_2 . In general, the combination and further reaction of diboron reagents, such as B_2pin_2 , B_2cat_2 or B_2neop_2 , with different alkoxide bases, e.g. $[OMe]^-$, $[OtBu]^-$ as well as $[F]^-$ leads to anionic sp^2 - sp^3 diboron adducts. Furthermore, the use of NHCs or phosphines (PR_3) leads to neutral sp^2 - sp^3 diboron adducts, which is shown in Figure 6.

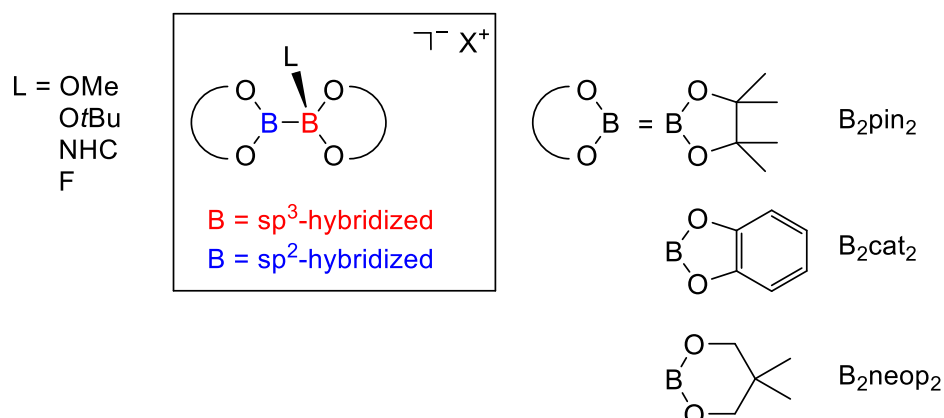
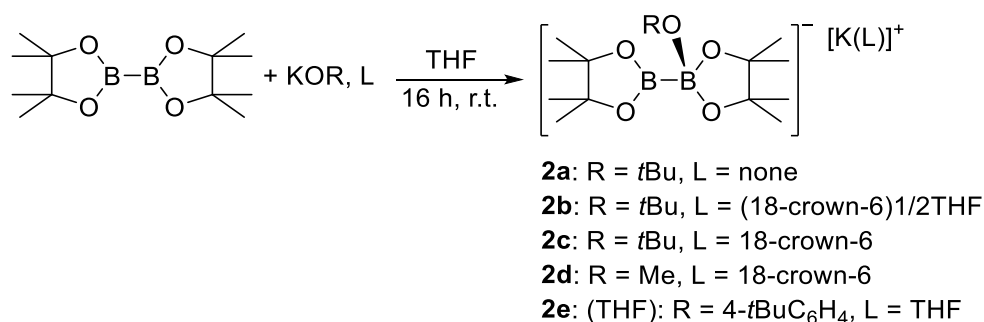


Figure 6: General scheme of anionic and neutral sp^2 - sp^3 diboron compounds.

1.2. Results and Discussion

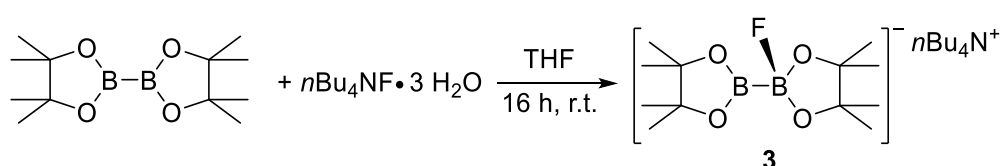
1.2.1. Studies on formation and reactivity of anionic sp^2 - sp^3 diboron adducts of the type $[B_2pin_2(OR)][M]$ **2a-2e** and $[B_2pin_2F][nBu_4N]$ **3**

In earlier studies, Marder *et al.* observed that the adduct of B_2pin_2 and $KOtBu$ is formed under the reaction conditions of the copper-catalyzed borylation of aryl-halides, as a sparingly soluble solid.^[80] This anionic adduct is responsible for low yields of aryl-Bpin *via* an un-catalyzed background reaction of aryl iodides. Further characterization of this adduct $[B_2pin_2(OtBu)]K$ showed that it is an anionic sp^2 - sp^3 diboron adduct. Furthermore, single X-ray diffraction and solid state NMR confirmed the existence of the anionic adduct. Lin, Kleeberg, Marder *et al.* reacted B_2pin_2 with other alkoxide bases, such as $[OMe]^-$ and $[4-tBuC_6H_4O]^-$ to obtain several anionic sp^2 - sp^3 diboron adducts (Scheme 29).^[74]



Scheme 29: Synthesis of several anionic sp^2 - sp^3 diboron adducts of B_2pin_2 and alkoxide bases.

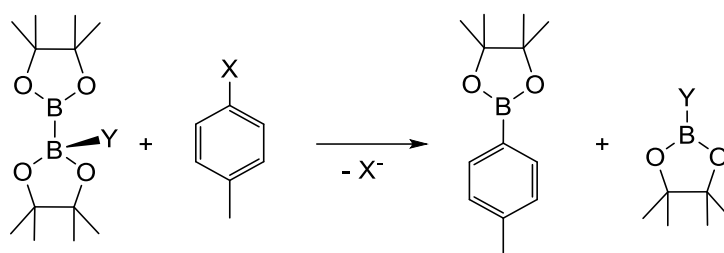
The presence of 18-crown-6 (18-C-6) improves the solubility of the anionic adducts significantly and the monomeric compounds can be obtained, such as $[(B_2pin_2OtBu)K][(18-C-6)(thf)_2K]$. The monomeric compounds $[(B_2pin_2OtBu)K][(18-C-6)]$ **2c** and $[(B_2pin_2OMe)K][(18-C-6)]$ **2d** are isolated in moderate to good yield. Furthermore, $[B_2pin_2O(4-tBuC_6H_4)]K$ **2e** is a polymeric compound and was isolated from the reaction of B_2pin_2 with $KO(4-tBuC_6H_4)$. The sterically more demanding phenolate $KO(4-Me-2,6-tBuC_6H_4)$ does not lead to the observation of an adduct. The reaction of $nBu_4NF \cdot 3 H_2O$ with B_2pin_2 led to the formation of the corresponding fluoride adduct $[B_2pin_2F][nBu_4N]$ **3** (Scheme 30).



Scheme 30: Synthesis of the anionic adduct $[B_2pin_2F][nBu_4N]$ **3**.

Marder and co-workers first examined the reactivity of the adducts with an aryl iodide and a diazonium $[BF_4]^-$ salt. The NMR spectra showed that the main-product is the corresponding

aryl-Bpin, but there were still more compounds detected, such as toluene and free diazonium $[\text{BF}_4]^-$ salt (Scheme 31).^[80]



Scheme 31: Reaction of the anionic $\text{sp}^2\text{-sp}^3$ diboron compound ($\text{Y} = [\text{OtBu}]^-$) with 4-methyl-phenyl diazonium tetrafluoroborate ($\text{X} = \text{N}_2^+$) and 4-methylphenyliodide ($\text{X} = \text{I}$).

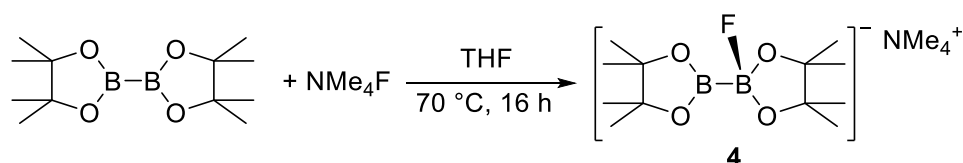
In contrast to the results of Zhu and Yamane in MeOH, Marder *et al.* did not observe any conversion in the reaction of phenyldiazonium tetrafluoroborate $[\text{C}_6\text{H}_5\text{N}_2][\text{BF}_4]$ with B_2pin_2 in acetonitrile at room temperature, although heating of the reaction produced 3% GC-MS yield.^[118] The conversion to the corresponding aryl-Bpin was observed only after adding a base to the reaction mixture or when the reaction was heated to 70 °C, but in each case the yield was low (3-40%), albeit, these results are in good agreement with the reported yield by Yamane and Zhu (45%).^[118]

1.2.2. Synthesis of the fluoride adducts of the type $[\text{B}_2(\text{OR})_4\text{F}][\text{NMe}_4]$

1.2.2.1. Synthesis of the anionic $\text{sp}^2\text{-sp}^3$ diboron adduct $[\text{B}_2\text{pin}_2\text{F}][\text{NMe}_4]$ 4

The main goals of this part of the work were the synthesis and characterization of other anionic adducts and examination of their reactivity towards various diazonium $[\text{BF}_4]^-$ salts and other electrophiles. In preliminary studies, Kleeberg worked on the synthesis and characterization of different adducts involving B_2pin_2 and alkoxide bases.^[74]

The initial focus was the reaction of B_2pin_2 with anhydrous NMe_4F . Therefore, one equivalent of B_2pin_2 and NMe_4F were dissolved in THF and heated overnight at 70 °C. After cooling to room temperature, a colorless solid was collected by filtration to obtain the anionic $\text{sp}^2\text{-sp}^3$ diboron adduct $[\text{B}_2\text{pin}_2\text{F}][\text{NMe}_4]$ 4 (Scheme 32).



Scheme 32: Synthesis of the anionic $\text{sp}^2\text{-sp}^3$ diboron adduct $[\text{B}_2\text{pin}_2\text{F}][\text{NMe}_4]$ 4.

The anionic sp^2 - sp^3 diboron adduct $[B_2pin_2F][NMe_4]$ **4** was characterized *via* 1H , $^{11}B\{^1H\}$, ^{19}F and $^{13}C\{^1H\}$ NMR spectroscopy as well as solid state NMR spectroscopy and elemental analysis. X-ray structure analysis confirmed the existence of the anionic sp^2 - sp^3 diboron adduct. The 1H NMR spectrum shows one broad singlet for the methyl-groups of the B_2pin_2 at 1.02 ppm and another singlet at 3.14 ppm for the methyl-groups of the amine. In the $^{11}B\{^1H\}$ NMR spectrum, the signal for the sp^3 -boron atom is detected at 7.68 ppm and the sp^2 -boron atom at 35.0 ppm, which is in good agreement with the signals of the $[B_2pin_2F][nBu_4N]$ adduct **3** (5.1 and 31.4 ppm) (Figure 7).

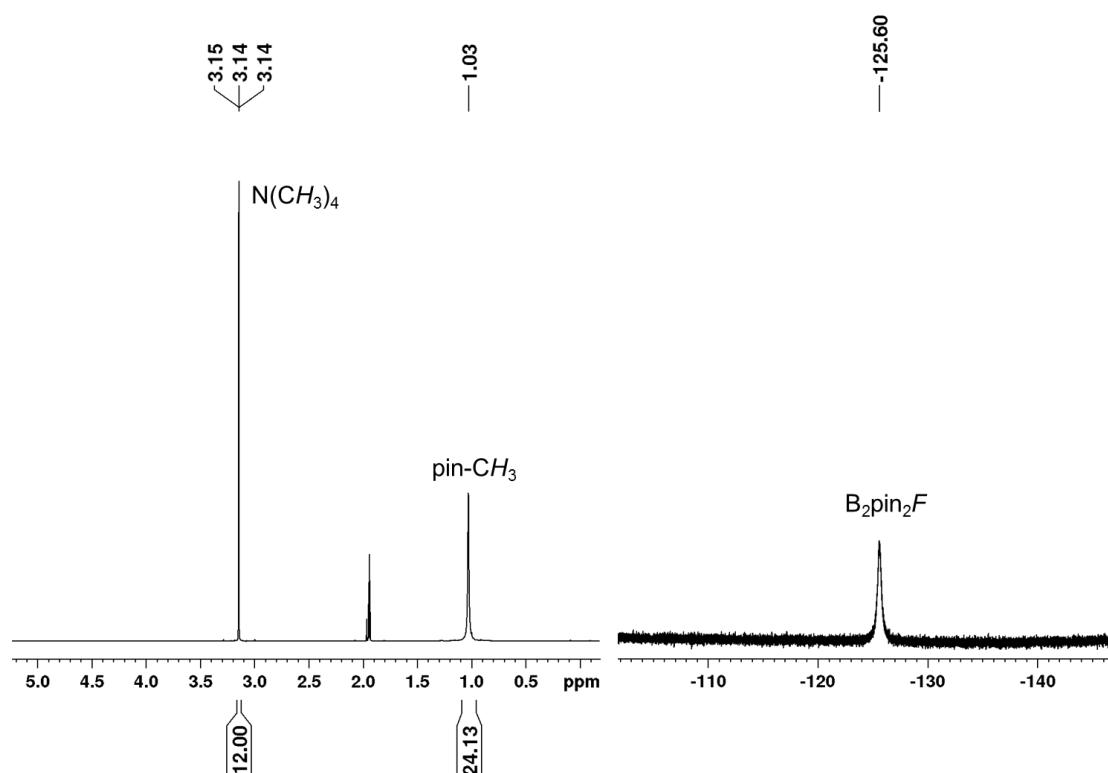


Figure 7: 1H (left) and ^{19}F (right) NMR spectra of compound $[B_2pin_2F][NMe_4]$ **4** in $MeCN-d_3$.

The resonance of the fluorine atom is detected at -125.6 ppm in the ^{19}F NMR spectrum, which is also comparable to the results of the similar adduct $[B_2pin_2F][nBu_4N]$ (-129.5 ppm). The $^{13}C\{^1H\}$ NMR spectrum shows one signal for the carbon atom of the methyl-groups in B_2pin_2 at 26.1 ppm as well as a triplet for the methyl-groups of the amine at 56.1 ppm ($^1J_{CN} = 3$ Hz). The quaternary carbon atom of the Bpin-moiety is detected at 79.4 ppm. As the 1H NMR spectrum showed only one signal for the methyl-groups of the two chemically different Bpin-moieties, the anionic sp^2 - sp^3 diboron adduct was also measured at lower temperature to obtain the signals for the methyl-groups in the expected ratio of 12:6:6 which was observed at -40 °C. Furthermore, to verify the results, the solid state NMR spectrum of compound **4** was recorded (Figure 8). As expected, two signals were observed in the solid state ^{11}B NMR spectrum, one

sharp signal at 5.0 ppm for the sp^3 -hybridized boron atom and one broad signal at 37.5 ppm for the sp^2 -hybridized boron atom.

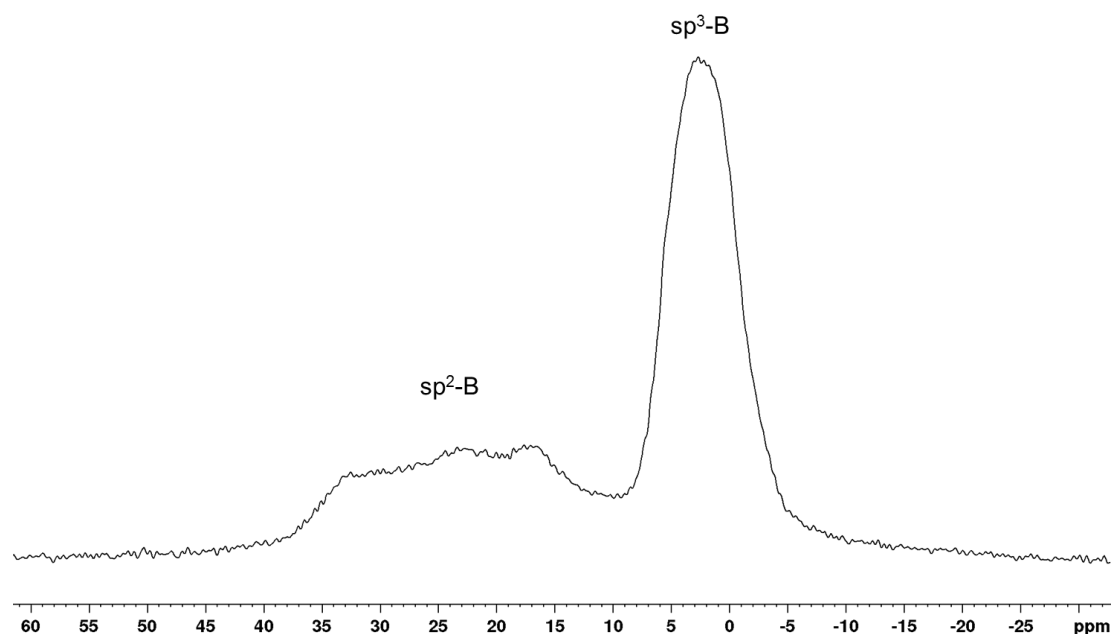


Figure 8: Solid state ^{11}B NMR spectrum of $[\text{B}_2\text{pin}_2\text{F}][\text{NMe}_4]$ **4**; reproduced from ref. [74] with permission from Wiley-VCH.

Additionally, single crystals of $[\text{B}_2\text{pin}_2\text{F}][\text{NMe}_4]$ **4** were obtained *via* heating adduct **4** and THF to 100 °C within 2 h. After 4 h at this temperature the sample was cooled to room temperature within 150 h. In the tube two types of crystals were found, colorless needles and prisms. A needle shaped crystal was used for X-ray diffraction to confirm the structure of the anionic part in $[\text{B}_2\text{pin}_2\text{F}][\text{NMe}_4]$ **4**. The molecular structure of adduct **4** is similar to those of the alkoxy adducts $[\text{B}_2\text{pin}_2(\text{OR})]\text{K}$ **2a-e** and similar to the fluoride adduct $[\text{B}_2\text{pin}_2\text{F}][\text{N}n\text{Bu}_4]$ **3**. The boron atom B1 is essentially planar, while B2 is tetrahedral (Figure 9). The B–B distance (1.736(8) Å) is slightly shorter than those found in the molecular alkoxy adduct $[\text{B}_2\text{pin}_2(\text{OMe})]\text{K}$ **2d** (1.753(2) Å).^[74] The longer B–F distance of 1.478(3) Å compared to simple $[\text{BF}_4]^-$ salts (1.369(5) Å on average)^[119-120] suggests a weaker bonding of the fluorine atom due to the increased donor capabilities of the alkoxy compared to the fluoride-group; however, the B–F bond is similar to this observed for the analogues adduct **3** (1.450(3) Å). The B–O distances are essentially similar to those observed for the alkoxy adducts **2a** and **2e**. The angles F1-B2-O3 and F1-B2-O4 are more similar to each other than the respective O5-B2-O3 and O5-B2-O4 angles in the alkoxy adducts, as they are not influenced by coordination to a potassium cation. All bond lengths and angles are comparable with those found in the analogous adduct $[\text{B}_2\text{pin}_2\text{F}][n\text{Bu}_4\text{N}]$ **3**.^[74]

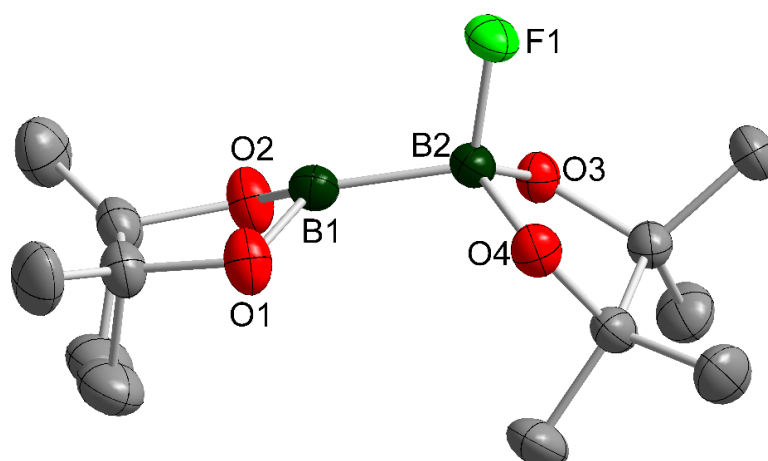
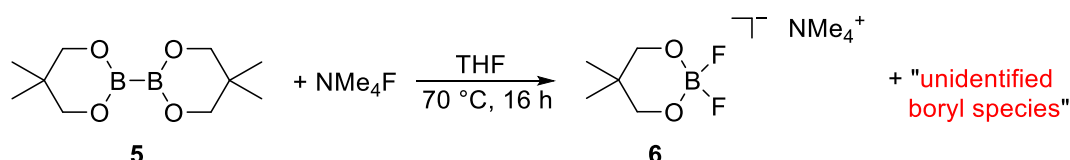


Figure 9: Perspective view of the anionic part of $[B_2pin_2F][Me_4N]$ **4** from **4(thf)**. Thermal ellipsoids are drawn at the 50% probability level; hydrogen atoms and the counter ion are omitted for clarity. Selected bond distances (Å) and angles ($^\circ$): B1–B2 1.736(8), F1–B2 1.478(2), O1–B1 1.389(2), O2–B1 1.394(2), O3–B2 1.472(2), O4–B2 1.468(2); O3–B2–O4 105.55(13) $^\circ$, O3–B2–F1 108.99(13), O4–B2–F1 106.79(13), O3–B2–B1 112.33(14), O4–B2–B1 115.50(14), F1–B2–B1 107.42(13); reproduced from ref. [74] with permission from Wiley-VCH.

1.2.2.2. Reaction of B_2neop_2 with NMe_4F

The reaction to form the anionic sp^2 - sp^3 diboron adduct $[B_2neop_2F][NMe_4]$ **7** was done under the same conditions as for adduct **4**. Stoichiometric amounts of B_2neop_2 **5** and NMe_4F were dissolved in THF and heated to 70 $^\circ C$ for 16 hours, due to the solubility of NMe_4F in refluxing THF (Scheme 33).



Scheme 33: Reaction of B_2neop_2 **5** with NMe_4F in THF.

The NMR spectra of the isolated solid did not correspond to the expected anionic sp^2 - sp^3 diboron adduct $[B_2neop_2F][NMe_4]$ **7**. The $^{11}B\{^1H\}$ NMR spectrum shows one sharp triplet at -0.32 ppm, and in the ^{19}F NMR spectrum, a quartet is detected at -150.8 ppm (Figure 10).

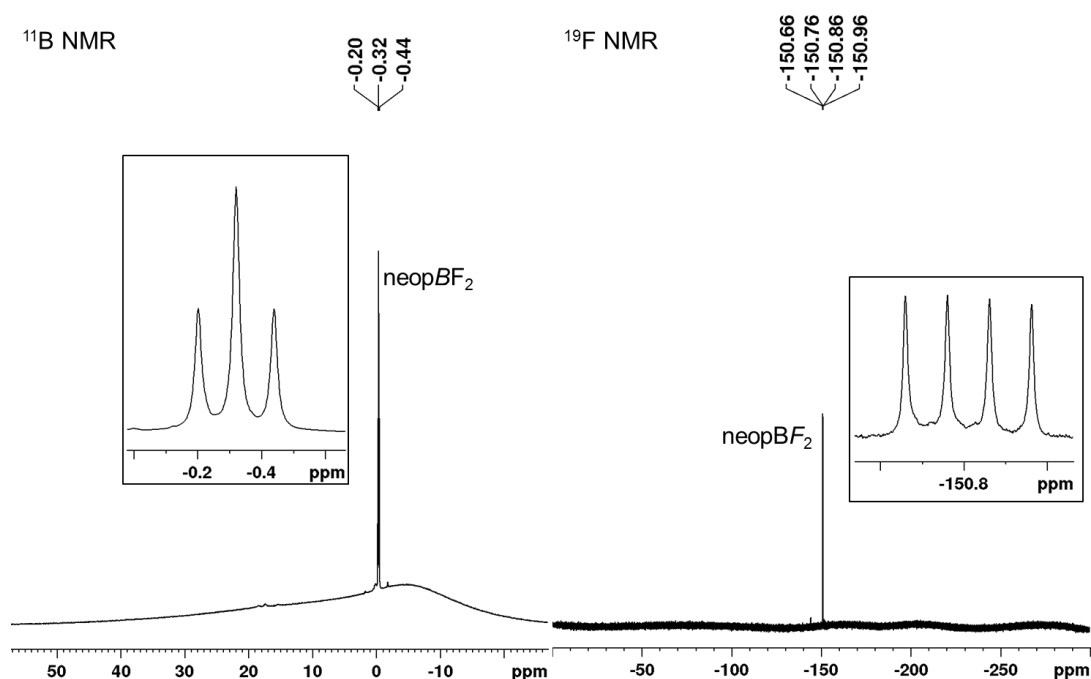


Figure 10: $^{11}\text{B}\{^1\text{H}\}$ (left) and ^{19}F (right) NMR spectra of $[\text{neopBF}_2][\text{NMe}_4]$ **6** (MeCN-d_3).

Furthermore, the ^1H NMR spectra reveals one singlet at 0.80 ppm with an integral of 6, which is assigned to the methyl-groups of the neop-moiety, and one further signal at 3.29 ppm with an integral of 4 for the CH_2 -group of the neop unit (Figure 11). In addition to the mentioned signals, one further signal for the methyl groups of NMe_4F are detected at 3.10 ppm. All of these NMR data indicate that the adduct $[\text{B}_2\text{neop}_2\text{F}][\text{NMe}_4]$ was not present; however, the measured NMR spectra suggested that the isolated compound is $[\text{neopBF}_2][\text{NMe}_4]$ **6**.

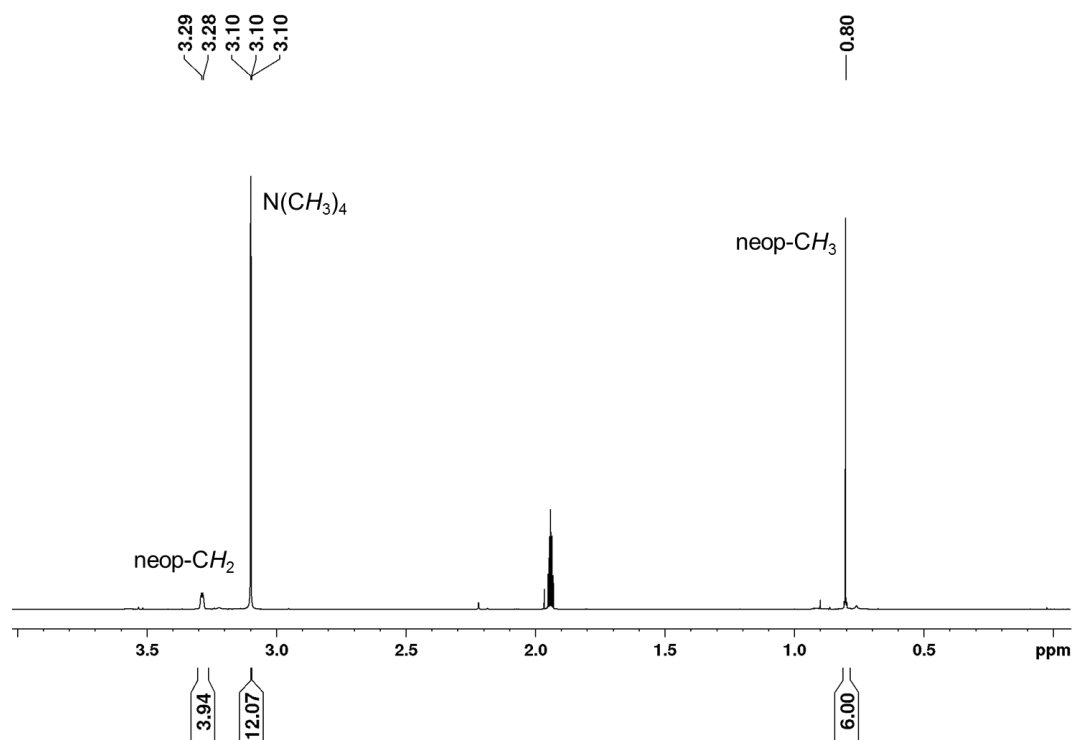
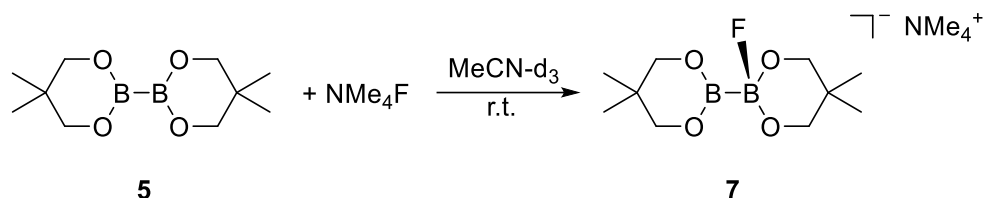


Figure 11: ^1H NMR spectrum of $[\text{neopBF}_2][\text{NMe}_4]$ **6** (MeCN-d_3 , 500 MHz).

Based on our knowledge that the NMe_4F salt is soluble in acetonitrile and furthermore, that the synthesized adduct **4** has also a good solubility in this solvent, the reaction of B_2neop_2 with NMe_4F was investigated on an NMR scale. Therefore, B_2neop_2 and NMe_4F were dissolved in 0.6 mL of MeCN-d_3 and NMR spectra of the reaction mixture were measured immediately (Scheme 34).



Scheme 34: NMR scale reaction of B_2neop_2 **5** with NMe_4F in MeCN-d_3 .

The NMR data indicate that the adduct formation of $[\text{B}_2\text{neop}_2\text{F}][\text{NMe}_4]$ **7** took place; however, both signals for the protons at the neop-moiety are significantly broadened, which could indicate that the decomposition of the “*in situ* formed” anionic $\text{sp}^2\text{-sp}^3$ diboron adduct had already occurred (Figure 12). Furthermore, the ^{19}F NMR spectra suggests the possible presence of the adduct $[\text{B}_2\text{neop}_2\text{F}][\text{NMe}_4]$ **7** as well as the decomposition product $[\text{neopBF}_2][\text{NMe}_4]$; however, in the $^{11}\text{B}\{^1\text{H}\}$ spectrum, the decomposition product, as well as B_2neop_2 , are detected. In the ^{19}F NMR spectrum, one broad singlet and a quartet are both observed at -150 ppm, where the quartet belongs to the decomposition product $[\text{neopBF}_2][\text{NMe}_4]$ **6** and the singlet to the “*in situ*” formed adduct **7** (Figure 13). Unfortunately, further investigations of the reaction of B_2neop_2 with NMe_4F did not lead to a better characterization of these two types of compounds.

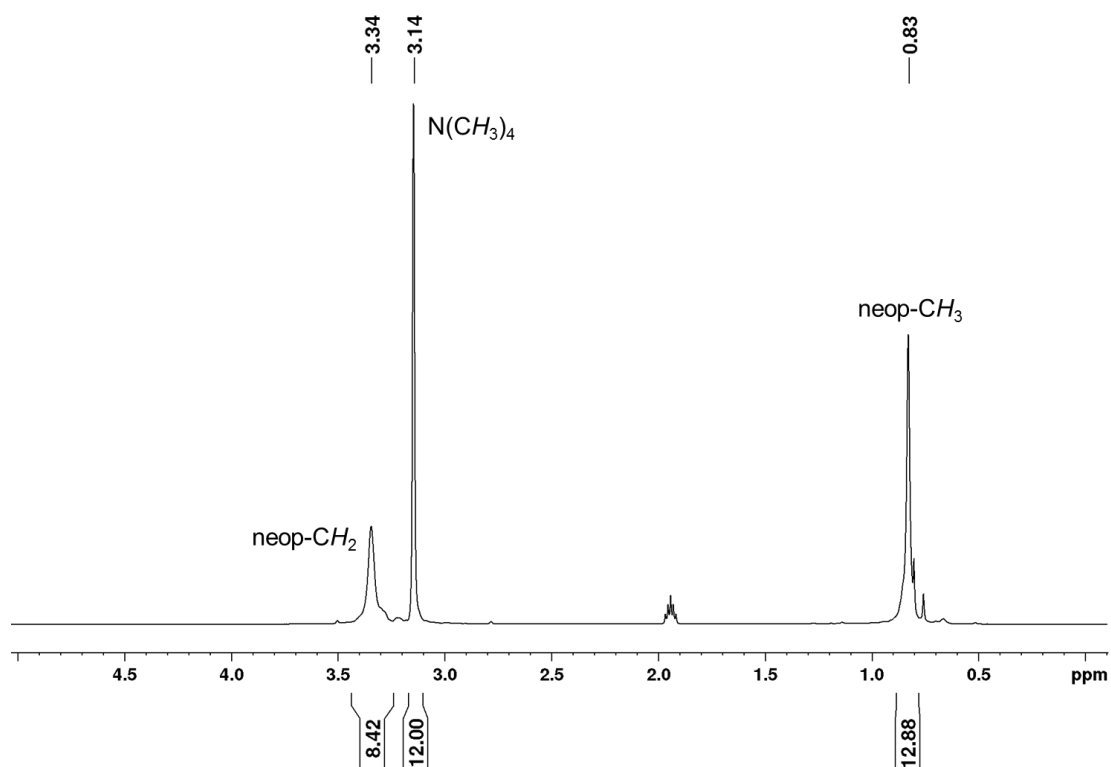


Figure 12: *In situ* ^1H NMR spectrum of the reaction of B_2neop_2 **5** with NMe_4F taken after 10 minutes at room temperature (reactant ratio: 1:1; 200 MHz, MeCN-d_3).

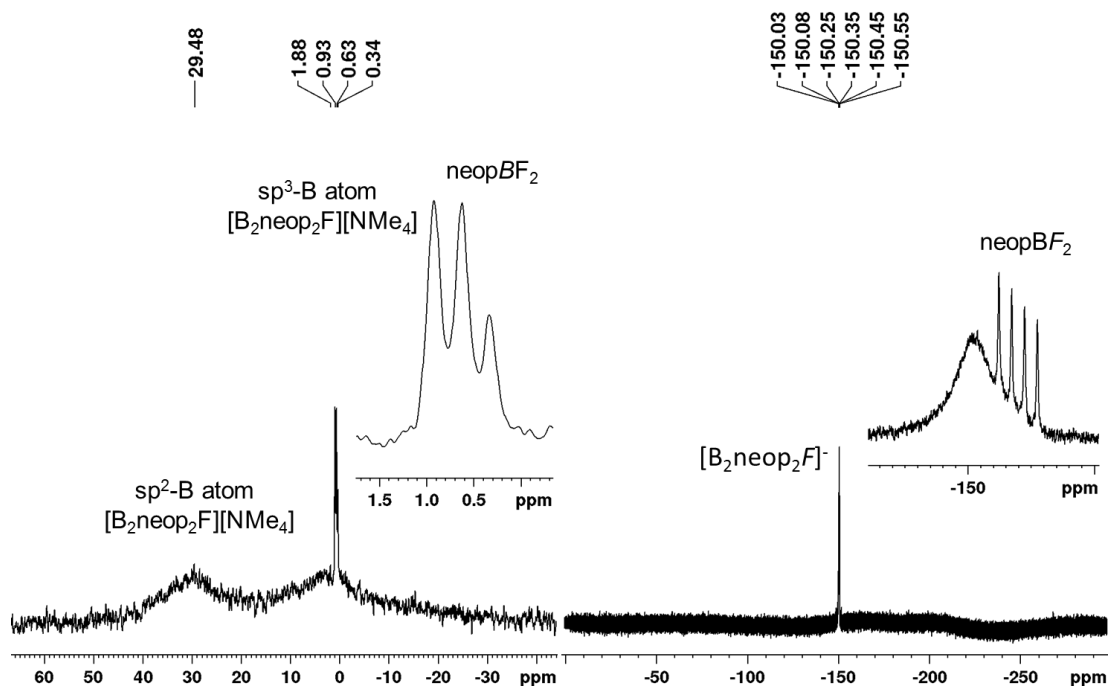


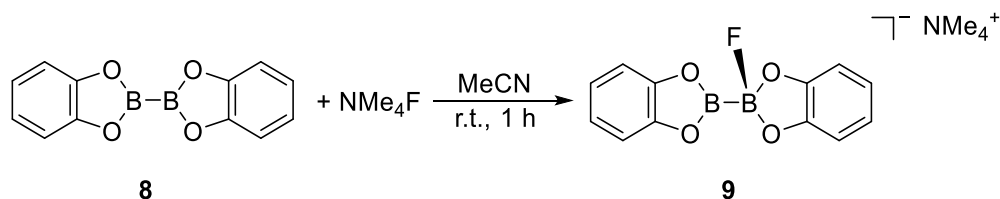
Figure 13: *In situ* $^{11}\text{B}\{^1\text{H}\}$ (left) and ^{19}F (right) NMR spectrum of the reaction of B_2neop_2 **5** with NMe_4F taken after 10 minutes at room temperature (reactant ratio: 1:1; MeCN-d_3).

1.2.2.3. Reaction of B₂cat₂ with NMe₄F

Based on the successful borylation reaction with adduct **4** and the *in situ* formed adduct [B₂neop₂F][NMe₄] **7** with the diboron reagents B₂pin₂ **1** and B₂neop₂ **5**, the next investigation was the reaction of B₂cat₂ **8** with NMe₄F to synthesize a third anionic sp²-sp³ diboron compound. Therefore, B₂cat₂ **8** and NMe₄F were dissolved in THF and heated to 70 °C for 16 hours. After work-up a colorless solid was isolated, which is soluble in MeCN-d₃.

The product was characterized *via* ¹H, ¹¹B{¹H} as well as ¹⁹F NMR spectroscopy; however, no signal is observed in the ¹⁹F NMR spectrum and the ¹¹B{¹H} NMR spectrum reveals a main signal at approximately 14 ppm, which belongs to well-known decomposition product [Bcat₂]⁻ with [NMe₄]⁺ as the counter ion. Nonetheless, there are further signals in the ¹¹B{¹H} NMR spectrum, which could not be assigned to specific compounds.

However, the synthesis of the anionic sp²-sp³ diboron adduct [B₂cat₂F][NMe₄] **9** was successful using acetonitrile as solvent (Scheme 35). The first investigation was an NMR scale reaction to monitor the desired compound *via* ¹H, ¹¹B{¹H} and ¹⁹F NMR spectroscopy.



Scheme 35: Reaction of B₂cat₂ **8** with NMe₄F in MeCN at room temperature.

[B₂cat₂F][NMe₄] **9** was characterized *via* solution and solid state NMR spectroscopy. The ¹H NMR spectrum shows one broad signal in the aromatic region for the catechol and a singlet for the methyl-groups for the [NMe₄]⁺ counter ion (Figure 14).

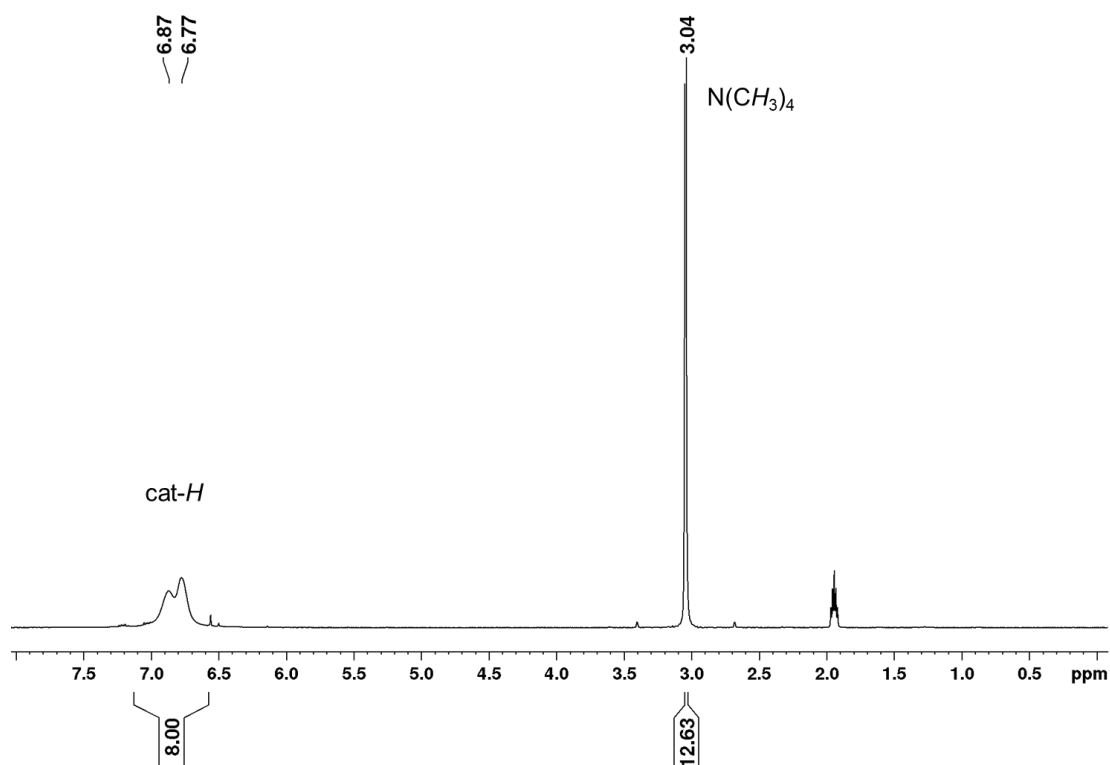


Figure 14: *In situ* ^1H NMR spectrum of $[\text{B}_2\text{cat}_2\text{F}][\text{NMe}_4]$ **9** (reactant ratio: 1:1; 200 MHz, MeCN-d_3).

In the $^{11}\text{B}\{^1\text{H}\}$ NMR, two broad signals are detected, one at 32.8 ppm which belongs to the sp^2 -hybridized boron atom and another one at 6.50 ppm for the sp^3 -hybridized boron atom. These observations are comparable with the NMR shifts of adduct **4**. Furthermore, the ^{19}F NMR spectrum shows one sharp signal at -129 ppm, which is also similar with the chemical shift of adduct **4** (Figure 15).

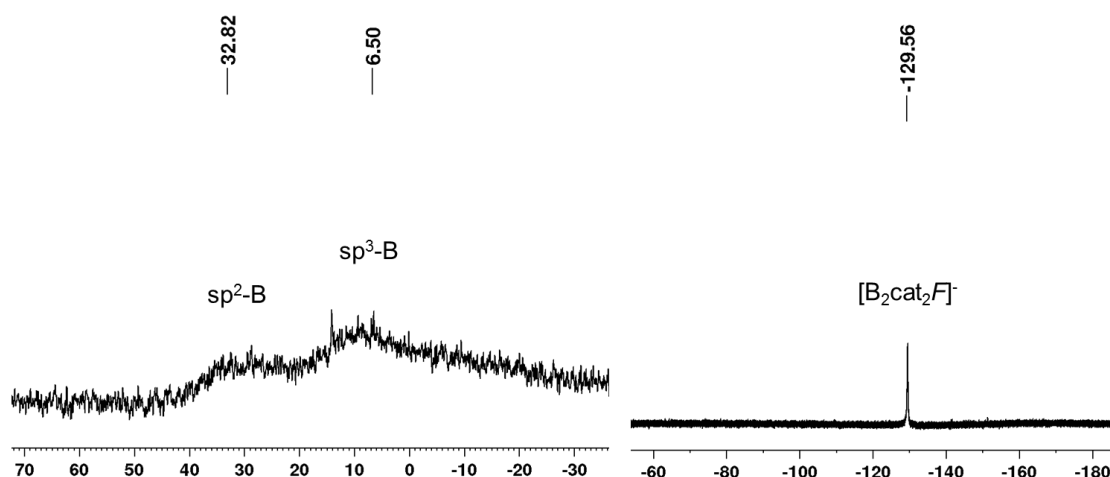


Figure 15: *In situ* $^{11}\text{B}\{^1\text{H}\}$ (left) and ^{19}F (right) NMR spectra of $[\text{B}_2\text{cat}_2\text{F}][\text{NMe}_4]$ **9** (reactant ratio: 1:1; MeCN-d_3).

Due to the fact that the solution NMR spectra give evidence for the decomposition product $[\text{Bcat}_2][\text{NMe}_4]$, compound **9** was also characterized *via* solid state NMR before further

application in any borylation reactions. The solid state ^{11}B NMR spectrum shows three signals, two signals belong to the anionic adduct, one signal for each boron atom, and the third sharp signal at 14 ppm belongs to compound $[\text{Bcat}_2][\text{NMe}_4]$; however, the main-product is the anionic $\text{sp}^2\text{-sp}^3$ diboron adduct **9**, which was used in following borylation reactions (Figure 16).

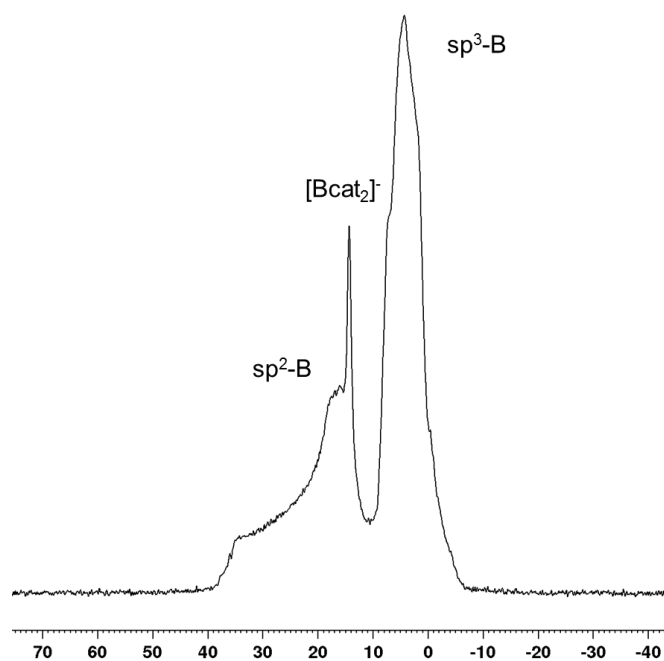
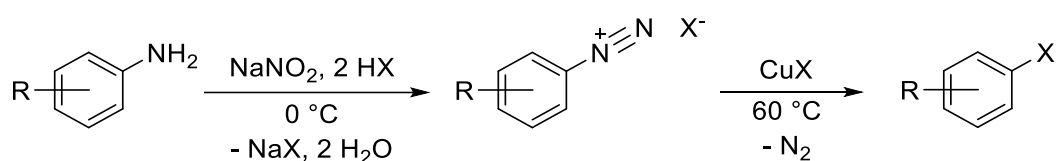


Figure 16: Solid state ^{11}B NMR spectrum of $[\text{B}_2\text{cat}_2\text{F}][\text{NMe}_4]$ **9**.

1.2.3. Reactivity of the anionic sp^2 - sp^3 diboron adducts

1.2.3.1. Metal-free borylation of aryl amines

The Sandmeyer reaction,^[121-123] which is shown in Scheme 36, is a classical two-step reaction to convert amino-groups into halogen-groups. The first step is the transformation of an amine substituent into a diazonium-group and the second step is the reaction with a copper(I) salt to give the halogenated arene. The advantage of this reaction is the application of arylamines, which are cheap and abundant. The synthesis of these compounds can be easily done by nitration and subsequent reduction of the appropriate arenes.^[121]



Scheme 36: The Sandmeyer reaction.

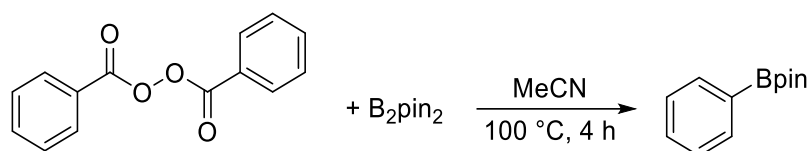
Wang *et al.* published a direct conversion of aryl amines to pinacol boronates under Sandmeyer reaction conditions.^[70] They used *tert*-butyl nitrite (*t*BuONO) as the ideal diazotization reagent for the transformation to aryl boronates. The best yield (40% GC-MS yield) was given by the use of aniline, B₂pin₂ and *t*BuONO in a 1:1:1 ratio in acetonitrile at 60 °C (Scheme 37).



Scheme 37: Reaction of aniline, B₂pin₂ and *t*BuONO in MeCN.

To increase the yield of the desired product, the same reaction was carried out with an additive, such as KOAc, as well as copper(I/II) salts. The reaction rate did not change; however, the use of the copper salts led to a conversion of 5 and 8% respective to the aryl boronates. However, the radical initiators 2,2'-azo-bis-*iso*-butyronitrile (AIBN) and benzoyl peroxide (BPO) (2%) could increase the yield up to 77% at room temperature. Furthermore, the *in situ* formed boronate product can be directly applied in the Pd-catalyzed Suzuki-Miyaura cross-coupling reaction^[17] without any further purification.

Due to the fact that it was not clear, whether or not the reaction took place *via* a radical mechanism, Wang *et al.* heated a stoichiometric mixture of B₂pin₂ with BPO in MeCN to 100 °C for one hour and obtained the phenyl boronate in 37% yield (Scheme 38).

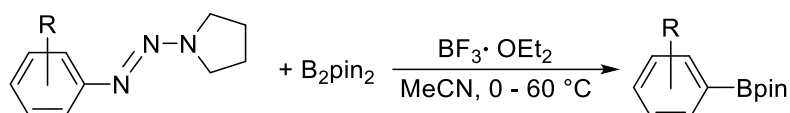


Scheme 38: Reaction of BPO with B₂pin₂ yielded the boronate ester.

Similar observations were reported by Yamane and Zhu, wherein the reaction of diazonium [BF₄]⁻ salts with B₂pin₂ in MeOH yielded the corresponding boronate in 45% yield (*vide infra*).^[118]

Recent reports by Wang *et al.* contain further transition-metal-free borylation reactions of tosylhydrazones,^[124] aryl amines^[125-126] as well as the synthesis of several aryl boronates *via* reaction of amines with B₂pin₂ and *t*BuONO.^[127]

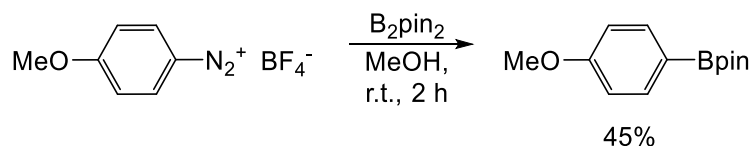
In 2010, Yamane and Zhu reported a transition-metal-free borylation of aryl triazenes mediated by BF₃•OEt₂ (Scheme 39).^[118]



Scheme 39: Borylation reaction of aryl triazenes with B₂pin₂.

They also proposed a potential mechanism for the borylation. Based on the formation of the triazene-BF₃-complex **A**, the next step is the formation of the arenediazonium salt **B**, which leads to the formation of anionic arenediazonium as a [B₂pin₂F]⁻ salt (**C**). After nucleophilic substitution of nitrogen in the arenediazonium salt, the favored borylation products (**D**) and an FBpin species would result; however, they did not observe it.

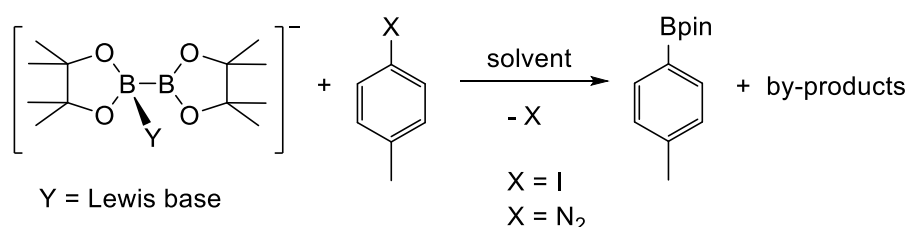
The reaction of diazonium [BF₄]⁻ salts with B₂pin₂ in pure methanol led to the same borylation product as in the aryl triazene reaction in 45% yield (Scheme 40).



Scheme 40: Borylation of an aryl-diazonium [BF₄]⁻ salt *via* reaction of [4-MeO-C₆H₄N₂][BF₄] with B₂pin₂ in pure MeOH.

1.2.3.2. Preliminary studies on the reactivity of adduct $[B_2pin_2(OR)K]$ **2a**, **2d** and $[B_2pin_2F][nBu_4N]$ **3**

Preliminary studies in our group had shown that several anionic sp^2 - sp^3 diboron adducts may act as nucleophilic boryl anions and react with electrophiles, such as aryl iodides or diazonium $[BF_4]^-$ salts, to form the desired boronates (Scheme 41).^[74]



Scheme 41: Reaction of several anionic sp^2 - sp^3 diboron compounds with aryl iodides and diazonium $[BF_4]^-$ salts.

During the studies on the copper-mediated borylation of aryl halides, it was observed that an un-catalyzed background reaction gave the desired aryl boronate ester in low yields. An *in situ* formed sp^2 - sp^3 anionic diboron adducts $[B_2pin_2(OtBu)K]$ **2a** is detected, which could be the active nucleophilic species, facilitating the transfer of a boron-moiety to the aryl iodide without the necessity of a metal catalyst.^[80]

The reactions of the anionic adducts $[B_2pin_2(OtBu)K]$ **2a**, $[B_2pin_2(OMe)K]$ **2d** and $[B_2pin_2F][nBu_4N]$ **3** with 4-methylphenyl iodide in THF are very slow and the conversion of the starting materials required higher temperatures. The use of $[B_2pin_2OMe]K$ **2a** gave the aryl boronate ester in 19% yield after 3 weeks at 60 °C. Almost no conversion of the starting materials was observed using $[B_2pin_2OMe]K$ **2a** or $[B_2pin_2F][nBu_4N]$ **3** as well as from the reaction of B_2pin_2 **1** with $[nBu_4P][OAc]$ (TBPE) (Figure 17).

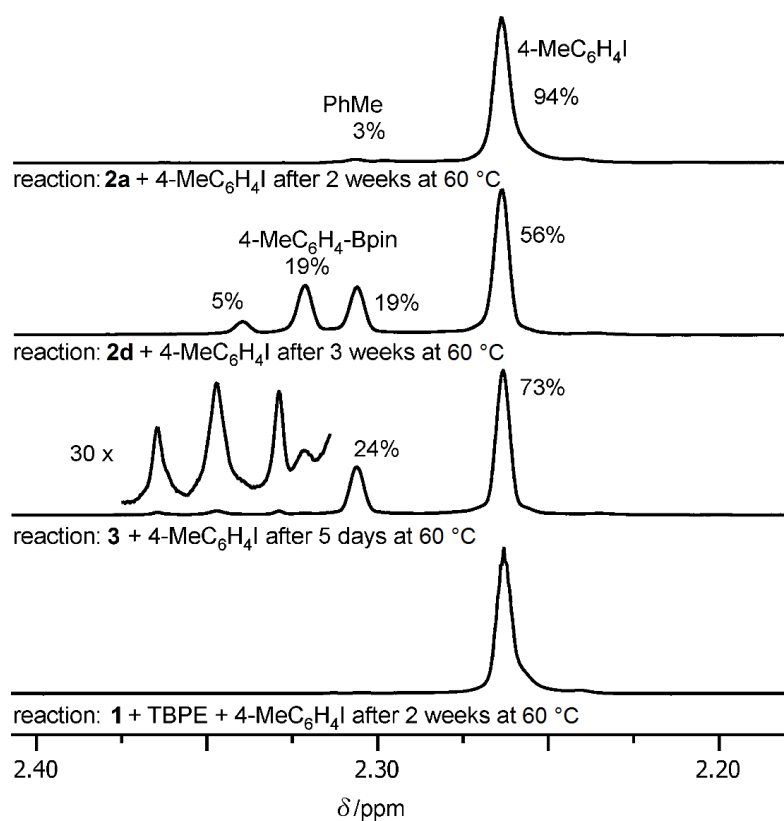


Figure 17: *In situ* ^1H NMR (400 MHz, THF-d_8) spectra (benzylic region) of the reaction of 4-Me- $\text{C}_6\text{H}_4\text{I}$ with $\text{sp}^2\text{-sp}^3$ diboron compounds (percentage with respect to all signals in the region shown, and all signals are assumed to be methyl-groups; signals with less than 3% intensity are not given, TBPE: $[\text{nBu}_4\text{P}][\text{OAc}]$); reproduced from ref. [74] with permission from Wiley-VCH.

In the case of compound **4**, no conversion of the starting material was observed; however, $[\text{B}_2\text{pin}_2\text{F}][\text{NMe}_4]$ decomposes at higher temperatures after several hours to give $[\text{pinBF}_2]^-$.^[74] Figure 18 shows the $^{11}\text{B}\{^1\text{H}\}$ NMR spectra of the reaction of adduct **4** with 4-Me- $\text{C}_6\text{H}_4\text{I}$. In the $^{11}\text{B}\{^1\text{H}\}$ NMR spectra, the resonance for B_2pin_2 is observed at approximately 30 ppm, and the resonance for $[\text{pinBF}_2]^-$ is observed as a sharp triplet at approximately 5 ppm.

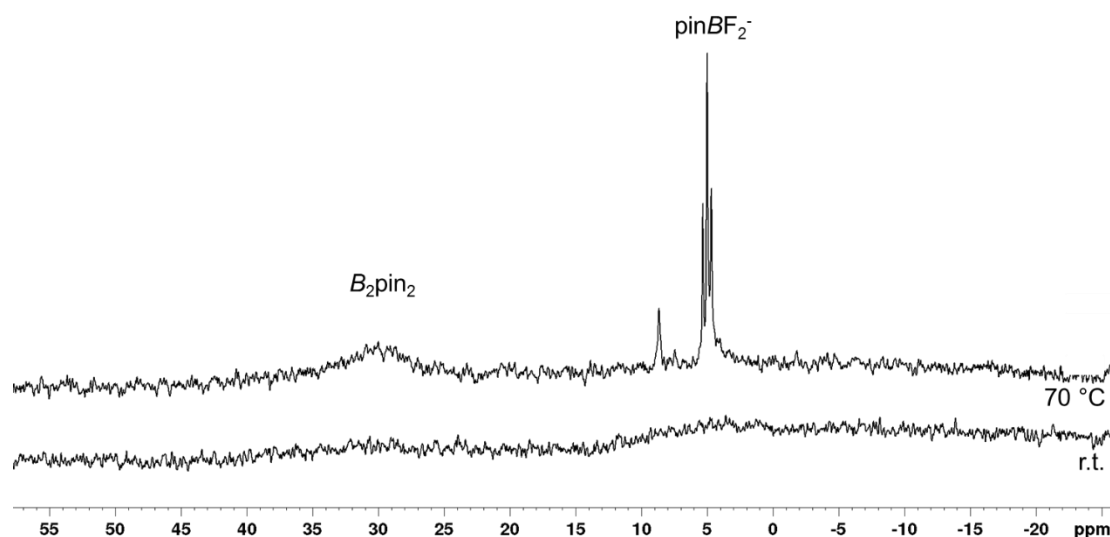


Figure 18: *In situ* $^{11}\text{B}\{^1\text{H}\}$ NMR spectrum taken at room temperature and after heating at 70 °C of the reaction of 4-Me-C₆H₄I with adduct **4** (Reactant ratio: 1:1; 64 MHz, MeCN-d₃); reproduced from ref. [74] with permission from Wiley-VCH.

As previously reported by Wang *et al.*, the borylation of amines is proceeded *via in situ* formation of a diazonium salt, B₂pin₂ and BPO as an additive as well as a postulated sp²-sp³ diboron compound.^[70, 125-128] Accordingly, the stable diazonium salt [4-Me-C₆H₄N₂][BF₄]⁻ was synthesized and was reacted with the previously synthesized anionic diboron compounds [B₂pin₂(OtBu)]K **2a**, [B₂pin₂(OMe)]K **2d** and [B₂pin₂F][nBu₄N] **3** as well as B₂pin₂ with TBPE (Figure 19). All four reactions showed conversion of the starting materials to the desired arylboronate ester; however, the best results were obtained, using TBPE as an additive. In the control reaction of the diazonium [BF₄]⁻ salt with KOMe, KOtBu and NMe₄F, as representative Lewis-bases, the by-products, in particularly toluene, were formed; however, this formation does not involve the diboron compounds nor the aryl boronate ester (Figure 19). Furthermore, reactions between an aryl boronate ester and KOMe or an aryl boronate ester and the diazonium [BF₄]⁻ salt (in the absence and presence of KOMe) neither gave product nor by-product.

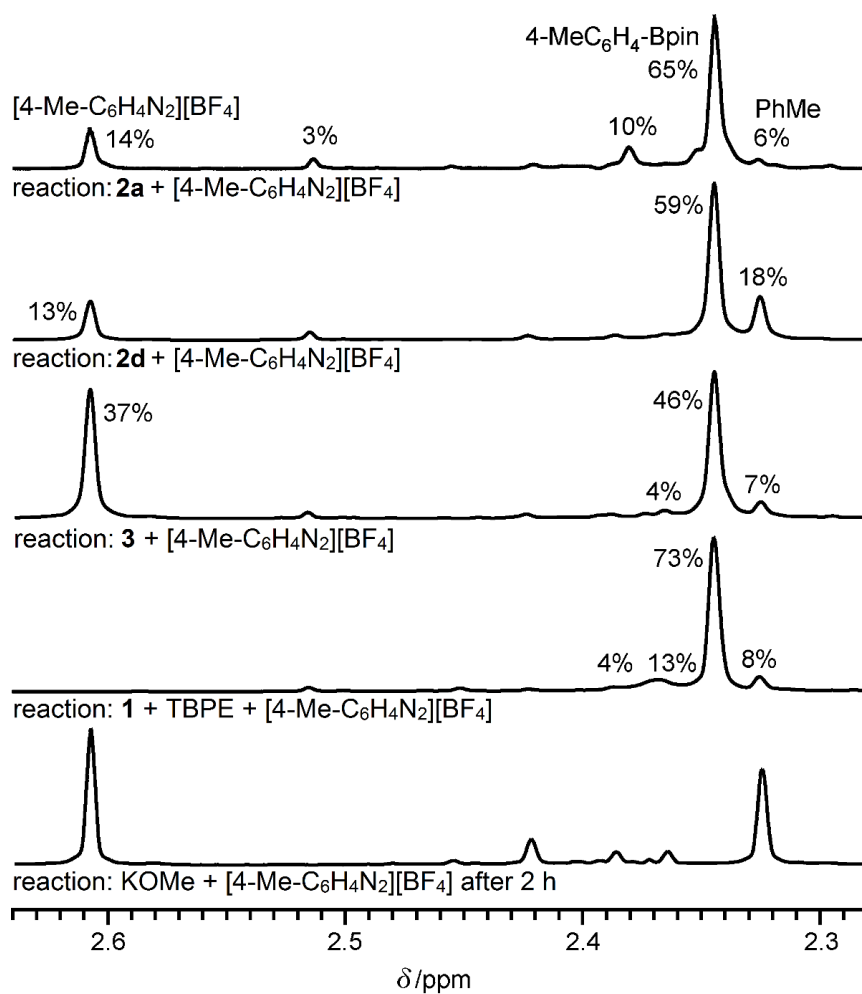
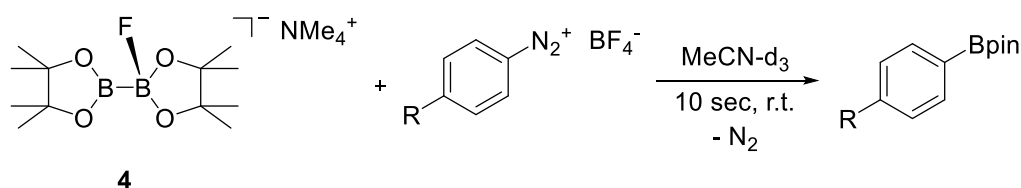


Figure 19: *In situ* ¹H NMR (400 MHz, MeCN-d₃) spectra (benzylic region) of the reaction of [4-Me-C₆H₄N₂][BF₄] with sp²-sp³ diboron compounds after 30 min at ambient temperature and with KOMe (percentage with respect to all signals in the region shown, and all signals are assumed to be methyl-groups; signals with less than 3% intensity are not given, TBPE: [*n*Bu₄P][OAc]); reproduced from ref. [74] with permission from Wiley-VCH.

1.2.3.3. Reactivity of adduct $[\text{B}_2\text{pin}_2\text{F}][\text{NMe}_4] \mathbf{4}$ towards diazonium $[\text{BF}_4]^-$ salts

Due to the fact that the anionic $\text{sp}^2\text{-sp}^3$ diboron adduct $\mathbf{4}$ is better soluble in solvents such as MeCN, further reactions of adduct $\mathbf{4}$ with different diazonium $[\text{BF}_4]^-$ salts were investigated in that solvent. Therefore, several diazonium $[\text{BF}_4]^-$ salts were synthesized, namely $[4\text{-R-C}_6\text{H}_4\text{N}_2][\text{BF}_4]$ ($\text{R} = \text{H, Me, OMe, NO}_2$ and Br), and were further reacted with adduct $\mathbf{4}$ in MeCN at room temperature (Scheme 42).^[74]



Scheme 42: Reaction of adduct $\mathbf{4}$ with $[4\text{-R-C}_6\text{H}_4\text{N}_2][\text{BF}_4]$ ($\text{R} = \text{H, Me, OMe, NO}_2$ and Br) in MeCN-d_3 at room temperature.

All reactions between adduct $\mathbf{4}$ and the diazonium $[\text{BF}_4]^-$ salts were first performed on an NMR scale to examine the reaction conditions and the stoichiometry (Figure 20).

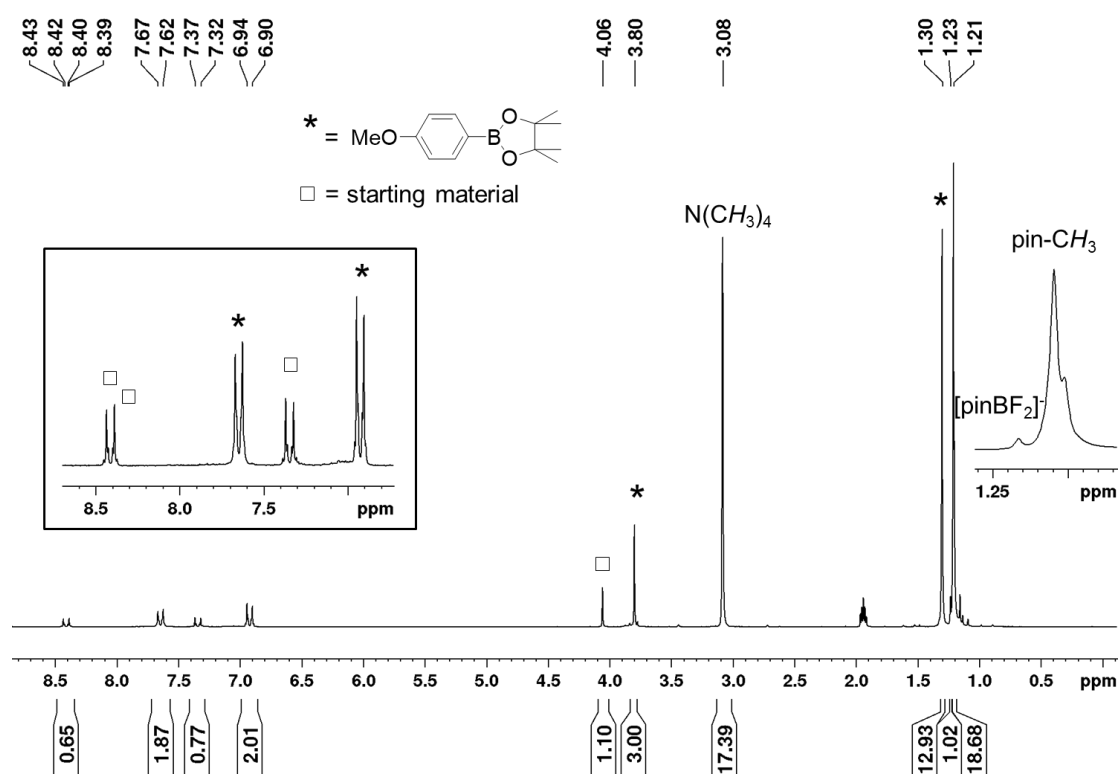
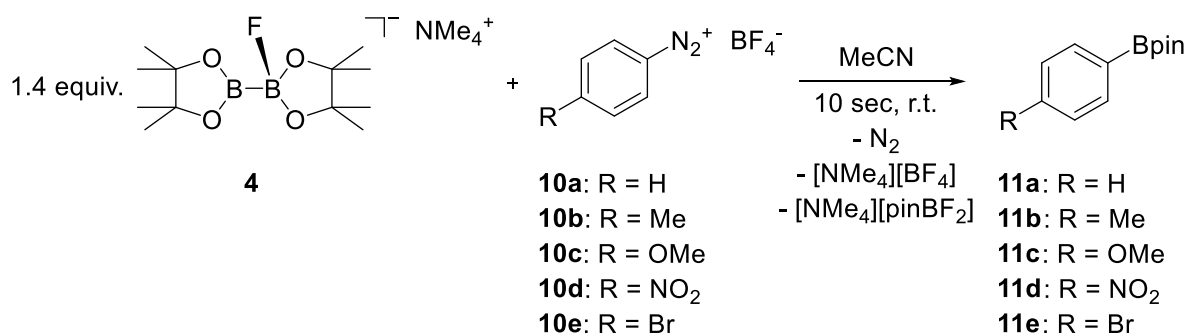


Figure 20: *In situ* ^1H NMR spectrum taken after 30 minutes of the borylation of $[4\text{-MeO-C}_6\text{H}_4\text{N}_2][\text{BF}_4]$ with adduct $\mathbf{4}$ (Reactant ratio: 1:1; 200 MHz, MeCN-d_3); reproduced from ref. [74] with permission from Wiley-VCH.

All NMR spectra revealed that the conversion of the starting materials (diazonium $[\text{BF}_4]^-$ salts) was constantly lower than 70%, therefore, to increase the conversion to 100%, as demonstrated by *in situ* NMR spectroscopy, all reactions were repeated using a 1.4:1 ratio, and the desired products were isolated (Scheme 43).^[74]



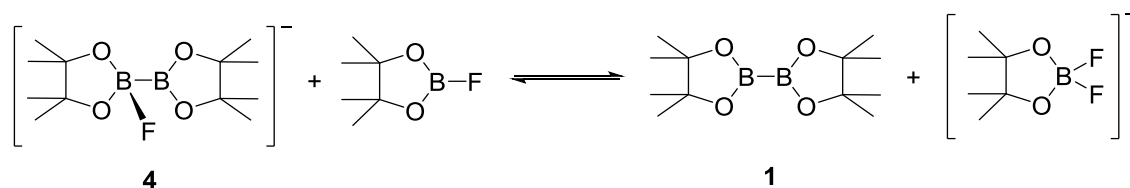
Scheme 43: Borylation reaction of adduct $[\text{B}_2\text{pin}_2\text{F}][\text{NMe}_4]$ **4** with different diazonium $[\text{BF}_4]^-$ salts in the ratio 1.4:1.

The borylation reactions gave the desired boronate esters in moderate to good isolated yields, which could be isolated *via* filtration of the $[\text{NMe}_4][\text{BF}_4]$ salt and further purification by column chromatography. In Table 1, the ^1H , $^{11}\text{B}\{^1\text{H}\}$ and $^{13}\text{C}\{^1\text{H}\}$ NMR data as well as the isolated yields are summarized.

^1H NMR [ppm]	1.32, 7.37-7.41, 7.46-7.51, 7.70-7.73	1.31, 2.35, 7.20-7.21, 7.59-7.61	1.30, 3.80, 6.91-6.93, 7.64-7.66	1.34, 7.88-7.90, 8.16-8.17	1.31, 7.54-7.56, 7.59-7.62
$^{11}\text{B}\{^1\text{H}\}$ NMR [ppm]	29.9	30.7	29.7	29.4	29.7
$^{13}\text{C}\{^1\text{H}\}$ NMR [ppm]	25.2, 84.8, 128.8, 132.3, 135.4	21.7, 25.2, 84.6, 129.5, 135.5, 142.5	25.2, 55.8, 84.5, 114.4, 137.2, 163.3	25.2, 85.6, 123.5, 136.4, 150.9	25.2, 85.1, 126.6, 132.9, 137.2
Isolated yield [%]	42	66	40	59	72

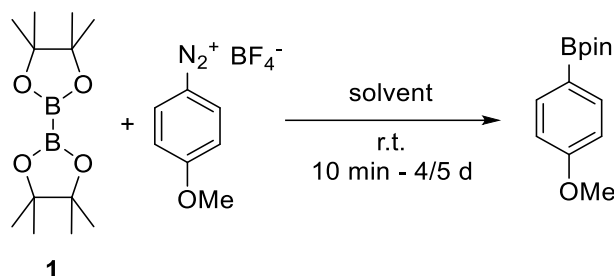
Table 1: ^1H , $^{11}\text{B}\{^1\text{H}\}$ and $^{13}\text{C}\{^1\text{H}\}$ NMR data as well as the yields of the isolated boronate esters.

All reactions, performed in a 1:1 ratio, adduct **4** : diazonium $[\text{BF}_4]^-$ salt, have in common the fact that the conversion of the starting material is approximately 70% and the expected by-product FBpin was not observed; however, the NMR spectra proved the existence of $[\text{pinBF}_2][\text{NMe}_4]$. Furthermore, the ^1H NMR spectrum revealed a signal for B_2pin_2 , but no signal for an “unreacted” fluoride adduct **4**, which may be explained by the possible equilibrium of the anionic adduct **4** and the “*in situ* formed” FBpin, this observation would also explain why the reaction is complete in a ratio of adduct **4** to substrate 1.4:1 (Scheme 44).^[74]



Scheme 44: Postulated equilibrium observed and involved in the reaction between adduct **4** and “*in situ* formed” FBpin.

Yamane and Zhu’s reported the metal-free borylation *via* reaction of the diazonium $[\text{BF}_4]^-$ salt $[\text{4-MeO-C}_6\text{H}_4\text{N}_2][\text{BF}_4]$ with B_2pin_2 in pure methanol at room temperature.^[118] Due to our knowledge concerning anionic $\text{sp}^2\text{-sp}^3$ diboron adducts, the reported reactions were repeated to verify the results. First, the reaction of B_2pin_2 **1** with $[\text{4-MeO-C}_6\text{H}_4\text{N}_2][\text{BF}_4]$ was investigated in aprotic solvents, such as MeCN-d_3 and acetone-d_6 (Scheme 45).



Scheme 45: Reaction of B_2pin_2 with $[\text{4-MeO-C}_6\text{H}_4\text{N}_2][\text{BF}_4]$ in MeCN-d_3 and acetone-d_6 at room temperature (reactant ratio: 1:1).

All NMR samples were recorded in 0.6 mL MeCN-d_3 or acetone-d_6 and were measured at different time intervals. The reported results by Yamane and Zhu by NMR study were verified; however, the reaction of B_2pin_2 with $[\text{4-MeO-C}_6\text{H}_4\text{N}_2][\text{BF}_4]$ in MeCN-d_3 or acetone-d_6 yielded only traces of the desired boronate ester after 4 days at room temperature.^[74] Figure 21 and 22 show the recorded ^1H NMR spectra at different time scales. After 10 minutes, 2 hours or even 20 hours, no conversion of the starting material could be observed; however, after 24 hours, traces of the desired boronate ester began to appear, and after 4 days, less than 4% of the boronate ester was observed. These observations are similar in both solvents, MeCN-d_3 and acetone-d_6 .

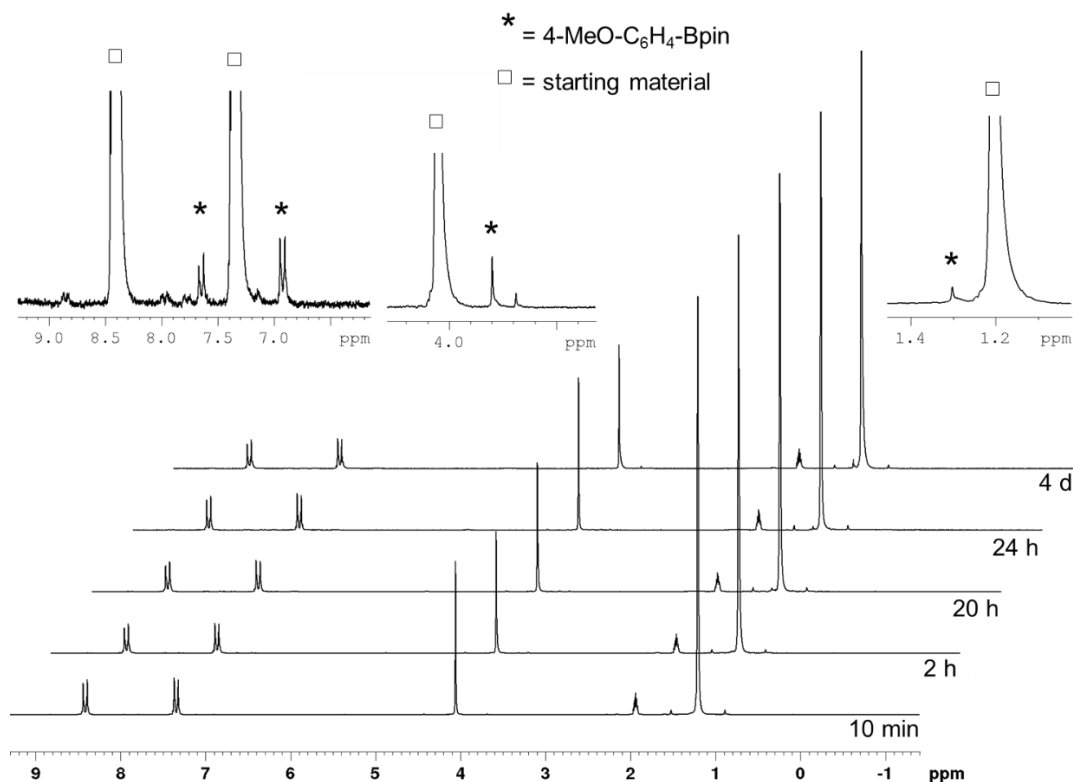


Figure 21: *In situ* ^1H NMR spectrum taken after 10 minutes, 2, 20 and 24 hours and 4 days of the reaction of $[\text{4-MeO-C}_6\text{H}_4\text{N}_2][\text{BF}_4]$ with B_2pin_2 **1** (reactant ratio: 1:1; 200 MHz, MeCN-d_3), which essentially shows that no reaction took place; reproduced from ref. [74] with permission from Wiley-VCH.

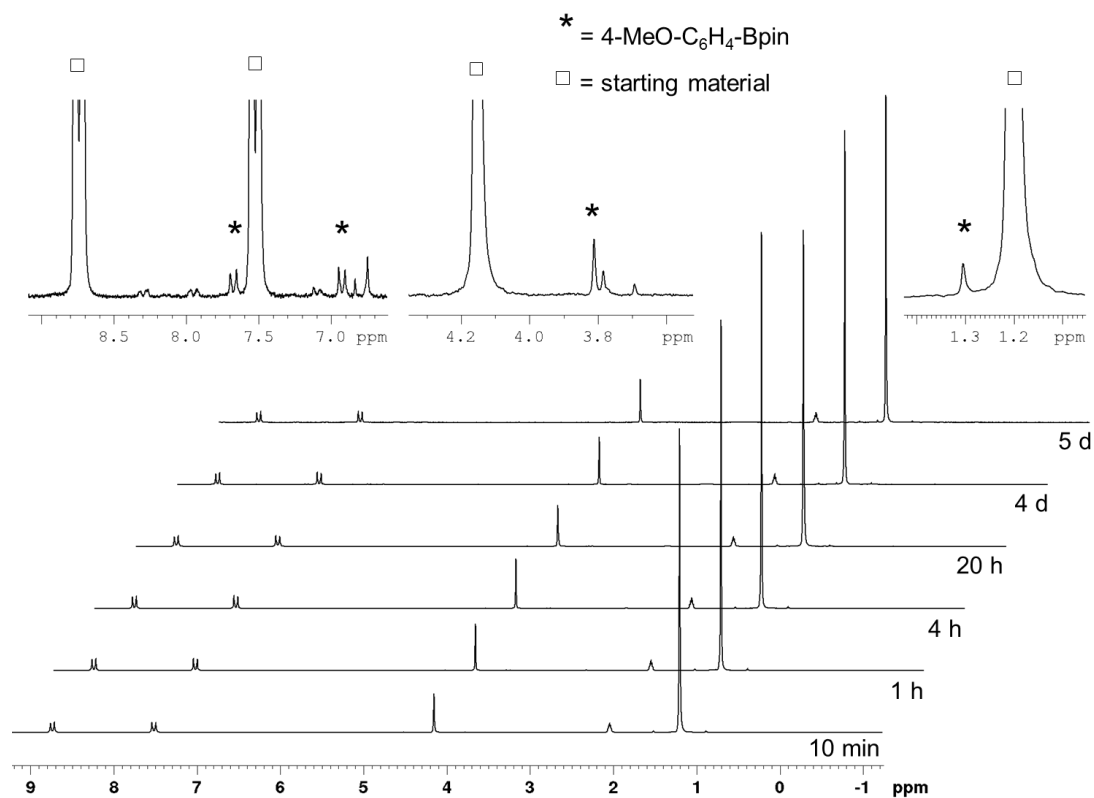
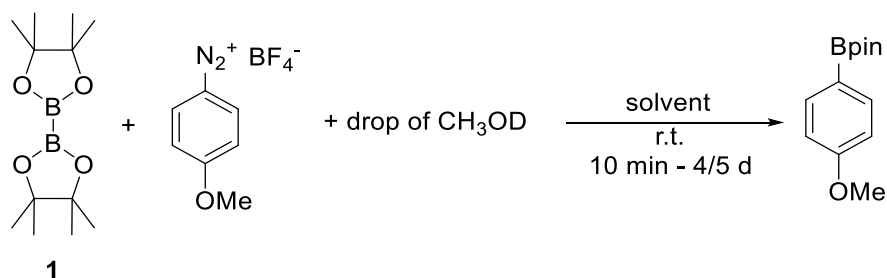


Figure 22: *In situ* ^1H NMR spectrum taken after 10 minutes, 1, 4 and 20 hours and 4 and 5 days of the reaction of $[\text{4-MeO-C}_6\text{H}_4\text{N}_2][\text{BF}_4]$ with B_2pin_2 **1** (reactant ratio: 1:1; 200 MHz, acetone-d_6), which essentially shows that no reaction took place; reproduced from ref. [74] with permission from Wiley-VCH.

Furthermore, the same reaction was repeated in MeCN-d₃ and acetone-d₆ with a drop of CH₃OD to the reaction mixture (Scheme 46). The reaction between B₂pin₂ and an aryl diazonium [BF₄]⁻ salt in pure methanol was reported previously, and therefore a drop of CH₃OD was added to the reactions in MeCN-d₃ and acetone-d₆ to see the effect on the rate of product formation.



Scheme 46: Reaction of B₂pin₂ **1** with [4-MeO-C₆H₄N₂]⁺[BF₄]⁻ in MeCN-d₃ or acetone-d₆ with a drop of CH₃OD (reactant ratio: 1:1:1; 200 MHz, MeCN-d₃).

The first NMR spectrum was measured after 10 minutes and then one drop of CH₃OD was added to the NMR sample (Figure 23 and 24). Afterwards, the sample was measured after 1 hour and 19 hours and finally after 4 days at room temperature. The final NMR spectrum of both reactions is enlarged to show the desired product signals. In the case of MeCN-d₃, the conversion was increased up to approximately 6%; however, the use of acetone-d₆ as the deuterated solvent yielded the desired boronate ester in circa 30%. These results also confirmed our results, that methanol could convert [BF₄]⁻ to F⁻ and MeOD/BF₃, which can activate the B–B bond of the diboron reagent (in this case B₂pin₂). In summary, borylation reaction only took place in coordinating solvents or in the presence of an alkoxide base, such as KOMe or KO^tBu, as well as fluoride-containing substrates, e.g. NMe₄F or *n*Bu₄NF•3 H₂O.

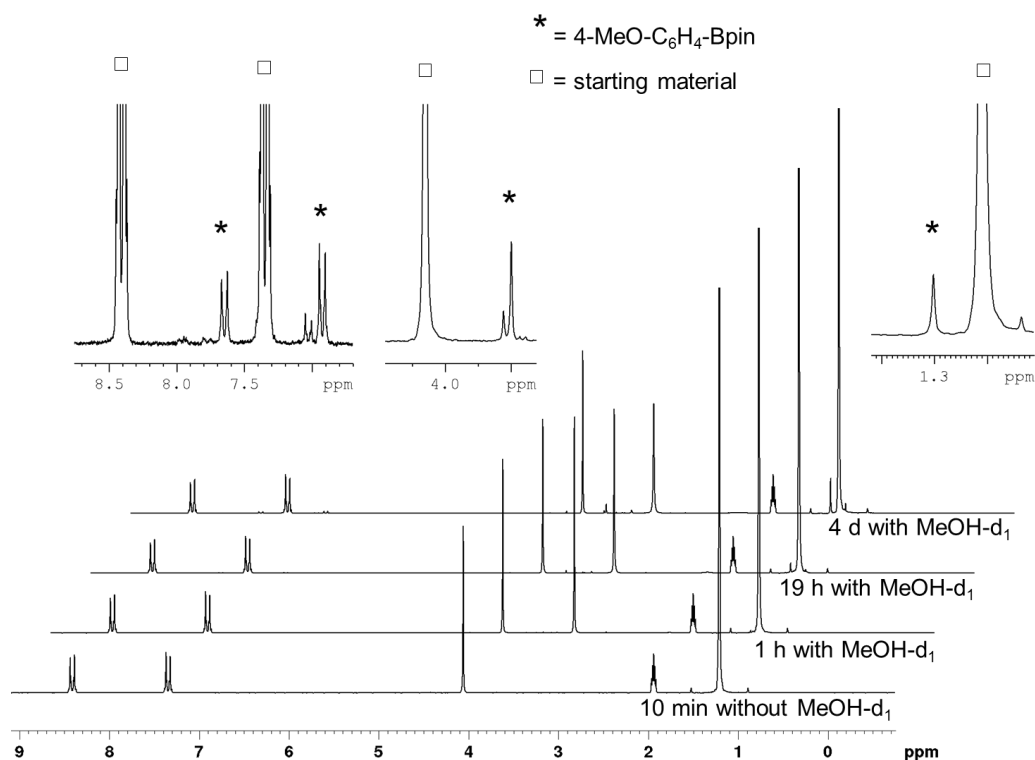


Figure 23: *In situ* ^1H NMR spectra taken after 10 minutes, one drop of MeOH-d_1 was added after 30 minutes, *in situ* ^1H NMR spectra taken after 1, 19 hours and 4 days of the reaction of $[\text{4-MeO-C}_6\text{H}_4\text{N}_2][\text{BF}_4]$ with B_2pin_2 **1** (reactant ratio: 1:1; 200 MHz, MeCN-d_3); reproduced from ref. [74] with permission from Wiley-VCH.

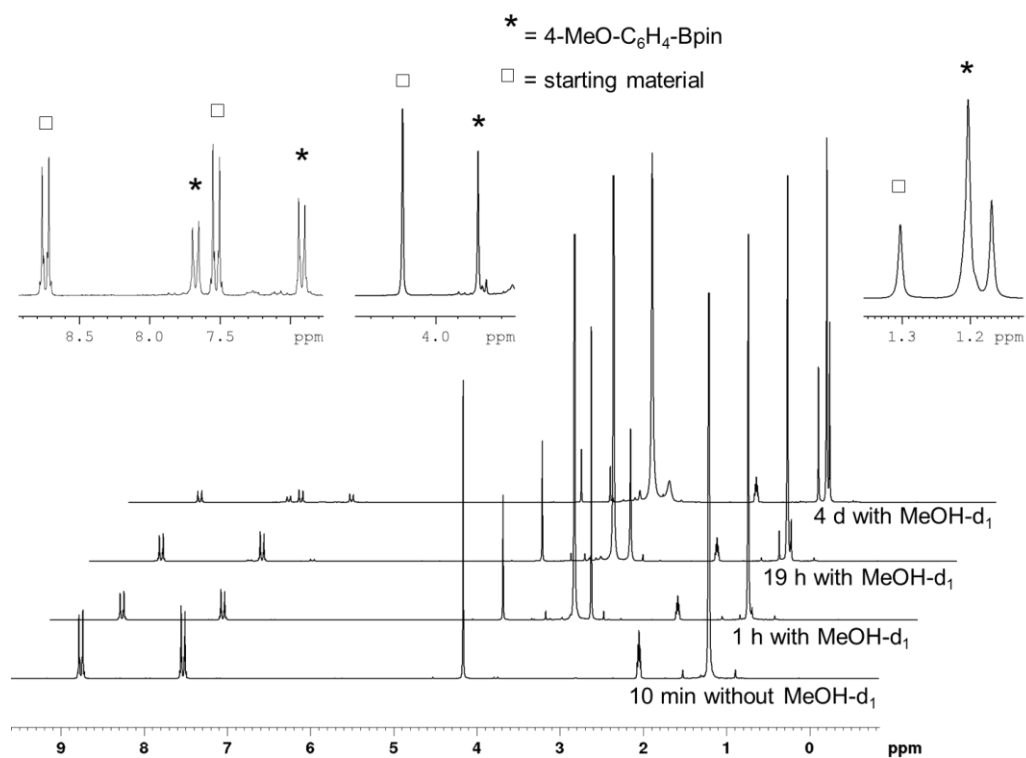
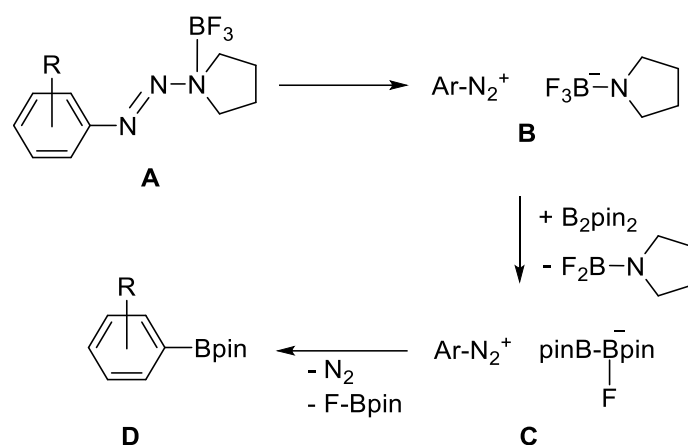


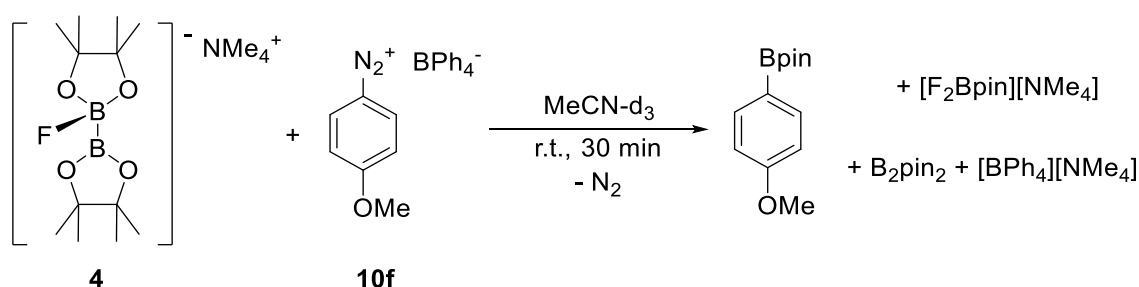
Figure 24: *In situ* ^1H NMR spectra taken after 10 minutes, one drop of MeOH-d_1 was added after 30 minutes, *in situ* ^1H NMR spectra taken after 1, 19 hours and 4 days of the reaction of $[\text{4-MeO-C}_6\text{H}_4\text{N}_2][\text{BF}_4]$ with B_2pin_2 **1** (reactant ratio: 1:1; 200 MHz, acetone-d_6 , RT); reproduced from ref. [74] with permission from Wiley-VCH.

The reaction of adduct **4** with diazonium $[\text{BF}_4]^-$ salts yielded the desired boronate ester, in accordance with the possible mechanism for the borylation reaction of aryltriazene reported by Yamane and Zhu. The first step is the adduct formation of the aryltriazene with BF_3 (**A**) followed by the decomposition to an *in situ* formed diazonium salts (**B**), which reacts with B_2pin_2 to give $[\text{B}_2\text{pin}_2\text{F}]^-$ (**C**) with $[\text{ArN}_2]^+$ as the counter ion. The last step is the elimination of FBpin and dinitrogen to form the desired product (**D**) (Scheme 47).^[118]



Scheme 47: Postulated mechanism for the borylation of aryltriazene.

The proposed intermediate **C** is similar to the adduct **4**, only the counter ion is different ($[\text{ArN}_2]^+$ instead of $[\text{NMe}_4]^+$); however, as already reported, the reaction of B_2pin_2 with $[\text{4-MeO-C}_6\text{H}_4\text{N}_2][\text{BF}_4]$ in aprotic solvents, such as acetonitrile or acetone, did not lead to any appreciable conversion of the starting material. This could be explained by the fact that MeOH activates the B-B bond, as was observed for isolated anionic $\text{sp}^2\text{-sp}^3$ diboron adduct **4**. To verify that the fluoride atom of adduct **4** is responsible for initiating the borylation reaction, and not a fluoride atom of the $[\text{BF}_4]^-$ counter ion, $[\text{BF}_4]^-$ was exchanged with $[\text{BPh}_4]^-$ (Scheme 48).^[74]



Scheme 48: Reaction of adduct **4** with $[\text{4-MeO-C}_6\text{H}_4\text{N}_2][\text{BPh}_4]$ **10f** to yield the desired boronate ester (reactant ratio: 1:1; 200 MHz, MeCN-d_3).

The reaction of adduct **4** with $[\text{4-MeO-C}_6\text{H}_4\text{N}_2][\text{BPh}_4]$ in MeCN-d_3 was monitored *via* ^1H , $^{11}\text{B}\{^1\text{H}\}$ and ^{19}F NMR spectroscopy. The reaction was complete within seconds after adding the solvent to the NMR tube, dinitrogen was formed, and the NMR spectrum was recorded (Figure 25).

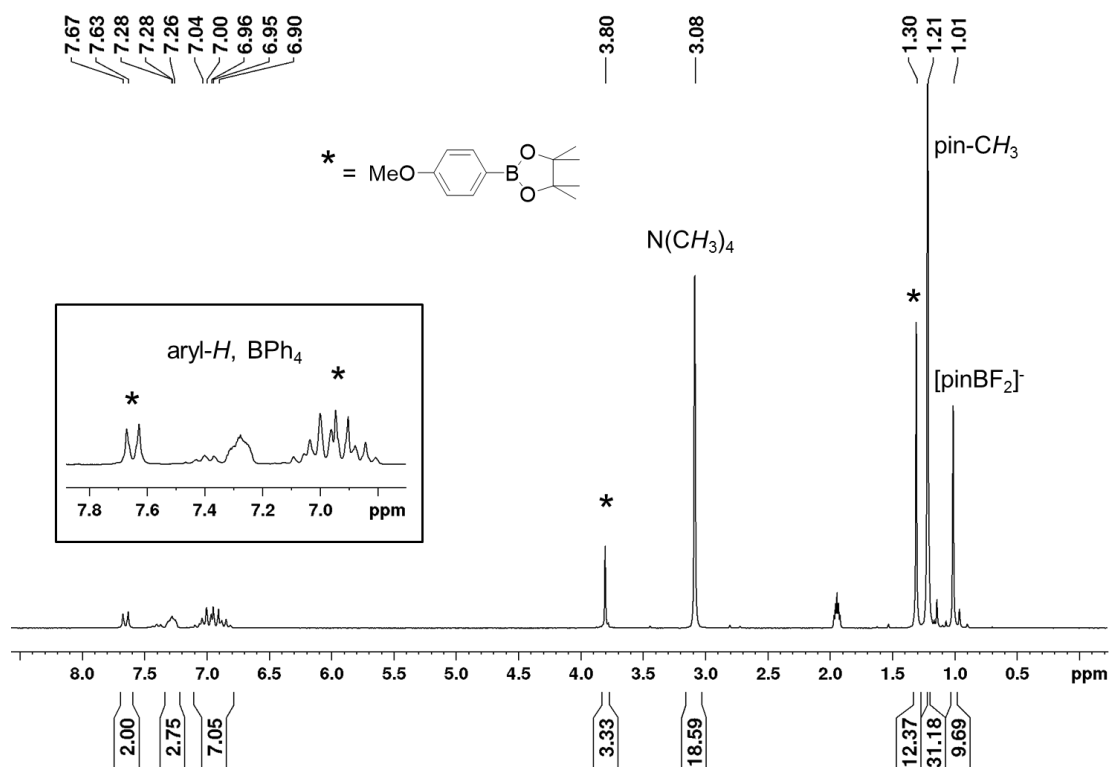


Figure 25: *In situ* ^1H NMR spectrum taken after 30 minutes of the borylation of $[4\text{-MeO-C}_6\text{H}_4\text{N}_2][\text{BPh}_4]$ with adduct **4** (reactant ratio: 1:1, 200 MHz, MeCN-d_3). During this particular reaction, a colorless precipitate was formed, which is proposed to be $[\text{NMe}_4][\text{BPh}_4]$; reproduced from ref. [74] with permission from Wiley-VCH.

In the ^1H NMR spectrum, the desired boronate ester $\text{MeO-C}_6\text{H}_4\text{-Bpin}$ is observed at 1.30 (pin- CH_3), 3.80 (OCH_3) and both signals in the aromatic region. Furthermore, at 1.01 ppm, the signal for the afore-mentioned $[\text{pinBF}_2]^-$ species is detected, which also gives rise to a sharp triplet at 4.99 ppm in the $^{11}\text{B}\{^1\text{H}\}$ NMR spectrum (*vide infra*) and a quartet at -141.5 ppm in the ^{19}F NMR spectrum (Figure 26).

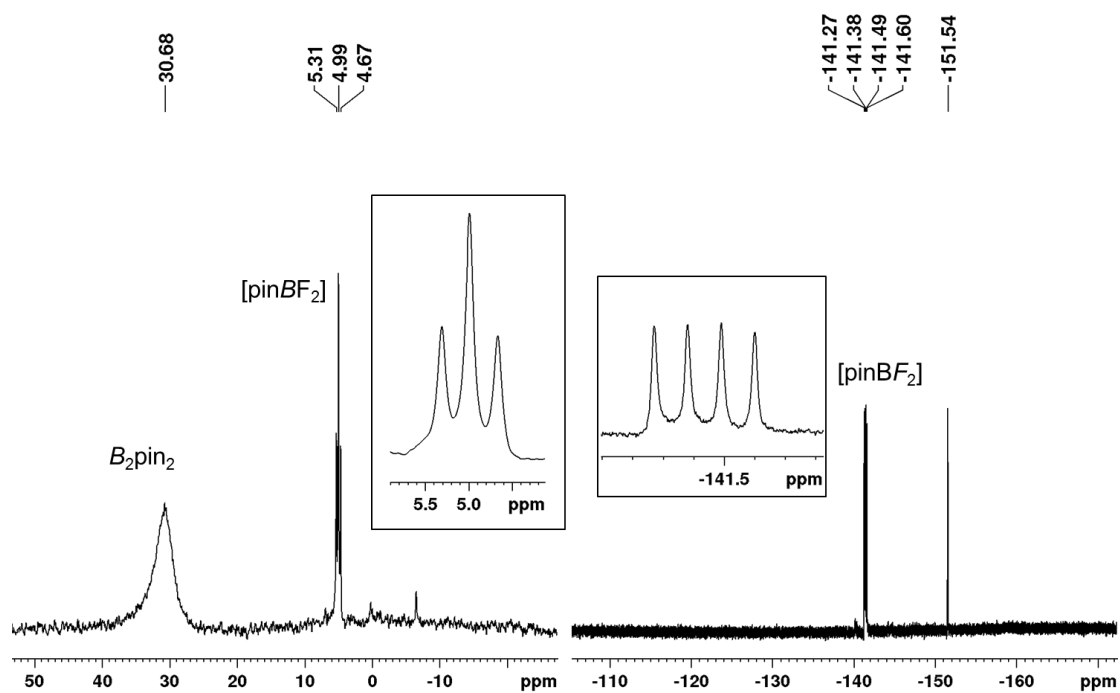
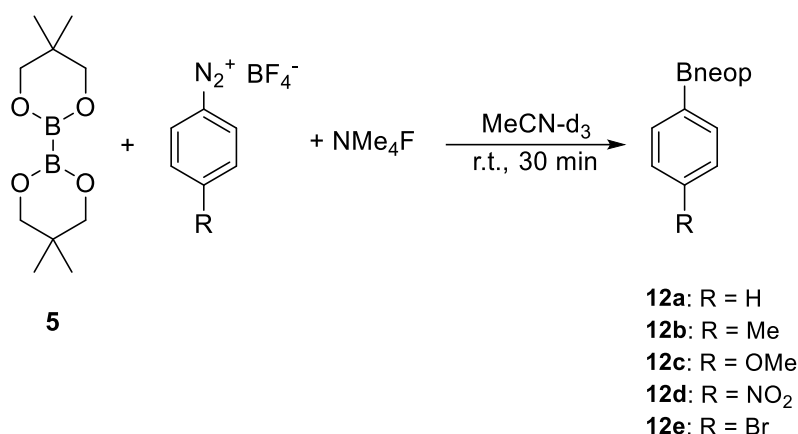


Figure 26: *In situ* $^{11}\text{B}\{^1\text{H}\}$ (left) and ^{19}F NMR (right) spectrum taken after 30 minutes of the borylation of $[\text{4-MeO-C}_6\text{H}_4\text{N}_2][\text{BPh}_4]$ with adduct **4** (reactant ratio: 1:1, MeCN-d_3); reproduced from ref. [74] with permission from Wiley-VCH.

1.2.3.4. Borylation reactions of B₂neop₂ with NMe₄F and diazonium [BF₄]⁻ salts

Due to further reported borylation reactions of adduct **4** with different diazonium [BF₄]⁻ salts, and the successful isolation and characterization of the boronate esters,^[74] the NMR scale reaction of B₂neop₂ and NMe₄F with [4-R-C₆H₄N₂][BF₄] (R = H, Me, OMe, NO₂ and Br) **10a-e** was investigated (Scheme 49). The reactions were monitored *via* NMR spectroscopy and GC-MS analysis; however, the desired boronate esters aryl-Bneop (**12a-e**) were only characterized using these two analytic methods.



Scheme 49: Reaction of B₂neop₂ **5** and NMe₄F with [4-R-C₆H₄N₂][BF₄] (R = H, Me, OMe, NO₂ and Br) at room temperature.

The reaction was monitored *via* ¹H and ¹¹B{¹H} NMR spectroscopy. The main-product of each reaction was the desired boronate ester aryl-Bneop (**12a-e**), which could also be characterized *via* GC-MS analysis. However, the borylation reaction proceeds not as clean as in the case of the reaction of adduct **4** with diazonium [BF₄]⁻ salts. In each reaction, unreacted B₂neop₂ **5** and the [4-R-C₆H₄N₂][BF₄] was observed, which is in accordance with the reported results.^[74] Figure 27 shows the ¹H NMR spectrum of the reaction of B₂neop₂ **5** and NMe₄F with [4-MeO-C₆H₄N₂][BF₄], and the product, 4-MeO-C₆H₄-Bneop **12c**, marked with asterisks (*).

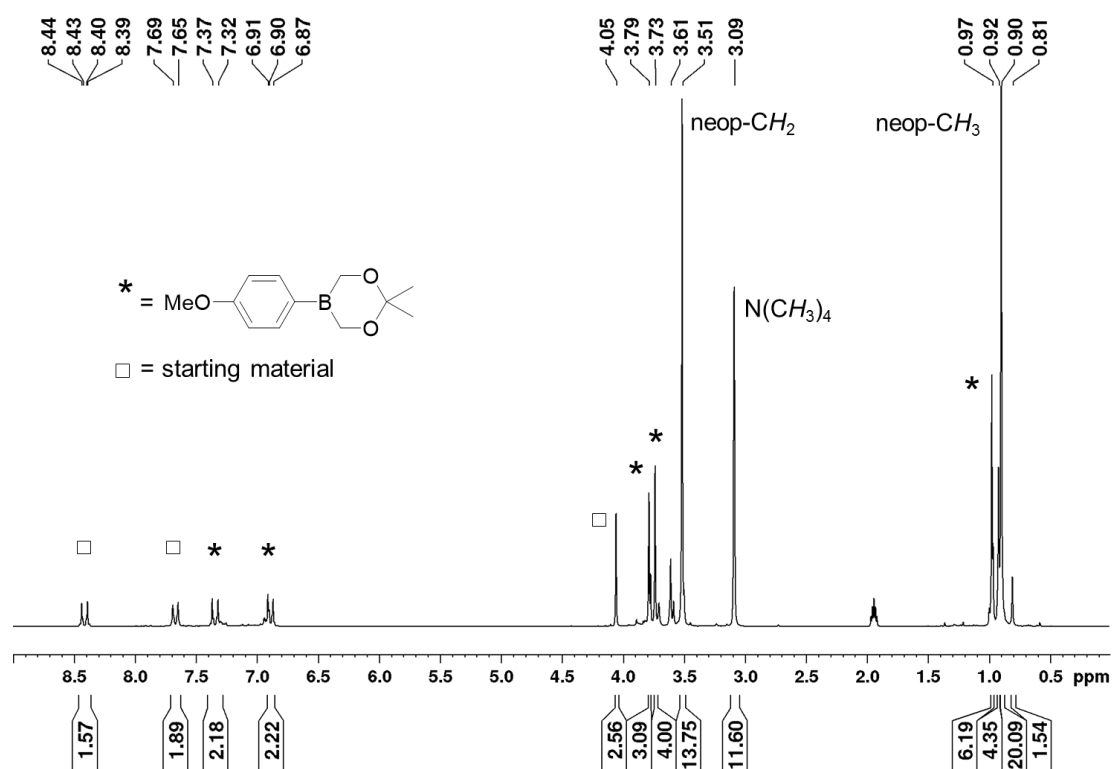


Figure 27: *In situ* ^1H NMR spectrum of the borylation reaction of B_2neop_2 **5** and NMe_4F with $[4\text{-MeO-C}_6\text{H}_4\text{N}_2][\text{BF}_4]$ at room temperature (Reactant ratio: 1:1; 200 MHz, MeCN-d_3).

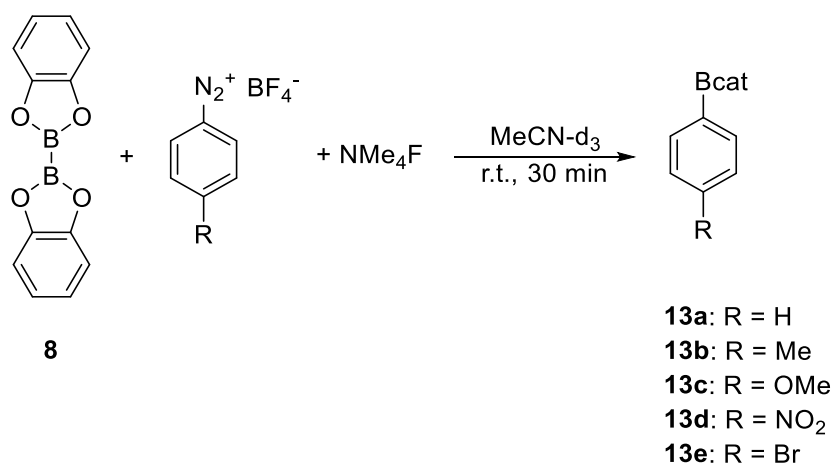
The obtained ^1H and $^{11}\text{B}\{^1\text{H}\}$ NMR data for the boronate ester aryl-Bneop (**12a-e**) are summarized in table 2 and are consistent with the data reported in literature.^[129-130]

	Bneop 	Bneop 	Bneop 	Bneop 	Bneop
^1H NMR [ppm]	0.99, 3.77, 7.32-7.44, 7.72-7.77	0.98, 2.33, 3.74, 7.17, 7.62	0.97, 3.73, 3.79, 6.89, 7.34	1.00, 3.80, 7.93, 8.16	0.98, 3.75, 7.49-7.53, 7.61-7.65
$^{11}\text{B}\{^1\text{H}\}$ NMR [ppm]	27.1	27.7	27.7	28.0	27.5
Mol-ion	190[M] ⁺	204[M] ⁺	220[M] ⁺	235[M] ⁺	268[M] ⁺

Table 2: ^1H and $^{11}\text{B}\{^1\text{H}\}$ NMR data and the molecular-ion peak in the mass spectrum of the aryl-Bneop boronate esters (**12a-e**).

1.2.3.5. Borylation reactions of B₂cat₂ with NMe₄F and diazonium [BF₄]⁻ salts

The borylation reactions of B₂cat₂ **8** and NMe₄F with different diazonium [BF₄]⁻ salts [4-R-C₆H₄N₂][BF₄] were done under the same conditions as the borylation reaction with diboron reagent B₂neop₂ **5** (Scheme 50). All reactions were carried out in MeCN-d₃ as the solvent and were monitored *via* ¹H and ¹¹B{¹H} NMR spectroscopy as well as GC-MS analysis.



Scheme 50: Reaction of B₂cat₂ **8** and NMe₄F with [4-R-C₆H₄N₂][BF₄] (R = H, Me, OMe, NO₂ and Br) at room temperature.

The main-product of each reaction is the respective boronate ester aryl-Bcat, which was characterized *via* ¹H and ¹¹B{¹H} NMR spectroscopy. Figure 28 shows the *in situ* ¹H NMR spectrum of the reaction of B₂cat₂ **8** and NMe₄F with [4-MeO-C₆H₄N₂][BF₄]. The main-product is the boronate ester aryl-Bcat **13a-e**; however, the starting materials, B₂cat₂ as well as the diazonium [BF₄]⁻ salts, are also detected.

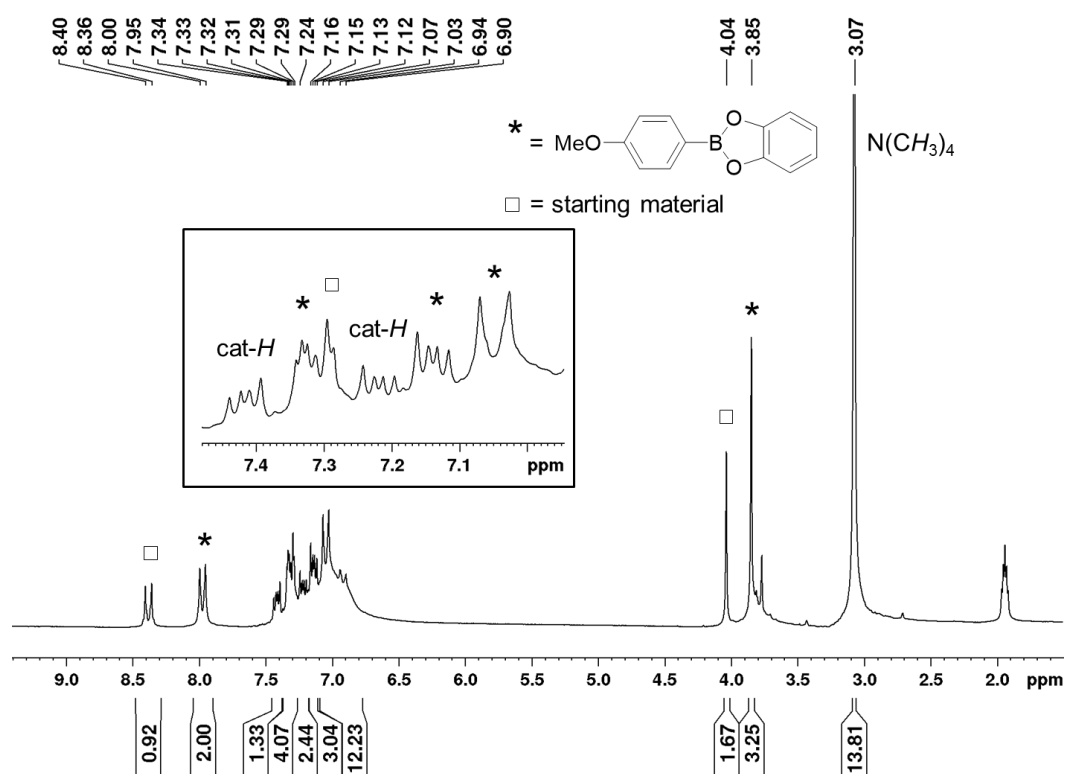


Figure 28: *In situ* ^1H NMR spectrum of the borylation reaction of B_2cat_2 **8** and NMe_4F with $[\text{4-MeO-C}_6\text{H}_4\text{N}_2][\text{BF}_4]$ at room temperature (Reactant ratio: 1:1; 200 MHz, MeCN-d_3).

^1H and $^{11}\text{B}\{^1\text{H}\}$ NMR data for the boronate esters aryl-Bcat (**13a-e**) are summarized in Table 3 and are consistent with the literature data.^[131]

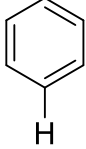
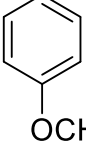
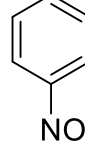
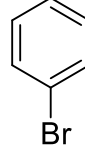
	Bcat 	Bcat 	Bcat 	Bcat 	Bcat 
^1H NMR [ppm]	7.15-7.19, 7.34-7.38, 7.52-7.60, 8.03-8.07	2.41, 7.13- 7.18, 7.32- 7.36, 7.93	3.85, 7.05, 7.12-7.16, 7.29-7.34, 7.97	7.69, 8.19-8.32	7.15-7.19, 7.33-7.37, 7.69, 7.93
$^{11}\text{B}\{^1\text{H}\}$ NMR [ppm]	32.2	32.4	31.3	31.2	32.2
Mol-ion	196[M] ⁺	210[M] ⁺	226[M] ⁺	241[M] ⁺	274[M] ⁺

Table 3: ^1H and $^{11}\text{B}\{^1\text{H}\}$ NMR data and the molecular-ion peak in the mass spectrum of the boronate esters aryl-Bcat (**13a-e**).

1.2.4. Experiments to obtain sp^3 - sp^3 diboron adducts

Due to the fact that studies of the working group^[51] and former reports by Hoveyda *et al.*^[18, 23] contain the syntheses of the neutral sp^2 - sp^3 diboron adduct $B_2pin_2 \cdot Cy_2Im$ and of anionic sp^2 - sp^3 diboron adducts were recently reported,^[74] the question of whether it is possible to synthesize and isolate possible anionic sp^3 - sp^3 diboron adducts of the type $[B_2pin_2(F)(NHC)][NMe_4]$ (NHC = *i*Pr₂Im, *n*Pr₂Im, Me₂Im, Me*i*PrIm) arises (Figure 29).

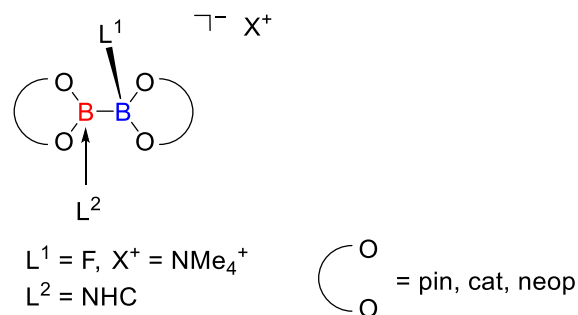
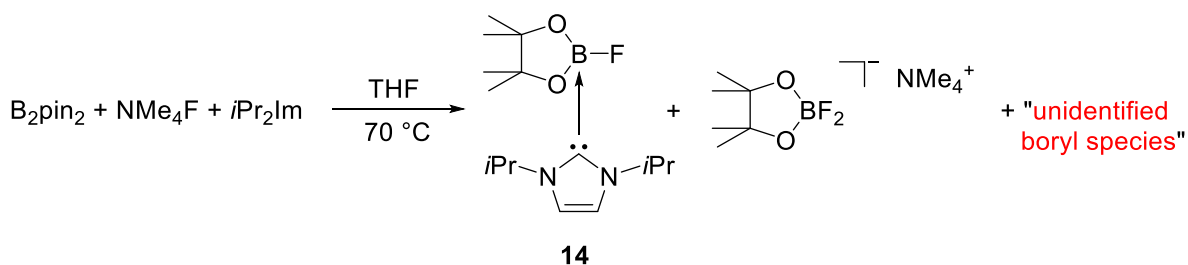


Figure 29: Possible anionic sp^3 - sp^3 diboron adduct $[B_2pin_2(F)(NHC)][NMe_4]$.

Based on the diboron adduct $B_2pin_2 \cdot Cy_2Im$ ^[51], the synthesis of the anionic sp^3 - sp^3 diboron adducts with B_2pin_2 **1** as the diboron reagent, NMe_4F as the base and several NHCs as the second coordinating ligand was investigated. The reaction conditions were the same in all reactions, in particular, the ratio of the starting materials was 1:1:1, THF was the solvent, and higher temperatures (up to 70 °C) were employed (NMe_4F is only soluble in MeCN for several minutes, and in refluxing THF).

First, the reaction with the NHC *i*Pr₂Im (*i*Pr₂Im = 1,3-di-*iso*-propyl-imidazolin-2-ylidene) was investigated, due to the fact that preliminary studies of the working group of Radius showed that B_2pin_2 **1** and *i*Pr₂Im form a neutral sp^2 - sp^3 diboron adduct. The reaction was carried out in THF at higher temperatures (Scheme 51).



Scheme 51: Reaction of B_2pin_2 **1** with NMe_4F and *i*Pr₂Im.

Two compounds were isolated from the reaction mixture. The first compound was an insoluble solid, which precipitated and was identified as the known compound $[pinBF_2][NMe_4]$ as the main-product (42%). However, the mother liquor was cooled to -30 °C and compound $FBpin \cdot iPr_2Im$ **14** could be isolated in very low yield (7%).

Compound **14** was characterized *via* ^1H , $^{11}\text{B}\{^1\text{H}\}$, $^{13}\text{C}\{^1\text{H}\}$ and ^{19}F NMR spectroscopy as well as elemental analysis. The ^1H NMR spectrum shows one set of signals for $i\text{Pr}_2\text{Im}$: The protons of the backbone are observed at 6.41 ppm and the methine proton $i\text{Pr-CH}$ at 6.03 ppm as a septet. The doublet resonance of the methyl-groups of the $i\text{Pr}_2\text{Im}$ is detected at 1.06 ppm. The pinacol-groups of the Bpin-moiety are detected at 1.20 and 1.57 ppm (Figure 30).

In the $^{13}\text{C}\{^1\text{H}\}$ NMR spectrum, the signals for the $i\text{Pr}_2\text{Im}$ NHC are detected at 23.2 ($i\text{Pr-CH}_3$), 49.3 ($i\text{Pr-CH}$) and 115.9 ppm (CHCH), and the carbene carbon atom are observed at 162.3 ppm. Furthermore, the methyl-groups of the pinacol are detected at 26.0 and 26.4 ppm, the resonance of the quaternary carbon atom is detected at 79.1 ppm. The $^{11}\text{B}\{^1\text{H}\}$ NMR spectrum shows one sharp doublet at 4.90 ppm and the fluorine atom resonates at -131 ppm as a quartet (Figure 31).

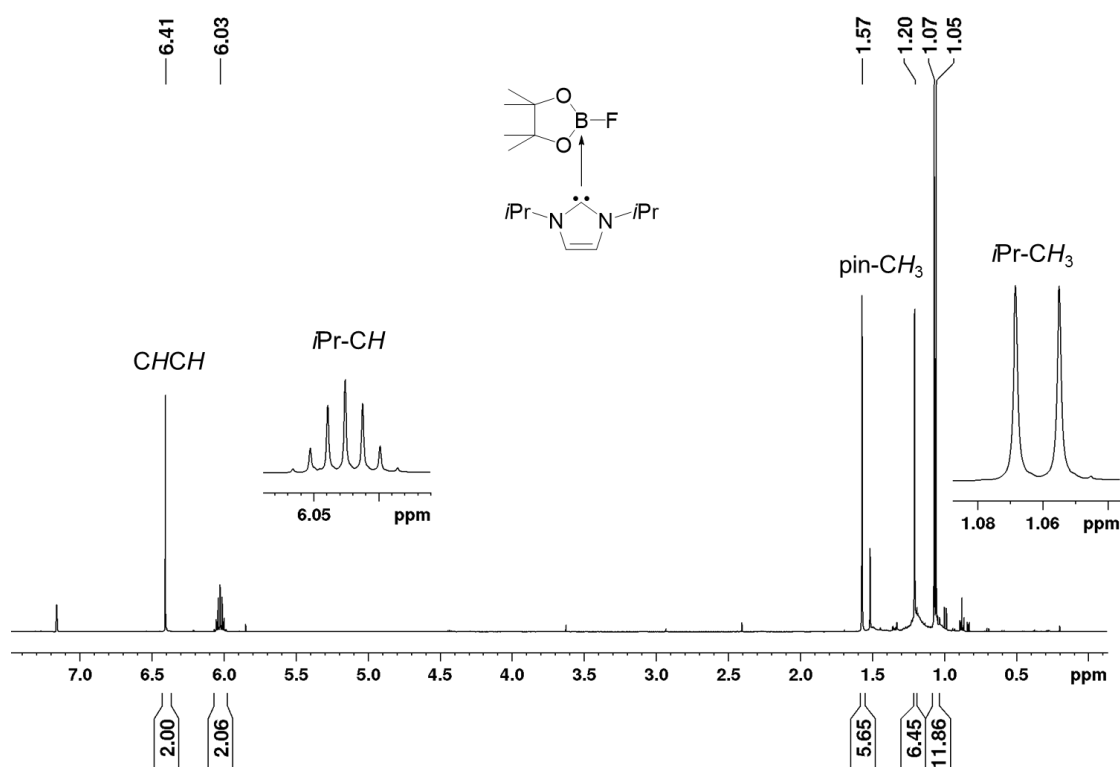


Figure 30: ^1H NMR spectrum of $\text{FBpin}\cdot i\text{Pr}_2\text{Im}$ **14** (500 MHz, C_6D_6).

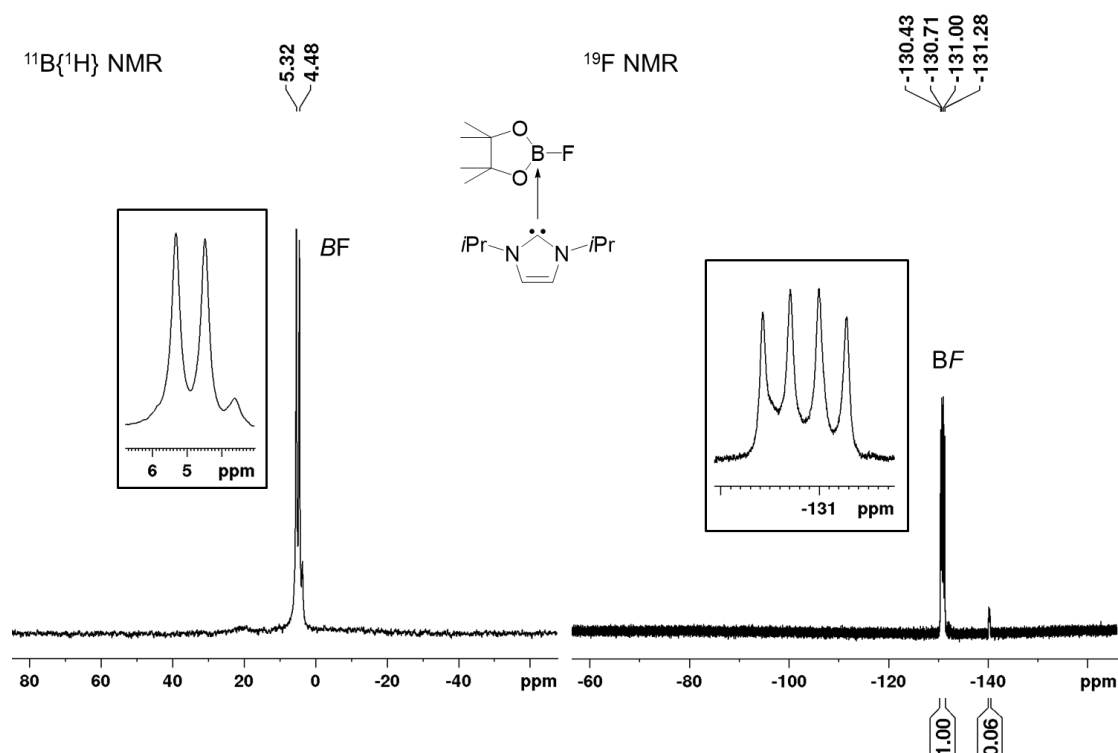
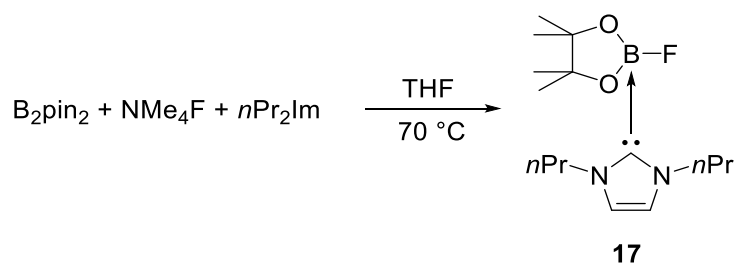


Figure 31: $^{11}\text{B}\{^1\text{H}\}$ (left) and ^{19}F (right) NMR spectra of $\text{FBpin}\cdot i\text{Pr}_2\text{Im}$ **14** (C_6D_6).

Similar results were obtained using Me_2Im ($\text{Me}_2\text{Im} = 1,3\text{-di-methyl-imidazolin-2-ylidene}$) and $\text{Me}i\text{PrIm}$ ($\text{Me}i\text{PrIm} = 1\text{-iso-propyl-3-methylimidazolin-2-ylidene}$) as the NHC. The main-product of both reactions was the salt $[\text{pinBF}_2][\text{NMe}_4]$; however, both adducts $\text{FBpin}\cdot\text{Me}_2\text{Im}$ **15** and $\text{FBpin}\cdot\text{Me}i\text{PrIm}$ **16** were characterized *via* ^1H , $^{11}\text{B}\{^1\text{H}\}$ and ^{19}F NMR spectroscopy. The obtained NMR data are summarized Table 4.

The reaction of B_2pin_2 **1** and NMe_4F with NHC $n\text{Pr}_2\text{Im}$ ($n\text{Pr}_2\text{Im} = 1,3\text{-di-}n\text{-propyl-imidazolin-2-ylidene}$) yielded the $\text{FBpin}\cdot n\text{Pr}_2\text{Im}$ **15** as the main-product, whereas no further signals were observed in the *in situ* $^{11}\text{B}\{^1\text{H}\}$ and ^{19}F NMR spectra, and the reaction mixture, compared to the reaction with $i\text{Pr}_2\text{Im}$, was a clear yellow solution (Scheme 52).



Scheme 52: Reaction of B_2pin_2 **1** with NMe_4F and $n\text{Pr}_2\text{Im}$.

$\text{FBpin}\cdot n\text{Pr}_2\text{Im}$ **15** was characterized *via* ^1H , $^{11}\text{B}\{^1\text{H}\}$, $^{13}\text{C}\{^1\text{H}\}$ and ^{19}F NMR spectroscopy as well as elemental analysis and X-ray diffraction. The ^1H NMR spectrum shows four signals for the $n\text{Pr}_2\text{Im}$ NHC, one singlet at 7.04 ppm for the protons at the backbone, one multiplet at 4.33 ppm and another one at 1.79 ppm for the methylene-groups of the NHC. The methyl-groups

resonate at 0.89 ppm as a triplet. The methyl-groups of the Bpin-moiety are split into two singlets at 0.93 and 1.12 ppm (Figure 32). In the $^{13}\text{C}\{^1\text{H}\}$ NMR spectrum, the signals for the $n\text{Pr}_2\text{Im}$ NHC are detected at 11.1 (CH_3), 25.0 (CH_2CH_3), 50.6 (N-CH_2) and 121.0 (CHCH), and the carbene carbon atom was observed *via* 2D NMR spectroscopy (HMBC) at 162.2 ppm. Furthermore, the pinacol methyl-groups are detected at 25.5 and 26.1 ppm, and the resonance of the quaternary carbon atom appears at 79.4 ppm. The $^{11}\text{B}\{^1\text{H}\}$ NMR spectrum shows one sharp doublet at 3.36 ppm and the fluorine atom resonates at -131 ppm as a quartet (Figure 33).

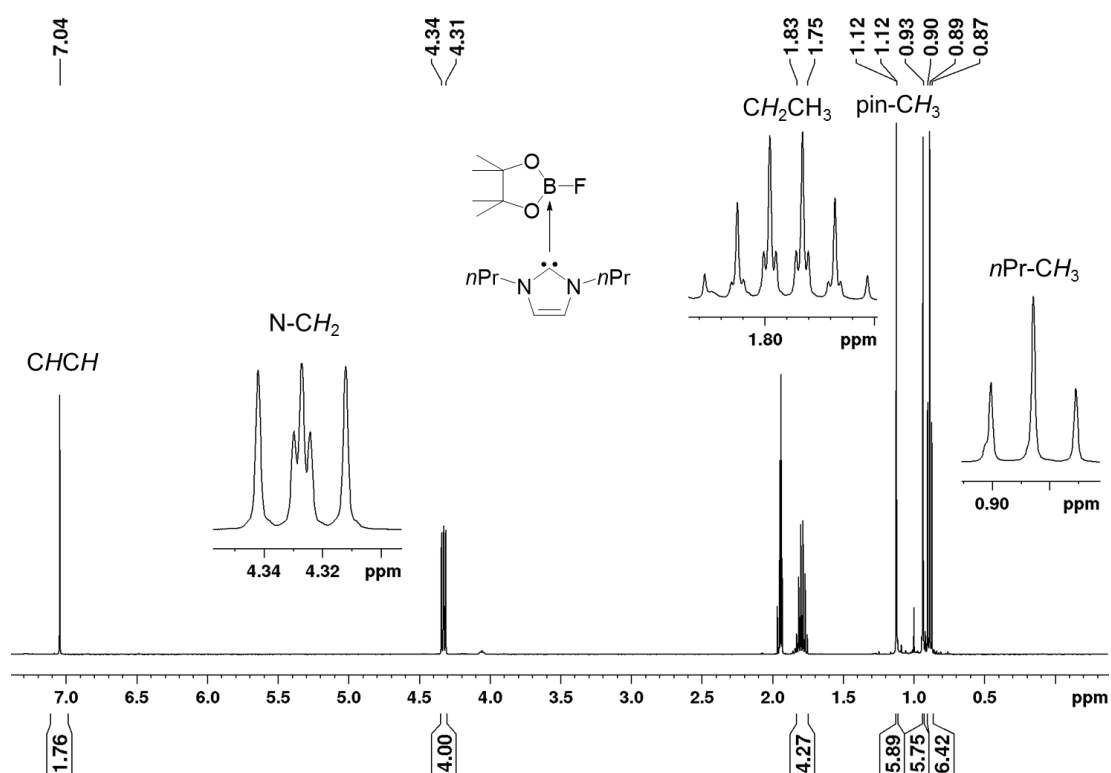


Figure 32: ^1H NMR spectrum of $\text{FBpin}\cdot n\text{Pr}_2\text{Im}$ **15** (500 MHz, MeCN-d_3).

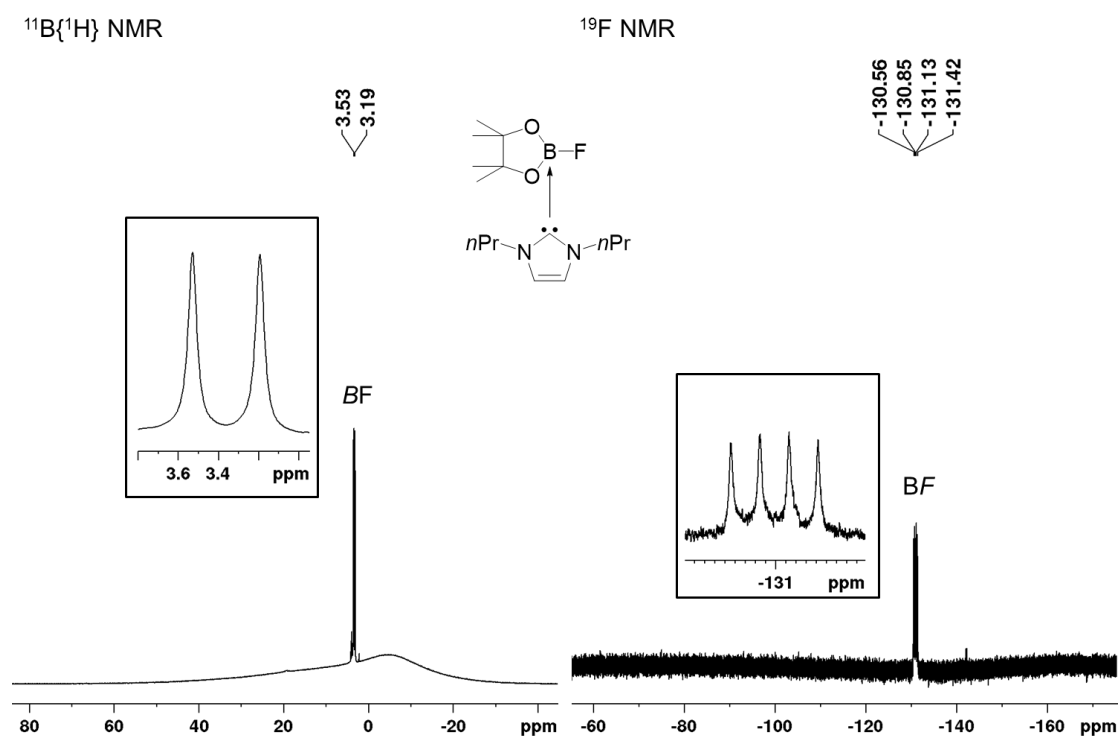


Figure 33: $^{11}\text{B}\{^1\text{H}\}$ (left) and ^{19}F (right) NMR spectra of $\text{FBpin}\cdot n\text{Pr}_2\text{Im}$ **15** (MeCN-d_3).

The X-ray structure of $\text{FBpin}\cdot n\text{Pr}_2\text{Im}$ **15** confirmed the solution structure obtained from the NMR data. The boron atom is tetrahedral coordinated with two oxygen atoms, one fluorine atom and the carbene carbon atom (Figure 34). The NHC binds to the boron atom and the B1–C1 bond distance of 1.667(2) Å is comparable to the bond length reported for the neutral $\text{sp}^2\text{-sp}^3$ diboron adduct $\text{B}_2\text{pin}_2\cdot\text{Cy}_2\text{Im}$ (1.673(2) Å).^[74] Furthermore, the B1–F1 (1.436(7) Å) distance is slightly shorter than that of the fluorine adduct $[\text{B}_2\text{pin}_2\text{F}][\text{NMe}_4]$ (1.478(2) Å).^[74] The B–O distances are comparable to those discussed earlier for the alkoxy adducts.^[74]

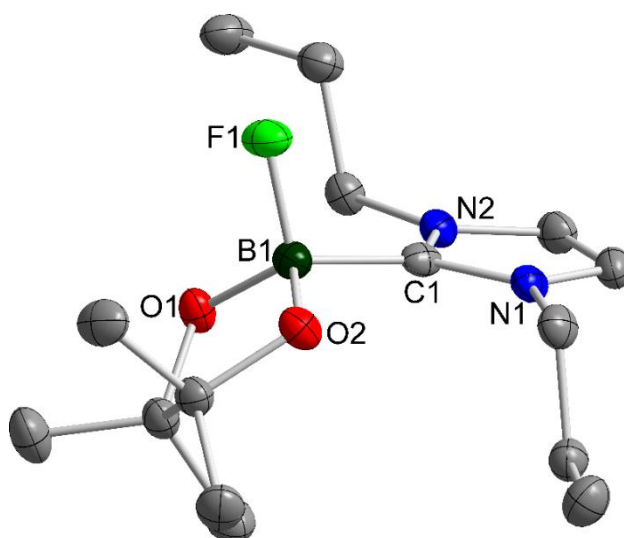


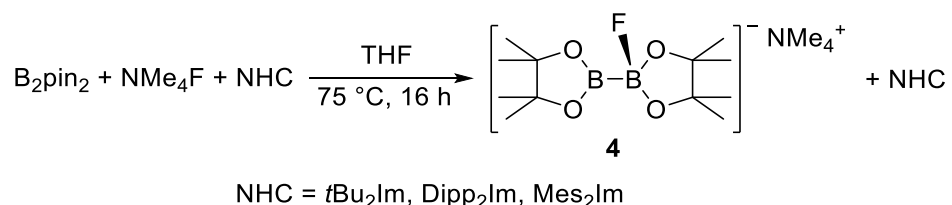
Figure 34: Perspective view of $\text{FBpin}\cdot n\text{Pr}_2\text{Im}$ **17**. Thermal ellipsoids are drawn at the 50% probability level; hydrogen atoms and the counter ion are omitted for clarity. Selected bond distances (Å) and angles ($^\circ$): B1–C1 1.667(2), B1–F1 1.436(7), B1–O1 1.454(10), B1–O2 1.445(9); F1–B1–C1 104.46(48), F1–B1–O1 108.58(49), F1–B1–O2 113.06(49).

The ^1H , $^{11}\text{B}\{^1\text{H}\}$, ^{19}F and $^{13}\text{C}\{^1\text{H}\}$ NMR spectroscopic data obtained for FBpin•*i*Pr₂Im **14**, FBpin•Me₂Im **15**, FBpin•Me*i*PrIm **16** and FBpin•*n*Pr₂Im **17** are summarized in Table 4.

NHC adduct	FBpin• <i>i</i> Pr ₂ Im 14	FBpin•Me ₂ Im 15	FBpin•Me <i>i</i> PrIm 16	FBpin• <i>n</i> Pr ₂ Im 17
^1H NMR [ppm]	1.60, 1.20, 1.57, 6.02, 6.40	0.94, 1.23, 3.90, 6.98	1.00, 1.20, 1.60, 3.55, 5.74, 5.91, 6.01	0.88, 0.92, 1.11, 1.78, 4.32, 7.03
$^{11}\text{B}\{^1\text{H}\}$ NMR [ppm]	4.90	4.25	4.85	3.35
$^{13}\text{C}\{^1\text{H}\}$ NMR [ppm]	NCN: 162.3			NCN: 162.2
^{19}F NMR [ppm]	-130.9	-133.6	-132.1	-131.0
Yield [%]	5	7	5	55

Table 4: Selected ^1H , $^{11}\text{B}\{^1\text{H}\}$, ^{19}F and $^{13}\text{C}\{^1\text{H}\}$ NMR data as well as the isolated yield of the mono-NHC adducts FBpin•*i*Pr₂Im **14**, FBpin•Me₂Im **15**, FBpin•Me*i*PrIm **16** and FBpin•*n*Pr₂Im **17**.

The reactions of B₂pin₂ (**1**), and NMe₄F with sterically more demanding NHCs, such as *t*Bu₂Im, Mes₂Im and Dipp₂Im, were also examined under the same conditions (higher temperatures and THF as the solvent). All reactions have in common that the anionic adduct [B₂pin₂F][NMe₄]**4** and the “free” NHC were isolated (Scheme 53).



Scheme 53: Reaction of B₂pin₂ **1**, NMe₄F and different sterically more demanding NHCs.

Chapter Two

Ring Expansion Reactions of Diboron(4)
Compounds with NHCs

“Bor-rings are anything but boring”

2. CHAPTER TWO: NEUTRAL ADDUCTS

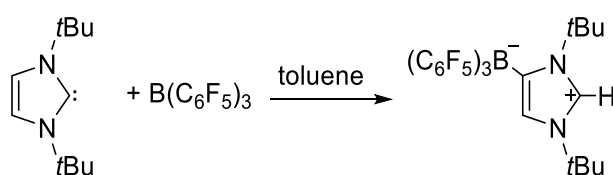
This year is the 25th anniversary of the first report of the isolation and characterization of a “bottleable” *N*-heterocyclic carbene (NHC).^[132] Since then, this class of compounds, as well as related molecules,^[133-142] e.g., cyclic alkylaminocarbenes (CAACs) and acyclic diaaminocarbenes (aDCs), have developed into an as yet unfinished success story par excellence in molecular chemistry. NHCs are heavily applied in main-group element^[143-147] and transition-metal chemistry,^[138, 148-149] especially to stabilize low-valent transition-metal^[150-151] and main-group element^[152-159] compounds, as ligands in homogeneous catalysis,^[160-163] or directly as organocatalysts.^[164-170] In all of these fields, NHCs are usually regarded as spectator ligands or reagents, but the latest developments have shown that they are not always inert, innocent bystanders. In some cases, NHCs react undergoing complete destruction of their core structure.

2.1. Introduction

2.1.1. Decomposition pathways of NHCs

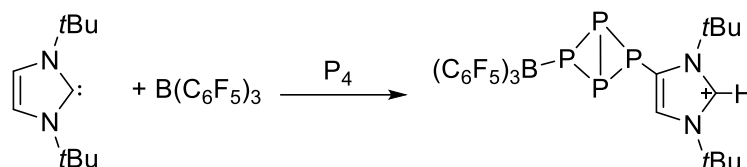
2.1.1.1. Exocyclic decomposition pathways

The application of NHCs as ligands or reagents in main-group element^[143-147] as well as in transition-metal^[138, 149, 171] chemistry is widespreadly known and was often reported. Generally, it is assumed that NHCs are inert; however, Tamm *et al.* reported the reaction of 1,3-di-*tert*-butyl-imidazolin-2-ylidene (*t*Bu₂Im) with B(C₆F₅)₃, yielding in the formation of the till then unexpected backbone activation of the NHC (Scheme 54).^[172]



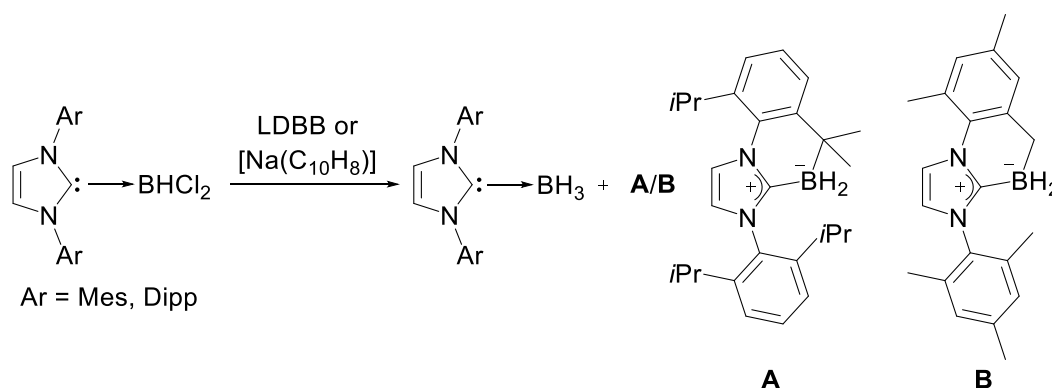
Scheme 54: Backbone activation of the NHC *via* reaction of *t*Bu₂Im with B(C₆F₅)₃.

Furthermore, during their study of frustrated Lewis pairs (FLPs),^[173-187] they were able to cleave one of the P–P bonds of the white phosphorus (P₄) *via* reaction of the FLP system *t*Bu₂Im/B(C₆F₅)₃ with P₄ (Scheme 55).^[188]

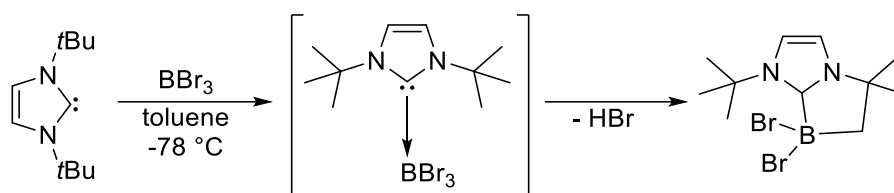
Scheme 55: P₄-activation *via* reaction of *t*Bu₂Im with B(C₆F₅)₃.

Many different exocyclic and endocyclic decomposition pathways are now well-established, with NHC-complexes of both main-group elements and transition-metals. These decomposition reactions include the activation of the backbone^[189-191] as well as *N*-alkyl activation^[192-202] e.g. C–H^[203-207], C–N^[192-193, 200, 208-209] and C–C^[210-211] bond activation reactions of the NHC. In the following paragraph, one example of the decomposition of an NHC is discussed.

Curran *et al.* observed an exocyclic decomposition of the NHC during their study of borylene chemistry in 2012.^[203] The alkyl-group at the *ortho*-position of the aromatic substituent on the nitrogen atom of the NHC was activated *via* reduction of HCl₂B•NHC (NHC = Mes₂Im or Dipp₂Im) with LDBB (LDBB = lithium di-*tert*-butylbiphenylide) or [Na(C₁₀H₈)], which resulted in the bonding of the methylene- or *i*Pr-group to the boron atom (Scheme 56).

Scheme 56: Reduction of NHC-stabilized HBCl₂ to form the isolable C–H insertion products **A** and **B**.

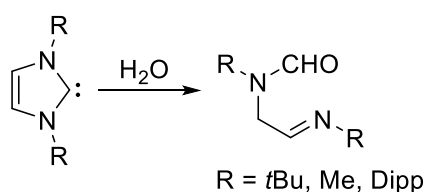
In 2011, Braunschweig and co-workers reported a further example of C–H activation of an *N*-alkyl-group.^[108] The reaction of *t*Bu₂Im with BBr₃ yielded in the formation of an *in situ* formed adduct Br₃B•*t*Bu₂Im, which was characterized by NMR spectroscopy at low temperature; however, this adduct is not stable at room temperature and spontaneously eliminates HBr to form the C–H activated product by further binding of the carbon atom to the boron atom (Scheme 57).



Scheme 57: Reaction of $t\text{Bu}_2\text{Im}$ with BBr_3 , which led to the C–H activated product.

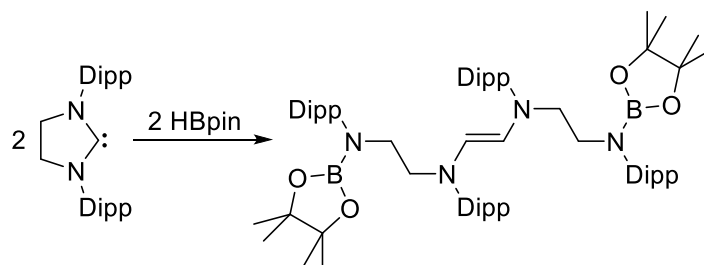
2.1.1.2. Solvolysis and ring-opening of NHCs

Treating NHCs and their corresponding imidazolium salts with water can lead to solvolytic ring-opening. In 2011, Nyulászi *et al.* reported several reactions of different carbenes in water or the reaction of NHCs with an equimolar amount of water in THF. The resulting products were formed *via* C–N cleavage of the NHC and further addition of H_2O across the C–N carbene bond to afford the corresponding aldehyde (Scheme 58).^[212]



Scheme 58: Hydrolysis of imidazolin-2-ylidenes.

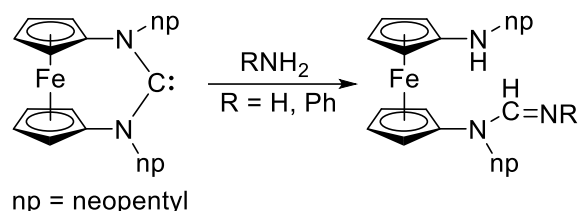
A similar ring-opened compound was reported by Bertrand and co-workers in 2010, during their study on the activation of several main-group hydrides with different CAACs and NHCs.^[213] The reactions of CAACs with silanes as well as boranes led to an oxidative addition of the substrate to the CAAC carbon atom; however, the reaction of Dipp_2Slm (1,3-bis(2,6-di-*iso*-propylphenyl)-imidazolidin-2-ylidene) with HBpin led to the unexpected ring-opening of the saturated NHC Dipp_2Slm at room temperature (Scheme 59).



Scheme 59: Reaction of Dipp_2Slm with HBpin forming the ring-opened product.

Ring-opening reactions of NHCs are also known involving transition-metal complexes, e.g. iron-complexes.^[144, 214] Siemeling and co-workers reported several C–N cleavage reactions of

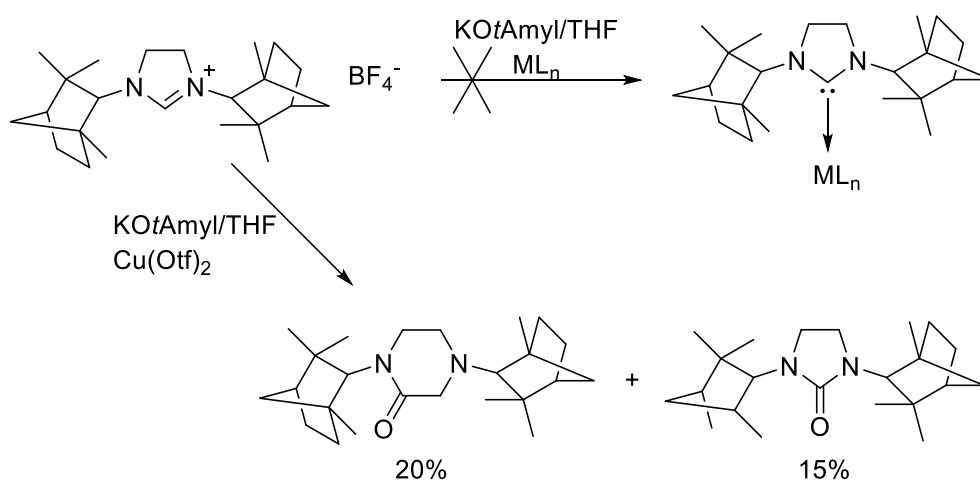
an interesting ferrocenyl-substituted carbene with ammonia or aniline (Scheme 60). In the case of both nitrogen-containing substrates, ring-opening products were observed, involving a proton migration to the *N*-alkyl-group and binding of the NPh or NH to the former carbene carbon atom.^[214]



Scheme 60: Reaction of $\text{Fe}(\text{Cp-Nnp})_2\text{C:}$ with aniline and ammonia.

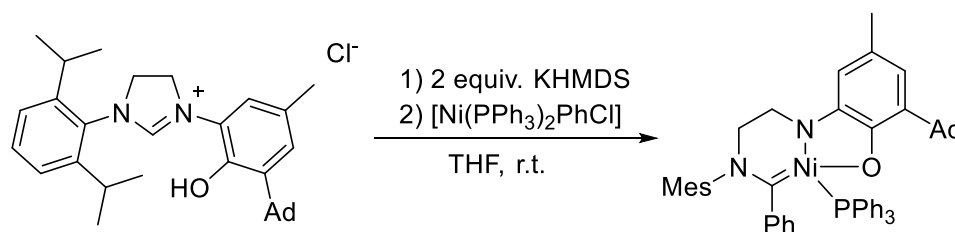
2.1.2. Metal-containing ring expansion reactions

Several examples of ring expansion reactions are also known for transition-metals.^[215-221] In 2006, Weaver and co-workers reported an unexpected ring expansion reaction of an enantiopure imidazolidinium salt during their study on copper-complexes with imidazolidin carbene ligands.^[215] The reaction of the difenchylimidazolidinium salt with potassium-*tert*-amylate (*KOtAmyl*) and copper(II) triflate did not lead to the formation of the expected copper-complex; however, they isolated a mixture of two organic compounds. One of them is the ring expanded product with one oxygen atom bound to the carbene carbon atom and the other one is an urea derivative. To confirm their results, they synthesized the ring expanded product *via* reaction of the corresponding amine with chloroacetyl chloride (Scheme 61).



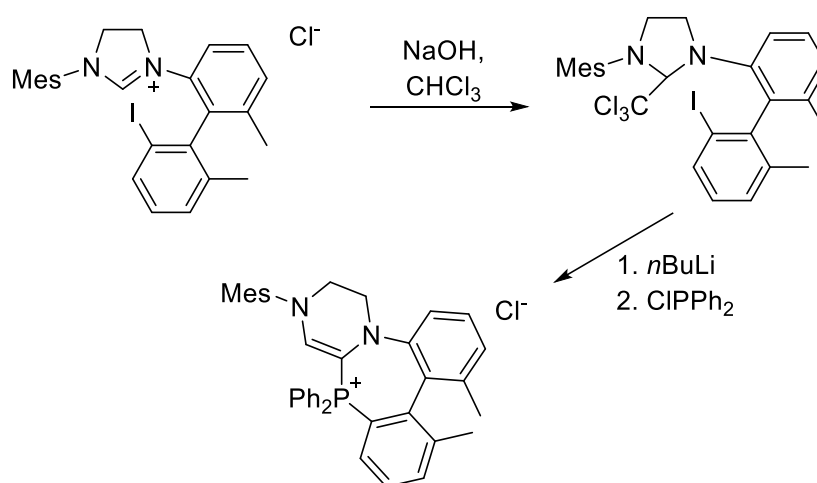
Scheme 61: Reaction of difenchylimidazolidinium salt with base and copper(II) triflate forming piperazinone and an urea derivative.

In the same year, Grubbs *et al.* published a similar reaction of an imidazolidinium salt with potassium hexamethyldisilazide (KHMDs) and $[\text{Ni}(\text{PPh}_3)_2\text{PhCl}]$ at room temperature.^[216] In this case, the C–N bond of the NHC is cleaved and the nickel atom inserts into the C–N bond (Scheme 62).



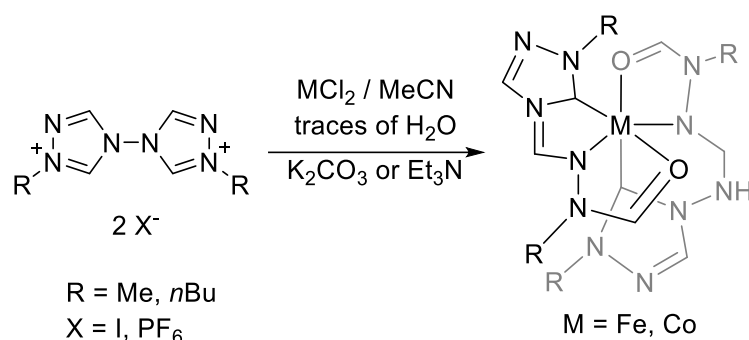
Scheme 62: Synthesis of the six-membered nickelacycle.

The product contains a six-membered nickelacycle including the migration of the phenyl substituent to the former carbene carbon atom. To prove that the migration of the alkyl-moiety depends on the size of the substituent, they carried out a similar reaction with the bulkier mesityl nickel-complex $[\text{Ni}(\text{PPh}_3)_2\text{MesBr}]$ and the corresponding product was an expected nickel-complex with an NHC coordinating to the metal. Grubbs *et al.* also reported the rearrangement of imidazolidin salts to phosphonium salts (Scheme 63).^[216]



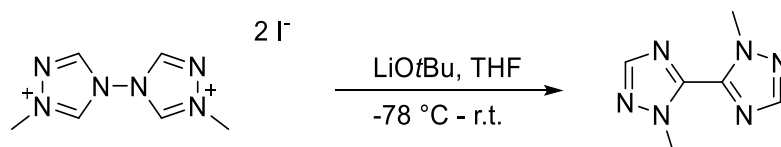
Scheme 63: Rearrangement of imidazolidin salts to phosphonium salts.

In 2012, Chen, Xue and co-workers reported the synthesis of stable iron and cobalt NHC-complexes including an unexpected ring-opening reaction and the *in situ* generation of a tridentate ligand.^[222] Based on the reaction of metal chlorides and bistriazolium salts with MeCN at 70 °C in the presence of base (K_2CO_3 or Et_3N), they obtained the metal-complexes in good yields (Scheme 64).

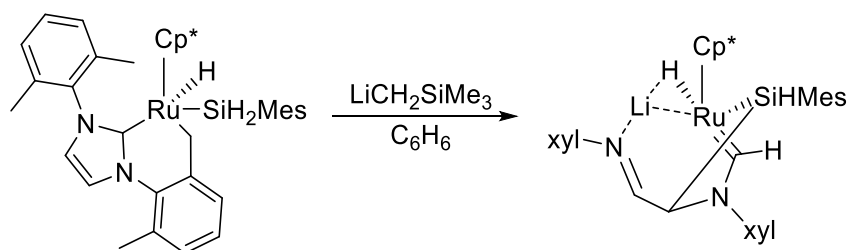


Scheme 64: Synthesis of Fe- and Co-NHC-complexes.

Crabtree *et al.* investigated the deprotonation of the imidazolium salt to transfer bistriazolium (bitz) to the metal precursors; however, the expected metal-complexes could not be observed. Therefore, the bitz salt was reacted with strong bases such as LiOtBu , which led to a rearranged product (Scheme 65).^[223] The molecular structure identified the isolated solid as a C–C linked bipyrazole, which is air and moisture stable.

Scheme 65: Rearrangement of bistriazolium salt (bitz) with LiOtBu .

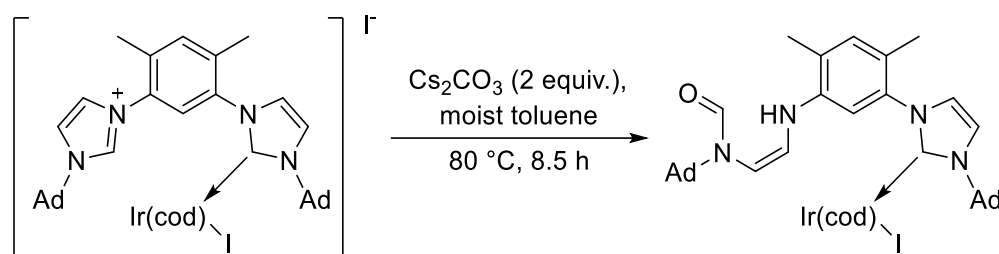
In 2014, Tilley *et al.* reported a ring expansion reaction, wherein ruthenium is involved as the metal atom. Based on their reactions of $[\text{RuCp}^*\text{L}(\text{N}_2)]$ with alkyl silanes, they obtained the corresponding silyl-Ru-complex (Scheme 66). Further reaction with $\text{LiCH}_2\text{SiMe}_3$ in benzene led to the formation of a ring-opened NHC-complex, including a C–N bond cleavage and C–Si bond formation on the former backbone carbon atom.^[219]



Scheme 66: Synthesis of the NHC ring-opened Ru-complex.

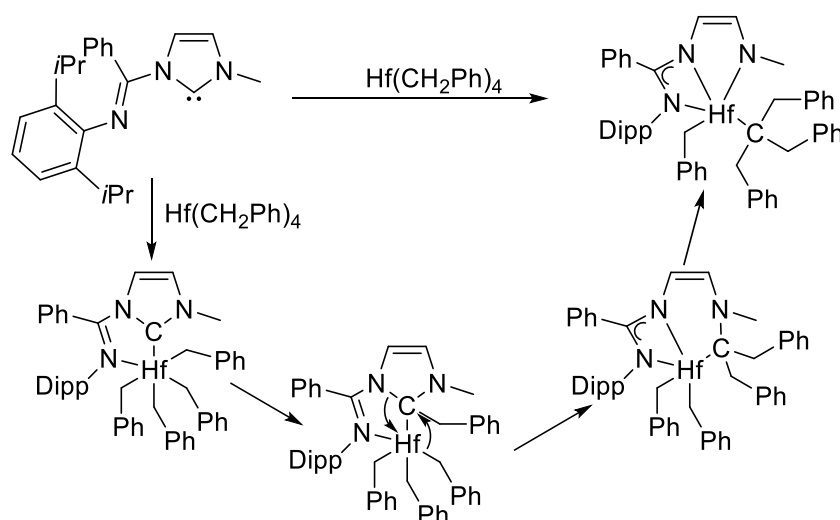
Interestingly, there are few examples of ring-opening reactions of NHCs in the literature which do not involve a six-membered heterocyclic ring in the product. These results were also reported by Braunstein and Zuo during their study on the synthesis of Ir(III) pincer-complexes with NHCs (Scheme 67).^[220] They reported two reactions, wherein ring-opened Ir-complexes could be observed. The first one was the reaction of the Ir-complex with Cs_2CO_3 in toluene,

which opened the non-coordinated imidazolium salt *via* formation of an aldehyde. Deprotonation of the imidazolium salts with strong bases indicated the presence of two chemically different heterocycles; however, storing an NMR sample overnight gave the ring-opened product as the major compound.



Scheme 67: Formation of ring-opened Ir-complex.

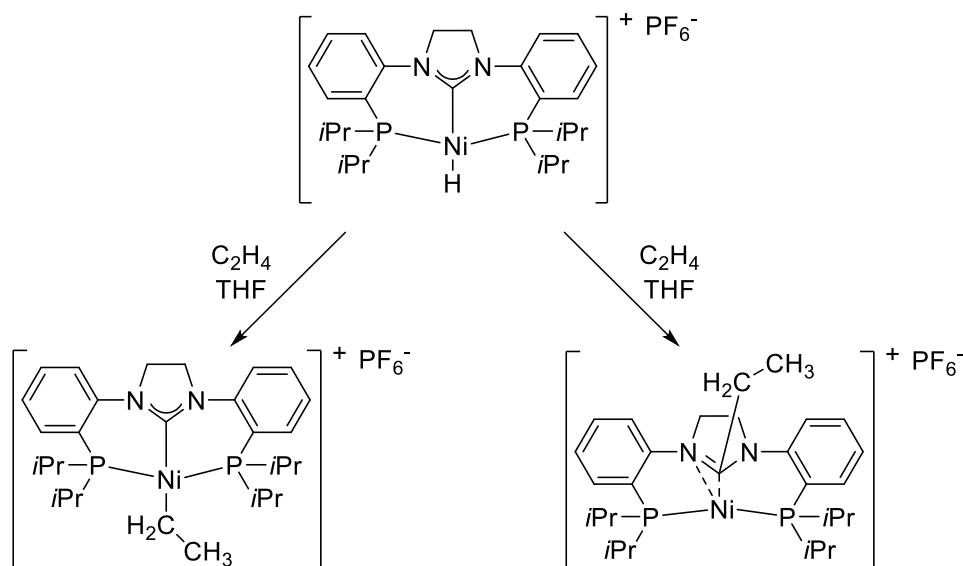
Recently, another interesting example of the complete removal of the carbene carbon atom from the ligand was reported by Slaughter *et al.*^[221] The reaction of an imino-imidazolium salt with KHMDS and tetrabenzyl-hafnium led to an eneamido–amidinato hafnium-complex which implies carbene carbon abstraction from the imino-*N*-heterocyclic carbene. A mechanism was postulated which includes an initial migration of two benzyl ligands from hafnium to the carbene carbon atom and subsequent Hf-insertion into the C–N bond. The last step of the sequence is the migration of a third benzyl-moiety, which led to the formation of a C(benzyl)₃ ligand coordinated to the hafnium atom (Scheme 68).



Scheme 68: Postulated mechanism for the formation of the Hf-complex.

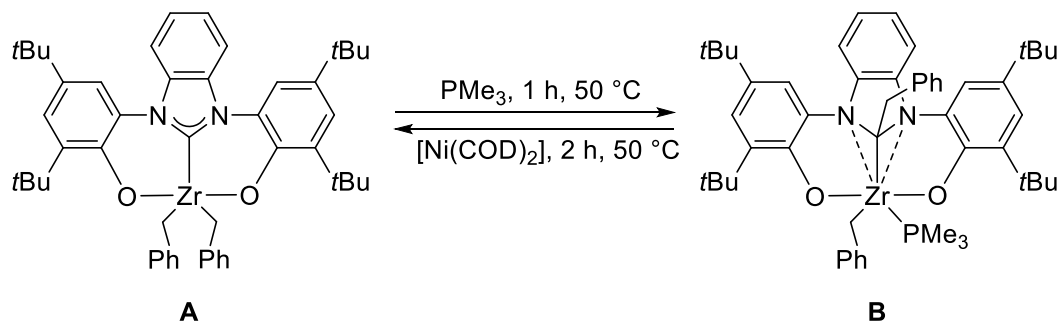
The initial and important step of ring expansion reactions is the activation of the E–X bond of the substrates; however, subsequent migration of hydrogen atoms, alkyl- or boryl-groups were reported. Furthermore, in transition-metal chemistry, migration to the carbene carbon atom is also observed. One example was reported in 2009 by Fryzuk, Green and co-workers, based

on the reaction of the nickel(II) hydride-complex $[\text{Ni}(\text{PCP})(\text{H})]\text{PF}_6$ (PCP = *o*-*i*Pr₂PC₆H₄(NC₃H₄N)*o*-C₆H₄P*i*Pr₂) with ethylene.^[198] The product can be formed by two possible reaction pathways. The first step is the formation of a Ni-complex with C₂H₄. The second step is divided into two different parts, insertion of ethylene into the Ni–C bond or into the Ni–H bond. However, after reductive elimination, the product in which an ethyl-group migrates to the carbene carbon atom, is formed (Scheme 69).



Scheme 69: Reaction of the nickel-hydride-complex leading to the unexpected migration of the ethyl-group to the carbene carbon atom.

Recently, similar results on the migration of a substituent to the NHC carbon atom were reported by Despagnet-Ayoub, Labinger, Bercaw *et al.* including the migration of one benzyl ligand from the zirconium atom to the carbene carbon atom of the ligand (Scheme 70).^[224] In comparison to the other reported example, the migration of the benzyl ligand is reversible; thus, heating complex **B** with $[\text{Ni}(\text{COD})_2]$ for 2 hours at 50 °C regenerates complex **A**.



Scheme 70: Migration of a benzyl ligand from the zirconium atom to the carbene carbon atom.

2.1.3. Main-group element-containing ring expansion reactions

Ring-opening reactions by solvolysis, e.g. with water or amines, can be regarded as E–H activations across the C–N (carbene) bond. In the last few years, another type of reaction with element hydrides and organyls has been reported several times involving expansion of the five membered NHC ring, either in solution or in the gas phase.^[225-226] Most reports of such ring expansion reactions (RER) have appeared quite recently, involving the main-group elements boron^[227-229], beryllium^[230-231] and silicon^[232] (Figure 35).

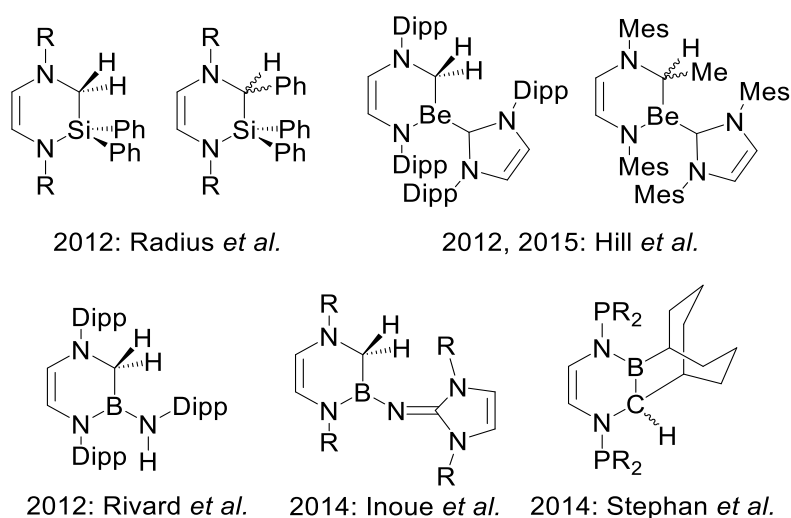
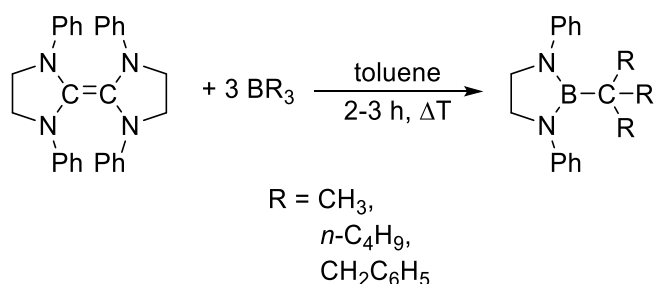


Figure 35: Overview of recently reported main-group element-promoted ring expansion reactions.

The first report of a closely related reaction dates back to 1965. Heese and Haag published the reactions of boralkyls with the dimeric carbene bis(1,3-diphenyl-imidazolidin-2-ylidene) (formally a carbene dimer) in toluene at elevated temperatures (Scheme 71).^[233]



Scheme 71: Reaction of dimeric carbenes with BR_3 (R = methyl, *n*-butyl, benzyl).

The reaction products are five-membered heterocycles with a boron/carbon atom exchange, which means that the three R-substituents bind finally to the former carbene carbon atom. They proposed a mechanism with four important steps: i) first, the formation of an adduct between the NHC and BR_3 (**A**); ii) the second step is the migration of one R-substituent to the carbene carbon atom (**B**); iii) simultaneous C–N bond cleavage of the NHC and insertion of

the boron atom with a further alkyl migration (**C**); iv) the last step is the ring contraction to the five-membered heterocycle and the resulting migration of the CR_3 -moiety to the boron atom (**D**).^[233]

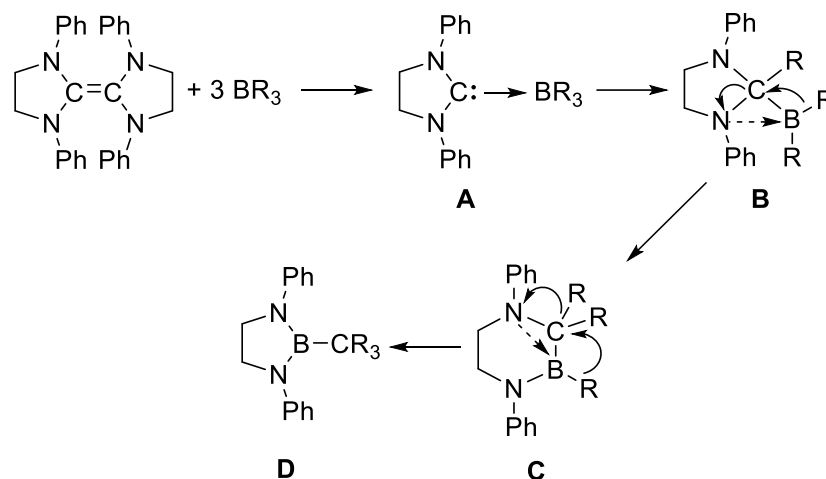
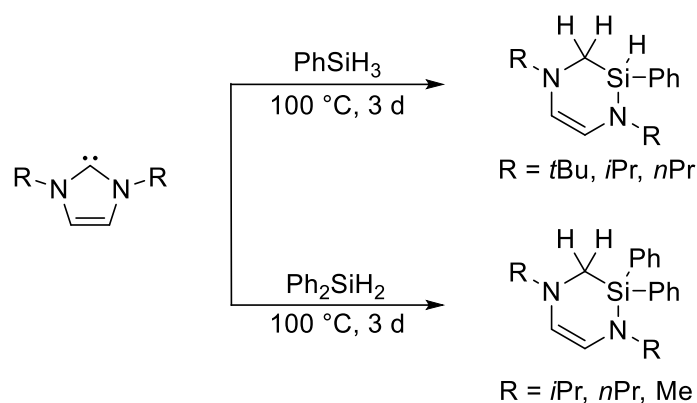


Figure 36: Postulated mechanism of the reaction of bis(1,3-diphenyl-imidazolidin-2-ylidene) with BR_3 ($\text{R} = \text{methyl}, n\text{-butyl}, \text{benzyl}$).

Although this reaction sequence was reported 50 years ago, and certainly needs to be verified, it already included some interesting and significant features which are apparent in recent reports. The first one is the concept of ring expansion reactions of NHCs; the majority of reaction pathways which have been proposed or calculated recently are, in a way, based on Figure 36. The second interesting feature here comprises the ring contraction from intermediate **C** to **D**, but this reaction is beyond the scope of the discussion.

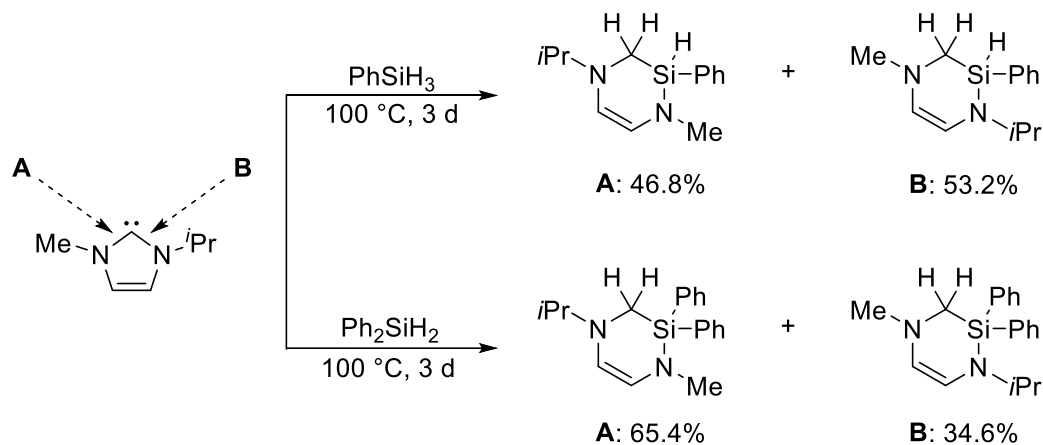
More and more examples of the incorporation of main-group elements into the NHC ring have appeared in the literature over the last four years. Most of these RERs lead to six-membered heterocyclic ring systems with the insertion of the main-group element (Be, Si or B) into the five membered ring. The first examples of these hydride-mediated ring expansion reactions were reported by Radius *et al.*^[232] and Hill *et al.*^[230] in 2012.

Radius *et al.* published a similar ring expansion reaction of NHCs with hydrosilanes at higher temperatures. Based on their study on the reactivity of nickel-complexes, e.g. $[\text{Ni}_2(\text{iPr}_2\text{Im})_4(\text{COD})]$ ^[234-241] with hydrosilanes $\text{H}_n\text{SiR}_{4-n}$ and reports that some NHCs could undergo insertion into the Si-H bond of several silanes, they were interested in stoichiometric reactions of NHCs with hydrosilanes (Scheme 72).



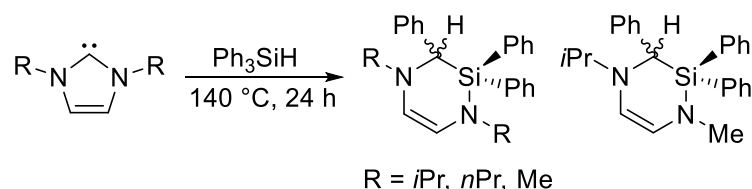
Scheme 72: Synthesis of the ring expanded product *via* reaction of NHCs with phenyl- and diphenylsilanes.

The reactions of NHCs with one equivalent of phenylsilanes ended in the formation of derivatives of 3,4-dihydro-2,5-diazasilinanes including the insertion of the silicon atom into the C–N bond and the migration of two hydrogen atoms to the former carbene carbon atom. In addition to the reported results, Radius and co-workers investigated the reactions of the unsymmetrically substituted $i\text{PrMeIm}$ with phenyl- and diphenylsilane. In the case of phenylsilane, the unexpected sterically more demanding product was the major product; however, the reaction with diphenylsilane led to an expected product ratio.



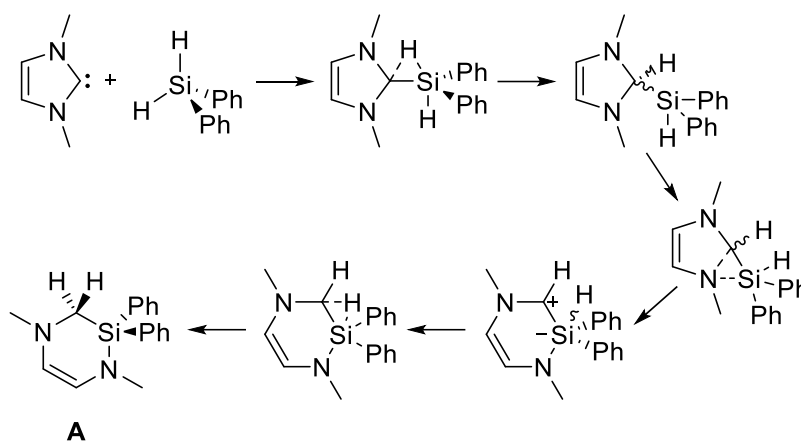
Scheme 73: Reaction of the unsymmetrical NHC $\text{Me}/i\text{PrIm}$ with phenyl- and diphenylsilane; reproduced from ref. [232] with permission from Wiley-VCH.

Thus, RERs seem to be a rather general process in NHC main-group chemistry which warrants further investigations. The isolated products were six-membered heterocycles which were formed *via* C–N bond cleavage within the NHC, migration of two hydrogen atoms to the (former) NHC carbene carbon atom and formal insertion of a silylene fragment into the C–N bond (Scheme 72 and 73). Moreover, for the reaction of Ph_3SiH , rather than mono- and diphenylsilane, migration of a phenyl-group was observed.



Scheme 74: Reaction of different NHCs with Ph_3SiH ; reproduced from ref. [232] with permission from Wiley-VCH.

A tentative mechanism for this reaction was proposed (Scheme 75), which was based on the experimental observations that the kinetics of the reaction of $i\text{Pr}_2\text{Im}$ with Ph_2SiH_2 follows a second order rate law (first order in both NHC and silane), whereas the RER of isolated 1,3-bis-(2,6-di-*iso*-propylphenyl)-2-(phenylsilyl)-imidazolin (**A**) follows first order kinetics.^[232] Furthermore, several DFT investigations^[242-247] based on the reported ring expansion reactions, mainly by the group of Wilson and Dutton, confirmed the results by Radius and co-workers.^[243]

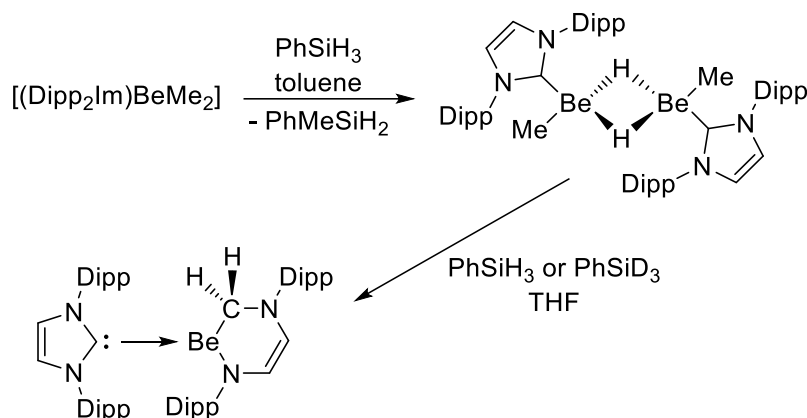


Scheme 75: Proposed mechanism of the reaction of the NHC Me_2Im with Ph_2SiH_2 , reproduced from ref. [232] with permission from Wiley-VCH.

Furthermore, Radius *et al.* reacted $i\text{Pr}_2\text{Im}$ with deuterated Ph_2SiD_2 and obtained deuteration exclusively at the NHC-carbene carbon atom. The reaction of $i\text{Pr}_2\text{Im}$ with a 1:1 ratio of Ph_2SiH_2 and Ph_2SiD_2 afforded a mixture of dideuterated and non-deuterated products and no H/D cross products were observed. These observations confirmed the calculated mechanism and the assumption that both protons which migrate to the former carbene carbon atom are originally from the silane.^[232]

Simultaneously, Hill and co-workers reported a ring expansion reaction during their study of organo-beryllium compounds at higher temperatures.^[230-231] Based on the reaction of two equivalents of methyl lithium with an equimolar solution of Dipp_2Im and BeCl_2 in diethylether, they isolated $[(\text{Dipp}_2\text{Im})\text{BeMe}_2]$ as the starting material for further reactions. The reaction of the starting material and PhSiH_3 led to the formation of the expected product PhMeSiH_2 ;

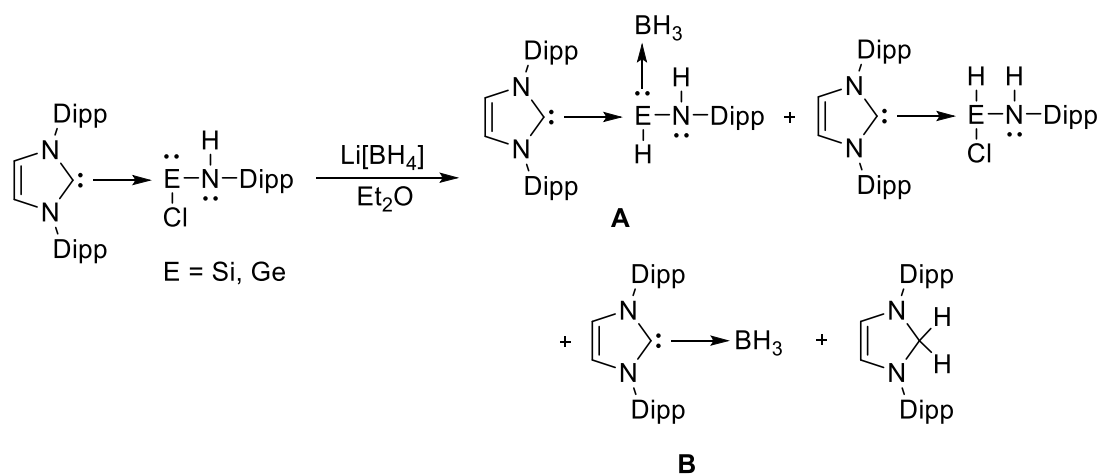
however, they isolated single crystals which were identified as a Be-H-Be bridged dimeric compound. The isolated dimeric compound is not soluble in common solvents, albeit heating the solid with PhSiH_3 in THF at 80 °C for six hours led to the formation of a ring expanded product, including the cleavage of the C–N bond, insertion of the beryllium atom and migration of two hydrogen atoms to the former carbene carbon atom (Scheme 76).^[230]



Scheme 76: Synthesis of the six-membered heterocycle.

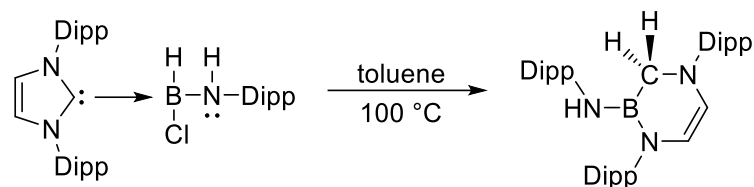
Furthermore, similar ring expanded products starting from Mes_2Im were reported by Hill and co-workers in 2015, including the observation of methyl migration from beryllium to the NHC carbon atom.^[231]

In 2012, Rivard *et al.* reported the hydride-mediated ring expansion reaction of NHCs with aminohydrides.^[227] Based on their observations on NHC-stabilized amidohydride-complexes of the general form $\text{Dipp}_2\text{Im}\cdot\text{EHNHDipp}$ (**A**) ($\text{E} = \text{Si}, \text{Ge}$ or Sn) which were present in the mixture arising from the reaction of $\text{Dipp}_2\text{Im}\cdot\text{E}(\text{Cl})\text{NHDipp}$ (**B**) with $\text{Li}[\text{BH}_4]$ and the following synthesis of carbene borane adducts, e.g. $\text{Dipp}_2\text{Im}\cdot\text{BH}_2\text{NHDipp}$ (**B**) (Scheme 77).



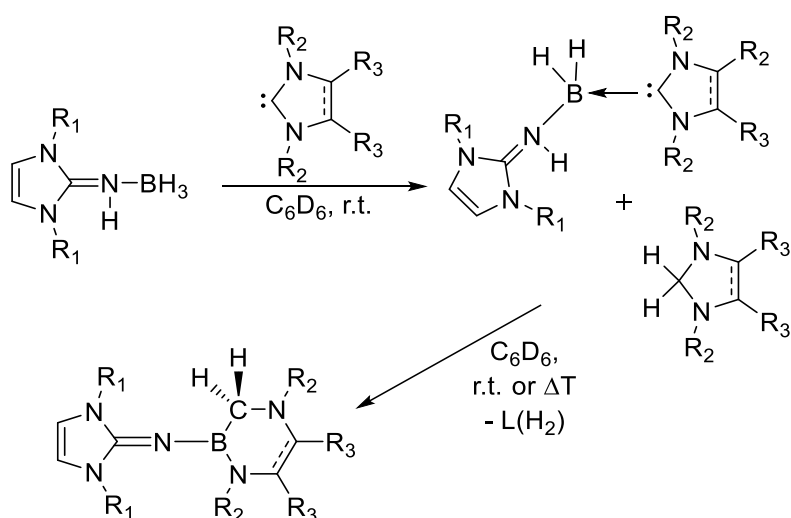
Scheme 77: Synthesis of silicon and germanium amidohydride-complexes.

The isolated carbene borane adduct $\text{Dipp}_2\text{Im}\cdot\text{BH}_2\text{NHDipp}$ was heated to $100\text{ }^\circ\text{C}$ and afterwards rearranged to the ring expanded product involving the cleavage of the C–N bond and insertion of the boron atom to form the six-membered heterocycle (Scheme 78).



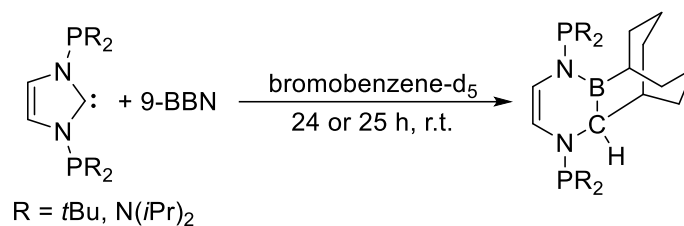
Scheme 78: Rearrangement of carbene borane adduct $\text{Dipp}_2\text{Im}\cdot\text{BH}_2\text{NHDipp}$ to the ring expanded product.

Similar results, including boron as the main-group element, were reported by Inoue *et al.* based on the adduct formation of an NHC with an iminoborane dihydride (Scheme 79).^[228] Keeping the adduct at room temperature or heating at elevated temperatures, depending on the used NHC, led to a rearrangement of the compound, including the insertion of a boron atom into the C–N bond and migration of two hydrogen atoms to the former carbene carbon atom.



Scheme 79: Synthesis of an NHC iminoborane adduct and further hydride-mediated ring expansion reaction.

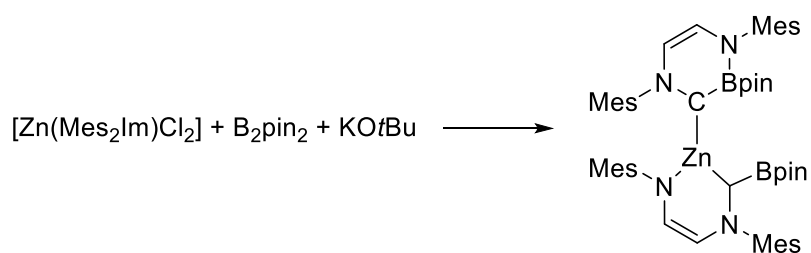
After characterization and isolation of the NHC adducts of 9-borabicyclo[3.3.1]nonane (9-BBN)^[248] the group of Stephan was interested in intramolecular borenium-phosphine FLPs with *N*-phosphorylated carbenes of the type $\text{C}_3\text{H}_2(\text{NPR}_2)_2$; however, these reactions yielded in a C–N bond cleavage and insertion of the boron atom into the C–N bond (Scheme 80).^[229]



Scheme 80: Reaction of 9-BBN with different NHCs.

In comparison to the ring expanded products reported by the working groups of Hill, Radius, Rivard and Inoue only one hydrogen atom migrates to the former carbene carbon atom and the reactions were carried out at room temperature.

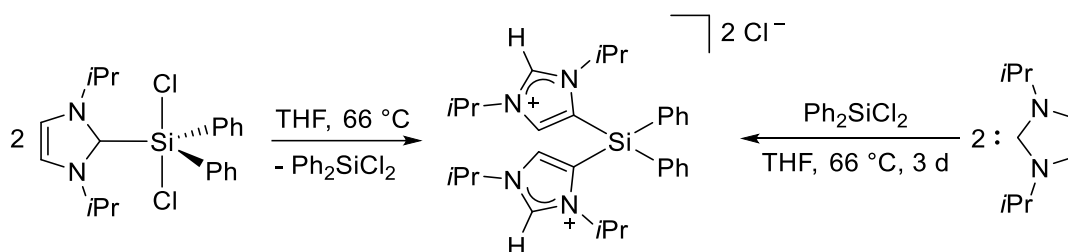
The preceding examples reveal that Lewis-acidic boron compounds may readily react with NHCs to give ring expanded products. Recently, Marder *et al.* presented another example of ring expansion reactions during their study on zinc-catalyzed borylation^[249] of primary, secondary and tertiary alkyl halides with alkoxy diboron reagents at room temperature. To explain the mechanism, they reacted [Zn(Mes₂Im)Cl₂] with B₂pin₂, but no conversion was observed; however, after adding KO*t*Bu to the reaction mixture a zinc-containing product was isolated (Scheme 81). The zinc-complex is formed *via* the cleavage of one C–N bond with insertion of one zinc atom into this bond and the migration of a Bpin-group to the former carbene carbon atom. Additionally, a second Bpin-moiety inserts into the C–N bond of another NHC ligand.



Scheme 81: Synthesis of the zinc-containing ring expanded product.

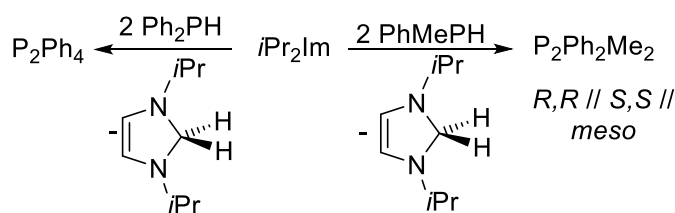
2.1.4. Limitation of ring expansion reactions

Currently, the appearance of ring expansion reactions depends on several factors, including: i) the Lewis-acidity of the substrates; ii) the presence of electropositive migrating groups, such as H, alkyl, phenyl or boryl-moieties. As already mentioned, Wilson, Dutton *et al.* demonstrated that RER depend also on energetically favorable bonding.^[242-245] DFT calculations showed that, for example, chlorosilanes are not able to undergo ring expansion reactions, due to the fact that the Si–Cl bond is energetically more favorable than a potential C–Cl bond. These observations were confirmed by Radius *et al.*, with the success using phenylsilanes and NHCs contrasting with recent reports by the same group which showed that similar reactions of NHCs with the substrate Ph_2SiCl_2 (electronegative) led to different reaction pathways,^[250] including the coordination of the silane to the backbone of the NHC (Scheme 82). Furthermore, the reduction of the imidazolium salt yielded in the isolated, abnormal NHC ($^a\text{iPr}_2\text{Im}$) $_2\text{SiPh}_2$.



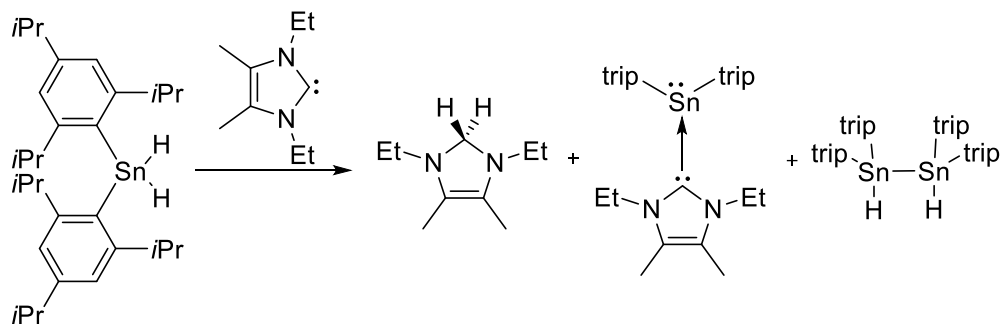
Scheme 82: Synthesis of ($^a\text{iPr}_2\text{Im}$) $_2\text{SiPh}_2$ with the abnormal coordination of two NHCs to a silylene-moiety.

In contrast to the reaction with silanes, which afforded RER products, the reaction of iPr_2Im with diphenylphosphine led to dehydrocoupling products.^[251] In the ^1H -NMR spectrum of the crude reaction mixture, iPr_2ImH_2 was observed as the hydrogen acceptor product with P_2Ph_4 being the phosphorus-containing product observed in the ^{31}P -NMR spectrum. Furthermore, the reaction of phenylmethylphosphine led to the formation of iPr_2ImH_2 and the corresponding *S,S,R,R* and *meso*-isomers of $\text{P}_2\text{Ph}_2\text{Me}_2$ (Scheme 83). The reaction of PhPH_2 with two or more equivalents of iPr_2Im led to four-, five-, and six-membered cyclic oligophosphines P_4R_4 , P_5R_5 and P_6R_6 as well as $\text{iPr}_2\text{Im}=\text{PR}$ ($\text{R} = \text{Ph}$ or *o*-Tol) and $\text{iPr}_2\text{Im}-\text{H}_2$.



Scheme 83: Hydrogen abstraction with an NHC forming diphosphines.

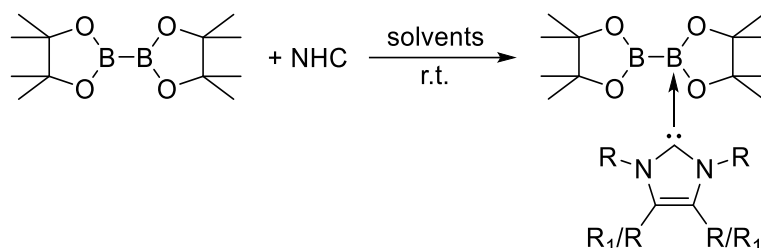
For group 14 chemistry, Wesemann and co-workers reported on hydrogen transfer from a stannane to NHCs.^[252-253] The reaction of $\text{Sntrip}_2\text{H}_2$ (trip = 2,4,6-tri-*iso*-propylphenyl) with the NHC $\text{Et}_2\text{Im}^{\text{Me}}$ led to NHC- H_2 , an NHC tin(II) adduct and the dimeric tin compound $[\text{Sntrip}_2\text{H}]_2$ (Scheme 84). The reaction of $\text{trip}_2\text{SnH}_2$ with two equivalents of the NHC led to the clean formation of the NHC-tin adduct.^[252] Recently, Wesemann *et al.* also reported the reaction of Ar^*SnH_3 with the bulky Ar^* ($\text{Ar}^* = 2,6\text{-}(2,4,6\text{-tri-}i\text{iso-propylphenyl})\text{C}_6\text{H}_3$) substituent with $\text{Me}_2\text{Im}^{\text{Me}}$, which led to the formation of $\text{Me}_2\text{Im}^{\text{Me}}\text{-H}_2$ and the tin(II) compound $\text{Ar}^*\text{SnH}(\text{NHC})$.^[253]



Scheme 84: Different reaction products of the reaction between Ar_2SnH_2 and an NHC.

2.2. Results and Discussion

Preliminary studies in the groups of Marder^[51] and Radius^[254-255] showed that it is possible to synthesize and characterize neutral sp^2 - sp^3 diboron adducts of the type $B_2pin_2 \cdot NHC$ (Scheme 85).



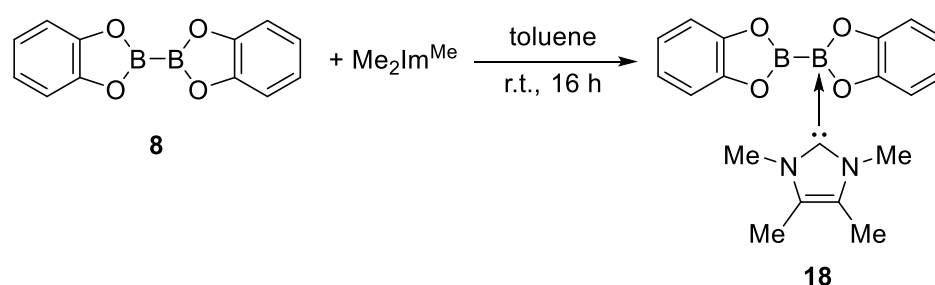
Scheme 85: Synthesis of different neutral sp^2 - sp^3 diboron adducts of the type $B_2pin_2 \cdot NHC$.

In the following chapter, the synthesis and characterization of different neutral sp^2 - sp^3 and sp^3 - sp^3 diboron adducts of B_2cat_2 and B_2neop_2 are discussed.

2.2.1. Mono- and bis-NHC adducts of diboron(4) compounds

2.2.1.1. Synthesis of mono-NHC adducts of the type $B_2cat_2 \cdot NHC$

The first investigation was the reaction of B_2cat_2 **8** with the NHC Me_2Im^{Me} . The stoichiometric reaction was carried out at room temperature, and after work-up, the desired neutral sp^2 - sp^3 diboron adduct $B_2cat_2 \cdot Me_2Im^{Me}$ **18** was obtained in good yield (79%) (Scheme 86).



Scheme 86: Synthesis of the mono-NHC adduct $B_2cat_2 \cdot Me_2Im^{Me}$ **18**.

$B_2cat_2 \cdot Me_2Im^{Me}$ **18** was fully characterized *via* NMR spectroscopy, in solution as well as in the solid state, X-ray diffraction and elemental analysis. The 1H NMR spectrum shows two singlets for each methyl-groups of the Me_2Im^{Me} , one at 1.03 ppm and the other one at 3.37 ppm (Figure 37). The protons of the catechol-moiety are detected as four multiplets in the aromatic region (6.80-6.81, 6.85-6.87, 7.12-7.13 and 7.14-7.15 ppm). In the $^{11}B\{^1H\}$ NMR spectrum, two signals are observed, one sharp signal for the sp^3 -boron atom at 7.11 ppm and one broad

signal at 38.6 ppm for the sp^2 -boron atom. The carbene carbon atom is detected at 160.4 ppm in the $^{13}C\{^1H\}$ NMR spectrum.^[256]

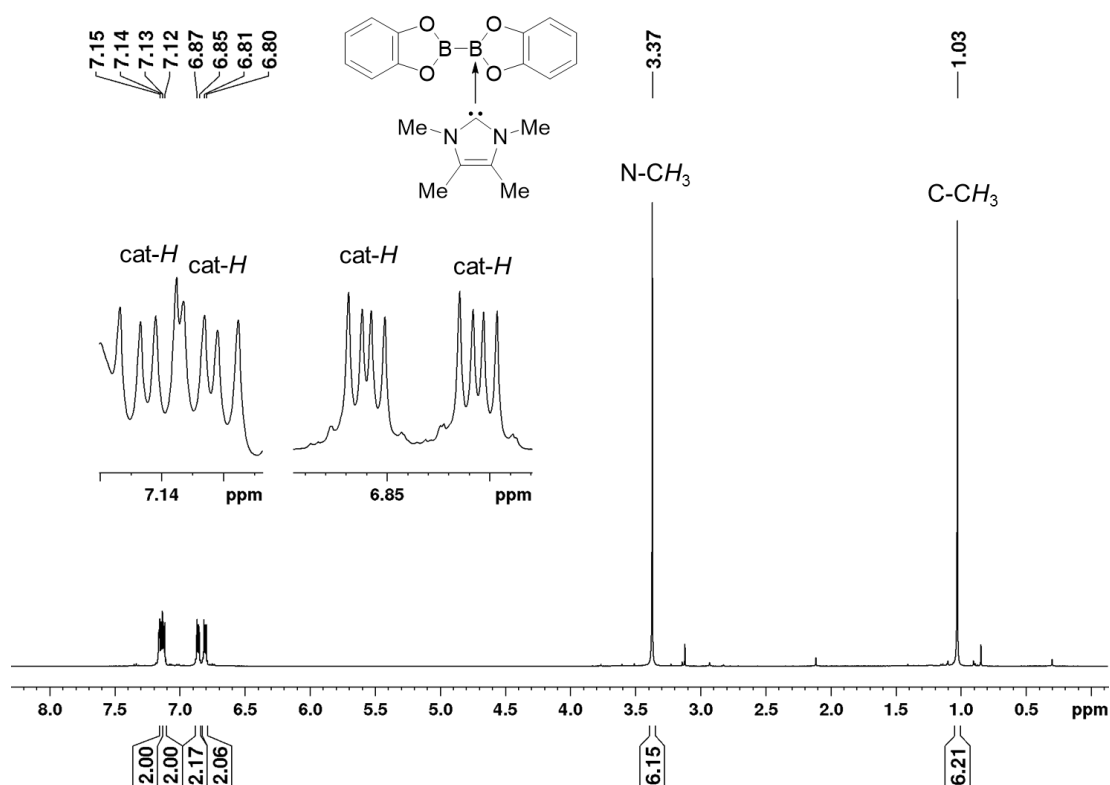


Figure 37: 1H NMR spectrum of $B_2cat_2 \cdot Me_2Im^{Me}$ **18** in C_6D_6 (500 MHz); reproduced from ref. [253] with permission from Wiley-VCH.

In addition to the recorded NMR spectra in solution, $B_2cat_2 \cdot Me_2Im^{Me}$ **18** was characterized *via* solid state NMR spectroscopy to confirm the existence of the mono-NHC diboron adduct **18**. In the ^{11}B solid state NMR spectra, two signals for the different boron atoms are observed, one at 3.82 ppm (sp^3 -boron atom) and the sp^2 -boron atom is detected at 34.1 ppm (Figure 38). Furthermore, the ^{13}C solid state NMR spectrum shows one signal for each methyl-group as well as for each carbon atom of the catechol-moiety. The quaternary carbon atoms are also observed as four signals between 147.9 and 154.7 ppm. The carbene carbon atom is detected as a broad signal (due to the quadrupole coupling of the boron atom) at 159.2 ppm. In addition to the ^{11}B and ^{13}C solid state NMR spectra, the ^{14}N solid state NMR spectra confirmed the results and showed two signals for the two nitrogen atoms (-204.6 and -207.1 ppm).^[256]

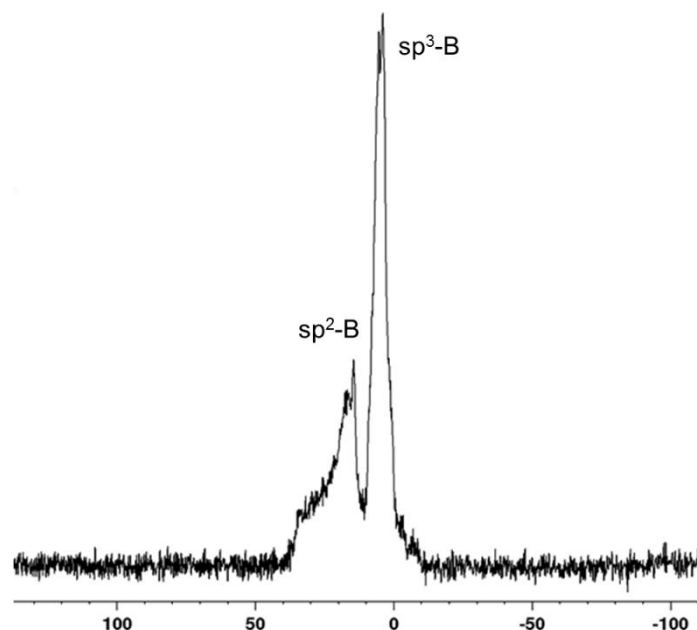


Figure 38: Solid state ^{11}B NMR of $\text{B}_2\text{cat}_2\cdot\text{Me}_2\text{Im}^{\text{Me}}$ **18**; reproduced from ref. [74] with permission from Wiley-VCH.

These results are different from the reported neutral $\text{sp}^2\text{-sp}^3$ diboron adducts,^[18, 23, 51, 254] in so far that in the ^{11}B NMR spectra, two signals are observed. In the case of the previous reported mono-NHC diboron adducts, only one signal is detected at room temperature, which can be explained by the fast exchange of the NHC between the two boron atoms (Figure 39).

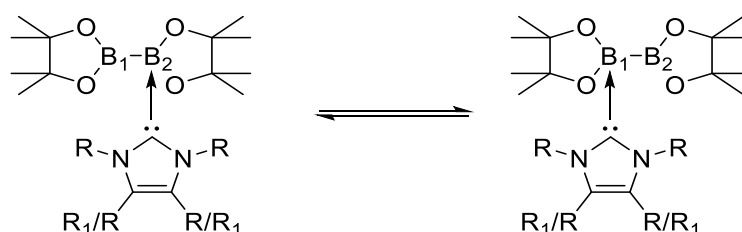


Figure 39: Exchange of the NHC between the two boron atoms of the diboron compound.

Based on the knowledge that “free” NHCs, including $\text{Me}_2\text{Im}^{\text{Me}}$, immediately react and further decompose in CH_2Cl_2 ^[257], compound $\text{B}_2\text{cat}_2\cdot\text{Me}_2\text{Im}^{\text{Me}}$ **18** was dissolved in CD_2Cl_2 and the reaction mixture was monitored *via* NMR spectroscopy. The ^1H as well as the ^{11}B NMR spectra showed no evidence for any decomposition reaction, which means that the mono-NHC adduct is dissolved and stable in this solvent. This observation is in good agreement with the reported results above that the NHC binds only to one boron atom.^[256]

Furthermore, single crystals were obtained to characterize compound **18** *via* X-ray diffraction, which confirmed the structure of the mono-NHC diboron adduct. The molecular structure of $\text{B}_2\text{cat}_2\cdot\text{Me}_2\text{Im}^{\text{Me}}$ **18** is similar to the reported structure of the diboron adduct $\text{B}_2\text{pin}_2\cdot\text{Cy}_2\text{Im}$.^[51] The boron atom B1 is essentially planar, while B2 is tetrahedral coordinated (Figure 40). The

B–B distance (B1–B2 1.729(3) Å) is slightly shorter than the distance found in the molecular $B_2pin_2 \cdot Cy_2Im$ (B1–B2 1.743(2) Å).^[51] The B–O distances are essentially comparable to those discussed earlier for the alkoxy and the fluoride adducts.^[74] The B2–C1 distance (1.647(2) Å) is similar to the distance found in $B_2pin_2 \cdot Cy_2Im$ (B2–C1 1.673(2) Å).^[256]

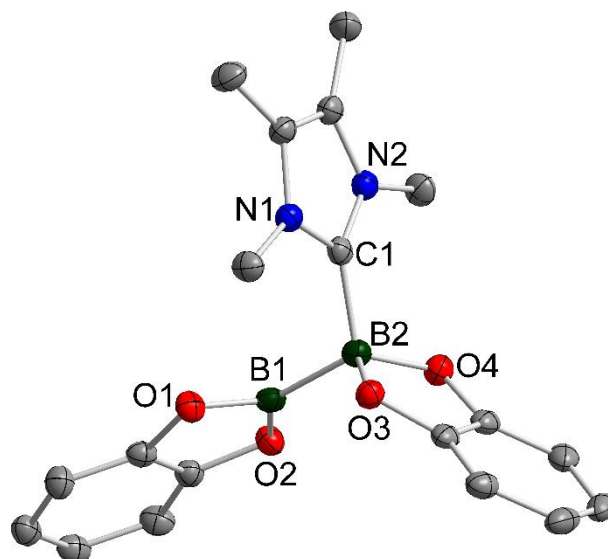
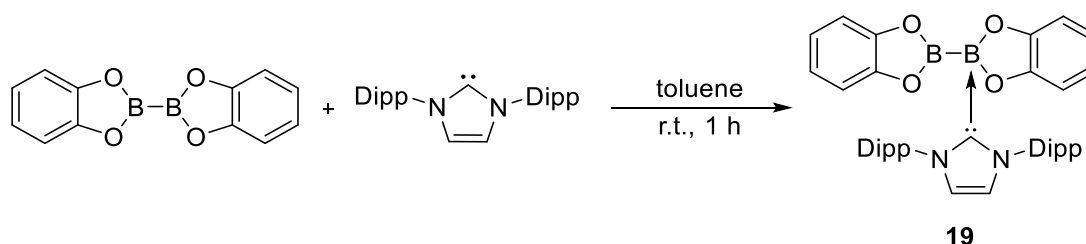


Figure 40: Molecular structure of $B_2cat_2 \cdot Me_2Im^{Me}$ **18** with thermal ellipsoids drawn at the 50% probability level; hydrogen atoms are omitted for clarity. Selected bond distances (Å) and angles (°): B2–C1 1.647(2), B1–B2 1.729(3), B1–O1 1.400(2), B1–O2 1.397(2), B2–O3 1.523(2), B2–O4 1.510(2); C1–B2–B1 110.48(12); reproduced from ref. [253] with permission from Wiley-VCH.

Based on the successful synthesis and characterization of $B_2cat_2 \cdot Me_2Im^{Me}$ **18**, the reaction of B_2cat_2 with the sterically more demanding NHC $Dipp_2Im$ was investigated. The stoichiometric reaction was carried out at room temperature, and after work-up, the mono-NHC diboron adduct $B_2cat_2 \cdot Dipp_2Im$ **19** was isolated in good yields (75%) (Scheme 87).



Scheme 87: Synthesis of the mono-NHC diboron adduct $B_2cat_2 \cdot Dipp_2Im$ **19**.

$B_2cat_2 \cdot Dipp_2Im$ **19** was characterized *via* 1H , $^{11}B\{^1H\}$ and $^{13}C\{^1H\}$ NMR spectroscopy and elemental analysis. The 1H NMR spectrum is similar to that recorded for the compound **18** (Figure 41). The signals for the catechol-groups are split into four multiplets (6.41–6.46, 6.48–6.53, 6.70–6.74 and 6.80–6.84 ppm). The *i*Pr-groups of the coordinating NHC $Dipp_2Im$ are detected as doublets at 0.99 and 1.41 ppm and the corresponding methine protons as septets

at 2.88 ppm. Additionally, the protons of the backbone of the NHC are observed at 6.38 ppm and the aryl protons as two multiplets at 6.93-6.94 and 6.97-7.02 ppm.

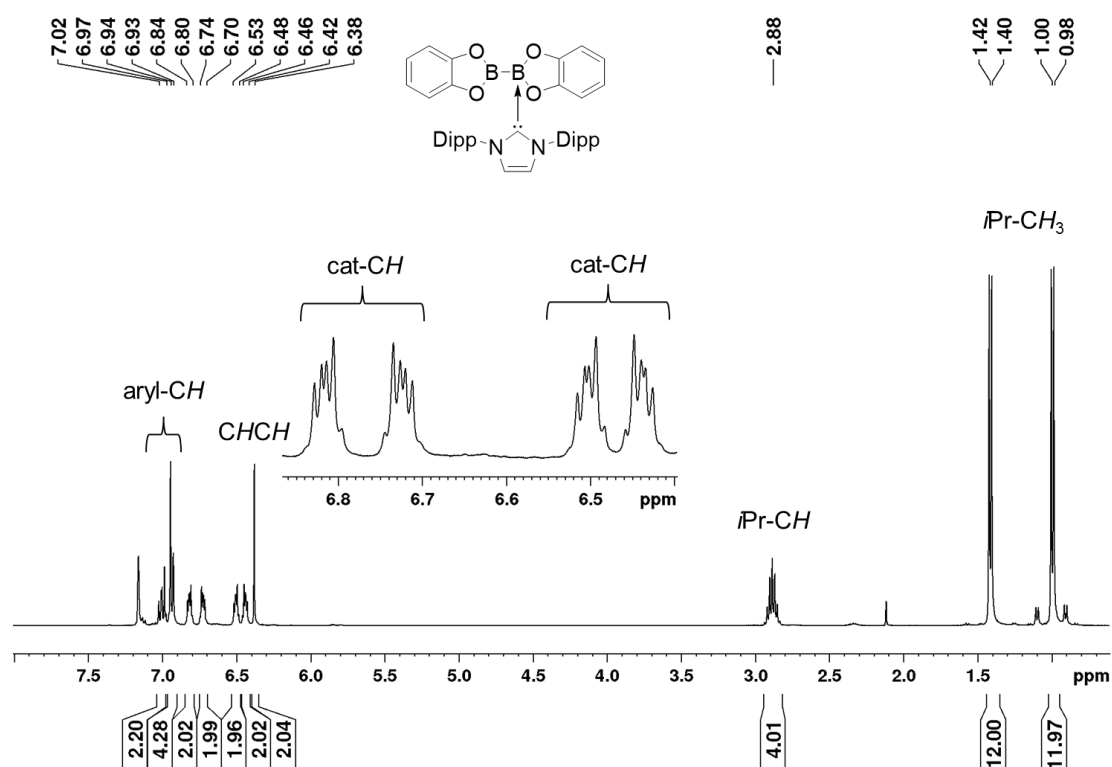


Figure 41: ¹H NMR spectrum of the mono-NHC diboron adduct B₂cat₂•Dipp₂Im **19** (400 MHz).

These observations are in good agreement with the obtained ¹¹B{¹H} NMR spectrum which shows two signals (Figure 42). One for the sp³-B atom at 6.78 ppm and the sp²-hybridized boron atom at 37.9 ppm. In the ¹³C{¹H} NMR spectrum, all signals are detected in the expected region; however, for the carbon atoms of the catechol-group are four signals observed. In comparison to the carbene carbon atom of the NHC Dipp₂Im, which is detected at 211.9 ppm, the carbene carbon atom of the coordinated NHC appears at 165.4 ppm.

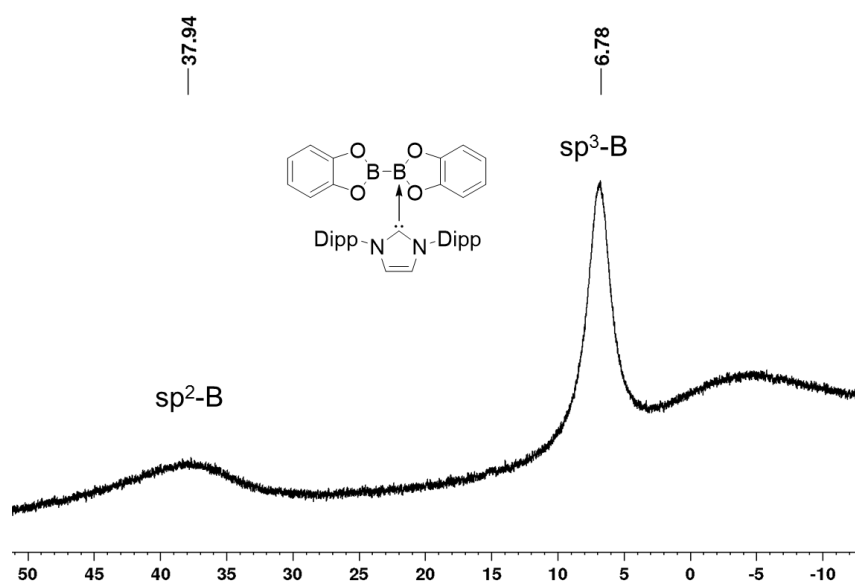
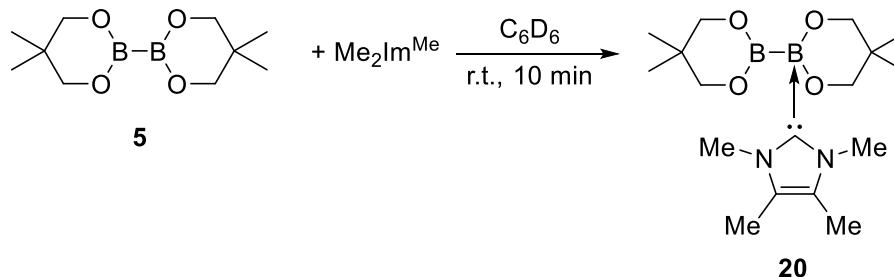


Figure 42: $^{11}\text{B}\{^1\text{H}\}$ NMR spectrum of the mono-NHC diboron adduct $\text{B}_2\text{cat}_2\cdot\text{Dipp}_2\text{Im}$ **19**.

2.2.1.2. Synthesis of mono-NHC adducts of the type $\text{B}_2\text{neop}_2\cdot\text{NHC}$

Based on the successful isolation and characterization of the mono-NHC diboron adducts $\text{B}_2\text{cat}_2\cdot\text{Me}_2\text{Im}^{\text{Me}}$ **18** and $\text{B}_2\text{cat}_2\cdot\text{Dipp}_2\text{Im}$ **19**, similar reactions using B_2neop_2 **5** as the diboron reagent were investigated. The reaction of B_2neop_2 **5** with the NHC $\text{Me}_2\text{Im}^{\text{Me}}$ was carried out under the same reactions conditions; however, the recorded NMR spectra of the isolated solid gave no evidence for the expected diboron adduct $\text{B}_2\text{neop}_2\cdot\text{Me}_2\text{Im}^{\text{Me}}$ **20**.

Therefore, the reaction of B_2neop_2 and $\text{Me}_2\text{Im}^{\text{Me}}$ was repeated on an NMR scale and was immediately monitored *via* ^1H and $^{11}\text{B}\{^1\text{H}\}$ NMR spectroscopy to observe any adduct formation between these two compounds (Scheme 88).



Scheme 88: Synthesis of the neutral $\text{sp}^2\text{-sp}^3$ diboron adduct $\text{B}_2\text{neop}_2\cdot\text{Me}_2\text{Im}^{\text{Me}}$ **20**.

In the *in situ* $^{11}\text{B}\{^1\text{H}\}$ NMR spectrum, two signals are observed; one broad signal belongs to the sp^2 -boron atom (29.3 ppm) and the other signal at 1.32 ppm to the sp^3 -boron atom (Figure 43).

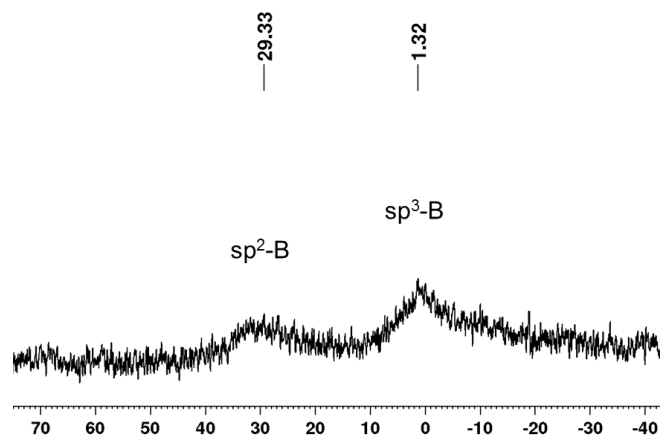


Figure 43: *In situ* $^{11}\text{B}\{^1\text{H}\}$ NMR spectrum of $\text{B}_2\text{neop}_2\cdot\text{Me}_2\text{Im}^{\text{Me}}$ **20**.

The *in situ* ^1H NMR spectrum also showed evidence for the desired $\text{sp}^2\text{-sp}^3$ diboron adduct $\text{B}_2\text{neop}_2\cdot\text{Me}_2\text{Im}^{\text{Me}}$ **20** (Figure 44). The signals for the two methyl-groups of the $\text{Me}_2\text{Im}^{\text{Me}}$ are detected at 1.20 and 3.77 ppm as singlets. The methyl-group of the neop-moieties are observed as a broad signal at 0.91 ppm, and the methylene-group is detected at 3.60 ppm also significantly broadened. However, the NMR spectrum recorded after several hours indicates no adduct formation, which signifies that $\text{B}_2\text{neop}_2\cdot\text{Me}_2\text{Im}^{\text{Me}}$ **20** is not stable over a longer time, and thus several attempts to isolate adduct **20** failed.

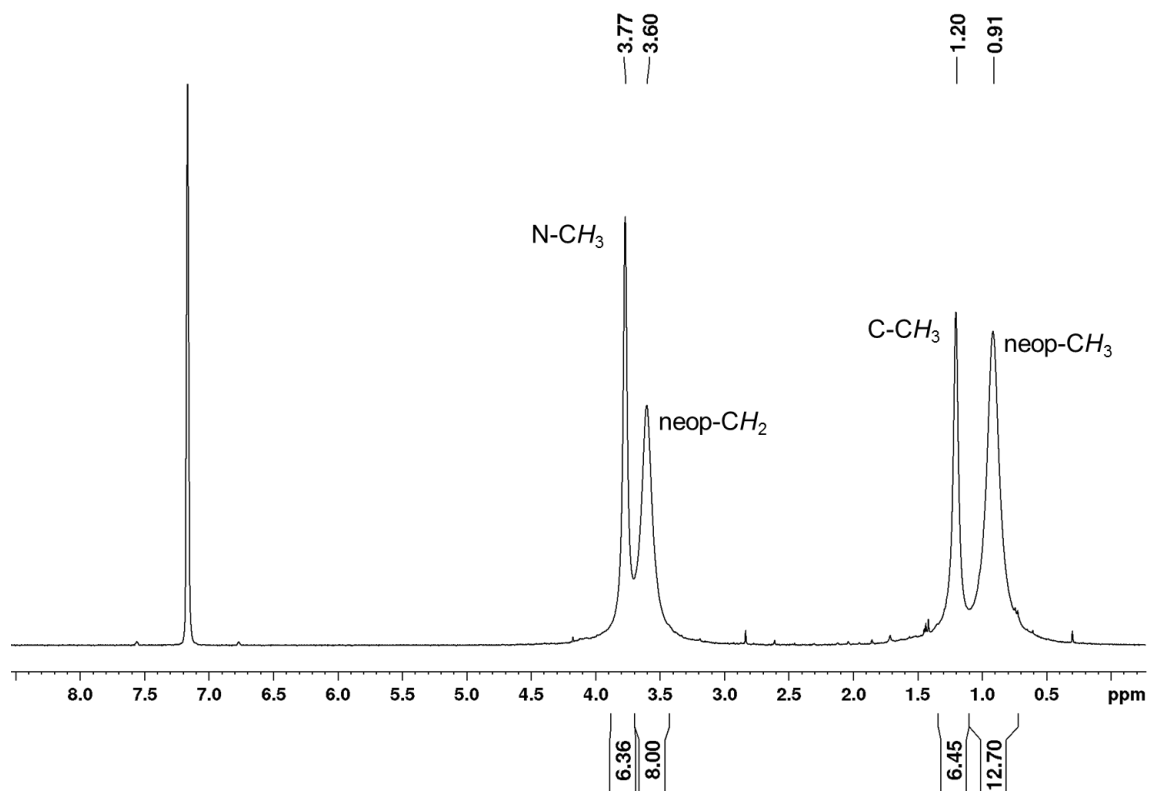


Figure 44: *In situ* ^1H NMR spectrum of $\text{B}_2\text{neop}_2\cdot\text{Me}_2\text{Im}^{\text{Me}}$ **20** in C_6D_6 (500 MHz).

Due to the fact, that the *in situ* ^1H NMR spectrum recorded at room temperature of the reaction of B_2neop_2 **5** and $\text{Me}_2\text{Im}^{\text{Me}}$ showed broad signals for the diboron adduct $\text{B}_2\text{neop}_2\cdot\text{Me}_2\text{Im}^{\text{Me}}$ **20** and neop-moieties of the diboron reagent are not split into a 2:2:4 ratio for the methylene-groups and 3:3:6 for the methyl-groups, the NMR spectrum of a stoichiometric mixture of B_2neop_2 **5** and $\text{Me}_2\text{Im}^{\text{Me}}$ was measured at lower temperatures ($-40\text{ }^\circ\text{C}$). Figure 45 shows the ^1H NMR spectrum, which shows one set of signals of the Me_2Im at 1.94 ppm for the methyl-groups at the backbone of the NHC, and the methyl-groups at the nitrogen atom are observed at 3.69 ppm. Furthermore, the signals for the neop $_\alpha$ -moiety are detected as doublets at 3.74 and 4.06 ppm (neop $_\alpha$ - CH_2) and the methyl-groups are observed as singlets at 1.25 and 1.27 ppm. The signals of the neop $_\beta$ -moiety bound to the sp^2 -hybridized boron atom are detected at 0.67 ppm for the methyl-groups and at 3.41 ppm for the methylene-group. In addition, further signals for unreacted starting material B_2neop_2 are detected at 0.51 and 3.19 ppm. Nevertheless, the recorded NMR spectra at room as well as at low temperature show evidence for the formation of the neutral diboron adduct $\text{B}_2\text{neop}_2\cdot\text{Me}_2\text{Im}^{\text{Me}}$ **20**.

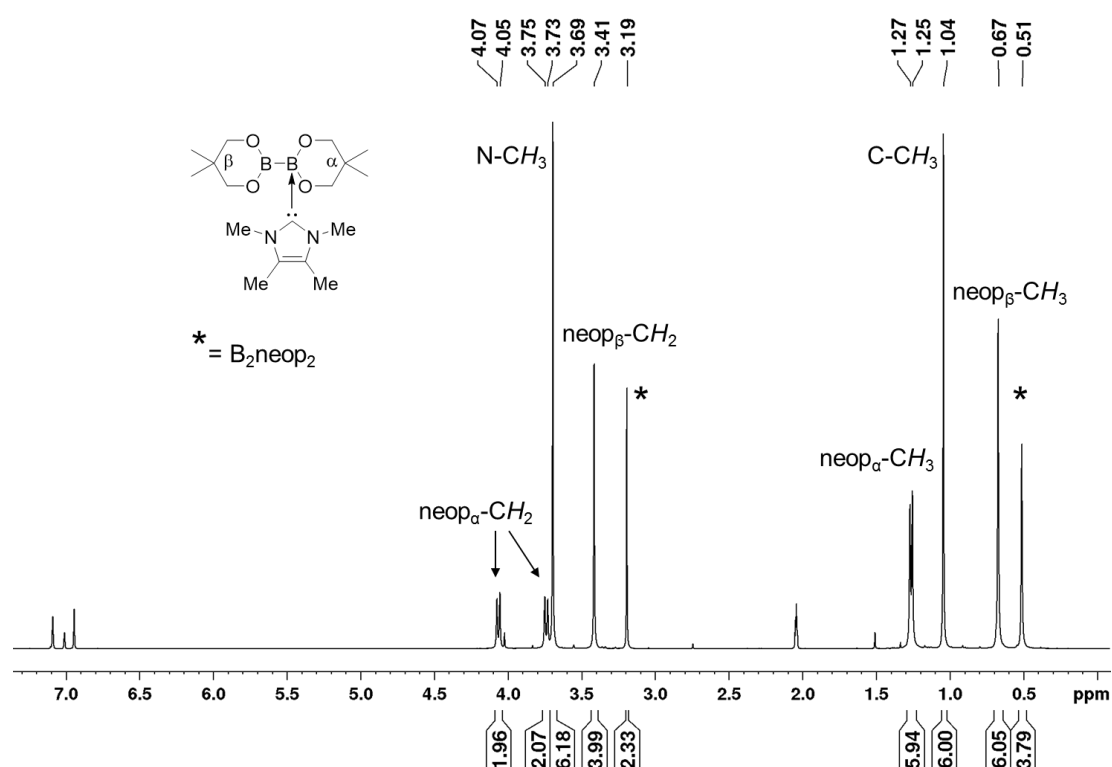
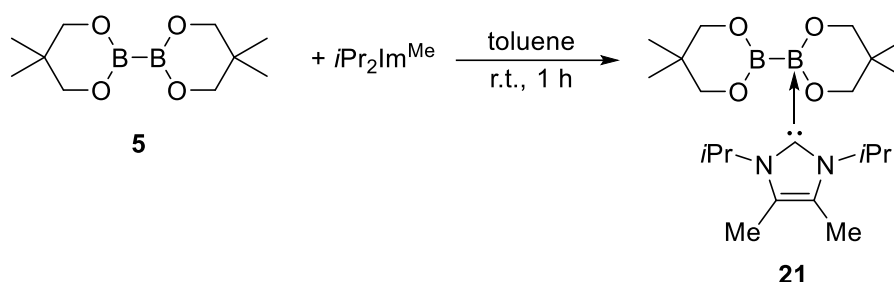


Figure 45: *In situ* ^1H NMR spectrum at $-40\text{ }^\circ\text{C}$ of the reaction of B_2neop_2 with $\text{Me}_2\text{Im}^{\text{Me}}$ in toluene- d_8 to characterize the adduct $\text{B}_2\text{neop}_2\cdot\text{Me}_2\text{Im}^{\text{Me}}$ **20** (500 MHz).

Based on the successful observation of the mono-NHC adduct $\text{B}_2\text{neop}_2\cdot\text{Me}_2\text{Im}^{\text{Me}}$ **20**, the reaction of B_2neop_2 and $i\text{Pr}_2\text{Im}^{\text{Me}}$ was carried out under the same reaction conditions to prove that the size of the NHC plays a role in the adduct formation. Therefore, the diboron reagent **5** and $i\text{Pr}_2\text{Im}^{\text{Me}}$ were dissolved in toluene and the reaction was worked-up after one hour

(Scheme 89). The obtained solid was characterized *via* NMR-spectroscopy and X-ray diffraction.



Scheme 89: Synthesis of the neutral $\text{sp}^2\text{-sp}^3$ diboron adduct $\text{B}_2\text{neop}_2\cdot i\text{Pr}_2\text{Im}^{\text{Me}}$ **21**.

The ^1H NMR spectrum of $\text{B}_2\text{neop}_2\cdot i\text{Pr}_2\text{Im}^{\text{Me}}$ **21** shows one set of signals for the $i\text{Pr}_2\text{Im}^{\text{Me}}$, the methyl-groups of the $i\text{Pr}$ -moiety are detected at 1.35 ppm as a doublet, the methyl-groups at the backbone at 1.69 ppm as a singlet (Figure 46). The methine protons are observed at 6.10 ppm and are significantly broadened. Furthermore, the methyl-groups of the neop-moieties are detected at 0.84 ppm and the methylene-groups at 3.53 ppm. The $^{11}\text{B}\{^1\text{H}\}$ NMR spectrum shows only one averaged signal at 21.6 ppm. The carbene carbon atom is observed at 191.0 ppm in the $^{13}\text{C}\{^1\text{H}\}$ NMR spectrum.

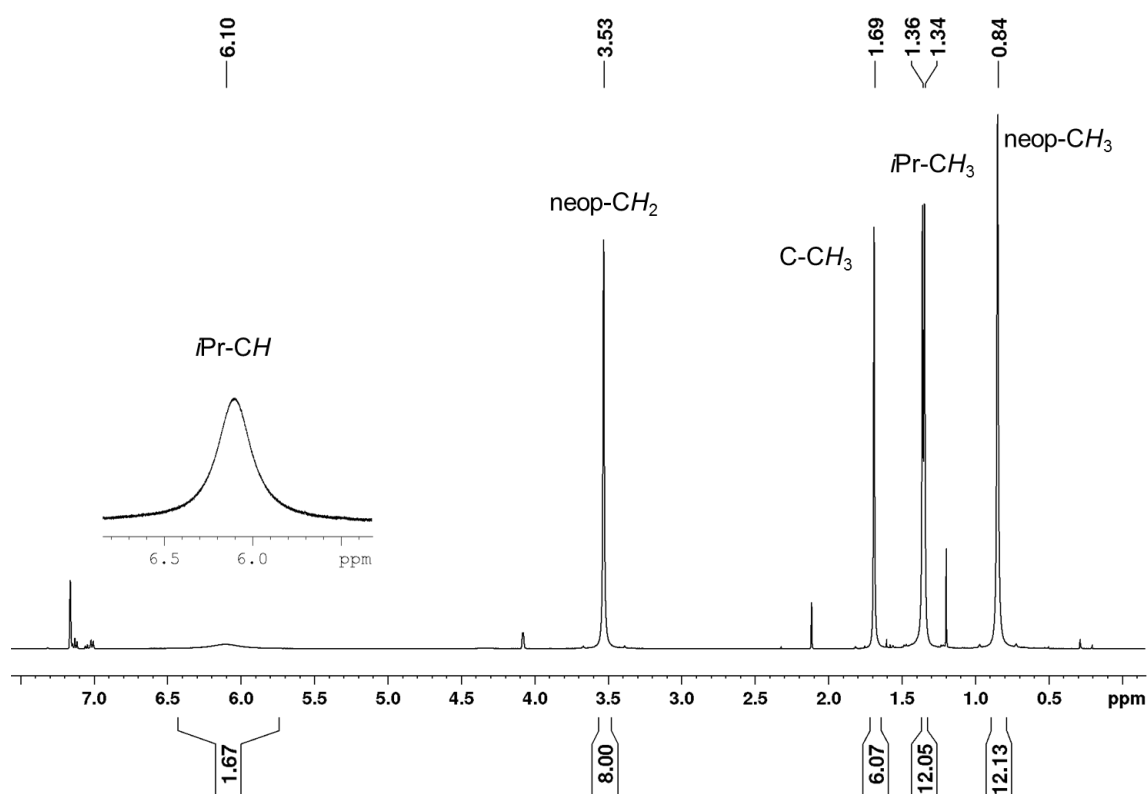


Figure 46: ^1H NMR spectrum of $\text{B}_2\text{neop}_2\cdot i\text{Pr}_2\text{Im}^{\text{Me}}$ **21** in C_6D_6 (500 MHz).

The molecular structure of $\text{B}_2\text{neop}_2\cdot i\text{Pr}_2\text{Im}^{\text{Me}}$ **21** is similar to the reported structure of the diboron adduct $\text{B}_2\text{pin}_2\cdot \text{Cy}_2\text{Im}$.^[51] The boron atom B1 is essentially planar, while B2 is

tetrahedral (Figure 47). The B–B distance (B1–B2 1.719(2) Å) is slightly shorter than the one found in the molecular $B_2pin_2 \cdot Cy_2Im$ (B1–B2 1.743(2) Å).^[51] The B–O distances are essentially comparable to those discussed earlier for the alkoxy and the fluoride adducts^[74] as well as for the reported adduct $B_2cat_2 \cdot Me_2Im^{Me}$.^[256] The B2–C1 distance of 1.647(2) Å is also comparable to the distance found in $B_2pin_2 \cdot Cy_2Im$ (B2–C1 1.673(2) Å) and $B_2cat_2 \cdot Me_2Im^{Me}$ **18** (B2–C1 1.647(2) Å).

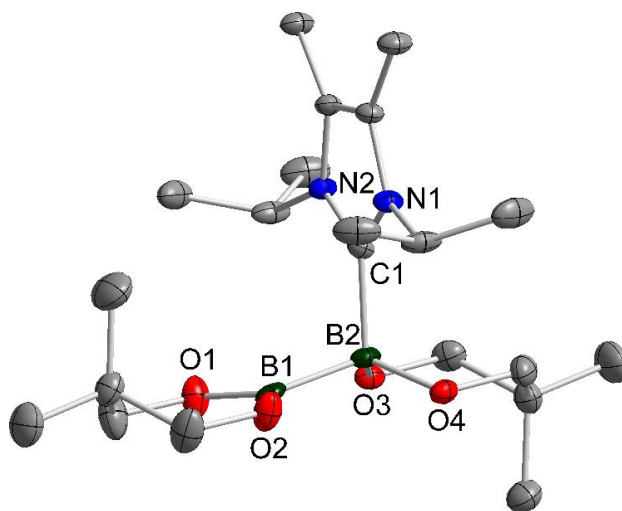
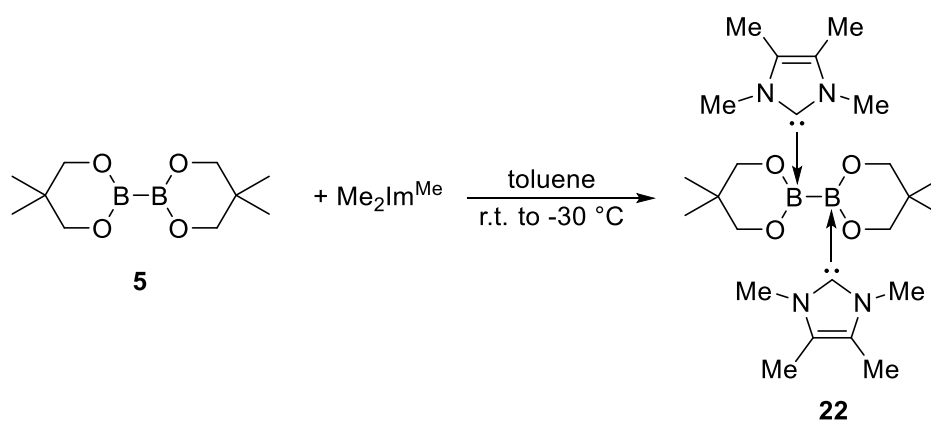


Figure 47: Molecular structure of $B_2neop_2 \cdot Pr_2Im^{Me}$ **21** with thermal ellipsoids drawn at the 50% probability level; hydrogen atoms are omitted for clarity. Selected bond distances (Å) and angles (°): B2–C1 1.709(2), B1–B2 1.719(2), B1–O1 1.371(2), B1–O2 1.371(2), B2–O3 1.482(2), B2–O4 1.482(2); C1–B2–B1 103.26(4), C1–B2–O3 109.18(8), C1–B2–O4 109.18(8).

2.2.1.3. Synthesis of the bis-NHC adducts of the type $B_2(OR)_2 \cdot (NHC)_2$

Based on our observations during the synthesis and characterization of neutral mono-NHC adducts of the type $B_2(OR)_4 \cdot NHC$ **18-21** that the adduct $B_2neop_2 \cdot Me_2Im^{Me}$ **20** is not stable, several attempts were made to crystallize the mono-NHC adduct $B_2neop_2 \cdot iPr_2Im^{Me}$ **21** from the reaction mixture. Therefore, a stoichiometric mixture of B_2neop_2 and Me_2Im^{Me} in toluene was cooled to -30 °C and single crystals were obtained, which were identified as the bis-NHC diboron adduct $B_2neop_2 \cdot (Me_2Im^{Me})_2$ **22** (Scheme 90).



Scheme 90: Reaction of B_2neop_2 **5** with Me_2Im^{Me} , which leads to the formation of the bis-NHC diboron adduct $B_2neop_2 \cdot (Me_2Im^{Me})_2$ **22**.

The molecular structure of $B_2neop_2 \cdot (Me_2Im^{Me})_2$ **22** is far different from the reported mono-NHC adducts **18** and **21** in that both boron atoms are sp^3 -hybridized and tetrahedral (Figure 48).^[256] The obtained B1–C1 distance of 1.662(2) Å is similar to those found in the mono-NHC diboron adducts (**18**: 1.647(2) Å and **21**: 1.709(2) Å) and the B1–B1' bond (1.770(2) Å) is also similar to the reported neutral diboron adducts (**18**: 1.729(3) Å and **21**: 1.719(2) Å).^[74, 256]

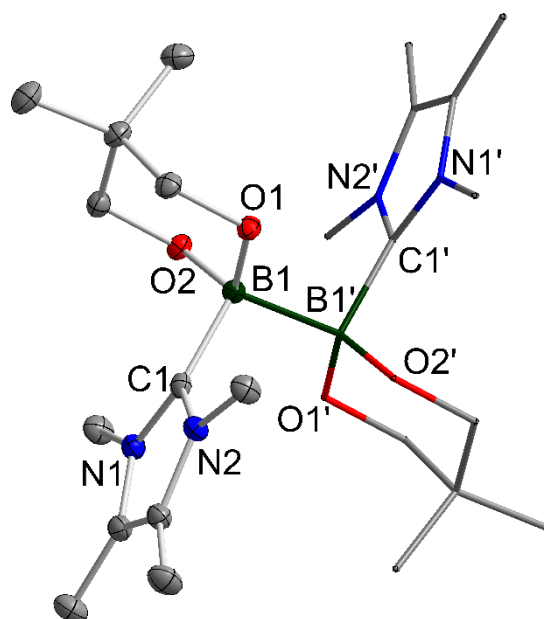
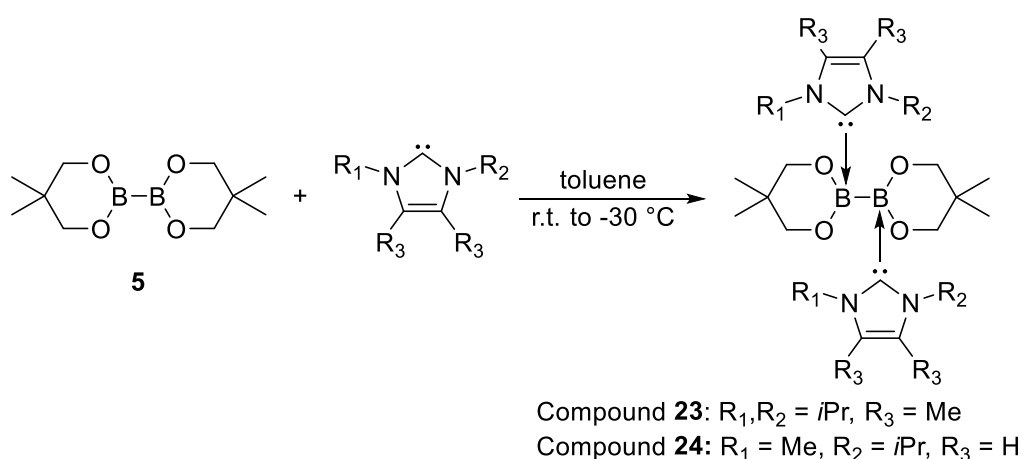


Figure 48: Molecular structure of $B_2neop_2 \cdot (Me_2Im^{Me})_2$ **22** with thermal ellipsoids drawn at the 50% probability level; hydrogen atoms are omitted and the second NHC and Bneop-moiety are drawn as wires/sticks for clarity. Selected bond distances (Å) and angles (°): B1–C1 1.662(2), B1–B1' 1.770(2), B1–O1 1.482(1), B1–O2 1.486(1); C1–B1–B1' 103.29(7), C1–B1–O1 109.82(8), C1–B1–O2 110.13(8).

Furthermore, the NHCs iPr_2Im^{Me} and $MeiPrIm$ were reacted with B_2neop_2 **5** in stoichiometric amounts and the reaction mixture was afterwards cooled to -30 °C. In both cases, single crystals for X-ray diffraction were obtained which were shown to be the bis-NHC diboron adducts $B_2neop_2 \cdot (iPr_2Im^{Me})_2$ **23** and $B_2neop_2 \cdot (MeiPrIm)_2$ **24** (Scheme 91). Further investigations on the synthesis and isolation of these three bis-NHC adducts **22-24** failed.



Scheme 91: Reaction of B_2neop_2 **5** with NHCs iPr_2Im^{Me} and $MeiPrIm$, which led to the compounds $B_2neop_2 \cdot (iPr_2Im^{Me})_2$ **23** and $B_2neop_2 \cdot (MeiPrIm)_2$ **24**.

Molecular structures of $B_2neop_2 \cdot iPr_2Im^{Me}$ **23** and $B_2neop_2 \cdot MeiPrIm$ **24** are comparable to that of the bis-NHC adduct $B_2neop_2 \cdot (Me_2Im^{Me})_2$ **22** (Figure 49). Both boron atoms are sp^3 -hybridized and the bond distances and angles are similar to those observed for the bis-NHC adduct **22**.

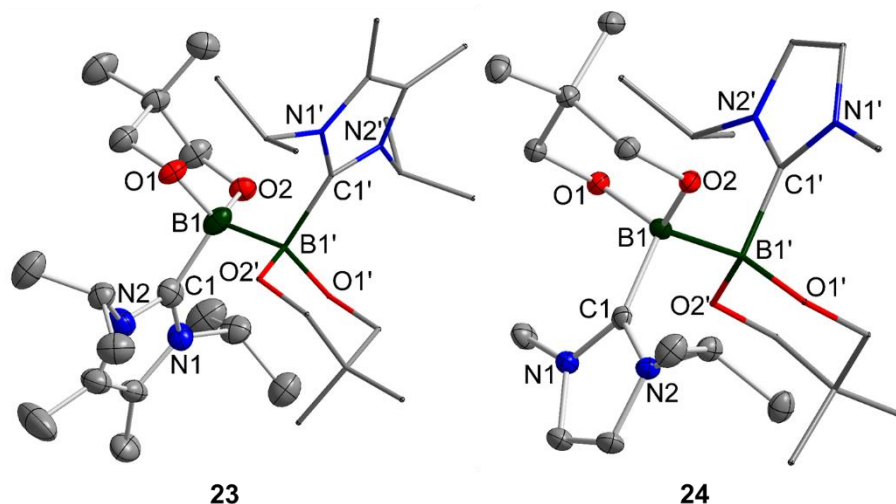


Figure 49: Left: molecular structure of $B_2neop_2 \cdot (iPr_2Im^{Me})_2$ **23** with thermal ellipsoids drawn at the 50% probability level; hydrogen atoms are omitted and the second NHC and Bneop-moiety are drawn as wires/sticks for clarity. Selected bond distances (Å) and angles (°): B1–C1 1.734(9), B1–B1' 1.727(9), B1–O1 1.494(10), B1–O2 1.450(11); C1–B1–B1' 103.81(52), C1–B1–O1 108.60(53), C1–B1–O2 109.27(51). Right: molecular structure of $B_2neop_2 \cdot (MeiPrIm)_2$ **24** with thermal ellipsoids drawn at the 50% probability level; hydrogen atoms are omitted and the second NHC and Bneop-moiety are drawn as wires/sticks for clarity. Selected bond distances (Å) and angles (°): B1–C1 1.734(9), B1–B1' 1.727(9), B1–O1 1.494(10), B1–O2 1.450(11); C1–B1–B1' 103.8(5), C1–B1–O1 108.6(5), C1–B1–O2 109.3(5).

Due to the fact that the NMR spectra of the isolated crystals of $B_2neop_2 \cdot (iPr_2Im^{Me})_2$ **23** show only evidence for the mono-NHC adduct $B_2neop_2 \cdot iPr_2Im^{Me}$ **21**, the NMR scale reaction of B_2neop_2 with iPr_2Im^{Me} was investigated in different stoichiometric ratios: 1:1, 1:2 and 1:3. All recorded *in situ* ¹H NMR spectra (Figure 50) showed only evidence for the mono-NHC adduct **21**; however, the chemical shift of the methine proton of the *i*Pr-group is at lower field in the 1:1 reaction. Furthermore, to confirm the existence of any adduct formation, the obtained NMR data were compared with those of “free” iPr_2Im^{Me} . A different shift of the methine proton was observed, and in comparison with the “free” NHC, the signal is very broad.

The bis-NHC adducts of the type $B_2neop_2 \cdot (NHC)_2$ are preferred in the solid state; however, in solution the dissociative exchange of the NHC between the two boron atoms is so fast that only the mono-NHC adduct could be observed.

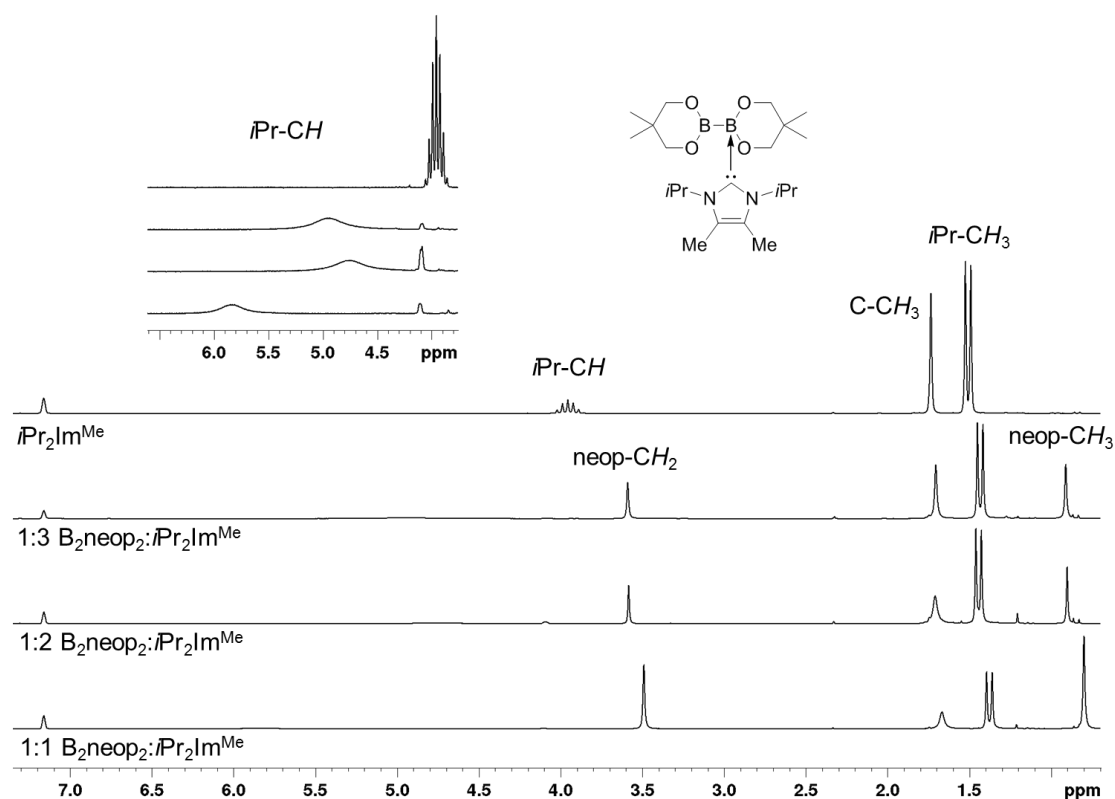


Figure 50: Reaction of B_2neop_2 **5** with different equivalents of iPr_2Im^{Me} (ratio 1:1, 1:2 and 1:3) at room temperature in C_6D_6 .

Additionally, B_2neop_2 and iPr_2Im^{Me} were reacted in the ratio 1:2 and cooled the reaction mixture to $-30\text{ }^\circ\text{C}$ to obtain crystals of the bis-NHC adduct $B_2neop_2 \cdot iPr_2Im^{Me}$ **23** and to characterize them by solid state NMR spectroscopy. Figure 51 displays the ^{13}C and ^{11}B solid state NMR of the isolated crystals. The solid state ^{11}B NMR spectrum shows three signals, two for the mono-NHC adduct **21**, one at 0 ppm for the sp^3 boron atom and one broad signal at circa 33 ppm for the sp^2 boron atom of the mono-NHC adduct $B_2neop_2 \cdot iPr_2Im^{Me}$. The third sharp signal at approximately 3 ppm belongs to the sp^3 boron atom of the bis-NHC adduct $B_2neop_2 \cdot (iPr_2Im^{Me})_2$ **23**. In addition, similar results were obtained in the solid state ^{13}C NMR spectrum, which shows two signals at 165 and 172 ppm in a 1:1.5 ratio for the two types of carbene carbon atoms (mono and bis-NHC diboron adduct). These observations confirmed the evidence for the bis-NHC adduct **23** as well as the existence of the mono-NHC adduct **21**; however, several attempts to isolate the bis-NHC adduct $B_2neop_2 \cdot (iPr_2Im^{Me})_2$ **23** failed.

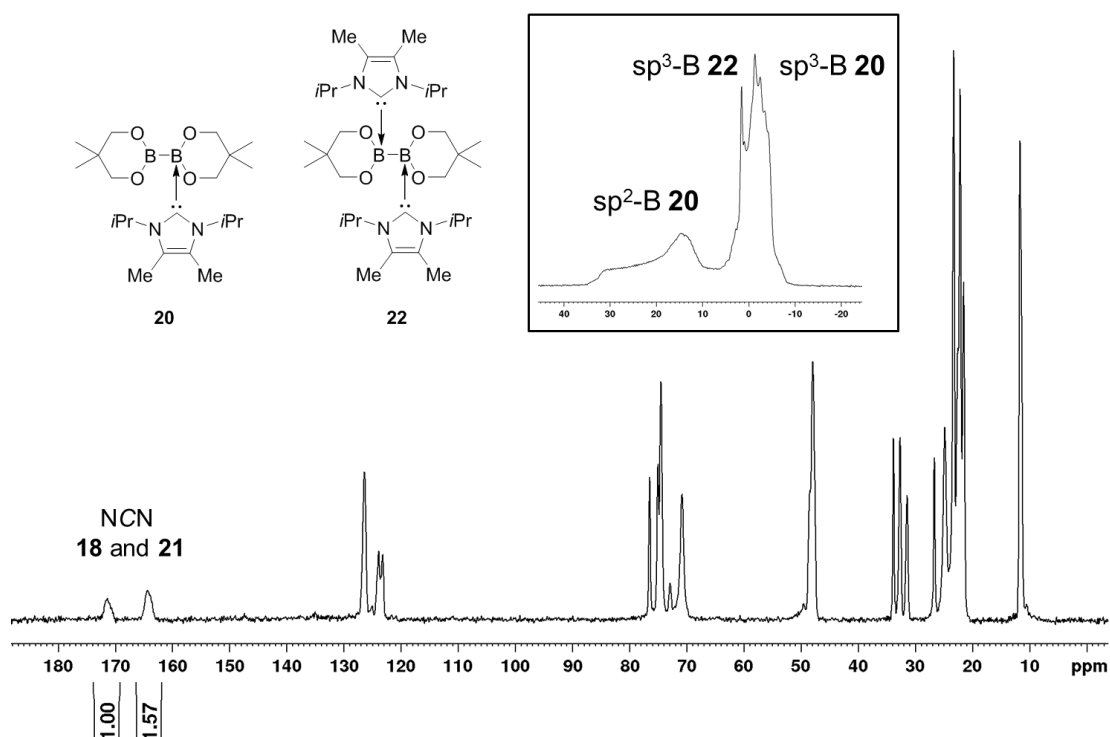
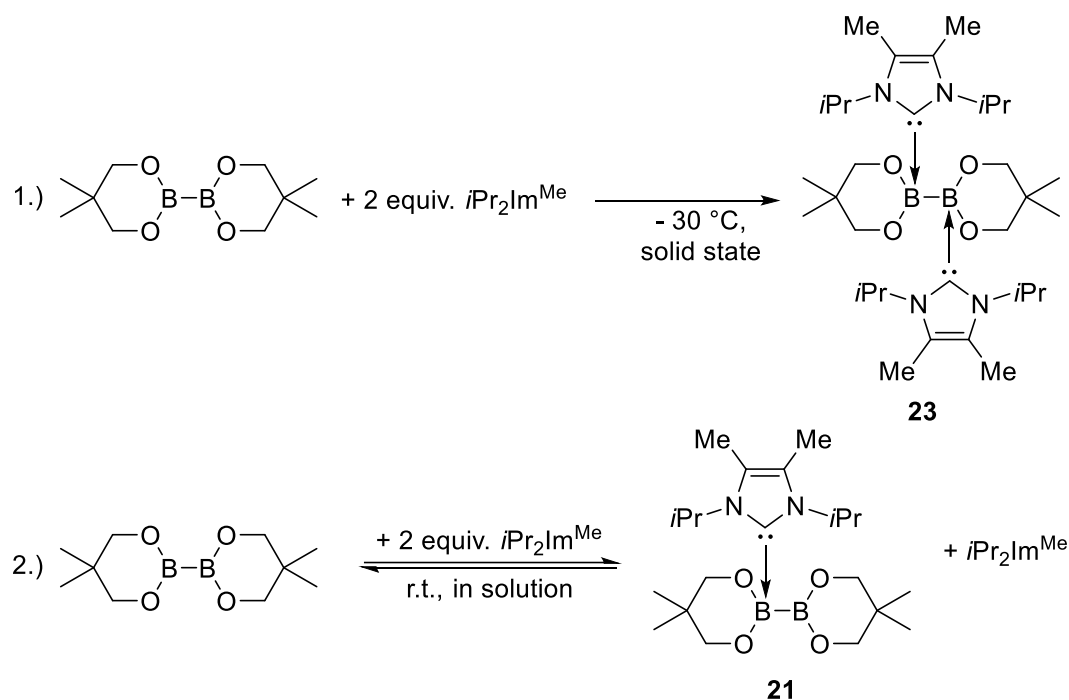


Figure 51: Solid state ^{13}C and ^{11}B NMR spectrum of the isolated crystals of the reaction of B_2neop_2 **5** and $i\text{Pr}_2\text{Im}^{\text{Me}}$ in a 1:1.5 ratio.

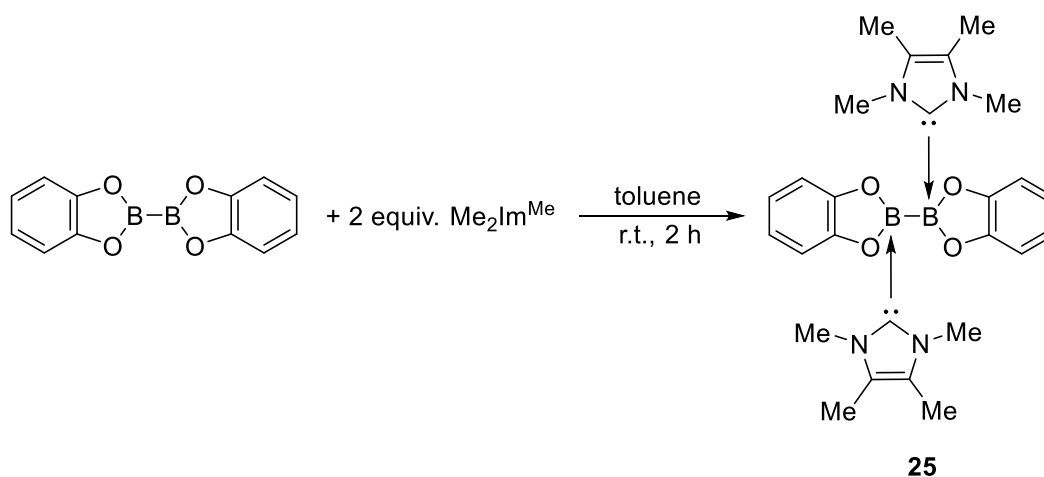
In summary, the synthesis and characterization of the mono-NHC diboron adducts of the type $\text{B}_2\text{neop}_2\cdot\text{NHC}$ was only possible using the sterically more demanding NHC $i\text{Pr}_2\text{Im}^{\text{Me}}$ which led to the formation of compound **21**. In the case of the smaller NHC $\text{Me}_2\text{Im}^{\text{Me}}$, the corresponding mono-NHC diboron adduct **20** could only be observed by *in situ* NMR spectroscopy at room and lower temperature. The reaction of B_2neop_2 with $i\text{Pr}_2\text{Im}$ in a 1:2 ratio yielded the corresponding bis-NHC diboron adduct $\text{B}_2\text{neop}_2\cdot(i\text{Pr}_2\text{Im}^{\text{Me}})_2$ **23**; however, compound **23** was only characterized by X-ray diffraction. The formation of the bis-NHC diboron adducts is favorable at lower temperature due to the gain of energy and as a result, higher symmetry of compound **23** (Scheme 92). Contrary observations were obtained in solution at room temperature. The bis-NHC diboron adduct dissociates to the mono-NHC diboron adduct $\text{B}_2\text{neop}_2\cdot i\text{Pr}_2\text{Im}^{\text{Me}}$ **21** and “free” $i\text{Pr}_2\text{Im}^{\text{Me}}$; however, in the ^1H NMR spectrum, no signals for the “free” NHC are detected (Figure 50).



Scheme 92: Reaction of B_2neop_2 with $i\text{Pr}_2\text{Im}$ in a 1:1 and 1.2 ratio. At lower temperature, the bis-NHC adduct $\text{B}_2\text{neop}_2 \cdot (i\text{Pr}_2\text{Im}^{\text{Me}})_2$ **23** was observed; however, in solution only the mono-NHC diboron adduct $\text{B}_2\text{neop}_2 \cdot i\text{Pr}_2\text{Im}^{\text{Me}}$ **21** is detectable.

2.2.1.4. Synthesis of the bis-NHC adducts $\text{B}_2\text{cat}_2 \cdot (\text{Me}_2\text{Im}^{\text{Me}})_2$

Based on the reported molecular structure of the type $\text{B}_2\text{neop}_2 \cdot (\text{NHC})_2$ **22-24**, the synthesis of further bis-NHC diboron adducts was investigated, using B_2cat_2 **8** as the diboron reagent and $\text{Me}_2\text{Im}^{\text{Me}}$ as the NHC. The reaction was carried out under the same reaction conditions applied for the synthesis of the mono-NHC adduct $\text{B}_2\text{cat}_2 \cdot \text{Me}_2\text{Im}^{\text{Me}}$ **18** and $\text{B}_2\text{cat}_2 \cdot \text{Dipp}_2\text{Im}$ **19** (Scheme 93). However, in contrast to compound **18** and **19**, which was a colorless reaction mixture, a bright yellow precipitate was formed, which was collected by filtration and washed with cold toluene.



Scheme 93: Synthesis of the bis-NHC diboron adduct $B_2cat_2 \cdot (Me_2Im^{Me})_2$ **25**.

Due to the fact that the obtained solid is insoluble in common deuterated solvents, the isolated solid was characterized *via* solid state NMR spectroscopy and was identified as the bis-NHC adduct $B_2cat_2 \cdot (Me_2Im^{Me})_2$ **25**. The solid state ^{11}B NMR spectrum shows one signal for both sp^3 -boron atoms at 2.72 ppm (Figure 52).^[256]

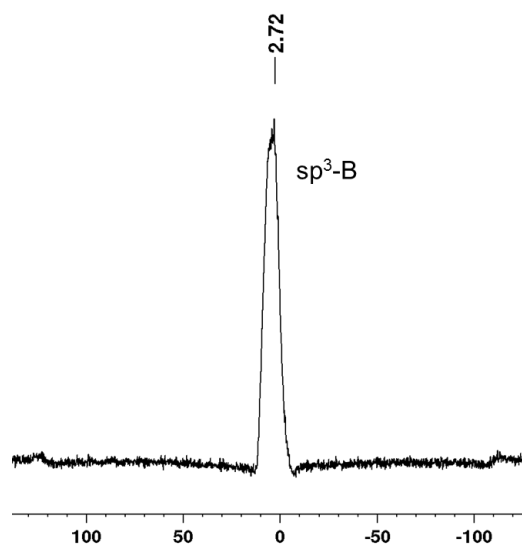


Figure 52: Solid state ^{11}B NMR spectrum of $B_2cat_2 \cdot (Me_2Im^{Me})_2$ **25**.

The solid state ^{13}C NMR spectrum also gives evidence for the formation of the bis-NHC adduct **25**. For each methyl-group of the NHC, at the backbone as well as at the nitrogen atoms, one signal is observed (4.91, 9.49, 33.1 and 34.9 ppm). The quaternary carbon atoms are detected at 123.8 and 124.2 ppm and the carbene carbon atoms at 166.4 ppm as a broad signal. The signal for the carbon atoms of the catechol-moiety are observed at 109.3, 110.5, 117.3 and 118.5 ppm. The quaternary carbon atoms of the catechol-groups are detected at 155.7 and 166.4 ppm (Figure 53). Furthermore, the solid state ^{15}N NMR spectrum of $B_2cat_2 \cdot (Me_2Im^{Me})_2$

25 shows two signals for the nitrogen atoms of the NHCs (-204.1 and -205.9 ppm), which also confirms the formation and the symmetry of the bis-NHC diboron adduct **25**.^[256]

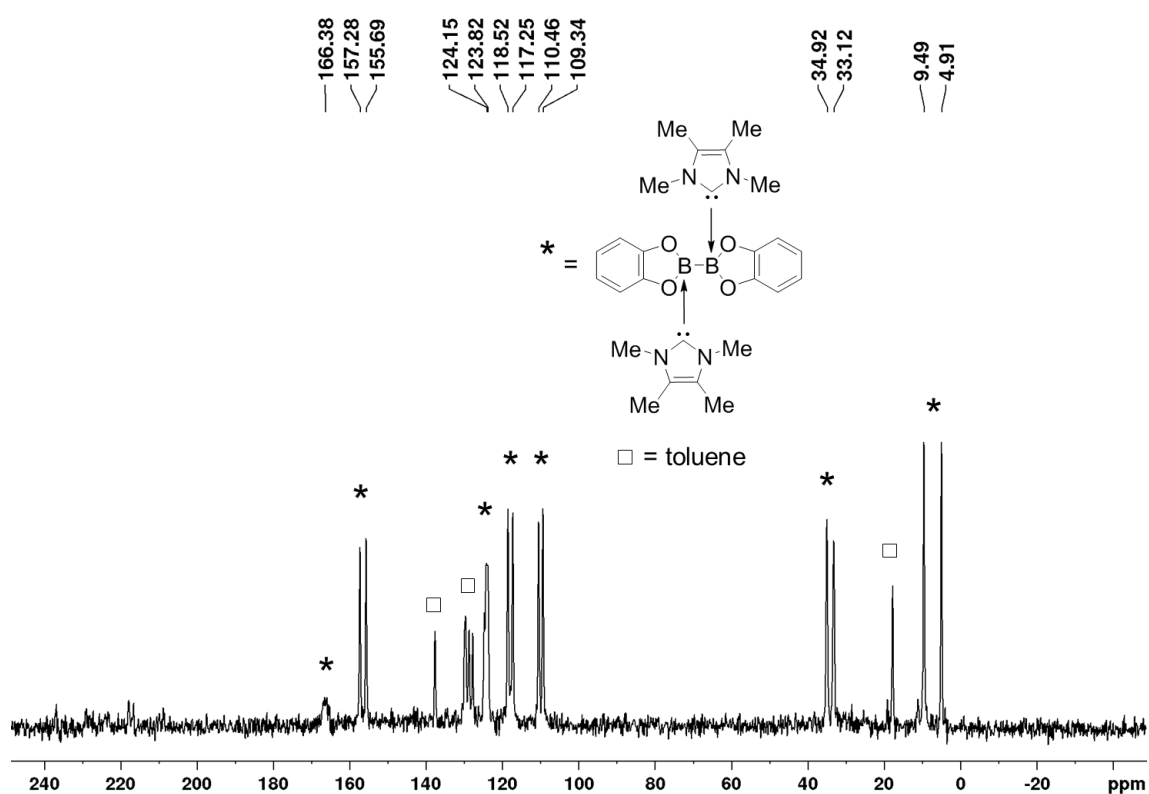


Figure 53: Solid state ¹³C NMR spectrum of B₂cat₂•(Me₂Im^{Me})₂ **25**.

In addition, single crystals of B₂cat₂•(Me₂Im^{Me})₂ **25** were obtained for X-ray diffraction, to confirm the results. Both boron atoms are sp³-hybridized and the B1–B1' distance (1.710(8) Å) is similar to the obtained data of the bis-NHC B₂neop₂ adducts **22–24** as well as the mono-NHC adduct B₂cat₂•Me₂Im^{Me} **18** (1.729(3) Å) (Figure 54).^[256] The B1–C1 bonds (1.658(9) Å) are slightly longer than observed in compound **18** (1.647(2) Å). Furthermore, the obtained data for the B1–O1 and B1–O2 distances (B1–O1 1.535(5) Å, B1–O2 1.537(5) Å) are similar to the bond lengths and angles in the mono-NHC adduct **18**.^[256]

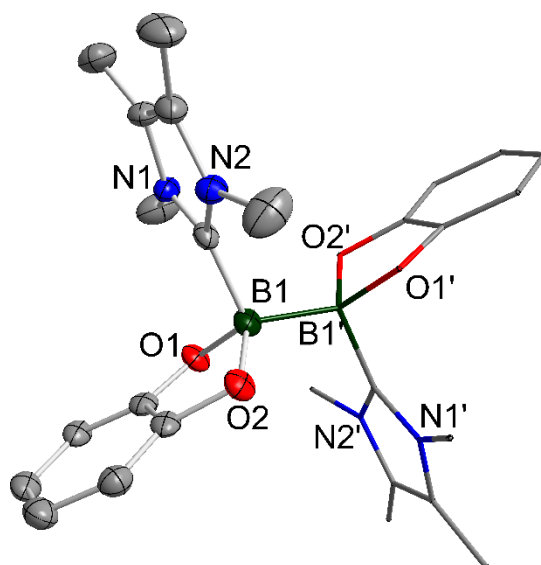


Figure 54: Molecular structure of $B_2cat_2 \cdot (Me_2Im^{Me})_2$ **25** with thermal ellipsoids drawn at the 50% probability level; hydrogen atoms are omitted and the second NHC and Bcat-moiety are drawn as wires/sticks for clarity. Selected bond distances (Å) and angles (°): B1–C1 1.662(2), B1–B1' 1.770(2), B1–O1 1.482(1), B1–O2 1.486(1); C1–B1–B1' 103.29(7), C1–B1–O1 109.82(8), C1–B1–O2 110.13(8).

In summary, the synthesis of the diboron compounds B_2cat_2 and B_2neop_2 with different NHCs in a 1:1 and 1:2 ratio led to the formation of the expected mono-NHC diboron adducts. In the case of B_2cat_2 , the mono-NHC adducts $B_2cat_2 \cdot Me_2Im^{Me}$ **18** and $B_2cat_2 \cdot Dipp_2Im$ **19** as well as the bis-NHC adduct $B_2cat_2 \cdot (Me_2Im^{Me})_2$ **25** were isolated and characterized. The obtained adducts are different in so far that the mono-NHC adducts **18** and **19** are very good soluble in benzene/toluene as well as dichloromethane (compound **18**); however, the bis-NHC adduct **25** is un-soluble in common solvents and decomposes in CH_2Cl_2 .

Using B_2neop_2 as the diboron reagent, formed the mono-NHC adduct $B_2neop_2 \cdot iPr_2Im^{Me}$ **21** which was fully characterized by NMR spectroscopy and X-ray diffraction. The NMR scale reaction of B_2neop_2 with the sterically less demanding NHC Me_2Im^{Me} yielded the *in situ* formed $B_2neop_2 \cdot Me_2Im^{Me}$ **21**; however, the mono-NHC adduct **21** is not stable and rearranges to the corresponding bis-NHC adduct $B_2neop_2 \cdot (Me_2Im^{Me})_2$ **22** which was characterized by X-ray diffraction. Related results were obtained in the reaction of B_2neop_2 with iPr_2Im^{Me} and $MeiPrIm$ in a 1:2 ratio. In both cases, the molecular structure was only confirmed by X-ray diffraction and by solid state NMR spectroscopy ($B_2neop_2 \cdot (iPr_2Im^{Me})_2$ **23**). Additionally, the recorded NMR spectra did not show any evidence for the bis-NHC adducts; however, the reaction of B_2neop_2 with iPr_2Im^{Me} in a 1:1, 1:2 and 1:3 ratio formed only the mono-NHC adduct $B_2neop_2 \cdot iPr_2Im^{Me}$ **21**. As a result, the obtained data indicate that the bis-NHC adducts of the type $B_2neop_2 \cdot (NHC)_2$ are preferred in the solid state; however, in solution, the mono-NHC adducts of B_2cat_2 and B_2neop_2 are favorable. In addition, using B_2pin_2 as the diboron reagent, instead of B_2cat_2 and B_2neop_2 , only forms mono-NHC adducts with different NHCs, namely $B_2pin_2 \cdot Me_2Im^{Me}$, $B_2pin_2 \cdot iPr_2Im$ and $B_2neop_2 \cdot iPr_2Im^{Me}$. Similar reactions in a 1:2 ratio did not lead to any further formation to bis-NHC adducts or ring expanded products.

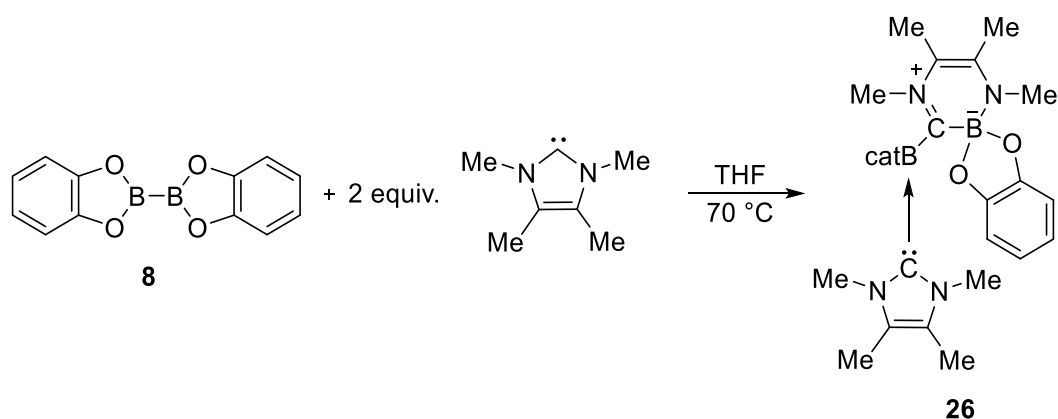
2.2.2. Ring expansion reactions

The reaction of B_2cat_2 **8** with one or two equivalents of the NHC Me_2Im^{Me} yielded the mono-NHC diboron adduct $B_2cat_2 \cdot Me_2Im^{Me}$ **18** and the bis-NHC diboron adduct $B_2cat_2 \cdot (Me_2Im^{Me})_2$ **25**. The NMR spectroscopic investigations showed that the behavior of these NHC diboron adducts in solution is different. $B_2cat_2 \cdot Me_2Im^{Me}$ **18** is soluble in C_6D_6 and CD_2Cl_2 , albeit, and also that it decomposes in dichloromethane. The bis-NHC adduct $B_2cat_2 \cdot (Me_2Im^{Me})_2$ **25** is not soluble in C_6D_6 and it decomposes in CD_2Cl_2 to the mono-NHC adduct as well as other compounds, which were not further characterized. The “free” NHC, such as Me_2Im^{Me} , reacts with dichloromethane and decomposes; however, this implicates that the Me_2Im^{Me} binds to one boron atom. Another difference is the stability at higher temperatures. While $B_2cat_2 \cdot Me_2Im^{Me}$ **18** is thermally stable in solution, the bis-NHC diboron adduct $B_2cat_2 \cdot (Me_2Im^{Me})_2$ **25** rearranges to a ring expanded product of the NHC with insertion of one boron-moiety into the C–N bond to form a six-membered heterocyclic ring, a so called “ring expansion reaction” (RER).^[256]

2.2.2.1. Ring expansion reactions involving B_2cat_2 as the diboron reagent

Synthesis of the ring expanded product RER- $B_2cat_2 \cdot (Me_2Im^{Me})_2$

The mentioned ring expanded products were obtained *via* reaction of B_2cat_2 **8** with two equivalents of the NHC Me_2Im^{Me} ; the reaction was carried out at higher temperature to re-dissolve the obtained solid in THF and, after work-up, the ring expanded product RER- $B_2cat_2 \cdot (Me_2Im^{Me})_2$ **26** was isolated (Scheme 94).^[256]



Scheme 94: Reaction of B_2cat_2 **8** with Me_2Im^{Me} , forming the ring expanded product RER- $B_2cat_2 \cdot (Me_2Im^{Me})_2$ **26**.

RER- $B_2cat_2 \cdot (Me_2Im^{Me})_2$ **26** was characterized *via* NMR-spectroscopy and elemental analysis as well as X-ray diffraction. The 1H NMR spectrum shows one set of signals for the six-membered heterocyclic ring as well as for the exocyclic Bcat-moiety and the coordinated NHC (Figure 55). The methyl-groups of the former backbone of the NHC are detected at 1.42 and

1.47 ppm ($\text{Me}_{b/c}\text{-CH}_3$). The methyl-moieties at the two nitrogen atoms are observed at 2.78 and 3.40 ppm ($\text{Me}_{a/d}\text{-CH}_3$). The protons of the catechol-groups are split into three signals; two multiplets at 6.83-6.85 and 7.06-7.07 ppm belong to the Bcat-moiety ($\text{B}_\alpha\text{cat}$), which was inserted into the ring. The other multiplet at 6.40-6.41 belongs to the Bcat-group (B_βcat), which was migrated to the former carbene carbon atom. The chemical shifts for the second NHC resonate at 1.09 ($\text{Me}_a\text{-CH}_3$) and 3.57 ppm ($\text{Me}_e\text{-CH}_3$).^[256]

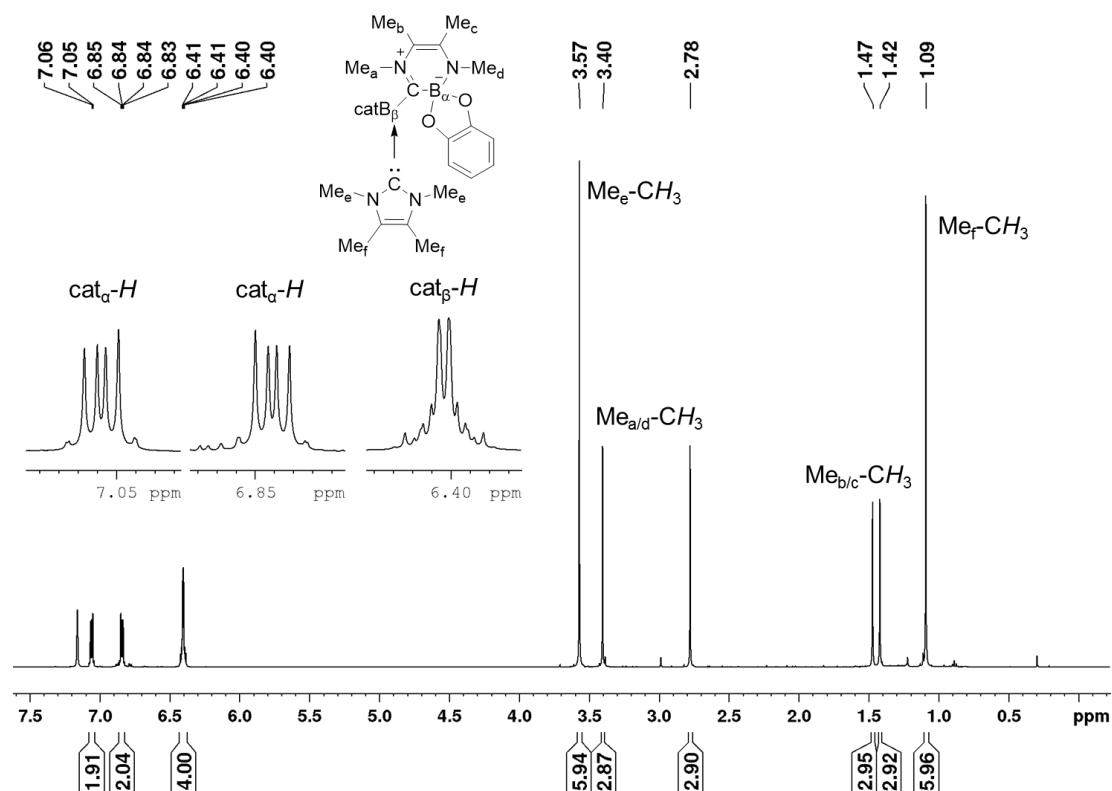


Figure 55: ^1H NMR of $\text{RER-B}_2\text{cat}_2\cdot(\text{Me}_2\text{Im}^{\text{Me}})_2$ **26** in C_6D_6 (500 MHz); reproduced from ref. [253] with permission from Wiley-VCH.

The $^{11}\text{B}\{^1\text{H}\}$ NMR spectrum of $\text{RER-B}_2\text{cat}_2\cdot(\text{Me}_2\text{Im}^{\text{Me}})_2$ **26** shows two sharp signals at 6.23 and 7.20 ppm, one for the inserted Bcat-moiety (B_α) and the other signal for the Bcat-group which migrates to the former carbene carbon atom (B_β) (Figure 56). The $^{13}\text{C}\{^1\text{H}\}$ NMR spectrum shows one signal for each methyl-group of the heterocyclic ring (15.4 ($\text{Me}_{b/c}\text{-CH}_3$), 15.5 ($\text{Me}_{b/c}\text{-CH}_3$), 31.4 ($\text{Me}_{a/d}\text{-CH}_3$) and 43.9 ($\text{Me}_{a/d}\text{-CH}_3$)). The quaternary carbene carbon atoms of the former backbone are observed at 110.2 and 140.6 ppm, and the former carbene carbon atom is detected at 184.2 ppm. In addition, the signals of the carbon atoms of the inserted Bcat-moiety are shown at 110.3 and 119.6 ppm ($\text{cat}_\alpha\text{-CH}$) and the inserted Bcat-group at 106.9 and 117.8 ppm ($\text{cat}_\beta\text{-CH}$). For the quaternary carbon atoms of the catechol-groups, two signals at 153.1 and 153.5 ppm (cat-C_q) are observed. The chemical shifts for the second NHC are detected at 7.76 ppm for methyl-groups at the backbone as well as one signal for the

methyl-groups at the nitrogen atom at 33.0 ppm; the backbone carbons resonate at 124.0 ppm and the carbene carbon atom at 158.8 ppm.^[256]

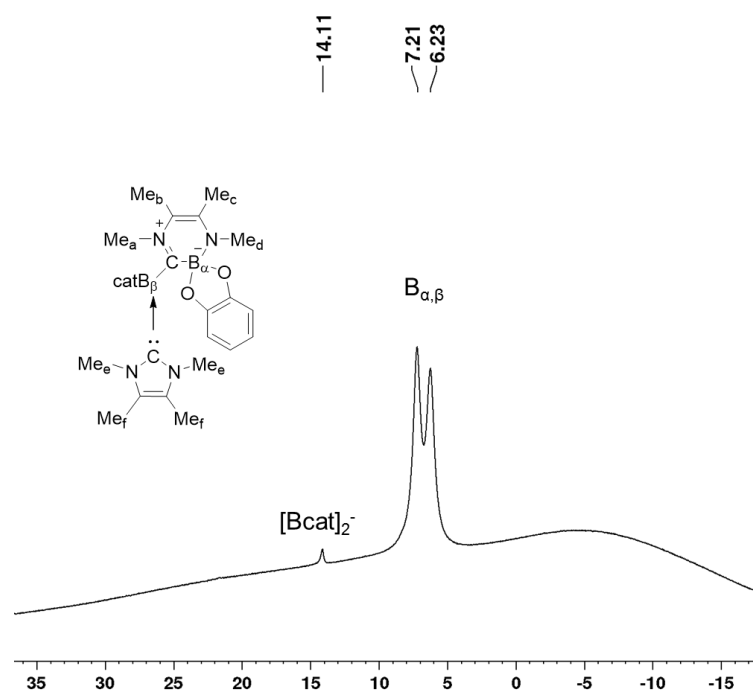


Figure 56: $^{11}\text{B}\{^1\text{H}\}$ NMR spectrum of $\text{RER-B}_2\text{cat}_2\cdot(\text{Me}_2\text{Im}^{\text{Me}})_2$ **26** in C_6D_6 ; reproduced from ref. [253] with permission from Wiley-VCH.

Single crystals of $\text{RER-B}_2\text{cat}_2\cdot(\text{Me}_2\text{Im}^{\text{Me}})_2$ **26** were obtained from a saturated solution of compound **26** in acetonitrile. The molecular structure confirmed the results for the six-membered heterocyclic ring as well as the migration of the second Bcat-moiety to the former carbene carbon atom and the coordination of the second NHC $\text{Me}_2\text{Im}^{\text{Me}}$ to the exocyclic Bcat-group (Figure 57). The C=C bond lengths in the six-membered heterocycle of compound **26** are 1.373(2) and 1.355(3) Å whereas N1–C2 (1.417(2) Å) is in the region of single bond lengths and C3–N2 (1.350(2) Å) and N1–C1 (1.323(1) Å) indicates some multiple bond character. The N2–B1 (1.517(2) Å) as well as all C–B distances are within the range of single bonds.^[256]

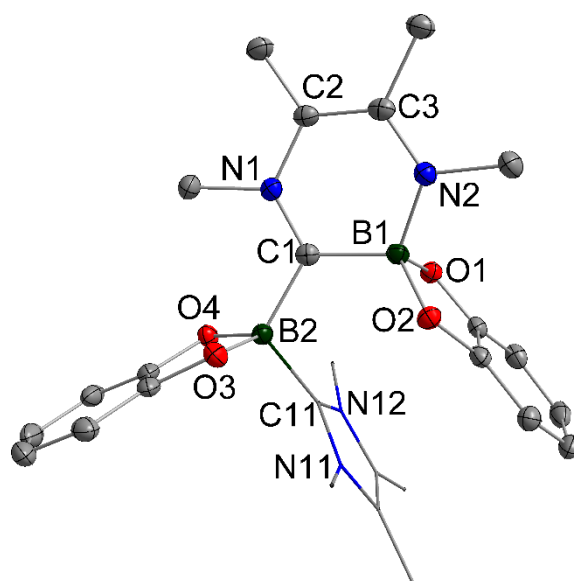
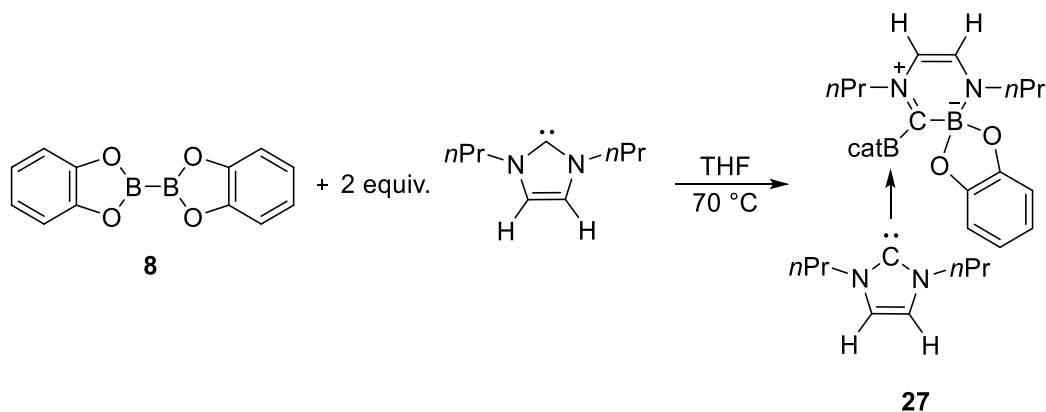


Figure 57: Molecular structure of RER-B₂cat₂•(Me₂Im^{Me})₂ **26** with thermal ellipsoids drawn at the 50% probability level; hydrogen atoms are omitted and the second NHC is drawn as wires/sticks for clarity. Selected bond distances (Å) and angles (°): B1–C1 1.604(2), C1–N1 1.3230(13), N1–C2 1.417(2), C2–C3 1.373(2), C3–N2 1.350(2), N2–B1 1.517(2), C1–B2 1.634(2), B2–C11 1.653(2); C1–B1–N2 109.32(10), B1–N2–C3 122.31(10), N2–C3–C2 121.96(11), C3–C2–N1 119.00(11), C2–N1–C1 124.46(10), N1–C1–B1 118.54(10), B1–C1–B2 120.10(10), C1–B2–C11 112.32(10). N1–C2–C3–N2//N1–B1–N2 16.14(6), N1–C2–C3–N2//N1–C1–N2 5.86(6); reproduced from ref. [253] with permission from Wiley-VCH.

Synthesis of the ring expanded product RER-B₂cat₂•(*n*Pr₂Im)₂

The successful synthesis and characterization of RER-B₂cat₂•(Me₂Im^{Me})₂ **26** raises the question whether the ring expansion process depends on the steric properties of the NHC. Therefore, the reaction of B₂cat₂ with *n*Pr₂Im was investigated. The reaction of B₂cat₂ **8** and *n*Pr₂Im was carried out under the same reaction conditions as used for compound **26**. Due to the fact that the solid precipitates at room temperature, the suspension was also heated to 70 °C to re-dissolve the solid, and afterwards RER-B₂cat₂•(*n*Pr₂Im)₂ **27** was isolated in good yield (71%) (Scheme 95).^[256]



Scheme 95: Reaction of B₂cat₂ **8** with *n*Pr₂Im to form the ring expanded product RER-B₂cat₂•(*n*Pr₂Im)₂ **27**.

RER-B₂cat₂•(nPr₂Im)₂ **27** was fully characterized *via* NMR spectroscopy as well as elemental analysis and X-ray diffraction. The ¹H NMR spectrum is similar to that of RER-B₂cat₂•(Me₂Im^{Me})₂ **26**. It shows one set of signals for the six-membered heterocycle as well as for the exocyclic Bcat-moiety and the second NHC (Figure 58). The backbone of the former NHC is detected at 5.19 (C_bH) and 6.10 ppm (C_cH) as two doublets. The signals for the nPr_a-moiety are observed at 0.73 (CH₃), 1.60 (CH₂CH₃) and 3.02 ppm (NCH₂) and the corresponding nPr_d-group at 0.60 (CH₃), 1.87 (CH₂CH₃) and 3.68 ppm (NCH₂). The protons of the catechol-moiety (cat_α-H) of the endocyclic boron atom resonate at 6.76-6.77 and 6.85-6.87 ppm and the signals for the exocyclic Bcat-moiety (cat_β-H) at 6.49-6.51 and 6.57-6.59 ppm. Furthermore, the signals for the coordinated NHC are detected at 0.74 (CH₃), 1.47 (CH₂CH₃) and 4.12 ppm (NCH₂) as well as at 5.54 ppm for the protons of the backbone (C_fH).^[256]

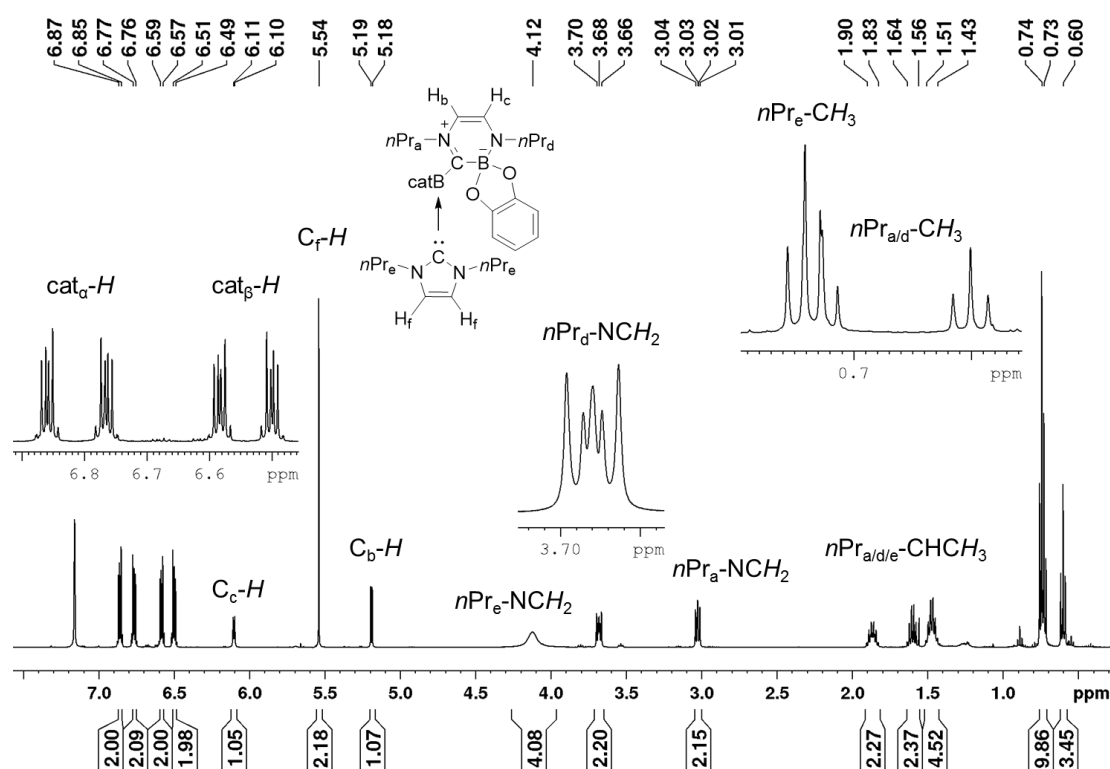


Figure 58: ¹H NMR spectrum of RER-B₂cat₂•(nPr₂Im)₂ **27** in C₆D₆ (500 MHz); reproduced from ref. [253] with permission from Wiley-VCH.

The ¹¹B{¹H} NMR spectrum of RER-B₂cat₂•(nPr₂Im)₂ **27** shows two sharp signals at 6.04 and 7.67 ppm, one for the inserted Bcat-moiety (B_α) and the other signal for the Bcat-group, which migrates to the former carbene carbon atom (B_β) (Figure 59). In the ¹³C{¹H} NMR spectrum, one signal for each carbon atom of the heterocyclic ring as well as one set of signals for the exocyclic Bcat-moiety and the coordinating NHC are observed. The chemical shifts for the backbone of the former NHC are detected at 105.6 (C_bH) and 136.1 (C_cH) ppm. The carbon atoms of the nPr_a-moiety are observed at 11.8 (CH₃), 25.8 (CH₂CH₃) and 51.9 (NCH₂) ppm

and the signals for the $n\text{Pr}_d$ -group at 11.5 (CH_3), 25.2 (CH_2CH_3) and 61.4 (NCH_2) ppm. The former carbene carbon atom is detected at 185.7 ppm and the NHC carbon atom at 160.7 ppm, which were assigned by 2D NMR spectroscopy (HMBC). In addition, the signals for the Bcat-moieties ($\text{cat}_{\alpha/\beta}\text{-CH}$) appear at 110.3 and 119.6 ppm for the inserted one and for the migrating Bcat-group at 107.5 and 118.1 ppm. The quaternary carbon atoms of the catechol-groups are observed at 152.9 and 153.3 ppm.^[256]

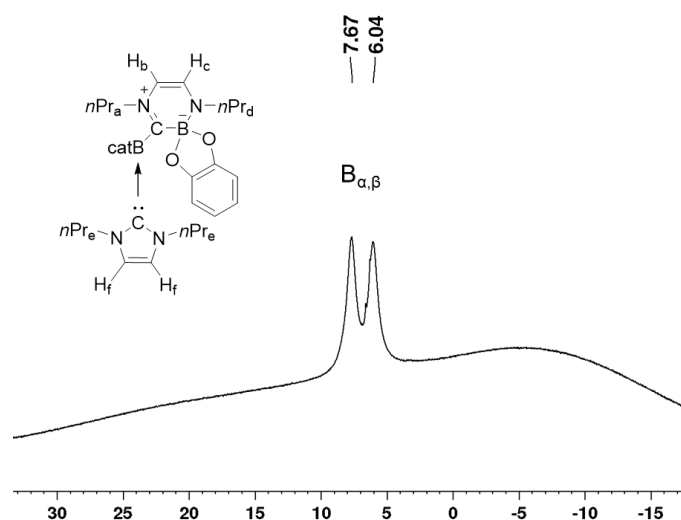


Figure 59: $^{11}\text{B}\{^1\text{H}\}$ NMR spectrum of $\text{RER-B}_2\text{cat}_2\cdot(n\text{Pr}_2\text{Im})_2$ **27** in C_6D_6 ; reproduced from ref. [253] with permission from Wiley-VCH.

The molecular structures of $\text{RER-B}_2\text{cat}_2\cdot(\text{Me}_2\text{Im}^{\text{Me}})_2$ **26** (Figure 57) and $\text{RER-B}_2\text{cat}_2\cdot(n\text{Pr}_2\text{Im})_2$ **27** (Figure 60) confirm the ring expansion of the NHC and the insertion of one Bcat-moiety into the C–N bond as well as the migration of the second Bcat-group to the former carbene carbon atom and further stabilization by a second $n\text{Pr}_2\text{Im}$. Both molecular structures show similar bond lengths and angles within the six-membered heterocyclic ring. The C=C bond lengths in the six-membered heterocycles are 1.373(2) Å and 1.355(3) Å whereas N1–C2 (**26**: 1.417(2) Å; **27**: 1.405(2) Å) are in the region of single bond lengths and C3–N2 (**26**: 1.350(2) Å; **27**: 1.340(2) Å), and N1–C1 (**26**: 1.323(1) Å; **27**: 1.326(2) Å) indicate some multiple bond character. The N2–B1 (1.517(2) Å and 1.533(3) Å) as well as all C–B distances are within the range of single bonds. Thus, compounds **26** and **27** contain one endocyclic Bcat within the new six-membered ring, as well as an exocyclic Bcat-moiety stabilized by complexation with a second NHC.^[256]

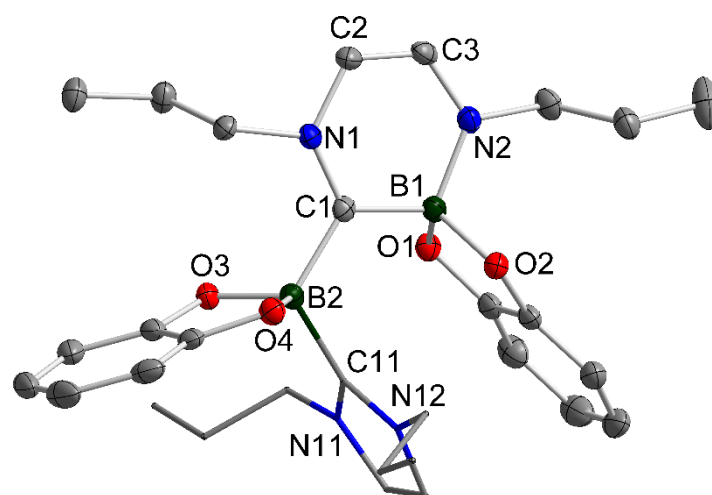


Figure 60: Molecular structure of RER-B₂cat₂•(*n*Pr₂Im)₂ **27** with thermal ellipsoids drawn at the 50% probability level; hydrogen atoms are omitted the second NHC is drawn as wires/sticks for clarity. Selected bond distances (Å) and angles (°): B1–C1 1.619(3), C1–N1 1.326(2), N1–C2 1.405(3), C2–C3 1.355(3), C3–N2 1.340(2), N2–B1 1.533(3), C1–B2 1.641(3), B2–C11 1.659(3); C1–B1–N2 111.02(15), B1–N2–C3 121.23(16), N2–C3–C2 124.06(18), C3–C2–N1 120.85(17), C2–N1–C1 123.59(15), B1–C1–B2 121.50(15), C1–B2–C11 112.39(15); N1–C2–C3–N2//N1–B1–N2 2.60(12), N1–C2–C3–N2//N1–C1–N2 1.42(13); reproduced from ref. [253] with permission from Wiley-VCH.

2.2.2.2. Exchange reactions

The successful ring expansion reaction of B₂cat₂ **8** with the two different NHCs Me₂Im^{Me} and *n*Pr₂Im yielding of the two ring expanded products RER-B₂cat₂•(Me₂Im^{Me})₂ **26** and RER-B₂cat₂•(*n*Pr₂Im)₂ **27**, showed that the opening of the C–N bond is not dependent on the size of the NHC. To demonstrate the strength of the bonding of the second NHC to the exocyclic Bcat-moiety, the reaction of RER-B₂cat₂•(*n*Pr₂Im)₂ **27** with one equivalent of Me₂Im^{Me} was investigated. In an NMR tube, RER-B₂cat₂•(*n*Pr₂Im)₂ **27** and one equivalent Me₂Im^{Me} were dissolved in 0.6 mL C₆D₆ and the solution was immediately monitored *via* NMR spectroscopy (Figure 61).^[256]

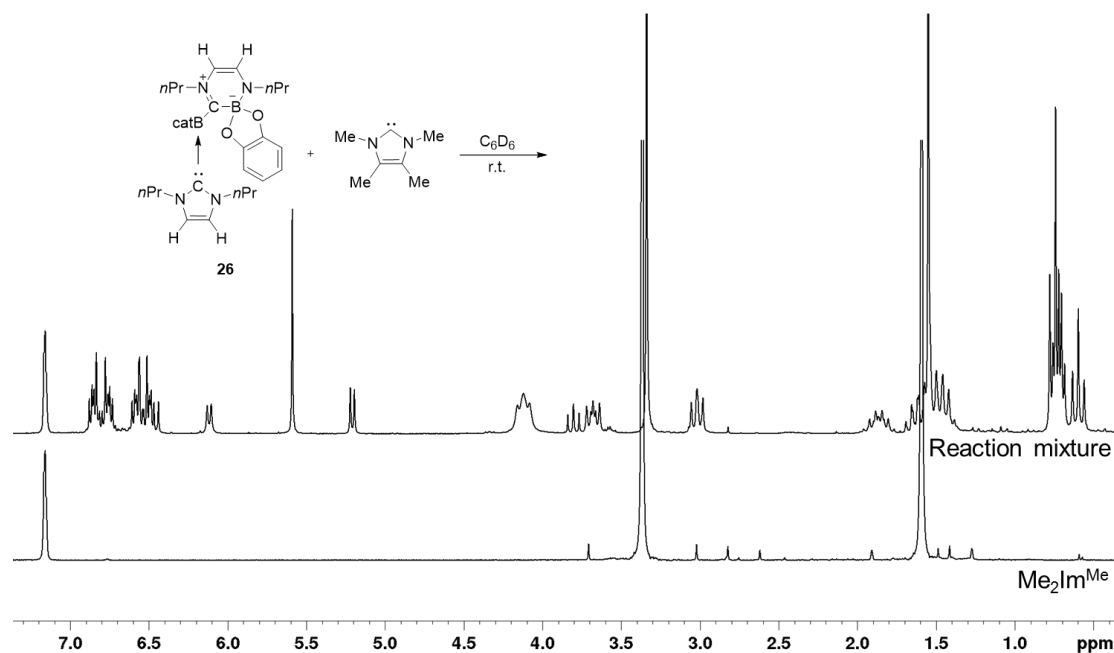
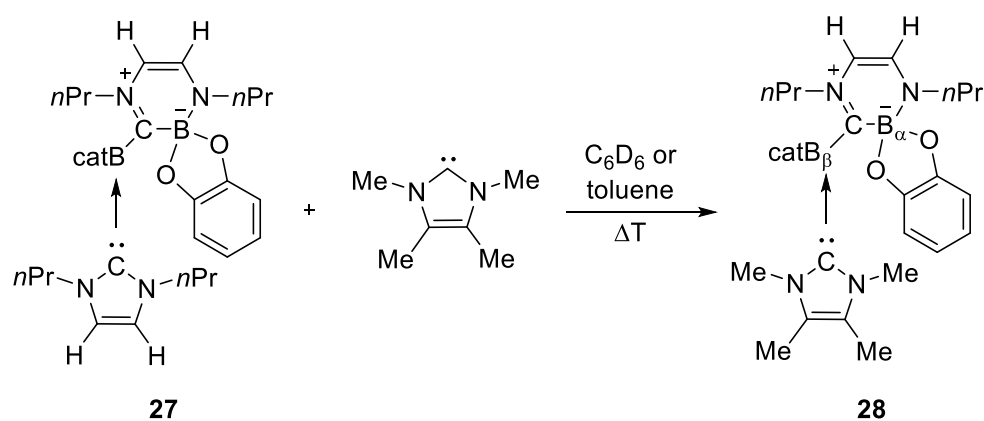


Figure 61: Reaction of RER-B₂cat₂·(nPr₂Im)₂ **27** with one equivalent Me₂Im^{Me} in C₆D₆ at room temperature (200 MHz); spectrum above: recorded reaction mixture, spectrum below: spectrum of the NHC Me₂Im^{Me} for comparison; reproduced from ref. [253] with permission from Wiley-VCH.

The ¹H NMR spectrum shows no evidence for the exchange of the nPr₂Im by the Me₂Im^{Me} at room temperature (Figure 61); however, heating the NMR tube to 70 °C for several hours changed the color from yellow to red and the desired ring expanded product RER-B₂cat₂·nPr₂Im·Me₂Im^{Me} **28** could be observed, as well as “free” NHC nPr₂Im in the ¹H NMR spectrum.

In addition to the NMR scale reaction, the reaction was carried out on a larger scale to isolate the ring expanded product and to characterize RER-B₂cat₂·nPr₂Im·Me₂Im^{Me} **28** (Scheme 96).^[256]



Scheme 96: Reaction of RER-B₂cat₂·(nPr₂Im)₂ **26** with Me₂Im^{Me} to form the ring expanded product RER-B₂cat₂·nPr₂Im·Me₂Im^{Me} **28**.

RER-B₂cat₂•nPr₂Im•Me₂Im^{Me} **28** was characterized *via* ¹H, ¹¹B{¹H} and ¹³C{¹H} NMR spectroscopy. The ¹H NMR spectrum shows two singlets for the exocyclic Me₂Im^{Me} NHC (Figure 62); the methyl-groups at the backbone are observed at 1.06 ppm and the corresponding methyl-groups at the nitrogen atom at 3.51 ppm. The signals of the heterocyclic ring as well as the second Bcat-moiety are detected in the same region as observed for the ring expanded product RER-B₂cat₂•(nPr₂Im)₂ **27**.^[256]

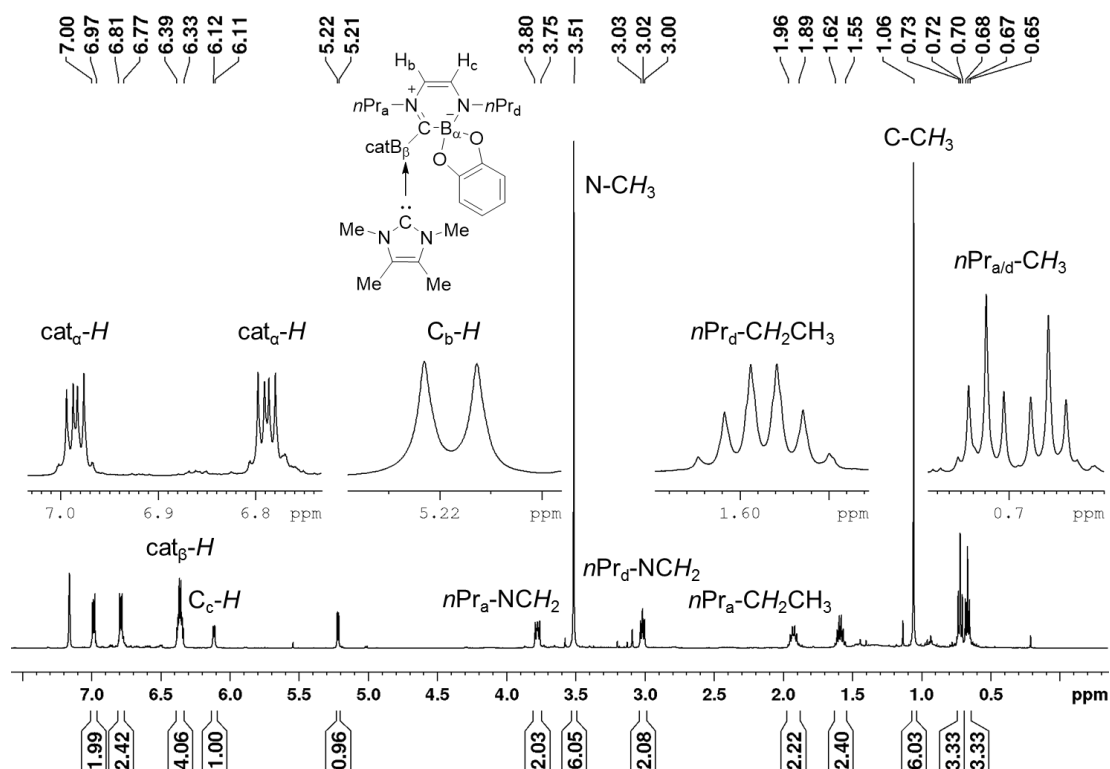


Figure 62: ¹H NMR spectrum of RER-B₂cat₂•nPr₂Im•Me₂Im^{Me} **28** in C₆D₆ (500 MHz); reproduced from ref. [253] with permission from Wiley-VCH.

The ¹¹B{¹H} NMR spectrum shows two signals for the two boron atoms (B_α and B_β) at 6.91 and 8.57 ppm (Figure 63). In the ¹³C{¹H} NMR spectrum, one signal for each carbon atom of the heterocyclic ring as well as one set of signals for the exocyclic Bcat-moiety and the coordinating NHC is detected. The methyl-groups of the exocyclic NHC are detected at 7.73 ppm (C-CH₃) and the methyl-groups at the nitrogen atom at 33.0 ppm, the signal of the carbon atoms of the backbone are observed at 123.9 ppm. The former carbene carbon atom appears at 186.8 ppm, which is also similar to the chemical shifts found in RER-B₂cat₂•(nPr₂Im)₂ **27**.^[256]

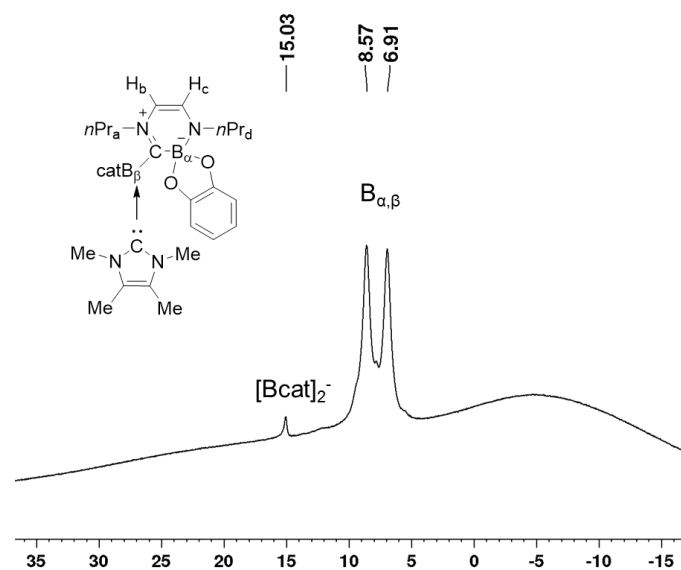
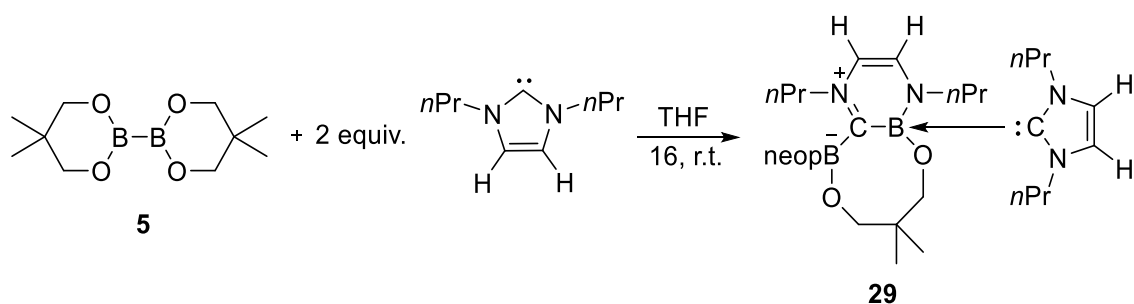


Figure 63: $^{11}\text{B}\{^1\text{H}\}$ NMR spectrum of RER- $\text{B}_2\text{cat}_2 \cdot n\text{Pr}_2\text{Im} \cdot \text{Me}_2\text{Im}^{\text{Me}}$ **28** in C_6D_6 ; reproduced from ref. [253] with permission from Wiley-VCH.

2.2.2.3. Ring expansion reactions involving B_2neop_2 as the diboron reagent

Based on the successful synthesis and characterization of the ring expanded products RER- $\text{B}_2\text{cat}_2 \cdot (\text{Me}_2\text{Im}^{\text{Me}})_2$ **26** and RER- $\text{B}_2\text{cat}_2 \cdot (n\text{Pr}_2\text{Im})_2$ **27** as well as RER- $\text{B}_2\text{cat}_2 \cdot n\text{Pr}_2\text{Im} \cdot \text{Me}_2\text{Im}^{\text{Me}}$ **28** at higher temperatures, the question arises whether the ring expansion is limited to the B_2cat_2 reagent or if similar results could be obtained using B_2neop_2 as the diboron compound.

Additionally, the reaction of B_2neop_2 with different NHCs was investigated. Based on our knowledge that the size of the NHC is not responsible for the success of the reaction, B_2neop_2 **5** and two equivalents of $n\text{Pr}_2\text{Im}$ were reacted under the same conditions which were used for the compounds **26** and **27**. In comparison to the reported ring expanded products RER- $\text{B}_2\text{cat}_2 \cdot (\text{Me}_2\text{Im}^{\text{Me}})_2$ **26** and RER- $\text{B}_2\text{cat}_2 \cdot (n\text{Pr}_2\text{Im})_2$ **27**, no solid precipitated at room temperature (Scheme 97). Therefore, an *in situ* NMR spectrum was obtained of the reaction mixture which showed, even at room temperature, two sharp signals at approximately 0 ppm, which implies a full conversion of the starting material (B_2neop_2 : ^{11}B NMR 29 ppm). After stirring the reaction mixture for 16 hours at room temperature, a yellow solid was obtained, which was identified as the ring expanded product RER- $\text{B}_2\text{neop}_2 \cdot (n\text{Pr}_2\text{Im})_2 \cdot \text{toluene}$ **29** via X-ray diffraction. While the $^{11}\text{B}\{^1\text{H}\}$ NMR spectrum indeed showed evidence for a ring expanded product, the ^1H NMR spectrum of the isolated solid was not comparable to the data found for compound **26** and **27**; however, single crystals of RER- $\text{B}_2\text{neop}_2 \cdot (n\text{Pr}_2\text{Im})_2 \cdot \text{toluene}$ **29** were obtained from a saturated solution of the solid in toluene.^[256]



Scheme 97: Reaction of B_2neop_2 **5** with two equivalents of $n\text{Pr}_2\text{Im}$, which led to the formation of the ring expanded product $\text{RER-B}_2\text{neop}_2 \cdot (n\text{Pr}_2\text{Im})_2 \cdot \text{toluene}$ **29**.

The molecular structure shows a six-membered heterocyclic ring, indicating the insertion of one boron atom into the C–N bond of the NHC *via* cleavage of the bond, which is similar to the reported ring expanded products containing B_2cat_2 as the diboron reagent ($\text{RER-B}_2\text{cat}_2 \cdot (\text{Me}_2\text{Im}^{\text{Me}})_2$ **26** and $\text{RER-B}_2\text{cat}_2 \cdot (n\text{Pr}_2\text{Im})_2$ **27**) (Figure 64). However, the coordination of the ligands is quite different from those previously reported. The second NHC coordinates to the endocyclic boron atom (B1) instead of coordinating to the exocyclic one. A further difference is the opening of the neopentane-glycolato-moiety of the boron atom B1, which is now bridged to the boron atom B2, giving six and eight-membered heterocyclic rings.^[256]

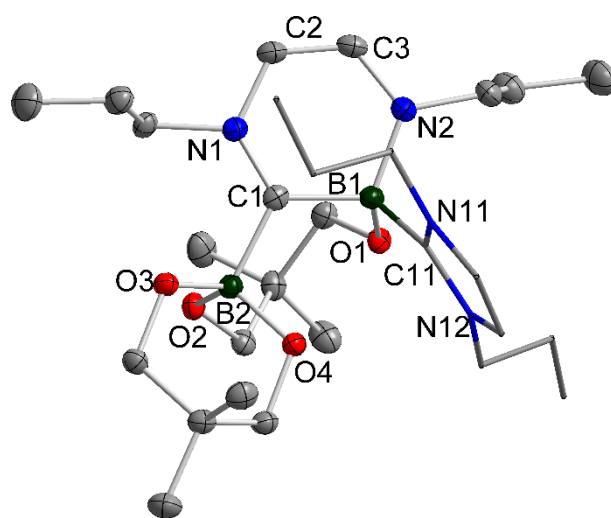


Figure 64: Molecular structure of $\text{RER-B}_2\text{neop}_2 \cdot (n\text{Pr}_2\text{Im})_2 \cdot \text{toluene}$ **29** with thermal ellipsoids drawn at the 50% probability level; hydrogen atoms are omitted the second NHC is drawn as wires/sticks for clarity. Selected bond distances (Å) and angles (°): C1–N1 1.315(2), N1–C2 1.416(2), C2–C3 1.345(2), C3–N2 1.346(2), N2–B1 1.548(2), B1–C1 1.635(2), B1–C11 1.647(2), C1–B2 1.652(2); C1–N1–C2 123.29(10), N1–C2–C3 121.19(11), C2–C3–N2 124.41(11), C3–N2–B1 120.55(10), N2–B1–C1 110.28(10), B1–C1–N1 119.06(10); N1–C2–C3–N2//N1–B1–N2 5.19(8); N1–C2–C3–N2//N1–C1–N2 1.97(8); reproduced from ref. [253] with permission from Wiley-VCH.

Based on the observed molecular structure, the solid was identified as the ring expanded product $\text{RER-B}_2\text{neop}_2 \cdot (n\text{Pr}_2\text{Im})_2 \cdot \text{toluene}$ **29**, which was subsequently fully characterized *via* NMR spectroscopy as well as elemental analysis. The ^1H NMR spectrum shows one signal for

each proton of one methylene-group as well as the methyl-groups of the neop-moiety, due to the fact that B1 is chiral resulting in the diastereotopic nature of the protons in compound **29**. The ^1H NMR spectrum (Figure 65, for an expanded view, see Figure 131-134) shows one set of signals for the exocyclic NHCs. The chemical shifts of the $n\text{Pr}_e$ -moiety are detected at 0.71-0.74 (CH_3 , overlapped with $n\text{Pr}_d\text{-CH}_3$), 1.25-1.36 (overlap with $n\text{Pr}_d\text{-CH}_2\text{CH}_3$) and 1.51-1.61 ppm (CH_2CH_3) and the two signals of the methylene-group at the nitrogen atom are observed at 3.07-3.12 and 3.29-3.35 (NCH_2) ppm. The resonances for the $n\text{Pr}_h$ -group are observed at 0.88 (CH_3), 1.67-1.77 and 1.78-1.87 (CH_2CH_3) and the signals for the $n\text{Pr}_h\text{-NCH}_2$ protons at 3.90-3.96 and 5.26-5.32 ppm. The signals of the protons of the backbone are detected as doublets at 6.02 (CH_f) and 6.08 ppm (CH_g).

In addition, the resonances of the two $n\text{Pr}$ -moieties of the heterocyclic ring are split into two sets of signals. The resonances of the $n\text{Pr}_a$ -group are detected at 0.99 ppm for the methyl-group, the signals for the methylene protons ($n\text{Pr}_a\text{-CH}_2\text{CH}_3$) appear at 2.08-2.16 and 2.17-2.24 ppm and the signals of the methylene-group at the nitrogen atom ($n\text{Pr}_a\text{-NCH}_2$) are detected at 4.07-4.13 and 4.91-4.97 ppm. The chemical shifts for the $n\text{Pr}_d$ -group are observed at 0.71-0.74 ppm for the methyl-group (overlapped with $n\text{Pr}_e\text{-CH}_3$), the methylene-group at 1.25-1.36 (overlapped with $n\text{Pr}_e\text{-CH}_3$) and 1.44-1.51 ppm and the methyl-group at the nitrogen atom ($n\text{Pr}_d\text{-NCH}_2$) at 2.41-2.47 and 2.61-2.67 ppm. The protons of the former NHC backbone are detected as doublets at 5.13 (CH_b) and 6.00 ppm (CH_c). Furthermore, based on the symmetry of the compound, each CMe_2 and CH_2 -group of the Bneop-moiety are split into two signals. The methyl-groups of the $\text{Bneop}_\alpha\text{-CH}_3$ are observed at 1.14 and 1.16 ppm as singlets and the methylene-groups as multiplets at 3.02-3.05 and 3.16-3.18 ppm ($\text{neop}_\alpha\text{-CH}_2$). The signals for the $\text{Bneop}_\beta\text{-CH}_3$ are detected as singlets at 0.75 and 1.12 ppm, and the methylene-groups at 2.86-2.88 and 3.79-3.81 ppm ($\text{neop}_\beta\text{-CH}_2$).^[256]

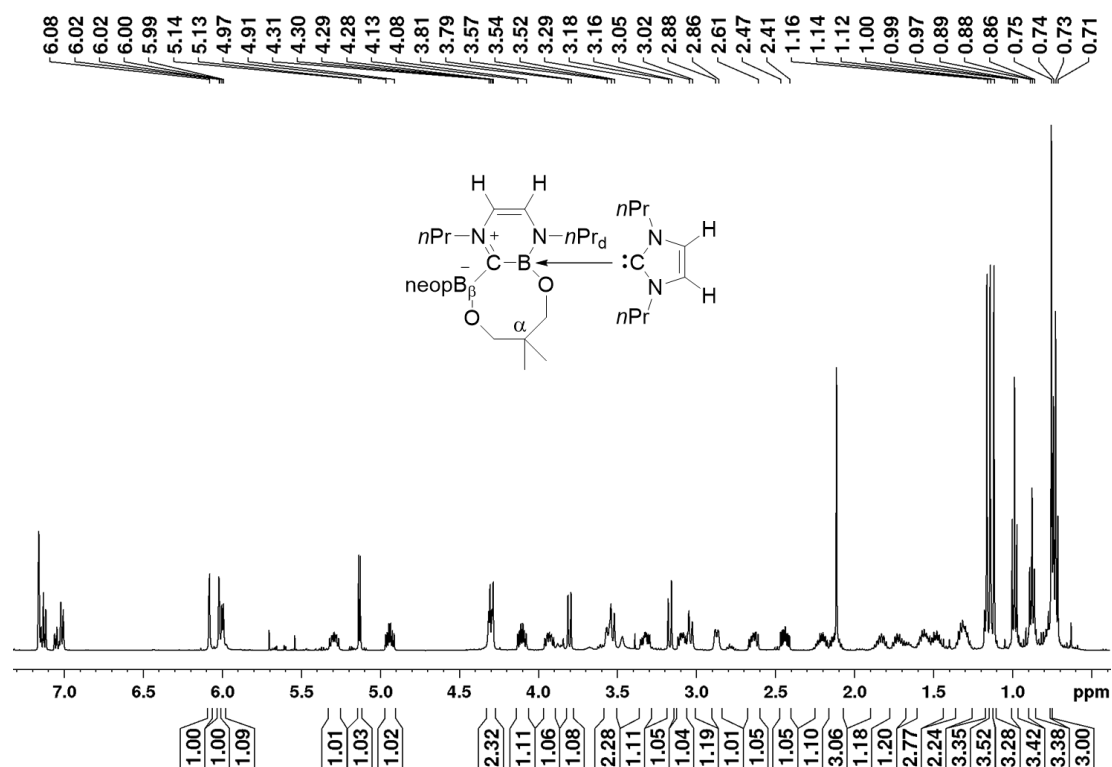


Figure 65: ^1H NMR spectrum of $\text{RER-B}_2\text{neop}_2 \cdot (\text{nPr}_2\text{Im})_2 \cdot \text{toluene}$ **29** in C_6D_6 ; reproduced from ref. [253] with permission from Wiley-VCH.

The $^{11}\text{B}\{^1\text{H}\}$ NMR spectrum of $\text{RER-B}_2\text{neop}_2 \cdot (\text{nPr}_2\text{Im})_2 \cdot \text{toluene}$ **29** shows two sharp signals at 1.03 and -2.35 ppm for the inserted (B_α) and the migrated boron atom (B_β) (Figure 66). In the $^{13}\text{C}\{^1\text{H}\}$ NMR spectrum, the resonance for the nPr_f -group of the exocyclic NHC is detected at 11.4 (CH_3), 24.6 (CH_2CH_3) and 50.5 ppm (NCH_2) and the signals for the nPr_e -group are observed at 11.7 (CH_3), 23.9 (CH_2CH_3) and 54.0 ppm (NCH_2). The resonances of the backbone appear at 118.0 (CH_f) and 120.1 ppm (CH_g) and the signal for the carbene carbon atom is found at 165.7 ppm. Furthermore, the signals for the nPr_a -group are observed at 12.0 (CH_3), 24.1 (CH_2CH_3) as well as 61.4 ppm (NCH_2). The signals for the nPr_d -group resonate at 12.0 (CH_3), 25.7 (CH_2CH_3) and 49.6 ppm (NCH_2). The chemical shifts of the carbon atoms of the former backbone are 102.6 (CH_b) and 135.0 ppm (CH_c) and the signal for the former carbene carbon atom occurs at 212.3 ppm. In addition, the signals for the carbon atoms of the inserted Bneop-moiety (Bneop_α) are observed at 23.8 and 24.7 ppm ($\text{neop}_\alpha\text{-CH}_3$) and the methylene-groups ($\text{neop}_\alpha\text{-CH}_2$) are detected at 68.9 and 70.5 ppm. The resonance of the migrated Bneop-group (Bneop_β) appears at 23.4 and 24.1 ppm for the methyl-groups ($\text{neop}_\beta\text{-CH}_3$) and the corresponding methylene-groups are observed at 71.5 and 72.9 ppm ($\text{neop}_\beta\text{-CH}_2$). Furthermore, the chemical shifts of the quaternary carbon atoms of each Bneop-moiety are detected at 37.7 ($\text{neop}_\alpha\text{-C}(\text{CH}_3)_2$) and 32.6 ppm ($\text{neop}_\beta\text{-C}(\text{CH}_3)_2$).^[256]

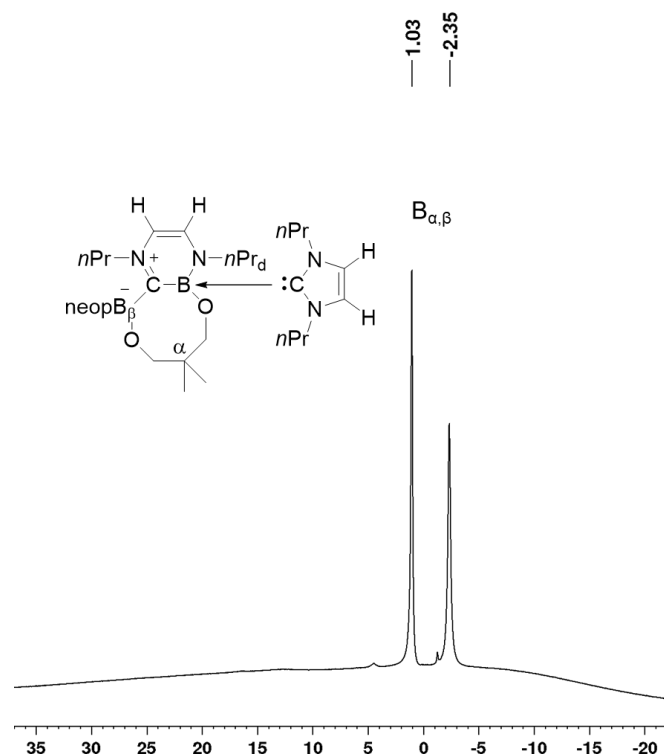
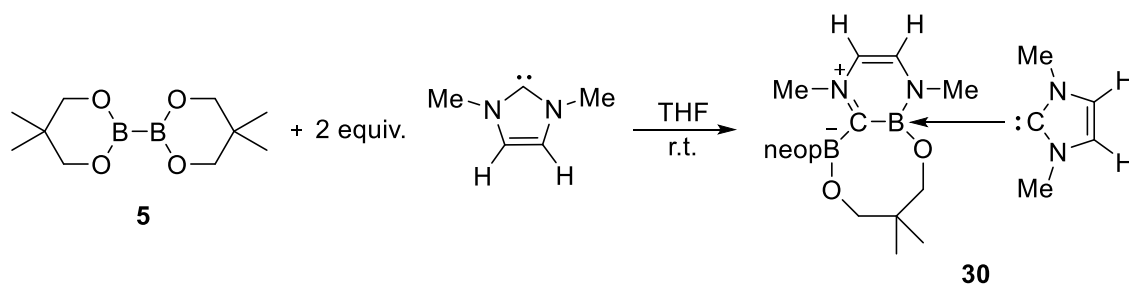


Figure 66: $^{11}\text{B}\{^1\text{H}\}$ NMR spectrum of $\text{RER-B}_2\text{neop}_2\cdot(\text{nPr}_2\text{Im})_2$ **29** in C_6D_6 (500 MHz); reproduced from ref. [253] with permission from Wiley-VCH.

Based on the successful isolation of the ring expanded product $\text{RER-B}_2\text{neop}_2\cdot(\text{nPr}_2\text{Im})_2$ **29**, similar reactions were investigated using the sterically less demanding NHCs Me_2Im and $\text{Me}_2\text{Im}^{\text{Me}}$. The reaction of B_2neop_2 **5** with two equivalents of Me_2Im yielded the ring expanded product $\text{RER-B}_2\text{neop}_2\cdot(\text{Me}_2\text{Im})_2$ **30**. (Scheme 98).

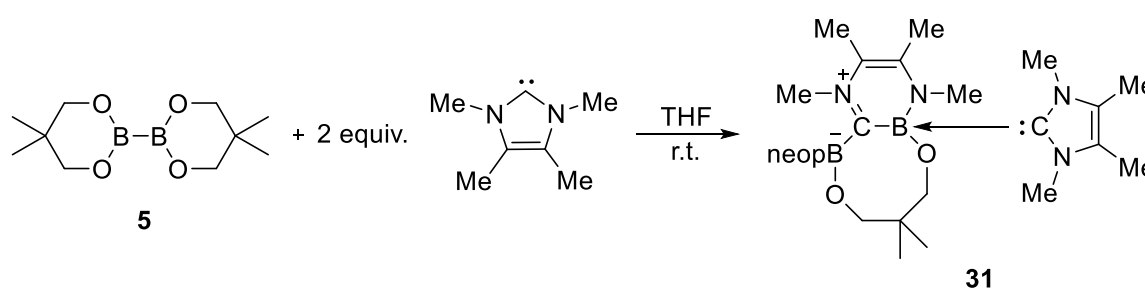


Scheme 98: Reaction of B_2neop_2 with two equivalents of Me_2Im , which led to the formation of the ring expanded product $\text{RER-B}_2\text{neop}_2\cdot(\text{Me}_2\text{Im})_2$ **30**.

$\text{RER-B}_2\text{neop}_2\cdot(\text{Me}_2\text{Im})_2$ **30** was characterized *via* ^1H , $^{11}\text{B}\{^1\text{H}\}$ and $^{13}\text{C}\{^1\text{H}\}$ NMR spectroscopy. The ^1H NMR spectrum of compound **30** shows similar splitting of the substituents as observed for $\text{RER-B}_2\text{neop}_2\cdot(\text{nPr}_2\text{Im})_2$ **29**. For each proton of the methylene-groups ($\text{neop}_{\alpha,\beta}\text{-CH}_2$) as well as for the methyl-groups ($\text{neop}_{\alpha,\beta}\text{-CH}_3$) one signal is detected. The chemical shifts for the heterocyclic ring are 2.36 and 4.03 ppm for the $\text{Me}_{a/d}\text{-CH}_3$ -moiety and the signals of the former backbone of the NHC ($\text{CH}_{b/c}$) are observed as doublets at 5.03 and 5.89 ppm. The coordinated NHC is detected at 3.68 ppm ($\text{Me}_{e/g}\text{-CH}_3$) and the protons of the backbone at 5.82 ppm ($\text{CH}_{f/g}$).

The $^{11}\text{B}\{^1\text{H}\}$ NMR spectrum shows one sharp signal for the inserted boron atom (B_α) and one for the migrating boron atom (B_β) at 0.93 and -2.51 ppm.

In comparison to $\text{RER-B}_2\text{neop}_2\cdot(\text{nPr}_2\text{Im})_2$ **29**, which is stable in solution for several days, the ring expanded product $\text{RER-B}_2\text{neop}_2\cdot(\text{Me}_2\text{Im})_2$ **30** was only stable for several hours in solution. In the case of NHC $\text{Me}_2\text{Im}^{\text{Me}}$, similar results were obtained; the reaction mixture turned from yellow to dark red, and after several hours, to dark brown. The *in situ* $^{11}\text{B}\{^1\text{H}\}$ NMR spectrum recorded after several minutes showed two sharp signals at 1.88 and -1.32 ppm for the two boron atoms (B_α and B_β), which confirm the formation of the ring expanded product; however, the NMR spectrum of the dark brown reaction mixture shows more signals, which could not be assigned to any known compound. Therefore, the reaction mixture was worked-up, while the reaction mixture was still yellow, and the ring expanded product $\text{RER-B}_2\text{neop}_2\cdot(\text{Me}_2\text{Im}^{\text{Me}})_2$ **31** was isolated (Scheme 99).



Scheme 99: Reaction of B_2neop_2 **5** with two equivalents of $\text{Me}_2\text{Im}^{\text{Me}}$ forming the ring expanded product $\text{RER-B}_2\text{neop}_2\cdot(\text{Me}_2\text{Im}^{\text{Me}})_2$ **31**.

$\text{RER-B}_2\text{neop}_2\cdot(\text{Me}_2\text{Im}^{\text{Me}})_2$ **31** was characterized *via* ^1H , $^{11}\text{B}\{^1\text{H}\}$ and $^{13}\text{C}\{^1\text{H}\}$ NMR spectroscopy. The ^1H NMR spectrum shows six signals in the region between 0.74 and 1.85 ppm, which belong to the methyl-groups of the neop-moiety as well as the methyl-groups at the backbone of the former NHC (Figure 67). Furthermore, in the region between 2.71 and 4.44 ppm, the corresponding signals for the methylene-groups of the neop-moiety could be detected. The methyl-groups of the nitrogen atoms in the heterocyclic ring are observed as sharp signals at 2.60 and 4.17 ppm. The corresponding chemical shifts for the exocyclic NHC are detected at 1.43 (C-CH_3) and 3.36 ppm (N-CH_3).

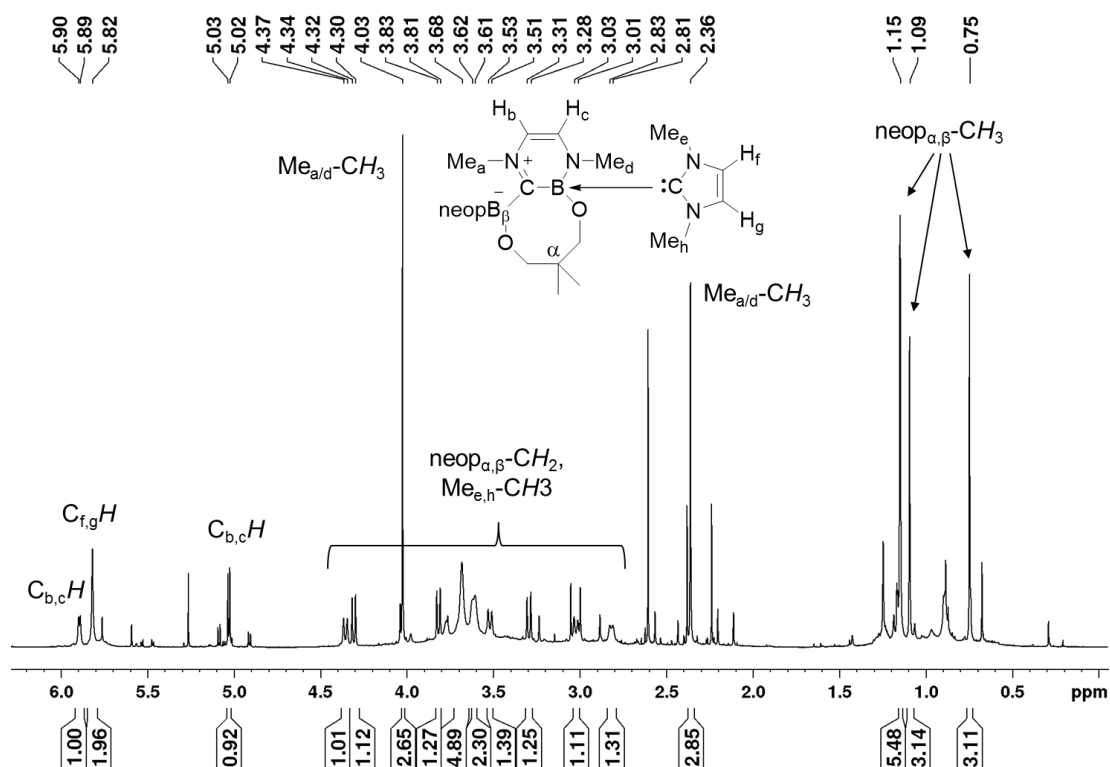


Figure 67: ^1H NMR spectrum of $\text{RER-B}_2\text{neop}_2\cdot(\text{Me}_2\text{Im}^{\text{Me}})_2$ **31** in C_6D_6 (500 MHz).

As already mentioned, in the $^{11}\text{B}\{^1\text{H}\}$ NMR spectrum, the two boron atoms (B_α and B_β) are observed at 1.88 and -1.32 ppm (Figure 68). Furthermore, the $^{13}\text{C}\{^1\text{H}\}$ NMR spectrum of $\text{RER-B}_2\text{neop}_2\cdot(\text{Me}_2\text{Im}^{\text{Me}})_2$ **31** shows the expected number of signals; however, due to the fact that compound **31** is not stable in solution for a long time, it was not possible to measure 2D NMR spectra (such as HBMBC, HSQC) to assign the signals to the corresponding carbon atoms. Nevertheless, the observed signals were compared with the ring expanded products $\text{RER-B}_2\text{neop}_2\cdot(n\text{Pr}_2\text{Im})_2$ **29** and $\text{RER-B}_2\text{neop}_2\cdot(\text{Me}_2\text{Im})_2$ **30**. The signals could be assigned to their respective carbon atoms.

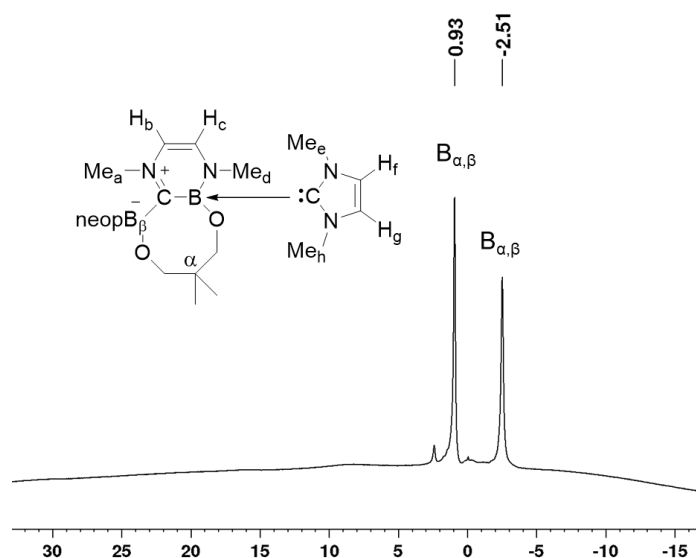


Figure 68: $^{11}\text{B}\{^1\text{H}\}$ NMR spectrum of RER- $\text{B}_2\text{neop}_2 \cdot (\text{Me}_2\text{Im}^{\text{Me}})_2$ **31** in C_6D_6 .

In summary, two different types of ring expanded products were obtained. Using B_2cat_2 as the diboron reagent led to the two ring expanded products RER- $\text{B}_2\text{cat}_2 \cdot (\text{Me}_2\text{Im}^{\text{Me}})_2$ **26** and RER- $\text{B}_2\text{cat}_2 \cdot (n\text{Pr}_2\text{Im})_2$ **27** at higher temperature. In contrast, ring expansion reactions using B_2neop_2 as the diboron compound yielded RER- $\text{B}_2\text{neop}_2 \cdot (n\text{Pr}_2\text{Im})_2$ **29** as well as RER- $\text{B}_2\text{neop}_2 \cdot (\text{NHC})_2$ (NHC = Me_2Im , $\text{Me}_2\text{Im}^{\text{Me}}$) **30** and **31**, even at room temperature. The core structure of both types is similar; however, they distinguish themselves in the coordination of the second Bcat-moiety and the exocyclic NHC. Whereas the NHC coordinates to the exo-Bcat-moiety in the case of the B_2cat_2 ring expanded product, the second NHC binds to the inserted Bneop-moiety, due to the ring-opening of the endocyclic neop-moiety, which led to the formation of the eight-membered heterocyclic ring (Figure 69).

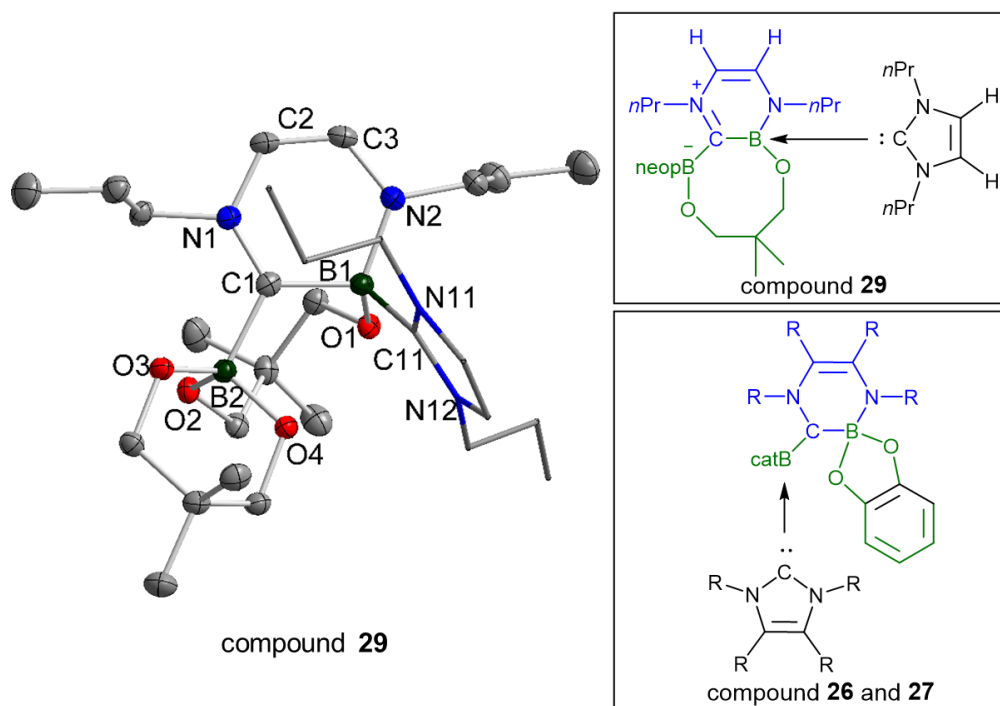
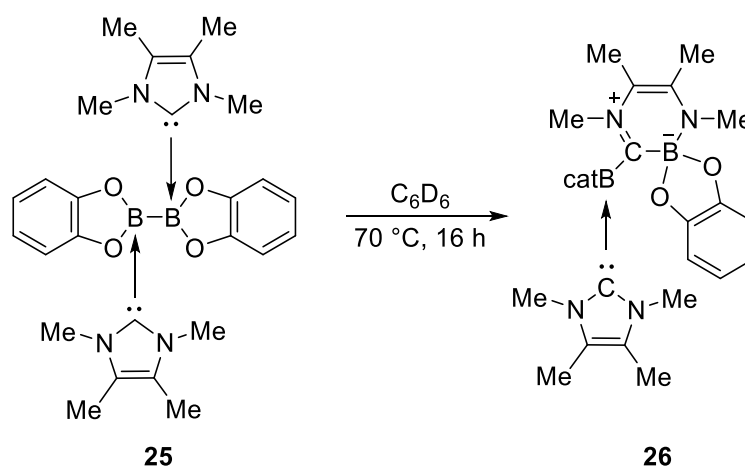


Figure 69: Comparison of ring expanded product $\text{RER-B}_2\text{neop}_2 \cdot (\text{nPr}_2\text{Im})_2$ **29** with the $\text{RER-B}_2\text{cat}_2 \cdot (\text{NHC})_2$ ($\text{NHC} = \text{Me}_2\text{Im}^{\text{Me}}$, nPr_2Im) **26** and **27**.

2.2.2.4. Experiments to determine the mechanism of the ring expansion reaction

The reactions of the diboron reagents B_2neop_2 **5** and B_2cat_2 **8** with different NHCs (Me_2Im^{Me} , nPr_2Im , Me_2Im , iPr_2Im^{Me}) in the ratio 1:1 and 1:2 yielded the mono-NHC adducts **18-21** and the bis-NHC adducts **22-25**. Furthermore, $B_2cat_2 \cdot Me_2Im^{Me}$ **18** and $B_2cat_2 \cdot (Me_2Im^{Me})_2$ **25** were compared, with respect to their stability in dichloromethane and the behavior at higher temperatures. As a result, the bis-NHC adduct **25** rearranges at higher temperature to the ring expanded product $RER-B_2cat_2 \cdot (Me_2Im^{Me})_2$ **26**, whereas the mono-NHC adduct **18** is stable for several hours.

To determine whether the bis-NHC-adduct **25** is a precursor to $RER-B_2cat_2 \cdot (Me_2Im^{Me})_2$ **26**, compound **25**•toluene was added to an NMR tube along with 0.6 ml C_6D_6 (Scheme 100). At room temperature, no reaction took place, but after heating the NMR tube at 70 °C overnight, the solid dissolved and the NMR spectra showed full conversion to the corresponding ring expanded product $RER-B_2cat_2 \cdot (Me_2Im^{Me})_2$ **26**.



Scheme 100: Rearrangement of the bis-NHC adduct $B_2cat_2 \cdot (Me_2Im^{Me})_2$ **25** at higher temperatures to form the ring expanded product $RER-B_2cat_2 \cdot (Me_2Im^{Me})_2$ **26**.

The corresponding 1H NMR spectra are depicted in Figure 70. The bottom shows the 1H NMR spectrum of compound **25**•toluene. Due to the fact that it is not soluble in C_6D_6 , only toluene was observed; however, heating the NMR tube to 70 °C led to a homogenous reaction mixture and the rearrangement to the corresponding ring expanded product and toluene were observed. To confirm these results, the obtained spectrum was compared to the 1H NMR spectrum of the isolated $RER-B_2cat_2 \cdot (Me_2Im^{Me})_2$ **26**.

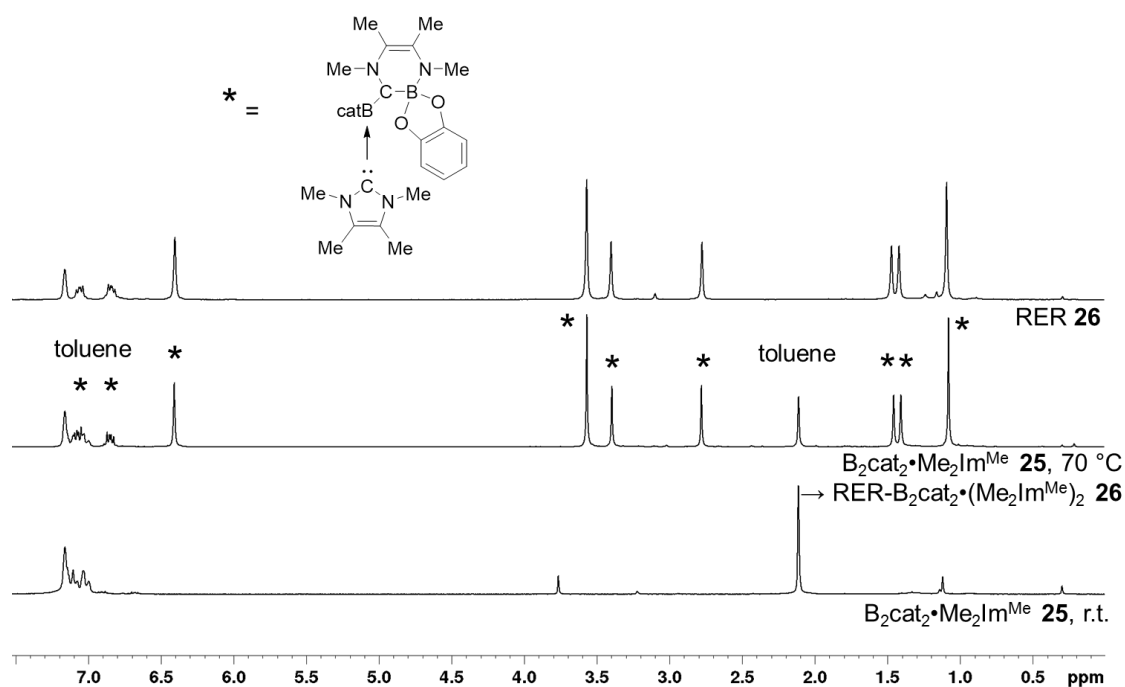
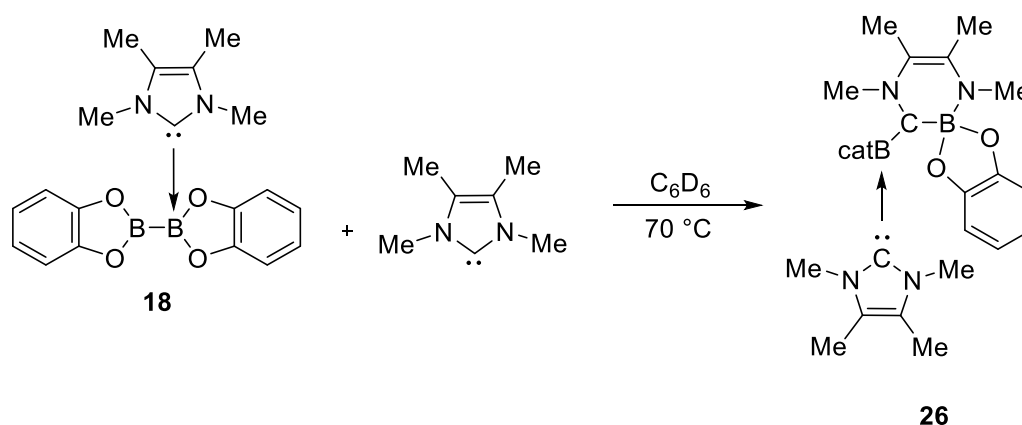


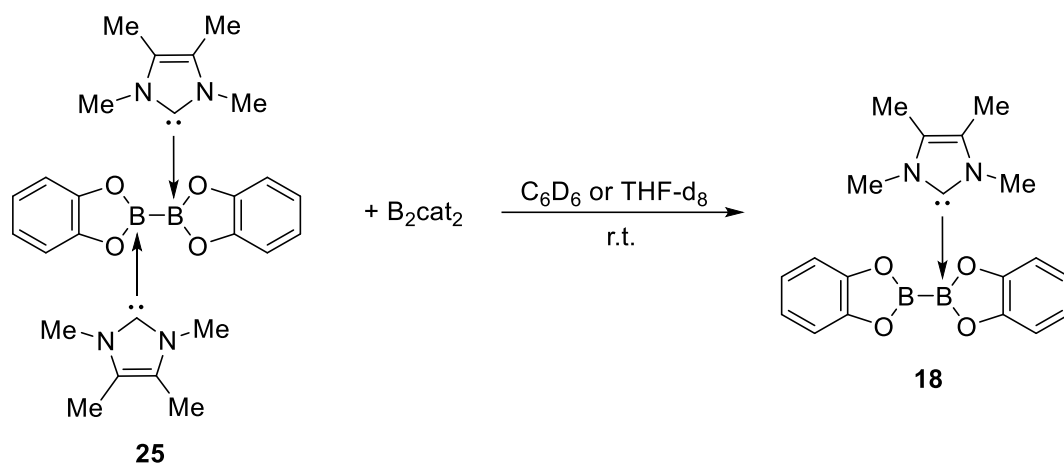
Figure 70: ^1H NMR spectra of the bis-NHC adduct $\text{B}_2\text{cat}_2\cdot(\text{Me}_2\text{Im}^{\text{Me}})_2$ **25** in C_6D_6 at room temperature, at $70\text{ }^\circ\text{C}$, which led to the ring expanded product $\text{RER-B}_2\text{cat}_2\cdot(\text{Me}_2\text{Im}^{\text{Me}})_2$ **26**, and for comparison see on the top the spectrum of the isolated $\text{RER-B}_2\text{cat}_2\cdot(\text{Me}_2\text{Im}^{\text{Me}})_2$ **26**; reproduced from ref. [253] with permission from Wiley-VCH.

Afterwards, the isolated mono-NHC adduct $\text{B}_2\text{cat}_2\cdot\text{Me}_2\text{Im}^{\text{Me}}$ **18** was reacted with the NHC $\text{Me}_2\text{Im}^{\text{Me}}$ to obtain the formation of the ring expanded product $\text{RER-B}_2\text{cat}_2\cdot(\text{Me}_2\text{Im}^{\text{Me}})_2$ **26** (Scheme 101). Immediately, a yellow solid precipitated; however, after heating the NMR tube at $70\text{ }^\circ\text{C}$ overnight, the solid re-dissolved in C_6D_6 and the ring expanded product $\text{RER-B}_2\text{cat}_2\cdot(\text{Me}_2\text{Im}^{\text{Me}})_2$ **26** was formed.



Scheme 101: Reaction of $\text{B}_2\text{cat}_2\cdot\text{Me}_2\text{Im}^{\text{Me}}$ **18** with $\text{Me}_2\text{Im}^{\text{Me}}$ at higher temperature to form the ring expanded product $\text{RER-B}_2\text{cat}_2\cdot(\text{Me}_2\text{Im}^{\text{Me}})_2$ **26**.

Furthermore, to determine whether the formation of the bis-NHC adduct $\text{B}_2\text{cat}_2\cdot(\text{Me}_2\text{Im}^{\text{Me}})_2$ **25** is reversible, NMR spectra of the reaction of the mono-NHC adduct $\text{B}_2\text{cat}_2\cdot\text{Me}_2\text{Im}^{\text{Me}}$ **18** and one equivalent B_2cat_2 were recorded (Scheme 102).



Scheme 102: Reaction of bis-NHC adduct $B_2cat_2 \cdot (Me_2Im^{Me})_2$ **25** with one equivalent B_2cat_2 to form the mono-NHC adduct $B_2cat_2 \cdot Me_2Im^{Me}$ **18**.

The bis-NHC diboron adduct $B_2cat_2 \cdot (Me_2Im^{Me})_2$ **25**•toluene immediately reacts with added B_2cat_2 to give the mono-NHC diboron adduct $B_2cat_2 \cdot Me_2Im^{Me}$ **18**. This observation was confirmed by 1H NMR spectroscopy. After 10 minutes, the mono-NHC adduct $B_2cat_2 \cdot Me_2Im^{Me}$ **18** (Figure 71).

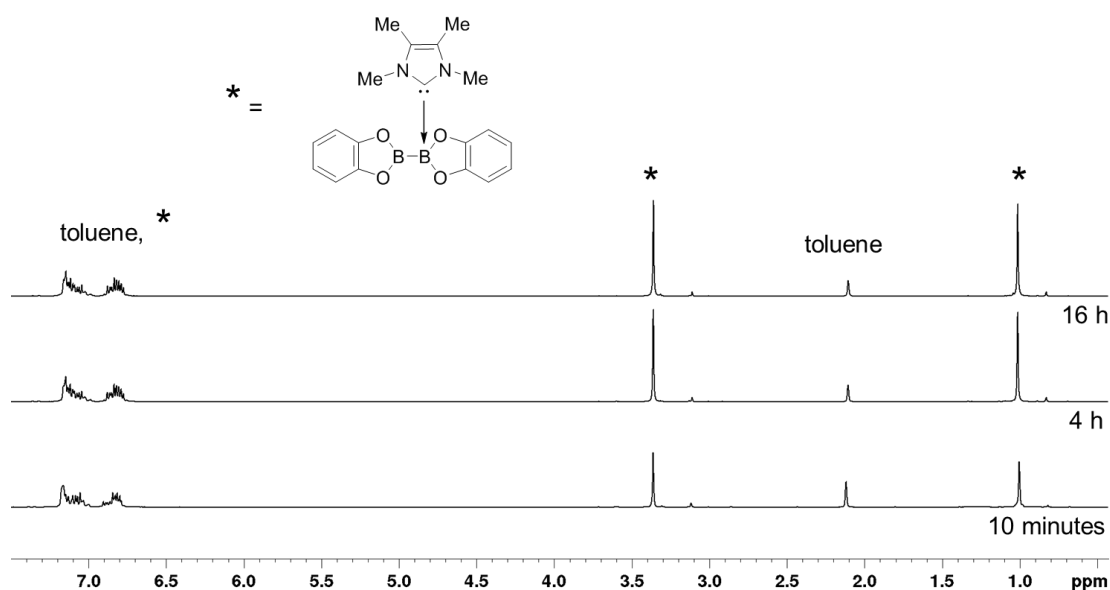


Figure 71: *In situ* 1H NMR spectrum of the reaction of bis-NHC adduct $B_2cat_2 \cdot (Me_2Im^{Me})_2$ **25** with one equivalent of B_2cat_2 in C_6D_6 to give the mono-NHC adduct $B_2cat_2 \cdot Me_2Im^{Me}$ **18**. The NMR spectra were measured at room temperature after 10 minutes, 4 and 16 hours; reproduced from ref. [253] with permission from Wiley-VCH.

2.2.2.5. Ring expansion reactions involving the saturated NHC Dipp₂SI_m and B₂cat₂ as the boron reagent

Theoretical investigations

Computational studies on the mechanism of borane, silane and beryllium hydride RERs disclosed that the ring insertion mechanisms are, in general, similar for these main-group element hydrides.^[242-247, 258] The principal mechanism can be divided into four steps that include: i) adduct formation between the Lewis-basic NHC and the Lewis-acidic element hydride; ii) hydride migration from the element hydride to the NHC carbene carbon atom; iii) C–N bond cleavage and ring expansion of the NHC with insertion of the main-group element moiety into the NHC ring; and iv) stabilization of the ring expanded NHC, for example *via* migration of another hydrogen atom to the (former) NHC carbene carbon atom (Figure 72). Moreover, the second step of this sequence, e.g. hydrogen migration to the NHC carbene carbon atom *via* activation of one of the E–H bonds of the main-group element hydride, is the rate limiting step according to these calculations, associated with the highest barrier on the energy surface. Calculations reported by Wilson and Dutton *et al.*^[243] for the reaction of the NHC Me₂Im with Ph₂SiH₂ have shown, that an initial, endothermic formation of an adduct SiH₂Ph₂•(Me₂Im), five-coordinated at silicon and repulsive on the energy hyper surface, is required. This adduct lies 56.4 kJ·mol⁻¹ above the starting materials. The crucial transition state for the hydrogen atom transfer may be described as an NHC-H-SiHPh₂ σ -complex, 113.4 kJ·mol⁻¹ higher in energy compared to the starting reactants. This barrier is in agreement with the experimentally observed high temperature conditions for the reaction. It is also in accordance with our experimental finding^[259] that the kinetics of the reaction of *t*Pr₂Im with Ph₂SiH₂ follows a second order rate law (first order in both, NHC and silane), whereas the ring expansion reaction of isolated 1,3-bis-(2,6-di-*iso*-propylphenyl)-2-(phenylsilyl)-imidazolidine follows first order kinetics.

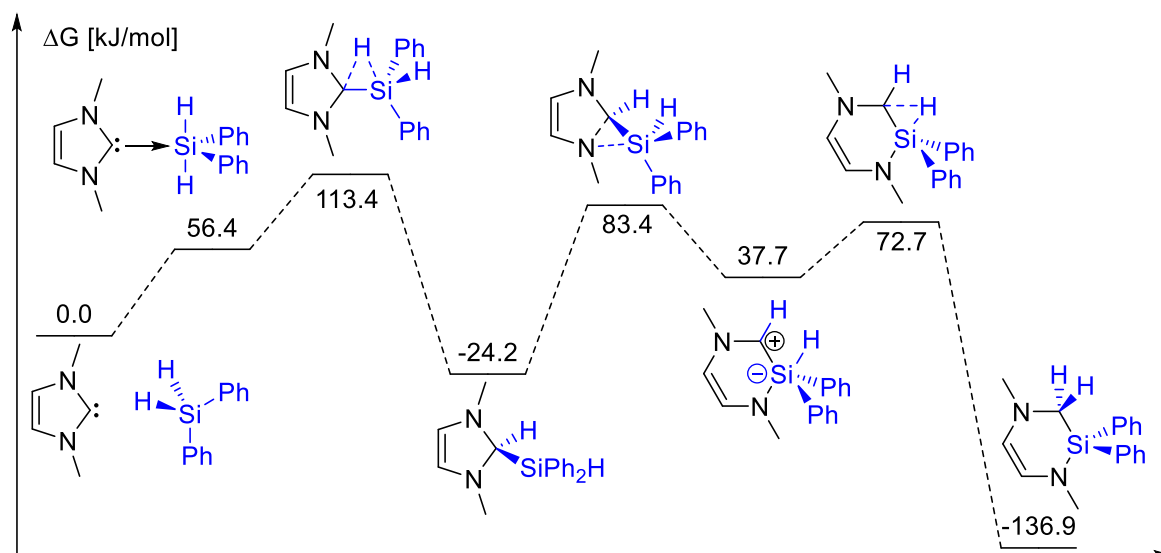
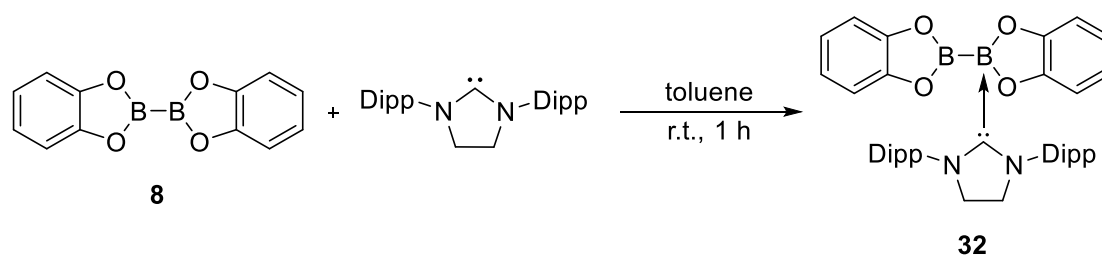


Figure 72: DFT investigations on the reaction mechanism of an NHC with H_2SiPh_2 .^[243]

Recently, Wilson, Dutton *et al.* reported DFT calculations on the reaction pathway using both NHCs, unsaturated and saturated at the backbone of the NHC.^[245] Their results confirmed the experimental observations by the groups of Bertrand *et al.* and Radius *et al.* that the reaction of the silane PhSiH_3 with the saturated NHC Dipp_2Slm yielded in the Si–H activation product $\text{Dipp}_2\text{Slm}(\text{H})\text{SiH}_2\text{Ph}$; however, heating the isolated product or the reaction mixture to $100\text{ }^\circ\text{C}$ for several days yielded the ring expanded product. Additionally, they reported that the ring expansion reaction should be faster using saturated NHCs, due to the lower energetically barrier. Thus, the Si–H activation product gives a lower barrier than the adduct formation between the silane and the NHC. Furthermore, another important observation is the aromatic character of the NHC, while saturated NHCs have a non-aromatic character, unsaturated NHCs lose their aromaticity *via* insertion of the main-group element and migration of the hydrides to the former carbene carbon atom.^[245]

Experimental investigations

To prove these theoretical results,^[245] the reaction of B_2cat_2 with the saturated NHC Dipp_2Slm was recorded at room and elevated temperatures (Scheme 103).



Scheme 103: Reaction of B_2cat_2 with the saturated NHC Dipp_2Slm to form the mono-NHC diboron adduct $\text{B}_2\text{cat}_2\cdot\text{Dipp}_2\text{Slm}$ **32** at room temperature.

The mono-NHC adduct $B_2cat_2 \cdot Dipp_2Slm$ **32** was characterized *via* NMR spectroscopy, elemental analysis and high resolution mass spectrometry as well as single X-ray diffraction. In the 1H NMR spectrum, two doublets for the methyl-groups of the Dipp-substituent are detected at 1.09 and 1.31 ppm as well as one septet at 3.35 ppm for the methine protons (Figure 73). The aryl-CH protons of the Dipp-moiety resonate as multiplets at 6.97-6.99 and 7.03-7.13 ppm. Furthermore, the saturated backbone CH_2 -groups of the NHC are observed as a singlet at 3.51 ppm. The chemical shifts for the catechol-groups of the B_2cat_2 are detected as four multiplets at 6.35-6.40, 6.48-6.53, 6.74-6.79 and 6.91-6.95 ppm.

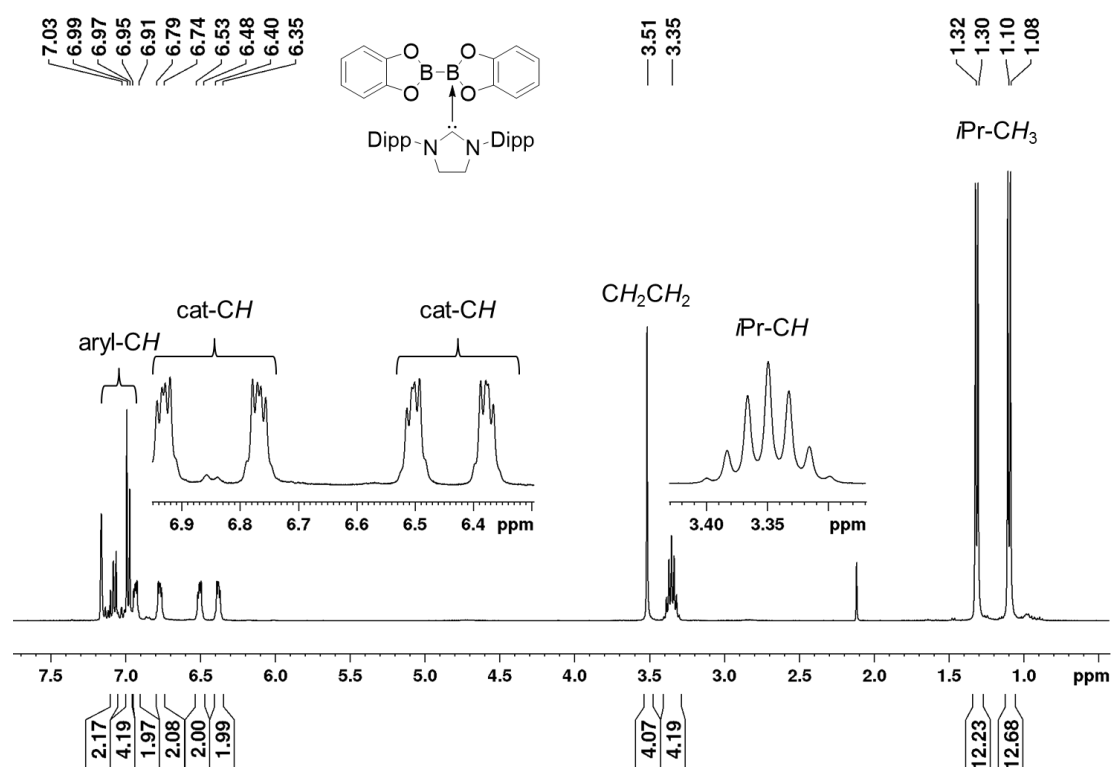


Figure 73: 1H NMR spectrum of the mono-NHC diboron adduct $B_2cat_2 \cdot Dipp_2Slm$ **32** in C_6D_6 (400 MHz).

In the $^{11}B\{^1H\}$ NMR spectrum, two signals are observed, one for the sp^3 -B atom at 7.10 ppm and one broad signal at 37.8 ppm for the sp^2 -B atom (Figure 74). The $^{13}C\{^1H\}$ NMR spectrum shows signals for the Dipp-substituent of the NHC as well as for the catechol-moiety of the B_2cat_2 . In comparison to the carbene carbon atom of the NHC $Dipp_2Slm$, which is detected at 244.0 ppm, the carbene carbon atom of the coordinated NHC resonates at 186.7 ppm. These results are in good agreement with the obtained data found for the mono-NHC diboron adducts $B_2cat_2 \cdot Me_2Im^{Me}$ **18** and $B_2cat_2 \cdot Dipp_2Im$ **19**.

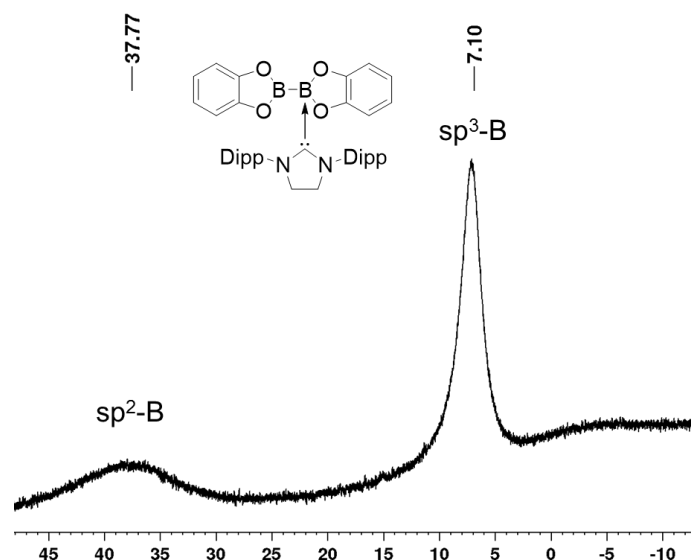


Figure 74: $^{11}\text{B}\{^1\text{H}\}$ NMR spectrum of the mono-NHC diboron adduct $\text{B}_2\text{cat}_2\cdot\text{Dipp}_2\text{Slm}$ **32** in C_6D_6 .

Furthermore, single crystals were obtained in order to characterize compound **32** via X-ray diffraction which confirmed the structure of the mono-NHC diboron adduct $\text{B}_2\text{cat}_2\cdot\text{Dipp}_2\text{Slm}$ **32** (Figure 75). Compound **32** crystallizes with two molecules in the asymmetric unit. The molecular structure of compound **32** is similar to the reported structures of $\text{B}_2\text{cat}_2\cdot\text{Me}_2\text{Im}^{\text{Me}}$ **18** and $\text{B}_2\text{cat}_2\cdot\text{Cy}_2\text{Im}$.^[51, 256] The boron atom B1 is essentially planar, while B2 is tetrahedral. The B–B distance (**32a**: 1.727(2) Å and **32b**: 1.731(2) Å) is shorter than the one found in the molecular structure of compound **18** and $\text{B}_2\text{pin}_2\cdot\text{Cy}_2\text{Im}$ (B1–B2: **18**: 1.729(3) Å; 1.743(2) Å),^[51, 256] but much longer in comparison to the B1–B2 distance in B_2cat_2 (1.678(3) Å)^[260]. The B2–C1 (**32a**: 1.645(2) Å and **32b**: 1.669(2) Å) distance is also slightly shorter than the one found in the other two mono-NHC adducts (C1–B2: **18**: 1.647(2) Å; 1.673(2) Å).

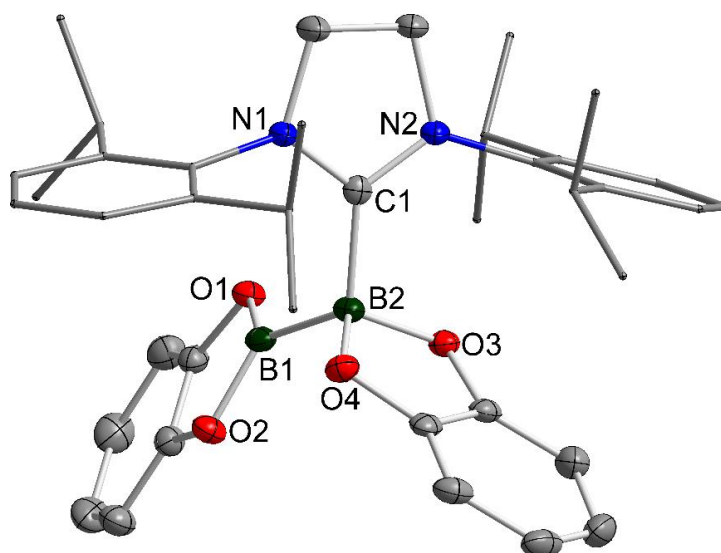
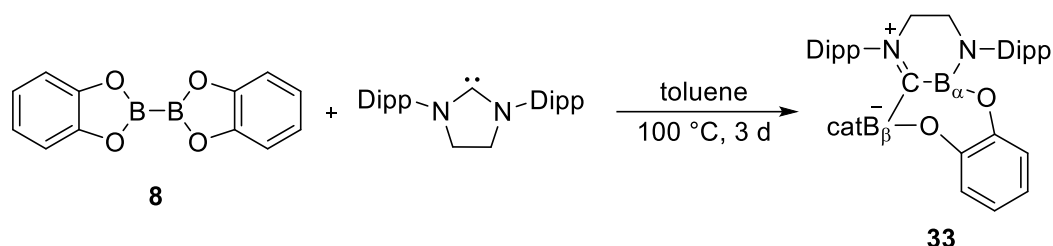


Figure 75: Molecular structure of $B_2cat_2 \cdot Dipp_2Slm$ **32** with thermal ellipsoids drawn at the 50% probability level; hydrogen atoms are omitted and the Dipp-substituents are drawn as wires/sticks for clarity. Compound **32** crystallizes with two molecules in the asymmetric unit. Selected bond distances (Å) and angles (°) for molecule **32a**: B2–C1 1.645(2), B1–B2 1.727(2), B1–O1 1.503(2), B1–O2 1.505(2), B2–O3 1.398(2), B2–O4 1.398(2); C1–B2–B1 112.53(11). Selected bond distances (Å) and angles (°) for molecule **32b**: B2–C1 1.669(2), B1–B2 1.731(2), B1–O1 1.501(2), B1–O2 1.497(2), B2–O3 1.395(2), B2–O4 1.398(2); C1–B2–B1 112.18(11).

The next step was the reaction of B_2cat_2 **8** and $Dipp_2Slm$ at elevated temperatures to determine whether 1) the mono-NHC adduct $B_2cat_2 \cdot Dipp_2Slm$ **32** is stable at elevated temperatures or 2) compound **32** rearranges to a further ring expanded product (Scheme 104).



Scheme 104: Reaction of B_2cat_2 with the saturated NHC $Dipp_2Slm$ which forms the ring expanded product $RER-B_2cat_2 \cdot Dipp_2Slm$ **33** at higher temperatures.

In comparison to the synthesis of the mono-NHC adduct $B_2cat_2 \cdot Dipp_2Slm$ **32** which gave a colorless reaction mixture, the solution of B_2cat_2 and $Dipp_2Slm$ in toluene changed from colorless to orange at higher temperatures. The *in situ* ^{11}B NMR spectrum, recorded after 3 days at 70 °C, showed two signals at 7.38 and 26.5 ppm which are slightly different from the observed signals for compound **32** (7.10 and 37.8 ppm). After work-up, an orange solid was isolated in good yield (72%) which was identified as the ring expanded product $RER-B_2cat_2 \cdot Dipp_2Slm$ **33**.

Compound **33** was characterized *via* NMR spectroscopy, elemental analysis and X-ray diffraction. In the 1H NMR spectrum, the signals of the methyl-groups of the *i*Pr-groups are split into four doublets at 0.94, 1.12, 1.26 and 1.37 ppm, due to the loss of symmetry (Figure 76).

Therefore, two septets for the methine protons were also detected at 2.75 and 3.26 ppm. The same effect is observed for the protons at the backbone of the NHC which resonate as two multiplets at 2.99-3.04 and 3.40-3.45 ppm. Additionally, the protons of the aryl-groups of the Dipp-substituent appear as multiplets between 6.49-7.29 ppm. The resonances of the catechol-moiety are split into three signals, two for the cat-group which opens at 6.49-6.54 and 6.55-6.60 ppm, and the cat_β-moiety resonates at 7.12-7.20 ppm.

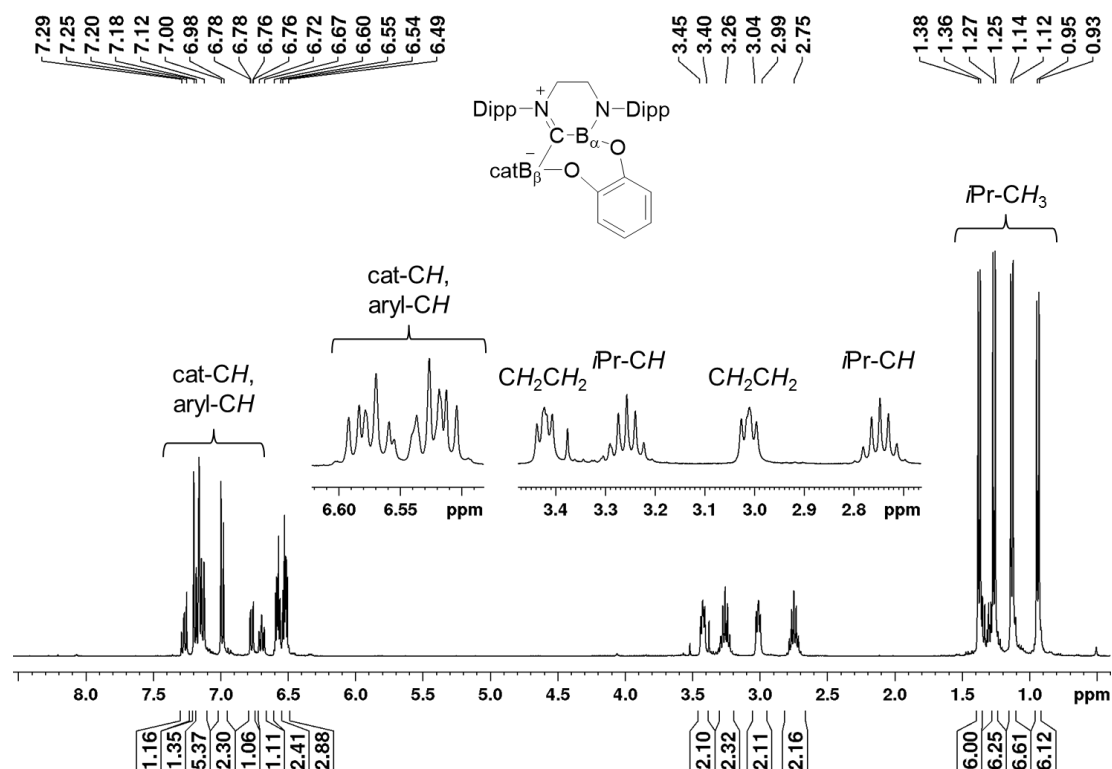


Figure 76: ¹H NMR spectrum of the ring expanded product RER-B₂cat₂•Dipp₂Slm **33** in C₆D₆ (400 MHz).

In the ¹¹B{¹H} NMR spectrum, one sharp signal for the sp³-B atom (B_β) is observed at 7.37 ppm and the boron which inserts into the C–N bond is detected as a broad signal at 26.6 ppm (Figure 77). Because of the lack of symmetry, in the ¹³C{¹H} NMR spectrum, separate signals are observed for the Dipp-substituents as well as for the two carbon atoms of the backbone. The former carbene carbon atom resonates at 215.8 ppm. The carbon atoms of the aryl-CH-groups are detected as six signals between 120.9 and 129.7 ppm. The corresponding quaternary carbon atoms resonate at 143.4-146.2 ppm. Additionally, the cat-CH-groups of the opened catechol-moiety are detected at 109.9 and 118.6 ppm. The carbon atoms of the catechol-group of the exocyclic boron resonates at 124.7 ppm. Furthermore, the quaternary carbon atoms of the catechol-groups are observed at 138.8, 141.3 and 152.7 ppm.

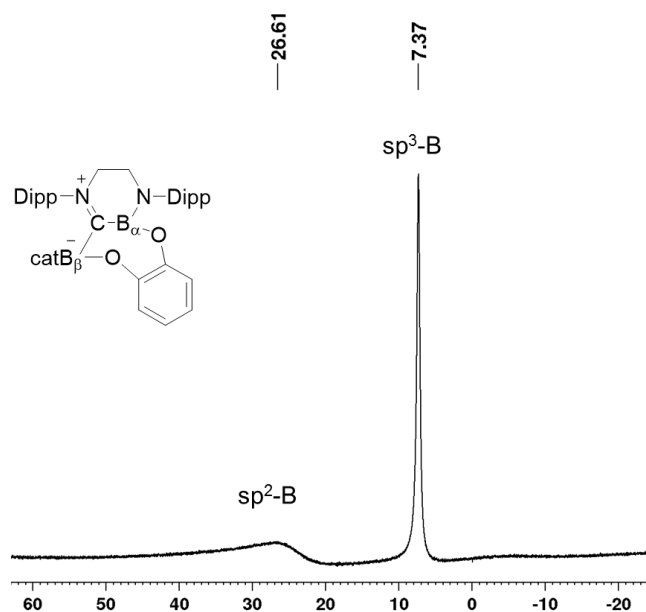


Figure 77: $^{11}\text{B}\{^1\text{H}\}$ NMR spectrum of the ring expanded product $\text{RER-B}_2\text{cat}_2\cdot\text{Dipp}_2\text{Slm}$ **33** in C_6D_6 .

The molecular structure of the ring expanded product $\text{RER-B}_2\text{cat}_2\cdot\text{Dipp}_2\text{Slm}$ **33** is similar to those of the ring expanded products involving B_2cat_2 and B_2neop_2 with unsaturated NHCs $\text{RER-B}_2\text{cat}_2\cdot(\text{NHC})_2$ **26** and **27** as well as $\text{RER-B}_2\text{neop}_2\cdot(n\text{Pr}_2\text{Im})_2$ **29** in so far as the core structure of the six-membered heterocyclic ring is similar (Figure 78).^[256]

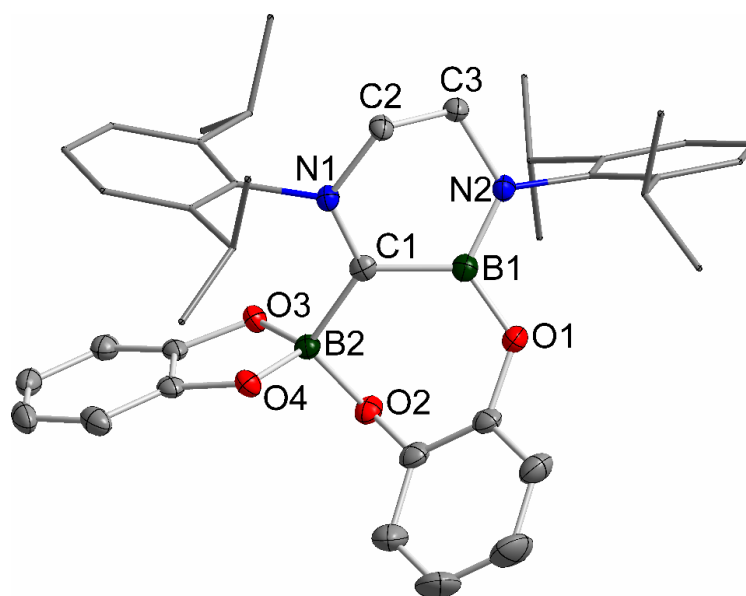


Figure 78: Molecular structure of $\text{RER-B}_2\text{cat}_2\cdot\text{Dipp}_2\text{Slm}$ **33** with thermal ellipsoids drawn at the 50% probability level; hydrogen atoms are omitted and the Dipp-substituents are drawn as wires/sticks for clarity. Selected bond distances (Å) and angles ($^\circ$): B1–C1 1.589(2), C1–N1 1.293(2), N1–C2 1.418(2), C2–C3 1.502(2), C3–N2 1.458(2), N2–B1 1.390(2), C1–B2 1.646(3), B1–O1 1.359(2), B2–O2 1.465(2), B2–O3 1.465(2), B2–O4 1.468(2); C1–B1–N2 116.19(13), B1–N2–C3 120.16(13), N2–C3–C2 110.39(13), C3–C2–N1 110.60(12), C2–N1–C1 120.53(12), N1–C1–B1 115.38(14), B1–C1–B2 121.50(12).

One boron atom inserts into the C–N bond of the NHC and the second boron atom migrates to the former carbene carbon atom. There are, however, two main differences. First, the

binding of the catechol-groups is different. In comparison to the ring expanded products **26** and **27**, the catechol-moiety of the inserted Bcat-group opens and coordinates to the exocyclic boron atom B_{β} ; however, these observations are similar to those seen in the molecular structure of $RER-B_2neop_2 \cdot (nPr_2Im)_2$ **29**. The second difference is the stabilization of the molecule. In compounds **26**, **27** and **29**, a second NHC coordinates to the exocyclic boron atom to give two sp^3 -hybridized boron atoms; however, in the case of $RER-B_2cat_2 \cdot Dipp_2Slm$ **33**, a second NHC is not needed to stabilize the molecule. In addition, a coordination of a second NHC to the endocyclic boron atom is sterically hindered due to the Dipp-substituent. The endocyclic sp^2 -hybridized boron atom is stabilized by the lone pair of the nitrogen atom as well as the former carbene carbon atom. The geometry of the exocyclic boron atom is tetragonal and is saturated by the three oxygen atoms and the former carbene carbon atom. Furthermore, to compare the experimental investigations with the theoretical studies, the reaction of B_2cat_2 with $Dipp_2Im$ (see, chapter 2.2.1.1) was repeated at higher temperatures; however, the obtained mono-NHC diboron adduct $B_2cat_2 \cdot Dipp_2Im$ **19** is stable and no formation of any ring expanded product is observed.

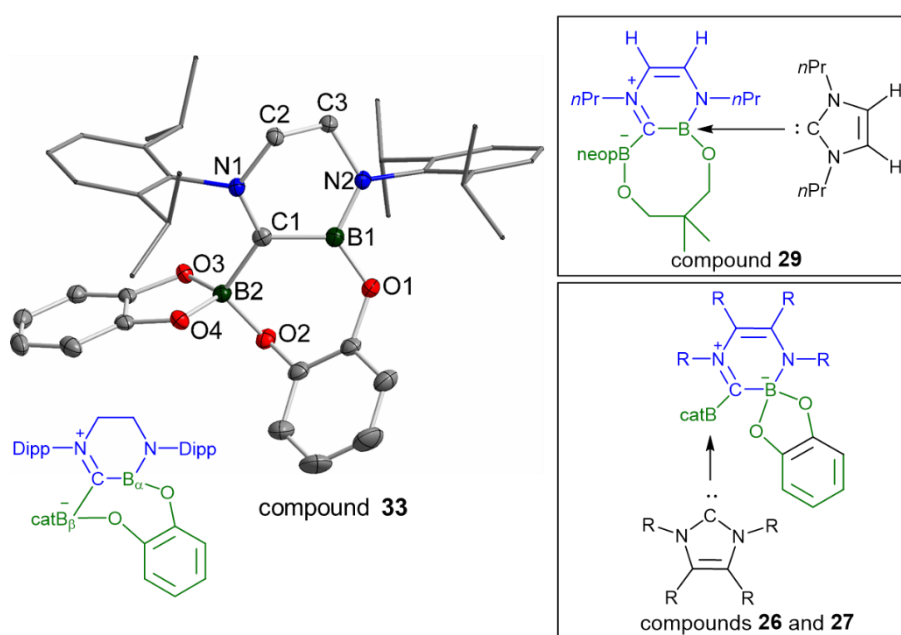


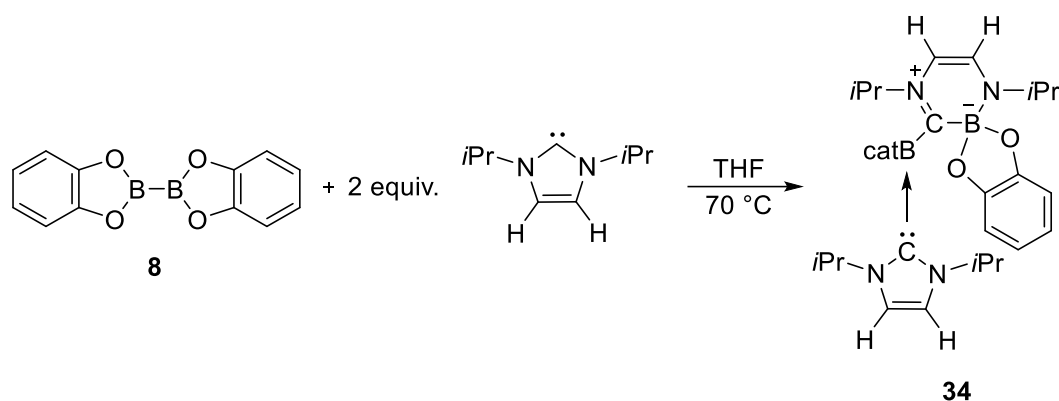
Figure 79: Comparison of ring expanded product $RER-B_2cat_2 \cdot Dipp_2Slm$ **33** with the ring expanded products involving B_2cat_2 or B_2neop_2 and unsaturated NHCs, $RER-B_2cat_2 \cdot (NHC)_2$ **26** and **27** as well as $RER-B_2neop_2 \cdot (nPr_2Im)_2$ **29**.

In summary, three different types of ring expanded products were obtained (Figure 79). The reaction of B_2cat_2 with unsaturated NHCs (Me_2Im^{Me} and nPr_2Im) yielded the ring expanded products $RER-B_2cat_2 \cdot (Me_2Im^{Me})_2$ **26** and $RER-B_2cat_2 \cdot (nPr_2Im)_2$ **27**. The reaction involving B_2neop_2 instead of B_2cat_2 yielded the ring expanded products $RER-B_2neop_2 \cdot (nPr_2Im)_2$ **29**, $RER-B_2neop_2 \cdot (Me_2Im)_2$ **30** and $RER-B_2neop_2 \cdot (Me_2Im^{Me})_2$ **31**. Furthermore, the mono-NHC

adduct $B_2cat_2 \cdot Dipp_2Slm$ **32** was synthesized which was identified as a precursor to the ring expanded product $RER-B_2cat_2 \cdot Dipp_2Slm$ **33**.

2.2.2.6. Additional molecular structures of products of ring expansion reactions

Based on our observation, that the reactions of the diboron reagents B_2cat_2 and B_2neop_2 with the Me_2Im^{Me} and nPr_2Im as well as Me_2Im at room or higher temperatures led to the ring expanded products $RER-B_2cat_2 \cdot (NHC)_2$ **26** and **27** as well as $RER-B_2neop_2 \cdot (NHC)_2$ **29-31**, further reactions were investigated with the NHC iPr_2Im and B_2cat_2 (Scheme 105).



Scheme 105: Reaction of B_2cat_2 **8** with two equivalents iPr_2Im at $70\text{ }^\circ\text{C}$.

The reaction was carried out under the same conditions as were used for the synthesis of $RER-B_2cat_2 \cdot (NHC)_2$ **26** and **27**; however, the reaction mixture turned dark red (instead of yellow) and the recorded $^{11}B\{^1H\}$ NMR spectrum shows more than the two expected signals at 6.39 and 7.00 ppm (Figure 80). The signal at 14.3 ppm belongs to the decomposition product $[Bcat_2]^-$.

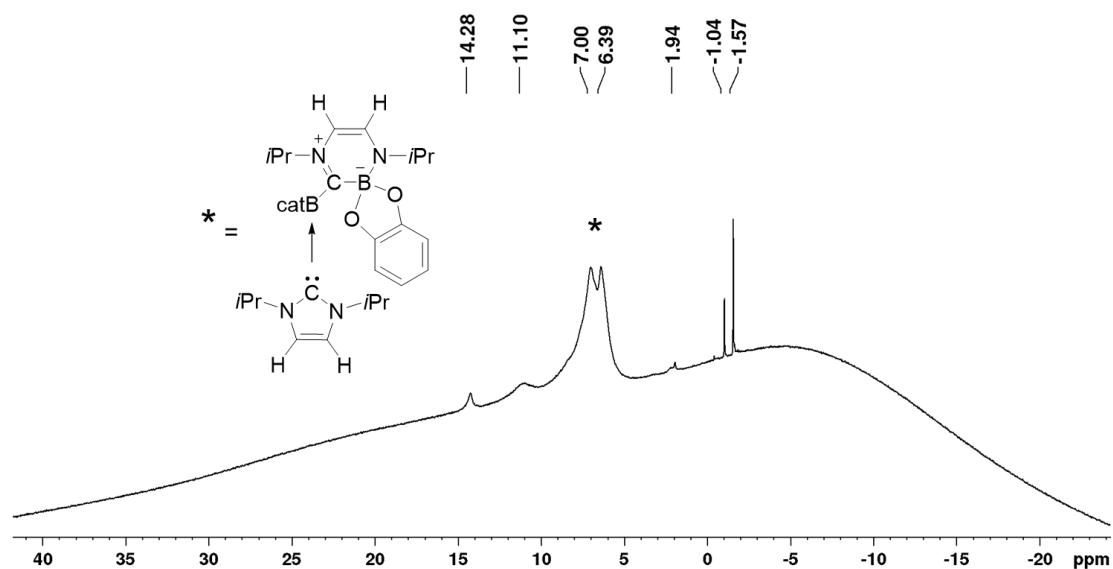


Figure 80: $^{11}\text{B}\{^1\text{H}\}$ NMR spectrum of the solid which was isolated after work-up of the reaction of B_2cat_2 with $i\text{Pr}_2\text{Im}$.

The mother liquor was cooled to $-30\text{ }^\circ\text{C}$ to obtain single crystals from the saturated solution of B_2cat_2 and two equivalents of $i\text{Pr}_2\text{Im}$; however, the molecular structure was characterized as the bis-NHC adduct of B_2cat_3 and $i\text{Pr}_2\text{Im}$, $\text{B}_2\text{cat}_3\cdot(i\text{Pr}_2\text{Im})_2$ **35** (Figure 81). The two Bcat-moieties are bridged by another catechol-group and one $i\text{Pr}_2\text{Im}$ is coordinated to each of the boron atoms. The analogous compound $\text{B}_2\text{eg}_3\cdot(i\text{Pr}_2\text{Im})_2$ was also observed as a decomposition product from the reaction of B_2eg_2 with $i\text{Pr}_2\text{Im}$ in a 1:2 ratio in the group lately.^[261]

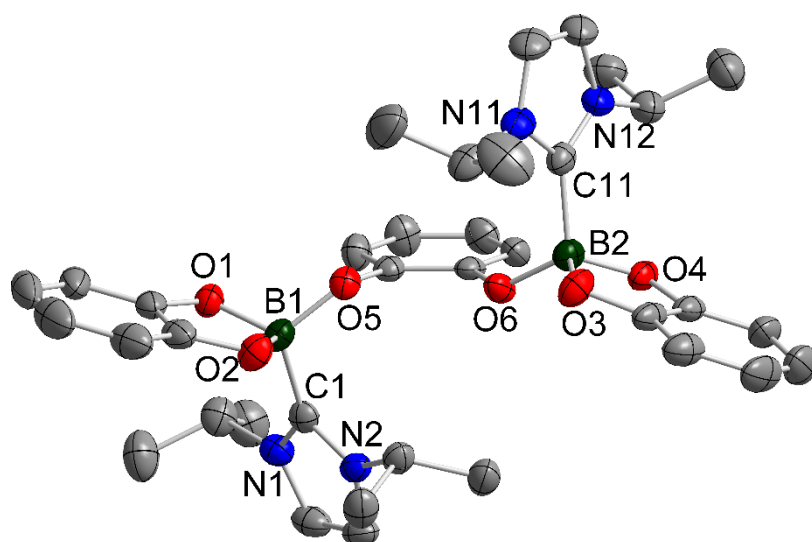


Figure 81: Molecular structure of $\text{B}_2\text{cat}_3\cdot(i\text{Pr}_2\text{Im})_2$ **35** with thermal ellipsoids drawn at the 50% probability level; hydrogen atoms are omitted for clarity. Selected bond distances (Å) and angles ($^\circ$): C1–B1 1.651(4), B1–O1 1.495(3), B1–O2 1.481(3), B1–O5 1.447(3), B2–C11 1.664(4), B2–O3 1.489(3), B2–O4 1.495(3), B2–O6 1.440(3); C1–B1–O1 110.62(19), C1–B1–O2 109.17(19), C1–B1–O5 110.14(19), C11–B2–O3 108.5(2), C11–B2–O4 109.78(19), C11–B2–O6 111.3(2).

In addition to the recorded NMR data and the decomposition product $B_2cat_3 \cdot (iPr_2Im)_2$ **35**, further single crystals for X-ray diffraction were obtained; however, the structure obtained was not the expected ring expanded product $RER-B_2cat_2 \cdot (iPr_2Im)_2$ **34**, but a related ring expanded compound $RER-HBcat \cdot (iPr_2Im)_2$ **36** (Figure 82). The core structure of both types is the same, the C–N bond of the NHC was cleaved and the Bcat-moiety inserted into the ring, albeit, the second NHC coordinated to the former carbene carbon atom and instead of the second Bcat-group a hydrogen atom is bound to the carbon atom.

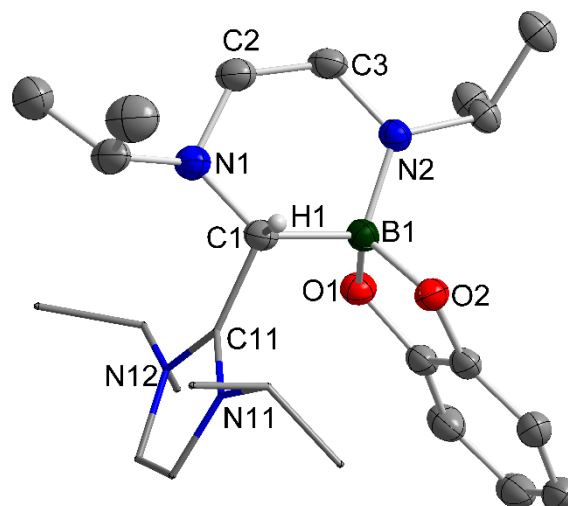


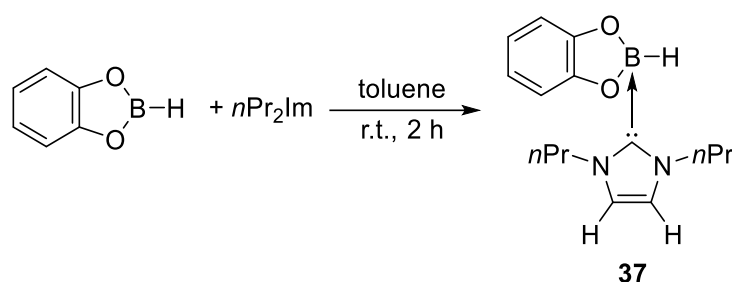
Figure 82: Molecular structure of compound $RER-HBcat \cdot (iPr_2Im)_2$ **36** with thermal ellipsoids drawn at the 50% probability level; hydrogen atoms (besides H1) are omitted and the exocyclic NHC is drawn as wires/sticks for clarity. Selected bond distances (Å) and angles (°): C1–N1 1.456(3), N1–C2 1.415(3), C2–C3 1.341(3), C3–N2 1.388(3), N2–B1 1.491(3), B1–C1 1.657(3), B1–C11 1.488(3); C1–N1–C2 112.36(16), N1–C2–C3 124.68(18), C2–C3–N2 125.40(18), C3–N2–B1 118.67(15), N2–B1–C1 108.27(10), B1–C1–N1 116.96(14); N1–C2–C3–N2//N1–B1–N2 6.549(97); N1–C2–C3–N2//N1–C1–N2 17.611(10).

The isolation of the expected ring expanded product $RER-B_2cat_2 \cdot (iPr_2Im)_2$ **34** was not successful; however, the molecular structure of $RER-HBcat \cdot (iPr_2Im)_2$ **36** led to the question, whether it is possible to synthesize the corresponding ring expanded products *via* reaction of $HB(OR)_2$ (HBcat and HBpin) with two equivalents of the NHC. These reactions will be discussed in the following chapter.

2.2.3. Reaction of HB(OR)₂ with saturated and unsaturated NHCs as well as CAAC^{Me}

2.2.3.1. Synthesis of NHC adducts of the type HBcat•NHC

The first investigation was the reaction of HBcat with one equivalent of the NHC *n*Pr₂Im in toluene at room temperature. Due to the fact that the ¹¹B NMR spectrum showed full conversion of the starting material, the reaction mixture was worked-up and the corresponding mono-NHC adduct HBcat•*n*Pr₂Im **37** was isolated in good yield (Scheme 106).



Scheme 106: Reaction of HBcat and *n*Pr₂Im to form the mono-NHC adduct HBcat•*n*Pr₂Im **37**.

HBcat•*n*Pr₂Im **37** was characterized *via* NMR spectroscopy, elemental analysis and X-ray diffraction. The ¹H NMR spectrum shows one set of signals for the *n*Pr₂Im and for the HBcat (Figure 83). The methyl-groups of *n*Pr-moieties are observed at 0.60 ppm as a triplet, the methylene-groups at 1.44 ppm as a sextet. The signals for the *n*Pr-NCH₂ protons are detected as a multiplet at 3.77-3.80 ppm and the protons at the backbone at 5.79 ppm. In addition, the resonances of the catechol-groups are observed at 6.82-6.84 and 7.03-7.05 ppm. The chemical shift of the proton at the boron atom is 5.06 ppm and appears as a quartet and as a singlet in the ¹H{¹¹B} NMR spectrum.

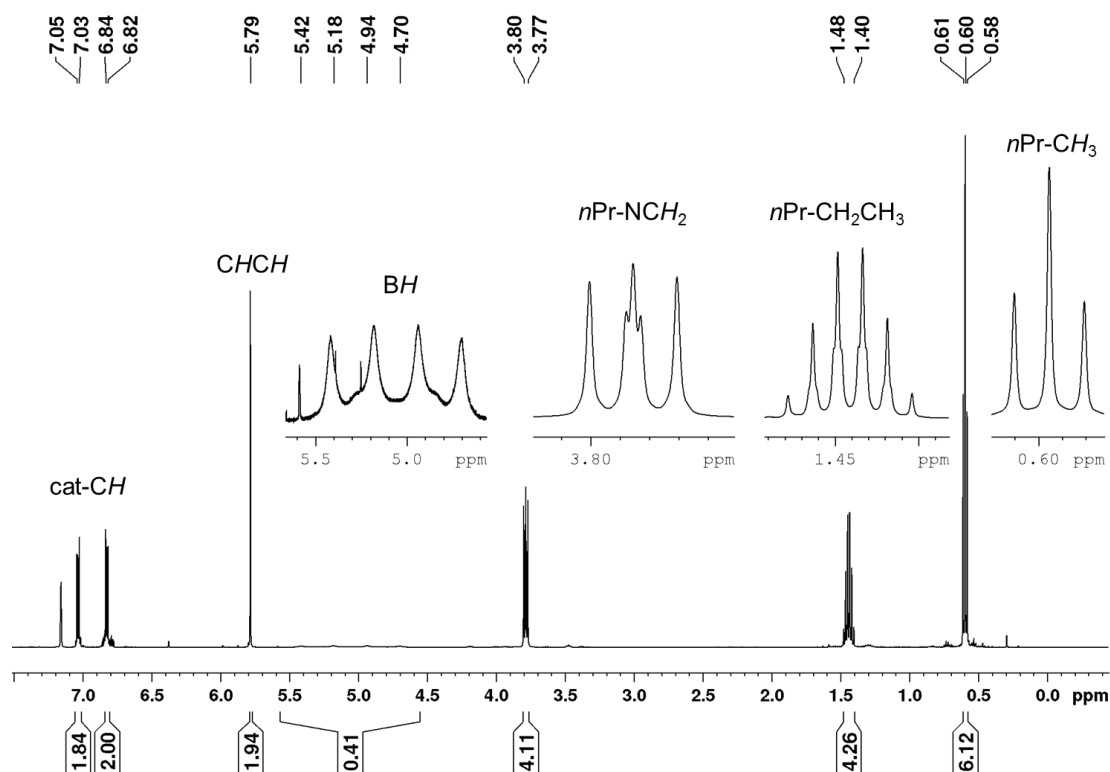


Figure 83: ^1H NMR spectrum of $\text{HBCat}\cdot n\text{Pr}_2\text{Im}$ **37** in C_6D_6 (500 MHz).

Furthermore, the ^{11}B NMR spectrum shows a doublet at 6.46 ppm ($^1J_{\text{BH}} = 119$ Hz) and the corresponding singlet in the proton decoupled NMR spectrum (Figure 84). The $^{13}\text{C}\{^1\text{H}\}$ NMR spectrum shows three signals for the carbon atom of the $n\text{Pr}$ -groups at 10.8 ($n\text{Pr-CH}_3$), 24.6 ($n\text{Pr-CH}_2\text{CH}_3$) and 50.2 ppm ($n\text{Pr-NCH}_2$) as well as one signal for the carbon atom at the backbone at 118.7 ppm. The resonances for the carbon atom of the catechol-groups are detected at 109.5 and 119.9 ppm. Furthermore, the quaternary carbon atom of the catechol-moieties is observed at 154.6 ppm and the carbene carbon atom at 161.0 ppm.

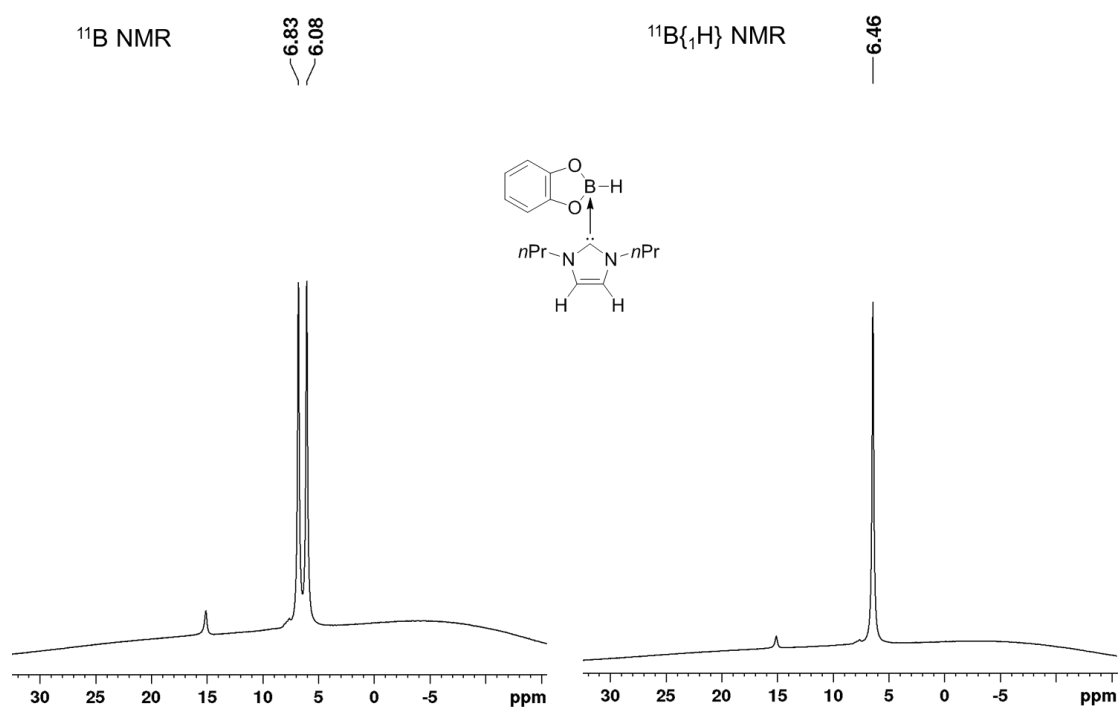


Figure 84: ^{11}B and $^{11}\text{B}\{^1\text{H}\}$ NMR spectrum of $\text{HBcat}\cdot n\text{Pr}_2\text{Im}$ **37** in C_6D_6 .

Additionally, single crystals for X-ray diffraction were obtained to confirm the structure of $\text{HBcat}\cdot n\text{Pr}_2\text{Im}$ **37** (Figure 85). The NHC $n\text{Pr}_2\text{Im}$ coordinates to the boron atom, which is then sp^3 -hybridized. The C1–B1 distance is with 1.631(3) Å in the range of the C1–B1 bond lengths as observed for the mono-NHC diboron adduct $\text{B}_2\text{cat}_2\cdot\text{Me}_2\text{Im}^{\text{Me}}$ **18**^[256] and $\text{B}_2\text{cat}_2\cdot\text{Dipp}_2\text{Im}$ **19** as well as $\text{B}_2\text{neop}_2\cdot i\text{Pr}_2\text{Im}^{\text{Me}}$ **21**.

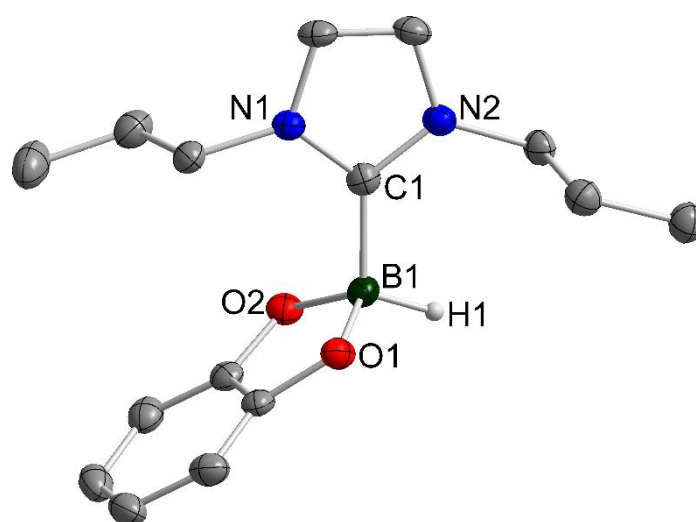
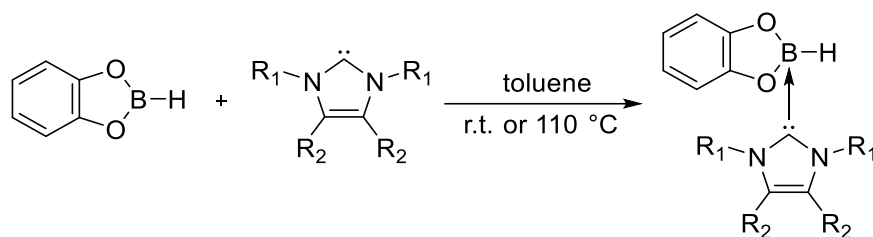


Figure 85: Molecular structure of $\text{HBcat}\cdot n\text{Pr}_2\text{Im}$ **37** with thermal ellipsoids drawn at the 50% probability level; hydrogen atoms (besides H1) are omitted for clarity. Selected bond distances (Å) and angles ($^\circ$): C1–B1 1.649(3), B1–O1 1.505(3), B1–O2 1.483(3); C1–B1–O1 109.85(16), C1–B1–O2 109.24(16).

In addition to the synthesized adduct $\text{HBcat}\cdot n\text{Pr}_2\text{Im}$ **37**, the reaction of HBcat with the NHCs $i\text{Pr}_2\text{Im}$ and $i\text{Pr}_2\text{Im}^{\text{Me}}$ yielded the mono-NHC adducts $\text{HBcat}\cdot i\text{Pr}_2\text{Im}$ **38** and $\text{HBcat}\cdot i\text{Pr}_2\text{Im}^{\text{Me}}$ **39**.

In comparison to both NHCs nPr_2Im and iPr_2Im , the reaction with iPr_2Im^{Me} was carried out at higher temperatures (Scheme 107).



Compound **38**: $R_1 = iPr$, $R_2 = H$

Compound **39**: $R_1 = iPr$, $R_2 = Me$

Scheme 107: Reaction of HBcat and iPr_2Im^R ($R = H$ **38**; Me **39**) to form the adduct HBcat• iPr_2Im **38** and HBcat• iPr_2Im^{Me} **39**.

HBcat• iPr_2Im **38** and HBcat• iPr_2Im^{Me} **39** were characterized by 1H , ^{11}B and $^{13}C\{^1H\}$ NMR spectroscopy as well as X-ray diffraction and elemental analysis and high resolution mass spectrometry (compound **39**). The obtained NMR data show similar chemical shifts as observed for HBcat• nPr_2Im **37**; however, the signals for the two NHCs are quite different. The resonances for the iPr -moiety of HBcat• iPr_2Im **38** are detected at 0.93 ($iPr-CH_3$) and 5.41 ppm ($iPr-CH$) and the backbone is observed at 6.21 ppm as a singlet. In the $^{13}C\{^1H\}$ NMR spectrum, the carbene carbon atom resonates at 160.0 ppm. The signals for the iPr_2Im^{Me} of the adduct HBcat• iPr_2Im^{Me} **39** are detected at 1.08 ($iPr-CH_3$) and 5.68 ppm ($iPr-CH$) and the methyl-group at the backbone resonates at 1.48 ppm. The carbene carbon atom is observed at 160.2 ppm, which is in good agreement with the data obtained for compounds **37** and **38**. In addition, the chemical shifts of the boron atoms are slightly different; the boron atom of HBcat• iPr_2Im **38** is detected at 6.62 ppm and the boron atom of adduct HBcat• iPr_2Im^{Me} **39** at 6.79 ppm.

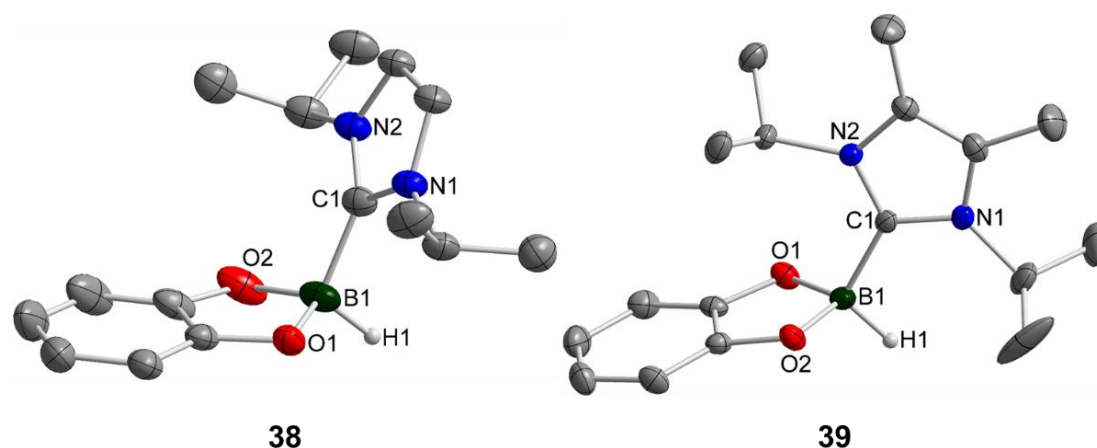
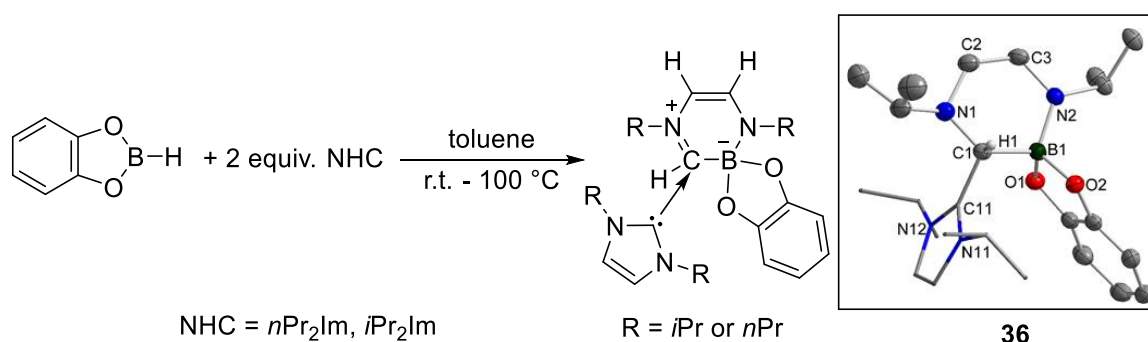


Figure 86: Left: molecular structure of HBcat·*iPr*₂Im **38** with thermal ellipsoids drawn at the 50% probability level; hydrogen atoms (besides H1) are omitted for clarity. Selected bond distances (Å) and angles (°): C1–B1 1.631(3), B1–O1 1.504(3), B1–O2 1.501(2); C1–B1–O1 110.33(16), C1–B1–O2 109.42(15). Right: molecular structure of HBcat·*iPr*₂Im^{Me} **39** with thermal ellipsoids drawn at the 50% probability level; hydrogen atoms (besides H1) are omitted for clarity. Selected bond distances (Å) and angles (°): C1–B1 1.646(2), B1–O1 1.501(2), B1–O2 1.510(2); C1–B1–O1 113.31(11), C1–B1–O2 107.18(10).

Additionally, single crystals for X-ray diffraction could be obtained for the mono-NHC adducts HBcat·*iPr*₂Im **38** and HBcat·*iPr*₂Im^{Me} **39** to confirm the results of the molecular structure (Figure 86). All bond length and angles are in good agreement with the data obtained for HBcat·*nPr*₂Im **37**.

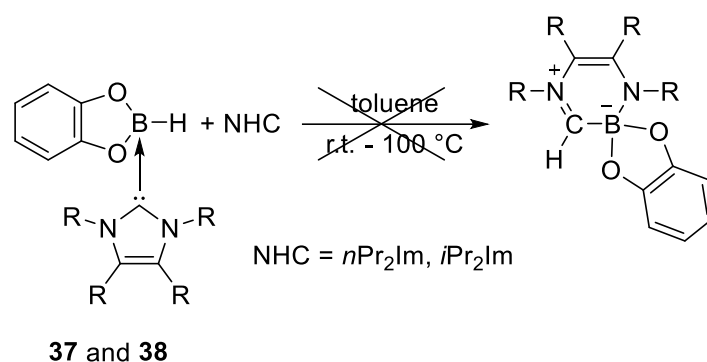
Based on the single crystal obtained from the reaction of B₂cat₂ with two equivalents of *iPr*₂Im, which was identified as the ring expanded product RER-HBcat·(*iPr*₂Im)₂ **36**, the reactions of HBcat and different NHCs in a 1:2 ratio were investigated at room as well as at higher temperatures (Scheme 108).



Scheme 108: Reactions of HBcat with two equivalents of NHC (NHC = *iPr*₂Im or *nPr*₂Im) to synthesize the ring expanded products RER-HBcat·(NHC)₂.

The reaction mixtures of HBcat and *nPr*₂Im as well as *iPr*₂Im were monitored *via in situ* ¹¹B and ¹¹B{¹H} NMR spectroscopy; however, the obtained spectra showed only signals for the two adducts HBcat·*nPr*₂Im **37** and HBcat·*iPr*₂Im **38** at room temperature. Therefore, the reaction

mixtures were heated to 100 °C for several hours. Nevertheless, the *in situ* $^{11}\text{B}/^{11}\text{B}\{^1\text{H}\}$ NMR spectra showed no evidence for any further conversion of the mono-NHC adduct **37** and **38**. Furthermore, the reaction of the isolated mono-NHC adduct $\text{HBcat}\cdot n\text{Pr}_2\text{Im}$ **37** and $\text{HBcat}\cdot i\text{Pr}_2\text{Im}$ **38** with one equivalent of the corresponding NHC ($n\text{Pr}_2\text{Im}$ or $i\text{Pr}_2\text{Im}$) were investigated to form the ring expanded product $\text{RER-HBcat}\cdot(i\text{Pr}_2\text{Im})_2$ **36**; however, no conversion to the expected ring expanded products were observed (Scheme 109).

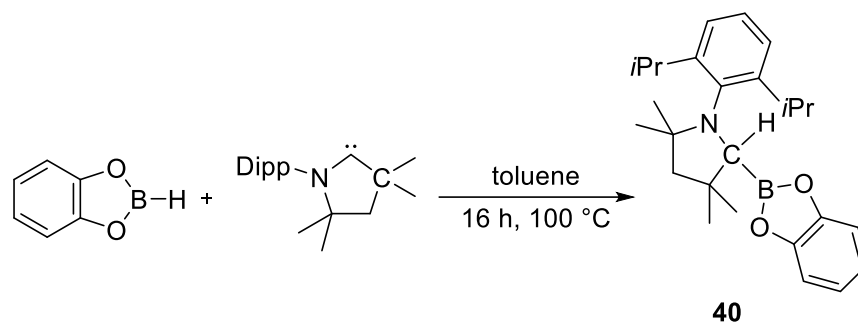


Scheme 109: Reaction of mono-NHC adduct $\text{HBcat}\cdot n\text{Pr}_2\text{Im}$ **37** or $\text{HBcat}\cdot i\text{Pr}_2\text{Im}$ **38** with one equivalent of the corresponding NHC ($n\text{Pr}_2\text{Im}$ or $i\text{Pr}_2\text{Im}$) to form the ring expanded product $\text{RER-HBcat}\cdot(i\text{Pr}_2\text{Im})_2$ **36**.

These results are also in good agreement with the DFT investigations reported by Brown *et al.*^[246] and Wilson, Dutton *et al.*^[245] The energy barrier between the adduct formation and the B–H activation is too high for any further activation. This is also comparable with the experimental investigations that even at elevated temperatures no conversion into the corresponding ring expanded product is observed.

2.2.3.2. Reaction of HBcat with CAAC^{Me} and the saturated NHC Dipp_2Sim

Based on the reaction of HBpin with the CAAC^{Me} which was reported by Bertrand *et al.* in 2010 to give the two compounds $\text{CAAC}^{\text{Cy}}(\text{H})\text{Bpin}$ and $\text{CAAC}^{\text{Menthyl}}(\text{H})\text{Bpin}$,^[213] a similar reaction of HBcat with CAAC^{Me} was investigated to obtain the corresponding B–H activation product $\text{CAAC}^{\text{Me}}(\text{H})\text{Bcat}$ **40**. The reaction mixture was heated to 100 °C overnight and, after work-up, the B–H activation product $\text{CAAC}^{\text{Me}}(\text{H})\text{Bcat}$ **40** was obtained (Scheme 110).



Scheme 110: Synthesis of the B–H activation product CAAC^{Me}(H)Bcat **40** by reaction of CAAC^{Me} with HBcat.

CAAC^{Me}(H)Bcat **40** was characterized *via* NMR-spectroscopy, high resolution mass spectroscopy and elemental analysis as well as X-ray diffraction. The ¹H NMR spectra shows, for each *iPr*-group of the two Dipp-substituents, one doublet with an integral of 3 (1.14, 1.24, 1.43 and 1.50 ppm) (Figure 87). The corresponding methine protons are detected at 3.50 and 4.35 ppm. Furthermore, the four methyl-groups of the CAAC^{Me} resonate at 1.12, 1.29, 1.33 and 1.34 ppm. The methylene-group is split into two multiplets, one at 1.76-1.79 ppm and the other one at 1.85-1.88 ppm. The signals of the aryl-CH-groups of the Dipp-substituent are observed as multiplets at 7.00-7.02, 7.12-7.14 and 7.24-7.26 ppm. Additionally, the protons of the Bcat-moiety are detected as two multiplets at 6.61-6.66 and 6.84-6.90 ppm. The signal for the proton at the CAAC carbon atom is observed at 4.22 ppm as a singlet.

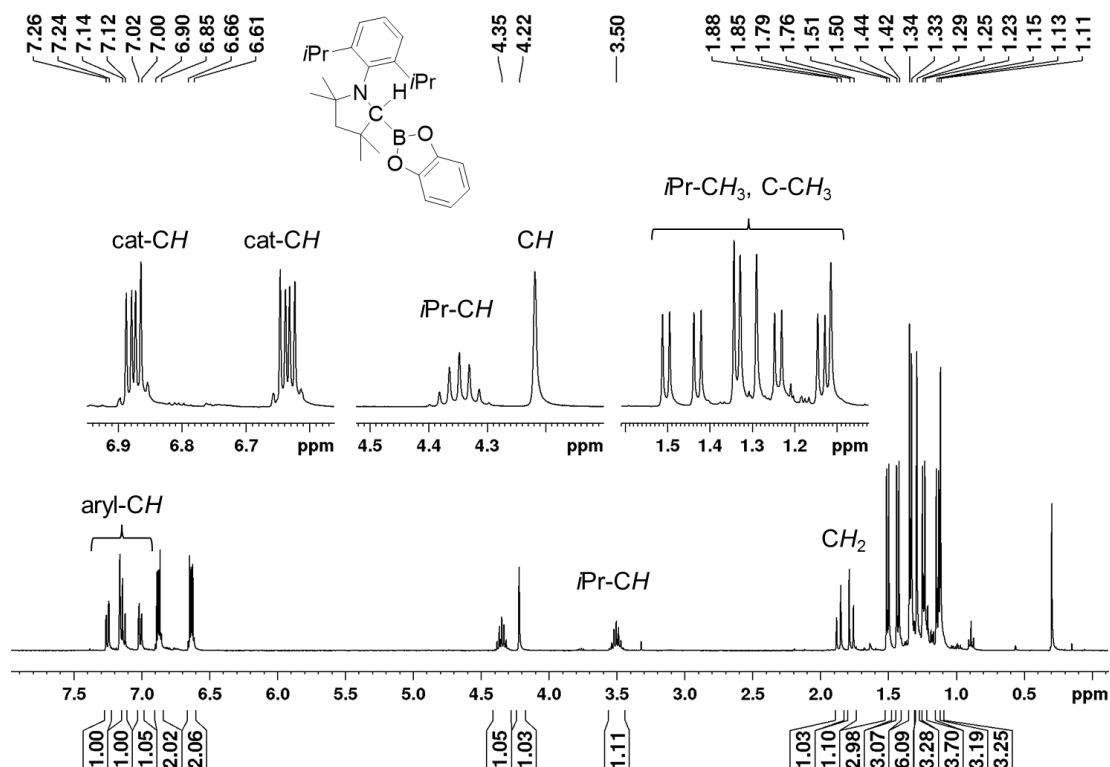


Figure 87: ¹H NMR spectrum of CAAC^{Me}(H)Bcat **40** in C₆D₆ (400 MHz).

The $^{11}\text{B}\{^1\text{H}\}$ NMR spectrum of $\text{CAAC}^{\text{Me}}(\text{H})\text{Bcat}$ **40** shows one broad singlet at 45.3 ppm for the $\text{sp}^2\text{-B}$ atom (Figure 88). Furthermore, in the $^{13}\text{C}\{^1\text{H}\}$ NMR spectrum, the signals for the methyl-groups of the Dipp-substituent are detected at 24.1, 25.3, 26.0 and 26.2 ppm, and the methine carbon atoms resonate at 28.1 and 29.5 ppm. The corresponding carbon atoms of the aryl rings are observed at 124.8, 124.9 and 127.0 ppm with the quaternary carbon atoms appearing at 139.8, 150.8 and 152.7 ppm. The four methyl-groups of the CAAC^{Me} are detected at 27.0, 28.7, 29.4 and 30.8 ppm. Additionally, the two quaternary carbon atoms resonate at 41.1 and 64.1 ppm. The methylene-group is detected at 58.4 ppm and the former CAAC^{Me} carbene carbon atom at 63.1 ppm as a broad signal. Furthermore, the signals for the catechol CH-groups are observed at 112.6 and 122.8 ppm and the corresponding quaternary carbon atoms at 148.2 ppm.

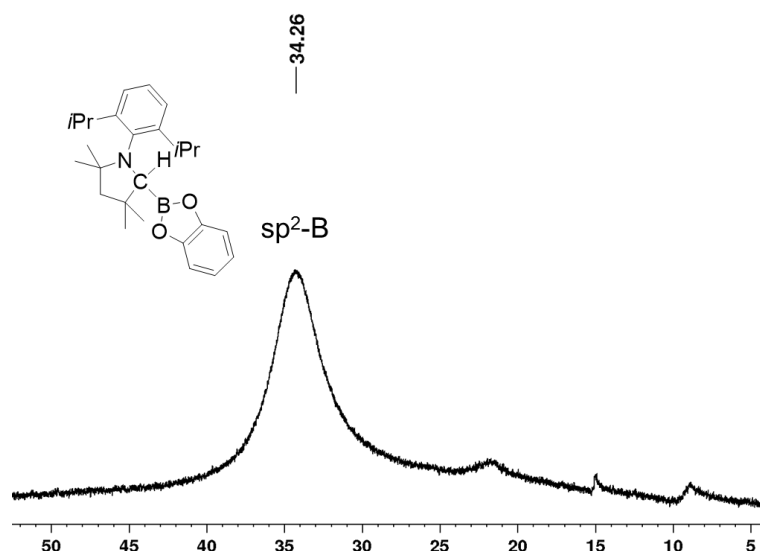


Figure 88: $^{11}\text{B}\{^1\text{H}\}$ NMR spectrum of $\text{CAAC}^{\text{Me}}(\text{H})\text{Bcat}$ **40** in C_6D_6 .

Single crystals of $\text{CAAC}^{\text{Me}}(\text{H})\text{Bcat}$ **40** were obtained from a saturated solution of compound **40** in *n*-hexane. The molecular structure confirmed the nature of the B–H activation product $\text{CAAC}^{\text{Me}}(\text{H})\text{Bcat}$ **40** (Figure 89). The Bcat-moiety binds to the former CAAC^{Me} carbene carbon atom and as a result, the proton of the HBcat migrated to the C1 carbon atom. The core structure of the CAAC^{Me} is still intact.

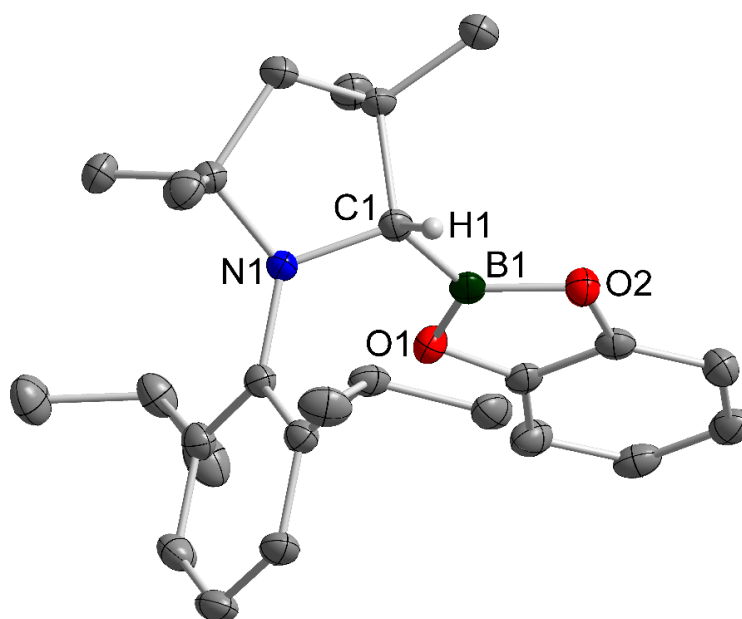
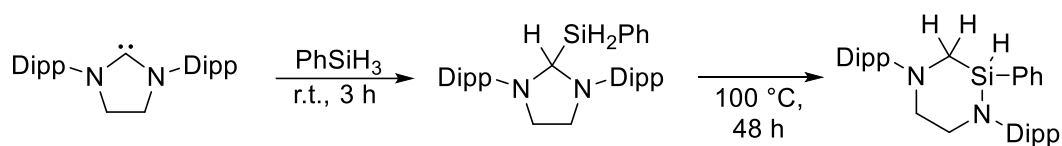
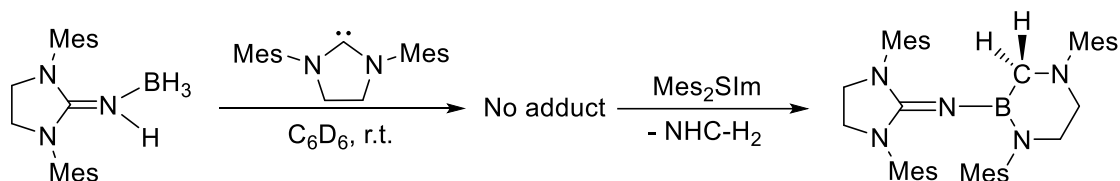


Figure 89: Molecular structure of $\text{CAAC}^{\text{Me}}(\text{H})\text{Bcat}$ **40** with thermal ellipsoids drawn at the 50% probability level; hydrogen atoms (besides H1) are omitted for clarity. Selected bond distances (Å) and angles (°): C1–B1 1.550(2), B1–O1 1.374(2), B1–O2 1.387(2); C1–B1–O1 126.38(15), C1–B1–O2 122.67(15).

The data obtained for the B–H activation product $\text{CAAC}^{\text{Me}}(\text{H})\text{Bcat}$ **40** are in good agreement with the data for the two compounds $\text{CAAC}^{\text{Cy}}(\text{H})\text{Bpin}$ and $\text{CAAC}^{\text{Menthyl}}(\text{H})\text{Bpin}$ reported by Bertrand *et al.*^[213]

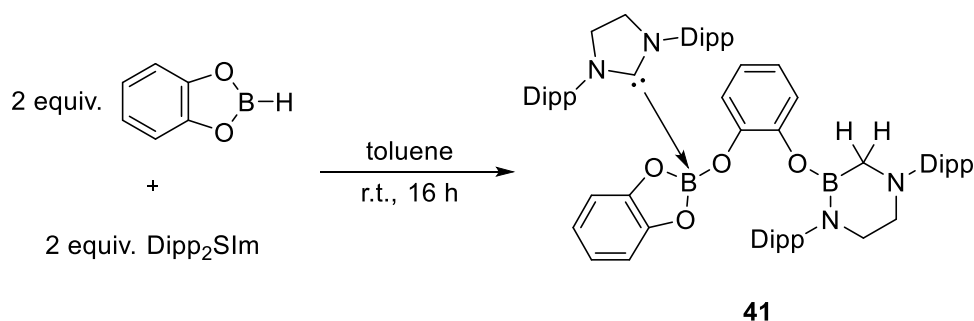
2.2.3.3. Reaction of HBcat with the saturated Dipp_2Slm and the unsaturated Dipp_2Im

Radius *et al.*^[232] and Inoue *et al.*^[228] reported the synthesis of ring expanded products *via* reaction of silanes and iminoborane dihydrides with different NHCs. Furthermore, the reactions of saturated NHCs, such as Dipp_2Slm and Mes_2Slm (1,3-bis(2,4,6-methyl)-imidazolidin-2-ylidene), yielded the corresponding ring expanded products; however, the reaction conditions are quite different. In the case of the silane-promoted ring expansion, the reactions were carried out at elevated temperatures; however, the conversion was complete in 2 days at 100 °C, instead of 3 days heating at 140 °C (Scheme 111, top). Similar observations were reported by Inoue *et al.*; using Mes_2Slm yielded the ring expanded product even at room temperature (Scheme 111, bottom).

Radius *et al.*Inoue *et al.*

Scheme 111: Ring expanded products reported by Radius *et al.* and Inoue *et al.* using saturated NHCs to obtain the RER products at milder conditions.

Based on our observations that the saturated NHC Dipp_2SIm reacts quite different with the diboron compound B_2cat_2 , the stoichiometric reaction of HBcat with Dipp_2SIm was investigated. First, the reaction was monitored *via* NMR spectroscopy; however, even at room temperature, full conversion of the starting material was observed and the ^{11}B NMR spectrum confirmed that the proton of the HBcat was removed by another main-group element. Additionally, the reaction was repeated on a larger scale to isolate the product (Scheme 112).



Scheme 112: Synthesis of the ring expanded product $\text{RER-Dipp}_2\text{SImB(H}_2\text{)-cat-Bcat}\cdot\text{Dipp}_2\text{SIm}$ **41** *via* stoichiometric reaction of HBcat with Dipp_2SIm .

The obtained solid was identified as the ring expanded product $\text{RER-Dipp}_2\text{SIm(H}_2\text{)B-cat-Bcat}\cdot\text{Dipp}_2\text{SIm}$ **41** and was isolated after work-up in 73% yield as a colorless solid. Additionally, compound **41** was characterized *via* NMR spectroscopy, elemental analysis and X-ray diffraction. The ^1H NMR spectrum of compound **41** shows signals for the six-membered heterocyclic ring, the bridged catechol-group with the oxygen-bound Bcat-moiety and for the coordinated NHC Dipp_2SIm (Figure 90). The resonances for the NHC appear in the expected region and, due to the symmetry of the NHC, the signals are not split. Additionally, for the two catechol-moieties, three multiplets are detected. One multiplet belongs to the Bcat-moiety which is observed at 7.07-7.13 ppm and the signals for the bridging catechol-group resonate as two multiplets between 6.23-6.39 ppm. Furthermore, the resonances of the *i*Pr-groups of

the heterocyclic ring are detected as four doublets at 1.30, 1.38, 1.47 and 1.51 ppm. The corresponding methine protons appear at 3.75-3.82 ppm. The aryl-CH protons of the Dipp-substituent resonate as multiplets between 6.23 and 7.36 ppm. The methylene-groups of the former backbone are observed as two multiplets at 3.22-3.35 and 3.48-3.53 ppm. The signal for the hydrogens which have migrated to the former carbene carbon atom appears as a singlet at 3.12 ppm.

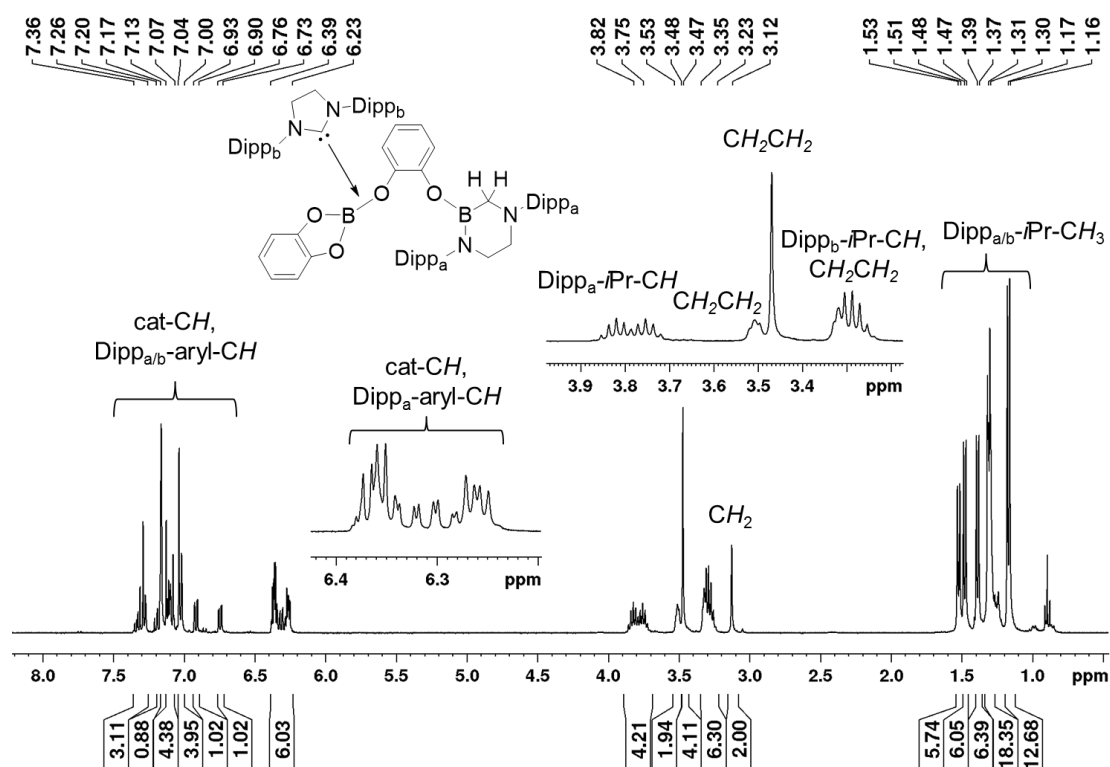


Figure 90: ¹H NMR spectrum of RER-Dipp₂Slm(H₂)B-cat-Bcat•Dipp₂Slm **41** in C₆D₆ (400 MHz).

In the ¹¹B NMR spectrum, only the signal for the sp³-hybridized boron atom is observed at 6.60 ppm. The resonance of the sp² boron atom in the heterocyclic ring is not obviously detected due to the fact that it is expected at ≥ 20 ppm and signal of the glass (≈ 40 ppm) was too intensive. Therefore, RER-Dipp₂Slm(H₂)B-cat-Bcat•Dipp₂Slm **41** was characterized *via* solid state ¹¹B NMR spectroscopy (Figure 91). The solid state ¹¹B shows one sharp signal at 7.22 ppm for the sp³-hybridized boron atom which is in good agreement with the solution ¹¹B NMR spectrum. Additionally, the sp² boron atom is detected as a broad signal at 32.6 ppm, due to the quadrupole coupling of the boron atom. The ¹³C{¹H} NMR spectrum of compound **41** shows one set of signals for the heterocyclic ring, the bridged catechol-group, the Bcat-moiety and the second NHC. The signals of the coordinating NHC resonates in the expected region; however, due to the binding to the boron atom, the resonance of the carbene carbon atom is shifted to higher field and is detected at 184.6 ppm (Dipp₂Slm: NCN 244.0 ppm). The carbon atoms of the catechol-group as well as the quaternary carbon atoms appear in the expected region. For each Dipp substituent of the heterocyclic ring is one set of signals

observed due to the loss of the symmetry. The carbon atoms of the *i*Pr-groups as well as the aromatic ring appear in the expected region. The backbone of the former NHC is detected at 52.8 and 54.7 ppm. In addition, the resonance for the former carbene carbon atom is shifted to higher field and is observed at 41.4 ppm.

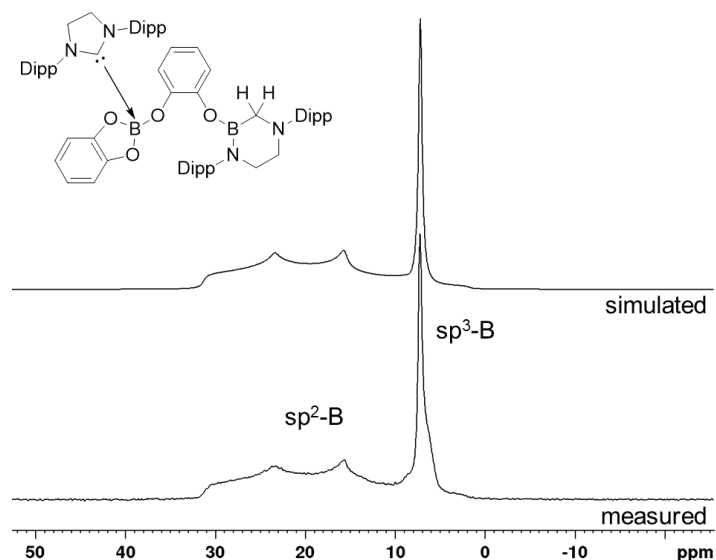


Figure 91: Solid state ^{11}B NMR spectra of RER-Dipp₂Slm(H₂)B-cat-Bcat•Dipp₂Slm (up: simulated, down: measured).

The molecular structure of RER-Dipp₂Slm(H₂)B-cat-Bcat•Dipp₂Slm **41** obtained by single crystal X-ray diffraction confirmed the ring expansion of the NHC Dipp₂Slm *via* insertion of one boron atom into the C–N bond as well as the migration of the two protons of the two equivalents of HBcat to the former carbene carbon atom (Figure 92). The catechol-group of the Bcat-moiety opens and binds to the second Bcat-group. Additionally, the second boron is stabilized *via* coordination of a second Dipp₂Slm which results in an sp³-hybridized boron atom.

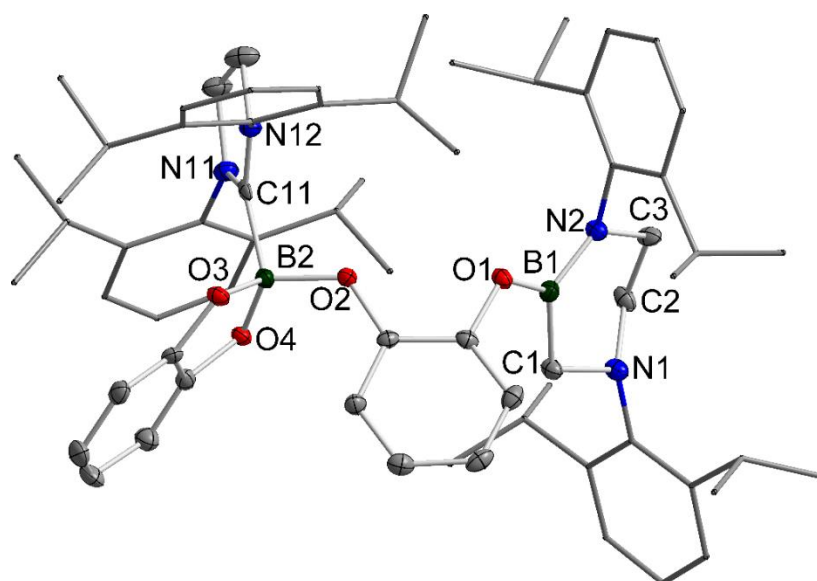


Figure 92: Molecular structure of RER-Dipp₂Slm(H₂)B-cat-Bcat•Dipp₂Slm **41** with thermal ellipsoids drawn at the 50% probability level; hydrogen atoms are omitted and the Dipp-substituents of the six-membered heterocyclic ring and of the second NHC are drawn as wires/sticks for clarity. Selected bond distances (Å) and angles (°): C1–N1 1.474(6), N1–C2 1.450(6), C2–C3 1.513(6), C3–N2 1.471(5), N2–B1 1.408(6), B1–C1 1.581(7), B1–O1 1.392(6), B2–O2 1.451(5), B2–O3 1.486(6), B2–O4 1.491(6), B2–C11 1.663(7); C1–N1–C2 113.4(4), N1–C2–C3 109.0(4), C2–C3–N2 111.3(3), C3–N2–B1 121.0(3), N2–B1–C1 119.7(4), B1–C1–N1 110.6(3), C11–B2–O2 103.7(3), C11–B2–O3 109.6(3), C11–B2–O4 110.4(3).

The core structure of the molecule is quite similar to the observed ring expanded product RER-B₂cat₂•Dipp₂Slm **33**, one Bcat-moiety inserts into the C–N bond of NHC and forms a six-membered heterocyclic ring; however, the oxygen atom O2 binds to the further HBcat molecule. Therefore, the hydride of the second HBcat could migrate to the former carbene carbon atom to neutralize the zwitterionic intermediate leading to compound **41**. Based on the stoichiometry of the reaction, a second NHC coordinates to the formal B(OR)₃-moiety (Figure 93).

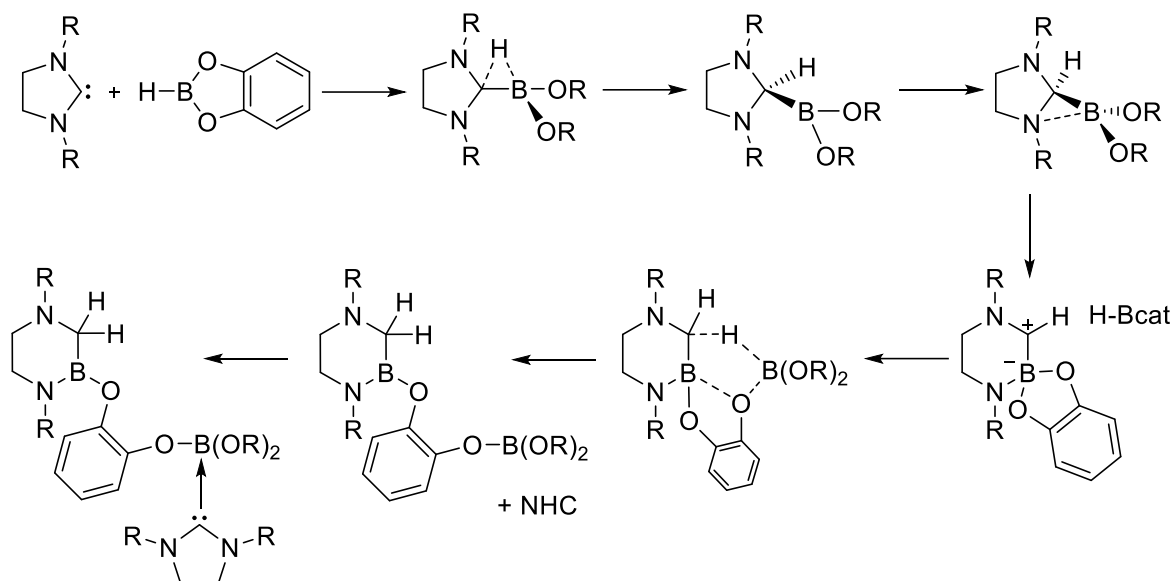


Figure 93: Postulated mechanism for the formation of the ring expanded product RER-Dipp₂SlmB-cat-Bcat•Dipp₂Slm **41**.

These experimental investigations confirmed the theoretical studies on the mechanism of ring expansion reactions.^[245] Wilson, Dutton *et al.* carried out DFT calculations on the reaction of silanes and boranes with saturated and unsaturated NHCs (Figure 94). They reported that the adduct formation between BR₃ and NHCs is favorable for H₂BMe (**A**), followed by HBMe₂ and BMe₃; however, the most stable adducts are formed with the backbone-methylated NHC. Furthermore, the energy barrier from the adduct formation **A** to the first transition state **T1** is lowest for the saturated NHC. For the overall reaction, starting with adduct formation, E–X bond activation, NHC ring expansion and further migration of the second substituent, the energy barrier is favorable with the saturated NHCs. The energy of the adduct formation is -96.9 kJ•mol⁻¹ and the ring expanded product is -211.5 kJ•mol⁻¹ which gives an energy difference of 114.6 kJ•mol⁻¹.

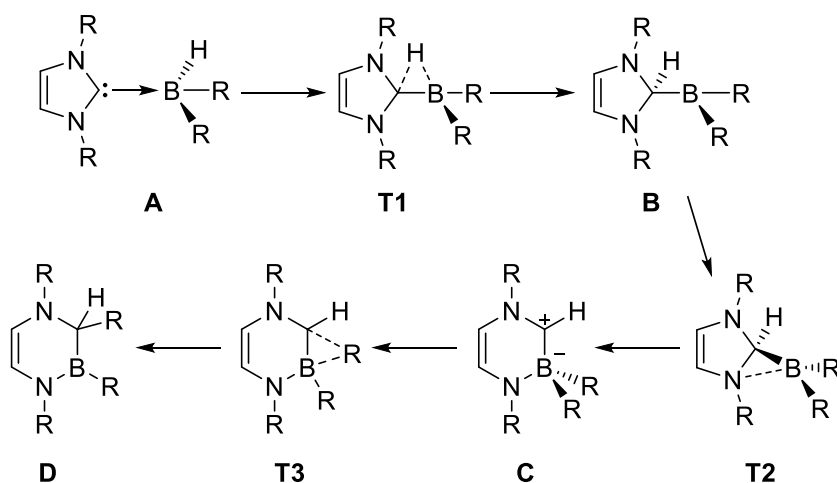
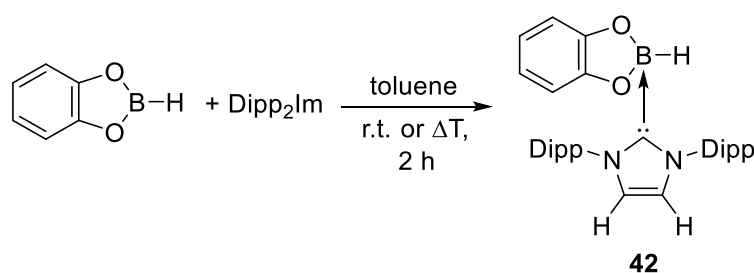


Figure 94: Calculated reaction pathway for ring expansion reactions of NHCs with BR₃ reported by Wilson, Dutton *et al.*

DFT investigations by Brown *et al.* also showed that, in the case of CAACs, E–X bond activation is the favorable reaction; however, the energy barrier for the insertion of the main-group element into the C–N bond of the NHC is too high.^[246] Therefore, only E–X bond activation is observed for the reactions of main-group hydrides with CAACs. These theoretical investigations were confirmed with experiments by Bertrand *et al.* in 2010.^[213] The group reported the reactions of silanes, phosphines and boranes with different CAACs which yielded the E–H bond activation products (E = Si, P, B).

In summary, the reactions of HBcat with the unsaturated NHCs nPr_2Im , iPr_2Im and iPr_2Im^{Me} yielded the mono-NHC adducts HBcat· nPr_2Im **37**, HBcat· iPr_2Im **38** and HBcat· iPr_2Im^{Me} **39**. A similar reaction, using CAAC^{Me} instead of an unsaturated NHC, yielded the B–H activation product CAAC^{Me}(H)Bcat **40**. These results are in good agreement with the DFT calculations reported by Wilson, Dutton *et al.*^[245] and Brown *et al.*^[246] that the energy barrier for any further ring expansion of the NHC and further migration of the boron atom into the C–N bond of the NHC is too high, or in the case of the reaction with the CAAC^{Me}, the B–H activation product is thermodynamically favored. However, the reaction of the saturated NHC Dipp₂Slm with HBcat showed that the ring opening of the saturated NHC is energetically favorable and, based on the lower energy barrier, the ring expanded product RER-Dipp₂Slm(H₂)B-cat-Bcat·Dipp₂Slm **41** was formed.

These observations were verified *via* reaction of unsaturated Dipp₂Im with HBcat at room and elevated temperatures; independent of the reaction conditions, the product was the mono-NHC adduct HBcat·Dipp₂Im **42** (Scheme 113).



Scheme 113: Reaction of HBcat with Dipp₂Im at room or elevated temperature to form the mono-NHC adduct HBcat·Dipp₂Im **42**.

HBcat·Dipp₂Im **42** was characterized *via* NMR spectroscopy and elemental analysis. The ¹H NMR spectrum shows one set of signals for the Dipp₂Im and for the HBcat (Figure 95). The methyl-groups of the Dipp-substituent are detected as doublets at 1.02 and 1.36 ppm, and the corresponding methine protons resonate at 2.68 ppm. The backbone of the NHC is observed at 6.32 ppm and the aryl-CH protons as two multiplets between 7.03 and 7.19 ppm. Additionally, the catechol-groups of the Bcat-moiety appear as two multiplets at 6.42-6.46 and 6.51-6.55 ppm. The hydride of the HBcat is detected as a quartet at 4.43 ppm.

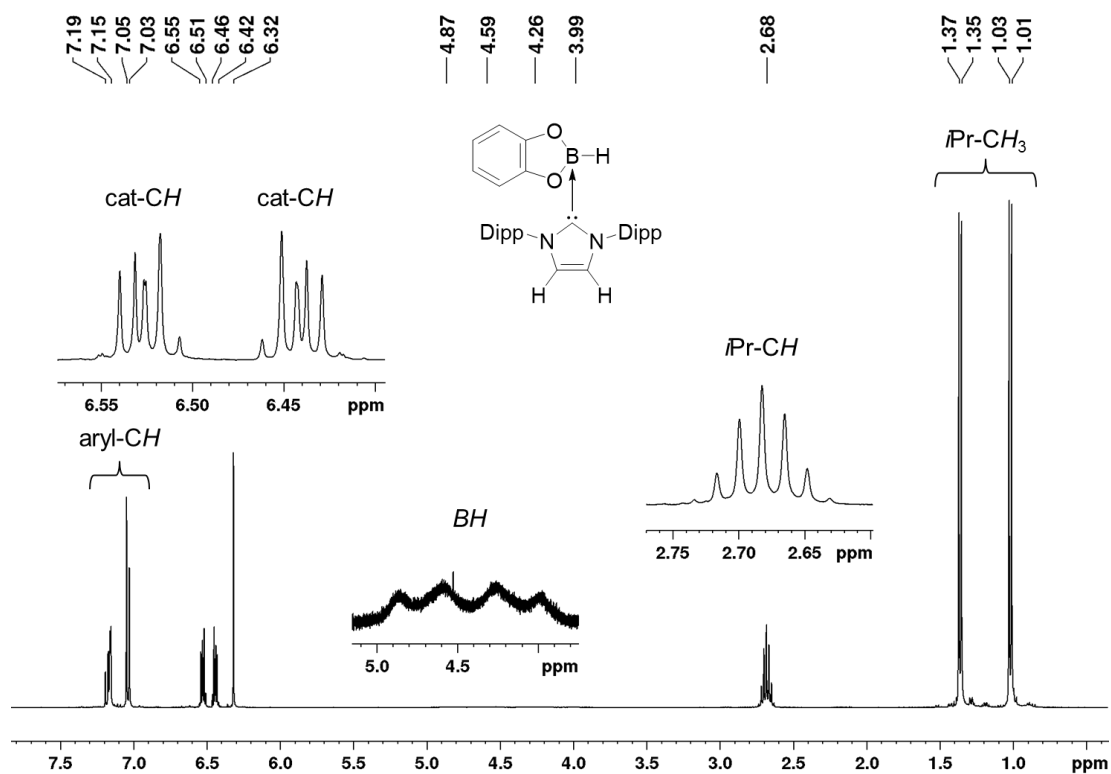


Figure 95: ^1H NMR spectrum of the mono-NHC adduct $\text{HBcat}\cdot\text{Dipp}_2\text{Im}$ **42** in C_6D_6 (400 MHz).

The ^{11}B NMR spectrum of $\text{HBcat}\cdot\text{Dipp}_2\text{Im}$ **42** shows a doublet at 6.03 ppm due to the B-H coupling in the molecule (Figure 96). The decoupled ^{11}B NMR spectrum ($^{11}\text{B}\{^1\text{H}\}$) shows a singlet. The data observed are in good agreement with those of the reported mono-NHC adducts $\text{HBcat}\cdot\text{NHC}$ **37-39**.

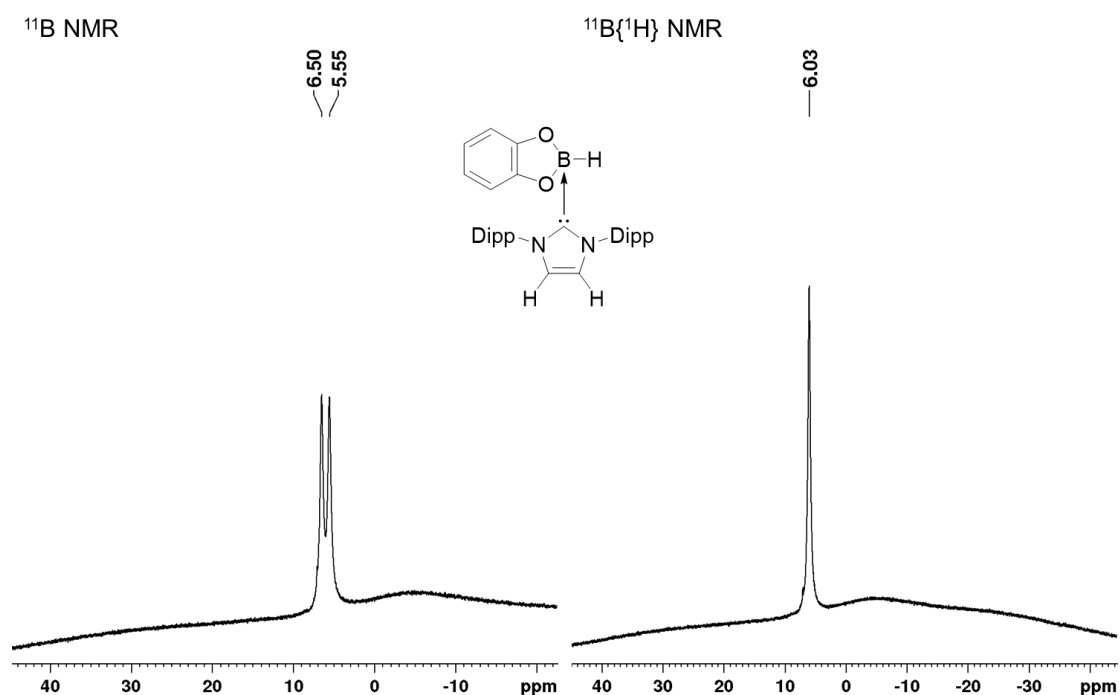


Figure 96: ^{11}B and $^{11}\text{B}\{^1\text{H}\}$ NMR spectrum of $\text{HBcat}\cdot\text{Dipp}_2\text{Im}$ **42** in C_6D_6 .

In the $^{13}\text{C}\{^1\text{H}\}$ NMR spectrum, the signals for the Dipp_2Im are detected in the expected region; however, the carbene carbon atom is shifted to higher field (165.8 ppm), due to the binding to the boron atom.

The synthesis of the mono-NHC adduct $\text{HBcat}\cdot\text{Dipp}_2\text{Im}$ **42** confirmed the expected results that the backbone of the NHC is important for the ring expansion of the NHC. Furthermore, these results verified the theoretical investigations on the mechanism of the ring expansion reaction.

For an overview, in table 4, the selected ^1H , $^{11}\text{B}/^{11}\text{B}$ Solid state and $^{13}\text{C}\{^1\text{H}\}$ NMR data as well as the isolated yield of the mono-NHC adducts $\text{HBcat}\cdot n\text{Pr}_2\text{Im}$ **37**, $\text{HBcat}\cdot i\text{Pr}_2\text{Im}$ **38**, $\text{HBcat}\cdot \text{Pr}_2\text{Im}^{\text{Me}}$ **39**, $\text{CAAC}^{\text{Me}}(\text{H})\text{Bcat}$ **40** and $\text{RER-Dipp}_2\text{SlmB-cat-Bcat}\cdot\text{Dipp}_2\text{Slm}$ **41** are summarized. For the mono-NHC adducts **37-39** similar results were obtained. The chemical shifts of the hydrides BH as well as the resonance in the $^{11}\text{B}/^{11}\text{B}\{^1\text{H}\}$ are comparable and the coupling constant is similar for each compound. The received data for the B–H activation product $\text{CAAC}^{\text{Me}}(\text{H})\text{Bcat}$ **40** is quite different for those observed in the reaction of HBcat with saturated and unsaturated NHCs. Due to the B–H activation, the hydride migrates to the former CAAC^{Me} carbon atom and as a result, the boron atom is still sp^2 -hybridized. Therefore, in the ^{11}B NMR spectrum, only one broad signal at 35.4 ppm is detected in the expected region. The reaction of HBcat with the saturated NHC Dipp_2Slm formed the ring expanded product $\text{RER-Dipp}_2\text{SlmB-cat-Bcat}\cdot\text{Dipp}_2\text{Slm}$ **41** via insertion of the boron atom into the C–N bond of the NHC and further migration of two hydrides to the former carbene carbon atom. As a results, in the solid state NMR spectrum, two signals appears; one broad signal for the sp^2 -hybridized boron atom in the heterocyclic ring at 32.6 ppm and one sharp signal for the sp^3 -hybridized boron atom at 7.22 ppm.

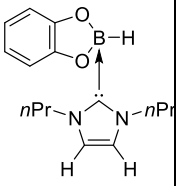
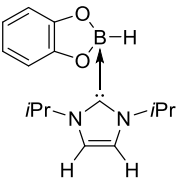
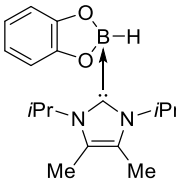
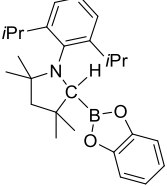
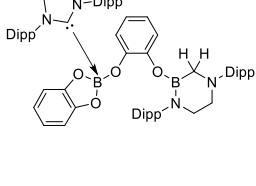
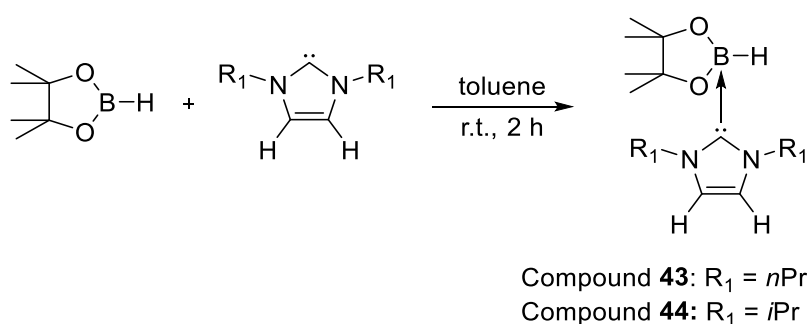
					
	37	38	39	40	41
¹H NMR [ppm]	BH: 5.06	BH: 5.17	BH: 5.23	CH: 4.22	CH ₂ : 3.12
¹¹B NMR [ppm]	6.46, ¹ J _{BH} = 119 Hz	6.62, ¹ J _{BH} = 118 Hz	6.81, ¹ J _{BH} = 117 Hz	35.4	¹¹B Solid state: 7.22 (sp ³ -B), 32.6 (sp ² -B).
¹³C{¹H} NMR [ppm]	NCN: 161.0	NCN: 160.0	NCN: 160.2	C-Bcat: 63.1	CH ₂ : 41.4 NCN: 184.6
Yield [%]	59	68	63	73	71

Table 5: Selected ¹H, ¹¹B/¹¹B Solid state and ¹³C{¹H} NMR data as well as the isolated yield of the mono-NHC adducts HBcat·*n*Pr₂Im **37**, HBcat·*i*Pr₂Im **38**, HBcat·*i*Pr₂Im^{Me} **39**, CAAC^{Me}(H)Bcat **40** and RER-Dipp₂Slm(H₂)B-cat-Bcat-Dipp₂Slm **41**.

2.2.3.4. Synthesis of NHC adducts of the type HBpin•NHC

Due to the successful synthesis of the mono-NHC adducts HBcat•NHC **37-39**, similar reactions of HBpin with the NHCs $n\text{Pr}_2\text{Im}$ and $i\text{Pr}_2\text{Im}$ in a 1:1 and 1:2 ratio were investigated to form the mono-NHC adduct of the type HBpin•NHC in the stoichiometric reaction and a possible RER-HBpin•(NHC)₂ in the 1:2 reaction ratio.

The first investigation was the stoichiometric reaction of HBpin with the NHCs $n\text{Pr}_2\text{Im}$ and $i\text{Pr}_2\text{Im}$, which yielded in the formation of the expected mono-NHC adducts HBpin• $n\text{Pr}_2\text{Im}$ **43** and HBpin• $i\text{Pr}_2\text{Im}$ **44**; however, adduct **44** was already obtained in an earlier diploma thesis in the group of Radius (Scheme 114).^[255]



Scheme 114: Synthesis of the mono-NHC adducts HBpin• $n\text{Pr}_2\text{Im}$ **43** and HBpin• $i\text{Pr}_2\text{Im}$ **44** via reaction of HBpin with the NHC $n\text{Pr}_2\text{Im}$ and $i\text{Pr}_2\text{Im}$.

HBpin• $n\text{Pr}_2\text{Im}$ **43** as well as HBpin• $i\text{Pr}_2\text{Im}$ **44** were characterized via ¹H, ¹¹B and ¹³C{¹H} NMR spectroscopy and the data obtained are similar to those of the mono-NHC adducts HBcat•NHC **37-39**. The ¹H NMR spectrum of compound **43** shows one set of signals for the NHC as well as for the HBpin (Figure 97). The chemical shifts of the *n*Pr-moieties are detected at 0.71 (*n*Pr-CH₃), 1.51-1.60 (*n*Pr-CH₂CH₃) the methylene-groups at the nitrogen atom at 4.17-4.21 ppm and the protons of the backbone at 5.87 ppm (compound **44**: 1.02 ppm *i*Pr-CH₃, 6.10 ppm *i*Pr-CH). Additionally, the resonances of the pinacol-groups are observed at 1.28 and 1.56 ppm (compound **44**: 1.30 and 1.58 ppm) as two singlets and the hydride (BH) at 4.44 ppm (compound **44**: 4.52 ppm) as a quartet.

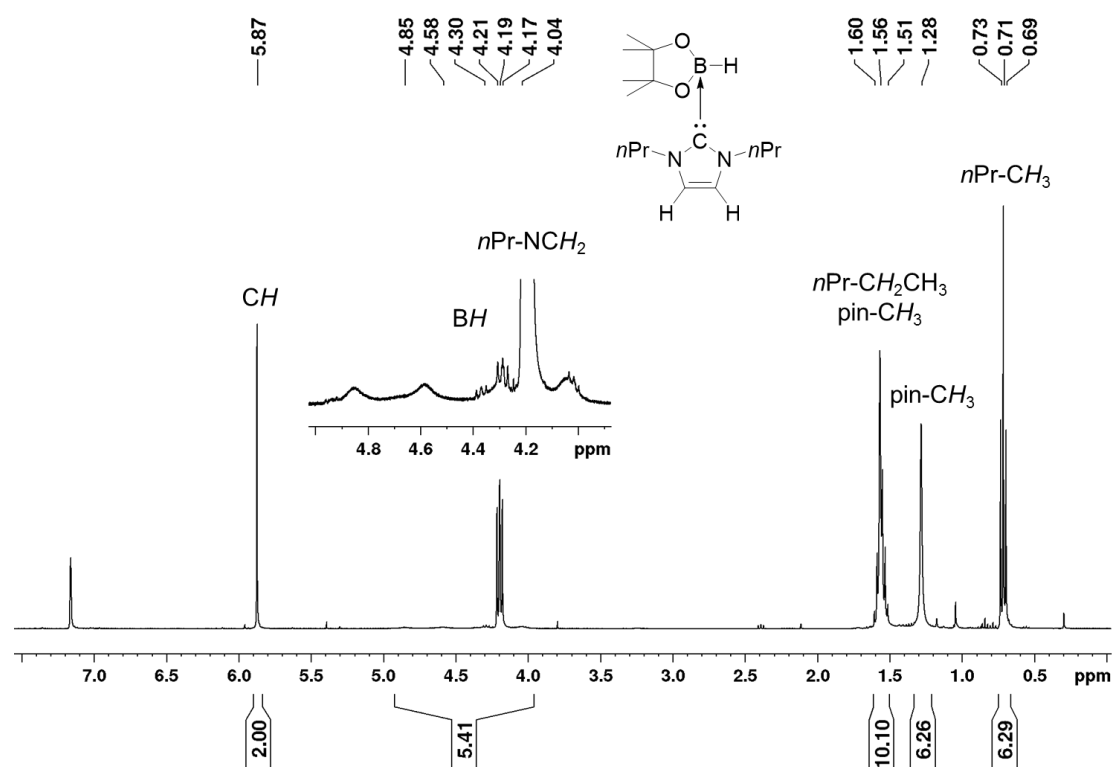


Figure 97: ^1H NMR spectrum of $\text{HBpin}\cdot n\text{Pr}_2\text{Im}$ **43** in C_6D_6 (400 MHz).

The ^{11}B NMR spectrum shows a doublet at 2.44 ppm ($^1J_{\text{BH}} = 108$ Hz), due to the coupling to the hydrogen atom (compound **44**: 2.51 ppm) (Figure 98). In the $^{13}\text{C}\{^1\text{H}\}$ the carbon atoms of the $n\text{Pr}$ -group are observed at 11.0 ($n\text{Pr-CH}_3$), 24.3 ($n\text{Pr-CH}_2\text{CH}_3$) and 49.7 ppm ($n\text{Pr-NCH}$) (compound **44**: 23.0 ($n\text{Pr-CH}_3$), 48.4 ($n\text{Pr-CH}$)). The backbone of the NHC as well as the carbene carbon atom are detected at 118.7 (NCCN) and 167.6 ppm (NCN) (compound **44**: 115.2 (NCCN), 166.4 (NCN), the carbene carbon atom was assigned *via* 2D NMR spectroscopy (HMBC)). For the pinacol-moieties, two signals for the methyl-group (25.6 and 25.7 ppm) are detected along with a signal at 78.2 ppm for the quaternary carbon atom (compound **44**: 25.5, 25.9 (pin- CH_3) and 78.1 (pin- C_q)).

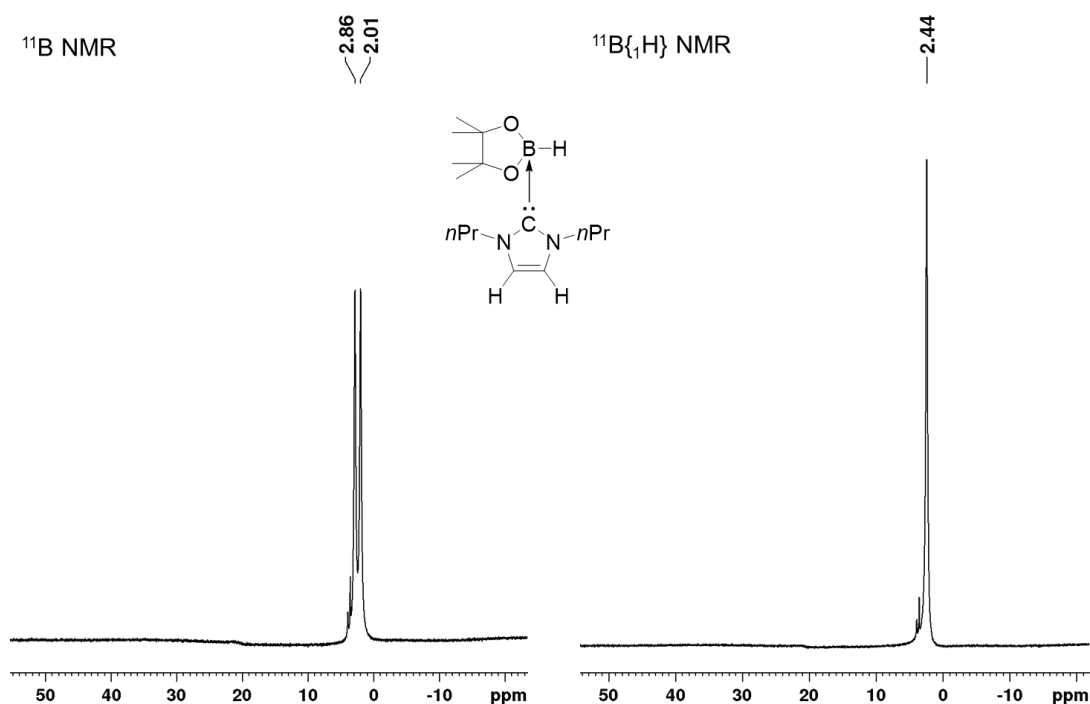


Figure 98: ^{11}B and $^{11}\text{B}\{^1\text{H}\}$ NMR spectra of $\text{HBpin}\cdot n\text{Pr}_2\text{Im}$ **43** in C_6D_6 .

In summary, the reactions of HBcat and HBpin with the unsaturated NHCs $n\text{Pr}_2\text{Im}$ and $i\text{Pr}_2\text{Im}$ yielded the expected mono-NHC adducts of the $\text{HB}(\text{OR})_2\cdot\text{NHC}$, namely $\text{HBcat}\cdot n\text{Pr}_2\text{Im}$ **37** and $\text{HBcat}\cdot i\text{Pr}_2\text{Im}$ **38** as well as $\text{HBpin}\cdot n\text{Pr}_2\text{Im}$ **43** and $\text{HBpin}\cdot i\text{Pr}_2\text{Im}$ **44** (Table 6). The obtained NMR spectroscopic data of all four mono-NHC adducts are similar. In the ^{11}B NMR spectrum, the signals for the boron atoms appear in the similar region; however, due to the different substituents at the boron atom (catechol and pinacol), the signals are only similar for the same borane. In comparison to the starting materials (HBcat and HBpin) which resonate at 28.8 and 28.4 ppm, the mono-NHC adducts of the type $\text{HBcat}\cdot\text{NHC}$ are detected at 6.46 and 6.46 ppm (compound **37** and **38**) and the corresponding adducts $\text{HBpin}\cdot n\text{Pr}_2\text{Im}$ **43** and $\text{HBpin}\cdot i\text{Pr}_2\text{Im}$ **44** at 2.44 and 4.52 ppm. Additionally, the coupling constant J_{BH} is also quite different to those of the starting material. The boron atoms in the mono-NHC adducts **37/38** and **43/44** are sp^3 -hybridized and in the starting material (HBcat and HBpin) sp^2 -hybridized. Therefore, the coupling constant J_{BH} in the mono-NHC adducts is smaller (compound **37**: 119 Hz, **38**: 118 Hz, **43**: 108 Hz and **44**: 110 Hz) than in HBcat (192 Hz) and HBpin (173 Hz)^[262] due to the dependence of the coupling constant to the hybridization.^[263-264] Related results were obtained in the ^1H NMR spectrum, the signal for the hydrides are similar for the same boranes; however, slightly different to each other. The resonances of the carbene carbon atom of all mono-NHC adducts **37/38** and **43/44** are in the same region (compound **37**: 161.0 ppm, **38**: 160.0 ppm, **43**: 167.6 ppm and **44**: 166.4 ppm).

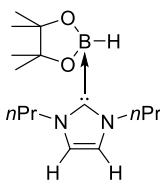
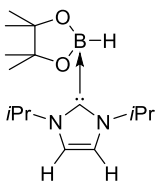
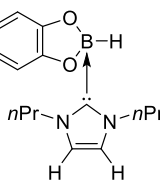
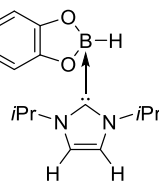
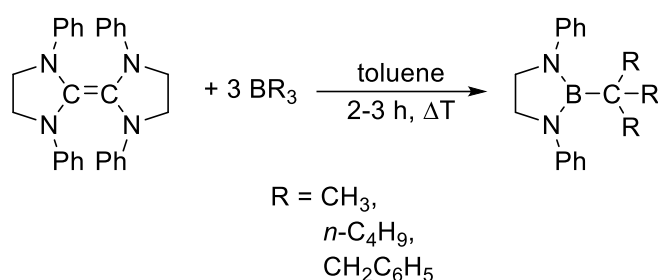
	 43	 44	 37	 38
¹ H NMR [ppm]	BH: 4.44	BH: 4.52	BH: 5.06	BH: 5.17
¹¹ B NMR [ppm]	2.44, ¹ J _{BH} = 108 Hz	2.51, ¹ J _{BH} = 110 Hz	6.46, ¹ J _{BH} = 119 Hz	6.62, ¹ J _{BH} = 118 Hz
¹³ C{ ¹ H} NMR [ppm]	NCN: 167.6	NCN: 166.4	NCN: 161.0	NCN: 160.0
Yield [%]	72	50	59	68

Table 6: Selected ¹H, ¹¹B and ¹³C{¹H} NMR data as well as the isolated yield of the mono-NHC adducts HBpin·*n*Pr₂Im **43** and HBpin·*i*Pr₂Im **44** as well as the mono-NHC adducts of the type HBcat·NHC, HBcat·*n*Pr₂Im **37** and HBcat·*i*Pr₂Im **38**.

2.2.4. Synthesis of mono-NHC adducts of the type $R_3B \cdot NHC$

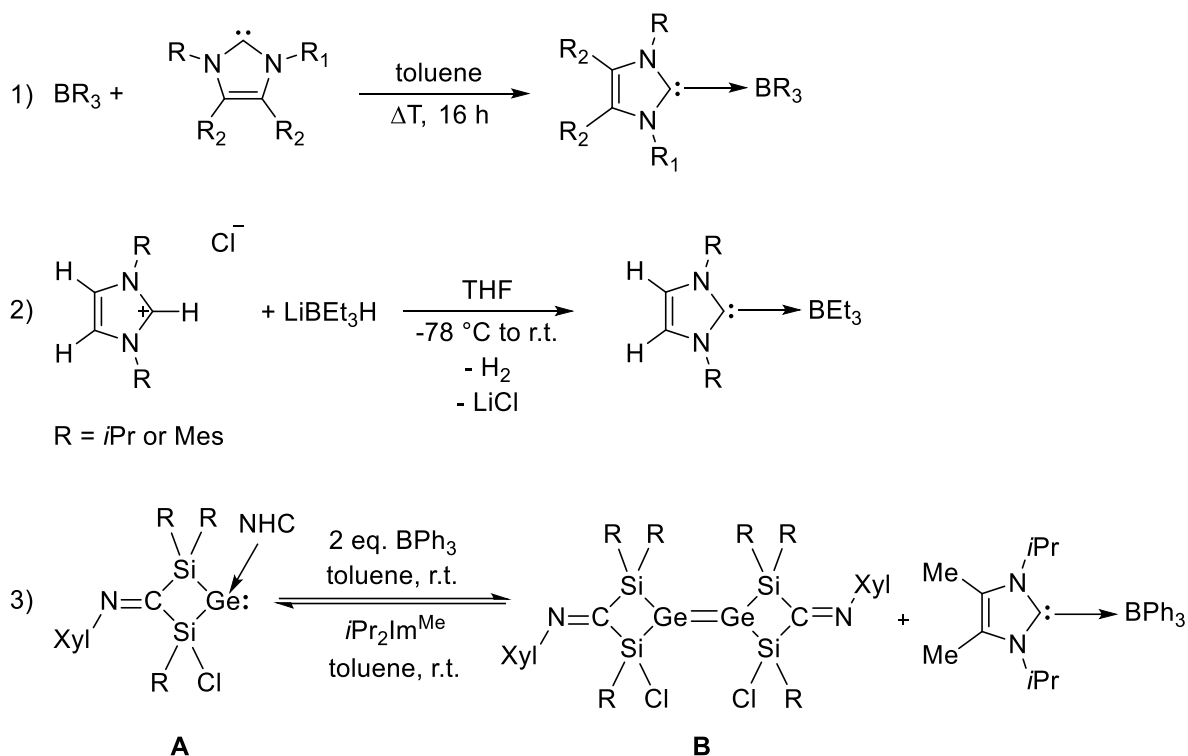
2.2.4.1. Synthesis according to literature procedure

The first report of a closely related reaction dates back to 1965. Heese and Haag reported the reactions of trialkylboranes with the electron-rich alkene bis(1,3-diphenyl-imidazolidin-2-ylidene) (formally a carbene dimer) in toluene at elevated temperatures (Scheme 115) to form five-membered heterocyclic rings.^[233] They also postulated a mechanism for the reaction, wherein the first step is adduct formation between the borane and the NHC.



Scheme 115: Reaction of the dimeric carbene with BR_3 ($R =$ methyl, n -butyl, benzyl).

These mono-NHC adducts of the type $R_3B \cdot NHC$ can be synthesized by three different routes. One direct synthesis is the reaction of the trialkylboranes with different isolated NHCs (Scheme 116).



Scheme 116: 1) Synthesis of the mono-NHC adducts *via* reaction of trialkylboranes with NHCs. 2) Reaction of the corresponding imidazolium salts NHC•HCl with LiBEt₃H to form the corresponding mono-NHC adduct. 3) Reversible reaction of the four membered cyclic germanium species **A** to form the digermene **B** and further formation of the mono-NHC adduct Ph₃B•*i*Pr₂Im^{Me}.

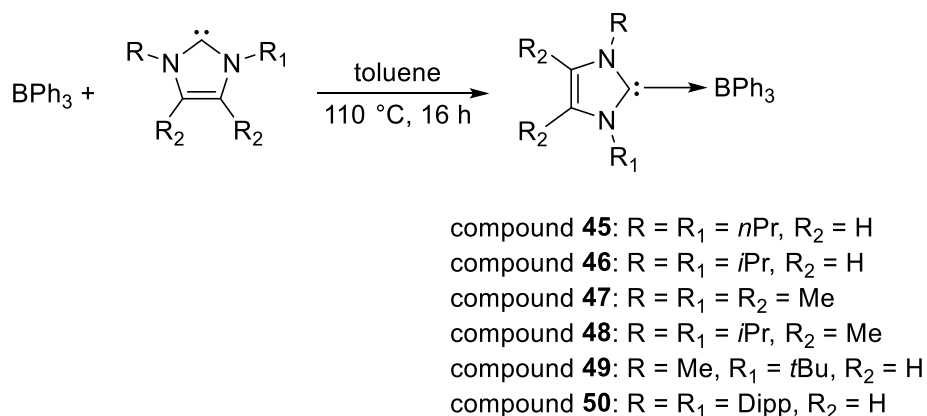
For an example, the direct reaction was reported by Curran, Malacria, Fensterbank and Lacôte in 2009. Using this method, the mono-NHC adducts Et₃B•Dipp₂Im and Ph₃B•Dipp₂Im were synthesized.^[265] The second possibility is the formation of the mono-NHC adduct *via* elimination of the corresponding salt. Therefore, the imidazolium salts NHC•HCl react with LiBEt₃H to form the corresponding mono-NHC adduct and LiCl as well as dihydrogen. For example, the mono-NHC adducts Et₃B•*i*Pr₂Im and Et₃B•Mes₂Im were obtained using this reaction route.^[266]

In addition, these mono-NHC adducts were also observed as by-products in different syntheses.^[267-269] For example, Scheschkewitz *et al.* reported the dimerization of a digermene. The reaction of an NHC adduct of the four-membered heterocyclic ring **A** with BPh₃ in toluene at room temperature gave the digermene **B** and the corresponding triphenyl borane adduct Ph₃B•*i*Pr₂Im^{Me}.^[267]

In the following section, reactions of two BR₃ compounds (BPh₃ and BEt₃) with different NHCs were explored.

2.2.4.2. Synthesis of mono-NHC adducts of the type $\text{Ph}_3\text{B}\cdot\text{NHC}$

Initially, the stoichiometric reaction of different NHCs with triphenylborane BPh_3 was examined. Each reaction was monitored *via in situ* ^{11}B NMR spectroscopy. Due to the fact that no conversion of the starting material took place at room temperature, the reaction mixture of each example was heated to $100\text{ }^\circ\text{C}$ overnight. In Scheme 117, the different reactions are summarized. The product of each reaction is the corresponding mono-NHC adduct.



Scheme 117: Synthesis of the mono-NHC adduct of the type $\text{Ph}_3\text{B}\cdot\text{NHC}$ **45-50** *via* reaction of BPh_3 with one equivalent of NHC (NHC = $n\text{Pr}_2\text{Im}$, $i\text{Pr}_2\text{Im}$, $\text{Me}_2\text{Im}^{\text{Me}^*}$, $i\text{Pr}_2\text{Im}^{\text{Me}}$, $\text{Me}t\text{Bulm}$ and Dipp_2Im).

As a result, six mono-NHC adducts of the type $\text{Ph}_3\text{B}\cdot\text{NHC}$, namely, $\text{Ph}_3\text{B}\cdot n\text{Pr}_2\text{Im}$ **45**, $\text{Ph}_3\text{B}\cdot i\text{Pr}_2\text{Im}$ **46**, $\text{Ph}_3\text{B}\cdot \text{Me}_2\text{Im}^{\text{Me}}$ **47**, $\text{Ph}_3\text{B}\cdot i\text{Pr}_2\text{Im}^{\text{Me}}$ **48**,^[267-268] $\text{Ph}_3\text{B}\cdot \text{Me}t\text{Bulm}$ **49** and $\text{Ph}_3\text{B}\cdot \text{Dipp}_2\text{Im}$ **50** were isolated in moderate to good yield and were characterized by NMR spectroscopy.^[265]

As an example, the characterization of the mono-NHC adduct $\text{Ph}_3\text{B}\cdot n\text{Pr}_2\text{Im}$ **45** will be discussed in the following paragraph. The ^1H NMR spectrum shows one set of signals of the $n\text{Pr}_2\text{Im}$ and the BPh_3 components (Figure 99). The resonances of the $n\text{Pr}$ -group are detected at 0.22 ($n\text{Pr}-\text{CH}_3$), 0.87-0.97 ppm ($n\text{Pr}-\text{CH}_2\text{CH}_3$) and the methylene-group at 3.18-3.22 ppm ($n\text{Pr}-\text{NCH}_2$). Additionally, the backbone of the NHC is observed at 5.93 ppm as a singlet. The resonances of the phenyl-group of the BPh_3 appear as multiplets in the expected region (7.16-7.20, 7.28-7.31 and 7.60-7.62 ppm).

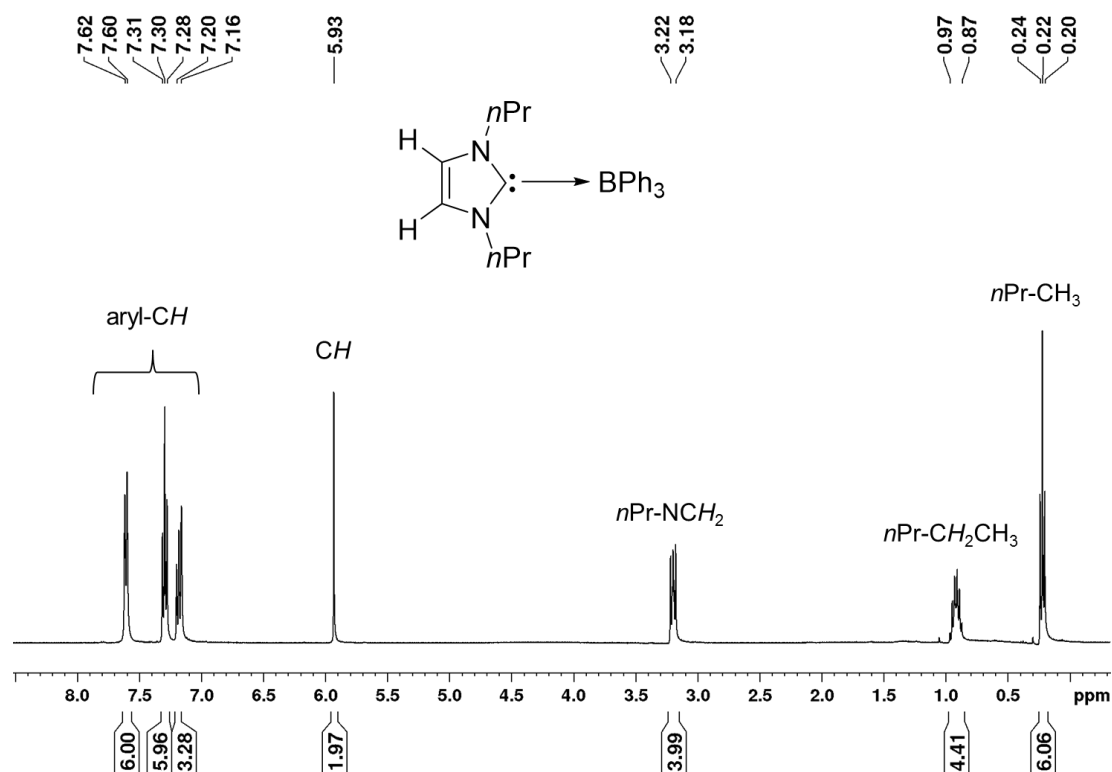


Figure 99: ^1H NMR spectrum of $\text{Ph}_3\text{B}\cdot n\text{Pr}_2\text{Im}$ **45** in C_6D_6 (400 MHz).

In the corresponding $^{11}\text{B}\{^1\text{H}\}$ NMR spectrum, the signal for the sp^3 -hybridized boron atom appears at -8.76 ppm, which is in the expected region for tetrahedral boron atoms (Figure 100). The $^{13}\text{C}\{^1\text{H}\}$ NMR spectrum also shows one set of signals for the $n\text{Pr}_2\text{Im}$ and for BPh_3 . The resonances for the $n\text{Pr}$ -group are observed at 10.7 ($n\text{Pr-CH}_3$), 24.0 ($n\text{Pr-CH}_2\text{CH}_3$) and 51.1 ppm ($n\text{Pr-NCH}_2$). The backbone of the NHC is detected at 119.8 and the carbene carbon atom at 169.7 ppm. In addition, the carbon atoms of the aryl-CH appear at 124.7 , 127.4 and 135.9 ppm and the corresponding quaternary carbon atoms resonate at 135.9 and 156.2 ppm.

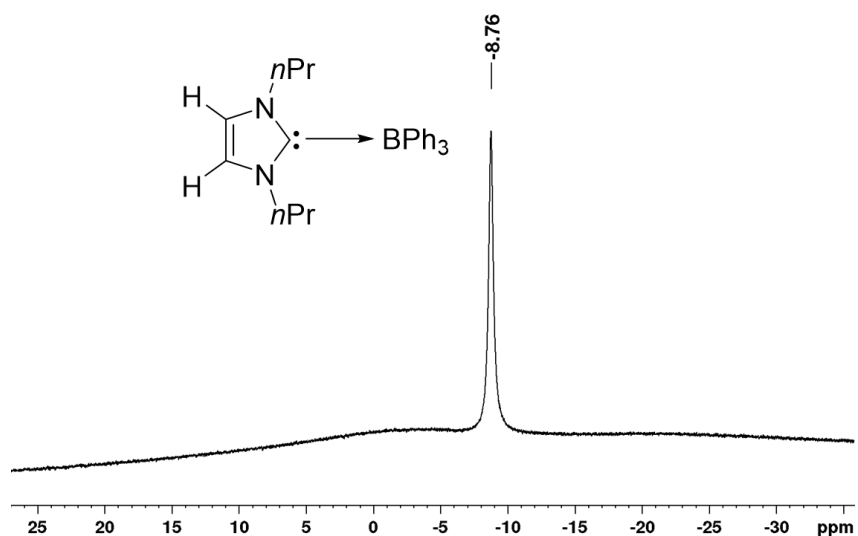


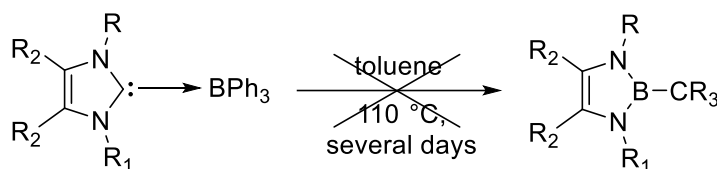
Figure 100: $^{11}\text{B}\{^1\text{H}\}$ NMR spectrum of $\text{Ph}_3\text{B}\cdot n\text{Pr}_2\text{Im}$ **45** in C_6D_6 .

Table 7 presents selected NMR spectroscopic data and isolated yields of the mono-NHC adducts $\text{Ph}_3\text{B}\cdot\text{iPr}_2\text{Im}$ **46**, $\text{Ph}_3\text{B}\cdot\text{Me}_2\text{Im}^{\text{Me}}$ **47**, $\text{Ph}_3\text{B}\cdot\text{iPr}_2\text{Im}^{\text{Me}}$ **48**, $\text{Ph}_3\text{B}\cdot\text{Me}^t\text{Bulm}$ **49** and $\text{Ph}_3\text{B}\cdot\text{Dipp}_2\text{Im}$ **50**. The spectroscopic data obtained are similar to those for the mono-NHC adduct $\text{Ph}_3\text{B}\cdot\text{iPr}_2\text{Im}$ **45**.

NHC adduct	$\text{Ph}_3\text{B}\cdot\text{iPr}_2\text{Im}$ 46	$\text{Ph}_3\text{B}\cdot\text{Me}_2\text{Im}^{\text{Me}}$ 47	$\text{Ph}_3\text{B}\cdot\text{iPr}_2\text{Im}^{\text{Me}}$ 48	$\text{Ph}_3\text{B}\cdot\text{Me}^t\text{Bulm}$ 49	$\text{Ph}_3\text{B}\cdot\text{Dipp}_2\text{Im}$ 50
^1H NMR [ppm]	0.60, 4.51, 6.17, 7.15-7.20, 7.28-7.32, 7.64-7.66	1.11, 2.63, 7.20-7.24, 7.33-7.37, 7.67-7.69	0.70, 1.52, 5.03, 7.16-7.20, 7.30-7.34, 7.67-7.69	1.06, 2.57, 5.72, 6.30, 7.16-7.20, 7.27-7.31, 7.56-7.58	0.92, 1.01, 2.99, 6.42, 6.74-6.76, 6.94-6.96, 6.98-7.00, 7.21-7.24
$^{11}\text{B}\{^1\text{H}\}$ NMR [ppm]	-8.61	-8.64	-8.09	-6.41	-6.47
$^{13}\text{C}\{^1\text{H}\}$ NMR [ppm]	NCN: 169.4	NCN: 168.8	NCN: 169.6	NCN: 174.2	NCN: 177.7
Yield [%]	53	58	49	64	74

Table 7: Selected ^1H , $^{11}\text{B}\{^1\text{H}\}$ and $^{13}\text{C}\{^1\text{H}\}$ NMR data as well as the isolated yield of the mono-NHC adducts $\text{Ph}_3\text{B}\cdot\text{iPr}_2\text{Im}$ **46**, $\text{Ph}_3\text{B}\cdot\text{Me}_2\text{Im}^{\text{Me}}$ **47**, $\text{Ph}_3\text{B}\cdot\text{iPr}_2\text{Im}^{\text{Me}}$ **48**, $\text{Ph}_3\text{B}\cdot\text{Me}^t\text{Bulm}$ **49** and $\text{Ph}_3\text{B}\cdot\text{Dipp}_2\text{Im}$ **50**.

The stability of all of these compounds **45-50** has been tested. Therefore, reactions were carried out at elevated temperatures to observe any ring expansion of the NHC and further ring contraction of the NHC and an exchange of the carbon atom with the boron atom. In each case; however, the corresponding mono-NHC adducts $\text{BPh}_3\cdot\text{NHC}$ **45-50** were shown to be stable even at elevated temperatures (Scheme 118).

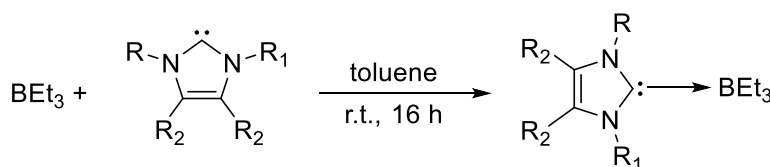


- compound **45**: R = R₁ = *n*Pr, R₂ = H
 compound **46**: R = R₁ = *i*Pr, R₂ = H
 compound **47**: R = R₁ = R₂ = Me
 compound **48**: R = R₁ = *i*Pr, R₂ = Me
 compound **49**: R = Me, R₁ = *t*Bu, R₂ = H
 compound **50**: R = R₁ = Dipp, R₂ = H

Scheme 118: The isolated mono-NHC adducts BPh₃•NHC **45-50** were heated to 110 °C for several days to obtain any further ring expansion or ring contraction reaction; however, in each case, no reaction took place.

2.2.4.3. Synthesis of the mono-NHC adducts of the type Et₃B•NHC

In addition to adducts of the type Ph₃B•NHC **45-50**, the stoichiometric reactions of BEt₃ and several NHCs were carried out at room temperature (Scheme 119). The corresponding mono-NHC adducts Et₃B•Me₂Im **51**, Et₃B•*i*Pr₂Im **52**,^[266] Et₃B•*i*Pr₂Im^{Me} **53** and Et₃B•Dipp₂Im **54**^[265, 270] as well as the mono-NHC adducts of the saturated NHC Et₃B•Dipp₂Slm were isolated and characterized.



- compound **51**: R = R₁ = Me, R₂ = H
 compound **52**: R = R₁ = *i*Pr, R₂ = H
 compound **53**: R = R₁ = *i*Pr, R₂ = Me
 compound **54**: R = R₁ = Dipp, R₂ = H
 compound **55**: R = R₁ = Dipp, R₂ = H₂

Scheme 119: Synthesis of the mono-NHC adduct Et₃B•NHC **51-55** via reaction of BEt₃ with one equivalent of NHC (NHC = Me₂Im, *i*Pr₂Im, *i*Pr₂Im^{Me} and Dipp₂Im as well as the saturated Dipp₂Slm).

The characterization of the mono-NHC adduct Et₃B•Me₂Im **51** will be discussed in detail in the following paragraph. The spectroscopic characterization of the remaining compounds is summarized in Table 8. In the ¹H NMR spectrum, one set of signals for the Me₂Im and the BEt₃-group is observed (Figure 101). The methyl-moiety of the NHC resonate at 3.18 ppm and the corresponding backbone at 5.54 ppm. The methylene-groups of the BEt₃-moiety appear

as a broad multiplet at 0.93-1.00 ppm and the methyl-groups are detected as a broad multiplet at 1.15-118 ppm.

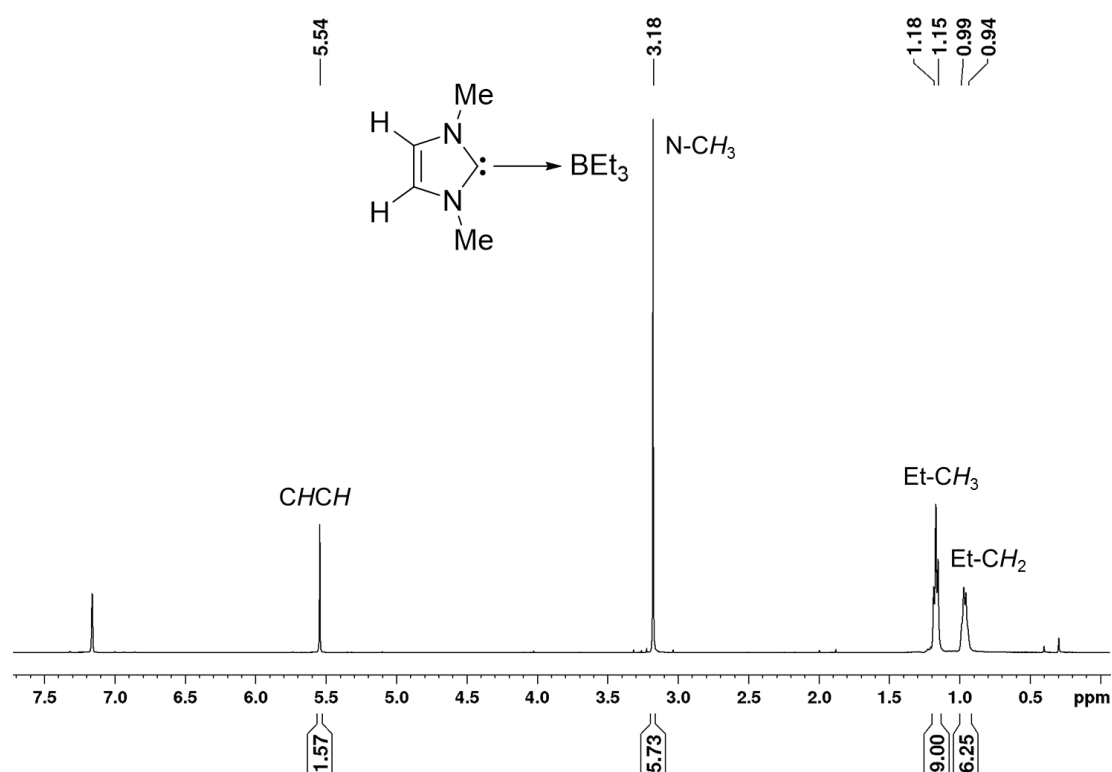


Figure 101: ¹H NMR spectrum of Et₃B•Me₂Im **51** in C₆D₆ (500 NMR).

The ¹¹B{¹H} NMR spectrum shows one sharp signal at -12.3 ppm which appears in the expected region for sp³-hybridized boron atoms (Figure 102). In the ¹³C{¹H} NMR spectrum, one set of signals is detected for the Me₂Im and for BEt₃. The methyl-group of the NHC is observed at 37.3 ppm and the carbon atoms of the backbone at 120.9 ppm. The carbene carbon atom is shifted to higher field due to the coordination to the boron atom and is detected at 176.9 ppm. Additionally, the methylene-groups of the BEt₃ appear at 15.1 ppm and the methyl-groups resonate at 12.1 ppm.

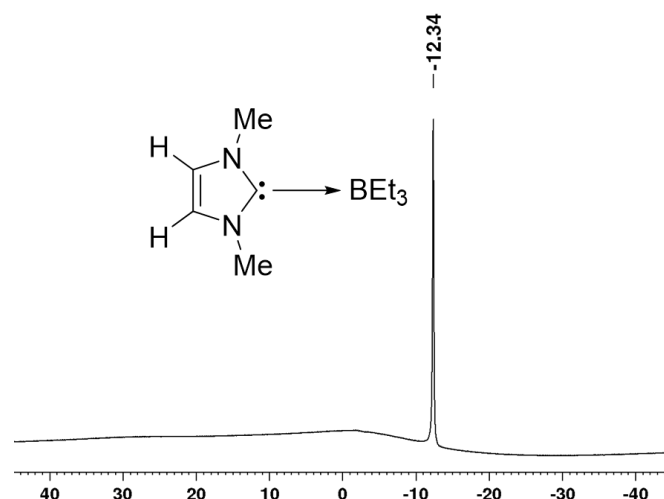


Figure 102: ^1H NMR spectrum of $\text{Et}_3\text{B}\cdot\text{Me}_2\text{Im}$ **51** in C_6D_6 .

Table 8 lists selected NMR spectroscopic data and isolated yields for the mono-NHC adducts $\text{Et}_3\text{B}\cdot i\text{Pr}_2\text{Im}$ **52**, $\text{Et}_3\text{B}\cdot i\text{Pr}_2\text{Im}^{\text{Me}}$ **53**, $\text{Et}_3\text{B}\cdot\text{Dipp}_2\text{Im}$ **54** and $\text{Et}_3\text{B}\cdot\text{Dipp}_2\text{SIm}$ **55**. The spectroscopic data obtained are comparable to those of the mono-NHC adduct $\text{Ph}_3\text{B}\cdot\text{Me}_2\text{Im}$ **51**.

NHC adduct	$\text{Et}_3\text{B}\cdot i\text{Pr}_2\text{Im}$ 52	$\text{Ph}_3\text{B}\cdot i\text{Pr}_2\text{Im}^{\text{Me}}$ 53	$\text{Ph}_3\text{B}\cdot\text{Dipp}_2\text{Im}$ 54	$\text{Ph}_3\text{B}\cdot\text{Dipp}_2\text{SIm}$ 55
^1H NMR [ppm]	0.98, 0.99-1.04, 1.17-1.20, 5.45, 6.19	1.03-1.08, 1.12, 1.23-1.26, 1.58, 5.78	0.44-0.48, 0.96, 1.07-1.10, 1.42, 2.96, 6.29, 7.08-7.09, 7.19-7.22	0.34-0.40, 1.03-1.09, 1.48-1.50, 3.33-3.44, 7.06-7.08, 7.14-7.18
$^{11}\text{B}\{^1\text{H}\}$ NMR [ppm]	-11.7	-11.2	-12.5	-12.6
$^{13}\text{C}\{^1\text{H}\}$ NMR [ppm]	NCN: 174.7	NCN: 174.5	NCN: 183.0	NCN:
Yield [%]	47	60	61	48

Table 8: Selected ^1H , $^{11}\text{B}\{^1\text{H}\}$ and $^{13}\text{C}\{^1\text{H}\}$ NMR data as well as the isolated yield of the mono-NHC adducts $\text{Et}_3\text{B}\cdot i\text{Pr}_2\text{Im}$ **52**, $\text{Et}_3\text{B}\cdot i\text{Pr}_2\text{Im}^{\text{Me}}$ **53**, $\text{Et}_3\text{B}\cdot\text{Dipp}_2\text{Im}$ **54** and $\text{Et}_3\text{B}\cdot\text{Dipp}_2\text{SIm}$ **55**.

In addition to the NMR spectroscopic data obtained of the mono-NHC adduct $\text{Et}_3\text{B}\cdot\text{NHC}$ **51-55**, single crystals for X-ray diffraction were obtained for compounds **51-53** and **55**. All four molecular structures confirmed adduct formation between BEt_3 and the different NHCs

(Figure 103). The bond lengths observed for all structures are comparable. For example, the C1–B1 bond distances are **51**: C1–B1 1.663(2) Å, **52**: C1–B1 1.681(2) Å, **53**: C1–B1 1.692(2) Å and **55**: C1–B1 1.686(3) Å.

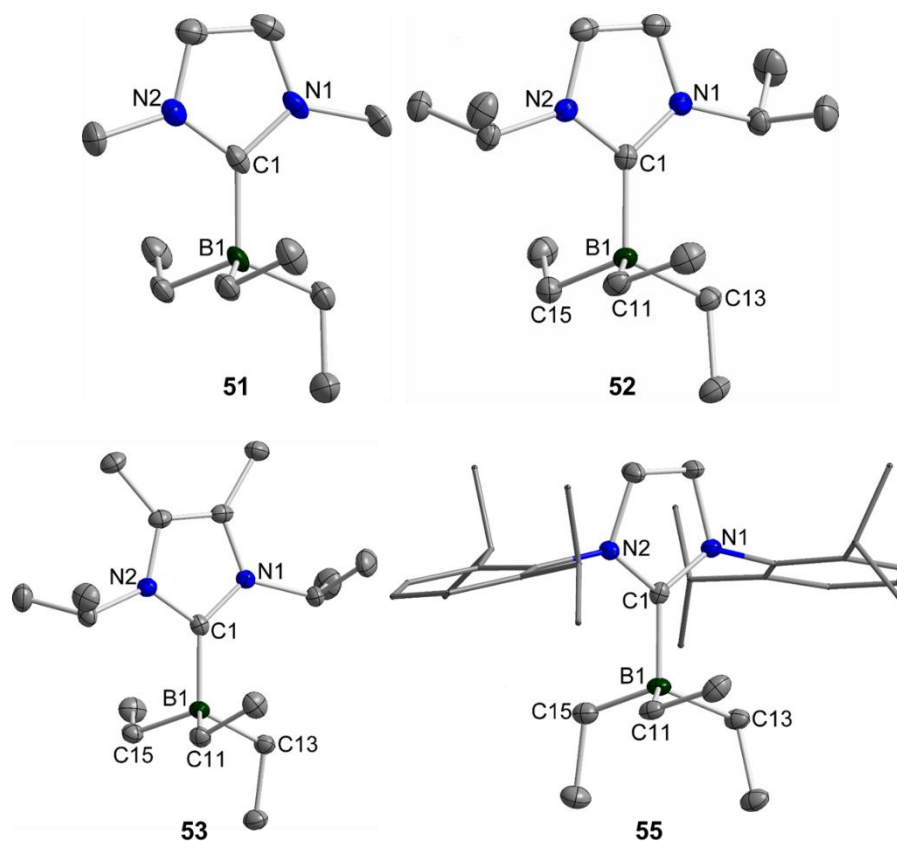
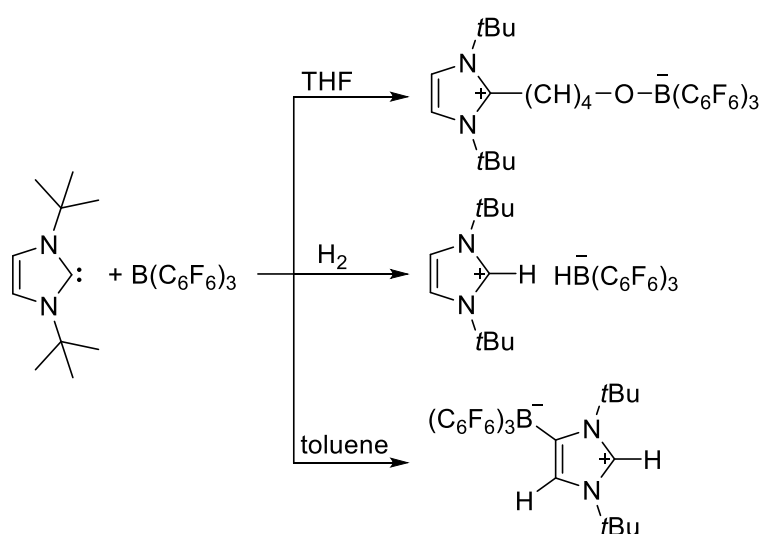


Figure 103: Top, left: molecular structure of $\text{Et}_3\text{B}\cdot\text{Me}_2\text{Im}$ **51** with thermal ellipsoids drawn at the 50% probability level; hydrogen atoms are omitted for clarity. Selected bond distances (Å) and angles ($^\circ$): C1–B1 1.663(2); C1–B1–C11 107.02(11), C1–B1–C13 111.92(11), C1–B1–C15 107.56(11). Top, right: molecular structure of $\text{Et}_3\text{B}\cdot i\text{Pr}_2\text{Im}$ **52** with thermal ellipsoids drawn at the 50% probability level; hydrogen atoms are omitted for clarity. Selected bond distances (Å) and angles ($^\circ$): C1–B1 1.681(2); C1–B1–C11 106.97(10), C1–B1–C13 113.22(10), C1–B1–C15 107.59(11). Bottom, left: molecular structure of $\text{Et}_3\text{B}\cdot i\text{Pr}_2\text{Im}^{\text{Me}}$ **53** with thermal ellipsoids drawn at the 50% probability level; hydrogen atoms are omitted for clarity. Selected bond distances (Å) and angles ($^\circ$): C1–B1 1.692(2); C1–B1–C11 107.33(10), C1–B1–C13 115.22(10), C1–B1–C15 107.29(10). Bottom, right: molecular structure of $\text{Et}_3\text{B}\cdot\text{Dipp}_2\text{SIm}$ **55** with thermal ellipsoids drawn at the 50% probability level; hydrogen atoms are omitted and the Dipp-substituents are drawn wires/sticks for clarity. Selected bond distances (Å) and angles ($^\circ$): C1–B1 1.686(3); C1–B1–C11 104.68(13), C1–B1–C13 111.00(13), C1–B1–C15 107.53(13).

Additionally, the isolated mono-NHC adducts **51–55** were also heated to 110 $^\circ\text{C}$ in toluene to observe whether any ring expansion or ring contraction reaction takes place; however, the adducts are stable at higher temperatures and no evidence for any further reaction was obtained.

2.2.5. Synthesis of the backbone-activated compounds of the type R_3B-tBu_2Im-H

In the last few years, several examples of the reactions of different substrates with the NHC tBu_2Im were reported which all show similar “abnormal” binding of tBu_2Im to the substrates (Scheme 120). “Abnormal” binding results from the coordination of the C4 carbon atom to the substrate, instead of the C2 carbon atom. Examples of such reported observations include metal-complexes^[271-277] and organic substrates. For example, Dagorne *et al.* reported reaction of $AlMe_3$ with tBu_2Im which yielded an “abnormal” adduct $Me_3Al-tBu_2Im-H$.^[277] Furthermore, the abnormal binding of the tBu_2Im NHC was also observed by Tamm *et al.*^[172, 174, 181, 188, 278-279] during their study on frustrated carbene-borane Lewis pairs (FLPs) in 2008.^[172] The reaction of tBu_2Im with $B(C_6F_6)_3$ in THF led to a ring opening of the THF and further binding of the former carbene carbon atom to the $(CH_2)_4$ -chain and the $B(C_6F_6)_3$ to the oxygen. The reaction of the FLP $tBu_2Im/B(C_6F_6)_3$ with dihydrogen (H_2) yielded the corresponding imidazolium borate. Additionally, stirring both compounds in toluene for two hours led to the observation of “abnormal” binding of the carbene ligand to the boron compound. Similar results were also reported using Ad_2Im (adamantyl-imidazolin-2-ylidene) as the NHC.^[278]

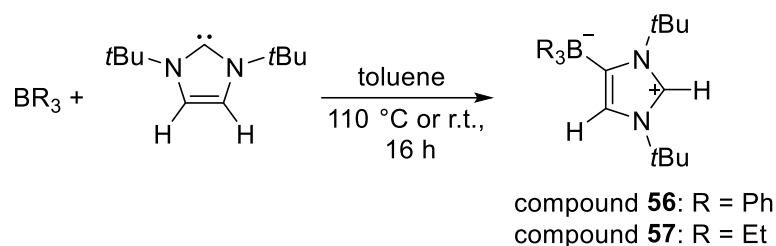


Scheme 120: Reaction of tBu_2Im with $B(C_6F_6)_3$ with THF, H_2 and in toluene.

Furthermore, one year later Tamm and co-workers also reported that the reaction of the corresponding saturated tBu_2SIIm with $B(C_6F_6)_3$ yielded similar results with THF and H_2 ; however, a similar “abnormal” ligand binding was not observed.^[181]

2.2.5.1. Synthesis of the backbone-activated compound $\text{Ph}_3\text{B}\cdot\text{tBu}_2\text{Im-H}$

Based on the synthesis of the mono-NHC adducts $\text{R}_3\text{B}\cdot\text{NHC}$ **45-55**, a similar reaction was conducted using tBu_2Im as the NHC (Scheme 121).



Scheme 121: Synthesis of the abnormal adducts of the type $\text{R}_3\text{B}\cdot\text{tBu}_2\text{Im-H}$ **56** and **57** *via* reaction of BR_3 (R = Ph, Et) with tBu_2Im at higher and room temperature.

Thus, the reaction of BPh_3 and tBu_2Im was carried out under the same reaction conditions; however, the NMR spectroscopic data obtained for the isolated solid were quite different to those observed for the mono-NHC adducts $\text{BPh}_3\cdot\text{NHC}$ **45-50**.

In the ^1H NMR spectrum of $\text{Ph}_3\text{B}\cdot\text{tBu}_2\text{Im-H}$ **56**, two signals with an integral of 9 are observed for the tBu -groups (0.64 and 1.03 ppm) and the backbone is also split into two signals, one doublet at 6.86 ppm and the other one between 7.38 and 7.41 ppm (overlapped with the signals of the aryl-CH-groups) (Figure 104). These observations confirm the loss of the symmetry of tBu_2Im which could be an evidence for a ring opening of the NHC and further insertion C–N bond of the NHC; however, the resonances of the three phenyl-groups of the BPh_3 are not split into further signals. This implies that the backbone activation of the NHC took place rather than a ring expansion reaction.

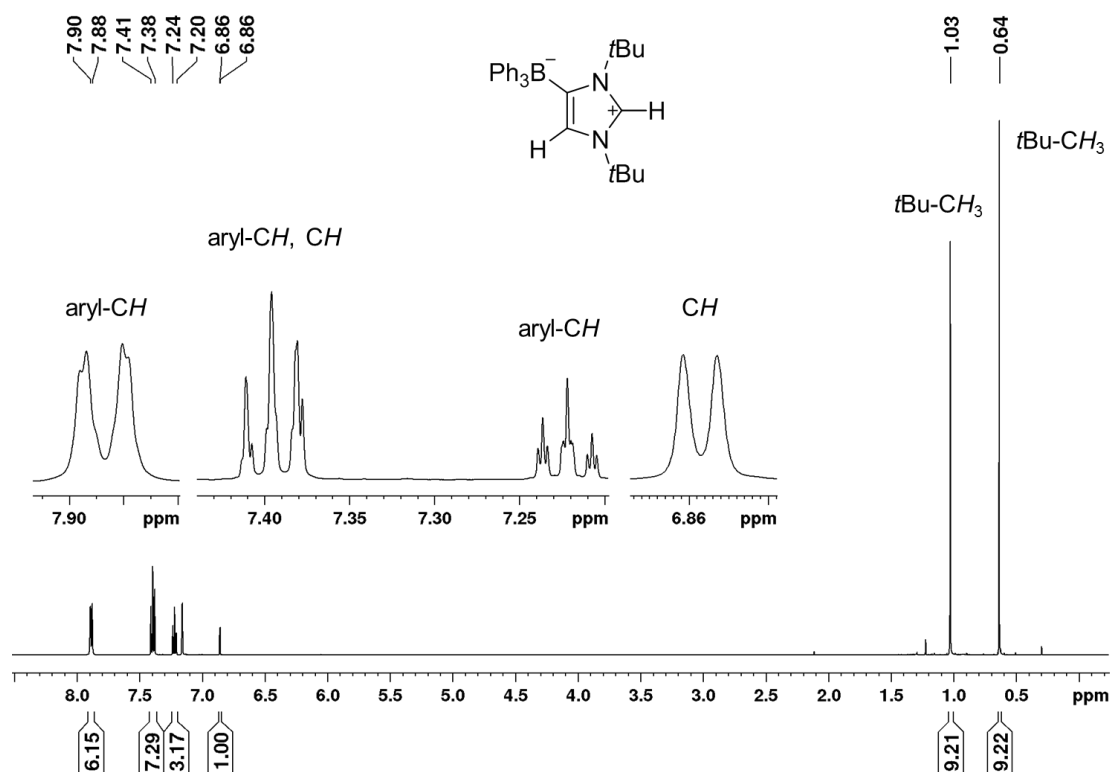


Figure 104: ^1H NMR spectrum of $\text{Ph}_3\text{B-tBu}_2\text{Im-H}$ **56** in C_6D_6 (500 MHz).

Additionally, the $^{11}\text{B}\{^1\text{H}\}$ NMR spectrum of the isolated solid shows one sharp signal at -7.96 ppm which is in good agreement with an sp^3 -hybridized boron atom (Figure 105).

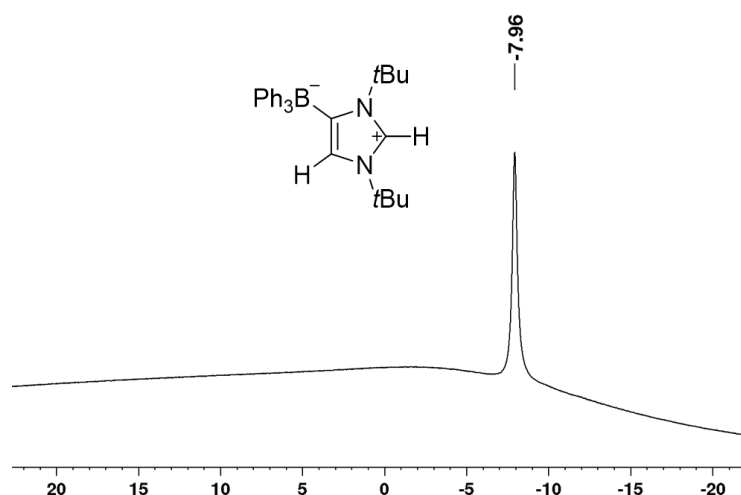


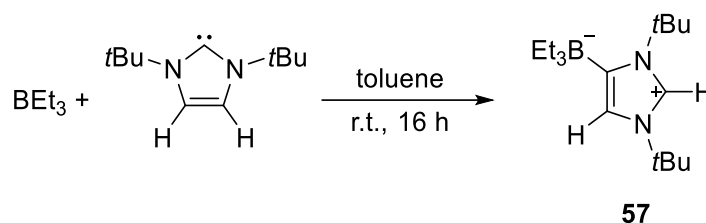
Figure 105: $^{11}\text{B}\{^1\text{H}\}$ NMR spectrum of $\text{Ph}_3\text{B-tBu}_2\text{Im-H}$ **56** in C_6D_6 .

The $^{13}\text{C}\{^1\text{H}\}$ NMR spectrum of the backbone-activated compound $\text{Ph}_3\text{B-tBu}_2\text{Im-H}$ **56** shows two signals for the carbon atoms of the *t*Bu-groups at 29.0 and 31.8 ppm as well as two signals for the quaternary carbon atoms of the *t*Bu-groups at 56.8 and 61.7 ppm. Additionally, the carbon atoms of the backbone the former carbene carbon atom resonate at 125.4 and 129.5 ppm and the quaternary carbon atom of the backbone at 159.9 ppm. The aryl-CH carbon

atoms of the BPh_3 resonate at 123.9 and 126.9 ppm and the corresponding quaternary carbon atoms at 136.5 ppm.

2.2.5.2. Synthesis of the backbone-activated compound $\text{Et}_3\text{B-tBu}_2\text{Im-H}$ **57**

The reaction of triethylborane (BEt_3) with tBu_2Im gave the similar abnormal adduct $\text{Et}_3\text{B-tBu}_2\text{Im-H}$ **57**, as described above for the triphenylborane (BPh_3). The reaction was carried out at room temperature and was monitored *via* $^{11}\text{B}\{^1\text{H}\}$ NMR spectroscopy to follow the conversion of the starting material. After work-up, the similar backbone-activated compound $\text{Et}_3\text{B-tBu}_2\text{Im-H}$ **57** was isolated (Scheme 122).



Scheme 122: Synthesis of the backbone-activated compound $\text{Et}_3\text{B-tBu}_2\text{Im-H}$ **57** *via* reaction of BEt_3 with tBu_2Im .

The ^1H and $^{13}\text{C}\{^1\text{H}\}$ NMR spectra of compound **57** are in good agreement with the abnormal binding of the two substrates. Therefore, the ^1H NMR spectrum indicates the presence of two different tBu -groups and CH-groups (Figure 106). One singlet of the tBu -group is observed at 0.78 ppm and the second one at 1.44 ppm. For the proton of the backbone one doublet is detected at 7.05 ppm, the proton attached to the former carbene carbon atom appears at 7.22 ppm. Additionally, the methyl-groups of the BEt_3 resonate as a multiplet at 1.35-1.38 ppm and the methylene-groups are observed as a multiplet at 1.10-1.15 ppm.

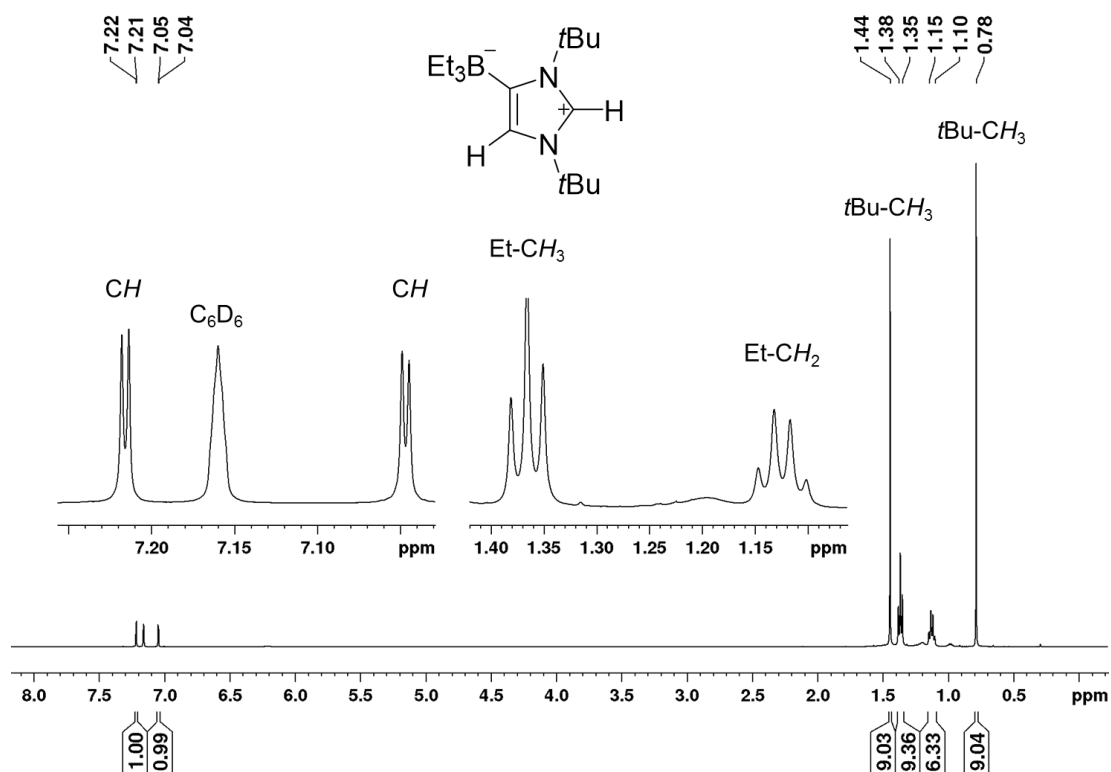


Figure 106: ^1H NMR spectrum of $\text{Et}_3\text{B-tBu}_2\text{Im-H}$ **57** in C_6D_6 (500 MHz).

The $^{11}\text{B}\{^1\text{H}\}$ NMR spectrum of $\text{Et}_3\text{B-tBu}_2\text{Im-H}$ **57** shows one sharp signal at -13.1 ppm which is in the expected region for an sp^3 -hybridized boron atom (Figure 107). In the $^{13}\text{C}\{^1\text{H}\}$ NMR spectrum, the signals for the methyl-groups of the tBu -moieties occur at 29.1 and 30.8 ppm and the corresponding quaternary carbon atoms at 56.1 and 59.3 ppm. The tertiary carbon atom of the backbone and of the former carbene carbon atom resonate at 123.7 and 126.4 ppm. The quaternary carbon atom of the backbone is detected at 163.1 ppm

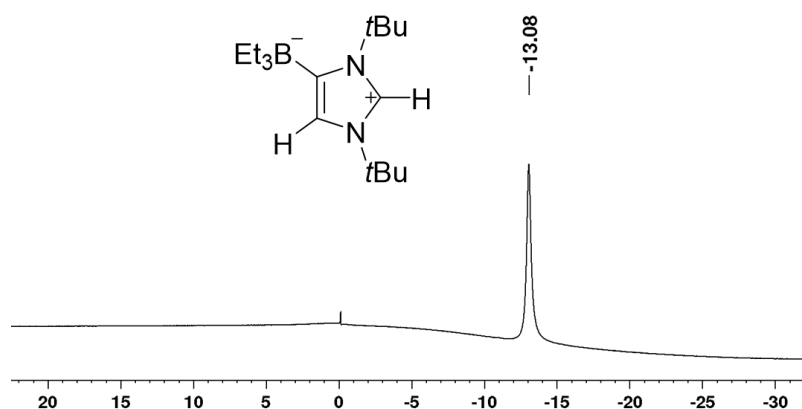


Figure 107: $^{11}\text{B}\{^1\text{H}\}$ NMR spectrum of $\text{Et}_3\text{B-tBu}_2\text{Im-H}$ **57** in C_6D_6 .

3. EXPERIMENTAL SECTION

3.1. General procedures

Unless otherwise noted, all manipulations were performed using standard Schlenk or glovebox (Innovative Technology Inc.) techniques under an atmosphere of dry nitrogen or argon. Reagent grade solvents (Fisher Scientific and J. T. Baker) were nitrogen saturated and were dried and deoxygenated using an Innovative Technology Inc. Pure-Solv 400 Solvent Purification System, and further deoxygenated by using the freeze-pump-thaw method.

Toluene was dried over potassium/benzophenone and freshly distilled before using. *n*-Hexane was dried over lithium aluminium hydride. MeCN was first dried over sodium hydride and distilled. Afterwards, dried over P₄O₁₀ and freshly distilled.

THF-d₈ and CH₃OD were obtained from Cambridge Isotope Laboratories and EURISOTOP and dried over CaH₂ or thoroughly dried 4 Å molecular sieves, respectively, followed by deoxygenating using the freeze-pump-thaw method. C₆D₆ was obtained from EURISOTOP and dried over potassium or sodium. MeCN-d₃ was first dried over sodium hydride and distilled. Afterwards, dried over P₄O₁₀ and freshly distilled.

Starting materials

All other reagents were purchased from commercial sources and were checked for purity by GC-MS.

The diboron reagents B₂pin₂, B₂cat₂ and B₂neop₂ were a generous gift from AllyChem Co. Ltd. NMe₄F salt was a generous gift from Prof. Dr. Maik Finze.

HBcat salt was a generous gift from Prof. Dr. Holger Braunschweig.

The NHCs Me₂Im, *n*Pr₂Im, *i*Pr₂Im, Me*i*PrIm, Me*t*Bulm, *t*Bu₂Im, Mes₂Im and Dipp₂Im as well as the saturated Dipp₂SIIm and the in the backbone methylated NHCs Me₂Im^{Me}, Me₂Im^{Me} were prepared according to literature procedures.^[235, 280]

CAAC^{Me} was prepared according to literature procedure.^[281]

3.2. Analytical methods

Elemental analysis

Elemental analyses (C, H, N, S) were measured with a 'vario Micro cube' from ELEMENTAR for combustion analysis.

Gas Chromatography (GC)

GC-MS analyses were performed using an Agilent 7890A gas chromatograph (column: HP-5MS, 30 m, Ø 0.25mm, film 0.25 µm; injector: 250 °C; oven: 40 °C (2 min), 40 °C to 250 °C

(20 °C min⁻¹), 280 °C (5 min); carrier gas: He (1.6 mL min⁻¹) equipped with an Agilent 5975C inert mass selective detector (MSD) operating in EI mode and an Agilent 7693A automatic liquid handling system (ALS) functioning as autosampler/injector.

Flash chromatography

Flash chromatography was performed with a Biotage® Isolera Four equipped with HP-Sil or KP-Sil cartridges and a diode array UV detector.

High-Resolution Mass Spectrometry (HRMS)

The high resolution mass analysis was measured on a Thermo Scientific Exactive Plus mass spectrometer, equipped with an Orbitrap Mass Analyzer. Measurements were accomplished using an ASAP/APCI source with a corona needle, and carrier-gas (N₂) temperature of 400 °C respectively 350 °C and 250 °C.

3.3. Spectroscopic methods

IR spectroscopy

All IR spectra were recorded on a NICOLET 380 FT-IR spectrometer using ATR. Dependent on the intensity of the vibration bands, the intensity was assigned to following abbreviations: very strong (vs), strong (s), middle (m), weak (w) and very weak (vw).

NMR-Spectroscopy

All NMR spectra were recorded on Bruker Avance 200, Avance 400, DRX-300 or Avance 500 spectrometers and were measured at 296 K. The chemical shifts are expressed in parts per million and are referenced to tetramethylsilane (¹H, ¹³C, ²⁹Si) and 85% H₃PO₄ (³¹P), Cl₃CF (¹⁹F) as the external standard *via* the residual proton signals of the deuterated solvent for the proton NMR spectra (¹H: C₆D₆, 7.16 ppm, THF-d₈ 1.72 ppm, CD₃CN 1.94 ppm) and the resonances of the naturally occurring ¹³C isotope in the carbon NMR spectra (¹³C: C₆D₆, 128.06 ppm, THF-d₈ 61.50 ppm, 126.28 ppm, CD₃CN 1.32 ppm, 118.26 ppm). All ¹³C NMR spectra are ¹H broadband decoupled. The coupling constants (J) are given in Hertz [Hz] without consideration of the sign. For multiplicities, the following abbreviations are used: s = singlet, d = doublet, t = triplet, m = multiplet, br = broad, v = very.

The solid-state magic-angle spinning (MAS) NMR spectra were recorded using a Bruker DSX-400 spectrometer operating at 128.38 MHz for ¹¹B, 400.15 MHz for ¹H and 100.6 MHz for ¹³C and with a 4 mm o. d. rotor. Chemical shifts were calibrated externally using adamantane (38.48 ppm).

3.4. Synthesis of starting materials

Following aryl-diazonium salts [R-C₆H₅N₂][BF₄] were synthesized according to literature procedure.^[282-284]

Compound 10a: phenyldiazonium-tetrafluoroborate [C₆H₅N₂][BF₄]

A solution of aniline (5.00 g, 0.05 mmol) in 5 mL of water and 50% tetrafluoroboric acid (32.0 g, 8.0 equiv.) was stirred at 0 °C and NaNO₂ (4.08 g, 0.06 mmol, 1.1 equiv.) was added slowly to the solution. The reaction mixture was stirred for 1 h at room temperature. Afterwards, the precipitate was collected *via* filtration and dried *in vacuo* to give 7.50 g of the product.

Yield: 7.50 g (72%) of a colorless solid.

¹H NMR (200 MHz, MeCN-d₃, 25 °C): δ_H / ppm = 7.89-7.97 (m, 2 H, CH), 8.22-8.30 (m, 1 H, CH), 8.47-8.51 (m, 2 H, CH).

¹¹B{¹H} NMR (64 MHz, MeCN-d₃, 25 °C): δ_B / ppm = 1.15 (s).

¹⁹F NMR (188 MHz, MeCN-d₃, 25 °C): δ_F / ppm = -151.3 (s).

Compound 10b: *p*-phenyl-diazonium-tetrafluoroborate [4-Me-C₆H₄N₂][BF₄]

A solution of *p*-toluidine (2.5 g, 0.02 mmol) in 5 mL of water and 50% tetrafluoroboric acid (12.3 g, 6.0 equiv.) was stirred at 0 °C and NaNO₂ (1.85 g, 0.03 mmol, 1.1 equiv.) was added slowly to the solution. The reaction mixture was stirred for 1 h at room temperature. Afterwards, the precipitate was collected *via* filtration and dried *in vacuo* to give 2.00 g of the product.

Yield: 2.00 g (42%) of a colorless solid.

¹H NMR (200 MHz, MeCN-d₃, 25 °C): δ_H / ppm = 2.60 (s, 3 H, CH₃), 7.73 (d, ³J_{HH} = 9 Hz, 2 H, CH), 8.37 (d, ³J_{HH} = 9 Hz, 2 H, CH).

¹¹B{¹H} NMR (64 MHz, MeCN-d₃, 25 °C): δ_B / ppm = 1.16 (s).

¹⁹F NMR (188 MHz, MeCN-d₃, 25 °C): δ_F / ppm = -151.3 (s).

Compound 10c: *p*-methoxyphenyldiazonium tetrafluoroborate [4-MeO-C₆H₄N₂][BF₄]

A solution of *p*-methoxyaniline (5.00 g, 0.04 mmol) in 5 mL of water and 50% tetrafluoroboric acid (22.0 g, 6.0 equiv.) was stirred at 0 °C and NaNO₂ (3.08 g, 0.04 mmol, 1.1 equiv.) was added slowly to the solution. The reaction mixture was stirred for 1 h at room temperature. Afterwards, the precipitate was collected *via* filtration and dried *in vacuo* to give 6.80 g of the product.

Yield: 6.80 g (75 %) of a red solid.

¹H NMR (200 MHz, MeCN-d₃, 25 °C): δ_H / ppm = 4.06 (s, 3 H, OCH₃), 7.35 (d, ³J_{HH} = 9 Hz, 2 H, CH), 8.42 (d, ³J_{HH} = 9 Hz, 2 H, CH).

¹¹B{¹H} NMR (64 MHz, MeCN-d₃, 25 °C): δ_B / ppm = 1.17 (s).

¹⁹F NMR (188 MHz, MeCN-d₃, 25 °C): δ_F / ppm = -151.4 (s).

Compound 10d: *p*-nitrophenyldiazonium tetrafluoroborate [4-O₂N-C₆H₄N₂][BF₄]

A solution of *p*-nitroaniline (5.00 g, 0.036 mmol) in 5 mL of water and 50% tetrafluoroboric acid (32.0 g, 8.0 equiv.) were stirred at 0 °C and NaNO₂ (2.75 g, 0.040 mmol, 1.1 equiv.) was added slowly to the solution. The reaction mixture was stirred for 1 h at room temperature. Afterwards, the precipitate was collected *via* filtration and dried *in vacuo* to give 7.85 g of the product.

Yield: 7.85 g (92%) of a green solid.

¹H NMR (200 MHz, MeCN-d₃, 25 °C): δ_H / ppm = 8.62 (d, ³J_{HH} = 9 Hz, 2 H, CH), 9 (d, ³J_{HH} = 9 Hz, 2 H, CH).

¹¹B{¹H} NMR (64 MHz, MeCN-d₃, 25 °C): δ_B / ppm = 1.18 (s).

¹⁹F NMR (188 MHz, MeCN-d₃, 25 °C): δ_F / ppm = -151.0 (s).

Compound 10f: *p*-methoxyphenyldiazonium tetraphenylborate [4-MeO-C₆H₄N₂][BPh₄]

A solution of *p*-methoxyaniline (0.50 g, 4.06 mmol) in 5 mL of water and 3 mL hydrochloric acid were mixed at ambient temperature and cooled to 0 °C. Afterwards, NaNO₂ (291 mg, 4.22 mmol) was added slowly to the solution and the excess HNO₂ was decomposed with sulfamic acid. Finally, NaBPh₄ (1.39 g, 4.06 mmol) was added to the reaction mixture and the precipitate was collected *via* filtration and dried *in vacuo* to give 1.47 g of the product.

Yield: 1.47 g (80%) of a yellow solid.

¹H NMR (200 MHz, MeCN-d₃, 25 °C): δ_H / ppm = 4.04 (s, 3 H, O-CH₃), 6.79-6.80 (m, 4 H, aryl-H, BPh₄), 6.94-7.05 (m, 8 H, aryl-H, BPh₄), 7.22-7.35 (m, 10 H, aryl-H, BPh₄, aryl-CH), 8.29-8.34 (m, 2 H, aryl-CH).

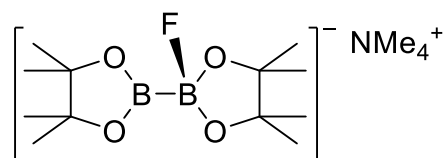
¹¹B{¹H} NMR (64 MHz, MeCN-d₃, 25 °C): δ_B / ppm = -6.61.

3.5. Synthesis of novel compounds

3.5.1. Synthesis of anionic sp^2 - sp^3 diboron adducts of the type $[B_2(OR)_4F][NMe_4]$

Compound 4: $[B_2pin_2F][NMe_4]$

NMe_4F (257 mg, 2.76 mmol, 1 equiv.) and B_2pin_2 (700 mg, 2.76 mmol, 1 equiv.) were combined in 60 mL of dry THF. After 16 h of stirring at 70 °C, the precipitate was collected



by filtration and washed twice with 5 mL of dry THF. The residue was crystallized from acetonitrile to obtain the product.

Yield: 565 mg (60%) of a colorless crystalline solid

For X-ray diffraction: In a flame-sealed ampoule $[B_2pin_2F][NMe_4]$ **4** and THF were heated to 100 °C within 2 h. After 4 h at this temperature the sample was cooled to room temperature within 150 h. In the tube two types of crystals were found colorless needles and prisms. A needle shaped crystal was used for this XRD.

1H NMR (500 MHz, $MeCN-d_3$, 25 °C): δ = 1.03 (s, 24 H, $C(CH_3)$), 3.14 (t, $^3J_{HN}$ = 1 Hz, 12 H, $N(CH_3)_4$)

^{11}B NMR (160 MHz, $MeCN-d_3$, 25 °C): δ = 5.7 (br s), 33.9 (v br s).

$^{13}C\{^1H\}$ NMR (175 MHz, $MeCN-d_3$, 25 °C): δ = 26.2 ($C(CH_3)$), 56.1 (t, $^3J_{CN}$ = 4 Hz, $N(CH_3)_4$), 78.9 (br, $C(CH_3)$).

^{19}F NMR (188 MHz, $MeCN-d_3$, 25 °C): δ = -125.6 (s).

1H NMR (200 MHz, $MeCN-d_3$, -30 °C): δ = 0.88 (s, 6 H, $C(CH_3)$), 0.96 (s, 6 H, $C(CH_3)$), 1.04 (s, 12 H, $C(CH_3)$), 3.10 (s, 12 H, $N(CH_3)_4$).

^{11}B SSNMR (128 MHz, 25 °C): δ = 5.5 (sp^3 -B atom), 37.5 (sp^2 -B atom).

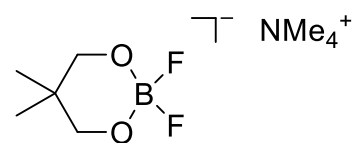
^{13}C SS NMR (100 MHz, 25 °C): δ = 25.9 (br, $C(CH_3)$), 54.9 ($N(CH_3)_4$), 77.0 (br, $C(CH_3)$), 80.2 (br, $C(CH_3)$).

^{19}F SS NMR (376 MHz, 25 °C): δ = -130.6.

Elemental analysis calcd (%) for $C_{16}H_{36}O_4NB_2F$: C 55.37, H 10.45, N 4.04; found: C 55.24, H 10.67, N 4.35.

Compound 6: $[neopBF_2][NMe_4]$

B_2neop_2 (200 mg, 0.88 mmol) and NMe_4F (82.4 mg, 0.88 mmol) were dissolved in 20 ml of dry THF and the reaction was stirred at 70 °C overnight. After cooling to room temperature, the precipitate was collected by filtration, washed twice with 5 mL of THF and dried *in vacuo* to obtain $[neopBF_2][NMe_4]$.



Yield: 95 mg (34%) colorless solid.

¹H NMR (500 MHz, MeCN-d₃, 25 °C): δ_H / ppm = 0.80 (s, 6 H, CH₃), 3.10 (t, J_{HH} = 1 Hz, 12 H, C(CH₃)), 3.28 (s, 4 H, CH₂).

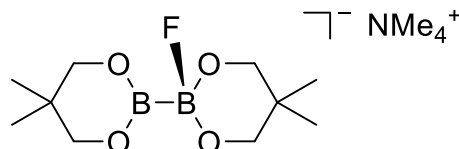
¹¹B NMR (160 MHz, MeCN-d₃, 25 °C): δ_B / ppm = 0.32 (t, ¹J_{BF} = 19 Hz).

¹⁹F NMR (188 MHz, MeCN-d₃, 25 °C): δ_F / ppm = -150.8 (q, ¹J_{FB} = 19 Hz).

¹³C NMR (125 MHz, MeCN-d₃, 25 °C): δ_C / ppm = 22.9 (CH₃), 32.7 (C_q), 56.0 (t, J = 4 Hz, N(CH₃)₄), 73.4 (t, J = 4 Hz, CH₂).

Compound 7: [B₂neop₂F][NMe₄]

NMR scale reaction: B₂neop₂ (20.0 mg, 89.0 μmol, 1 equiv.) and NMe₄F (8.30 mg, 88.5 μmol, 1 equiv.) were dissolved in 0.6 mL MeCN-d₃ and the reaction mixture



was immediately monitored *via* NMR-spectroscopy. Compound **6** as well as the anionic adduct [B₂neop₂F][NMe₄] **7** were observed.

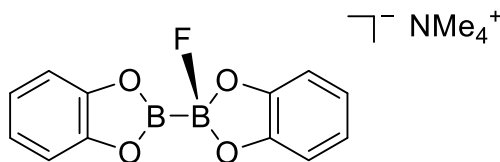
¹H NMR (200 MHz, MeCN-d₃, 25 °C): δ_H / ppm = 0.83 (s, 12 H, neop-CH₃), 3.14 (s, 12 H, N(CH₃)₄), 3.34 (s br, 8 H, neop-CH₂).

¹¹B{¹H} NMR (64 MHz, MeCN-d₃, 25 °C): δ_B / ppm = these are the signals of compounds [neopBF₂][NMe₄] **8** (0.32 ppm) and [B₂neop₂F][NMe₄] **7** (29.4 ppm (sp²) and 1.88 ppm (sp³)).

¹⁹F NMR (188 MHz, MeCN-d₃, 25 °C): δ_F / ppm = -150 ppm (s).

Compound 9: [B₂cat₂F][NMe₄]

NMe₄F (39.0 mg, 420 μmol, 1 equiv.) and B₂cat₂ (100 mg, 420 μmol, 1 equiv.) were combined in 20 mL of dry MeCN. After 1 h of stirring at room



temperature, the solvent was removed *in vacuo* and the colorless solid was isolated.

Yield: 100 mg (72%) of a colorless solid.

¹H NMR (200 MHz, MeCN-d₃, 25 °C): δ = 3.04 (N(CH₃)₄), 6.77-6.87 (m, 8 H, cat-CH).

¹¹B NMR (64 MHz, MeCN-d₃, 25 °C): δ = 6.50 (v br s), 32.8 (br s).

¹⁹F NMR (188 MHz, MeCN-d₃, 25 °C): δ = -129.6 (s).

¹¹B SSNMR (128 MHz, 25 °C): δ = 5.6 (sp³-B atom), 35.2 (sp²-B atom).

¹³C SS NMR (100 MHz, 25 °C): δ = 54.5 (br, N(CH₃)₄), 108.4 (cat-CH), 111.8 (cat-CH), 117.8 (cat-CH), 125.0 (cat-CH), 147.9 (cat-C), 152.3 (cat-CH).

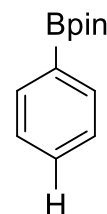
¹⁹F SS NMR (376 MHz, 25 °C): δ = -121.4.

3.5.2. Reactivity of adduct **4** and the in situ formed adducts **7** and **9** with different diazonium $[\text{BF}_4]^-$ salts

3.5.2.1. Reactivity of $[\text{B}_2\text{pin}_2\text{F}][\text{NMe}_4]$ with different diazonium $[\text{BF}_4]^-$ salts

Compound **11a**: 2-phenyl-4,4,5,5-tetramethyl-1,3,2-dioxaborane

$[\text{B}_2\text{pin}_2\text{F}][\text{NMe}_4]$ **4** (400 mg, 1.15 mmol, 1.4 equiv.) and freshly prepared phenyldiazonium-tetrafluoroborate $[\text{C}_6\text{H}_5\text{N}_2][\text{BF}_4]$ **5a** (158 mg, 0.83 mmol, 1 equiv.) were combined in 20 mL of acetonitrile to give a dark red solution and dinitrogen formed was vented from the Schlenk tube. Afterwards, the reaction mixture was quenched with 10 mL of Et_2O and the solution was filtered to remove the precipitate ($[\text{NMe}_4][\text{BF}_4]$). The solvent was evaporated under vacuum and the residue was re-dissolved in 20 mL of *n*-hexane. The solution was filtered to remove any insoluble materials and the product was purified by automated flash chromatography (*n*-hexane/ Et_2O).



Yield: 70 mg (42%) of a colorless solid.

$^1\text{H NMR}$ (500 MHz, MeCN-d_3 , 25 °C): δ_{H} / ppm = 1.32 (s, 12 H, CH_3), 7.37-7.41 (m, 2 H, CH), 7.46-7.51 (m, 1 H, CH), 7.70-7.73 (m, 2 H, CH).

$^{11}\text{B}\{^1\text{H}\}$ NMR (160 MHz, MeCN-d_3 , 25 °C): δ_{B} / ppm = 29.9 (s).

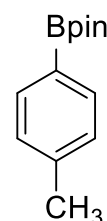
$^{13}\text{C}\{^1\text{H}\}$ NMR (125 MHz, MeCN-d_3 , 25 °C): δ_{C} / ppm = 25.2 (CH_3), 84.8 (OCC_3), 128.8 (CH), 132.3 (CH), 135.4 (CH).

IR (ATR): $[\tilde{\nu} / \text{cm}^{-1}]$: 857 (m), 962 (w), 1025 (m), 1091 (s), 1139 (s), 1165 (w), 1210 (w), 1265 (w), 1355 (vs, C=C), 1392 (m), 1438 (m), 1499 (w), 1603 (w), 2980 (s, C-H).

GC-MS: Ret.: 4.264 min; m/z : 204 $[\text{M}]^+$, 189 $[\text{M}-\text{CH}_3]^+$, 118 $[\text{M}-\text{C}_5\text{H}_{10}\text{O}]^+$, 105 $[\text{M}-\text{C}_6\text{H}_{11}\text{O}]^+$.

Compound **11b**: 2-(4-methylphenyl)-4,4,5,5-tetramethyl-1,3,2-dioxaborane

$[\text{B}_2\text{pin}_2\text{F}][\text{NMe}_4]$ **4** (300 mg, 0.865 mmol) and freshly prepared 4-methylphenyldiazonium-tetrafluoroborate $[\text{4-Me-C}_6\text{H}_4\text{N}_2][\text{BF}_4]$ **5b** (127 mg, 0.617 mmol) were combined in 20 mL of acetonitrile to give a dark red solution and dinitrogen formed was vented from the Schlenk tube. Afterwards, the reaction mixture was quenched with 10 mL of Et_2O and the solution was filtered to remove the precipitate ($[\text{NMe}_4][\text{BF}_4]$). The solvent was evaporated under vacuum and the residue was re-dissolved in 20 mL of *n*-hexane. The solution was filtered to remove any insoluble materials and the product was purified by automated flash chromatography (*n*-hexane/ Et_2O).



Yield: 90 mg (66%) of a yellow solid.

$^1\text{H NMR}$ (500 MHz, MeCN-d_3 , 25 °C): δ_{H} / ppm = 1.31 (s, 12 H, CH_3), 2.35 (s, 3 H, CH_3), 7.20-7.21 (d, $^3J_{\text{HH}} = 8$ Hz, 2 H, CH), 7.59-7.61 (d, $^3J_{\text{HH}} = 8$ Hz, 2 H, CH).

$^{11}\text{B}\{^1\text{H}\}$ NMR (160 MHz, MeCN-d_3 , 25 °C): δ_{B} / ppm = 30.7.

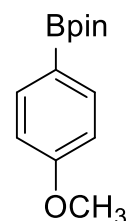
$^{13}\text{C}\{^1\text{H}\}$ NMR (125 MHz, MeCN- d_3 , 25 °C): δ_C / ppm = 21.7 (Ph- CH_3), 25.2 (CH_3), 84.6 (OCC_3), 129.5 (CH), 135.5 (CH), 142.5 (CCH_3).

IR (ATR): [$\tilde{\nu}$ / cm^{-1}]: 815 (m), 858 (m), 963 (w), 1022 (w), 1089 (s), 1142 (s), 1213 (w), 1266 (m), 1320 (s), 1357 (vs), 1398 (m), 1612 (m, C=C), 2977 (m, C-H).

GC-MS: Ret.: 4.989 min; m/z: 218 [M] $^+$, 203 [$\text{M}-\text{CH}_3$] $^+$, 132 [$\text{M}-\text{C}_5\text{H}_{10}\text{O}$] $^+$, 119 [$\text{M}-\text{C}_6\text{H}_{11}\text{O}$] $^+$.

Compound 11c: 2-(4-methoxyphenyl)-4,4,5,5-tetramethyl-1,3,2-dioxaborane

[$\text{B}_2\text{pin}_2\text{F}$][NMe_4] **4** (500 mg, 1.44 mmol) and freshly prepared 4-methoxyphenyldiazonium-tetrafluoroborate [$4\text{-MeO-C}_6\text{H}_4\text{N}_2$][BF_4] **5c** (229 mg, 1.03 mmol) were combined in 20 mL of acetonitrile to give a dark red solution and dinitrogen formed was vented from the Schlenk tube. Afterwards, the reaction mixture was quenched with 10 mL of Et_2O and the solution was filtered to remove the precipitate ([NMe_4][BF_4]). The solvent was evaporated under vacuum and the residue was re-dissolved in 20 mL of *n*-hexane. The solution was filtered to remove any insoluble materials and the product was purified by automated flash chromatography (*n*-hexane/ Et_2O).



Yield: 96 mg (40%) of a yellow oil.

^1H NMR (500 MHz, MeCN- d_3 , 25 °C): δ_H / ppm = 1.30 (s, 12 H, CH_3), 3.80 (s, 3 H, O- CH_3), 6.91-6.93 (d, $^3J_{\text{HH}} = 9$ Hz, 2 H, CH), 7.64-7.66 (d, $^3J_{\text{HH}} = 9$ Hz, 2 H, CH).

$^{11}\text{B}\{^1\text{H}\}$ NMR (160 MHz, MeCN- d_3 , 25 °C): δ_B / ppm = 29.7 (s).

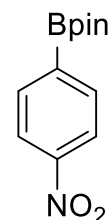
$^{13}\text{C}\{^1\text{H}\}$ NMR (125 MHz, MeCN- d_3 , 25 °C): δ_C / ppm = 25.2 (CH_3), 55.8 (O- CH_3), 84.5 (OCC_3), 114.4 (CH), 137.2 (CH), 163.3 (C- OCH_3).

IR (ATR): [$\tilde{\nu}$ / cm^{-1}]: 830 (w), 859 (w), 962 (w), 1030 (w), 1091 (m), 1141 (s), 1175 (w), 1214 (vw), 1245 (s, C-O), 1277 (w), 1317 (m), 1357 (s), 1395 (w), 1409 (w), 1465 (vw), 1518 (vw), 1570 (vw), 1604 (s, C=C), 2838 (vw), 2935 (vw), 2977 (w, C-H).

GC-MS: Ret.: 5.962 min; m/z: 234 [M] $^+$, 219 [$\text{M}-\text{CH}_3$] $^+$, 148 [$\text{M}-\text{C}_5\text{H}_{10}\text{O}$] $^+$, 134 [$\text{M}-\text{C}_6\text{H}_{12}\text{O}$] $^+$.

Compound 11d: 2-(4-nitrophenyl)-4,4,5,5-tetramethyl-1,3,2-dioxaborane

[$\text{B}_2\text{pin}_2\text{F}$][NMe_4] **4** (300 mg, 0.865 mmol) and freshly prepared *p*-nitrophenyldiazonium tetrafluoroborate [$4\text{-O}_2\text{N-C}_6\text{H}_4\text{N}_2$][BF_4] **5d** (146 mg, 0.617 mmol) were combined in 20 mL of acetonitrile to give a dark red solution and dinitrogen formed was vented from the Schlenk tube. Afterwards, the reaction mixture was quenched with 10 mL of Et_2O and the solution was filtered to remove the precipitate ([NMe_4][BF_4]). The solvent was evaporated under vacuum and the residue was re-dissolved in 20 mL of *n*-hexane. The solution was filtered to remove any insoluble materials and the product was purified by automated flash chromatography (*n*-hexane/ Et_2O).



Yield: 90 mg (59%) of a colorless solid.

¹H NMR (500 MHz, MeCN-d₃, 25 °C): δ_H / ppm = 1.34 (s, 12 H, CH₃), 7.88-7.90 (d, ³J_{HH} = 9 Hz, 2 H, CH), 8.16-8.17 (d, ³J_{HH} = 9 Hz, 2 H, CH).

¹¹B{¹H} NMR (160 MHz, MeCN-d₃, 25 °C): δ_B / ppm = 29.4.

¹³C{¹H} NMR (125 MHz, MeCN-d₃, 25 °C): δ_C / ppm = 25.2 (CH₃), 85.6 (OCC₃), 123.5 (CH), 136.4 (CH), 150.9 (C-NO₂).

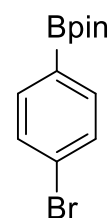
IR (ATR): [ν̃ / cm⁻¹]: 811 (w), 852 (m), 963 (w), 1013 (w), 1085 (m), 1144 (m), 1214 (w), 1270 (m), 1306 (m), 1347 (s, NO₂), 1362 (m), 1397 (m), 1493 (w), 1515 (s), 1597 (w, C=C), 2932 (w), 2976 (w, C-H).

Elemental analysis calcd (%) for C₁₂H₁₆BNO₄: C 57.87, H 6.47, N 5.62; found: C 57.64, H 6.63, N 5.49.

GC-MS: Ret.: 6.725 min; m/z: 249 [M]⁺, 234 [M-CH₃]⁺, 163 [M-C₅H₁₀O]⁺, 150 [M-C₆H₁₁O]⁺.

Compound 11e: 2-(4-Bromophenyl)-4,4,5,5-tetramethyl-1,3,2-dioxaborane

[B₂pin₂F][NMe₄] **4** (300 mg, 0.865 mmol) and *p*-bromophenyldiazonium tetrafluoroborate [4-Br-C₆H₄N₂][BF₄] **5e** (167 mg, 0.617 mmol) were combined in 20 mL of acetonitrile to give a dark red solution and dinitrogen formed was vented from the Schlenk tube. Afterwards, the reaction mixture was quenched with 10 mL of Et₂O and the solution was filtered to remove the precipitate ([NMe₄][BF₄]). The solvent was evaporated under vacuum and the residue was re-dissolved in 20 mL of *n*-hexane. The solution was filtered to remove any insoluble materials and the product was purified by automated flash chromatography (*n*-hexane/Et₂O).



Yield: 125 mg (72%) of an orange solid.

¹H NMR (500 MHz, MeCN-d₃, 25 °C): δ_H / ppm = 1.31 (s, 12 H, CH₃), 7.54-7.56 (m, 2 H, CH), 7.59-7.62 (m, 2 H, CH).

¹¹B{¹H} NMR (160 MHz, MeCN-d₃, 25 °C): δ_B / ppm = 29.7 (s).

¹³C{¹H} NMR (125 MHz, MeCN-d₃, 25 °C): δ_C / ppm = 25.2 (CH₃), 85.1 (OCC₃), 126.6 (C-Br), 132.0 (CH), 137.2 (CH).

IR (ATR): [ν̃ / cm⁻¹]: 821 (m), 858 (w), 963 (w), 1010 (m), 1087 (s), 1141 (s), 1167 (w), 1215 (w), 1258 (w), 1274 (w), 1296 (vw), 1327 (s), 1357 (s), 1389 (s), 1469 (vw), 1587 (s, C=C), 2932 (vw), 2978 (w, C-H).

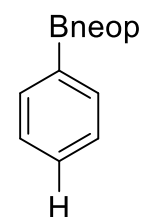
Elemental analysis calcd (%) for C₈H₈BBrO₂: C 50.93, H 5.70, N 5.62; found: C 50.79, H 5.90, N 5.49.

GC-MS: Ret.: 5.949 min; m/z: 284 [M]⁺, 269 [M-CH₃]⁺, 198 [M-C₆H₁₂]⁺, 183 [M-C₆H₁₂O]⁺, 103 [M-C₆H₁₂BrO]⁺.

3.5.2.2. Reactivity of B₂neop₂ and NMe₄F with diazonium [BF₄]⁻ salts

Compound 12a: Characterization of C₆H₅-Bneop

NMR scale reaction: B₂neop₂ (20.0 mg, 89.0 μmol, 1 equiv.), NMe₄F (8.30 mg, 89.0 μmol, 1 equiv.) and [C₆H₅N₂][BF₄] (17.0 mg, 89.0 μmol, 1 equiv.) were dissolved in 0.6 mL of MeCN-d₃ and the reaction mixture was immediately monitored *via* NMR-spectroscopy and afterwards *via* GC-MS analysis.



Spectroscopic yield: 71%

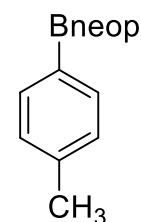
¹H NMR (200 MHz, MeCN-d₃, 25 °C): δ_H / ppm = 0.99 (s, 6 H, CH₃), 3.77 (s, 4 H, CH₂), 7.32-7.44 (m, 3 H, aryl-CH, para-CH), 7.72-7.77 (m, 2 H, aryl-CH).

¹¹B{¹H} NMR (64 MHz, MeCN-d₃, 25 °C): δ_B / ppm = 27.1 (s).

GC-MS: Ret.: 4.664 min; m/z: 190 [M]⁺, 175 [M-CH₃]⁺, 160 [M-C₂H₆]⁺, 147 [M-C₃H₇]⁺, 132 [M-C₄H₁₀]⁺, 118 [M-C₅H₁₂]⁺, 105 [M-C₆H₁₃]⁺, 91 [M-C₇H₁₅]⁺, 77 [M-C₈H₁₇]⁺, 65 [M-C₉H₁₇]⁺. By-product: B₂neop₂; Ret.: 5.427 min.

Compound 12b: Characterization of 4-H₃C-C₆H₄-Bneop

NMR scale reaction: B₂neop₂ (20.0 mg, 89.0 μmol, 1 equiv.), NMe₄F (8.30 mg, 89.0 μmol, 1 equiv.) and [4-CH₃-C₆H₄N₂][BF₄] (18.2 mg, 89.0 μmol, 1 equiv.) were dissolved in 0.6 mL of MeCN-d₃ and the reaction mixture was immediately monitored *via* NMR-spectroscopy and afterwards *via* GC-MS analysis.



Spectroscopic yield: 86%

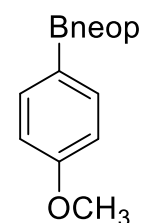
¹H NMR (200 MHz, MeCN-d₃, 25 °C): δ_H / ppm = 0.98 (s, 6 H, CH₃), 2.33 (s, 3 H, CH₃), 3.74 (s, 4 H, CH₂), 7.17 (d, ³J_{HH} = 8 Hz, 2 H, aryl-CH), 7.62 (d, ³J_{HH} = 8 Hz, 2 H, aryl-CH).

¹¹B{¹H} NMR (64 MHz, MeCN-d₃, 25 °C): δ_B / ppm = 27.7 (s).

GC-MS: Ret.: 5.413 min; m/z: 204 [M]⁺, 189 [M-CH₃]⁺, 173 [M-CH₃O]⁺, 161 [M-C₂H₃O]⁺, 146 [M-C₃H₆O]⁺, 132 [M-C₄H₈O]⁺, 119 [M-C₅H₉O]⁺. By-product: 4,4'-dimethyl-1,1'-biphenyl.; Ret.: 5.723 min.

Compound 12c: Characterization of 4-MeO-C₆H₄-Bneop

NMR scale reaction: B₂neop₂ (20.0 mg, 89.0 μmol, 1 equiv.), NMe₄F (8.30 mg, 89.0 μmol, 1 equiv.) and [4-MeO-C₆H₄N₂][BF₄] (19.7 mg, 89.0 μmol, 1 equiv.) were dissolved in 0.6 mL of MeCN-d₃ and the reaction mixture was immediately monitored *via* NMR-spectroscopy and afterwards *via* GC-MS analysis.



Spectroscopic yield: 56%

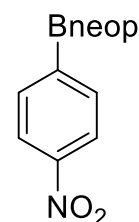
¹H NMR (200 MHz, MeCN-d₃, 25 °C): δ_H / ppm = 0.97 (s, 6 H, CH₃), 3.73 (s, 4 H, CH₂), 3.79 (s, 3 H, CH₃), 6.89 (d, ³J_{HH} = 9 Hz, 2 H, aryl-CH), 7.34 (d, ³J_{HH} = 9 Hz, 2 H, aryl-CH).

¹¹B{¹H} NMR (64 MHz, MeCN-d₃, 25 °C): δ_B / ppm = 27.7 (s).

GC-MS: Ret.: 6.355 min; m/z: 220 [M]⁺, 205 [M-CH₃]⁺, 189 [M-CH₃O]⁺, 177 [M-C₂H₃O]⁺, 162 [M-C₃H₆O]⁺, 149 [M-C₄H₇O]⁺, 134 [M-C₅H₁₀O]⁺. By-product: B₂neop₂; Ret.: 5.427 min.

Compound 12d: Characterization of 4-O₂N-C₆H₄-Bneop

NMR scale reaction: B₂neop₂ (20.0 mg, 89.0 μmol, 1 equiv.), NMe₄F (8.30 mg, 88.5 μmol, 1 equiv.) and [4-O₂N-C₆H₄N₂][BF₄] (21.0 mg, 88.5 μmol, 1 equiv.) were dissolved in 0.6 mL of MeCN-d₃ and the reaction mixture was immediately monitored *via* NMR-spectroscopy and afterwards *via* GC-MS analysis.



Spectroscopic yield: 56%

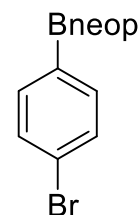
¹H NMR (200 MHz, MeCN-d₃, 25 °C): δ_H / ppm = 1.00 (s, 6 H, CH₃), 3.80 (s, 4 H, CH₂), 7.93 (d, ³J_{HH} = 9 Hz, 2 H, aryl-CH), 8.16 (d, ³J_{HH} = 9 Hz, 2 H, aryl-CH).

¹B{¹H} NMR (64 MHz, MeCN-d₃, 25 °C): δ_B / ppm = 28.0 (s).

GC-MS: Ret.: 7.156 min; m/z: 235 [M]⁺, 220 [M-CH₃]⁺, 205 [M-C₂H₆]⁺, 192 [M-C₃H₇]⁺. By-product: B₂neop₂; Ret.: 5.427 min.

Compound 12e: Characterization of 4-Br-C₆H₄-Bneop

NMR scale reaction: B₂neop₂ (20.0 mg, 89.0 μmol, 1 equiv.), NMe₄F (8.30 mg, 89.0 μmol, 1 equiv.) and [4-O₂N-C₆H₄N₂][BF₄] (24.0 mg, 89.0 μmol, 1 equiv.) were dissolved in 0.6 mL of MeCN-d₃ and the reaction mixture was immediately monitored *via* NMR-spectroscopy and afterwards *via* GC-MS analysis.



Spectroscopic yield: 94%

¹H NMR (200 MHz, MeCN-d₃, 25 °C): δ_H / ppm = 0.98 (s, 6 H, CH₃), 3.75 (s, 4 H, CH₂), 7.49-7.53 (m, 2 H, aryl-CH), 7.61-7.65 (m, 2 H, aryl-CH).

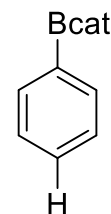
¹B{¹H} NMR (64 MHz, MeCN-d₃, 25 °C): δ_B / ppm = 27.5 (s).

GC-MS: Ret.: 6.392 min; m/z: 268 [M]⁺, 253 [M-CH₃]⁺, 239 [M-C₂H₅]⁺, 225 [M-C₃H₇]⁺, 212 [M-C₄H₈]⁺, 197 [M-C₅H₁₁]⁺. By-product: B₂neop₂; Ret.: 5.427 min.

3.5.2.3. Reactivity of B₂cat₂ and NMe₄F with diazonium [BF₄]⁻ salts

Compound 13a: Characterization of C₆H₅-Bcat

NMR scale reaction: B₂cat₂ (20.0 mg, 84.0 μmol, 1 equiv.), NMe₄F (16.1 mg, 84.1 μmol, 1 equiv.) and [C₆H₅N₂][BF₄] (16.1 mg, 84.1 μmol, 1 equiv.) were dissolved in 0.6 mL of MeCN-d₃ and the reaction mixture was immediately monitored *via* NMR-spectroscopy and afterwards *via* GC-MS analysis.



Spectroscopic yield: 82%

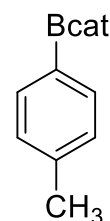
¹H NMR (200 MHz, MeCN-d₃, 25 °C): δ_H / ppm = 7.15-7.19 (m, 2 H, cat-CH), 7.34-7.38 (m, 2 H, cat-CH), 7.52-7.60 (m, 3 H, aryl-CH, para-CH), 8.03-8.07 (m, 2 H, aryl-CH).

¹¹B{¹H} NMR (64 MHz, MeCN-d₃, 25 °C): δ_B / ppm = 32.2 (s).

GC-MS: Ret.: 5.744 min; m/z: 196 [M]⁺, 181 [M-O]⁺, 168 [M-CHO]⁺, 157 [M-CHOB]⁺, 144 [M-C₂H₂OB]⁺. No by-product

Compound 13b: Characterization of 4-H₃C-C₆H₅-Bcat

NMR scale reaction: B₂cat₂ (20.0 mg, 84.1 μmol, 1 equiv.), NMe₄F (7.83 mg, 84.1 μmol, 1 equiv.) and [4-H₃C-C₆H₄N₂][BF₄] (17.3 mg, 84.1 μmol, 1 equiv.) were dissolved in 0.6 mL of MeCN-d₃ and the reaction mixture was immediately monitored *via* NMR-spectroscopy and afterwards *via* GC-MS analysis.



Spectroscopic yield: 63%

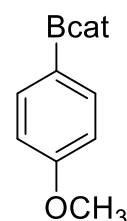
¹H NMR (200 MHz, MeCN-d₃, 25 °C): δ_H / ppm = 2.41 (s, 3 H, CH₃), 7.13-7.18 (m, 2 H, cat-CH), 7.32-7.36 (m, 4 H, aryl-CH, cat-CH), 7.93 (d, ³J_{HH} = 8 Hz, 2 H, aryl-CH).

¹¹B{¹H} NMR (64 MHz, MeCN-d₃, 25 °C): δ_B / ppm = 32.4 (s).

GC-MS: Ret.: 6.441 min; m/z: 210 [M]⁺, 194 [M-O]⁺, 181 [M-CO]⁺, 165 [M-CO₂]⁺, 153 [M-C₂O₂]⁺.
By-product: B₂cat₂; Ret.: 7.305 min.

Compound 13c: Characterization of 4-MeO-C₆H₅-Bcat

NMR scale reaction: B₂cat₂ (20.0 mg, 84.1 μmol, 1 equiv.), NMe₄F (7.83 mg, 84.1 μmol, 1 equiv.) and [4-MeO-C₆H₄N₂][BF₄] (18.7 mg, 84.1 μmol, 1 equiv.) were dissolved in 0.6 mL of MeCN-d₃ and the reaction mixture was immediately monitored *via* NMR-spectroscopy and afterwards *via* GC-MS analysis.



Spectroscopic yield: 67%

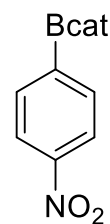
¹H NMR (200 MHz, MeCN-d₃, 25 °C): δ_H / ppm = 3.85 (s, 3 H, OCH₃), 7.05 (d, ³J_{HH} = 9 Hz, 2 H, aryl-CH), 7.12-7.16 (m, 2 H, cat-CH), 7.29-7.34 (m, 2 H, cat-CH), 7.97 (d, ³J_{HH} = 9 Hz, 2 H, aryl-CH).

¹¹B{¹H} NMR (64 MHz, MeCN-d₃, 25 °C): δ_B / ppm = 31.3 (s).

GC-MS: Ret.: 7.344 min; m/z: 226 [M]⁺, 211 [M-CH₃]⁺, 195 [M-OCH₃]⁺. No by-product.

Compound 13d: Characterization of 4-O₂N-C₆H₅-Bcat

NMR scale reaction: B₂cat₂ (20.0 mg, 84.1 μmol, 1 equiv.), NMe₄F (7.83 mg, 84.1 μmol, 1 equiv.) and [4-O₂N-C₆H₄N₂][BF₄] (19.9 mg, 84.1 μmol, 1 equiv.) were dissolved in 0.6 mL of MeCN-d₃ and the reaction mixture was immediately monitored *via* NMR-spectroscopy and afterwards *via* GC-MS analysis.



Spectroscopic yield: 54%

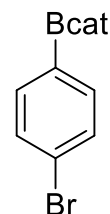
¹H NMR (200 MHz, MeCN-d₃, 25 °C): δ_H / ppm = 7.69 (d, ³J_{HH} = 8.44 Hz, 2 H, aryl-CH), 8.19-8.32 (m, 6 H, aryl-CH, cat-CH).

¹¹B{¹H} NMR (64 MHz, MeCN-d₃, 25 °C): δ_B / ppm = 31.2(s).

GC-MS: Ret.: 8.002 min; m/z: 241 [M]⁺, 211 [M-CH₂O]⁺, 195 [M-CH₂O₂]⁺, 183 [M-C₂H₂O₂]⁺, 167 [M-C₂H₂O₃]⁺, 151 [M-C₂H₂O₄]⁺. By-product: B₂cat₂; Ret.: 7.307 min.

Compound 13e: Characterization of 4-Br-C₆H₅-Bcat

NMR scale reaction: B₂cat₂ (20.0 mg, 84.1 μmol, 1 equiv.), NMe₄F (7.83 mg, 84.1 μmol, 1 equiv.) and [4-Br-C₆H₄N₂][BF₄] (22.8 mg, 84.1 μmol, 1 equiv.) were dissolved in 0.6 mL of MeCN-d₃ and the reaction mixture was immediately monitored *via* NMR-spectroscopy and afterwards *via* GC-MS analysis.



Spectroscopic yield: 81%

¹H NMR (200 MHz, MeCN-d₃, 25 °C): δ_H / ppm = 7.15-7.19 (m, 2 H, cat-CH), 7.33-7.37 (m, 2 H, cat-CH), 7.69 (d, ³J_{HH} = 8 Hz, 2 H, aryl-CH), 7.93 (d, ³J_{HH} = 8 Hz, 2 H, aryl-CH).

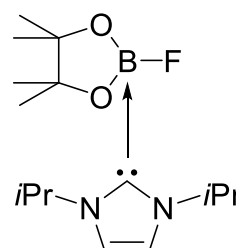
¹¹B{¹H} NMR (64 MHz, MeCN-d₃, 25 °C): δ_B / ppm = 32.2 (s).

GC-MS: Ret.: 7.326 min; m/z: 276 [M]⁺, 195 [M-Br]⁺. No by-product

3.5.3. Synthesis of FBpin•NHC adducts

Compound 14: FBpin•*i*Pr₂Im

B₂pin₂ (500 mg, 1.97 mmol, 1 equiv.) and NMe₄F (183 mg, 1.97 mmol, 1 equiv.) were dissolved in 20 mL of THF and *i*Pr₂Im (300 μL, 300 mg, 1.97 mmol, 1 equiv.) was added to the reaction mixture, which immediately turned from colorless to bright yellow. It was heated to 70 °C for 16 h. The solvent was removed *in vacuo* and the residue was re-dissolved in 10 mL of *n*-hexane. A colorless solid precipitated, which was identified as [pinBF₂][NMe₄F]. The yellow mother liquor was cooled to -30 °C to obtain the adduct FBpin•*i*Pr₂Im.



Yield: 65 mg (5%) of yellow crystals.

¹H NMR (500 MHz, C₆D₆, 25 °C): δ_H / ppm = 1.60 (d, ³J_{HH} = 7 Hz, 12 H, *i*Pr-CH₃), 1.20 (s, 6 H, pin-CH₃), 1.57 (s, 6 H, pin-CH₃), 6.02 (sept., ³J_{HH} = 7 Hz, 2 H, *i*Pr-CH), 6.40 (s, 2 H, CH).

¹¹B{¹H} NMR (160 MHz, C₆D₆, 25 °C): δ_B / ppm = 4.90 (d, ¹J_{BF} = 54 Hz)

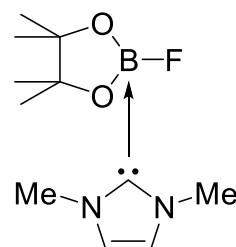
¹⁹F NMR (188 MHz, C₆D₆, 25 °C): δ_F / ppm = -130.9 (q, ¹J_{FB} = 54 Hz)

¹³C{¹H} NMR (125 MHz, C₆D₆, 25 °C): δ_C / ppm = 23.2 (*i*Pr-CH₃), 26.0 (pin-CH₃), 26.4 (pin-CH₃), 49.3 (*i*Pr-CH), 79.1 (pin-C), 115.9 (CHCH), 162.3 (NCN) with line broadening (lb 12).

Elemental analysis calcd (%) for C₁₅H₂₈O₂N₂BF: C 60.42, H 9.46, N 9.39; found: C 60.91, H 9.65, N 9.20.

Compound 15: FBpin•Me₂Im

B₂pin₂ (500 mg, 1.97 mmol, 1 equiv.) and NMe₄F (183 mg, 1.97 mmol, 1 equiv.) were dissolved in 20 mL of THF and Me₂Im (189 μL, 189 mg, 1.97 mmol, 1 equiv.) was added to the reaction mixture, which immediately turned from colorless to red. It was heated to 70 °C for 16 h. The solvent was removed *in vacuo* and the residue was re-dissolved in 10 mL of *n*-hexane. A colorless solid precipitated, which was identified as a mixture of [pinBF₂][NMe₄F] and the product FBpin•Me₂Im. The mixture of both compounds was re-dissolved in MeCN and afterwards, FBpin•Me₂Im was isolated as yellow crystals in very low yield; however, the decomposition product [pinBF₂][NMe₄F] stayed in the mother liquor, therefore, the two compounds were separated.



Yield: 40 mg (7%) of yellow crystals.

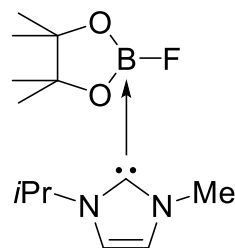
¹H NMR (200 MHz, MeCN-d₃, 25 °C): δ_H / ppm = 0.94 (s, 6 H, pin-CH₃), 1.23 (s, 6 H, pin-CH₃), 3.90 (s, 6 H, Me-CH₃), 6.98 (s, 2 H, CH).

¹¹B{¹H} NMR (64 MHz, MeCN-d₃, 25 °C): δ_B / ppm = 4.25 (d, ¹J_{BF} = 54 Hz)

¹⁹F NMR (188 MHz, MeCN-d₃, 25 °C): δ_F / ppm = -133.6 (q, ¹J_{FB} = 54 Hz)

Compound 16: FBpin•Me*i*Pr₂Im

B₂pin₂ (200 mg, 788 μmol, 1 equiv.) and NMe₄F (73.4 mg, 788 μmol, 1 equiv.) were dissolved in 20 mL of THF and Me*i*Pr₂Im (98.0 μL, 98.0 mg, 788 μmol, 1 equiv.) was added to the reaction mixture, which immediately turned from colorless to orange. It was heated to 70 °C for 16 h. The solvent was removed *in vacuo* and the residue was re-dissolved in 10 mL *n*-hexane. A colorless solid precipitated, which was identified as [pinBF₂][NMe₄F]. The orange mother liquor was cooled to -30 °C to obtain the adduct FBpin•Me*i*Pr₂Im.



Yield: 20 mg (5%) of an orange solid.

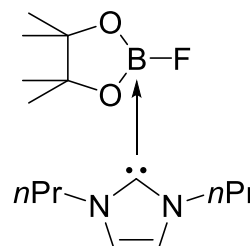
¹H NMR (200 MHz, C₆D₆, 25 °C): δ_H / ppm = 1.00 ppm (d, ³J_{HH} = 7 Hz, 6 H, *i*Pr-CH₃), 1.20 (s, 6 H, pin-CH₃), 1.60 (s, 6 H, pin-CH₃), 3.55 (s, 6 H, Me-CH₃), 5.74 (d, ³J_{HH} = 2 Hz, 1 H, CH), 5.91 (sept, ³J_{HH} = 7 Hz, 1 H, *i*Pr-CH), 6.01 (d, ³J_{HH} = 2 Hz, 1 H, CH).

¹¹B{¹H} NMR (64 MHz, C₆D₆, 25 °C): δ_B / ppm = 4.85 (d, ¹J_{BF} = 54 Hz).

¹⁹F NMR (188 MHz, C₆D₆, 25 °C): δ_F / ppm = -132.1 (q, ¹J_{FB} = 54 Hz).

Compound 17: FBpin•*n*Pr₂Im

B₂pin₂ (200 mg, 788 μmol, 1 equiv.) and NMe₄F (73.4 mg, 788 μmol, 1 equiv.) were dissolved in 20 mL of THF and *n*Pr₂Im (120 μL, 120 mg, 788 μmol, 1 equiv.) was added to the reaction mixture, which immediately turned from colorless to bright yellow. It was heated to 70 °C for 16 h. The solvent was removed *in vacuo* and the residue was re-dissolved in 10 mL of *n*-hexane. A yellow solid precipitated, which was identified as the adduct FBpin•*n*Pr₂Im.



For X-ray diffraction: A saturated solution of FBpin•*n*Pr₂Im in *n*-hexane was cooled to -30 °C to obtain single crystals for X-ray diffraction.

Yield: 213 mg (55%) of a colorless solid.

¹H NMR (500 MHz, MeCN-d₃, 25 °C): δ_H / ppm = 0.88 ppm (t, ³J_{HH} = 7 Hz, 6 H, CH₃), 0.92 (s, 6 H, pin-CH₃), 1.11 (s, 6 H, pin-CH₃), 1.78 (sext., ³J_{HH} = 7 Hz, 4 H, CH₂), 4.32 (t, ³J_{HH} = 7 Hz, 4 H, N-CH₂), 7.03 (s, 2 H, CHCH).

¹¹B{¹H} NMR (64 MHz, MeCN-d₃, 25 °C): δ_B / ppm = 3.35 (d, ¹J_{BF} = 54 Hz).

¹⁹F NMR (188 MHz, MeCN-d₃, 25 °C): δ_F / ppm = -131.0 (q, ¹J_{FB} = 54 Hz).

¹³C{¹H} NMR (50 MHz, MeCN-d₃, 25 °C): δ_C / ppm = 11.1 (CH₃), 25.0 (CH₂), 25.5 (pin-CH₃), 26.1 (pin-CH₃), 50.6 (N-CH₂), 79.4 (pin-C), 121.0 (CHCH), 162.2 (NCN) assigned *via* 2D NMR spectroscopy (HMBC).

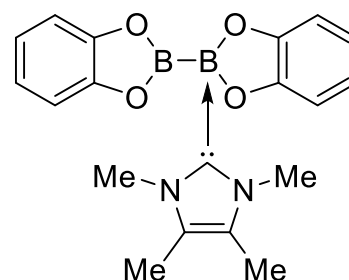
Elemental analysis calcd (%) for C₁₅H₂₈O₂N₂BF: C 60.42, H 9.46, N 9.39; found: C 60.16, H 9.39, N 9.47.

3.5.4. Synthesis of Mono-NHC diboron adducts

3.5.4.1. Synthesis of the mono-NHC adducts of the type $B_2cat_2 \cdot NHC$

Compound 18: $B_2cat_2 \cdot Me_2Im^{Me}$

Me_2Im^{Me} (52.0 mg, 0.42 mmol) was added to a stirred solution of B_2cat_2 (100 mg, 0.42 mmol) in 10 mL of toluene. After stirring the reaction mixture for 16 h at room temperature all volatiles were removed *in vacuo*. Afterwards, the residue was washed with 10 mL of *n*-hexane to obtain the product.



For X-ray diffraction: A saturated solution of $B_2cat_2 \cdot Me_2Im^{Me}$ in toluene was cooled to $-30\text{ }^\circ\text{C}$ to obtain single crystals for X-ray diffraction.

Yield: 120 mg (79%) of a colorless solid

$^1\text{H NMR}$ (500 MHz, C_6D_6 , $25\text{ }^\circ\text{C}$): $\delta = 1.03$ (s, 6 H, CH_3), 3.37 (s, 6 H, NCH_3), 6.80-6.81 (m, 2 H, cat-CH), 6.85-6.87 (m, 2 H, cat-CH), 7.12-7.13 (m, 2 H, cat-CH), 7.14-7.15 (m, 2 H, cat-CH).

$^{11}\text{B}\{^1\text{H}\}$ NMR (160 MHz, C_6D_6 , $25\text{ }^\circ\text{C}$): $\delta = 7.11$ (s, $sp^3\text{-B}$), 38.6 (s_{br} , $sp^2\text{-B}$).

$^1\text{H NMR}$ (200 MHz, CD_2Cl_2 , $25\text{ }^\circ\text{C}$): $\delta = 2.00$ (s, 6 H, C- CH_3), 3.80 (s, 6 H, N- CH_3), 6.41-6.48 (m, 2 H, cat-CH), 6.51-6.59 (m, 2 H, cat-CH), 6.90-6.99 (m, 2 H, cat-CH), 7.07-7.16 (m, 2 H, cat-CH).

$^{11}\text{B}\{^1\text{H}\}$ NMR (64 MHz, C_6D_6 , $25\text{ }^\circ\text{C}$): $\delta = 6.87$ (s, $sp^3\text{-B}$), 38.3 (s_{br} , $sp^2\text{-B}$)

$^{13}\text{C}\{^1\text{H}\}$ NMR (125 MHz, C_6D_6 , $25\text{ }^\circ\text{C}$): $\delta = 7.47$ (CH_3), 32.1 (NCH_3), 109.7 (cat-CH), 112.5 (cat-CH), 118.9 (cat-CH), 122.3 (cat-CH), 124.3 ($NCCN$), 149.3 (cat- C_q), 154.6 (cat- C_q), 160.4 (NCN).

$^{11}\text{B SS NMR}$ (128 MHz, $25\text{ }^\circ\text{C}$): $\delta = 8.99$ ($sp^3\text{-B}$), 35.5 ($sp^2\text{-B}$).

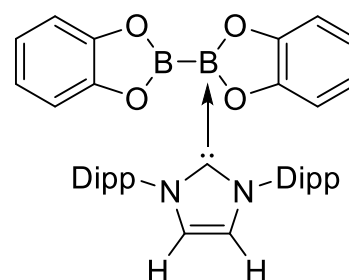
$^{13}\text{C SS NMR}$ (100 MHz, $25\text{ }^\circ\text{C}$): $\delta = 6.10$ (CH_3), 7.37 (CH_3), 32.7 (NCH_3), 34.8 (NCH_3), 109.0 (cat-CH), 109.5 (cat-CH), 112.6 (cat-CH), 113.7 (cat-CH), 118.1 (cat-CH), 123.2 (cat-CH), 124.7 ($NCCN$), 125.5 ($NCCN$), 147.9 (C_q), 148.5 (C_q), 154.0 (C_q), 154.7 (C_q), 158.9 (NCN).

$^{15}\text{N SS NMR}$ (40 MHz, $25\text{ }^\circ\text{C}$): $\delta = -204.6$, -207.2 .

Elemental analysis calcd (%) for $C_{19}H_{20}B_2N_4O_4$: C 63.04, H 5.57, N 7.74; found: C 62.87, H 5.60, N 7.63.

Compound 19: $B_2cat_2 \cdot Dipp_2Im$

$Dipp_2Im$ (240 mg, 0.65 mmol) and B_2cat_2 (150 mg, 0.65 mmol) were dissolved in 10 mL of toluene. After stirring the reaction mixture for 1 h at room temperature all volatiles were removed *in vacuo*. Afterwards, the residue was washed with 10 mL of *n*-hexane to obtain the product.



Yield: 291 mg (75%) of a colorless solid.

^1H NMR (400 MHz, C_6D_6 , 25 °C): δ = 0.99 (d, $^3J_{\text{HH}}$ = 7 Hz, 12 H, Dipp-*i*Pr- CH_3), 1.41 (d, $^3J_{\text{HH}}$ = 7 Hz, 12 H, Dipp-*i*Pr- CH_3), 2.88 (sept, $^3J_{\text{HH}}$ = 7 Hz, 5 H, Dipp-*i*Pr- CH), 6.38 (s, 4 H, CHCH), 6.41-6.46 (m, 2 H, cat- CH), 6.48-6.53 (m, 2 H, cat- CH), 6.70-6.74 (m, 2 H, cat- CH), 6.80-6.84 (m, 2 H, cat- CH), 6.92-6.94 (m, 4 H, Dipp-aryl- CH), 6.97-7.02 (m, 4 H, Dipp-aryl- CH).

$^{11}\text{B}\{^1\text{H}\}$ NMR (128 MHz, C_6D_6 , 25 °C): δ = 6.78 (s, $\text{sp}^3\text{-B}$), 37.9 (s_{br} , $\text{sp}^2\text{-B}$).

$^{13}\text{C}\{^1\text{H}\}$ NMR (100 MHz, C_6D_6 , 25 °C): δ = 22.3 (Dipp-*i*Pr- CH_3), 26.1 (Dipp-*i*Pr- CH_3), 29.4 (Dipp-*i*Pr- CH), 109.4 (cat- CH), 112.0 (cat- CH), 117.8 (cat- CH), 121.4 (cat- CH), 123.9 (CHCH , Dipp-aryl- CH), 130.5 (Dipp-aryl- CH), 133.6 (Dipp-aryl- C_q), 145.5 (Dipp-aryl- C_q), 149.2 (cat- C_q), 154.2 (cat- C_q), 165.4 (NCN).

Elemental analysis calcd (%) for $\text{C}_{39}\text{H}_{44}\text{B}_2\text{N}_2\text{O}_4$: C 74.78, H 7.08, N 4.47; found: C 74.27, H 7.08, N 4.12.

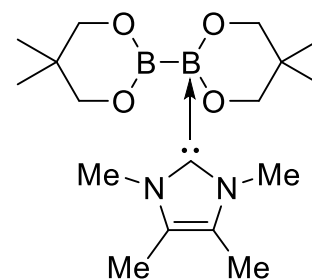
3.5.4.2. Synthesis of the mono-NHCs adducts of the type $\text{B}_2\text{neop}_2\cdot\text{NHC}$

Compound 20: $\text{B}_2\text{neop}_2\cdot\text{Me}_2\text{Im}^{\text{Me}}$

NMR-scale reaction: $\text{Me}_2\text{Im}^{\text{Me}}$ (16.0 mg, 129 μmol) and B_2neop_2 (15.0 mg, 129 μmol) were dissolved in 0.6 mL of C_6D_6 . The reaction was immediately monitored *via* ^1H and $^{11}\text{B}\{^1\text{H}\}$ NMR spectroscopy.

^1H NMR (200 MHz, C_6D_6 , 25 °C): δ = 0.91 (s_{br} , 12 H, neop- CH_3), 1.20 (s_{br} , 8 H, C- CH_3), 3.60 (s_{br} , 8 H, neop- CH_2), 3.77 (s_{br} , 6 H, N- CH_3).

$^{11}\text{B}\{^1\text{H}\}$ NMR (64 MHz, C_6D_6 , 25 °C): δ = 1.32 ($\text{sp}^3\text{-B}$), 29.3 ($\text{sp}^2\text{-B}$).



Compound 21: $\text{B}_2\text{neop}_2\cdot\text{iPr}_2\text{Im}^{\text{Me}}$

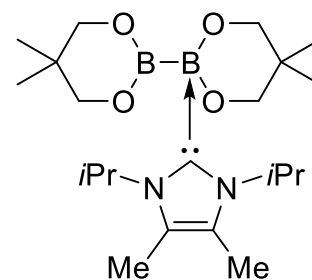
*i*Pr $_2$ Im $^{\text{Me}}$ (239 mg, 1.33 mmol, 1 equiv.) and B_2neop_2 (300 mg, 1.33 mmol) were dissolved in 20 mL of toluene. After stirring the reaction mixture for 1 h at room temperature, all volatiles were removed *in vacuo*. Afterwards, the residue was washed with 10 mL of *n*-hexane to obtain the product.

For X-ray diffraction: A saturated solution of $\text{B}_2\text{neop}_2\cdot\text{iPr}_2\text{Im}^{\text{Me}}$ in toluene was cooled to -30 °C to obtain single crystals for X-ray diffraction.

Yield: 310 mg (58%) of a colorless solid.

^1H NMR (500 MHz, C_6D_6 , 25 °C): δ = 0.83 (s, 12 H, neop- CH_3), 1.36 (d, $^3J_{\text{HH}}$ = 7 Hz, 12 H, *i*Pr- CH_3), 1.67 (s, 6 H, C- CH_3), 3.52 (s, 8 H, neop- CH_2), 6.0 (s_{br} , 2 H, *i*Pr- CH).

$^{11}\text{B}\{^1\text{H}\}$ NMR (160 MHz, C_6D_6 , 25 °C): δ = 21.6 ($\text{B}_{\alpha,\beta}$).



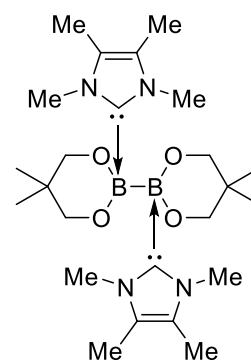
$^{13}\text{C}\{^1\text{H}\}$ NMR (125 MHz, C_6D_6 , 25 °C): δ = 10.0 (C- CH_3), 22.7 (*i*Pr- CH_3), 22.8 (neop- CH_3), 32.2 (neop- C_q), 48.4 (*i*Pr-CH), 72.6 (neop- CH_2), 123.9 (CHCH), 191.0 (NCN) assigned *via* 2D NMR spectroscopy (HMBC).

3.5.4.3. Synthesis of the bis-NHC adducts of the type $\text{B}_2\text{neop}_2\cdot(\text{NHC})_2$

The bis-NHC diboron adducts $\text{B}_2\text{neop}_2\cdot(\text{Me}_2\text{Im}^{\text{Me}})_2$ **22**, $\text{B}_2\text{neop}_2\cdot(\text{iPr}_2\text{Im}^{\text{Me}})_2$ **23** and $\text{B}_2\text{neop}_2\cdot(\text{MeiPrIm})_2$ **24** were only characterized by X-ray diffraction. Single crystals were obtained from the reaction mixture of B_2neop_2 with the corresponding NHC; however, none of these bis-NHC diboron adducts **22-24** were further characterized by NMR spectroscopy or elemental analysis based on the dissociation of the second NHC in solution.

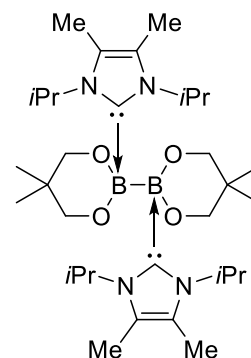
Compound 22: $\text{B}_2\text{neop}_2\cdot(\text{Me}_2\text{Im}^{\text{Me}})_2$

$\text{Me}_2\text{Im}^{\text{Me}}$ (150 mg, 1.21 mmol, 1 equiv.) and B_2neop_2 (273 mg, 1.21 mmol, 1 equiv.) were dissolved in 10 mL of toluene. After stirring the reaction mixture for 1 h at room temperature, the reaction mixture was cooled to -30 °C to obtain single crystals for X-ray diffraction from the saturated solution.



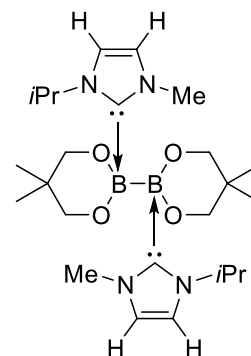
Compound 23: $\text{B}_2\text{neop}_2\cdot(\text{iPr}_2\text{Im}^{\text{Me}})_2$

$\text{iPr}_2\text{Im}^{\text{Me}}$ (150 mg, 1.66 mmol, 2 equiv.) and B_2neop_2 (376 mg, 0.83 mmol, 1 equiv.) were dissolved in 10 mL of toluene. After stirring the reaction mixture for 1 h at room temperature, the reaction mixture was cooled to -30 °C to obtain single crystals for X-ray diffraction from the saturated solution.



Compound 24: $\text{B}_2\text{neop}_2\cdot(\text{MeiPrIm})_2$

MeiPrIm (150 mg, 2.42 mmol, 2 equiv.) and B_2neop_2 (273 mg, 1.21 mmol, 1 equiv.) were dissolved in 10 mL of toluene. After stirring the reaction mixture for 1 h at room temperature, the reaction mixture was cooled to -30 °C to obtain single crystals for X-ray diffraction from the saturated solution.



3.5.4.4. Synthesis of the bis-NHC adducts of the type $B_2cat_2 \cdot (NHC)_2$

Compound 25: $B_2cat_2 \cdot (Me_2Im^{Me})_2$

Me_2Im^{Me} (156 mg, 1.26 mol) was added to a stirred solution of B_2cat_2 (150 mg, 630 mmol) in 15 mL of toluene. After stirring the reaction mixture for 2 h at room temperature, the light yellow solid which precipitated was collected by filtration and washed three times with 5 mL of toluene to obtain the product.

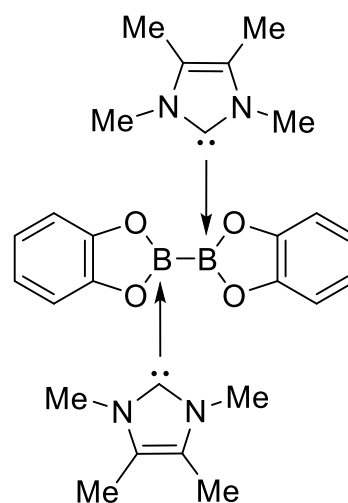
Yield: 250 mg (84%) of a light yellow solid.

$B_2cat_2 \cdot (Me_2Im^{Me})_2$ **25** is un-soluble in common solvents, such as C_6D_6 , toluene- d_8 and THF- d_3 , additionally, it decomposes in CD_2Cl_2 . Therefore, compound **24** was only characterized by solid state NMR spectroscopy.

^{11}B SS NMR (128 MHz, 25 °C): $\delta = 2.72$ (sp^3 -B).

^{13}C SS NMR (100 MHz, 25 °C): $\delta = 4.91$ (CH_3), 9.49 (CH_3), 33.1 (NCH_3), 34.9 (NCH_3), 109.3 (cat-CH), 110.5 (cat-CH), 117.3 (cat-CH), 118.5 (cat-CH), 123.8 (NCCN), 124.2 (NCCN), 155.7 (C_q), 157.3 (C_q), 166.4 (br, NCN).

^{15}N SS NMR (40 MHz, 25 °C): $\delta = -204.1, -205.9$.



3.5.5. Synthesis of the ring expanded products (RER)

3.5.5.1. Synthesis of the ring expanded products containing B₂cat₂

Compound 26: RER-B₂cat₂•(Me₂Im^{Me})₂

Me₂Im^{Me} (209 mg, 1.68 mmol, 2 equiv.) was added to a stirred solution of B₂cat₂ (200 mg, 0.84 mmol, 1 equiv.) in 40 mL of THF. After stirring the resulting reaction mixture for 16 h at 70 °C, all volatiles were removed *in vacuo*. Afterwards, the residue was washed with 20 mL of *n*-hexane to obtain the product.

For X-ray diffraction: A saturated solution of RER-B₂cat₂•(Me₂Im^{Me})₂ in *n*-hexane was cooled to -30 °C to obtain single crystals for X-ray diffraction.

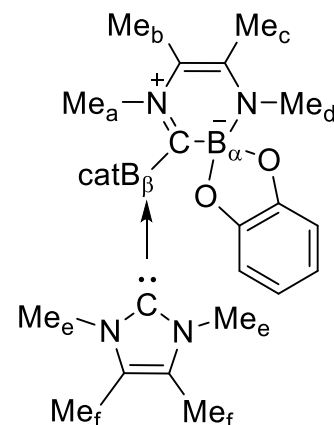
Yield: 325 mg (80%) of a yellow solid.

¹H NMR (500 MHz, C₆D₆, 25 °C): δ = 1.09 (s, 6 H, Me_f-CH₃), 1.42 (s, 3 H, Me_{b/c}-CH₃), 1.47 (s, 3 H, Me_{b/c}-CH₃), 2.78 (s, 3 H, Me_{a/d}-CH₃), 3.40 (s, 3 H, Me_{a/d}-CH₃), 3.57 (s, 6 H, Me_e-CH₃), 6.40-6.41 (m, 4 H, C_βH), 6.83-6.84 (m, 2 H, C_αH), 7.05-7.07 (m, 2 H, C_αH).

¹¹B{¹H} NMR (160 MHz, C₆D₆, 25 °C): δ = 6.23 (s, B_{α/β}), 7.20 (s, B_{α/β}).

¹³C{¹H} NMR (125 MHz, C₆D₆, 25 °C): δ = 7.76 (Me_f-CH₃), 15.4 (Me_{b/c}-CH₃), 15.5 (Me_{b/c}-CH₃), 31.4 (Me_{a/d}-CH₃), 33.0 (Me_e-CH₃), 43.9 (Me_{a/d}-CH₃), 106.9 (cat_β-CH), 110.2 (C_{b/c}H), 110.3 (cat_α-CH), 117.8 (cat_β-CH), 119.6 (cat_α-CH), 124.0 (C_fH), 140.6 (C_{b/c}H), 153.1 (cat-C_q), 153.5 (cat-C_q), 158.8 (NCN), 184.2 (C_q).

Elemental analysis calcd (%) for C₂₆H₃₂B₂N₄O₄: C 64.23, H 6.63, N 11.52; found: C 63.98 H 6.70, N 11.83



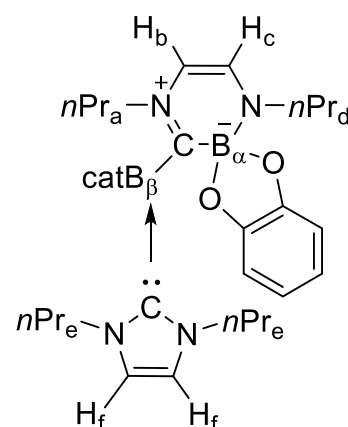
Compound 27: RER-B₂cat₂•(*n*Pr₂Im)₂

*n*Pr₂Im (448 μl, 448 mg, 2.94 mmol, 2 equiv.) was added to a stirred solution of B₂cat₂ (350 mg, 1.47 mmol, 1 equiv.) in 40 mL of THF. After stirring the resulting reaction mixture for 16 h at 70 °C, all volatiles were removed *in vacuo*. Afterwards, the residue was washed with 20 mL of *n*-hexane to obtain the product.

For X-ray diffraction: A saturated solution of RER-B₂cat₂•(*n*Pr₂Im)₂ in *n*-hexane was cooled to -30 °C to obtain single crystals for X-ray diffraction.

Yield: 565 mg (71%) of a yellow solid.

¹H NMR (500 MHz, C₆D₆, 25 °C): δ = 0.60 (t, ³J_{HH} = 7 Hz, 3 H, *n*Pr_d-CH₃), 0.73 (t, ³J_{HH} = 7 Hz, 3 H, *n*Pr_a-CH₃), 0.74 (t, ³J_{HH} = 7 Hz, 6 H, *n*Pr_e-CH₃), 1.47 (sext, ³J_{HH} = 7 Hz, 4 H, *n*Pr_e-CH₂CH₃), 1.60 (sext, ³J_{HH} = 7 Hz, 2 H, *n*Pr_a-CH₂CH₃), 1.87 (m, 2 H, *n*Pr_d-CH₂CH₃), 3.02 (m, 2 H, *n*Pr_a-



NCH_2CH_2), 3.68 (m, 2 H, $n\text{Pr}_d\text{-NCH}_2\text{CH}_2$), 4.12 (s_{br}, 4 H, $n\text{Pr}_e\text{-NCH}_2\text{CH}_2$), 5.19 (d, $^3J_{\text{HH}} = 5$ Hz, 1 H, C_bH), 5.54 (s, 2 H, C_fH), 6.10 (d, $^3J_{\text{HH}} = 5$ Hz, 1 H, C_cH), 6.49-6.51 (m, 2 H, $\text{cat}_\beta\text{-CH}$), 6.57-6.59 (m, 2 H, $\text{cat}_\beta\text{-CH}$), 6.76-6.77 (m, 2 H, $\text{cat}_\alpha\text{-CH}$), 6.85-6. (m, 2 H, $\text{cat}_\alpha\text{-CH}$).

$^{11}\text{B}\{^1\text{H}\}$ NMR (160 MHz, C_6D_6 , 25 °C): $\delta = 6.04$ (s, $B_{\alpha/\beta}$), 7.67 (s, $B_{\alpha/\beta}$).

$^{13}\text{C}\{^1\text{H}\}$ NMR (125 MHz, C_6D_6 , 25 °C): $\delta = 11.2$ ($n\text{Pr}_e\text{-CH}_3$), 11.5 ($n\text{Pr}_d\text{-CH}_3$), 11.8 ($n\text{Pr}_a\text{-CH}_3$), 24.4 ($n\text{Pr}_e\text{-CH}_2\text{CH}_3$), 25.2 ($n\text{Pr}_d\text{-CH}_2\text{CH}_3$), 25.8 ($n\text{Pr}_a\text{-CH}_2\text{CH}_3$), 51.4 ($n\text{Pr}_e\text{-NCH}_2\text{CH}_2$), 51.9 ($n\text{Pr}_a\text{-NCH}_2\text{CH}_2$), 61.4 ($n\text{Pr}_d\text{-NCH}_2\text{CH}_2$), 105.6 (C_bH), 107.5 ($\text{cat}_\beta\text{-CH}$), 110.3 ($\text{cat}_\alpha\text{-CH}$), 118.1 ($\text{cat}_\beta\text{-CH}$), 119.0 (C_fH), 119.6 ($\text{cat}_\alpha\text{-CH}$), 136.1 (C_cH), 152.9 (cat-C_q), 153.3 (cat-C_q), 160.7 (NCN), 185.7 (C_q)

Elemental analysis calcd (%) for $\text{C}_{30}\text{H}_{40}\text{B}_2\text{N}_4\text{O}_4$: C 66.44, H 7.43, N 10.33; found: C H 66.37, H 7.43, N 10.29.

Compound 28: RER-B₂cat₂•nPr₂Im•Me₂Im^{Me}

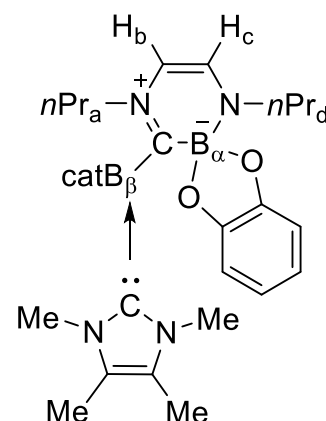
$\text{Me}_2\text{Im}^{\text{Me}}$ (30 mg, 240 μmol) was added to a stirred solution of RER-B₂cat₂•nPr₂Im **26** (130 mg, 240 μmol) in 10 mL of dry toluene. After heating the reaction mixture for 16 h at 110 °C, all volatiles were removed *in vacuo*. Afterwards, the residue was washed with 10 mL of *n*-hexane to obtain the product.

Yield: 70 mg (57%) of a yellow solid.

^1H NMR (500 MHz, C_6D_6 , 25 °C): $\delta = 0.67$ (t, $^3J_{\text{HH}} = 7$ Hz, 3 H, $n\text{Pr}_a\text{-CH}_3$), 0.72 (t, $^3J_{\text{HH}} = 7$ Hz, 3 H, $n\text{Pr}_d\text{-CH}_3$), 1.06 (s, 6 H, Me-CH_3), 1.59 (sext, $^3J_{\text{HH}} = 7$ Hz, 2 H, $n\text{Pr}_d\text{-CH}_2\text{CH}_3$), 1.89-1.96 (m, 2 H, $n\text{Pr}_a\text{-CH}_2\text{CH}_3$), 3.00-3.03 (m, 2 H, $n\text{Pr}_d\text{-NCH}_2$), 3.51 (s, 6 H, Me-NCH_3), 3.75-3.80 (m, 2 H, $n\text{Pr}_a\text{-NCH}_2$), 5.22 (d, $^3J_{\text{HH}} = 5$ Hz, 1 H, C_bH), 6.11 (d, $^3J_{\text{HH}} = 5$ Hz, 1 H, C_cH), 6.33-6.39 (m, 4 H, $\text{cat}_\beta\text{-CH}$), 6.77-6.81 (m, 2 H, $\text{cat}_\alpha\text{-CH}$), 6.97-7.00 (m, 2 H, $\text{cat}_\alpha\text{-CH}$).

$^{11}\text{B}\{^1\text{H}\}$ NMR (160 MHz, C_6D_6 , 25 °C): $\delta = 6.91$ (s, $B_{\alpha/\beta}$), 8.57 (s, $B_{\alpha/\beta}$).

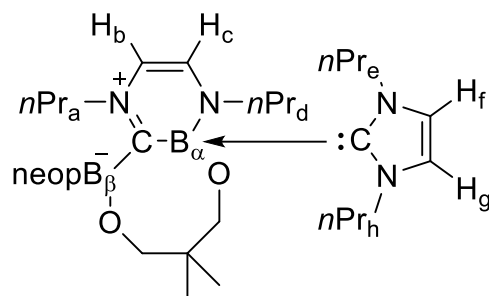
$^{13}\text{C}\{^1\text{H}\}$ NMR (125 MHz, C_6D_6 , 25 °C): $\delta = 7.73$ (Me-CH_3), 11.5 ($n\text{Pr}_a\text{-CH}_3$), 11.8 ($n\text{Pr}_d\text{-CH}_3$), 25.3 ($n\text{Pr}_e\text{-CH}_2\text{CH}_3$), 25.7 ($n\text{Pr}_d\text{-CH}_2\text{CH}_3$), 33.0 (Me-NCH_3), 51.8 ($n\text{Pr}_d\text{-CH}_3$), 61.4 ($n\text{Pr}_a\text{-CH}_3$), 105.6 (C_bH), 106.7 ($\text{cat}_\beta\text{-CH}$), 110.3 ($\text{cat}_\alpha\text{-CH}$), 117.9 ($\text{cat}_\beta\text{-CH}$), 119.6 ($\text{cat}_\alpha\text{-CH}$), 123.9 (NCCN), 136.0 (C_cH), 152.9 (cat-C_q), 153.1 (cat-C_q), 158.5 (NCN).



3.5.5.2. Synthesis of the ring expanded products containing B₂neop₂

Compound 29: RER-B₂neop₂•(nPr₂Im)₂

nPr₂Im (404 μl, 270 mg, 266 mmol, 2 equiv.) was added to a stirred solution of B₂neop₂ (300 mg, 133 mmol, 1 equiv.) in 12 mL of dry THF. After stirring the reaction mixture for 16 h at room temperature, all volatiles were removed *in vacuo*. Afterwards, the residue was washed with 20 mL of *n*-hexane to obtain the product.



For X-ray diffraction: nPr₂Im (197 μl, 197 mg, 1.22 mmol, 2 equiv.) and B₂neop₂ (150 mg, 0.66 mmol, 1 equiv.) were mixed in dry toluene (5 mL). After 20 min, the mixture was concentrated to ca. 2 mL and left at -30 °C to crystallize. The mother liquor was decanted and the colorless X-ray quality single crystals were used for the diffraction study.

Yield: 106 mg (21%) of a yellow solid.

¹H NMR (500 MHz, C₆D₆, 25 °C): δ = 0.71-0.74 (m, 6 H, nPr_{d/e}-CH₃), 0.75 (s, 3 H, neop_β-CH₃), 0.88 (t, ³J_{HH} = 7 Hz, 3 H, nPr_h-CH₃), 0.99 (t, ³J_{HH} = 7 Hz, 3 H, nPr_a-CH₃), 1.12 (s, 3 H, neop_β-CH₃), 1.14 (s, 3 H, neop-CH₃), 1.16 (s, 3 H, neop_α-CH₃), 1.25-1.36 (m, 2 H, nPr_{d/e}-CH₂CH₃), 1.44-1.51 (m, 1 H, nPr_d-CH₂CH₃), 1.51-1.61 (m, 1 H, nPr_e-CH₂CH₃), 1.67-1.77 (m, 1 H, nPr_h-CH₂CH₃), 1.78-1.87 (m, 1 H, nPr_h-CH₂CH₃), 2.08-2.16 (m, 1 H, nPr_a-CH₂CH₃), 2.17-2.24 (m, 1 H, nPr_a-CH₂CH₃), 2.41-2.47 (m, 1 H, nPr_d-NCH₂), 2.61-2.67 (m, 1 H, nPr_d-NCH₂), 2.86-2.88 (m, 1 H, neop_β-CH₂), 3.02-3.05 (m, 1 H, neop_α-CH₂), 3.07-3.12 (m, 1 H, nPr_e-NCH₂), 3.16-3.18 (m, 1 H, neop_α-CH₂), 3.29-3.35 (m, 1 H, nPr_e-NCH₂), 3.52-3.57 (m, 2 H, neop_{α/β}-CH₂), 3.79-3.81 (m, 1 H, neop_α-CH₂), 3.90-3.96 (m, 1 H, m, 1 H, nPr_h-NCH₂), 4.07-4.13 (m, 1 H, nPr_a-NCH₂), 4.28-4.31 (m, 2 H, neop_{α/β}-CH₂), 4.91-4.97 (m, 1 H, nPr_a-NCH₂), 5.13 (d, ³J_{HH} = 5 Hz, 1 H, CH_b), 5.26-5.32 (m, 1 H, nPr_h-NCH₂), 6.00 (d, ³J_{HH} = 5 Hz, 1 H, CH_c), 6.02 (d, ³J_{HH} = 2 Hz, 1 H, CH_f), 6.08 (d, ³J_{HH} = 2 Hz, 1 H, CH_g).

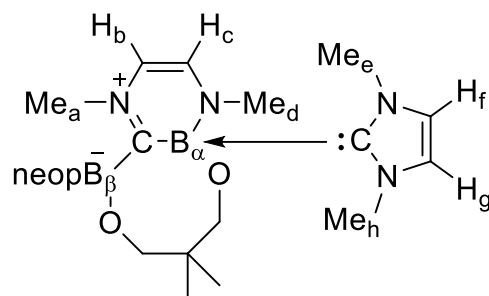
¹¹B{¹H} NMR (160 MHz, C₆D₆, 25 °C): δ = -2.35 (s, B_{α/β}), 1.03 (s, B_{α/β}).

¹³C{¹H} NMR (125 MHz, C₆D₆, 25 °C): δ = 11.4 (nPr_h-CH₃), 11.7 (nPr_e-CH₃), 12.0 (nPr_a-CH₃), 12.0 (nPr_d-CH₃), 23.4 (neop_β-CH₃), 23.8 (neop_α-CH₃), 23.9 (nPr_e-CH₂CH₃), 24.1 (nPr_a-CH₂CH₃), 24.1 (neop_β-CH₃), 24.6 (nPr_h-CH₂CH₃), 24.7 (neop_α-CH₃), 25.7 (nPr_d-CH₂CH₃), 32.6 (neop_β-C(CH₃)₂), 37.7 (neop_α-C(CH₃)₂), 49.6 (nPr_d-NCH₂), 50.5 (nPr_h-NCH₂), 54.0 (nPr_e-NCH₂), 61.4 (nPr_a-NCH₂), 68.9 (neop_α-CH₂), 70.5 (neop_α-CH₃), 71.5 (neop_β-CH₃), 72.9 (neop_β-CH₃), 102.6 (CH_b), 118.0 (CH_f), 120.1 (CH_f), 135.0 (CH_c), 165.7 (NCN), 212.3 (C_q).

Elemental analysis calcd (%) for C₂₈H₅₂B₂N₄O₄: C 63.41, H 9.88, N 10.56; found: C 63.66 H 9.93, N 10.62

Compound 30: RER-B₂neop₂•(Me₂Im)₂

Me₂Im (170 μl, 170 mg, 1.47 mmol, 2 equiv.) was added to a stirred solution of B₂neop₂ (200 mg, 890 μmol, 1 equiv.) in 20 mL of toluene. After stirring the resulting reaction mixture for 2 h at room temperature, all volatiles were removed *in vacuo*. Afterwards, the residue was washed with 15 mL of *n*-hexane to obtain the desired product.



Yield: 222 mg (60%) of a colorless solid.

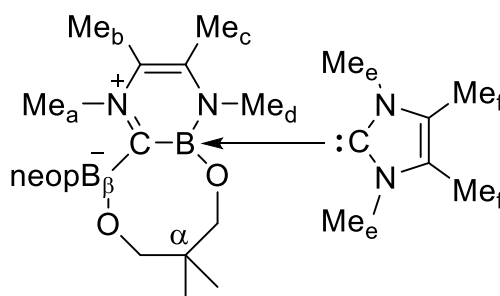
¹H NMR (500 MHz, C₆D₆, 25 °C): δ = 0.75 (s, 3 H, neop_{α,β}-CH₃), 1.09 (s, 3 H, neop_{α,β}-CH₃), 1.15 (s, 6 H, neop_{α,β}-CH₃), 2.36 (s, 3 H, Me_{a,d}-CH₃), 2.81-2.83 (m, 1 H, neop_{α,β}-CH₂), 3.01-3.03 (m, 1 H, neop_{α,β}-CH₂), 3.28-3.31 (m, 1 H, neop_{α,β}-CH₂), 3.51-3.53 (m, 1 H, neop_{α,β}-CH₂), 3.61-3.62 (m, 1 H, neop_{α,β}-CH₂), 3.68 (s_{br}, 6 H, Me_{e,h}-CH₃), 3.81-3.83 (m, 1 H, neop_{α,β}-CH₂), 4.03 (s, 3 H, Me_{a,d}-CH₃), 4.30-4.32 (m, 1 H, neop_{α,β}-CH₂), 4.34-4.37 (m, 1 H, neop_{α,β}-CH₂), 5.03 (d, ³J_{HH} = 5 Hz, 1 H, CH_{b,c}), 5.82 (s, 2 H, CH_{f,g}), 5.89 (d, ³J_{HH} = 5 Hz, 1 H, CH_{b,c}).

¹¹B{¹H} NMR (160 MHz, C₆D₆, 25 °C): δ = -2.51 (s, B_{α/β}), 0.93 (s, B_{α/β}).

¹³C{¹H} NMR (125 MHz, C₆D₆, 25 °C): δ = 23.2 (neop_{α,β}-CH₃), 23.7 (neop_{α,β}-CH₃), 23.9 (neop_{α,β}-CH₃), 24.9 (neop_{α,β}-CH₃), 32.8 (neop_{α,β}-C_q), 36.0 (Me_{e,h}-CH₃), 37.6 (Me_{a,d}-CH₃), 37.8 (neop_{α,β}-C_q), 47.1 (Me_{a,d}-CH₃), 68.6 (neop_{α,β}-CH₂), 70.5 (neop_{α,β}-CH₂), 71.5 (neop_{α,β}-CH₂), 73.0 (neop_{α,β}-CH₂), 103.7 (CH_{b,c}), 120.3 (CH_{f,g}), 136.0 (CH_{b,c}), 165.0 (NCN), 212.9 (C_q).

Compound 31: RER-B₂neop₂•(Me₂Im^{Me})₂

Me₂Im^{Me} (110 mg, 890 μmmol, 2 equiv.) and B₂neop₂ (100 mg, 445 μmol, 1 equiv.) were dissolved in 20 mL of THF. After stirring the resulting reaction mixture for 2 h at room temperature, all volatiles were removed *in vacuo*. Afterwards, the residue was washed with 15 mL of *n*-hexane to obtain the desired product.



Yield: 90 mg (43%) of a colorless solid.

¹H NMR (500 MHz, C₆D₆, 25 °C): δ = 0.74 (s, 3 H, neop_{α,β}-CH₃), 1.02 (s, 3 H, neop_{α,β}-CH₃), 1.21 (s, 3 H, neop_{α,β}-CH₃), 1.22 (s, 3 H, neop_{α,β}-CH₃), 1.43 (s, 6 H, Me_f-CH₃), 1.70 (s, 3 H, Me_{b,c}-CH₃), 1.85 (s, 3 H, Me_{b,c}-CH₃), 2.60 (s, 3 H, Me_{a,d}-CH₃), 2.73 (m, 1 H, neop_{α,β}-CH₂), 3.08 (m, 1 H, neop_{α,β}-CH₂), 3.31 (m, 1 H, neop_{α,β}-CH₂), 3.34 (s, 6 H, Me_e-CH₃), 3.56 (m, 1 H, neop_{α,β}-CH₂), 3.62 (m, 1 H, neop_{α,β}-CH₂), 3.85 (d, ³J_{HH} = 10 Hz, 1 H, neop_{α,β}-CH₂), 4.12 (s, 3 H, Me_{a,d}-CH₃), 4.36 (d, ³J_{HH} = 10 Hz, 1 H, neop_{α,β}-CH₂), 4.43 (d, ³J_{HH} = 10 Hz, 1 H, neop_{α,β}-CH₂).

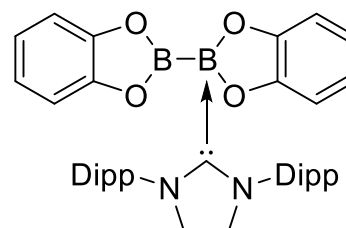
¹¹B{¹H} NMR (160 MHz, C₆D₆, 25 °C): δ = -1.31 (s, B_{α/β}), 1.83 (s, B_{α/β}).

$^{13}\text{C}\{^1\text{H}\}$ NMR (125 MHz, C_6D_6 , 25 °C): δ = 7.92 ($\text{Me}_f\text{-CH}_3$), 15.5 ($\text{Me}_{b/c}\text{-CH}_3$), 15.5 ($\text{Me}_{b/c}\text{-CH}_3$), 23.1 ($\text{neop}_{\alpha,\beta}\text{-CH}_3$), 23.9 ($\text{neop}_{\alpha,\beta}\text{-CH}_3$), 24.0 ($\text{neop}_{\alpha,\beta}\text{-CH}_3$), 25.1 ($\text{neop}_{\alpha,\beta}\text{-CH}_3$), 31.8 ($\text{Me}_{a/d}\text{-CH}_3$), 32.4 ($\text{neop}_{\alpha,\beta}\text{-C}_q$), 33.3 ($\text{Me}_e\text{-CH}_3$), 38.0 ($\text{neop}_{\alpha,\beta}\text{-C}_q$), 45.7 ($\text{Me}_{a/d}\text{-CH}_3$), 68.7 ($\text{neop}_{\alpha,\beta}\text{-CH}_2$), 70.1 ($\text{neop}_{\alpha,\beta}\text{-CH}_2$), 71.5 ($\text{neop}_{\alpha,\beta}\text{-CH}_2$), 73.0 ($\text{neop}_{\alpha,\beta}\text{-CH}_3$), 105.2 ($\text{C}_b\text{-CH}$), 123.1 (NCCN), 137.8 ($\text{C}_c\text{-CH}$), 164.1 (NCN), 210.6 (C_q).

3.5.5.3. Reactions of B_2cat_2 with the saturated NHC Dipp_2Slm

Compound 32: $\text{B}_2\text{cat}_2 \cdot \text{Dipp}_2\text{Slm}$

Dipp_2Slm (162 mg, 0.42 mmol) and B_2cat_2 (100 mg, 0.42 mmol) were dissolved in 10 mL of toluene. After stirring the reaction mixture for 1 h at room temperature all volatiles were removed *in vacuo*. Afterwards, the residue was washed with 10 mL of *n*-hexane to obtain the product.



For X-ray diffraction: A saturated solution of $\text{B}_2\text{cat}_2 \cdot \text{Dipp}_2\text{Slm}$ in toluene was cooled to -30 °C to obtain single crystals for X-ray diffraction.

Yield: 180 mg (69%) of a colorless solid.

^1H NMR (400 MHz, C_6D_6 , 25 °C): δ = 1.09 (d, $^3J_{\text{HH}} = 7$ Hz, 12 H, $\text{Dipp-}i\text{Pr-CH}_3$), 1.31 (d, $^3J_{\text{HH}} = 7$ Hz, 12 H, $\text{Dipp-}i\text{Pr-CH}_3$), 3.35 (sept, $^3J_{\text{HH}} = 7$ Hz, 5 H, $\text{Dipp-}i\text{Pr-CH}$), 3.51 (s, 4 H, CH_2CH_2), 6.35-6.40 (m, 2 H, cat-CH), 6.48-6.53 (m, 2 H, cat-CH), 6.74-6.79 (m, 2 H, cat-CH), 6.91-6.95 (m, 2 H, cat-CH), 6.97-6.99 (m, 4 H, Dipp-aryl-CH), 7.03-7.13 (m, 2 H, Dipp-aryl-CH).

$^{11}\text{B}\{^1\text{H}\}$ NMR (128 MHz, C_6D_6 , 25 °C): δ = 7.10 (s, $\text{sp}^3\text{-B}$), 37.8 (s_{br} , $\text{sp}^2\text{-B}$).

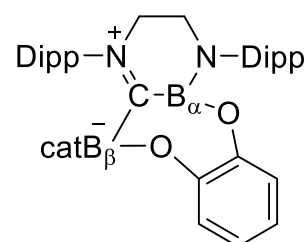
$^{13}\text{C}\{^1\text{H}\}$ NMR (100 MHz, C_6D_6 , 25 °C): δ = 23.1 ($\text{Dipp-}i\text{Pr-CH}_3$), 26.5 ($\text{Dipp-}i\text{Pr-CH}_3$), 29.2 ($\text{Dipp-}i\text{Pr-CH}$), 53.5 (CH_2CH_2), 109.5 (cat-CH), 112.2 (cat-CH), 118.0 (cat-CH), 121.7 (cat-CH), 124.4 (Dipp-aryl-CH), 129.7 (Dipp-aryl-CH), 134.2 (Dipp-aryl-C_q), 146.5 (Dipp-aryl-C_q), 149.2 (cat-C_q), 154.1 (cat-C_q), 186.7 (NCN).

Elemental analysis calcd (%) for $\text{C}_{39}\text{H}_{46}\text{B}_2\text{N}_2\text{O}_4$: C 74.54, H 7.38, N 4.46; found: C 74.74, H 7.58, N 4.08.

HRMS-ASAP (m/z): $[\text{M} + \text{H}]^+$ calcd for $\text{C}_{39}\text{H}_{46}\text{B}_2\text{N}_2\text{O}_4$, 629.3729; found, 629.3712.

Compound 33: $\text{RER-B}_2\text{cat}_2 \cdot \text{Dipp}_2\text{Slm}$

Dipp_2Slm (240 mg, 630 μmol , 1 equiv.) and B_2cat_2 (150 mg, 630 μmol , 1 equiv.) in 20 mL of toluene. After stirring the reaction mixture for 3 d at 100 °C, all volatiles were removed *in vacuo*. Afterwards, the residue was washed with 20 mL of *n*-hexane to obtain the product.



For X-ray diffraction: A saturated solution of $\text{B}_2\text{cat}_2 \cdot \text{Dipp}_2\text{Slm}$ in *n*-hexane was cooled to -30 °C to obtain single crystals for X-ray diffraction.

Yield: 280 mg (72%) of an orange solid.

^1H NMR (400 MHz, C_6D_6 , 25 °C): δ = 0.94 (d, $^3J_{\text{HH}}$ = 7 Hz, 6 H, Dipp-*i*Pr- CH_3), 1.12 (d, $^3J_{\text{HH}}$ = 7 Hz, 6 H, Dipp-*i*Pr- CH_3), 1.26 (d, $^3J_{\text{HH}}$ = 7 Hz, 6 H, Dipp-*i*Pr- CH_3), 1.37 (d, $^3J_{\text{HH}}$ = 7 Hz, 6 H, Dipp-*i*Pr- CH_3), 2.75 (sept, $^3J_{\text{HH}}$ = 7 Hz, 2 H, Dipp-*i*Pr- CH), 2.99-3.04 (m, 2 H, CH_2CH_2), 3.26 (sept, $^3J_{\text{HH}}$ = 7 Hz, 2 H, Dipp-*i*Pr- CH), 3.40-3.45 (m, 2 H, CH_2CH_2), 6.49-6.54 (m, 3 H, cat- CH , Dipp-aryl- CH), 6.55-6.60 (m, 2 H, cat- CH), 6.67-6.72 (m, 1 H, Dipp-aryl- CH), 6.76-6.78 (m, 1 H, Dipp-aryl- CH), 6.98-7.00 (m, 2 H, Dipp-aryl- CH), 7.12-7.20 (m, 4 H, cat- CH), 7.19 (s, 1 H, Dipp-aryl- CH), 7.25-7.29 (m, 1 H, Dipp-aryl- CH).

$^{11}\text{B}\{^1\text{H}\}$ NMR (128 MHz, C_6D_6 , 25 °C): δ = 7.37 (s, B_β), 26.6 (s, B_α).

$^{13}\text{C}\{^1\text{H}\}$ NMR (100 MHz, C_6D_6 , 25 °C): δ = 22.8 (Dipp-*i*Pr- CH_3), 24.2 (Dipp-*i*Pr- CH_3), 25.4 (Dipp-*i*Pr- CH_3), 25.7 (Dipp-*i*Pr- CH_3), 29.3 (Dipp-*i*Pr- CH), 29.4 (Dipp-*i*Pr- CH), 48.0 (CH_2CH_2), 58.8 (CH_2CH_2), 109.9 (cat- CH), 118.6 (cat- CH), 120.9 (Dipp-aryl- CH), 121.0 (Dipp-aryl- CH), 124.3 (Dipp-aryl- CH), 124.4 (Dipp-aryl- CH), 124.7 (cat- CH), 128.5 (Dipp-aryl- CH), 129.7 (Dipp-aryl- CH), 138.8 (cat- C_q), 141.3 (cat- C_q), 143.4 (Dipp-aryl- C_q), 144.8 (Dipp-aryl- C_q), 145.6 (Dipp-aryl- C_q), 146.2 (Dipp-aryl- C_q), 152.7 (cat- C_q), 215.8 (C_q , assigned *via* 2D NMR spectroscopy).

Elemental analysis calcd (%) for $\text{C}_{39}\text{H}_{46}\text{B}_2\text{N}_2\text{O}_4$: C 74.54, H 7.38, N 4.46; found: C 74.54, H 7.40, N 4.46.

3.5.5.4. Additional molecular structures of products of ring expansion reactions

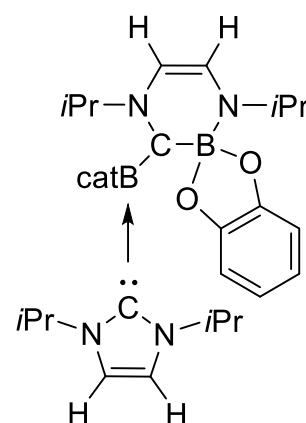
Compound 34: RER- $\text{B}_2\text{cat}_2 \cdot (\text{iPr}_2\text{Im})_2$

iPr $_2$ Im (224 μL , 224 mg, 1.47 mmol, 2 equiv.) was added to a stirred solution of B_2cat_2 (175 mg, 74.0 μmol , 1 equiv.) in 40 mL of THF. After stirring the resulting reaction mixture for 16 h at 70 °C, all volatiles were removed *in vacuo*. Afterwards, the residue was washed with 20 mL of *n*-hexane to obtain a yellow solid.

Yield: 100 mg (25%) of a yellow solid.

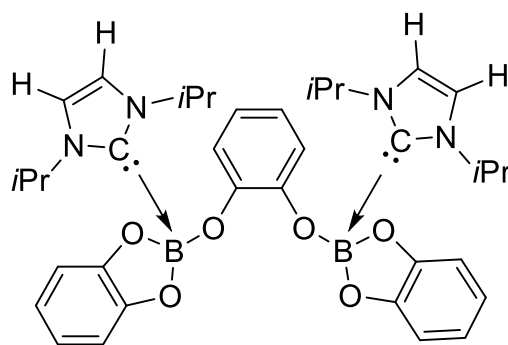
^1H NMR (500 MHz, C_6D_6 , 25 °C): δ = 1.04 (d, $^3J_{\text{HH}}$ = 7 Hz, 12 H, *i*Pr- CH_3), 1.05 (d, $^3J_{\text{HH}}$ = 7 Hz, 6 H, *i*Pr- CH_3), 1.18 (d, $^3J_{\text{HH}}$ = 7 Hz, 6 H, *i*Pr- CH_3), 3.77 (sept, $^3J_{\text{HH}}$ = 7 Hz, 1 H, *i*Pr- CH), 4.98 (sept, $^3J_{\text{HH}}$ = 7 Hz, 1 H, *i*Pr- CH), 5.28 (sept, $^3J_{\text{HH}}$ = 7 Hz, 2 H, *i*Pr- CH), 5.60 (d, $^3J_{\text{HH}}$ = 3 Hz, 1 H, CH), 6.07 (s, 2 H, CH), 6.47 (d, $^3J_{\text{HH}}$ = 3 Hz, 1 H, CH), 6.55-6.59 (m, 2 H, cat- CH), 6.64-6.68 (m, 2 H, cat- CH), 6.76-6.80 (m, 2 H, cat- CH), 6.86-6.89 (m, 2 H, cat- CH).

$^{11}\text{B}\{^1\text{H}\}$ NMR (160 MHz, C_6D_6 , 25 °C): δ = 6.39 (s, $B_{\alpha/\beta}$), 7.00 (s, $B_{\alpha/\beta}$).



Compound 35: $B_2cat_3 \cdot (iPr_2Im)_2$

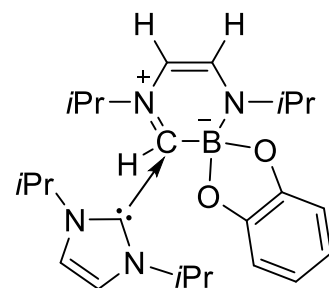
iPr_2Im (224 μ l, 224 mg, 1.47 mmol, 2 equiv.) was added to a stirred solution of B_2cat_2 (175 mg, 74.0 μ mol, 1 equiv.) in 40 mL of THF. After stirring the resulting reaction mixture for 16 h at 70 °C, all volatiles were removed *in vacuo*. Afterwards, the residue was washed with 20 mL of *n*-hexane to obtain a yellow solid.



For X-ray diffraction: A saturated solution of $RER-B_2cat_2 \cdot (iPr_2Im)_2$ in toluene was cooled to -30 °C to obtain single crystals for X-ray diffraction which were identified as the bis-NHC adduct of B_2cat_3 .

Compound 36: $RER-HBcat \cdot (iPr_2Im)_2$

iPr_2Im (224 μ l, 224 mg, 1.47 mmol, 2 equiv.) was added to a stirred solution of B_2cat_2 (175 mg, 74.0 μ mol, 1 equiv.) in 40 mL of THF. After stirring the resulting reaction mixture for 16 h at 70 °C, all volatiles were removed *in vacuo*. Afterwards, the residue was washed with 20 mL of *n*-hexane to obtain a yellow solid.



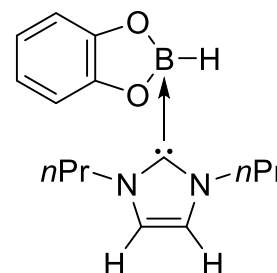
For X-ray diffraction: A saturated solution of $RER-B_2cat_2 \cdot (iPr_2Im)_2$ in toluene was cooled to -30 °C to obtain single crystals for X-ray diffraction which were identified as the ring-expanded product $RER-HBcat \cdot (iPr_2Im)_2$ **36**.

3.5.6. Reactions of HBcat with different unsaturated NHCs and CAAC^{Me}

3.5.6.1. Synthesis of NHC adducts of the type HBcat•NHC

Compound 37: HBcat•*n*Pr₂Im

*n*Pr₂Im (330 mg, 330 μL, 2.17 mmol, 1 equiv.) was added to a stirred solution of HBcat (260 mg, 2.17 mmol, 1 equiv.) in 10 mL of toluene. After stirring the reaction mixture for 2 h at room temperature, all volatiles were removed *in vacuo*. Afterwards, the residue was washed with 10 mL of *n*-hexane to obtain the desired product.



For X-ray diffraction: A saturated solution of HBcat•*n*Pr₂Im in *n*-hexane was cooled to -30 °C to obtain single crystals for X-ray diffraction.

Yield: 350 mg (59%) of a colorless solid.

¹H NMR (500 MHz, C₆D₆, 25 °C): δ = 0.60 (t, ³J_{HH} = 7 Hz, 6 H, *n*Pr-CH₃), 1.44 (sext, 4 H, *n*Pr-CH₂CH₃), 3.77-3.80 (m, 4 H, *n*Pr-NCH₂), 5.06 (quart, ¹J_{HB} = 119 Hz, 1 H, BH), 5.79 (s, 2 H, CHCH), 6.82-6.84 (m, 2 H, cat-CH), 7.03-7.5 (m, 2 H, cat-CH).

¹H{¹¹B} NMR (500 MHz, C₆D₆, 25 °C): δ = 5.06 (s, 1 H, BH).

¹¹B NMR (160 MHz, C₆D₆, 25 °C): δ = 6.46 (d, ¹J_{BH} = 119 Hz, sp³-B, BH).

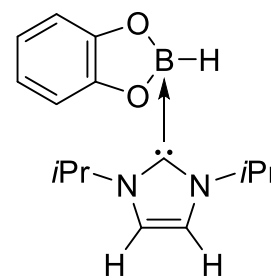
¹¹B{¹H} NMR (160 MHz, C₆D₆, 25 °C): δ = 6.46 (s, sp³-B, BH).

¹³C{¹H} NMR (100 MHz, C₆D₆, 25 °C): δ = 10.8 (*n*Pr-CH₃), 24.6 (*n*Pr-CH₂CH₃), 50.2 (*n*Pr-NCH), 109.5 (cat-CH), 118.7 (NCCN), 119.9 (cat-CH), 154.6 (cat-C_q), 161.0 (NCN).

Elemental analysis calcd (%) for C₁₅H₂₁BN₂O₂: C 66.20, H 7.78, N 10.29; found: C 66.61 H 7.87, N 10.19.

Compound 38: HBcat•*i*Pr₂Im

*i*Pr₂Im (253 mg, 253 μL, 1.66 mmol, 1 equiv.) was added to a stirred solution of HBcat (200 mg, 1.66 mmol, 1 equiv.) in 10 mL of toluene. After stirring the reaction mixture for 2 h at room temperature, all volatiles were removed *in vacuo*. Afterwards, the residue was washed with 10 mL of *n*-hexane to obtain the desired product.



For X-ray diffraction: A saturated solution of HBcat•*i*Pr₂Im in *n*-hexane was cooled to -30 °C to obtain single crystals for X-ray diffraction.

Yield: 310 mg (68%) of a colorless solid.

¹H NMR (500 MHz, C₆D₆, 25 °C): δ = 0.93 (d, ³J_{HH} = 7 Hz, 12 H, *i*Pr-CH₃), 5.17 (quart, ¹J_{HB} = 118 Hz, 1 H, BH), 5.41 (s br, 2 H, *i*Pr-CH), 6.21 (s, 2 H, CHCH), 6.82-6.84 (m, 2 H, cat-CH), 7.05-7.07 (m, 2 H, cat-CH).

¹H{¹¹B} NMR (400 MHz, C₆D₆, 25 °C): δ = 5.17 (s, 1 H, BH).

¹¹B NMR (160 MHz, C₆D₆, 25 °C): δ = 6.62 (d, ¹J_{BH} = 118 Hz, sp³-B, BH).

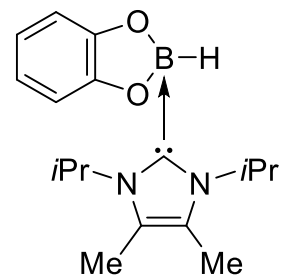
$^{11}\text{B}\{^1\text{H}\}$ NMR (160 MHz, C_6D_6 , 25 °C): $\delta = 6.62$ (s, $\text{sp}^3\text{-B}$, BH).

$^{13}\text{C}\{^1\text{H}\}$ NMR (100 MHz, C_6D_6 , 25 °C): $\delta = 22.9$ (*i*Pr- CH_3), 49.7 (*i*Pr-CH), 109.6 (cat-CH), 116.2 (NCCN), 118.8 (cat-CH), 154.6 (cat- C_q), 160.0 (NCN).

Elemental analysis calcd (%) for $\text{C}_{15}\text{H}_{21}\text{BN}_2\text{O}_2$: C 66.20, H 7.78, N 10.29; found: C 66.83 H 7.73, N 10.08.

Compound 39: HBcat·*i*Pr₂Im^{Me}

*i*Pr₂Im^{Me} (330 mg, 1.83 mmol, 1 equiv.) was added to a stirred solution of HBcat (220 mg, 1.83 mmol, 1 equiv.) in 20 mL of toluene. After stirring the reaction mixture for 2 h at 110 °C, all volatiles were removed *in vacuo*. Afterwards, the residue was washed with 10 mL of *n*-hexane to obtain the desired product.



For X-ray diffraction: A saturated solution of HBcat·*i*Pr₂Im^{Me} in *n*-hexane was cooled to -30 °C to obtain single crystals for X-ray diffraction.

Yield: 385 mg (63%) of a colorless solid.

^1H NMR (400 MHz, C_6D_6 , 25 °C): $\delta = 1.07$ (d, $^3J_{\text{HH}} = 7$ Hz, 12 H, *i*Pr- CH_3), 1.48 (s, 6 H, C- CH_3), 5.23 (quart, $^1J_{\text{HB}} = 117$ Hz, 1 H, BH), 5.68 (br s, 2 H, *i*Pr-CH), 6.83-6.87 (m, 2 H, cat-CH), 7.06-7.10 (m, 2 H, cat-CH).

$^1\text{H}\{^{11}\text{B}\}$ NMR (400 MHz, C_6D_6 , 25 °C): $\delta = 5.21$ (s, 1 H, BH).

^{11}B NMR (128 MHz, C_6D_6 , 25 °C): $\delta = 6.81$ (d, $^1J_{\text{BH}} = 117$ Hz, $\text{sp}^3\text{-B}$, BH).

$^{11}\text{B}\{^1\text{H}\}$ NMR (128 MHz, C_6D_6 , 25 °C): $\delta = 6.81$ (s, $\text{sp}^3\text{-B}$, BH)

$^{13}\text{C}\{^1\text{H}\}$ NMR (100 MHz, C_6D_6 , 25 °C): $\delta = 9.93$ (C- CH_3), 21.5 (*i*Pr- CH_3), 49.7 (*i*Pr-CH), 109.5 (cat-CH), 118.7 (cat-CH), 124.9 (NCCN), 154.6 (cat- C_q), 160.2 (NCN).

HRMS-ASAP (m/z): $[\text{M} - \text{H}]^+$ calcd for $\text{C}_{17}\text{H}_{24}\text{BN}_2\text{O}_2$, 299.1925; found, 299.1923.

Elemental analysis calcd (%) for $\text{C}_{17}\text{H}_{25}\text{BN}_2\text{O}_2$: C 68.24, H 8.09, N 9.36; found: C 67.94 H 8.36, N 9.31.

3.5.6.2. Synthesis of the B–H activation product CAAC^{Me}(H)Bcat 40

Compound 40: CAAC^{Me}(H)Bcat

CAAC^{Me} (202 mg, 708 μmol, 1 equiv.) was added to a stirred solution of HBcat (85 mg, 708 μmol, 1 equiv.) in 20 mL of toluene. After stirring the reaction mixture for 16 h at 100 °C, all volatiles were removed *in vacuo* to obtain the desired product.

For X-ray diffraction: A saturated solution of CAAC^{Me}(H)Bcat in toluene was cooled to -30 °C to obtain single crystals for X-ray diffraction.

Yield: 210 mg (73%) of a colorless solid.

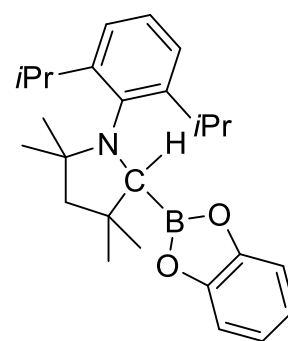
¹H NMR (400 MHz, C₆D₆, 25 °C): δ = 1.12 (s, 3 H, CH₃), 1.14 (d, ³J_{HH} = 7 Hz, 3 H, Dipp-*i*Pr-CH₃), 1.24 (d, ³J_{HH} = 7 Hz, 3 H, Dipp-*i*Pr-CH₃), 1.29 (s, 3 H, CH₃), 1.33 (s, 3 H, CH₃), 1.34 (s, 3 H, CH₃), 1.43 (d, ³J_{HH} = 7 Hz, 3 H, Dipp-*i*Pr-CH₃), 1.50 (d, ³J_{HH} = 7 Hz, 3 H, Dipp-*i*Pr-CH₃), 1.76-1.79 (m, 1 H, CH₂), 1.85-1.88 (m, 1 H, CH₂), 3.50 (sept, ³J_{HH} = 7 Hz, 1 H, Dipp-*i*Pr-CH), 4.22 (s, 1 H, C-H), 4.35 (sept, ³J_{HH} = 7 Hz, 1 H, Dipp-*i*Pr-CH), 6.61-6.66 (m, 2 H, cat-CH), 6.84-6.90 (m, 2 H, cat-CH), 7.00-7.02 (m, 1 H, Dipp-aryl-CH), 7.12-7.14 (m, 1 H, Dipp-aryl-CH), 7.24-7.26 (m, 1 H, Dipp-aryl-CH).

¹¹B{¹H} NMR (128 MHz, C₆D₆, 25 °C): δ = 35.4 (s br, sp²-B, C-Bcat)

¹³C{¹H} NMR (100 MHz, C₆D₆, 25 °C): δ = 24.1 (Dipp-*i*Pr-CH₃), 25.3 (Dipp-*i*Pr-CH₃), 26.0 (Dipp-*i*Pr-CH₃), 26.2 (Dipp-*i*Pr-CH₃), 27.0 (C-CH₃), 28.1 (Dipp-*i*Pr-CH), 28.7 (C-CH₃), 29.4 (C-CH₃), 29.5 (Dipp-*i*Pr-CH), 30.8 (C-CH₃), 41.1 (C-(CH₃)₂), 58.4 (CH₂), 63.1 (C-Bcat), 64.1 (C-(CH₃)₂), 112.6 (cat-CH), 122.8 (cat-CH), 124.8 (Dipp-aryl-CH), 124.9 (Dipp-aryl-CH), 127.0 (Dipp-aryl-CH), 139.8 (Dipp-aryl-C_q), 148.2 (cat-C_q), 150.8 (Dipp-aryl-C_q), 152.7 (Dipp-aryl-C_q).

Elemental analysis calcd (%) for C₂₆H₃₆BNO₂: C 77.03, H 8.95, N 3.46; found: C 76.53 H 9.07, N 3.29.

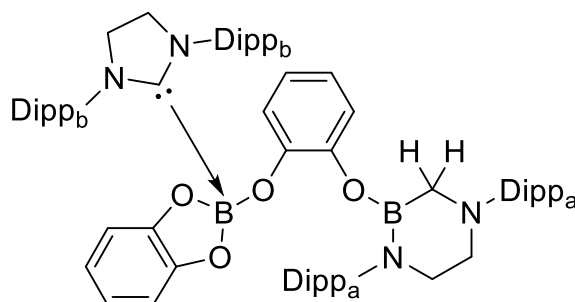
HRMS-ASAP (m/z): [M + H]⁺ calcd for C₂₆H₃₈BNO₂, 406.2917; found, 406.2905.



3.5.6.3. Synthesis of the ring expanded product RER-Dipp₂SlmB-cat-Bcat-Dipp₂Slm 41

Compound 41: RER-Dipp₂Slm(H₂)B-cat-Bcat-Dipp₂Slm

Dipp₂Slm (320 mg, 0.83 mmol, 1 equiv.) was added to a stirred solution of HBcat (100 mg, 0.83 μmol, 1 equiv.) in 20 mL of toluene. After stirring the reaction mixture for 16 h at room temperature, all volatiles were removed *in vacuo* to obtain the desired product.



For X-ray diffraction: A saturated solution of RER-Dipp₂SlmB-cat-Bcat-Dipp₂Slm in toluene was cooled to -30 °C to obtain single crystals for X-ray diffraction.

Yield: 300 mg (71%) of a colorless solid.

¹H NMR (400 MHz, C₆D₆, 25 °C): δ = 1.16 (d, ³J_{HH} = 7 Hz, 12 H, Dipp_b-*i*Pr-CH₃), 1.30 (m, 18 H, Dipp_a-*i*Pr-CH₃, Dipp_b-*i*Pr-CH₃), 1.38 (d, ³J_{HH} = 7 Hz, 6 H, Dipp_a-*i*Pr-CH₃), 1.47 (d, ³J_{HH} = 7 Hz, 6 H, Dipp_a-*i*Pr-CH₃), 1.51 (d, ³J_{HH} = 7 Hz, 6 H, Dipp_a-*i*Pr-CH₃), 3.12 (s, 2 H, CH₂), 3.22-3.35 (m, 6 H, CH₂CH₂, Dipp_b-*i*Pr-CH), 3.47 (s, 4 H, Dipp_b-CH₂CH₂), 3.48-3.53 (m, 2 H, CH₂CH₂), 3.75-3.82 (m, 4 H, Dipp_a-*i*Pr-CH), 6.23-6.39 (m, 6 H, cat-CH, Dipp_a-aryl-CH), 6.73-6.76 (m, 1 H, Dipp_a-aryl-CH), 6.90-6.93 (m, 1 H, Dipp_a-aryl-CH), 7.00-7.04 (m, 4 H, Dipp_b-aryl-CH), 7.07-7.13 (m, 4 H, cat-CH), 7.17-7.20 (m, 1 H, Dipp_a-aryl-CH), 7.26-7.36 (m, 3 H, Dipp_{a/b}-aryl-CH).

¹¹B{¹H} NMR (128 MHz, C₆D₆, 25 °C): δ = 6.60 (sp³-B), sp²-B atom was not detectable.

¹¹B SS NMR (128 MHz, 25 °C): δ = 7.22 (sp³-B), 32.6 (sp²-B).

¹³C{¹H} NMR (100 MHz, C₆D₆, 25 °C): δ = 23.5 (Dipp_b-*i*Pr-CH₃), 24.5 (Dipp_a-*i*Pr-CH₃), 25.3 (Dipp_a-*i*Pr-CH₃), 25.5 (Dipp_a-*i*Pr-CH₃), 25.6 (Dipp_a-*i*Pr-CH₃), 26.6 (Dipp_b-*i*Pr-CH₃), 28.6 (Dipp_a-*i*Pr-CH), 28.8 (Dipp_a-*i*Pr-CH), 29.1 (Dipp_b-*i*Pr-CH₃), 41.4 (CH₂), 52.8 (Dipp_a-CH₂CH₂), 53.3 (Dipp_b-CH₂CH₂), 54.7 (Dipp_a-CH₂CH₂), 109.0 (cat-CH), 118.1 (cat-CH), 119.8 (Dipp_a-aryl-CH), 121.5 (Dipp_a-aryl-CH), 122.9 (Dipp_a-aryl-CH), 123.4 (Dipp_a-aryl-CH), 124.3 (Dipp_b-aryl-CH), 126.6 (Dipp_a-aryl-CH), 127.0 (Dipp_a-aryl-CH), 129.6 (cat-CH), 135.0 (Dipp-aryl-C), 142.8 (Dipp-aryl-C), 146.1 (Dipp-aryl-C), 146.6 (cat-C_q), 146.7 (Dipp-aryl-C), 148.2 (Dipp-aryl-C), 148.5 (Dipp-aryl-C), 148.7 (Dipp-aryl-C), 152.4 (cat-C_q), 184.6 (NCN, assigned *via* 2D NMR spectroscopy (HMBC)).

Elemental analysis calcd (%) for C₆₆H₈₆B₂N₄O₄: C 77.64, H 8.49, N 5.49; found: C 77.87 H 8.84, N 5.25.

3.5.6.4. Synthesis of the mono-NHC adduct HBcat•Dipp₂Im

Compound 42: HBcat•Dipp₂Im

Dipp₂Im (517 mg, 1.33 mmol, 1 equiv.) was added to a stirred solution of HBcat (160 mg, 1.33 mmol, 1 equiv.) in 20 mL of toluene. After stirring the reaction mixture for 2 h at room temperature, all volatiles were removed *in vacuo*. Afterwards, the residue was washed with 10 mL of *n*-hexane to obtain the desired product.

Yield: 400 mg (59%) of a colorless solid.

¹H NMR (400 MHz, C₆D₆, 25 °C): δ = 1.02 (d, ³J_{HH} = 7 Hz, 12 H, Dipp-*i*Pr-CH₃), 1.36 (d, ³J_{HH} = 7 Hz, 12 H, Dipp-*i*Pr-CH₃), 2.68 (sept, ³J_{HH} = 7 Hz, 4 H, Dipp-*i*Pr-CH), 4.43 (m, 1 H, BH), 6.32 (s, 2 H, CHCH), 6.42-6.46 (m, 2 H, cat-CH), 6.51-6.55 (m, 2 H, cat-CH), 7.03-7.05 (m, 4 H, Dipp-aryl-CH), 7.15-7.19 (m, 2 H, Dipp-aryl-CH).

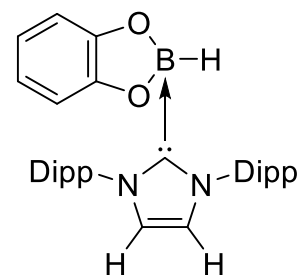
¹H{¹¹B} NMR (400 MHz, C₆D₆, 25 °C): δ = 4.43 (s, 1 H, BH).

¹¹B NMR (128 MHz, C₆D₆, 25 °C): δ = 6.03 (d, ¹J_{BH} = 123 Hz, sp³-B, BH).

¹¹B{¹H} NMR (128 MHz, C₆D₆, 25 °C): δ = 6.03 (s, sp³-B, BH)

¹³C{¹H} NMR (100 MHz, C₆D₆, 25 °C): δ = 22.7 (Dipp-*i*Pr-CH₃), 25.4 (Dipp-*i*Pr-CH₃), 29.2 (Dipp-*i*Pr-CH), 108.9 (cat-CH), 117.7 (cat-CH), 123.2 (CHCH), 123.9 (Dipp-aryl-CH), 130.5 (Dipp-aryl-CH), 133.7 (Dipp-aryl-C_q), 145.3 (Dipp-aryl-C_q), 154.2 (cat-C_q), 165.8 (NCN, assigned *via* 2D NMR spectroscopy (HMBC)).

Elemental analysis calcd (%) for C₃₃H₄₁BN₂O₂: C 77.95, H 8.13, N 5.51; found: C 78.07 H 8.10, N 5.44.



3.5.7. Synthesis of the NHC adducts of the type HBpin•NHC

Compound 43: HBpin•*n*Pr₂Im

*n*Pr₂Im (237 mg, 237 μL, 1.56 mmol, 1 equiv.) was added to a stirred solution of HBpin (200 mg, 1.56 mmol, 1 equiv.) in 10 mL of toluene. After stirring the reaction mixture for 2 h at room temperature, all volatiles were removed *in vacuo*. Afterwards, the residue was washed with 10 mL of *n*-hexane to obtain the desired product.

Yield: 315 mg (72%) of a light yellow solid.

¹H NMR (400 MHz, C₆D₆, 25 °C): δ = 0.71 (t, ³J_{HH} = 7 Hz, 6 H, *n*Pr-CH₃), 1.27 (s, 6 H, pin-CH₃), 1.51-1.60 (m, 4 H, *n*Pr-CH₂CH₃), 1.56 (s, 6 H, pin-CH₃), 4.17-4.21 (m, 4 H, *n*Pr-NCH₂), 4.44 (quart, ¹J_{HB} = 108 Hz, 1 H, BH), 5.87 (s, 2 H, CHCH).

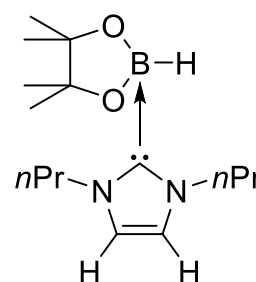
¹H{¹¹B} NMR (500 MHz, C₆D₆, 25 °C): δ = 4.44 (s, 1 H, BH).

¹¹B NMR (160 MHz, C₆D₆, 25 °C): δ = 2.44 (d, ¹J_{BH} = 108 Hz, sp³-B, BH).

¹¹B{¹H} NMR (160 MHz, C₆D₆, 25 °C): δ = 2.44 (s, sp³-B, BH).

¹³C{¹H} NMR (100 MHz, C₆D₆, 25 °C): δ = 11.0 (*n*Pr-CH₃), 24.3 (*n*Pr-CH₂CH₃), 25.6 (pin-CH₃), 25.7 (pin-CH₃), 49.7 (*n*Pr-NCH), 78.2 (pin-C_q), 118.7 (NCCN), 167.6 (NCN, assigned *via* 2D NMR spectroscopy (HMBC)).

Elemental analysis calcd (%) for C₁₅H₂₉BN₂O₂: C 64.29, H 10.43, N 10.00; found: C 64.36 H 10.68, N 9.77.



Compound 44: HBpin•*i*Pr₂Im

Synthesis according to the reported procedure.^[255]

*i*Pr₂Im (175 mg, 175 μL, 1.15 mmol, 1 equiv.) was added to a stirred solution of HBpin (147 mg, 1.15 mmol, 1 equiv.) in 10 mL of toluene. After stirring the reaction mixture for 2 h at room temperature, all volatiles were removed *in vacuo*. Afterwards, the residue was washed with 10 mL of *n*-hexane to obtain the desired product.

Yield: 160 mg (50%) of a light yellow solid.

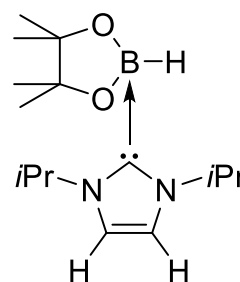
¹H NMR (400 MHz, C₆D₆, 25 °C): δ = 1.02 (d, ³J_{HH} = 7 Hz, 12 H, *i*Pr-CH₃), 1.30 (s, 6 H, pin-CH₃), 1.58 (s, 6 H, pin-CH₃), 4.52 (quart, ¹J_{HB} = 110 Hz, 1 H, BH), 6.10 (s br, 2 H, *i*Pr-CH), 6.19 (s, 2 H, CHCH).

¹H{¹¹B} NMR (400 MHz, C₆D₆, 25 °C): δ = 4.52 (s, 1 H, BH).

¹¹B NMR (160 MHz, C₆D₆, 25 °C): δ = 2.51 (d, ¹J_{BH} = 110 Hz, sp³-B, BH).

¹¹B{¹H} NMR (160 MHz, C₆D₆, 25 °C): δ = 2.51 (s, sp³-B, BH).

¹³C{¹H} NMR (100 MHz, C₆D₆, 25 °C): δ = 23.0 (*i*Pr-CH₃), 25.5 (pin-CH₃), 25.9 (pin-CH₃), 48.4 (*i*Pr-CH), 78.1 (pin-C_q), 115.2 (NCCN), 166.4 (NCN, assigned *via* 2D NMR spectroscopy (HMBC)).

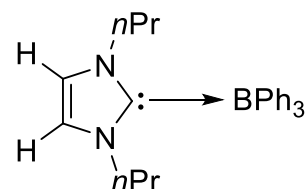


Elemental analysis calcd (%) for $C_{15}H_{29}BN_2O_2$: C 64.29, H 10.43, N 10.00; found: C 63.86 H 10.49, N 9.22.

3.5.8. Synthesis of the NHC adducts of the type $Ph_3B \cdot NHC$

Compound 45: $Ph_3B \cdot nPr_2Im$

nPr_2Im (50.0 μ l, 50.0 mg, 0.33 mmol) was added to a stirred solution of BPh_3 (80.0 mg, 0.33 mmol) in 15 mL of toluene. After stirring the resulting reaction mixture for 16 h at 110 °C, all volatiles were removed *in vacuo*. Afterwards, the residue was washed with 10 mL of *n*-hexane to obtain the desired product.



Yield: 69 mg (53%) of a yellow solid.

1H NMR (400 MHz, C_6D_6 , 25 °C): δ = 0.22 (t, $^3J_{HH}$ = 7 Hz, 6 H, $nPr-CH_3$), 0.92 (sext, $^3J_{HH}$ = 7 Hz, 4 H, $nPr-CH_2CH_3$), 3.18-3.22 (m, 4 H, N- CH_2), 5.93 (s, 2 H, CH), 7.16-7.18 (m, 3 H, aryl-CH), 7.28-7.31 (m, 6 H, aryl-CH), 7.60-7.62 (m, 6 H, aryl-CH).

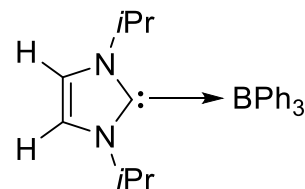
$^{11}B\{^1H\}$ NMR (128 MHz, C_6D_6 , 25 °C): δ = -8.76 (sp^3 -B).

$^{13}C\{^1H\}$ NMR (100 MHz, C_6D_6 , 25 °C): δ = 10.7 ($nPr-CH_3$), 24.0 ($nPr-CH_2CH_3$), 51.1 (N- CH_2), 119.8 (NCCN), 124.7 (aryl-CH), 127.4 (aryl-CH), 135.9 (aryl-CH), 156.2 (aryl-C), 169.7 (NCN).

Elemental analysis calcd (%) for $C_{25}H_{27}BN_2$: C 82.23, H 7.92, N 7.10; found: C 71.57 H 7.54, N 7.08.

Compound 46: $Ph_3B \cdot iPr_2Im$

iPr_2Im (50.0 μ l, 50.0 mg, 0.33 mmol) was added to a stirred solution of BPh_3 (80.0 mg, 0.33 mmol) in 15 mL of toluene. After stirring the resulting reaction mixture for 16 h at 110 °C, all volatiles were removed *in vacuo*. Afterwards, the residue was washed with 10 mL of *n*-hexane to obtain the desired product.



Yield: 69.0 mg (53%) of a yellow solid.

1H NMR (400 MHz, C_6D_6 , 25 °C): δ = 0.60 (d, $^3J_{HH}$ = 7 Hz, 12 H, $iPr-CH_3$), 4.51 (sept, $^3J_{HH}$ = 7 Hz, 2 H, $iPr-CH$), 6.17 (s, 2 H, CH), 7.15-7.20 (m, 3 H, aryl-CH), 7.28-7.32 (m, 6 H, aryl-H), 7.64-7.66 (m, 6 H, aryl-CH).

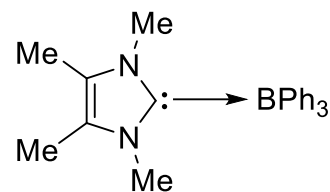
$^{11}B\{^1H\}$ NMR (128 MHz, C_6D_6 , 25 °C): δ = -8.61 (sp^3 -B).

$^{13}C\{^1H\}$ NMR (100 MHz, C_6D_6 , 25 °C): δ = 22.7 ($iPr-CH_3$), 49.5 ($iPr-CH$), 116.6 (NCCN), 124.7 (aryl-CH), 127.4 (aryl-CH), 135.8 (aryl-CH), 156.1 (aryl-C), 169.4 (NCN, *via* increasing the line broadening to lb of 16)).

Elemental analysis calcd (%) for $C_{25}H_{27}BN_2$: C 82.23, H 7.92, N 7.10; found: C 63.61 H 7.63, N 7.88.

Compound 47: Ph₃B•Me₂Im^{Me}

Me₂Im^{Me} (41.0 mg, 0.33 mmol) and BPh₃ (80.0 mg, 0.33 mmol) were stirred in 15 mL of toluene. After stirring the reaction mixture for 16 h at 110 °C, all volatiles were removed *in vacuo*. Afterwards, the residue was washed with 10 mL of *n*-hexane to obtain the desired product.



Yield: 70 mg (58%) of a colorless solid.

¹H NMR (400 MHz, C₆D₆, 25 °C): δ = 1.11 (C-CH₃), 2.63 (N-CH₃), 7.20-7.24 (m, 3 H, aryl-CH), 7.33-7.37 (m, 6 H, aryl-CH), 7.67-7.69 (m, 6 H, aryl-H).

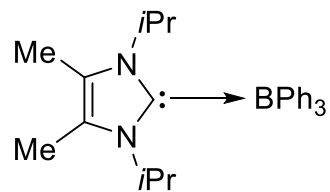
¹¹B{¹H} NMR (128 MHz, C₆D₆, 25 °C): δ = -8.64 (sp³-B).

¹³C{¹H} NMR (100 MHz, C₆D₆, 25 °C): δ = 8.11 (C-CH₃), 34.5 (N-CH₃), 124.3 (C-CH₃), 124.6 (aryl-CH), 127.5 (aryl-CH), 135.7 (aryl-CH), 156.7 (aryl-C), 168.8 (NCN, with line broadening (lb 16)).

Elemental analysis calcd (%) for C₂₅H₂₇BN₂: C 81.97, H 7.43, N 7.65; found: C 63.75 H 7.21, N 7.28.

Compound 48: Ph₃B•*i*Pr₂Im^{Me}

*i*Pr₂Im^{Me} (75.0 mg, 0.41 mmol) and BPh₃ (100.0 mg, 0.41 mmol) were stirred in 15 mL of toluene. After stirring the reaction mixture for 16 h at 110 °C, all volatiles were removed *in vacuo*. Afterwards, the residue was washed with 10 mL of *n*-hexane to obtain the desired product.



Yield: 85 mg (49%) of a colorless solid.

¹H NMR (400 MHz, C₆D₆, 25 °C): δ = 0.70 (d, ³J_{HH} = 7 Hz, 12 H, *i*Pr-CH₃), 1.52 (s, 6 H, C-CH₃), 5.03 (sept, ³J_{HH} = 7 Hz, 2 H, *i*Pr-CH), 7.16-7.20 (m, 3 H, aryl-CH), 7.30-7.34 (m, 6 H, aryl-CH), 7.67-7.69 (m, 6 H, aryl-CH).

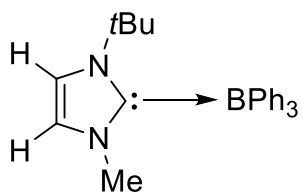
¹¹B{¹H} NMR (128 MHz, C₆D₆, 25 °C): δ = -8.09 (sp³-B).

¹³C{¹H} NMR (100 MHz, C₆D₆, 25 °C): δ = 10.3 (C-CH₃), 20.9 (*i*Pr-CH₃), 49.5 (*i*Pr-CH), 124.5 (aryl-CH), 125.1 (C-CH₃), 127.4 (aryl-CH), 135.8 (aryl-CH), 157.0 (aryl-C), 169.6 (NCN).

Elemental analysis calcd (%) for C₂₅H₂₇BN₂: C 82.46, H 8.35, N 6.63; found: C 62.81 H 7.46, N 7.02.

Compound 49: Ph₃B•Me*t*Bulm

Me*t*Bulm (57.0 mg, 0.41 mmol) and BPh₃ (100 mg, 0.41 mmol) were stirred in 15 mL of toluene. After stirring the reaction mixture for 16 h at 110 °C, all volatiles were removed *in vacuo*. Afterwards, the residue was washed with 10 mL of *n*-hexane to obtain the desired product.



Yield: 100 mg (64%) of a colorless solid.

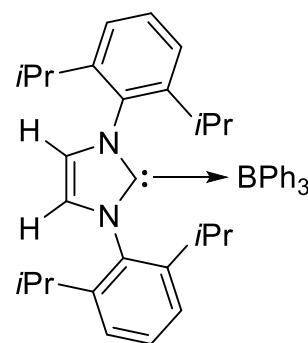
^1H NMR (400 MHz, C_6D_6 , 25 °C): δ = 1.06 (s, 9 H, *t*Bu- CH_3), 2.57 (s, 3 H, Me- CH_3), 5.72 (d, $^3J_{\text{HH}}$ = 2 Hz, 1 H, CH), 6.30 (d, $^3J_{\text{HH}}$ = 2 Hz, 1 H, CH), 7.16-7.20 (m, 3 H, aryl-CH), 7.27-7.31 (m, 6 H, aryl-CH), 7.56-7.58 (m, 6 H, aryl-CH).

$^{11}\text{B}\{^1\text{H}\}$ NMR (128 MHz, C_6D_6 , 25 °C): δ = -6.41 (sp³-B).

$^{13}\text{C}\{^1\text{H}\}$ NMR (100 MHz, C_6D_6 , 25 °C): δ = 31.6 (*t*Bu- CH_3), 40.3 (Me- CH_3), 60.0 (*t*Bu-C), 117.5 (CH), 20.9 (CH), 124.7 (aryl-CH), 127.2 (aryl-CH), 136.6 (aryl-CH), 157.8 (aryl-C), 174.2 (NCN).

Compound 50: $\text{Ph}_3\text{B}\cdot\text{Dipp}_2\text{Im}$

Dipp₂Im (128 mg, 0.33 mmol) and BPh₃ (80.0 mg, 0.33 mmol) were stirred in 15 mL of toluene. After stirring the reaction mixture for 16 h at room temperature, all volatiles were removed *in vacuo*. Afterwards, the residue was washed with 10 mL of *n*-hexane to obtain the desired product.



Yield: 153 mg (74%) of a colorless solid.

^1H NMR (400 MHz, C_6D_6 , 25 °C): δ = 0.92 (d, $^3J_{\text{HH}}$ = 7 Hz, 12 H, *i*Pr- CH_3), 1.01 (d, $^3J_{\text{HH}}$ = 7 Hz, 12 H, *i*Pr- CH_3), 2.99 (sept, $^3J_{\text{HH}}$ = 7 Hz, 2 H, *i*Pr-CH), 6.42 (s, 2 H, CHCH), 6.74-6.76 (m, 4 H, aryl-CH), 6.94-6.96 (m, 8 H, aryl-CH), 6.98-7.00 (m, 3 H, aryl-CH), 7.21-7.24 (m, 6 H, aryl-CH).

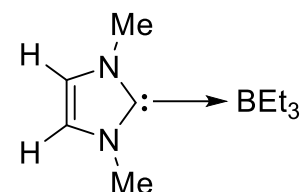
$^{11}\text{B}\{^1\text{H}\}$ NMR (128 MHz, C_6D_6 , 25 °C): δ = -6.74 (sp³-B).

$^{13}\text{C}\{^1\text{H}\}$ NMR (100 MHz, C_6D_6 , 25 °C): δ = 22.0 (*i*Pr- CH_3), 26.5 (*i*Pr- CH_3), 28.8 (*i*Pr-CH), 123.9 (aryl-CH; NHC), 124.0 (aryl-CH, NHC), 125.4 (CH, NHC), 125.8 (aryl-CH, BPh₃), 130.3 (aryl-CH, BPh₃), 137.2 (aryl-CH, BPh₃), 137.5 (aryl-CH, NHC), 145.0 (aryl-C_q, NHC), 153.7 (aryl-C_q, BPh₃) 177.7 (NCN, assigned *via* 2D NMR spectroscopy (HMBC)).

3.5.9. Synthesis of the mono-NHC adducts of the type $\text{Et}_3\text{B}\cdot\text{NHC}$

Compound 51: $\text{Et}_3\text{B}\cdot\text{Me}_2\text{Im}$

BEt_3 (147 μl , 100 mg, 1.02 mmol) was added to a stirred solution of Me_2Im (98.0 μl , 98.0 mg, 1.02 mmol) in 20 mL of toluene. After stirring the reaction mixture for 16 h at room temperature, all volatiles were removed *in vacuo*. Afterwards the residue was washed with 10 ml *n*-hexane to obtain the desired product.



For X-ray diffraction: A saturated solution of $\text{Et}_3\text{B}\cdot\text{Me}_2\text{Im}$ in toluene was cooled to $-30\text{ }^\circ\text{C}$ to obtain single crystals for X-ray diffraction.

Yield: 263 mg (66%) of a colorless solid.

$^1\text{H NMR}$ (500 MHz, C_6D_6 , $25\text{ }^\circ\text{C}$): δ = 0.93-1.00 (m, 6 H, Et-CH_2), 1.15-1.18 (m, 9 H, Et-CH_3), 3.18 (s, 6 H, CH_3), 5.54 (s, 2 H, CH).

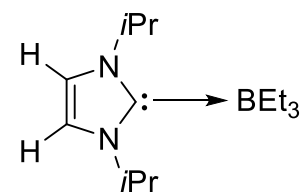
$^{11}\text{B}\{^1\text{H}\}$ NMR (160 MHz, C_6D_6 , $25\text{ }^\circ\text{C}$): δ = -12.3 ($\text{sp}^3\text{-B}$).

$^{13}\text{C}\{^1\text{H}\}$ NMR (125 MHz, C_6D_6 , $25\text{ }^\circ\text{C}$): δ = 12.1 (Et-CH_3), 15.1 (Et-CH_2), 37.3 (CH_3), 120.9 (NCCN), 176.9 (NCN).

Elemental analysis calcd (%) for $\text{C}_{29}\text{H}_{35}\text{BN}_2$: C 68.06, H 11.94, N 14.43; found: C 68.11 H 12.14, N 14.46.

Compound 52: $\text{Et}_3\text{B}\cdot i\text{Pr}_2\text{Im}$

BEt_3 (443 μl , 300 mg, 3.06 mmol) was added to a stirred solution of $i\text{Pr}_2\text{Im}$ (466 μl , 466 mg, 3.06 mmol) in 20 ml toluene. After stirring the reaction mixture for 16 h at room temperature all volatiles were removed *in vacuo*. Afterwards the residue was washed with 10 ml *n*-hexane to obtain the desired product.



For X-ray diffraction: A saturated solution of $\text{Et}_3\text{B}\cdot i\text{Pr}_2\text{Im}$ in toluene was cooled to $-30\text{ }^\circ\text{C}$ to obtain single crystals for X-ray diffraction.

Yield: 375 mg (47%) of a colorless solid.

$^1\text{H NMR}$ (500 MHz, C_6D_6 , $25\text{ }^\circ\text{C}$): δ = 0.98 (d, $^3J_{\text{HH}} = 7\text{ Hz}$, 12 H, $i\text{Pr-CH}_3$), 0.99-1.04 (m, 6 H, Et-CH_2), 1.17-1.20 (m, 9 H, Et-CH_3), 5.45 (sept, $^3J_{\text{HH}} = 7\text{ Hz}$, 2 H, $i\text{Pr-CH}$), 6.19 (s, 2 H, CH).

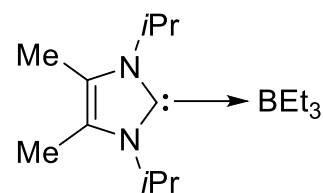
$^{13}\text{C}\{^1\text{H}\}$ NMR (125 MHz, C_6D_6 , $25\text{ }^\circ\text{C}$): δ = 12.2 (Et-CH_3), 15.2 (Et-CH_2), 23.6 ($i\text{Pr-CH}_3$), 48.5 ($i\text{Pr-CH}$), 116.0 (NCCN), 174.7 (NCN).

$^{11}\text{B}\{^1\text{H}\}$ NMR (160 MHz, C_6D_6 , $25\text{ }^\circ\text{C}$): δ = -11.7 ($\text{sp}^3\text{-B}$).

Elemental analysis calcd (%) for $\text{C}_{29}\text{H}_{35}\text{BN}_2$: C 72.00, H 12.49, N 11.20; found: C 72.15 H 12.56, N 11.30.

Compound 53: Et₃B•iPr₂Im^{Me}

BEt₃ (148 μl, 100 mg, 1.02 mmol) was added to a stirred solution of iPr₂Im^{Me} (184 mg, 1.02 mmol) in 20 ml toluene. After stirring the reaction mixture for 16 h at 110 °C all volatiles were removed *in vacuo*. Afterwards the residue was washed with 10 ml *n*-hexane to obtain the desired product.



For X-ray diffraction: A saturated solution of Et₃B•iPr₂Im^{Me} in toluene was cooled to -30 °C to obtain single crystals for X-ray diffraction.

Yield: 170 mg (60%) of a colorless solid.

¹H NMR (500 MHz, C₆D₆, 25 °C): δ = 1.03-1.08 (m, 6 H, Et-CH₂), 1.12 (d, ³J_{HH} = 7 Hz, 12 H, iPr-CH₃), 1.23-1.26 (m, 9 H, Et-CH₃), 1.58 (s, 6 H, C-CH₃), 5.78 (sept, ³J_{HH} = 7 Hz, 2 H, iPr-CH).

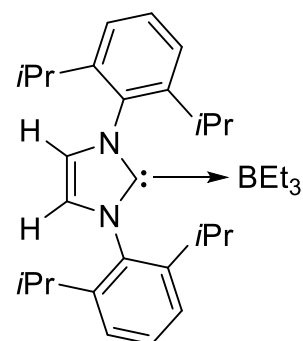
¹¹B{¹H} NMR (160 MHz, C₆D₆, 25 °C): δ = -11.2 (sp³-B).

¹³C{¹H} NMR (125 MHz, C₆D₆, 25 °C): δ = 10.5 (C-CH₃), 12.6 (Et-CH₃), 15.9 (Et-CH₂), 21.7 (iPr-CH₃), 47.9 (iPr-CH), 124.4 (NCCN), 174.5 (NCN).

Elemental analysis calcd (%) for C₂₉H₃₅BN₂: C 73.37, H 12.68, N 10.07; found: C 74.06 H 12.81, N 9.74.

Compound 54: Et₃B•Dipp₂Im

BEt₃ (148 μl, 100 mg, 1.02 mmol) was added to a stirred solution of Dipp₂Im (397 mg, 1.02 mmol) in 20 ml toluene. After stirring the reaction mixture for 16 h at room temperature, all volatiles were removed *in vacuo*. Afterwards the residue was washed with 10 ml *n*-hexane to obtain the desired product.



Yield: 305 mg (61%) of a colorless solid.

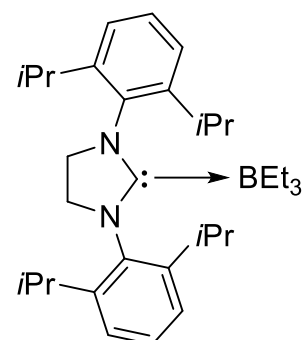
¹H NMR (500 MHz, C₆D₆, 25 °C): δ = 0.44-0.48 (m, 6 H, Et-CH₂), 0.96 (d, ³J_{HH} = 7 Hz, 12 H, Dipp-iPr-CH₃), 1.07-1.10 (m, 9 H, Et-CH₃), 1.42 (d, ³J_{HH} = 7 Hz, 12 H, iPr-CH₃), 2.96 (sept, ³J_{HH} = 7 Hz, 2 H, Dipp-iPr-CH), 6.29 (s, 2 H, CHCH), 7.08-7.09 (m, 4 H, Dipp-aryl-CH), 7.19-7.22 (m, 2 H, Dipp-aryl-CH).

¹¹B{¹H} NMR (160 MHz, C₆D₆, 25 °C): δ = -12.5 (sp³-B).

¹³C{¹H} NMR (125 MHz, C₆D₆, 25 °C): δ = 12.4 (Et-CH₃), 14.9 (Et-CH₂), 22.5 (Dipp-iPr-CH₃), 26.4 (Dipp-iPr-CH₃), 29.0 (Dipp-iPr-CH), 123.8 (Dipp-aryl-CH), 124.1 (CHCH), 130.4 (Dipp-aryl-CH), 137.1 (Dipp-aryl-C_q), 146.0 (Dipp-aryl-C_q), 183.0 (NCN).

Compound 55: Et₃B•Dipp₂SIm

BEt₃ (38.0 μl, 25.0 mg, 256 μmol) was added to a stirred solution of Dipp₂SIm (100 mg, 256 μmol) in 20 ml toluene. After stirring the reaction mixture for 16 h at room temperature, all volatiles were removed *in vacuo*. Afterwards the residue was washed with 10 ml *n*-hexane to obtain the desired product.



For X-ray diffraction: A saturated solution of Et₃B•Dipp₂SIm in toluene was cooled to -30 °C to obtain single crystals for X-ray diffraction.

Yield: 60 mg (48%) of a colorless solid.

¹H NMR (500 MHz, C₆D₆, 25 °C): δ = 0.34-0.40 (m, 6 H, Et-CH₂), 1.03-1.09 (m, 21 H, Dipp-*i*Pr-CH₃, Et-CH₃), 1.48-1.50 (d, ³J_{HH} = 7 Hz, 12 H, Dipp-*i*Pr-CH₃), 3.33-3.44 (m, 8 H, Dipp-*i*Pr-CH, CH₂CH₂), 7.06-7.08 (m, 4 H, Dipp-aryl-CH), 7.14-7.18 (m, 2 H, Dipp-aryl-CH).

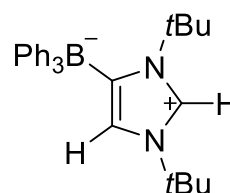
¹¹B{¹H} NMR (160 MHz, C₆D₆, 25 °C): δ = -12.6 (sp³-B).

¹³C{¹H} NMR (125 MHz, C₆D₆, 25 °C): δ = 12.3 (Et-CH₃), 14.7 (Et-CH₂), 23.2 (Dipp-*i*Pr-CH₃), 26.8 (Dipp-*i*Pr-CH₃), 28.9 (Dipp-*i*Pr-CH), 54.1 (CH₂CH₂), 124.3 (Dipp-aryl-CH), 129.5 (Dipp-aryl-CH), 137.7 (Dipp-aryl-C_q), 146.6 (Dipp-aryl-C_q), 205.9 (NCN).

3.5.10. Synthesis of the backbone-activated products of the type R₃B-*t*Bu₂Im-H

Compound 56: Ph₃B-*t*Bu₂Im-H

*t*Bu₂Im (60.0 mg, 0.33 mmol) and BPh₃ (80.0 mg, 0.33 mmol) were stirred in 15 mL of toluene. After stirring the reaction mixture for 16 h at 110 °C, all volatiles were removed *in vacuo*. Afterwards, the residue was washed with 10 mL of *n*-hexane to obtain Ph₃B-*t*BuIm-H.



Yield: 86 mg (62%) of a colorless solid.

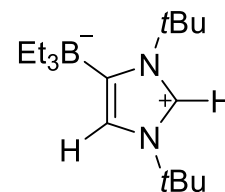
¹H NMR (500 MHz, C₆D₆, 25 °C): δ = 0.64 (s, 9 H, *t*Bu-CH₃), 1.03 (s, 9 H, *t*Bu-CH₃), 6.86 (d, ³J_{HH} = 2 Hz, 1 H, CH), 7.20-7.26 (m, 3 H, aryl-CH), 7.38-7.41 (m, 7 H, CH, aryl-CH), 7.88-7.90 (m, 6 H, aryl-CH).

¹¹B{¹H} NMR (160 MHz, C₆D₆, 25 °C): δ = -7.96 (sp³-B).

¹³C{¹H} NMR (125 MHz, C₆D₆, 25 °C): δ = 29.0 (*t*Bu-CH₃), 31.8 (*t*Bu-CH₃), 56.8 (*t*Bu-C), 61.7 (*t*Bu-C), 123.9 (aryl-CH), 125.4 (CH), 126.9 (aryl-CH), 129.5 (CH), 136.5 (aryl-C), 159.8 (C-BPh₃).

Compound 57: Et₃B-*t*Bu₂Im-H

BEt₃ (148 μl, 100 mg, 1.02 mmol) was added to a stirred solution of *t*Bu₂Im (184 mg, 1.02 mmol) in 20 ml toluene. After stirring the reaction mixture for 16 h at 110 °C all volatiles were removed *in vacuo*. Afterwards the residue was washed with 10 ml *n*-hexane to obtain the desired product.



Yield: 86 mg (62%) of a colorless solid.

¹H NMR (500 MHz, C₆D₆, 25 °C): δ = 0.78 (s, 9 H, *t*Bu-CH₃), 1.10-1.15 (m, 6 H, Et-CH₂), 1.35-1.38 (m, 9 H, Et-CH₃), 1.44 (s, 9 H, *t*Bu-CH₃), 7.04 (d, ³J_{HH} = 2 Hz, 1 H, CH), 7.22 (d, ³J_{HH} = 2 Hz, 1 H, CH).

¹¹B{¹H} NMR (160 MHz, C₆D₆, 25 °C): δ = -13.1 (sp³-B).

¹³C{¹H} NMR (125 MHz, C₆D₆, 25 °C): δ = 12.2 (Et-CH₃), 17.3 (Et-CH₂), 29.1 (*t*Bu-CH₃), 30.8 (*t*Bu-CH₃), 56.1 (*t*Bu-C), 59.3 (*t*Bu-C), 123.7 (CH), 126.4 (CH), 163.1 (C-BEt₃).

4. CRYSTALLOGRAPHIC DATA

4.1. Crystallographic data collection parameters

Crystals were immersed in a film of perfluoropolyether oil on a glass fiber and transferred to a Bruker X8 Apex-2 diffractometer, with CCD area detector and mirror-monochromated Mo-K α radiation, equipped with an Oxford Cryosystems low-temperature device. Data were collected at 100 K. The images were processed with the Bruker software packages and equivalent reflections were merged. Corrections for Lorentz-polarization effects and absorption were performed if necessary and the structures were solved by direct methods. Subsequent difference Fourier syntheses revealed the positions of all other non-hydrogen atoms, and hydrogen atoms were included in calculated positions and refined using a riding model. Extinction corrections were applied as required. Crystallographic calculations were performed using the SHELXTL software package.^[285] All non-hydrogen atoms were refined anisotropically. Hydrogen atoms were assigned to idealized positions and were included in structure factors calculations.

Data for [B₂pin₂F][NMe₄] **4** was recorded on Bruker SMART 6000 diffractometer (ω scans, 0.3° width) using CuK α radiation ($\lambda = 1.54184 \text{ \AA}$) was used employing an Oxford Diffraction Gemini Ultra and Oxford Diffraction Nova A instrument, respectively (ω scans). The structure was solved by direct methods and refined by full-matrix least squares on all F² data (SHELX^[286]). Unless specified, all non-hydrogen atoms were refined with anisotropic displacement parameters and hydrogen atoms were included in calculated positions and refined using a riding model. Refinement, analysis of the structures and the preparation of graphics were performed using SHELXTL^[286], ORTEP 3,^[287] DIAMOND,^[288] WinGX^[289] and PLATON.^[290]

Data for B₂cat₂•Me₂Im^{Me} **18** and B₂cat₂•(Me₂Im^{Me})₂ **25** were recorded on a Bruker APEX-II diffractometer, with CuK α radiation (graphite monochromator, $\lambda = 1.5418 \text{ \AA}$). The Bruker APEX2 software package was used for data collection,^[291] and the CrysAlisPro software package was used for cell refinement and data reduction.^[292] The CrysAlisPro software package was used for empirical absorption corrections, which were applied using spherical harmonics, implemented in SCALE3 ABSPACK scaling algorithm. Structures were solved using direct^[293] methods and refined against F² using the Crystals^[285] software package. Non-hydrogen atoms were refined anisotropically. Hydrogen atoms were all located in a difference map and repositioned geometrically.

4.2. CCDC-numbers of published compounds

The crystallographic data (cif-files) of the published compounds were uploaded to the CAMBRIDGE CRYSTALLOGRAPHIC DATA CENTRE (CCDC) and can be downloaded via <http://www.ccdc.cam.ac.uk>. Table 9 lists the corresponding CCDC-numbers.

Compound	CCDC-number
[B₂pin₂F][NMe₄] 4	1028949
B₂cat₂•Me₂Im^{Me} 18	1047166
B₂cat₂•(Me₂Im^{Me})₂ 25	1058480
RER-B₂cat₂•(Me₂Im^{Me})₂ 26	1054810
RER-B₂cat₂•(nPr₂Im)₂ 27	1054811
RER-B₂neop₂•(nPr₂Im)₂ 29	1054812

Table 9: CCDC-numbers of published compounds.

4.3. Crystallographic data collection parameters

Table 10: Crystallographic data collection parameters for adduct [B₂pin₂F][NMe₄] **4** · C₄H₈O

	[B ₂ pin ₂ F][NMe ₄] 4 · C ₄ H ₈ O
Chemical formula	C ₁₆ H ₃₆ B ₂ FNO ₄ ·C ₄ H ₈ O
Formula mass /g · mol ⁻¹	419.18
Crystal size /mm ³	0.52×0.08×0.07
Crystal system	monoclinic
Space group, Z	<i>P</i> 2 ₁ / <i>n</i> , 4
<i>a</i> /Å	14.6595(6)
<i>b</i> /Å	8.1665(3)
<i>c</i> /Å	20.9451(8)
<i>α</i>	90°
<i>β</i>	99.525(4)°
<i>γ</i>	90°
Volume /Å ³	2472.91(17))
ρ_{calcd} /g · cm ⁻³	1.126
<i>T</i> /K	150(2)
μ /mm ⁻¹ , Radiation	0.663 CuK α
Measured reflns	39523
Indep. reflns	5111
param./restraints	295/20
θ range	3.429° – 75.574°
GoF on <i>F</i> ²	1.077
<i>R</i> _{int}	0.0552
<i>R</i> ₁ [<i>I</i> > 2 σ (<i>I</i>)]	0.0608
w <i>R</i> ₂ (all data)	0.1805
max / min peaks /e Å ⁻³	0.473, -0.223
CCDC number	1028949

Table 11: Crystallographic data collection parameters for FBpin•*n*Pr₂Im **17**.

	FBpin• <i>n</i> Pr ₂ Im 17
Chemical formula	C ₁₅ H ₂₈ BFN ₂ O ₂
Formula mass /g · mol ⁻¹	298.20
Crystal size/mm ³	0.25x0.12x0.11
Crystal system	trigonal
Space group, Z	<i>R</i> 3 <i>c</i> , 18
<i>a</i> /Å	24.782(3)
<i>b</i> /Å	24.782(3)
<i>c</i> /Å	14.2177(17)
<i>α</i>	90°
<i>β</i>	90°
<i>γ</i>	120°
Volume /Å ³	7561.7(19)
ρ_{calcd} /g · cm ⁻³	1.179
<i>T</i> /K	100(2)
μ /mm ⁻¹ , Radiation	0.084 MoK α
Measured reflns	25045
Indep. reflns	2994
param./restraints	197/1
θ range	2.846° – 26.019°
GoF on <i>F</i> ²	1.622
<i>R</i> _{int}	0.0344
<i>R</i> ₁ [<i>I</i> > 2σ(<i>I</i>)]	0.0524
w <i>R</i> ₂ (all data)	0.1653
max / min peaks /e Å ⁻³	0.452, -0.287

Table 12: Crystallographic data collection parameters for B₂cat₂•Me₂Im^{Me} **18**.

	B ₂ cat ₂ •Me ₂ Im ^{Me} 18
Chemical formula	C ₁₉ H ₂₀ B ₂ N ₂ O ₄
Formula mass /g · mol ⁻¹	361.99
Crystal size /mm ³	0.25x0.30x0.50
Crystal system	orthorhombic
Space group, Z	<i>Pca</i> 2 ₁ , 8
<i>a</i> /Å	13.16172(16)
<i>b</i> /Å	15.76793(16)
<i>c</i> /Å	17.33231(18)
<i>α</i>	90°
<i>β</i>	90°
<i>γ</i>	90°
Volume /Å ³	3597.03(7)
ρ_{calcd} /g · cm ⁻³	1.337
<i>T</i> /K	100(2)
μ /mm ⁻¹ , Radiation	0.749 CuK α
Measured reflns	14277
Indep. reflns	5782
param./restraints	488/1
θ range	2.802° – 74.678°
GoF on <i>F</i> ²	0.9855
<i>R</i> _{int}	0.020
<i>R</i> ₁ [<i>I</i> > 2 σ (<i>I</i>)]	0.0260
w <i>R</i> ₂ (all data)	0.0704
max / min peaks /e Å ⁻³	0.22, -0.15
CCDC number	1047166

Table 13: Crystallographic data collection parameters for B₂neop₂•iPr₂Im^{Me} **21**.

B ₂ neop ₂ •iPr ₂ Im ^{Me} 21	
Chemical formula	C ₂₁ H ₄₀ B ₂ N ₂ O ₄
Formula mass /g · mol ⁻¹	406.17
Crystal system	orthorhombic
Space group, Z	<i>Cmc</i> 2 ₁ , 8
<i>a</i> /Å	11.5133(13)
<i>b</i> /Å	12.4703(13)
<i>c</i> /Å	16.7390(19)
<i>α</i>	90°
<i>β</i>	90°
<i>γ</i>	90°
Volume /Å ³	2403.3(5)
ρ_{calcd} /g · cm ⁻³	1.123
<i>T</i> /K	100(2)
μ /mm ⁻¹ , Radiation	0.075 MoK α
Measured reflns	8643
Indep. reflns	2497
param./restraints	153/1
θ range	2.408° – 26.029 °
GoF on <i>F</i> ²	1.118
<i>R</i> _{int}	0.0429
<i>R</i> ₁ [<i>I</i> > 2 σ (<i>I</i>)]	0.0482
w <i>R</i> ₂ (all data)	0.1230
max / min peaks /e Å ⁻³	0.321, -0.218

Table 14: Crystallographic data collection parameters for $B_2neop_2 \cdot (Me_2Im^{Me})_2$ **22**.

$B_2neop_2 \cdot (Me_2Im^{Me})_2$ 22 • 2(toluene)	
Chemical formula	$C_{24}H_{44}B_2N_4O_4 \cdot 2(C_7H_8)$
Formula mass /g · mol ⁻¹	658.52
Crystal size /mm ³	0.23x0.22x0.15
Crystal system	monoclinic
Space group, Z	$P2_1/n$, 4
a /Å	8.4650(4)
b /Å	16.1068(8)
c /Å	13.6527(6)
α	90°
β	95.327(2)°
γ	90°
Volume /Å ³	1853.43(15)
ρ_{calcd} /g · cm ⁻³	1.180
T /K	100(2)
μ /mm ⁻¹ , Radiation	0.075 MoK α
Measured reflns	24084
Indep. reflns	3681
param./restraints	224/0
θ range	1.960° – 26.093°
GoF on F^2	1.060
R_{int}	0.0199
R_1 [$I > 2\sigma(I)$]	0.0359
wR ₂ (all data)	0.0963
max / min peaks /e Å ⁻³	0.458, -0.181

Table 15: Crystallographic data collection parameters for $B_2neop_2 \cdot (iPr_2Im^{Me})_2$ **23**.

	$B_2neop_2 \cdot (iPr_2Im^{Me})_2$ 23
Chemical formula	$C_{32}H_{60}B_2N_4O_4$
Formula mass /g · mol ⁻¹	586.46
Crystal size /mm ³	0.16x0.12x0.11
Crystal system	triclinic
Space group, Z	$P\bar{1}$, 2
<i>a</i> /Å	9.7049(19)
<i>b</i> /Å	10.167(2)
<i>c</i> /Å	10.957(2)
α	102.22(3)°
β	112.21(3)°
γ	110.29(3)°
Volume /Å ³	862.6(4)
ρ_{calcd} /g · cm ⁻³	1.129
<i>T</i> /K	100(2)
μ /mm ⁻¹ , Radiation	0.073 MoK α
Measured reflns	3218
Indep. reflns	3218
param./restraints	199/0
θ range	2.185° – 26.050°
GoF on F^2	0.999
R_{int}	0.0708
R_1 [$I > 2\sigma(I)$]	0.1016
wR ₂ (all data)	0.3098
max / min peaks /e Å ⁻³	0.527, -0.394

Table 16: Crystallographic data collection parameters for B₂neop₂•(MeⁱPrIm)₂ **24**.

	B ₂ neop ₂ •(Me ⁱ PrIm) ₂ 24
Chemical formula	C ₃₈ H ₆₀ B ₂ N ₄ O ₄
Formula mass /g · mol ⁻¹	658.52
Crystal size /mm ³	0.17x0.07x0.05
Crystal system	monoclinic
Space group, Z	<i>P</i> 2 ₁ / <i>n</i> , 4
<i>a</i> /Å	9.0255(4)
<i>b</i> /Å	17.1950(8)
<i>c</i> /Å	12.2519(6)
<i>α</i>	90°
<i>β</i>	93.833(2)°
<i>γ</i>	90°
Volume /Å ³	1897.16(15)
ρ_{calcd} /g · cm ⁻³	1.153
<i>T</i> /K	100(2)
μ /mm ⁻¹ , Radiation	0.073 MoK α
Measured reflns	24761
Indep. reflns	3754
param./restraints	233/0
θ range	2.044° – 26.084°
GoF on <i>F</i> ²	1.035
<i>R</i> _{int}	0.0300
<i>R</i> ₁ [<i>I</i> > 2 σ (<i>I</i>)]	0.0370
w <i>R</i> ₂ (all data)	0.0963
max / min peaks /e Å ⁻³	0.368, -0.196

Table 17: Crystallographic data collection parameters for $B_2cat_2 \cdot (Me_2Im^{Me})_2$ **25**.

	$B_2cat_2 \cdot (Me_2Im^{Me})_2$ 25 • $2(C_4H_8O)$
Chemical formula	$C_{26}H_{32}B_2N_4O_4 \cdot 2(C_4H_8O)$
Formula mass /g · mol ⁻¹	630.40
Crystal size /mm ³	0.15x0.25x0.50
Crystal system	triclinic
Space group, Z	$P\bar{1}$, 2
<i>a</i> /Å	8.6337(7)
<i>b</i> /Å	9.7684(9)
<i>c</i> /Å	11.0680(12)
α	111.448(9)°
β	95.692(8)°
γ	102.121(7)°
Volume /Å ³	833.40(16)
ρ_{calcd} /g · cm ⁻³	1.256
<i>T</i> /K	150.01(11)
μ /mm ⁻¹ , Radiation	0.085 MoK α
Measured reflns	5745
Indep. reflns	3321
param./restraints	245/12
θ range	3.469° – 27.880°
GoF on F^2	0.88
R_{int}	0.033
R_1 [$I > 2\sigma(I)$]	0.073
wR ₂ (all data)	0.19
max / min peaks /e Å ⁻³	0.57, -0.36
CCDC number	1058480

Table 18: Crystallographic data collection parameters for RER-B₂cat₂•(Me₂Im^{Me})₂ **26**.

	RER-B ₂ cat ₂ •(Me ₂ Im ^{Me}) ₂ 26
Chemical formula	C ₂₆ H ₃₂ B ₂ N ₄ O ₄
Formula mass /g · mol ⁻¹	486.18
Crystal size/mm ³	0.42x0.30x0.29
Crystal system	triclinic
Space group, Z	$P\bar{1}$, 2
<i>a</i> /Å	8.3570(4)
<i>b</i> /Å	11.6526(6)
<i>c</i> /Å	13.3526(7)
α	98.1640(15)°
β	100.5530(15)°
γ	102.2480(15)°
Volume /Å ³	1226.86(11)
ρ_{calcd} /g · cm ⁻³	1.316
<i>T</i> /K	100(2)
μ /mm ⁻¹ , Radiation	0.088 MoK α
Measured reflns	16156
Indep. reflns	4845
param./restraints	333/0
θ range	1.580° – 26.031°
GoF on F^2	1.037
R_{int}	0.0196
R_1 [$I > 2\sigma(I)$]	0.0349
wR ₂ (all data)	0.0891
max / min peaks /e Å ⁻³	0.332, -0.261
CCDC number	1054810

Table 19: Crystallographic data collection parameters for RER-B₂cat₂•(nPr₂Im)₂ **27**.

	RER-B ₂ cat ₂ •(nPr ₂ Im) ₂ 27
Chemical formula	C ₃₀ H ₄₀ B ₂ N ₄ O ₄
Formula mass /g · mol ⁻¹	542.28
Crystal size /mm ³	0.65x0.34x0.30
Crystal system	monoclinic
Space group, Z	<i>P</i> 2 ₁ / <i>n</i> , 4
<i>a</i> /Å	11.1173(8)
<i>b</i> /Å	14.0629(10)
<i>c</i> /Å	19.5476(14)
<i>α</i>	90°
<i>β</i>	106.520(2)°
<i>γ</i>	90°
Volume /Å ³	2929.9(4)
ρ_{calcd} /g · cm ⁻³	1.229
<i>T</i> /K	100(2)
μ /mm ⁻¹ , Radiation	0.081 MoK α
Measured reflns	38639
Indep. reflns	5740
param./restraints	365/0
θ range	1.810° – 25.980°
GoF on <i>F</i> ²	1.103
<i>R</i> _{int}	0.0576
<i>R</i> ₁ [<i>I</i> > 2 σ (<i>I</i>)]	0.0419
w <i>R</i> ₂ (all data)	0.1306
max / min peaks /e Å ⁻³	0.310, -0.294
CCDC number	1054811

Table 20: Crystallographic data collection parameters for RER-B₂neop₂•(nPr₂Im)₂ **29**.

	RER-B ₂ neop ₂ •(nPr ₂ Im) ₂ 29
Chemical formula	C ₂₈ H ₅₂ B ₂ N ₄ O ₄
Formula mass /g · mol ⁻¹	530.36
Crystal size /mm ³	0.38x0.16x0.14
Crystal system	monoclinic
Space group, Z	<i>P</i> 2 ₁ / <i>n</i> , 4
<i>a</i> /Å	11.0462(4)
<i>b</i> /Å	16.8693(6)
<i>c</i> /Å	18.0015(6)
α	90°
β	92.7030(10)°
γ	90°
Volume /Å ³	3350.7(2)
ρ_{calcd} /g · cm ⁻³	1.051
<i>T</i> /K	100(2)
μ /mm ⁻¹ , Radiation	0.069 MoK α
Measured reflns	31788
Indep. reflns	6621
param./restraints	351/0
θ range	1.655° – 26.073°
GoF on <i>F</i> ²	1.064
<i>R</i> _{int}	0.0264
<i>R</i> ₁ [<i>I</i> > 2 σ (<i>I</i>)]	0.0381
w <i>R</i> ₂ (all data)	0.0956
max / min peaks /e Å ⁻³	0.291, -0.190
CCDC number	1054812

Table 21: Crystallographic data collection parameters for the mono-NHC adduct B₂cat₂•Dipp₂Slm **32**.

B ₂ cat ₂ •Dipp ₂ Slm 32 • C ₇ H ₈	
Chemical formula	C ₃₉ H ₄₆ B ₂ N ₂ O ₄ •C ₇ H ₈
Formula mass /g · mol ⁻¹	784.61
Crystal system	triclinic
Space group, Z	$P\bar{1}$, 2
<i>a</i> /Å	12.395(2)
<i>b</i> /Å	14.186(2)
<i>c</i> /Å	23.450(4)
α	90.354(4)°
β	96.904(4)°
γ	98.937(4)°
Volume /Å ³	4042.6(11)
ρ_{calcd} /g · cm ⁻³	1.108
<i>T</i> /K	100(2)
μ /mm ⁻¹ , Radiation	0.069 MoK α
Measured reflns	45957
Indep. reflns	16035
param./restraints	928/0
θ range	1.453° – 26.097°
GoF on F^2	1.014
R_{int}	0.0207
R_1 [$I > 2\sigma(I)$]	0.0414
wR ₂ (all data)	0.1124
max / min peaks /e Å ⁻³	0.398, -0.304

Table 22: Crystallographic data collection parameters for RER-B₂cat₂•Dipp₂Slm **33**.

RER-B ₂ cat ₂ •Dipp ₂ Slm 33 • 2(C ₆ H ₆)	
Chemical formula	C ₃₉ H ₄₆ B ₂ N ₂ O ₄ •2(C ₆ H ₆)
Formula mass /g · mol ⁻¹	784.61
Crystal system	orthorhombic
Space group, Z	<i>P</i> 2 ₁ 2 ₁ 2 ₁ , 4
<i>a</i> /Å	14.1723(9)
<i>b</i> /Å	16.4694(11)
<i>c</i> /Å	18.9434(12)
α	90°
β	90°
γ	90°
Volume /Å ³	4421.6(5)
ρ_{calcd} /g · cm ⁻³	1.179
<i>T</i> /K	296(2)
μ /mm ⁻¹ , Radiation	0.073 MoK α
Measured reflns	49313
Indep. reflns	10243
param./restraints	540/0
θ range	1.638° – 27.608°
GoF on <i>F</i> ²	1.010
<i>R</i> _{int}	0.0516
<i>R</i> ₁ [<i>I</i> > 2 σ (<i>I</i>)]	0.0360
w <i>R</i> ₂ (all data)	0.0888
max / min peaks /e Å ⁻³	0.249, -0.244

Table 23: Crystallographic data collection parameters for B₂cat₃•(iPr₂Im)₂ **35**.

	B ₂ cat ₃ •(iPr ₂ Im) ₂ 35
Chemical formula	C ₄₈ H ₅₆ B ₂ N ₄ O ₆
Formula mass /g · mol ⁻¹	806.58
Crystal size /mm ³	0.48x0.15x0.09
Crystal system	monoclinic
Space group, Z	<i>P</i> 2 ₁ / <i>n</i> , 4
<i>a</i> /Å	13.6001(9)
<i>b</i> /Å	15.4857(10)
<i>c</i> /Å	21.2461(16)
<i>α</i>	90°
<i>β</i>	91.861(2)°
<i>γ</i>	90°
Volume /Å ³	4472.2(5)
ρ_{calcd} /g · cm ⁻³	1.198
<i>T</i> /K	100(2)
μ /mm ⁻¹ , Radiation	0.074 MoK α
Measured reflns	38413
Indep. reflns	8845
param./restraints	549/0
θ range	1.628° – 26.083°
GoF on <i>F</i> ²	1.017
<i>R</i> _{int}	0.0345
<i>R</i> ₁ [<i>I</i> > 2 σ (<i>I</i>)]	0.0612
w <i>R</i> ₂ (all data)	0.1746
max / min peaks /e Å ⁻³	0.387, -0.223

Table 24: Crystallographic data collection parameters for RER-HBcat·(*i*Pr₂Im)₂ **36**.

	RER-HBcat·(<i>i</i> Pr ₂ Im) ₂ 36
Chemical formula	C ₂₄ H ₃₇ BN ₄ O ₂
Formula mass /g · mol ⁻¹	424.38
Crystal size/mm ³	0.15x0.14x0.07
Crystal system	triclinic
Space group, Z	<i>P</i> $\bar{1}$, 2
<i>a</i> /Å	9.4793(8)
<i>b</i> /Å	9.8725(9)
<i>c</i> /Å	13.4421(11)
α	79.620(2)°
β	78.062(2)°
γ	87.549(2)°
Volume /Å ³	1210.60(18)
ρ_{calcd} /g · cm ⁻³	1.164
<i>T</i> /K	100(2)
μ /mm ⁻¹ , Radiation	0.074 MoK α
Measured reflns	14459
Indep. reflns	4819
param./restraints	288/0
θ range	1.573° – 26.127°
GoF on <i>F</i> ²	1.044
<i>R</i> _{int}	0.0252
<i>R</i> ₁ [<i>I</i> > 2 σ (<i>I</i>)]	0.0512
w <i>R</i> ₂ (all data)	0.1354
max / min peaks /e Å ⁻³	0.910, -0.272

Table 25: Crystallographic data collection parameters for HBcat•*n*Pr₂Im **37**.

	HBcat• <i>n</i> Pr ₂ Im 37
Chemical formula	C ₁₅ H ₂₁ BN ₂ O ₂
Formula mass /g · mol ⁻¹	272.15
Crystal size /mm ³	0.13x0.10x0.06
Crystal system	triclinic
Space group, Z	<i>P</i> $\bar{1}$, 4
<i>a</i> /Å	7.7836(8)
<i>b</i> /Å	10.6918(12)
<i>c</i> /Å	18.959(2)
α	73.738(3)°
β	81.952(3)°
γ	80.351(3)°
Volume /Å ³	1486.0(3)
ρ_{calcd} /g · cm ⁻³	1.216
<i>T</i> /K	100(2)
μ /mm ⁻¹ , Radiation	0.080 MoK α
Measured reflns	15858
Indep. reflns	5872
param./restraints	377/0
θ range	2.002° – 26.055°
GoF on <i>F</i> ²	1.017
<i>R</i> _{int}	0.0332
<i>R</i> ₁ [<i>I</i> > 2 σ (<i>I</i>)]	0.0441
w <i>R</i> ₂ (all data)	0.1116
max / min peaks /e Å ⁻³	0.284, -0.204

Table 26: Crystallographic data collection parameters for HBcat•Pr₂Im **38**.

	HBcat•Pr ₂ Im 38
Chemical formula	C ₁₅ H ₂₁ BN ₂ O ₂
Formula mass /g · mol ⁻¹	272.15
Crystal size /mm ³	0.18x0.12x0.07
Crystal system	monoclinic
Space group, Z	<i>P</i> 2 ₁ / <i>n</i> , 4
<i>a</i> /Å	7.2810(8)
<i>b</i> /Å	31.467(4)
<i>c</i> /Å	8.3453(9)
<i>α</i>	90°
<i>β</i>	113.110(4)°
<i>γ</i>	90°
Volume /Å ³	1758.6(3)
ρ_{calcd} /g · cm ⁻³	1.028
<i>T</i> /K	100(2)
μ /mm ⁻¹ , Radiation	0.067 MoK α
Measured reflns	22611
Indep. reflns	3460
param./restraints	187/0
θ range	2.589° – 26.041°
GoF on <i>F</i> ²	1.052
<i>R</i> _{int}	0.0605
<i>R</i> ₁ [<i>I</i> > 2 σ (<i>I</i>)]	0.0500
w <i>R</i> ₂ (all data)	0.1283
max / min peaks /e Å ⁻³	0.211, -0.189

Table 27: Crystallographic data collection parameters for HBcat•iPr₂Im^{Me} **39**.

	HBcat•iPr ₂ Im ^{Me} 39
Chemical formula	C ₁₇ H ₂₅ BN ₂ O ₂
Formula mass /g · mol ⁻¹	300.20
Crystal size/mm ³	0.61x0.52x0.37
Crystal system	monoclinic
Space group, Z	<i>P</i> 2 ₁ / <i>c</i> , 4
<i>a</i> /Å	10.2485(5)
<i>b</i> /Å	12.9496(7)
<i>c</i> /Å	13.5363(7)
<i>α</i>	90°
<i>β</i>	109.8810(10)°
<i>γ</i>	90°
Volume /Å ³	1689.39(15)
ρ_{calcd} /g · cm ⁻³	1.180
<i>T</i> /K	100(2)
μ /mm ⁻¹ , Radiation	0.076 MoK α
Measured reflns	17198
Indep. reflns	3586
param./restraints	230/0
θ range	2.113° – 26.768°
GoF on <i>F</i> ²	1.018
<i>R</i> _{int}	0.0305
<i>R</i> ₁ [<i>I</i> > 2 σ (<i>I</i>)]	0.0403
w <i>R</i> ₂ (all data)	0.1076
max / min peaks /e Å ⁻³	0.254, -0.265

Table 28: Crystallographic data collection parameters for CAAC^{Me}(H)Bcat **40**.

CAAC ^{Me} (H)Bcat 40	
Chemical formula	C ₂₆ H ₃₆ BNO ₂
Formula mass /g · mol ⁻¹	405.37
Crystal size/mm ³	0.29x0.16x0.07
Crystal system	monoclinic
Space group, Z	<i>P</i> 2 ₁ / <i>n</i> , 4
<i>a</i> /Å	10.9700(17)
<i>b</i> /Å	13.1181(19)
<i>c</i> /Å	15.538(2)
<i>α</i>	90°
<i>β</i>	91.623(5)°
<i>γ</i>	90°
Volume /Å ³	2235.1(6)
<i>ρ</i> _{calcd} /g · cm ⁻³	1.205
<i>T</i> /K	100(2)
<i>μ</i> /mm ⁻¹ , Radiation	0.074 MoK _α
Measured reflns	19699
Indep. reflns	4489
param./restraints	279/0
<i>θ</i> range	2.032° – 26.300°
GoF on <i>F</i> ²	1.077
<i>R</i> _{int}	0.0747
<i>R</i> ₁ [<i>I</i> > 2σ(<i>I</i>)]	0.0522
w <i>R</i> ₂ (all data)	0.1484
max / min peaks /e Å ⁻³	0.351, -0.290

Table 29: Crystallographic data collection parameters for RER-Dipp₂Slm(H₂)B-cat-Bcat•Dipp₂Slm **41**.

RER-Dipp ₂ Slm(H ₂)B-cat-Bcat•Dipp ₂ Slm 41 • C ₆ H ₁₄	
Chemical formula	C ₆₆ H ₈₆ B ₂ N ₄ O ₄ •C ₆ H ₁₄
Formula mass /g · mol ⁻¹	1107.17
Crystal size /mm ³	0.41x0.21x0.11
Crystal system	monoclinic
Space group, Z	<i>P</i> 2 ₁ / <i>c</i> , 4
<i>a</i> /Å	14.4886(10)
<i>b</i> /Å	33.966(2)
<i>c</i> /Å	15.4292(10)
<i>α</i>	90°
<i>β</i>	98.096(2)°
<i>γ</i>	90°
Volume /Å ³	7517.4(9)
ρ_{calcd} /g · cm ⁻³	0.978
<i>T</i> /K	100(2)
μ /mm ⁻¹ , Radiation	0.059 MoK α
Measured reflns	81590
Indep. reflns	14815
param./restraints	757/0
θ range	1.541° – 26.051°
GoF on <i>F</i> ²	1.086
<i>R</i> _{int}	0.0458
<i>R</i> ₁ [<i>I</i> > 2 σ (<i>I</i>)]	0.0821
w <i>R</i> ₂ (all data)	0.2227
max / min peaks /e Å ⁻³	0.512, -0.440

Table 30: Crystallographic data collection parameters for Et₃B•Me₂Im **51**.

Et ₃ B•Me ₂ Im 51	
Chemical formula	C ₁₁ H ₂₃ BN ₂
Formula mass /g · mol ⁻¹	194.12
Crystal size /mm ³	0.48x0.38x0.21
Crystal system	monoclinic
Space group, Z	<i>P</i> 2 ₁ / <i>n</i> , 4
<i>a</i> /Å	7.9478(8)
<i>b</i> /Å	11.1662(10)
<i>c</i> /Å	14.4393(14)
<i>α</i>	90°
<i>β</i>	105.024(2)°
<i>γ</i>	90°
Volume /Å ³	1237.6(2)
ρ_{calcd} /g · cm ⁻³	1.042
<i>T</i> /K	100(2)
μ /mm ⁻¹ , Radiation	0.060 MoK α
Measured reflns	8809
Indep. reflns	2442
param./restraints	132/0
θ range	2.337° – 26.053°
GoF on <i>F</i> ²	1.046
<i>R</i> _{int}	0.0502
<i>R</i> ₁ [<i>I</i> > 2 σ (<i>I</i>)]	0.0516
w <i>R</i> ₂ (all data)	0.1498
max / min peaks /e Å ⁻³	0.330, -0.329

Table 31: Crystallographic data collection parameters for Et₃B•iPr₂Im **52**.

	Et ₃ B•iPr ₂ Im 52
Chemical formula	C ₁₅ H ₃₁ BN ₂
Formula mass /g · mol ⁻¹	250.23
Crystal size /mm ³	0.49x0.45x0.23
Crystal system	monoclinic
Space group, Z	<i>P</i> 2 ₁ / <i>c</i> , 4
<i>a</i> /Å	9.7161(7)
<i>b</i> /Å	10.5855(8)
<i>c</i> /Å	15.9916(11)
<i>α</i>	90°
<i>β</i>	95.032(2)°
<i>γ</i>	90°
Volume /Å ³	1638.4(2)
ρ_{calcd} /g · cm ⁻³	1.014
<i>T</i> /K	100(2)
μ /mm ⁻¹ , Radiation	0.058 MoK α
Measured reflns	3266
Indep. reflns	3266
param./restraints	170/0
θ range	2.104° – 26.032°
GoF on <i>F</i> ²	1.032
<i>R</i> _{int}	0.0269
<i>R</i> ₁ [<i>I</i> > 2 σ (<i>I</i>)]	0.0358
w <i>R</i> ₂ (all data)	0.0954
max / min peaks /e Å ⁻³	0.225, -0.169

Table 32: Crystallographic data collection parameters for Et₃B•iPr₂Im^{Me} **53**.

	Et ₃ B•iPr ₂ Im ^{Me} 53
Chemical formula	C ₁₇ H ₃₅ BN ₂
Formula mass /g · mol ⁻¹	278.28
Crystal size /mm ³	0.52x0.32x0.05
Crystal system	monoclinic
Space group, Z	<i>P</i> 2 ₁ / <i>n</i> , 4
<i>a</i> /Å	11.441(2)
<i>b</i> /Å	9.2240(17)
<i>c</i> /Å	17.891(3)
<i>α</i>	90°
<i>β</i>	106.843(5)°
<i>γ</i>	90°
Volume /Å ³	1807.1(6)
ρ_{calcd} /g · cm ⁻³	1.023
<i>T</i> /K	100(2)
μ /mm ⁻¹ , Radiation	0.058 MoK α
Measured reflns	12142
Indep. reflns	3557
param./restraints	205/0
θ range	1.895° – 26.030°
GoF on <i>F</i> ²	1.026
<i>R</i> _{int}	0.0319
<i>R</i> ₁ [<i>I</i> > 2 σ (<i>I</i>)]	0.0409
w <i>R</i> ₂ (all data)	0.1098
max / min peaks /e Å ⁻³	0.297, -0.174

Table 33: Crystallographic data collection parameters for Et₃B•Dipp₂Slm **55**.

	Et ₃ B•Dipp ₂ Slm 55
Chemical formula	C ₃₃ H ₅₃ BN ₂
Formula mass /g · mol ⁻¹	488.58
Crystal size /mm ³	0.12x0.12x0.03
Crystal system	triclinic
Space group, Z	$P\bar{1}$, 2
<i>a</i> /Å	9.5555(9)
<i>b</i> /Å	12.4380(11)
<i>c</i> /Å	12.6084(12)
α	92.671(3)°
β	91.435(3)°
γ	93.446(3)°
Volume /Å ³	1493.6(2)
ρ_{calcd} /g · cm ⁻³	1.014
<i>T</i> /K	100(2)
μ /mm ⁻¹ , Radiation	0.061 MoK α
Measured reflns	19575
Indep. reflns	5967
param./restraints	336/0
θ range	1.617° – 26.239°
GoF on F^2	1.064
R_{int}	0.0316
R_1 [$I > 2\sigma(I)$]	0.0532
wR ₂ (all data)	0.1458
max / min peaks /e Å ⁻³	0.313, -0.213

5. SUMMARY

The present work aims first at the synthesis and characterization of anionic sp^2 - sp^3 diboron compounds of the type $[B_2(OR)_4F][NMe_4]$ (OR_2 = pinacol, catechol and neopentyl) and an examination of their reactivity with aryl diazonium salts. The second part explores the reactions of different diboron reagents with saturated and unsaturated NHCs to form mono- and bis-NHC adducts of the type $B_2(OR)_4 \cdot NHC$ and $B_2(OR)_4 \cdot (NHC)_2$ and to study their behavior at elevated temperatures.

5.1. Chapter One: Borylation Reactions

The anionic sp^2 - sp^3 diboron adducts $[B_2pin_2F][NMe_4]$ **4** and $[B_2cat_2F][NMe_4]$ **9** were synthesized *via* reaction of B_2pin_2 or B_2cat_2 with NMe_4F . The adduct $[B_2neop_2F][NMe_4]$ **7** was only observed in the *in situ* 1H and ^{11}B NMR spectra; however, a decomposition product was identified as $[neopBF_2][NMe_4]$ **6** (Figure 108).

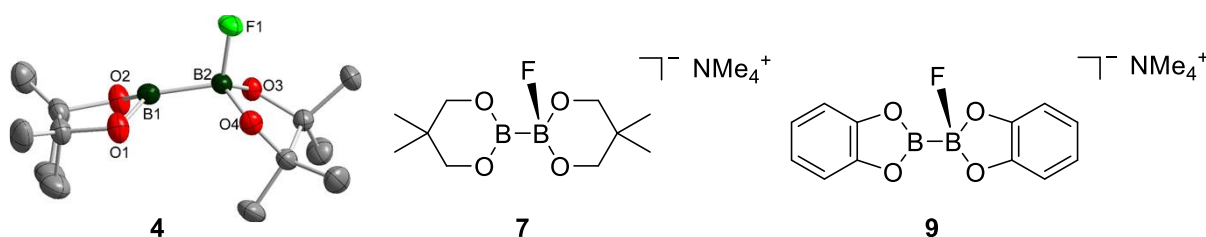
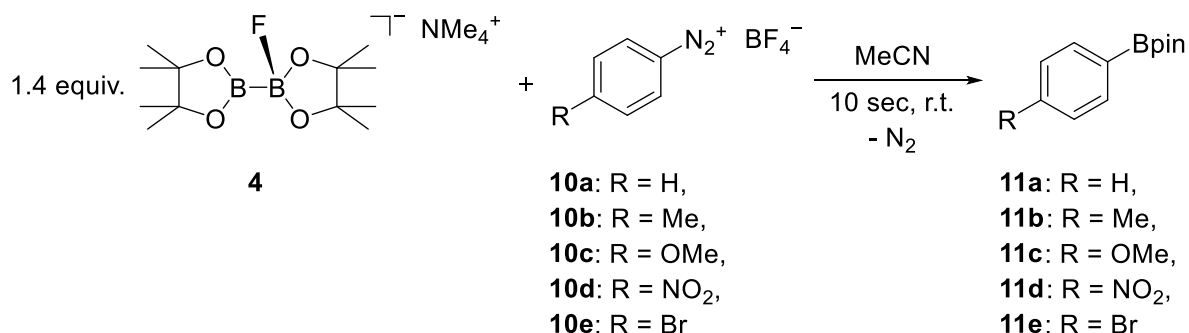


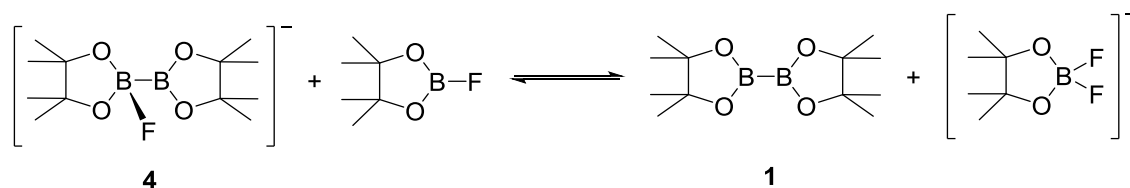
Figure 108: Anionic sp^2 - sp^3 diboron adducts, namely, $[B_2pin_2F][NMe_4]$ **4**, $[B_2neop_2F][NMe_4]$ **7** and $[B_2cat_2F][NMe_4]$ **9**.

The next investigation was the reaction of the isolated $[B_2pin_2F][NMe_4]$ **4** with freshly prepared aryl-diazonium $[BF_4]^-$ salts to transfer a nucleophilic pinB-moiety to the organic electrophiles, hence acting as a formal source of boryl anions. The borylation reactions of adduct **4** with $[R-C_6H_5N_2][BF_4]$ (R = H, Me, OMe, NO_2 and Br) **10a-10e** formed the corresponding aryl-Bpin compounds **11a-11e** in moderate to good yield (Scheme 123).



Scheme 123: Borylation reaction of adduct $[B_2pin_2F][NMe_4]$ **4** with different diazonium $[BF_4]^-$ salts in a 1.4:1 ratio.

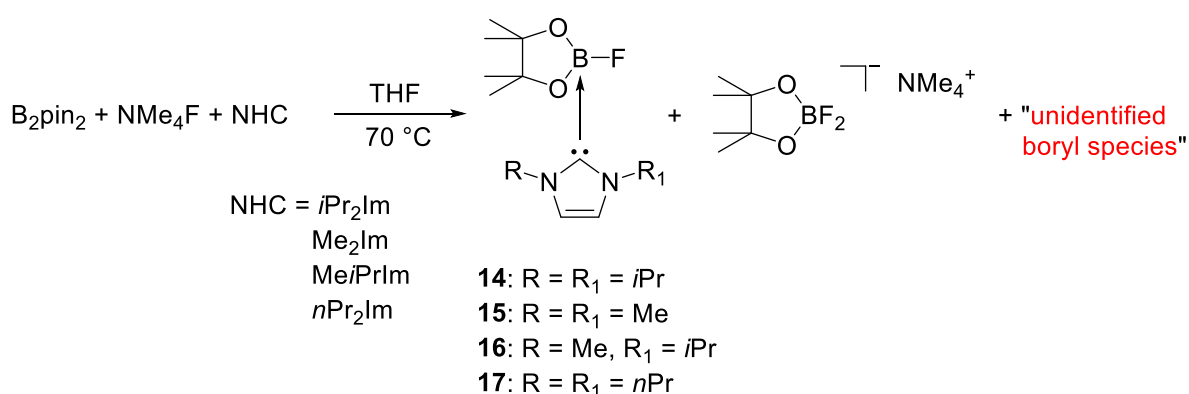
All reactions performed in a 1:1 ratio of adduct **4** : diazonium $[\text{BF}_4]^-$ salt, had in common the fact that the conversion of the starting material is approximately 70% and the expected by-product FBpin was not observed; however, the NMR spectra confirmed the existence of $[\text{pinBF}_2][\text{NMe}_4]$. Furthermore, the ^1H NMR spectrum revealed a signal for B_2pin_2 , but no signal for “unreacted” fluoride adduct **4**, which may be explained by the possible equilibrium of the anionic adduct **4** and the “*in situ* formed” FBpin (Scheme 124). This observation would also explain why the reaction is complete when a ratio of adduct **4** to substrate of 1.4:1 was used.



Scheme 124: Postulated equilibrium observed and involved in the reaction between adduct **4** and “*in situ* formed” FBpin.

The borylation reactions using B_2neop_2 **5** and B_2cat_2 **8** and NMe_4F , of different diazonium $[\text{BF}_4]^-$ salts $[4\text{-R-C}_6\text{H}_4\text{N}_2][\text{BF}_4]$ **10a-e** were done under the same conditions as the borylation reaction with the diboron reagent B_2pin_2 **1**. All reactions were carried out in MeCN-d_3 as the solvent at room temperature. The desired aryl-Bneop **12a-e** and aryl-Bcat **13a-e** esters were characterized by *in situ* ^1H and $^{11}\text{B}\{^1\text{H}\}$ NMR spectroscopy as well as GC-MS analysis.

In addition to the obtained $\text{sp}^2\text{-sp}^3$ diboron adducts, the question of whether it is possible to synthesize and isolate possible anionic $\text{sp}^3\text{-sp}^3$ diboron adducts of the type $[\text{B}_2\text{pin}_2(\text{F})(\text{NHC})][\text{NMe}_4]$ ($\text{NHC} = i\text{Pr}_2\text{Im}$, Me_2Im , $\text{Me}i\text{PrIm}$ and $n\text{Pr}_2\text{Im}$) arises. The reactions of B_2pin_2 **1** and NMe_4F with different NHCs led to the formation of the adducts $\text{FBpin}\cdot i\text{Pr}_2\text{Im}$ **14**, $\text{FBpin}\cdot \text{Me}_2\text{Im}$ **15**, $\text{FBpin}\cdot \text{Me}i\text{PrIm}$ **16** and $\text{FBpin}\cdot n\text{Pr}_2\text{Im}$ **17**; however, in the first three reactions, the decomposition compound $[\text{pinBF}_2][\text{NMe}_4]$ was observed as a by-product (Scheme 125).



Scheme 125: Synthesis of the $\text{FBpin}\cdot i\text{Pr}_2\text{Im}$ **14**, $\text{FBpin}\cdot \text{Me}_2\text{Im}$ **15**, $\text{FBpin}\cdot \text{Me}i\text{PrIm}$ **16** and $\text{FBpin}\cdot n\text{Pr}_2\text{Im}$ **17** via reaction of B_2pin_2 **1** and NMe_4F with different NHCs.

5.2. Chapter Two: Ring Expansion Reactions

Furthermore, the synthesis of neutral mono-NHC diboron adducts were investigated. The stoichiometric reactions of B_2cat_2 **8** with Me_2Im^{Me} or $Dipp_2Im$ led to the formation of the expected adducts, namely, $B_2cat_2 \cdot Me_2Im^{Me}$ **18** and $B_2cat_2 \cdot Dipp_2Im$ **19** which were characterized by NMR spectroscopy and elemental analysis. Additionally, the molecular structure of adduct **18** was confirmed by X-ray diffraction (Figure 109).

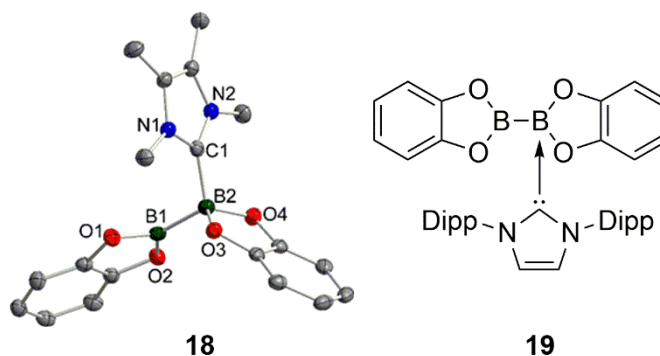


Figure 109: Left: molecular structure of $B_2cat_2 \cdot Me_2Im^{Me}$ **18**; Right: structure of $B_2cat_2 \cdot Dipp_2Im$ **19**.

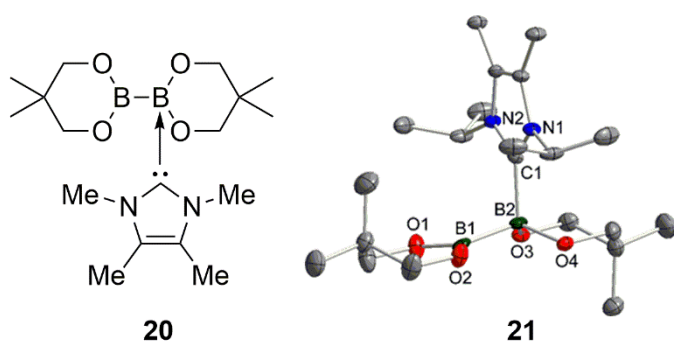


Figure 110: Left: structure of $B_2neop_2 \cdot Me_2Im^{Me}$ **20**; Right: molecular structure of $B_2neop_2 \cdot iPr_2Im^{Me}$ **21**.

Similar results were obtained using B_2neop_2 as the diboron reagent. In the case of the NHC iPr_2Im , the expected mono-NHC $B_2neop_2 \cdot iPr_2Im^{Me}$ **21** was isolated after work-up. The similar adduct $B_2neop_2 \cdot Me_2Im^{Me}$ **20** was only observed by *in situ* NMR spectroscopy at room and below temperature (Figure 110).

In addition to the mono-NHC adducts **20** and **21**, the bis-NHC adducts $B_2neop_2 \cdot (Me_2Im^{Me})_2$ **22**, $B_2neop_2 \cdot (iPr_2Im^{Me})_2$ **23** and $B_2neop_2 \cdot (MeiPrIm)_2$ **24** were characterized by X-ray diffraction (Figure 111).

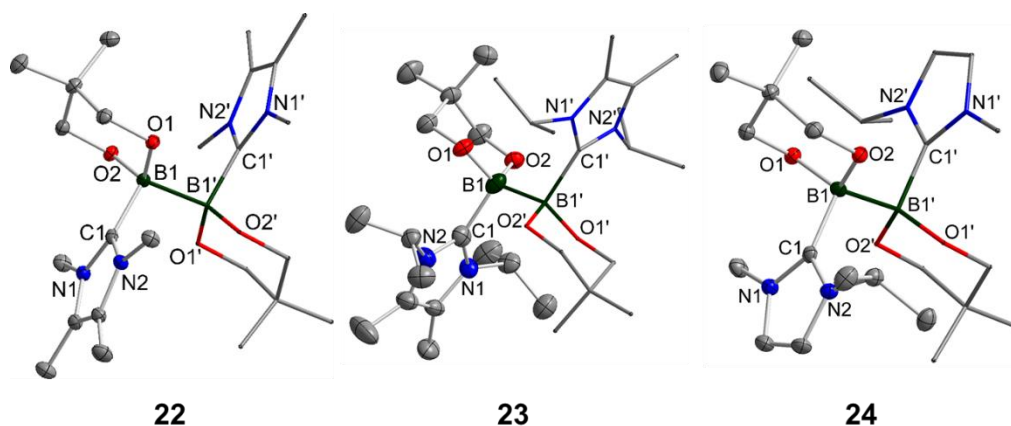


Figure 111: Molecular structure of the bis-NHC diboron adducts $B_2neop_2 \cdot (Me_2Im^{Me})_2$ **22**, $B_2neop_2 \cdot (iPr_2Im^{Me})_2$ **23** and $B_2neop_2 \cdot (MeiPrIm)_2$ **24**.

The reaction of B_2cat_2 **8** with two equivalents of the NHC Me_2Im^{Me} gave the bis-NHC diboron adduct $B_2cat_2 \cdot (Me_2Im^{Me})_2$ **25** (Figure 112). The NMR spectroscopic investigations showed that the behavior of the bis-NHC diboron adduct **25** is different than $B_2cat_2 \cdot Me_2Im^{Me}$ **18**. The mono-NHC adduct **18** is soluble in C_6D_6 and CD_2Cl_2 . The bis-NHC adduct $B_2cat_2 \cdot (Me_2Im^{Me})_2$ **25** is not soluble in C_6D_6 and it decomposes in CD_2Cl_2 to the mono-NHC adduct and NHC decomposition products, which were not further characterized. Another difference between **18** and **25** is their stability at higher temperatures. While $B_2cat_2 \cdot Me_2Im^{Me}$ **18** is thermally stable in solution, the bis-NHC diboron adduct $B_2cat_2 \cdot (Me_2Im^{Me})_2$ **25** rearranges to a ring expanded product of the NHC with insertion of one boron-moiety into the C–N bond to form a six-membered heterocyclic ring, a so called “ring expansion reaction” (RER).

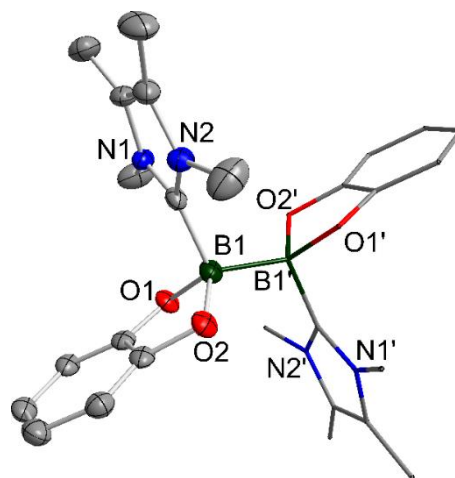


Figure 112: Molecular structure of $B_2cat_2 \cdot (Me_2Im^{Me})_2$ **25**.

Further ring expanded products were obtained *via* reaction of B_2cat_2 **8** with two equivalents of Me_2Im^{Me} or nPr_2Im at elevated temperatures which formed the RER- $B_2cat_2 \cdot (Me_2Im^{Me})_2$ **26** and RER- $B_2cat_2 \cdot (nPr_2Im)_2$ **27**. In addition, the observed ring expanded products showed that the opening of the C–N bond is not dependent on the size of the NHC. To examine the strength of the bonding of the second NHC to the exocyclic Bcat-moiety, the reaction of RER- $B_2cat_2 \cdot (nPr_2Im)_2$ **27** with one equivalent of Me_2Im^{Me} was investigated which formed the NHC-exchanged product RER- $B_2cat_2 \cdot nPr_2Im \cdot Me_2Im^{Me}$ **28** (Figure 113).

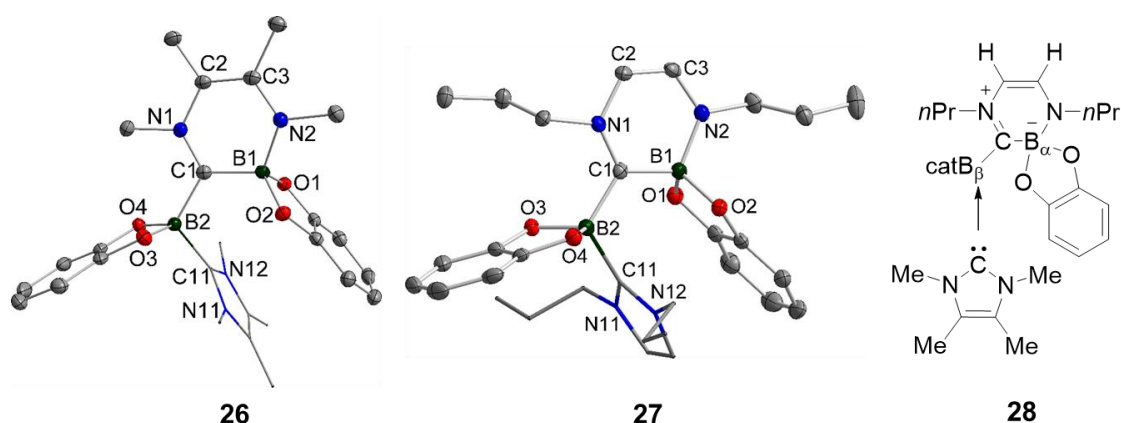


Figure 113: Molecular structure of RER- $B_2cat_2 \cdot (Me_2Im^{Me})_2$ **26** and RER- $B_2cat_2 \cdot (nPr_2Im)_2$ **27** as well as the structure of RER- $B_2cat_2 \cdot nPr_2Im \cdot Me_2Im^{Me}$ **28**.

Additionally, B_2neop_2 **5** and two equivalents of nPr_2Im were reacted under the same conditions which were used for compounds **26** and **27** to determine whether the ring expansion of the

NHC depends on the diboron reagent. In comparison to the reported ring expanded products $\text{RER-B}_2\text{cat}_2 \cdot (\text{Me}_2\text{Im}^{\text{Me}})_2$ **26** and $\text{RER-B}_2\text{cat}_2 \cdot (n\text{Pr}_2\text{Im})_2$ **27**, no solid precipitated immediately at room temperature and ring expanded products $\text{RER-B}_2\text{neop}_2 \cdot (n\text{Pr}_2\text{Im})_2$, $\text{RER-B}_2\text{neop}_2 \cdot \text{Me}_2\text{Im}$ **30** and $\text{RER-B}_2\text{neop}_2 \cdot \text{Me}_2\text{Im}^{\text{Me}}$ **31** were isolated (Figure 114).

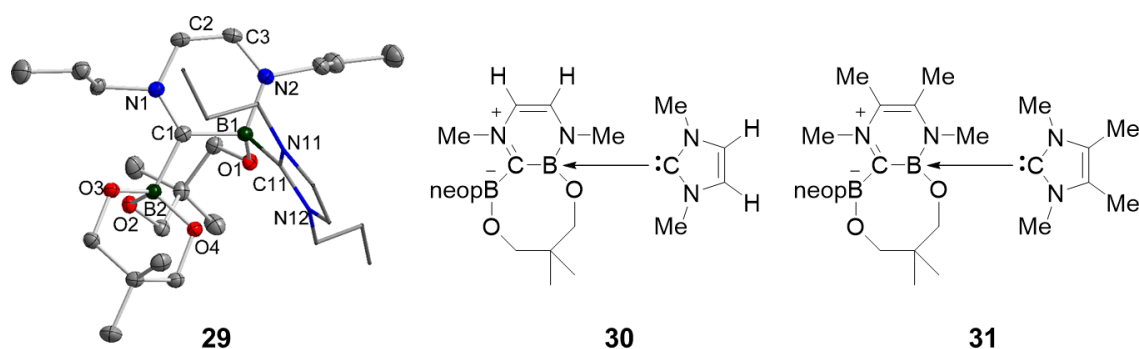


Figure 114: Molecular structure of $\text{RER-B}_2\text{neop}_2 \cdot (n\text{Pr}_2\text{Im})_2$ **29** as well as the structure of $\text{RER-B}_2\text{neop}_2 \cdot \text{Me}_2\text{Im}$ **30** and $\text{RER-B}_2\text{neop}_2 \cdot \text{Me}_2\text{Im}^{\text{Me}}$ **31**.

A further investigation was the reaction of B_2cat_2 **8** with the saturated NHC Dipp_2Slm to determine whether the saturated backbone of the NHC changes the reaction conditions required or the obtained products. At room temperature, the mono-NHC adduct $\text{B}_2\text{cat}_2 \cdot \text{Dipp}_2\text{Slm}$ **32** was isolated and characterized; however, heating the adduct **32** to 100 °C for three days led to an unexpected ring expanded product $\text{RER-B}_2\text{cat}_2 \cdot \text{Dipp}_2\text{Slm}$ **33** (Figure 115).

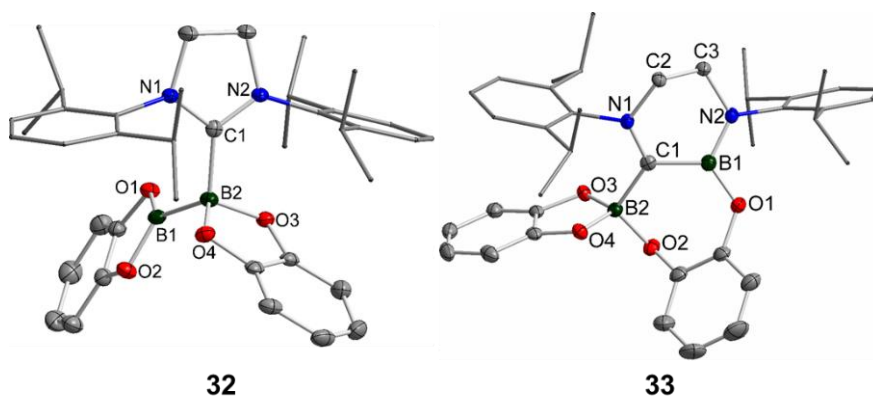


Figure 115: Molecular structures of $\text{B}_2\text{cat}_2 \cdot \text{Dipp}_2\text{Slm}$ **32** and $\text{RER-B}_2\text{cat}_2 \cdot \text{Dipp}_2\text{Slm}$ **33**.

The stoichiometric reaction of *HBcat* with the NHCs *nPr*₂*Im*, *iPr*₂*Im* and *iPr*₂*Im*^{Me} resulted in the formation of the expected mono-NHC adducts *HBcat*·*nPr*₂*Im* **37**, *HBcat*·*iPr*₂*Im* **38** and *HBcat*·*iPr*₂*Im*^{Me} **39** (Figure 116).

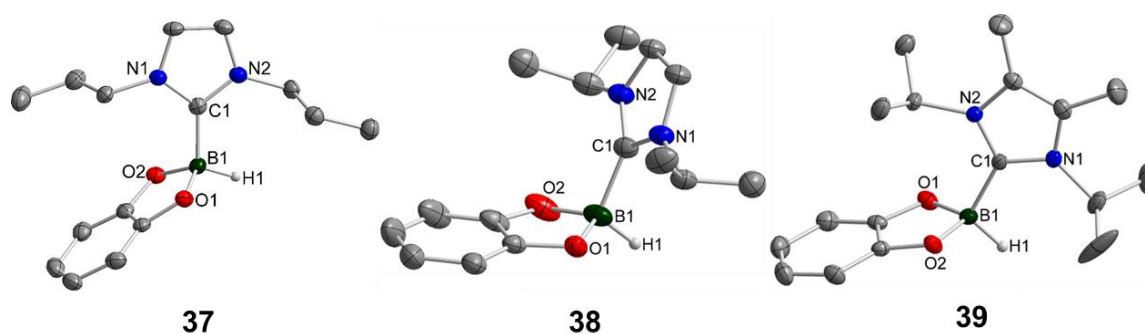


Figure 116: Molecular structures of HBcat·*n*Pr₂Im **37**, HBcat·*i*Pr₂Im **38** and HBcat·*i*Pr₂Im^{Me} **39**.

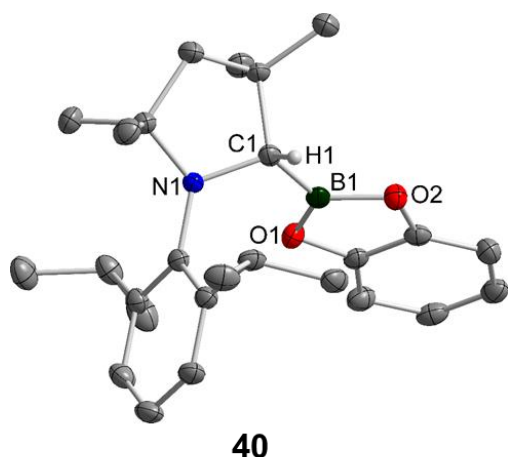


Figure 117: Molecular structure of CAAC^{Me}(H)Bcat **40**.

A similar reaction, using CAAC^{Me} instead of an unsaturated NHC, yielded the B–H activation product CAAC^{Me}(H)Bcat **40** (Figure 117). These results are in good agreement with the DFT calculations reported by Wilson, Dutton *et al.*^[245] and Brown *et al.*^[246] that the energy barrier for ring expansion of the NHC involving insertion of the boron atom into the C–N bond of the NHC is too high, or in the case of the reaction with the CAAC^{Me}, the B–H activation product is thermodynamically favored.

The reaction of the saturated NHC Dipp₂Slm with HBcat led to the formation of the ring expanded product RER-Dipp₂Slm(H₂)B-cat-Bcat·Dipp₂Slm **41** (Figure 118). These observations were verified *via* reaction of unsaturated Dipp₂Im with HBcat at room and elevated temperatures; independent of the reaction conditions, the product was the mono-NHC adduct HBcat·Dipp₂Im **42**.

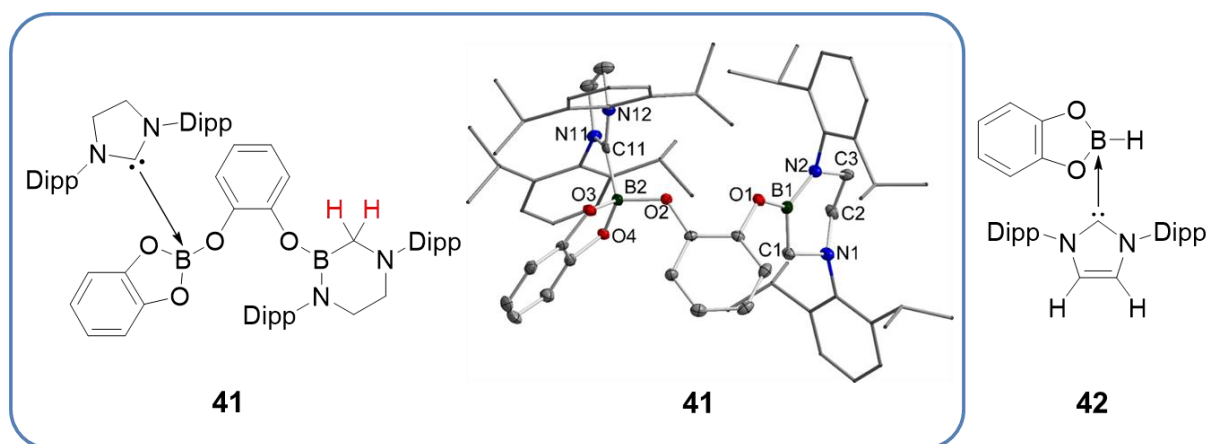


Figure 118: Molecular structure of RER-Dipp₂Slm(H₂)B-cat-Bcat·Dipp₂Slm **41** and the structure of HBcat·Dipp₂Im **42**.

The stoichiometric reactions yielded in the formation of the expected mono NHC adducts of the type $\text{Ph}_3\text{B}\cdot\text{NHC}$, namely, $\text{Ph}_3\text{B}\cdot n\text{Pr}_2\text{Im}$ **45**, $\text{Ph}_3\text{B}\cdot i\text{Pr}_2\text{Im}$ **46**, $\text{Ph}_3\text{B}\cdot\text{Me}_2\text{Im}^{\text{Me}}$ **47**, $\text{Ph}_3\text{B}\cdot i\text{Pr}_2\text{Im}^{\text{Me}}$ **48**, $\text{Ph}_3\text{B}\cdot\text{Me}t\text{Bulm}$ **49**, $\text{Ph}_3\text{B}\cdot\text{Dipp}_2\text{Im}$ **50** and $\text{Et}_3\text{B}\cdot\text{NHC}$, namely, $\text{Et}_3\text{B}\cdot\text{Me}_2\text{Im}$ **51**, $\text{Et}_3\text{B}\cdot i\text{Pr}_2\text{Im}$ **52**, $\text{Et}_3\text{B}\cdot i\text{Pr}_2\text{Im}^{\text{Me}}$ **53**, $\text{Et}_3\text{B}\cdot\text{Dipp}_2\text{Im}$ **54** and $\text{Et}_3\text{B}\cdot\text{Dipp}_2\text{Slm}$ **55**. However, even at higher temperatures, no further rearrangement to any ring expanded products took place. In addition, the reaction of BPh_3 and BEt_3 led to the abnormal binding of the $t\text{Bu}_2\text{Im}$ to the alkylborane to form the two compounds $\text{Ph}_3\text{B}-t\text{Bu}_2\text{Im}-\text{H}$ **56** and $\text{Et}_3\text{B}-t\text{Bu}_2\text{Im}-\text{H}$ **57** (Figure 119).

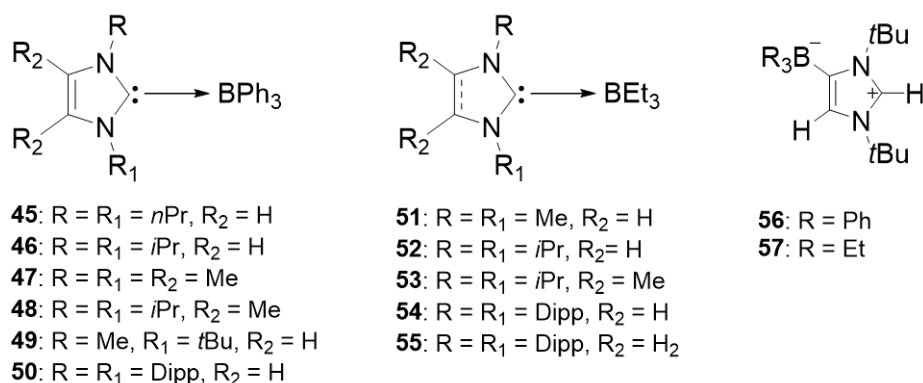


Figure 119: Left: structure of the type $\text{R}_3\text{B}\cdot\text{NHC}$ ($\text{R} = \text{Ph}$), $\text{Ph}_3\text{B}\cdot n\text{Pr}_2\text{Im}$ **45**, $\text{Ph}_3\text{B}\cdot i\text{Pr}_2\text{Im}$ **46**, $\text{Ph}_3\text{B}\cdot\text{Me}_2\text{Im}^{\text{Me}}$ **47**, $\text{Ph}_3\text{B}\cdot i\text{Pr}_2\text{Im}^{\text{Me}}$ **48**, $\text{Ph}_3\text{B}\cdot\text{Me}t\text{Bulm}$ **49**, $\text{Ph}_3\text{B}\cdot\text{Dipp}_2\text{Im}$ **50**. Middle: structure of the type $\text{Et}_3\text{B}\cdot\text{NHC}$, $\text{Et}_3\text{B}\cdot\text{Me}_2\text{Im}$ **51**, $\text{Et}_3\text{B}\cdot i\text{Pr}_2\text{Im}$ **52**, $\text{Et}_3\text{B}\cdot i\text{Pr}_2\text{Im}^{\text{Me}}$ **53**, $\text{Et}_3\text{B}\cdot\text{Dipp}_2\text{Im}$ **54** and $\text{Et}_3\text{B}\cdot\text{Dipp}_2\text{Slm}$ **55**. Right: Structure of $\text{Ph}_3\text{B}-t\text{Bu}_2\text{Im}-\text{H}$ **56** and $\text{Et}_3\text{B}-t\text{Bu}_2\text{Im}-\text{H}$ **57**.

6. ZUSAMMENFASSUNG

Im Rahmen der vorliegenden Arbeit wurde die Synthese und das Reaktionsverhalten Lewis-Säuren/Lewis-Basen-Addukte von Diboran(4)-Verbindungen als Lewis-Säuren untersucht. Als Lewis-Basen dienten zum einem das Fluorid-Ion, zum anderen *N*-Heterozyklische Carbene. Ein Ziel der vorliegenden Arbeit war somit die Synthese und Charakterisierung anionischer sp^2 - sp^3 -Diboran-Verbindungen des Typs $[B_2(OR)_4F][NMe_4]$ (OR_2 = Pinakol, Catechol und Neopentyl), die auf ihre Eigenschaft als „Boryl-Übertragungsreagenz“ gegenüber Diazoniumsalzen überprüft wurden.

Der zweite Teil der Arbeit untersucht die Reaktion von Diboranen (B_2cat_2 und B_2neop_2) mit gesättigten und ungesättigten *N*-Heterozyklischen Carbenen (NHCs). Die neutralen, einfach- und zweifach-substituierten NHC-Addukte des Typs $B_2(OR)_4 \cdot NHC$ und $B_2(OR)_4 \cdot (NHC)_2$ wurden anschließend auf ihre thermische Stabilität untersucht.

6.1. Kapitel Eins: Anionische Addukte

Die anionische sp^2 - sp^3 Diboran Addukte $[B_2pin_2F][NMe_4]$ **4** und $[B_2cat_2F][NMe_4]$ **9** (Abbildung 120) wurden durch die Reaktion von B_2pin_2 bzw. B_2cat_2 mit NMe_4F dargestellt, isoliert und charakterisiert. $[B_2neop_2F][NMe_4]$ **7** konnte ausgehend von B_2neop_2 und NMe_4F lediglich 1H - und ^{11}B - NMR-spektroskopisch nachgewiesen werden. Als Hauptprodukt dieser Reaktion wurde $[neopBF_2][NMe_4]$ **6** identifiziert (Abbildung 120).

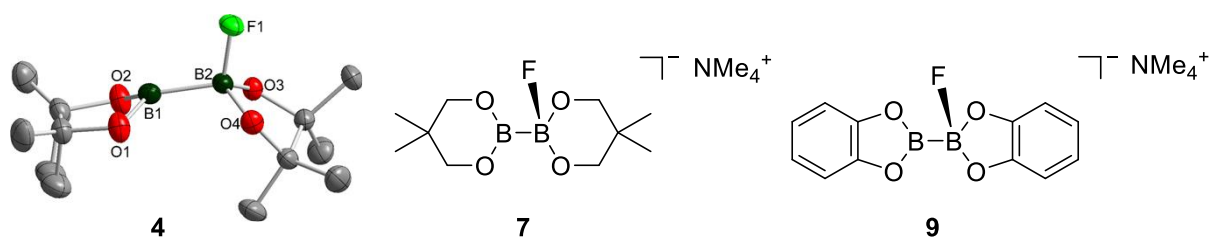
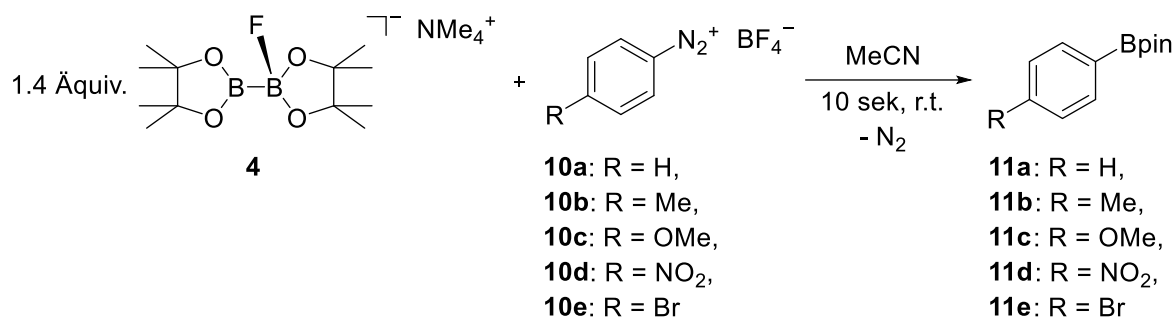
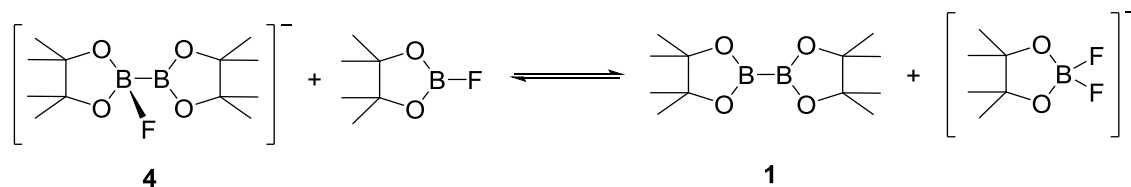


Abbildung 120: Die anionischen sp^2 - sp^3 -Diboran-Addukte, $[B_2pin_2F][NMe_4]$ **4**, $[B_2neop_2F][NMe_4]$ **7** und $[B_2cat_2F][NMe_4]$ **9**.

Die Addukte **4**, **7** und **9** wurden anschließend auf ihre Reaktivität gegenüber Diazoniumsalzen $[R-C_6H_5N_2][BF_4]$ **10a-e** getestet. Hierbei wurde nachgewiesen, dass die „Bpin“-Einheit als Quelle für Boryl-Anionen verwendet werden kann. Durch Borylierung von **10a-e** mit Addukt **4** wurden die entsprechenden Boronsäureester **11a-e** dargestellt (Schema 126).

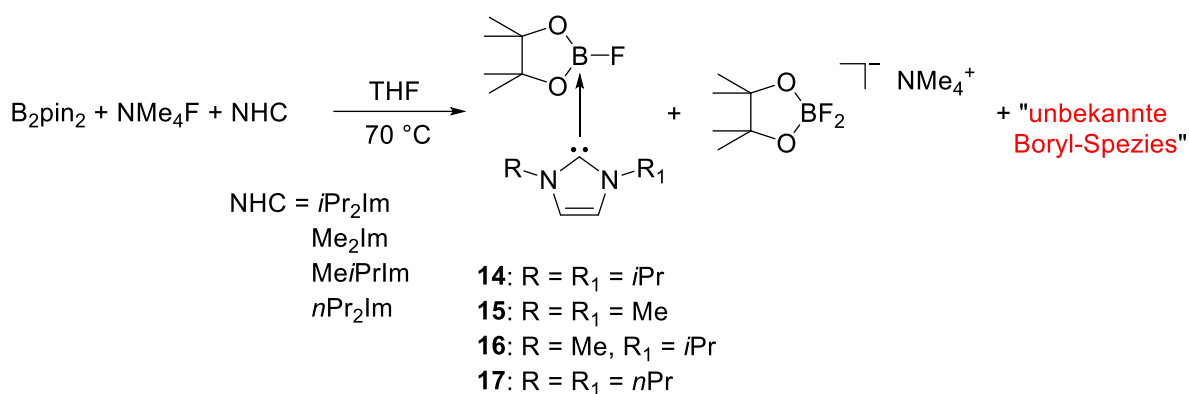
Schema 126: Borylierung unterschiedlicher Diazoniumsalze mit Addukt **4**.

Alle stöchiometrischen Reaktionen im Verhältnis Diazoniumsalz : Addukt **4** von 1:1 zeigten einen Umsatz des Diazoniumsalzes von ungefähr 70%. Das erwartete Nebenprodukt FBpin bzw. überschüssiges $[\text{B}_2\text{pin}_2\text{F}][\text{NMe}_4]$ **4** konnte nicht nachgewiesen werden. Verbindung **4** scheint also zu einem Gleichgewicht mit dem *in situ* gebildeten FBpin zu B_2pin_2 und $[\text{pinBF}_2][\text{NMe}_4]$ zu reagieren, welches NMR-spektroskopisch in allen Reaktionen nachgewiesen wurde (Schema 127). Um eine vollständige Umsetzung der Startmaterialien zu gewährleisten, wurden die Reaktionen des Adduktes **4** mit den Diazoniumsalzen **10a-e** im stöchiometrischen Verhältnis 1.4:1 durchgeführt.

Schema 127: Mögliches Gleichgewicht zwischen dem "in situ gebildeten" FBpin und $[\text{B}_2\text{pin}_2\text{F}][\text{NMe}_4]$ **4**.

Die Borylierung der Diazoniumsalze **10a-e** wurde ebenso mit stöchiometrischen Mengen an B_2neop_2 bzw. B_2cat_2 und wasserfreiem NMe_4F bei Raumtemperatur durchgeführt. Alle Reaktionen wurden NMR-spektroskopisch und durch GC-MS Analyse verfolgt um die erhaltenen Boronsäureester Aryl-Bneop **12a-e** und Aryl-Bcat **13a-e** zu charakterisieren.

Ferner wurde versucht, Addukte des Typs $[\text{B}_2\text{pin}_2(\text{NHC})\text{F}][\text{NMe}_4]$ durch Umsetzung von B_2pin_2 mit NMe_4F und unterschiedlichen NHCs zu synthetisieren. Die Reaktionen mit den NHCs *i*Pr₂Im, Me₂Im, Me*i*PrIm und *n*Pr₂Im lieferten jedoch lediglich die Addukte FBpin•*i*Pr₂Im **14**, FBpin•Me₂Im **15**, FBpin•Me*i*PrIm **16** und FBpin•*n*Pr₂Im **17** in geringen Mengen (Schema 128). Als Hauptprodukt der jeweiligen Umsetzungen wurde das Zersetzungsprodukt $[\text{pinBF}_2][\text{NMe}_4]$ isoliert (ausgenommen FBpin•*n*Pr₂Im **17**). Verbindung **17** konnte zusätzlich strukturell charakterisiert werden.



Schema 128: Reaktion von B₂pin₂ mit NMe₄F und den NHCs *i*Pr₂Im, Me₂Im, Me*i*PrIm und *n*Pr₂Im.

6.2. Kapitel Zwei: Neutrale Addukte

Ferner wurden neutrale, einfach- und zweifach-substituierte NHC-Addukte des Typs B₂(OR)₄•NHC und B₂(OR)₄•(NHC)₂ dargestellt. Aus der stöchiometrischen Reaktion von B₂cat₂ mit Me₂Im^{Me} und Dipp₂Im wurden die entsprechenden Mono-NHC Diboran Addukte B₂cat₂•Me₂Im^{Me} **18** und B₂cat₂•Dipp₂Im **19** isoliert, wobei **18** strukturell belegt werden konnte. (Abbildung 121).

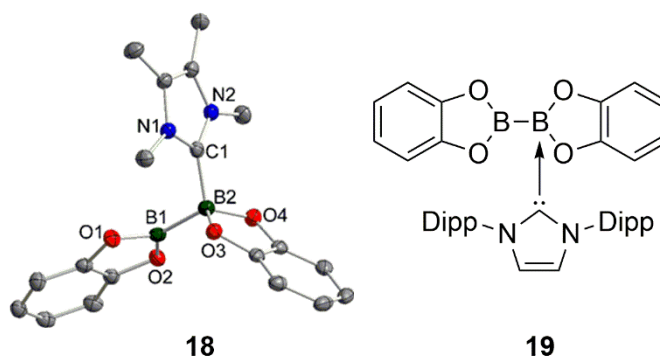


Abbildung 121: Links: Molekülstruktur von B₂cat₂•Me₂Im^{Me} **18**; Rechts: Struktur von B₂cat₂•Dipp₂Im **19**.

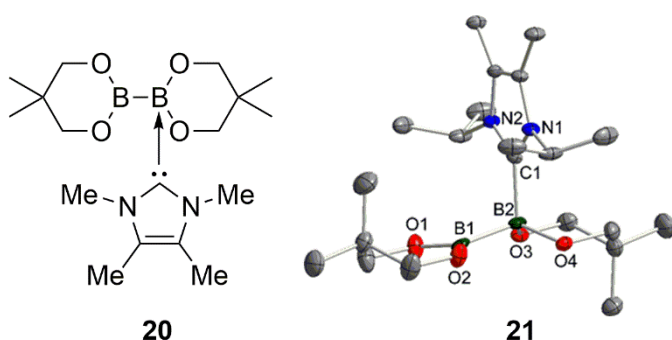


Abbildung 122: Links: Struktur von B₂neop₂•Me₂Im^{Me} **20**; Rechts: Molekülstruktur von B₂neop₂•*i*Pr₂Im^{Me} **21**.

Die Reaktion von B₂neop₂ mit *i*Pr₂Im^{Me} liefert das isolierbare, neutrale Addukt B₂neop₂•*i*Pr₂Im^{Me} **21**, während B₂neop₂•Me₂Im^{Me} **20** nicht isolierbar und nur anhand *in situ* aufgenommener ¹H- und ¹¹B-NMR-Spektren bei Raumtemperatur bzw. tiefen Temperaturen charakterisiert werden konnte (Abbildung 122).

Zusätzlich zu **20** und **21** konnten die zweifach-substituierten NHC-Addukte $B_2neop_2 \cdot (Me_2Im^{Me})_2$ **22**, $B_2neop_2 \cdot (iPr_2Im^{Me})_2$ **23** und $B_2neop_2 \cdot (MeiPrIm)_2$ **24** synthetisiert und kristallographisch charakterisiert werden (Abbildung 123).

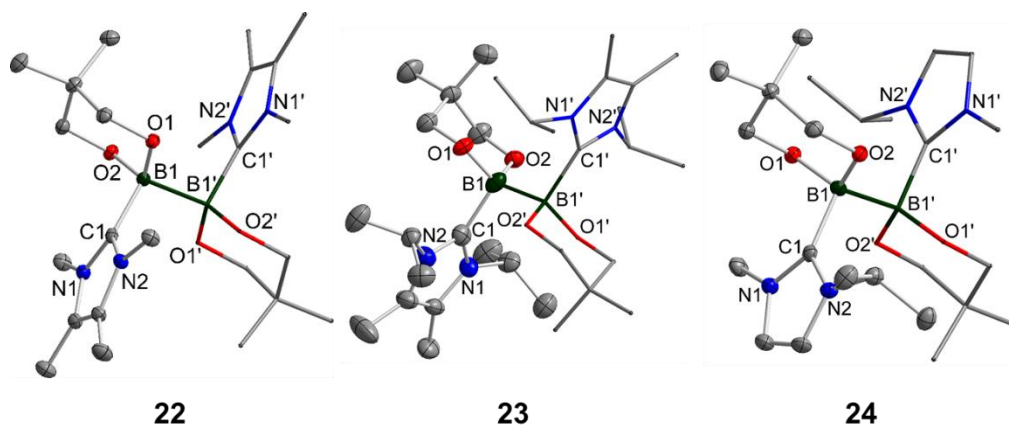


Abbildung 123: Molekülstruktur von $B_2neop_2 \cdot (Me_2Im^{Me})_2$ **22**, $B_2neop_2 \cdot (iPr_2Im^{Me})_2$ **23** und $B_2neop_2 \cdot (MeiPrIm)_2$ **24**.

Die Reaktion von B_2cat_2 mit Me_2Im^{Me} im Verhältnis 1:2 lieferte $B_2cat_2 \cdot (Me_2Im^{Me})_2$ **25** (Abbildung 124). $B_2cat_2 \cdot Me_2Im^{Me}$ **18** und $B_2cat_2 \cdot (Me_2Im^{Me})_2$ **25** zeigen unterschiedliches Verhalten in Lösung: Während $B_2cat_2 \cdot Me_2Im^{Me}$ **18** in Dichlormethan (DCM) stabil und löslich ist, zersetzt sich **25** in DCM. Ein weiterer Unterschied ist das Verhalten von **18** und **25** bei erhöhter Temperatur: Während **18** bei thermischer Belastung stabil ist, lagert sich **25** in einer Ringerweiterungsreaktion (RER) zu einem sechs-gliedrigen Heterozyklus um.

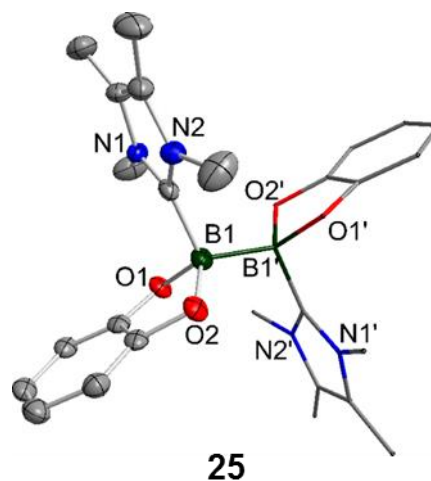


Abbildung 124: Molekülstruktur von $B_2cat_2 \cdot (Me_2Im^{Me})_2$ **25**.

Weitere Ringerweiterungsprodukte wurden durch die Reaktion von B_2cat_2 mit zwei Äquivalenten Me_2Im^{Me} und nPr_2Im bei erhöhten Temperaturen erhalten. RER- $B_2cat_2 \cdot (Me_2Im^{Me})_2$ **26** und RER- $B_2cat_2 \cdot (nPr_2Im)_2$ **27** belegen, dass die RER unabhängig von der Größe des NHCs ist. Aus RER- $B_2cat_2 \cdot (nPr_2Im)_2$ **27** lässt sich durch Umsetzung mit einem Äquivalent Me_2Im^{Me} das an B2 (Abbildung 125) gebundene nPr_2Im durch Me_2Im^{Me} unter Ausbildung von RER- $B_2cat_2 \cdot nPr_2Im \cdot Me_2Im^{Me}$ **28** ersetzen (Abbildung 125).

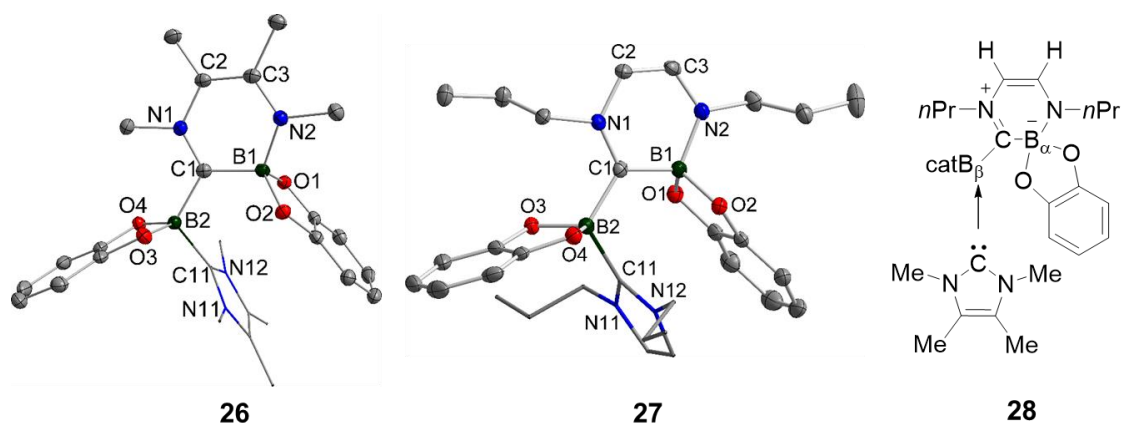


Abbildung 125: Molekülstruktur von RER-B₂cat₂•(Me₂Im^{Me})₂ **26** und RER-B₂cat₂•(nPr₂Im)₂ **27** und die Struktur von RER-B₂cat₂•nPr₂Im•Me₂Im^{Me} **28**.

Entsprechende Reaktionen der NHCs mit B₂neop₂ anstelle von B₂cat₂ belegen, dass die Ringerweiterungsprodukte hin zu RER-B₂neop₂•(nPr₂Im)₂ **29**, RER-B₂neop₂•Me₂Im **30** und RER-B₂neop₂•Me₂Im^{Me} **31** bereits bei Raumtemperatur stattfinden (Abbildung 126). Das Grundgerüst der RER-Produkte **29-31** ist identisch zu demjenigen von RER-B₂cat₂•(Me₂Im^{Me})₂ **26** und RER-B₂cat₂•(nPr₂Im)₂ **27**. Diese Verbindungen unterscheiden sich jedoch in der Koordination des zusätzlichen Carben-Liganden sowie des Dialat-Substituenten.

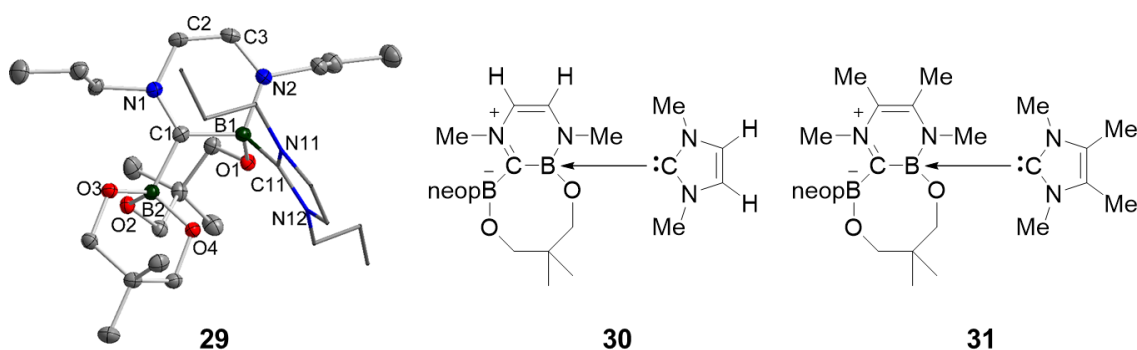


Abbildung 126: Molekülstruktur von RER-B₂neop₂•(nPr₂Im)₂ **29** und die Strukturen von RER-B₂neop₂•Me₂Im **30** und RER-B₂neop₂•Me₂Im^{Me} **31**.

Die Umsetzung von B₂cat₂ mit Dipp₂Slm führt bei Raumtemperatur zur Bildung des Mono-NHC Adduktes B₂cat₂•Dipp₂Slm **32**. Allerdings ist Verbindung **32** im Vergleich zu den beiden Addukten B₂cat₂•Me₂Im^{Me} **18** und B₂cat₂•Dipp₂Im **19** bei höheren Temperaturen nicht stabil und lagert nach drei Tagen bei 100 °C zu RER-B₂cat₂•Dipp₂Slm **33** um (Abbildung 127).

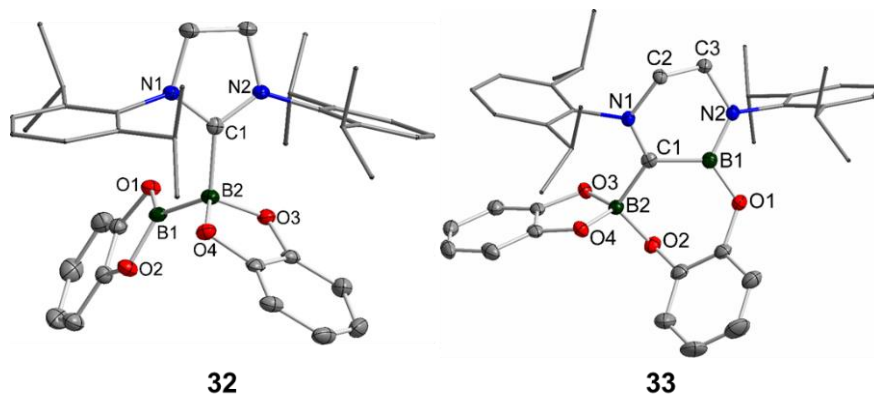


Abbildung 127: Molekülstruktur von $B_2cat_2 \cdot Dipp_2SIIm$ **32** und RER- $B_2cat_2 \cdot Dipp_2SIIm$ **33**.

Die stöchiometrischen Reaktionen von HBcat mit den NHCs nPr_2Im , iPr_2Im und iPr_2Im^{Me} führten zur Bildung der entsprechenden einfach-substituierten-NHC-Addukten $HBcat \cdot nPr_2Im$ **37**, $HBcat \cdot iPr_2Im$ **38** und $HBcat \cdot iPr_2Im^{Me}$ **39** (Abbildung 128).

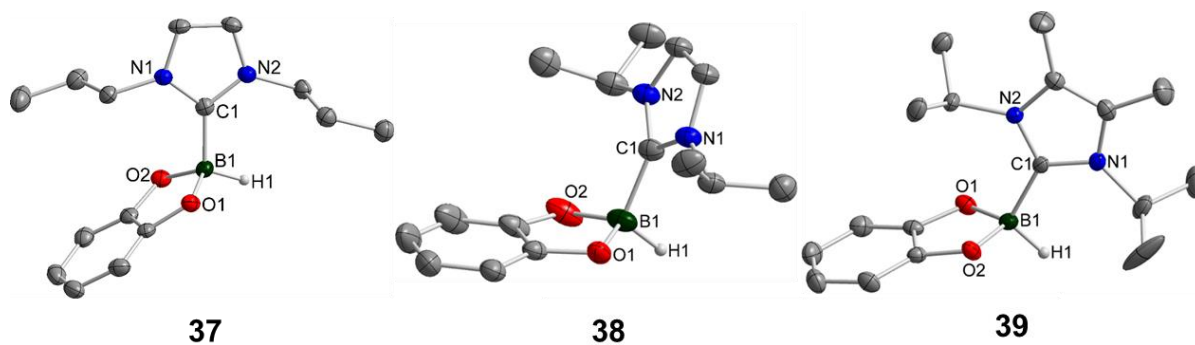


Abbildung 128: Molekülstruktur von $HBcat \cdot nPr_2Im$ **37**, $HBcat \cdot iPr_2Im$ **38** und $HBcat \cdot iPr_2Im^{Me}$ **39**.

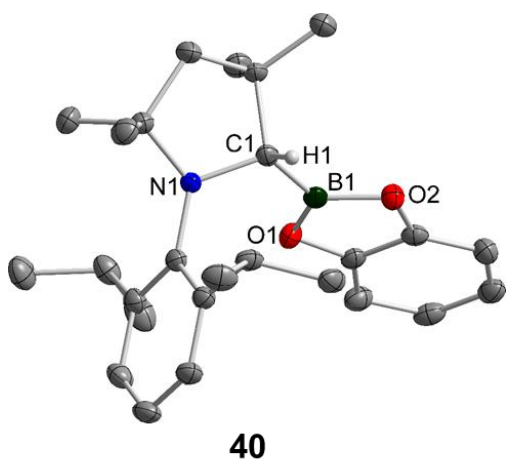


Abbildung 129: Molekülstruktur von $CAAC^{Me}(H)Bcat$ **40**.

Wird anstelle des NHCs das cyclische Alkyl-Amino-Carben $CAAC^{Me}$ eingesetzt, so findet unter B–H Bindungsaktivierung eine oxidative Addition des Catecholborans an das Carben-Kohlenstoffatom statt (Abbildung 129).

Im Gegensatz dazu führt die Reaktion von HBcat mit dem gesättigten NHC Dipp₂Slm bei Raumtemperatur zum RER-Produkt RER-Dipp₂Slm(H₂)B-cat-Bcat•Dipp₂Slm **41**. Wird hingegen anstelle von Dipp₂Slm das analoge NHC mit ungesättigtem Rückgrat eingesetzt, wird das thermisch stabile Mono-NHC-Addukt HBcat•Dipp₂Im **42** isoliert (Abbildung 130). Diese Reaktionsunterschiede sind durch Wilson und Dutton anhand theoretischer Rechnungen vorhergesagt worden und wurden in dieser Arbeit erstmals bestätigt.

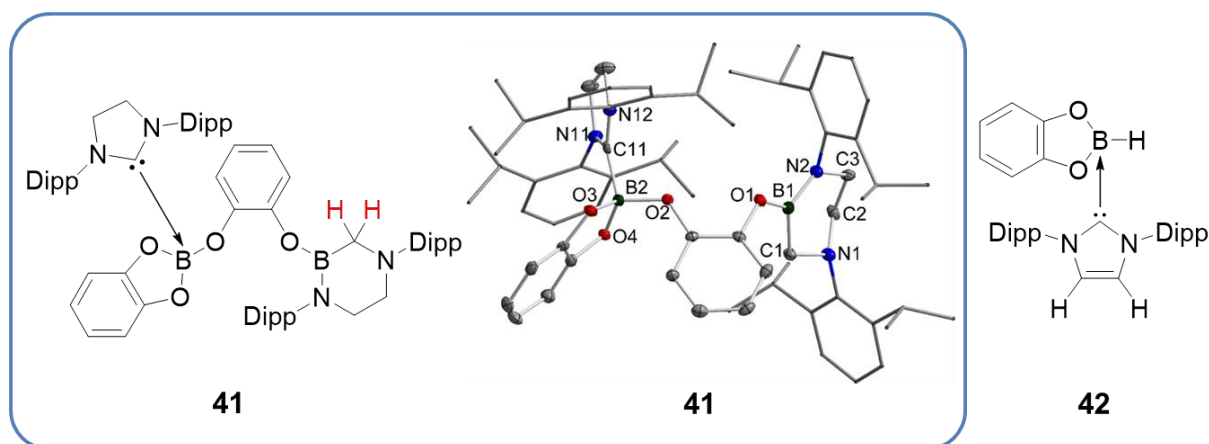


Abbildung 130: Molekülstruktur von RER-Dipp₂Slm(H₂)B-cat-Bcat•Dipp₂Slm **41** und die Struktur von HBcat•Dipp₂Im **42**.

Aus der Reaktion verschiedener NHCs mit den Trialkylboranen BPh₃ und BEt₃ wurden die Produkte Ph₃B•*n*Pr₂Im **45**, Ph₃B•*i*Pr₂Im **46**, Ph₃B•Me₂Im^{Me} **47**, Ph₃B•*i*Pr₂Im^{Me} **48**, Ph₃B•Me*t*Bulm **49** und Ph₃B•Dipp₂Im **50**, sowie Et₃B•Me₂Im **51**, Et₃B•*i*Pr₂Im **52**, Et₃B•*i*Pr₂Im^{Me} **53**, Et₃B•Dipp₂Im **54** und Et₃B•Dipp₂Slm **55** isoliert (Abbildung 131). Diese wurden auf ihre thermische Stabilität hin untersucht. Eine Ringerweiterungsreaktion konnte bei keiner dieser Verbindungen beobachtet werden. Die analogen Reaktionen von BPh₃ und BEt₃ mit dem NHC *t*Bu₂Im lieferten die Verbindungen Ph₃B-*t*Bu₂Im-H **56** und Et₃B-*t*Bu₂Im-H **57**. In diesem Falle bindet das Carben „abnormal“ über das Kohlenstoffatom C4 und nicht über das Carben-Kohlenstoffatom an das Trialkylboran.

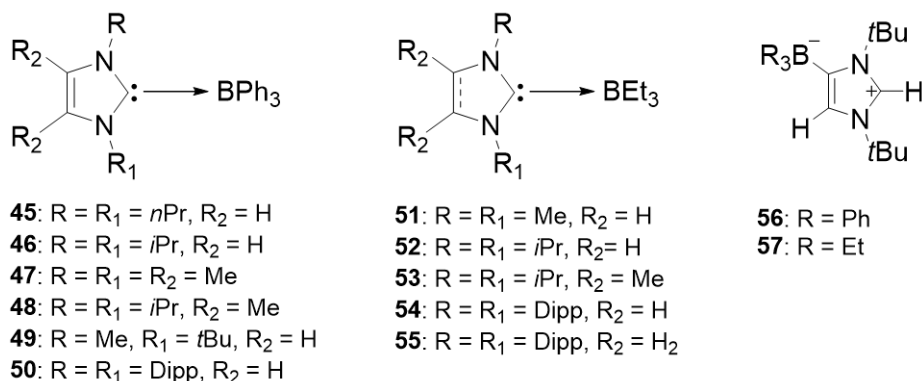


Abbildung 131: NHC-Addukte von BPh₃ und BEt₃.

Die Ergebnisse dieser Arbeit zeigen zum einem, dass anionische Addukte des Typs $[\text{B}_2(\text{OR})_4\text{F}][\text{NMe}_4]$ **4**, **7** und **9** als „Boryl-Übertragungsreagenzien“ eingesetzt werden können. Ferner lassen sich ausgehend von Diboran(4)-Verbindungen durch die Umsetzung mit *N*-Heterozyklischen Carbenen die einfach- und zweifach-substituierten NHC-Addukte $\text{B}_2(\text{OR})_4\cdot\text{NHC}$ und $\text{B}_2(\text{OR})_4\cdot(\text{NHC})_2$ synthetisieren. Diese sind zum Teil instabil gegenüber einer Ringerweiterungsreaktion unter Insertion einer Boryleinheit in die C–N-Bindung des Carbens. Untersuchungen an NHC-Addukten von Boranen BR_3 und $\text{HB}(\text{OR})_2$ zeigen weiterhin, dass die Addukte $\text{Ph}_3\text{B}\cdot\text{NHC}$ gegenüber solchen Ringerweiterungen stabil sind. Die Addukte $\text{HB}(\text{OR})_2\cdot\text{NHC}$ sind je nach eingesetztem Carben und Boran entweder stabil oder reagieren unter B–H-Bindungsaktivierung zur Ringerweiterung des Carbens.

7. APPENDIX

7.1. Abbreviations

Substituents

Ad	adamantyl
Ar	aryl
cat	catecholato
Cy	cyclohexyl
Dipp	2,6-di- <i>iso</i> -propylphenyl
Et	ethyl
<i>i</i> Pr	<i>iso</i> -propyl
<i>n</i> Pr	<i>n</i> -propyl
Me	methyl
MeO	methoxy
Mes	mesityl
neop	neopentylglycolato
Ph	phenyl
pin	pinacolato
<i>t</i> Bu	<i>tert</i> -butyl
<i>t</i> BuO	<i>tert</i> -butoxy

Solvents

C ₆ D ₆	deuterated benzene
DCM	dichloromethane
DMF	dimethylformamide
Et ₂ O	diethylether
MeCN	acetonitrile
MeOH	methanol
THF	tetrahydrofurane

Diboron compounds:

B ₂ pin ₂	bis(pinacolato)diboron
B ₂ cat ₂	bis(catecholato)diboron
⁵ B ₂ neop ₂	bis(neopentylglycolato)diboron
B ₂ eg ₂	bis(ethylenglycolato)diboron
B ₂ (NMe ₂) ₄	tetra(dimethylamino)diboron
B ₂ (OMe) ₄	(tetramethoxy)diboron

N-heterocyclic carbenes

Notice: The corresponding imidazolium- and imidazolidinium-chlorides are depicted as the HCl-adducts of the “free” NHC (e.g. Me₂Im•HCl).

Me ₂ Im	1,3-Dimethylimidazolin-2-ylidene
<i>n</i> Pr ₂ Im	1,3-Di- <i>n</i> -propylimidazolin-2-ylidene
<i>i</i> Pr ₂ Im	1,3-Di- <i>iso</i> -propylimidazolin-2-ylidene
<i>t</i> Bu ₂ Im	1,3-Di- <i>tert</i> -butylimidazolin-2-ylidene
Cy ₂ Im	1,3-Dicyclohexylimidazolin-2-ylidene
Mes ₂ Im	1,3-Dimesitylimidazolin-2-ylidene
Me ₂ Im ^{Me}	1,3,4,5-Tetramethylimidazolin-2-ylidene
<i>i</i> Pr ₂ Im ^{Me}	1,3-Di- <i>iso</i> -propyl-4,5-dimethylimidazolin-2-ylidene
Dipp ₂ Im	1,3-(2,6-Di- <i>iso</i> -propylphenyl)imidazolin-2-ylidene
Dipp ₂ SIm	1,3-(2,6-Di- <i>iso</i> -propylphenyl)imidazolidine-2-ylidene
Ad ₂ Im	1,3-Diadamanthylimidazol-2-ylidene

Analytically abbreviations

COSY	correlation spectroscopy
CSD	Cambridge Structural Database
d	doublet (in NMR spectroscopy); days
DFT	density functional theory
equiv.	equivalent
GC	gas chromatography
h	hour
HMBC	heteronuclear multiple bond correlation
HSQC	heteronuclear single quantum coherence
m	multiplet (in NMR spectroscopy)
min	minute
NMR	nuclear magnetic resonance
q	quartet in NMR spectroscopy
r.t.	room temperature
s	singlet (in NMR spectroscopy)
sec	second
sept	septet (in NMR spectroscopy)
t	triplet (in NMR spectroscopy)

7.2. Symbols and non-SI units

Å	Ångström, $1 \text{ Å} = 10^{-10} \text{ m}$
J	J -coupling constant in NMR spectroscopy, Hz
M^+	molecular ion peak in MS
M	molar concentration, $1 \text{ M} = 1 \text{ mol dm}^{-3}$
mol%	percentage by amount
m/z	mass to charge ratio in MS
ppm	parts per million
Z	atomic number
wt%	per cent by weight
δ	chemical shift in NMR spectroscopy, ppm
ν	frequency, s^{-1}

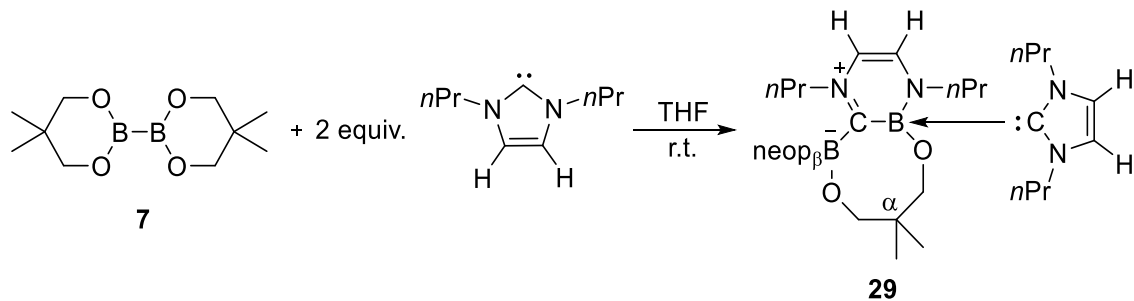
7.3. List of compounds

Compound 1:	B ₂ pin ₂
Compound 2a:	[B ₂ pin ₂ (OtBu)]K
Compound 2b:	{[B ₂ pin ₂ (OtBu)] ₂ K}{[(18-C-6)(thf) ₂]K}
Compound 2c:	[B ₂ pin ₂ (OtBu)]K(18-C-6)
Compound 2d:	[B ₂ pin ₂ (OMe)]K
Compound 2e:	[B ₂ pin ₂ (O(4-tBuC ₆ H ₄))]K
Compound 3:	[B ₂ pin ₂ F][NnBu ₄]
Compound 4:	[B ₂ pin ₂ F][NMe ₄]
Compound 5:	B ₂ neop ₂
Compound 6:	[neopBF ₂][NMe ₄]
Compound 7:	[B ₂ neop ₂ F][NMe ₄]
Compound 8:	B ₂ cat ₂
Compound 9:	[B ₂ cat ₂ F][NMe ₄]
Compound 10a:	[C ₆ H ₅ N ₂][BF ₄]
Compound 10b:	[4-H ₃ C-C ₆ H ₄ N ₂][BF ₄]
Compound 10c:	[4-MeO-C ₆ H ₄ N ₂][BF ₄]
Compound 10d:	[4-O ₂ N-C ₆ H ₄ N ₂][BF ₄]
Compound 10e:	[4-Br-C ₆ H ₄ N ₂][BF ₄]
Compound 10f:	[4-MeO-C ₆ H ₄ N ₂][BPh ₄]
Compound 11a:	C ₆ H ₅ -Bpin
Compound 11b:	4-H ₃ C-C ₆ H ₄ -Bpin
Compound 11c:	4-MeO-C ₆ H ₄ -Bpin
Compound 11d:	4-O ₂ N-C ₆ H ₄ -Bpin
Compound 11e:	4-Br-C ₆ H ₄ -Bpin
Compound 12a:	C ₆ H ₅ -Bneop
Compound 12b:	4-H ₃ C-C ₆ H ₄ -Bneop
Compound 12c:	4-MeO-C ₆ H ₄ -Bneop
Compound 12d:	4-O ₂ N-C ₆ H ₄ -Bneop
Compound 12e:	4-Br-C ₆ H ₄ -Bneop
Compound 13a:	C ₆ H ₅ -Bcat
Compound 13b:	4-H ₃ C-C ₆ H ₄ -Bcat
Compound 13c:	4-MeO-C ₆ H ₄ -Bcat
Compound 13d:	4-O ₂ N-C ₆ H ₄ -Bcat
Compound 13e:	4-Br-C ₆ H ₄ -Bcat
Compound 14:	FBpin•iPr ₂ Im
Compound 15:	FBpin•Me ₂ Im

Compound 16:	FBpin•Me <i>i</i> PrIm
Compound 17:	FBpin• <i>n</i> Pr ₂ Im
Compound 18:	B ₂ cat ₂ •Me ₂ Im ^{Me}
Compound 19:	B ₂ cat ₂ •Dipp ₂ Im
Compound 20:	B ₂ neop ₂ •Me ₂ Im ^{Me}
Compound 21:	B ₂ neop ₂ • <i>i</i> Pr ₂ Im ^{Me}
Compound 22:	B ₂ neop ₂ •(Me ₂ Im ^{Me}) ₂
Compound 23:	B ₂ neop ₂ •(<i>i</i> Pr ₂ Im ^{Me}) ₂
Compound 24:	B ₂ neop ₂ •(<i>i</i> PrMelm) ₂
Compound 25:	B ₂ cat ₂ •(Me ₂ Im ^{Me}) ₂
Compound 26:	RER-B ₂ cat ₂ •(Me ₂ Im ^{Me}) ₂
Compound 27:	RER-B ₂ cat ₂ •(<i>n</i> Pr ₂ Im) ₂
Compound 28:	RER-B ₂ cat ₂ • <i>n</i> Pr ₂ Im•Me ₂ Im ^{Me}
Compound 29:	RER-B ₂ neop ₂ •(<i>n</i> Pr ₂ Im) ₂
Compound 30:	RER-B ₂ neop ₂ •(Me ₂ Im) ₂
Compound 31:	RER-B ₂ neop ₂ •(Me ₂ Im ^{Me}) ₂
Compound 32:	B ₂ cat ₂ •Dipp ₂ SIIm
Compound 33:	RER-B ₂ cat ₂ •Dipp ₂ SIIm
Compound 34:	RER-B ₂ cat ₂ •(<i>i</i> Pr ₂ Im) ₂
Compound 35:	B ₂ cat ₃ •(<i>i</i> Pr ₂ Im) ₂
Compound 36:	RER-HBcat•(<i>i</i> Pr ₂ Im) ₂
Compound 37:	HBcat• <i>n</i> Pr ₂ Im
Compound 38:	HBcat• <i>i</i> Pr ₂ Im
Compound 39:	HBcat• <i>i</i> Pr ₂ Im ^{Me}
Compound 40:	CAAC ^{Me} (H)Bcat
Compound 41:	RER-Dipp ₂ SIIm(H ₂)B-cat-Bcat•Dipp ₂ SIIm
Compound 42:	HBcat•Dipp ₂ SIIm
Compound 43:	HBpin• <i>n</i> Pr ₂ Im
Compound 44:	HBpin• <i>i</i> Pr ₂ Im
Compound 45:	Ph ₃ B• <i>n</i> Pr ₂ Im
Compound 46:	Ph ₃ B• <i>i</i> Pr ₂ Im
Compound 47:	Ph ₃ B•Me ₂ Im ^{Me}
Compound 48:	Ph ₃ B• <i>i</i> Pr ₂ Im ^{Me}
Compound 49:	Ph ₃ B•Me <i>t</i> Bulm
Compound 50:	Ph ₃ B•Dipp ₂ Im
Compound 51:	Et ₃ B•Me ₂ Im
Compound 52:	Et ₃ B• <i>i</i> Pr ₂ Im

Compound 53 :	$\text{Et}_3\text{B}\cdot\text{iPr}_2\text{Im}^{\text{Me}}$
Compound 54 :	$\text{Et}_3\text{B}\cdot\text{Dipp}_2\text{Im}$
Compound 55 :	$\text{Et}_3\text{B}\cdot\text{Dipp}_2\text{SIm}$
Compound 56 :	$\text{Ph}_3\text{B}\cdot\text{tBu}_2\text{Im-H}$
Compound 57 :	$\text{Et}_3\text{B}\cdot\text{tBu}_2\text{Im-H}$

7.4. Additional NMR spectra

7.4.1. Compound 29: RER-B₂neop₂•(nPr₂Im)₂•toluene

Scheme 129: Reaction of B₂neop₂ with two equivalents of nPr₂Im, which led to the formation of the ring expanded product RER-B₂neop₂•(nPr₂Im)₂•toluene **29**.

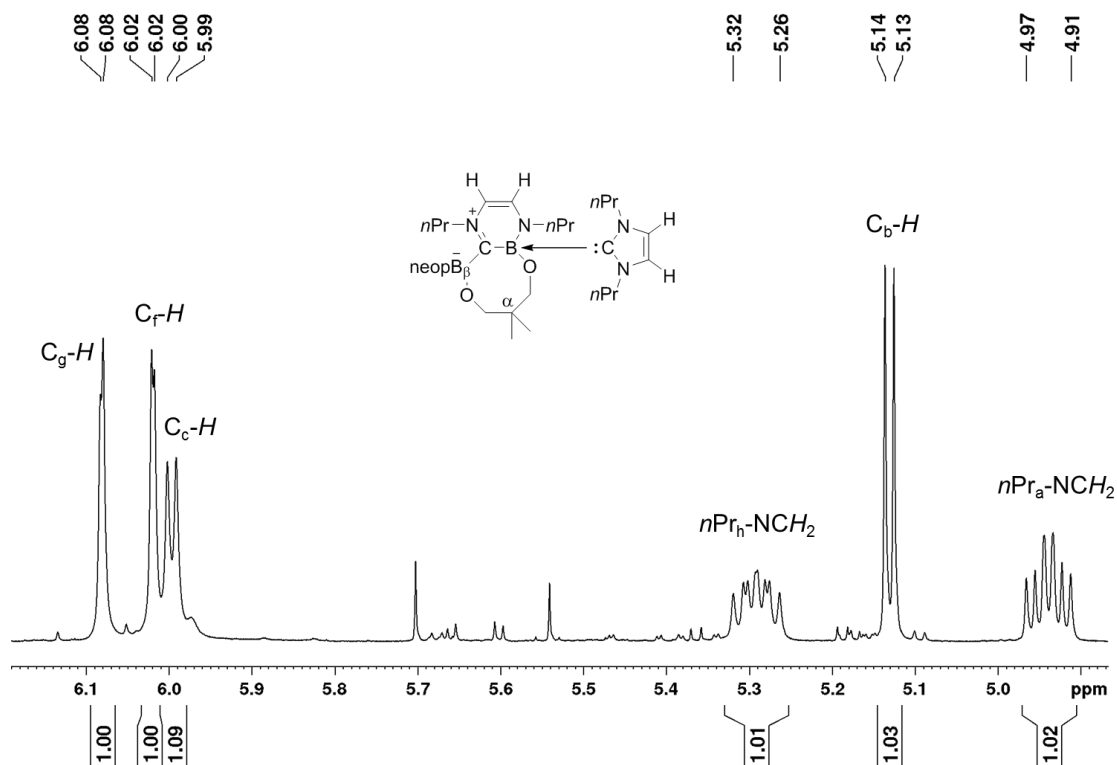
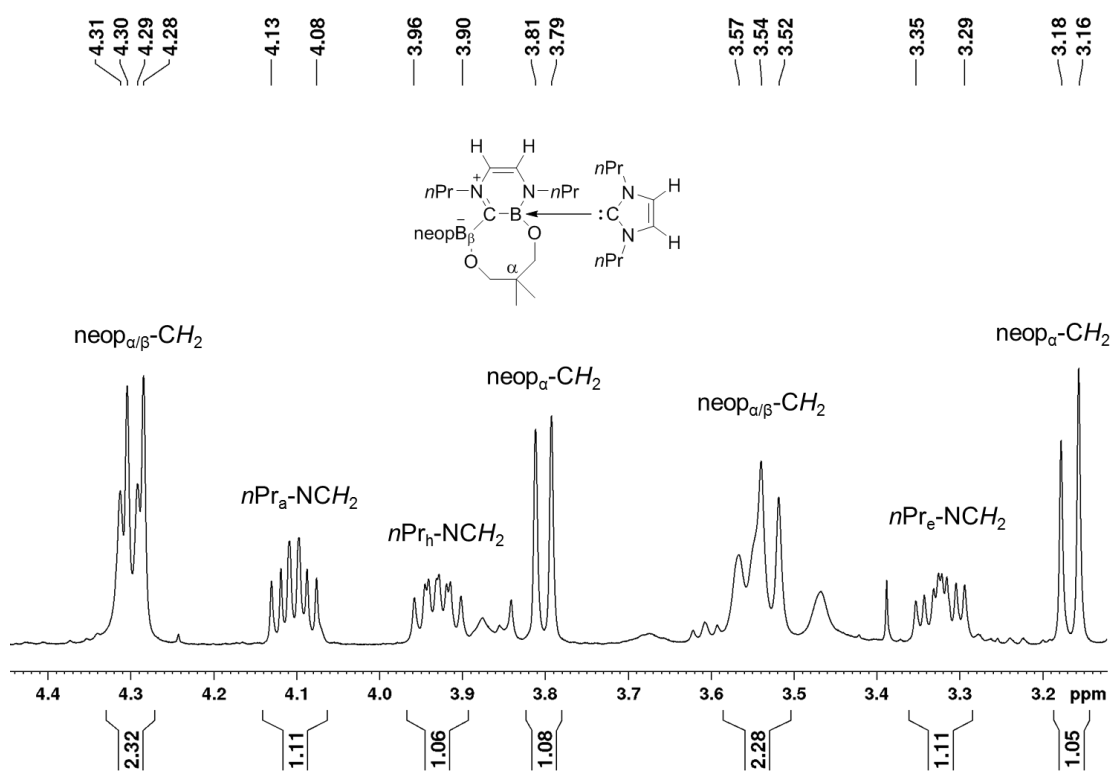
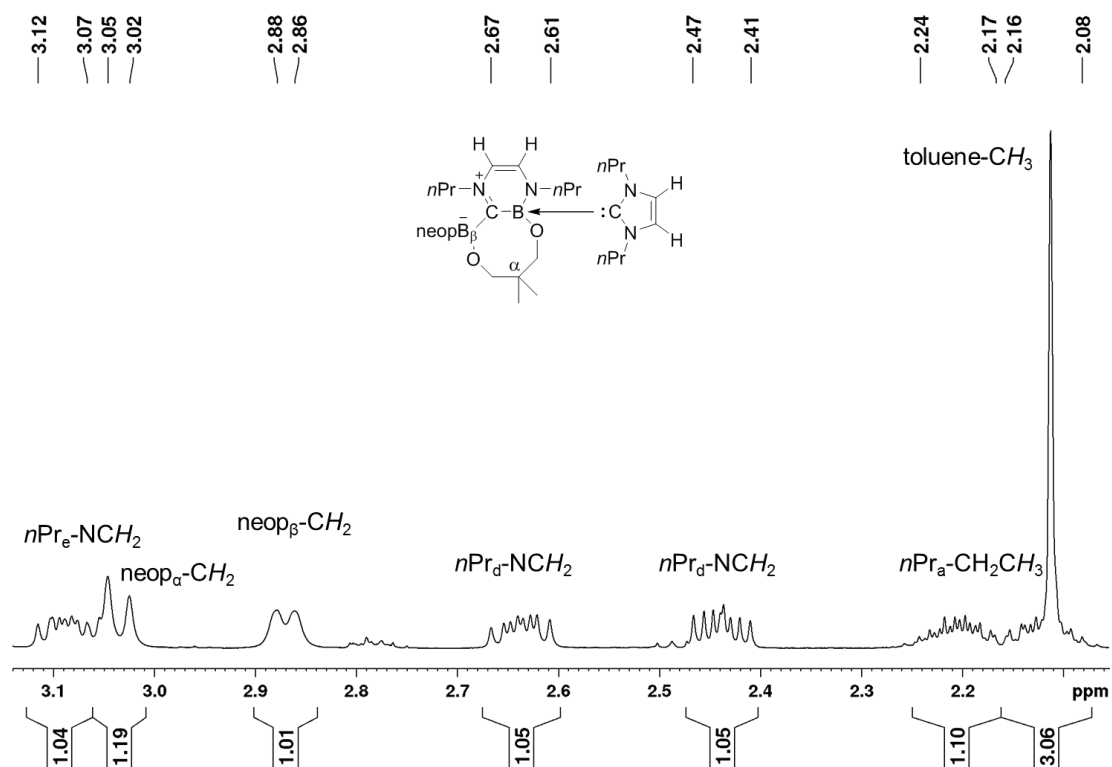
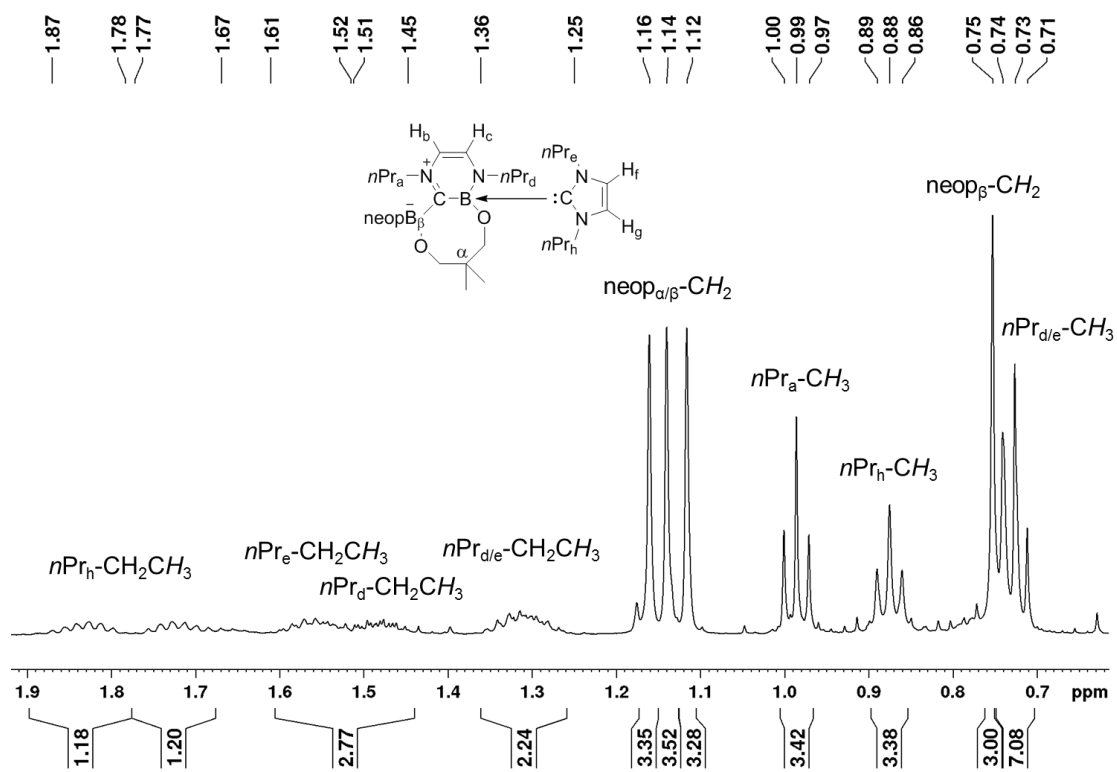


Figure 131: ¹H NMR spectrum of RER-B₂neop₂•(nPr₂Im)₂•toluene **29** in C₆D₆ (500 MHz).

Figure 132: ¹H NMR spectrum of RER-B₂neop₂•(nPr₂Im)₂•toluene **29** in C₆D₆ (500 MHz).Figure 133: ¹H NMR spectrum of RER-B₂neop₂•(nPr₂Im)₂•toluene **29** in C₆D₆ (500 MHz).

Figure 134: ^1H NMR spectrum of $\text{RER-B}_2\text{neop}_2 \cdot (\text{nPr}_2\text{Im})_2 \cdot \text{toluene}$ **29** in C_6D_6 (500 MHz).

8. REFERENCES

- [1] P. Ceron, A. Finch, J. Frey, J. Kerrigan, T. Parsons, G. Urry, H. I. Schlesinger, *J. Am. Chem. Soc.* **1959**, *81*, 6368-6371.
- [2] W. Biffar, H. Nöth, H. Pommerening, B. Wrackmeyer, *Chem. Ber.* **1980**, *113*, 333-341.
- [3] H. Nöth, *Z. Naturforsch., Teil B* **1984**, *39*, 1463-1466.
- [4] T. Ishiyama, M. Murata, T. Ahiko, N. Miyaoura, *Org. Synth.* **2000**, *77*, 176-182.
- [5] C. N. Welch, S. G. Shore, *Inorg. Chem.* **1968**, *7*, 225-230.
- [6] P. Nguyen, G. Lesley, N. J. Taylor, T. B. Marder, N. L. Pickett, W. Clegg, M. R. J. Elsegood, N. C. Norman, *Inorg. Chem.* **1994**, *33*, 4623-4624.
- [7] T. Ishiyama, N. Matsuda, N. Miyaoura, A. Suzuki, *J. Am. Chem. Soc.* **1993**, *115*, 11018-11019.
- [8] T. Ishiyama, N. Matsuda, M. Murata, F. Ozawa, A. Suzuki, N. Miyaoura, *Organometallics* **1996**, *15*, 713-720.
- [9] T. Ishiyama, M. Yamamoto, N. Miyaoura, *Chem. Commun.* **1996**, 2073-2074.
- [10] T. Ishiyama, M. Yamamoto, N. Miyaoura, *Chem. Commun.* **1997**, 689-690.
- [11] R. T. Baker, J. C. Calabrese, S. A. Westcott, P. Nguyen, T. B. Marder, *J. Am. Chem. Soc.* **1993**, *115*, 4367-4368.
- [12] R. T. Baker, P. Nguyen, T. B. Marder, S. A. Westcott, *Angew. Chem.* **1995**, *107*, 1451-1452; *Angew. Chem. Int. Ed. Engl.* **1995**, *34*, 1336-1338.
- [13] G. Lesley, P. Nguyen, N. J. Taylor, T. B. Marder, A. J. Scott, W. Clegg, N. C. Norman, *Organometallics* **1996**, *15*, 5137-5154.
- [14] C. N. Iverson, M. R. Smith, *J. Am. Chem. Soc.* **1995**, *117*, 4403-4404.
- [15] C. N. Iverson, M. R. Smith, *Organometallics* **1996**, *15*, 5155-5165.
- [16] C. N. Iverson, M. R. Smith, *Organometallics* **1997**, *16*, 2757-2759.
- [17] N. Miyaoura, A. Suzuki, *Chem. Rev.* **1995**, *95*, 2457-2483.
- [18] K.-S. Lee, A. R. Zhugralin, A. H. Hoveyda, *J. Am. Chem. Soc.* **2009**, *131*, 7253-7255.
- [19] A. Bonet, H. Gulyás, E. Fernández, *Angew. Chem.* **2010**, *122*, 5256-5260; *Angew. Chem. Int. Ed.* **2010**, *49*, 5130-5134.
- [20] A. Bonet, C. Pubill-Ulldemolins, C. Bo, H. Gulyás, E. Fernández, *Angew. Chem.* **2011**, *123*, 7296-7299; *Angew. Chem. Int. Ed.* **2011**, *50*, 7158-7161.
- [21] I. Ibrahim, P. Breistein, A. Córdova, *Chem. Eur. J.* **2012**, *18*, 5175-5179.
- [22] H. Wu, S. Radomkit, J. M. O'Brien, A. H. Hoveyda, *J. Am. Chem. Soc.* **2012**, *134*, 8277-8285.
- [23] K.-S. Lee, A. R. Zhugralin, A. H. Hoveyda, *J. Am. Chem. Soc.* **2010**, *132*, 12766.
- [24] Y. G. Lawson, M. J. G. Lesley, N. C. Norman, C. R. Rice, T. B. Marder, *Chem. Commun.* **1997**, 2051-2052.
- [25] R. van Asselt, C. J. Elsevier, W. J. J. Smeets, A. L. Spek, *Inorg. Chem.* **1994**, *33*, 1521-1531.
- [26] B. Liu, M. Gao, L. Dang, H. Zhao, T. B. Marder, Z. Lin, *Organometallics* **2012**, *31*, 3410-3425.
- [27] H. A. Ali, I. Goldberg, M. Srebnik, *Organometallics* **2001**, *20*, 3962-3965.
- [28] G. W. Kabalka, B. C. Das, S. Das, *Tetrahedron Lett.* **2002**, *43*, 2323-2325.
- [29] H. Ito, H. Yamanaka, J.-I. Tateiwa, A. Hosomi, *Tetrahedron Lett.* **2000**, *41*, 6821-6825.
- [30] K. Takahashi, T. Ishiyama, N. Miyaoura, *J. Organomet. Chem.* **2001**, *625*, 47-53.
- [31] L. Dang, H. Zhao, Z. Lin, T. B. Marder, *Organometallics* **2008**, *27*, 1178-1186.
- [32] L. Dang, Z. Lin, T. B. Marder, *Organometallics* **2008**, *27*, 4443-4454.
- [33] J. A. Schiffner, K. Müther, M. Oestreich, *Angew. Chem.* **2010**, *122*, 1214-1216; *Angew. Chem. Int. Ed.* **2010**, *49*, 1194-1196.
- [34] E. Hartmann, D. J. Vyas, M. Oestreich, *Chem. Commun.* **2011**, *47*, 7917-7932.
- [35] V. Lillo, A. Bonet, E. Fernández, *Dalton Trans.* **2009**, 2899-2908.
- [36] S. Mun, J.-E. Lee, J. Yun, *Org. Lett.* **2006**, *8*, 4887-4889.
- [37] J.-E. Lee, J. Yun, *Angew. Chem.* **2008**, *120*, 151-153; *Angew. Chem. Int. Ed.* **2008**, *47*, 145-147.
- [38] H.-S. Sim, X. Feng, J. Yun, *Chem. Eur. J.* **2009**, *15*, 1939-1943.
- [39] V. Lillo, A. Prieto, A. Bonet, M. M. Díaz-Requejo, J. Ramírez, P. J. Pérez, E. Fernández, *Organometallics* **2009**, *28*, 659-662.

References

- [40] W. J. Fleming, H. Muller-Bunz, V. Lillo, E. Fernández, P. J. Guiry, *Org. Biomol. Chem.* **2009**, *7*, 2520-2524.
- [41] A. Bonet, V. Lillo, J. Ramirez, M. M. Diaz-Requejo, E. Fernández, *Org. Biomol. Chem.* **2009**, *7*, 1533-1535.
- [42] I. H. Chen, L. Yin, W. Itano, M. Kanai, M. Shibasaki, *J. Am. Chem. Soc.* **2009**, *131*, 11664-11665.
- [43] M. Gao, S. B. Thorpe, W. L. Santos, *Org. Lett.* **2009**, *11*, 3478-3481.
- [44] M. Gao, S. B. Thorpe, C. Kleeberg, C. Slebodnick, T. B. Marder, W. L. Santos, *J. Org. Chem.* **2011**, *76*, 3997-4007.
- [45] S. B. Thorpe, X. Guo, W. L. Santos, *Chem. Commun.* **2011**, *47*, 424-426.
- [46] S. B. Thorpe, J. A. Calderone, W. L. Santos, *Org. Lett.* **2012**, *14*, 1918-1921.
- [47] J. Plotzitzka, C. Kleeberg, *Organometallics* **2014**, *33*, 6915-6926.
- [48] L. Dang, Z. Lin, T. B. Marder, *Chem. Commun.* **2009**, 3987-3995.
- [49] A. D. J. Calow, A. Whiting, *Org. Biomol. Chem.* **2012**, *10*, 5485-5497.
- [50] N. J. Bell, A. J. Cox, N. R. Cameron, J. S. O. Evans, T. B. Marder, M. A. Duin, C. J. Elsevier, X. Bauchere, A. A. D. Tulloch, R. P. Tooze, *Chem. Commun.* **2004**, 1854-1855.
- [51] C. Kleeberg, A. G. Crawford, A. S. Batsanov, P. Hodgkinson, D. C. Apperley, M. S. Cheung, Z. Lin, T. B. Marder, *J. Org. Chem.* **2012**, *77*, 785-789.
- [52] S. Radomkit, A. H. Hoveyda, *Angew. Chem.* **2014**, *126*, 3455-3459; *Angew. Chem. Int. Ed.* **2014**, *53*, 3387-3391.
- [53] E. M. Vieira, M. L. Snapper, A. H. Hoveyda, *J. Am. Chem. Soc.* **2011**, *133*, 3332-3335.
- [54] J. M. O'Brien, K.-S. Lee, A. H. Hoveyda, *J. Am. Chem. Soc.* **2010**, *132*, 10630-10633.
- [55] F. Meng, H. Jang, A. H. Hoveyda, *Chem. Eur. J.* **2013**, *19*, 3204-3214.
- [56] F. Meng, B. Jung, F. Haeffner, A. H. Hoveyda, *Org. Lett.* **2013**, *15*, 1414-1417.
- [57] F. Meng, H. Jang, B. Jung, A. H. Hoveyda, *Angew. Chem.* **2013**, *125*, 5150-5155; *Angew. Chem. Int. Ed.* **2013**, *52*, 5046-5051.
- [58] F. Meng, F. Haeffner, A. H. Hoveyda, *J. Am. Chem. Soc.* **2014**, *136*, 11304-11307.
- [59] F. Gao, A. H. Hoveyda, *J. Am. Chem. Soc.* **2010**, *132*, 10961-10963.
- [60] A. O. Larsen, W. Leu, C. N. Oberhuber, J. E. Campbell, A. H. Hoveyda, *J. Am. Chem. Soc.* **2004**, *126*, 11130-11131.
- [61] K.-S. Lee, M. K. Brown, A. W. Hird, A. H. Hoveyda, *J. Am. Chem. Soc.* **2006**, *128*, 7182-7184.
- [62] M. K. Brown, T. L. May, C. A. Baxter, A. H. Hoveyda, *Angew. Chem.* **2007**, *119*, 1115-1118; *Angew. Chem. Int. Ed.* **2007**, *46*, 1097-1100.
- [63] Y. Lee, H. Jang, A. H. Hoveyda, *J. Am. Chem. Soc.* **2009**, *131*, 18234-18235.
- [64] K.-S. Lee, A. H. Hoveyda, *J. Org. Chem.* **2009**, *74*, 4455-4462.
- [65] A. Guzman-Martinez, A. H. Hoveyda, *J. Am. Chem. Soc.* **2010**, *132*, 10634-10637.
- [66] H. Wu, J. M. Garcia, F. Haeffner, S. Radomkit, A. R. Zhugralin, A. H. Hoveyda, *J. Am. Chem. Soc.* **2015**, *137*, 10585-10602.
- [67] K.-S. Lee, A. H. Hoveyda, *J. Am. Chem. Soc.* **2010**, *132*, 2898-2900.
- [68] J. M. O'Brien, A. H. Hoveyda, *J. Am. Chem. Soc.* **2011**, *133*, 7712-7715.
- [69] K.-S. Lee, H. Wu, F. Haeffner, A. H. Hoveyda, *Organometallics* **2012**, *31*, 7823-7826.
- [70] F. Mo, Y. Jiang, D. Qiu, Y. Zhang, J. Wang, *Angew. Chem.* **2010**, *122*, 1890-1893; *Angew. Chem. Int. Ed.* **2010**, *49*, 1846-1849.
- [71] C. Pubill-Ulldemolins, A. Bonet, H. Gulyás, C. Bo, E. Fernández, *Org. Biomol. Chem.* **2012**, *10*, 9677-9682.
- [72] T. B. Marder, presented at the Euroboron 5 conference, Edinburgh, UK, September 2010.
- [73] C. Kleeberg, P. Hodgkinson, D. Apperley, F. Mo, D. Qiu, M. S. Cheung, L. Dang, J. Wang, Z. Lin, T. B. Marder, presented at the IMEBORON XIV conference, Niagara Falls, Canada, September 2011.
- [74] S. Pietsch, E. C. Neeve, D. C. Apperley, R. Bertermann, F. Mo, D. Qiu, M. S. Cheung, L. Dang, J. Wang, U. Radius, Z. Lin, C. Kleeberg, T. B. Marder, *Chem. Eur. J.* **2015**, *21*, 7082-7098.
- [75] W. Clegg, C. Dai, F. J. Lawlor, T. B. Marder, P. Nguyen, N. C. Norman, N. L. Pickett, W. P. Power, A. J. Scott, *J. Chem. Soc., Dalton Trans.* **1997**, 839-846.

References

- [76] P. Nguyen, C. Dai, N. J. Taylor, W. P. Power, T. B. Marder, N. L. Pickett, N. C. Norman, *Inorg. Chem.* **1995**, *34*, 4290-4291.
- [77] H. Gulyás, A. Bonet, C. Pubill-Ulldemolins, C. Solé, J. Cid, E. Fernández, *Pure Appl. Chem.* **2012**, *84*, 2219-2231.
- [78] C. Pubill-Ulldemolins, A. Bonet, C. Bo, H. Gulyás, E. Fernández, *Chem. Eur. J.* **2012**, *18*, 1121-1126.
- [79] J. Cid, J. J. Carbó, E. Fernández, *Chem. Eur. J.* **2012**, *18*, 12794-12802.
- [80] C. Kleeberg, L. Dang, Z. Lin, T. B. Marder, *Angew. Chem.* **2009**, *121*, 5454-5458; *Angew. Chem. Int. Ed.* **2009**, *48*, 5350-5354.
- [81] B. A. D'Sa, J. G. Verkade, *J. Am. Chem. Soc.* **1996**, *118*, 12832-12833.
- [82] P. B. Kisanga, B. A. D'Sa, J. G. Verkade, *J. Org. Chem.* **1998**, *63*, 10057-10059.
- [83] P. B. Kisanga, J. G. Verkade, *J. Org. Chem.* **1999**, *64*, 4298-4303.
- [84] J.-S. Tang, J. G. Verkade, *Angew. Chem.* **1993**, *105*, 934-936; *Angew. Chem. Int. Ed. Engl.* **1993**, *32*, 896-898.
- [85] X. Sanz, G. M. Lee, C. Pubill-Ulldemolins, A. Bonet, H. Gulyás, S. A. Westcott, C. Bo, E. Fernández, *Org. Biomol. Chem.* **2013**, *11*, 7004-7010.
- [86] A. B. Cuenca, J. Cid, D. Garcia-Lopez, J. J. Carbo, E. Fernández, *Org. Biomol. Chem.* **2015**, *13*, 9659-9664.
- [87] N. Miralles, R. M. Romero, E. Fernández, K. Muniz, *Chem. Commun.* **2015**, *51*, 14068-14071.
- [88] G. Palau-Lluch, X. Sanz, E. La Cascia, M. G. Civit, N. Miralles, A. B. Cuenca, E. Fernández, *Pure Appl. Chem.* **2015**, *87*, 181-193.
- [89] E. L. Cascia, X. Sanz, C. Bo, A. Whiting, E. Fernández, *Org. Biomol. Chem.* **2015**, *13*, 1328-1332.
- [90] J. Cid, H. Gulyás, J. J. Carbo, E. Fernández, *Chem. Soc. Rev.* **2012**, *41*, 3558-3570.
- [91] C. Solé, H. Gulyás, E. Fernández, *Chem. Commun.* **2012**, *48*, 3769-3771.
- [92] A. Bonet, C. Sole, H. Gulyás, E. Fernández, *Org. Biomol. Chem.* **2012**, *10*, 6621-6623.
- [93] J. Cid, J. J. Carbó, E. Fernández, *Chem. Eur. J.* **2014**, *20*, 3616-3620.
- [94] D. S. Laitar, P. Müller, J. P. Sadighi, *J. Am. Chem. Soc.* **2005**, *127*, 17196-17197.
- [95] D. S. Laitar, E. Y. Tsui, J. P. Sadighi, *Organometallics* **2006**, *25*, 2405-2408.
- [96] D. S. Laitar, E. Y. Tsui, J. P. Sadighi, *J. Am. Chem. Soc.* **2006**, *128*, 11036-11037.
- [97] T. Wartik, R. Moore, H. I. Schlesinger, *J. Am. Chem. Soc.* **1949**, *71*, 3265-3266.
- [98] A. Finch, H. I. Schlesinger, *J. Am. Chem. Soc.* **1958**, *80*, 3573-3574.
- [99] T. Wartik, E. F. Apple, *J. Am. Chem. Soc.* **1958**, *80*, 6155-6158.
- [100] W. VanDorne, A. W. Cordes, G. W. Hunt, *Inorg. Chem.* **1973**, *12*, 1686-1689.
- [101] B. M. Graybill, J. K. Ruff, *J. Am. Chem. Soc.* **1962**, *84*, 1062-1063.
- [102] R. Schaeffer, Q. Johnson, J. Kane, *J. Am. Chem. Soc.* **1970**, *92*, 7614-7615.
- [103] G. Urry, J. Kerrigan, T. D. Parsons, H. I. Schlesinger, *J. Am. Chem. Soc.* **1954**, *76*, 5299-5301.
- [104] C. P. Brock, M. K. Das, R. P. Minton, K. Niedenzu, *J. Am. Chem. Soc.* **1988**, *110*, 817-822.
- [105] W. Haubold, U. Kraatz, G. Sawitzki, *Z. Naturforsch., Teil B* **1984**, 1027-1031.
- [106] W. Haubold, U. Kraatz, W. Einholz, *Z. Anorg. Allg. Chem.* **1991**, *592*, 35-41.
- [107] W. Keller, L. G. Sneddon, W. Einholz, A. Gemmler, *Chem. Ber.* **1992**, *125*, 2343-2346.
- [108] P. Bissinger, H. Braunschweig, A. Damme, R. D. Dewhurst, T. Kupfer, K. Radacki, K. Wagner, *J. Am. Chem. Soc.* **2011**, *133*, 19044-19047.
- [109] H. Braunschweig, A. Damme, J. O. C. Jimenez-Halla, T. Kupfer, K. Radacki, *Angew. Chem.* **2012**, *124*, 6372-6376; *Angew. Chem. Int. Ed.* **2012**, *51*, 6267-6271.
- [110] H. Braunschweig, A. Damme, T. Kupfer, *Chem. Commun.* **2013**, *49*, 2774-2776.
- [111] K. Takahashi, T. Ishiyama, N. Miyaura, *Chem. Lett.* **2000**, *29*, 982-983.
- [112] R. D. Dewhurst, E. C. Neeve, H. Braunschweig, T. B. Marder, *Chem. Commun.* **2015**, *51*, 9594-9607.
- [113] D. Curtis, M. J. G. Lesley, N. C. Nicholas, A. G. Orpen, J. Starbuck, *J. Am. Chem. Soc.* **1999**, 1687-1694.
- [114] I. A. Cade, W. Y. Chau, I. Vitorica-Yrezabal, M. J. Ingleson, *Dalton Trans.* **2015**, *44*, 7506-7511.
- [115] G. L. Brubaker, S. G. Shore, *Inorg. Chem.* **1969**, *8*, 2804-2806.

References

- [116] W. Clegg, T. R. F. Johann, T. B. Marder, N. C. Norman, A. G. Orpen, T. M. Peakman, M. J. Quayle, C. R. Rice, A. J. Scott, *J. Am. Chem. Soc.* **1998**, 1431-1438.
- [117] M. J. G. Lesley, N. C. Norman, A. G. Orpen, J. Starbuck, *New J. Chem.* **2000**, 24, 115-117.
- [118] C. Zhu, M. Yamane, *Org. Lett.* **2012**, 14, 4560-4563.
- [119] K. M. Anderson, A. E. Goeta, K. S. B. Hancock, J. W. Steed, *Chem. Commun.* **2006**, 2138-2140.
- [120] K. Gotoh, R. Ishikawa, H. Ishida, *Acta Crystallogr. Sect. E* **2005**, 61, o4016-o4017.
- [121] H. H. Hodgson, *Chem. Rev.* **1947**, 40, 251-277.
- [122] C. Galli, *Chem. Rev.* **1988**, 88, 765-792.
- [123] E. B. Merkushev, *Synthesis* **1988**, 923-937.
- [124] H. Li, L. Wang, Y. Zhang, J. Wang, *Angew. Chem.* **2012**, 124, 2997-3000; *Angew. Chem. Int. Ed.* **2012**, 51, 2943-2946.
- [125] D. Qiu, Y. Zhang, J. Wang, *Org. Chem. Front.* **2014**, 1, 422-425.
- [126] D. Qiu, F. Meng, L. Jin, S. Tang, S. Wang, F. Mo, J. Zhang, J. B. Wang, *Org. Synth.* **2014**, 91, 106-115.
- [127] D. Qiu, L. Jin, Z. Zheng, H. Meng, F. Mo, X. Wang, Y. Zhang, J. Wang, *J. Org. Chem.* **2013**, 78, 1923-1933.
- [128] D. Qiu, S. Wang, S. Tang, H. Meng, L. Jin, F. Mo, Y. Zhang, J. Wang, *J. Org. Chem.* **2014**, 79, 1979-1988.
- [129] J. Takaya, N. Iwasawa, *ACS Catalysis* **2012**, 2, 1993-2006.
- [130] H. Kinuta, Y. Kita, E. Rémond, M. Tobisu, N. Chatani, *Synthesis* **2012**, 44, 2999-3002.
- [131] A. Del Grosso, R. G. Pritchard, C. A. Muryn, M. J. Ingleson, *Organometallics* **2010**, 29, 241-249.
- [132] A. J. Arduengo, R. L. Harlow, M. Kline, *J. Am. Chem. Soc.* **1991**, 113, 361-363.
- [133] W. A. Herrmann, C. Köcher, *Angew. Chem.* **1997**, 109, 2256-2282; *Angew. Chem. Int. Ed.* **1997**, 36, 2162-2187.
- [134] A. J. Arduengo, *Acc. Chem. Rev.* **1999**, 32, 913-921.
- [135] D. Bourissou, O. Guerret, F. P. Gabbaï, G. Bertrand, *Chem. Rev.* **2000**, 100, 39-92.
- [136] W. A. Herrmann, *Angew. Chem.* **2002**, 114, 1342-1363; *Angew. Chem. Int. Ed.* **2002**, 41, 1290-1309.
- [137] F. E. Hahn, M. C. Jahnke, *Angew. Chem.* **2008**, 120, 3166-3216; *Angew. Chem. Int. Ed.* **2008**, 47, 3122-3172.
- [138] O. Schuster, L. Yang, H. G. Raubenheimer, M. Albrecht, *Chem. Rev.* **2009**, 109, 3445-3478.
- [139] J. Vignolle, X. Cattoën, D. Bourissou, *Chem. Rev.* **2009**, 109, 3333-3384.
- [140] M. Melaimi, M. Soleilhavoup, G. Bertrand, *Angew. Chem.* **2010**, 122, 8992-9032; *Angew. Chem. Int. Ed.* **2010**, 49, 8810-8849.
- [141] M. Asay, C. Jones, M. Driess, *Chem. Rev.* **2011**, 111, 354-396.
- [142] M. N. Hopkinson, C. Richter, M. Schedler, F. Glorius, *Nature* **2014**, 510, 485-496.
- [143] Y. Wang, G. H. Robinson, *Chem. Commun.* **2009**, 5201-5213.
- [144] U. Siemeling, *Aust. J. Chem.* **2011**, 64, 1109-1112.
- [145] D. Martin, M. Soleilhavoup, G. Bertrand, *Chem. Sci.* **2011**, 2, 389-399.
- [146] Y. Wang, G. H. Robinson, *Inorg. Chem.* **2011**, 50, 12326-12337.
- [147] Y. Wang, G. H. Robinson, *Dalton Trans.* **2012**, 41, 337-345.
- [148] S. Díez-González, N. Marion, S. P. Nolan, *Chem. Rev.* **2009**, 109, 3612-3676.
- [149] M. Poyatos, J. A. Mata, E. Peris, *Chem. Rev.* **2009**, 109, 3677-3707.
- [150] F. Hering, J. Nitsch, U. Paul, A. Steffen, F. M. Bickelhaupt, U. Radius, *Chem. Sci.* **2015**, 6, 1426-1432.
- [151] F. Hering, U. Radius, *Organometallics* **2015**, 34, 3236-3245.
- [152] R. J. Baker, R. D. Farley, C. Jones, M. Kloth, D. M. Murphy, *Chem. Commun.* **2002**, 1196-1197.
- [153] Y. Wang, Y. Xie, P. Wei, R. B. King, H. F. Schaefer, P. v. R. Schleyer, G. H. Robinson, *Science* **2008**, 321, 1069-1071.
- [154] Y. Wang, Y. Xie, P. Wei, R. B. King, H. F. Schaefer, P. v. R. Schleyer, G. H. Robinson, *J. Am. Chem. Soc.* **2008**, 130, 14970-14971.
- [155] A. Sidiropoulos, C. Jones, A. Stasch, S. Klein, G. Frenking, *Angew. Chem.* **2009**, 121, 9881-9884; *Angew. Chem. Int. Ed.* **2009**, 48, 9701-9704.

References

- [156] M. Y. Abraham, Y. Wang, Y. Xie, P. Wei, H. F. Schaefer, P. v. R. Schleyer, G. H. Robinson, *Chem. Eur. J.* **2010**, *16*, 432-435.
- [157] N. Holzmann, A. Stasch, C. Jones, G. Frenking, *Chem. Eur. J.* **2011**, *17*, 13517-13525.
- [158] D. J. D. Wilson, S. A. Couchman, J. L. Dutton, *Inorg. Chem.* **2012**, *51*, 7657-7668.
- [159] H. Braunschweig, R. D. Dewhurst, K. Hammond, J. Mies, K. Radacki, A. Vargas, *Science* **2012**, *336*, 1420-1422.
- [160] S. P. Nolan, *N-Heterocyclic Carbenes in Synthesis*, Wiley-VCH, Weinheim, **2006**.
- [161] F. Glorius, *N-Heterocyclic Carbenes in Transition Metal Catalysis: Topics in Organometallic Chemistry, Vol. 21*, Springer, Berlin, **2007**.
- [162] D. Enders, O. Niemeier, A. Henseler, *Chem. Rev.* **2007**, *107*, 5606-5655.
- [163] S. Díez-Gonzalez, *N-Heterocyclic Carbenes: From Laboratory Curiosities to Efficient Synthetic Tools*, RSC, Cambridge, **2010**.
- [164] N. Marion, S. Díez-González, S. P. Nolan, *Angew. Chem.* **2007**, *119*, 3046-3058; *Angew. Chem. Int. Ed.* **2007**, *46*, 2988-3000.
- [165] V. Nair, S. Vellalath, B. P. Babu, *Chem. Soc. Rev.* **2008**, *37*, 2691-2698.
- [166] E. M. Phillips, A. Chan, K. A. Scheidt, *Aldrichimica Acta* **2009**, *42*, 55-66.
- [167] J. L. Moore, T. Rovis, *Top. Curr. Chem.* **2010**, *291*, 77-144.
- [168] C. S. J. Cazin, *N-Heterocyclic Carbenes in Organocatalysis, N-Heterocyclic Carbenes in Transition Metal Catalysis and Organocatalysis, Catalysis by Metal Complexes*, Springer, Dordrecht, **2011**.
- [169] A. T. Biju, N. Kuhl, F. Glorius, *Acc. Chem. Rev.* **2011**, *44*, 1182-1195.
- [170] P. Chauhan, D. Enders, *Angew. Chem.* **2014**, *126*, 1509-1511; *Angew. Chem. Int. Ed.* **2014**, *53*, 1485-1487.
- [171] S. Díez-Gonzalez, N. Marion, S. P. Nolan, *Chem. Rev.* **2009**, 3612-3676.
- [172] D. Holschumacher, T. Bannenberg, C. G. Hrib, P. G. Jones, M. Tamm, *Angew. Chem.* **2008**, *120*, 7538-7542; *Angew. Chem. Int. Ed.* **2008**, *47*, 7428-7432.
- [173] G. Erker, *Pure Appl. Chem.* **2012**, *84*, 2203-2217.
- [174] E. L. Kolychev, E. Theuergarten, M. Tamm, *Top. Curr. Chem.* **2013**, *334*, 121-155.
- [175] G. Kehr, S. Schwendemann, G. Erker, *Top. Curr. Chem.* **2013**, *332*, 45-83.
- [176] D. W. Stephan, *J. Am. Chem. Soc.* **2015**, *137*, 10018-10032.
- [177] D. W. Stephan, G. Erker, *Angew. Chem.* **2015**, *127*, 6498-6541; *Angew. Chem. Int. Ed.* **2015**, *54*, 6400-6441.
- [178] D. W. Stephan, *Acc. Chem. Rev.* **2015**, *48*, 306-316.
- [179] P. A. Chase, D. W. Stephan, *Angew. Chem.* **2008**, *120*, 7543-7547; *Angew. Chem. Int. Ed.* **2008**, *47*, 7433-7437.
- [180] P. A. Chase, A. L. Gille, T. M. Gilbert, D. W. Stephan, *Dalton Trans.* **2009**, 7179-7188.
- [181] D. Holschumacher, C. Taouss, T. Bannenberg, C. G. Hrib, C. G. Daniliuc, P. G. Jones, M. Tamm, *Dalton Trans.* **2009**, 6927-6929.
- [182] G. C. Welch, R. R. S. Juan, J. D. Masuda, D. W. Stephan, *Science* **2006**, *314*, 1124-1126.
- [183] G. C. Welch, D. W. Stephan, *J. Am. Chem. Soc.* **2007**, *129*, 1880-1881.
- [184] P. Spies, G. Erker, G. Kehr, K. Bergander, R. Fröhlich, S. Grimme, D. W. Stephan, *Chem. Commun.* **2007**, 5072-5074.
- [185] A. E. Ashley, A. L. Thompson, D. O'Hare, *Angew. Chem.* **2009**, *121*, 10023-10027; *Angew. Chem. Int. Ed.* **2009**, *48*, 9839-9843.
- [186] C. M. Mömming, E. Otten, G. Kehr, R. Fröhlich, S. Grimme, D. W. Stephan, G. Erker, *Angew. Chem.* **2009**, *121*, 6770-6773; *Angew. Chem. Int. Ed.* **2009**, *48*, 6643-6646.
- [187] S. Grimme, H. Kruse, L. Goerigk, G. Erker, *Angew. Chem.* **2010**, *122*, 1444-1447; *Angew. Chem. Int. Ed.* **2010**, *66*, 1402-1405.
- [188] D. Holschumacher, T. Bannenberg, K. Ibrom, C. G. Daniliuc, P. G. Jones, M. Tamm, *Dalton Trans.* **2010**, *39*, 10590-10592.
- [189] B. M. Day, T. Pugh, D. Hendriks, C. F. Guerra, D. J. Evans, F. M. Bickelhaupt, R. A. Layfield, *J. Am. Chem. Soc.* **2013**, *135*, 13338-13341.
- [190] B. M. Day, K. Pal, T. Pugh, J. Tuck, R. A. Layfield, *Inorg. Chem.* **2014**, *53*, 10578-10584.

References

- [191] M. Wagner, T. Zoller, W. Hiller, M. H. Prosenc, K. Jurkschat, *Chem. Commun.* **2013**, *49*, 8925-8927.
- [192] S. Caddick, F. G. N. Cloke, P. B. Hitchcock, A. K. de K. Lewis, *Angew. Chem.* **2004**, *116*, 5948-5951; *Angew. Chem. Int. Ed.* **2004**, *43*, 5824-5827.
- [193] S. Burling, M. F. Mahon, R. E. Powell, M. K. Whittlesey, J. M. J. Williams, *J. Am. Chem. Soc.* **2006**, *128*, 13702-13703.
- [194] J. Ruiz, B. F. Perandones, *J. Am. Chem. Soc.* **2007**, *129*, 9298-9299.
- [195] M. A. Huertos, J. Pérez, L. Riera, *J. Am. Chem. Soc.* **2008**, *130*, 5662-5663.
- [196] Y. Han, Y.-T. Hong, H. V. Huynh, *J. Organomet. Chem.* **2008**, *693*, 3159-3165.
- [197] J. A. Cabeza, I. del Río, D. Miguel, M. G. Sánchez-Vega, *Angew. Chem.* **2008**, *120*, 1946-1948; *Angew. Chem. Int. Ed.* **2008**, *47*, 1920-1922.
- [198] T. Steinke, B. K. Shaw, H. Jong, B. O. Patrick, M. D. Fryzuk, J. C. Green, *J. Am. Chem. Soc.* **2009**, *131*, 10461-10466.
- [199] L. J. L. Häller, M. J. Page, S. Erhardt, S. A. Macgregor, M. F. Mahon, M. A. Naser, A. Vélez, M. K. Whittlesey, *J. Am. Chem. Soc.* **2010**, *132*, 18408-18416.
- [200] L. Xiang, J. Xiao, L. Deng, *Organometallics* **2011**, *30*, 2018-2025.
- [201] M. Brill, J. Díaz, M. A. Huertos, R. López, J. Pérez, L. Riera, *Chem. Eur. J.* **2011**, *17*, 8584-8595.
- [202] T. Hatanaka, Y. Ohki, K. Tatsumi, *Angew. Chem.* **2014**, *126*, 2765-2767; *Angew. Chem. Int. Ed.* **2014**, *53*, 2727-2729.
- [203] D. P. Curran, A. Boussonnière, S. J. Geib, E. Lacôte, *Angew. Chem.* **2012**, *124*, 1634-1637; *Angew. Chem. Int. Ed.* **2012**, *51*, 1602-1605.
- [204] Y. Ohki, T. Hatanaka, K. Tatsumi, *J. Am. Chem. Soc.* **2008**, *130*, 17174-17186.
- [205] R. Wolf, M. Plois, A. Hepp, *Eur. J. Inorg. Chem.* **2010**, *2010*, 918-925.
- [206] M. Würtemberger, T. Ott, C. Döring, T. Schaub, U. Radius, *Eur. J. Inorg. Chem.* **2011**, *2011*, 405-415.
- [207] N. Bramanathan, E. Mas-Marzá, F. E. Fernández, C. E. Ellul, M. F. Mahon, M. K. Whittlesey, *Eur. J. Inorg. Chem.* **2012**, *2012*, 2213-2219.
- [208] L.-J. Liu, F. Wang, M. Shi, *Eur. J. Inorg. Chem.* **2009**, 1723-1728.
- [209] Y.-C. Hu, C.-C. Tsai, W.-C. Shih, G. P. A. Yap, T.-G. Ong, *Organometallics* **2010**, *29*, 516-518.
- [210] B. R. Galan, M. Gembicky, P. M. Dominiak, J. B. Keister, S. T. Diver, *J. Am. Chem. Soc.* **2005**, *127*, 15702-15703.
- [211] B. R. Galan, M. Pitak, M. Gembicky, J. B. Keister, S. T. Diver, *J. Am. Chem. Soc.* **2009**, *131*, 6822-6832.
- [212] O. Hollóczki, P. Terleczy, D. Szieberth, G. Mourgas, D. Gudat, L. Nyulászi, *J. Am. Chem. Soc.* **2011**, *133*, 780-789.
- [213] G. D. Frey, J. D. Masuda, B. Donnadieu, G. Bertrand, *Angew. Chem.* **2010**, *122*, 9634-9637; *Angew. Chem. Int. Ed.* **2010**, *49*, 9444-9447.
- [214] U. Siemeling, C. Farber, C. Bruhn, M. Leibold, D. Selent, W. Baumann, M. von Hopffgarten, C. Goedecke, G. Frenking, *Chem. Sci.* **2010**, *1*, 697-704.
- [215] A. S. Pelegrí, M. R. J. Elsegood, V. McKee, G. W. Weaver, *Org. Lett.* **2006**, *8*, 3049-3051.
- [216] A. W. Waltman, T. Ritter, R. H. Grubbs, *Organometallics* **2006**, *25*, 4238-4239.
- [217] D. Pugh, A. Boyle, A. A. Danopoulos, *Dalton Trans.* **2008**, 1087-1094.
- [218] A. Kaiho, H. Suzuki, *Angew. Chem.* **2012**, *124*, 1437-1440; *Angew. Chem. Int. Ed.* **2012**, *51*, 1408-1411.
- [219] H.-J. Liu, M. S. Ziegler, T. D. Tilley, *Polyhedron* **2014**, *84*, 203-208.
- [220] W. Zuo, P. Braunstein, *Dalton Trans.* **2012**, *41*, 636-643.
- [221] D. Prema, Y. L. N. M. Arachchige, R. E. Murray, L. M. Slaughter, *Chem. Commun.* **2015**, *51*, 6753-6756.
- [222] G.-F. Wang, X.-J. Song, F. Chen, Y.-Z. Li, X.-T. Chen, Z.-L. Xue, *Dalton Trans.* **2012**, *41*, 10919-10922.
- [223] M. Poyatos, W. McNamara, C. Incarvito, E. Clot, E. Peris, R. H. Crabtree, *Organometallics* **2008**, *27*, 2128-2136.

References

- [224] E. Despagnet-Ayoub, M. K. Takase, J. A. Labinger, J. E. Bercaw, *J. Am. Chem. Soc.* **2015**, *137*, 10500-10503.
- [225] P. Hemberger, A. Bodi, T. Gerber, M. Würtemberger, U. Radius, *Chem. Eur. J.* **2013**, *19*, 7090-7099.
- [226] P. Hemberger, A. Bodi, J. H. J. Berthel, U. Radius, *Chem. Eur. J.* **2015**, *21*, 1434-1438.
- [227] S. M. I. Al-Rafia, R. McDonald, M. J. Ferguson, E. Rivard, *Chem. Eur. J.* **2012**, *18*, 13810-13820.
- [228] D. Franz, S. Inoue, *Chem. Asian J.* **2014**, *9*, 2083-2087.
- [229] T. Wang, D. W. Stephan, *Chem. Eur. J.* **2014**, *20*, 3036-3039.
- [230] M. Arrowsmith, M. S. Hill, G. Kociok-Köhn, D. J. MacDougall, M. F. Mahon, *Angew. Chem.* **2012**, *124*, 2140-2142; *Angew. Chem. Int. Ed.* **2012**, *51*, 2098-2100.
- [231] M. Arrowsmith, M. S. Hill, G. Kociok-Köhn, *Organometallics* **2015**, *34*, 653-662.
- [232] D. Schmidt, J. H. J. Berthel, S. Pietsch, U. Radius, *Angew. Chem.* **2012**, *124*, 9011-9015; *Angew. Chem. Int. Ed.* **2012**, *51*, 8881-8885.
- [233] G. Hesse, A. Haag, *Tetrahedron Lett.* **1965**, *6*, 1123-1125.
- [234] T. Schaub, U. Radius, *Chem. Eur. J.* **2005**, *11*, 5024-5030.
- [235] T. Schaub, M. Backes, U. Radius, *Organometallics* **2006**, *25*, 4196-4206.
- [236] T. Schaub, M. Backes, U. Radius, *Chem. Commun.* **2007**, 2037-2039.
- [237] T. Schaub, C. Döring, U. Radius, *Dalton Trans.* **2007**, 1993-2002.
- [238] T. Schaub, M. Backes, O. Plietzsch, U. Radius, *Dalton Trans.* **2009**, 7071-7079.
- [239] T. Zell, T. Schaub, K. Radacki, U. Radius, *Dalton Trans.* **2011**, *40*, 1852-1854.
- [240] P. Fischer, K. Götz, A. Eichhorn, U. Radius, *Organometallics* **2012**, *31*, 1374-1383.
- [241] D. Schmidt, T. Zell, T. Schaub, U. Radius, *Dalton Trans.* **2014**, *43*, 10816-10827.
- [242] K. J. Iversen, D. J. D. Wilson, J. L. Dutton, *Organometallics* **2013**, *32*, 6209-6217.
- [243] K. J. Iversen, D. J. D. Wilson, J. L. Dutton, *Dalton Trans.* **2013**, *42*, 11035-11038.
- [244] K. J. Iversen, D. J. D. Wilson, J. L. Dutton, *Dalton Trans.* **2014**, *43*, 12820-12823.
- [245] K. J. Iversen, D. J. D. Wilson, J. L. Dutton, *Dalton Trans.* **2015**, *44*, 3318-3325.
- [246] M. R. Momeni, E. Rivard, A. Brown, *Organometallics* **2013**, *32*, 6201-6208.
- [247] M.-D. Su, *Inorg. Chem.* **2014**, *53*, 5080-5087.
- [248] J. M. Farrell, J. A. Hatnean, D. W. Stephan, *J. Am. Chem. Soc.* **2012**, *134*, 15728-15731.
- [249] S. K. Bose, K. Fucke, L. Liu, P. G. Steel, T. B. Marder, *Angew. Chem.* **2014**, *126*, 1829-1834; *Angew. Chem. Int. Ed.* **2014**, *53*, 1799-1784.
- [250] H. Schneider, D. Schmidt, U. Radius, *Chem. Eur. J.* **2015**, *21*, 2793-2797.
- [251] H. Schneider, D. Schmidt, U. Radius, *Chem. Commun.* **2015**, *51*, 10138-10141.
- [252] C. P. Sindlinger, L. Wesemann, *Chem. Sci.* **2014**, *5*, 2739-2746.
- [253] C. P. Sindlinger, L. Wesemann, *Chem. Commun.* **2015**, *51*, 11421-11424.
- [254] A. Eichhorn, U. Radius, T. B. Marder, unpublished results.
- [255] A. Eichhorn, Diplomarbeit, Julius-Maximilians-Universität Würzburg, **2012**.
- [256] S. Pietsch, U. Paul, I. A. Cade, M. J. Ingleson, U. Radius, T. B. Marder, *Chem. Eur. J.* **2015**, *21*, 9018-9021.
- [257] A. J. Arduengo, F. Davidson, H. V. R. Dias, J. R. Goerlich, D. Khasnis, W. J. Marshall, T. K. Prakasha, *J. Am. Chem. Soc.* **1997**, *119*, 12742-12749.
- [258] R. Fang, L. Yang, Q. Wang, *Organometallics* **2014**, *33*, 53-60.
- [259] D. Schmidt, Doktorarbeit, Julius-Maximilians-Universität Würzburg, **2013**.
- [260] W. Clegg, M. R. J. Elsegood, F. J. Lawlor, N. C. Norman, N. L. Pickett, E. G. Robins, A. J. Scott, P. Nguyen, N. J. Taylor, T. B. Marder, *Inorg. Chem.* **1998**, *37*, 5289-5293.
- [261] M. Eck, T. B. Marder unpublished results.
- [262] H. Braunschweig, F. Guethlein, L. Mailänder, T. B. Marder, *Chem. Eur. J.* **2013**, *19*, 14831-14835.
- [263] J. Kroner, B. Wrackmeyer, *J. Chem. Soc., Faraday Trans. 2* **1976**, *72*, 2283-2290.
- [264] B. Wrackmeyer, *Prog. NMR Spectrosc.* **1979**, *12*, 227-259.
- [265] J. Monot, M. M. Brahmi, S.-H. Ueng, C. Robert, M. D.-E. Murr, D. P. Curran, M. Malacria, L. Fensterbank, E. Lacôte, *Org. Lett.* **2009**, *11*, 4914-4917.
- [266] Y. Yamaguchi, T. Kashiwabara, K. Ogata, Y. Miura, Y. Nakamura, K. Kobayashi, T. Ito, *Chem. Commun.* **2004**, 2160-2161.

References

- [267] A. Jana, V. Huch, H. S. Rzepa, D. Scheschkewitz, *Angew. Chem.* **2015**, *127*, 291-295; *Angew. Chem. Int. Ed.* **2015**, *54*, 289-292.
- [268] H. Cui, J. Zhang, C. Cui, *Organometallics* **2013**, *32*, 1-4.
- [269] A. C. Filippou, O. Chernov, K. W. Stumpf, G. Schnakenburg, *Angew. Chem.* **2010**, *122*, 6851-6851; *Angew. Chem. Int. Ed.* **2010**, *49*, 3296-3300.
- [270] M. Chen, Y. Wang, R. J. Gilliard, Jr, P. Wei, N. A. Schwartz, G. H. Robinson, *Dalton Trans.* **2014**, *43*, 14211-14214.
- [271] C. E. Ellul, M. F. Mahon, O. Saker, M. K. Whittlesey, *Angew. Chem.* **2007**, *119*, 6459-6461; *Angew. Chem. Int. Ed.* **2007**, *46*, 6343-6345.
- [272] M. R. Crittall, C. E. Ellul, M. F. Mahon, O. Saker, M. K. Whittlesey, *Dalton Trans.* **2008**, 4209-4211.
- [273] G. C. Fortman, N. M. Scott, A. Linden, E. D. Stevens, R. Dorta, S. P. Nolan, *Chem. Commun.* **2010**, *46*, 1050-1052.
- [274] Y. Liu, R. Ganguly, H. V. Huynh, W. K. Leong, *Angew. Chem.* **2013**, *125*, 12332-12335; *Angew. Chem. Int. Ed.* **2013**, *52*, 12110-12113.
- [275] P. Jochmann, D. W. Stephan, *Chem. Eur. J.* **2014**, *20*, 8370-8378.
- [276] A. K. Guha, S. Sarmah, A. K. Phukan, *Dalton Trans.* **2010**, *39*, 7374-7383.
- [277] A.-L. Schmitt, G. Schnee, R. Welter, S. Dagonne, *Chem. Commun.* **2010**, *46*, 2480-2482.
- [278] S. Kronig, E. Theuergarten, D. Holschumacher, T. Bannenberg, C. G. Daniliuc, P. G. Jones, M. Tamm, *Inorg. Chem.* **2011**, *50*, 7344-7359.
- [279] E. Theuergarten, T. Bannenberg, M. D. Walter, D. Holschumacher, M. Freytag, C. G. Daniliuc, P. G. Jones, M. Tamm, *Dalton Trans.* **2014**, *43*, 1651-1662.
- [280] N. Kuhn, T. Kratz, *Synthesis* **1993**, *1993*, 561-562.
- [281] V. Lavallo, Y. Canac, A. DeHope, B. Donnadiou, G. Bertrand, *Angew. Chem.* **2005**, *117*, 7402-7405; *Angew. Chem. Int. Ed.* **2005**, *44*, 7236-7239.
- [282] M. P. Brown, A. E. Dann, D. W. Hunt, H. B. Silver, *J. Am. Chem. Soc.* **1962**, 4648-4652.
- [283] P. Hanson, J. R. Jones, A. B. Taylor, P. H. Walton, A. W. Timms, *J. Chem. Soc., Perkin Trans. 2* **2002**, 1135-1150.
- [284] M. Svobodová, P. Šimůnek, V. Macháček, L. Štruncová, A. Růžička, *Tetrahedron* **2012**, *68*, 2052-2060.
- [285] P. W. Betteridge, J. R. Carruthers, R. I. Cooper, K. Prout, D. J. Watkin, *J. Appl. Cryst.* **2003**, *36*, 1487.
- [286] G. Sheldrick, *Acta Crystallogr. Sect. A* **2008**, *64*, 112-122.
- [287] L. Farrugia, *J. Appl. Crystallogr.* **1997**, *30*, 565.
- [288] K. Brandenburg, **1997**, Crystal Impact GbR, Diamond 3.2i, Bonn Germany.
- [289] L. Farrugia, *J. Appl. Crystallogr.* **1999**, *32*, 837-838.
- [290] P. van der Sluis, A. L. Spek, *Acta Crystallogr. Sect. A* **1990**, *46*, 194-201.
- [291] I. Bruker Analytical X-ray Systems, **2006**, *Apex2*; Version 2 User Manual, M86-E01078. Madison, WI.
- [292] CrysAlisPro, Agilent Technologies, Version 1.171.35.19 (release 27-10-2011 Crsyalis171 NET) (compiled Oct. 2011, 15.02.11).
- [293] A. Altomare, G. Cascarano, C. Giacovazzo, A. Guagliardi, M. C. Burla, G. Polidori, M. Camalli, *J. Appl. Cryst.* **1994**, *27*, 435.

9. ACKNOWLEDGMENT

Dear Todd, Dear Udo,

I thank you so much for the last years being a PhD student in both groups. Thanks for your support, your help, your discussion, the never ending meetings and the opportunity to give me a topic with so much freedom of decision. I also want to thank you for being part of the "Marder Family" and the "Ak Radius", it is still an honor to have such a great cooperation with both of you.

I also want to thank the whole "Marder Family", thanks for the good time, the discussion and the time we shared on several conferences. Especially, I want to thank the "catalysis subgroup", namely, Martin, Shubhankar, Emily, Lujia, Jing and Toni, for the help, the discussion and the good time we shared.

Many thanks to Dr. Christian Kleeberg, we first met in Warschau and I will not forget the time we shared on several conferences. Thanks for helping me with the anionic adducts and the never ending discussions, how to drink wodka (you are right, some are warm better than others ☺).

I also want to thank Dr. Michael Ingleson and Dr. Ian Cade for the cooperation which led to a really good publication.

Weiterhin möchte ich mich bei Ulli, Nicola, Heidi, Toni, Matze und Rumpel für das Korrekturlesen meiner Arbeit bedanken, vielen Dank an euch alle für den letzten Feinschliff.

Ein riesen Dank geht an den ganzen Ak Radius, Ulli, Johannes, Heidi, Toni, Mirjam, Max und Katha für die Zeit, die wir hier oben zusammen hatten, es war ein unbeschreiblich tolle Zeit.

Ganz besonders möchte ich mich bei euch vieren, Ulli, Rumpel, Heidi und Toni, bedanken, die letzten 4 Jahren waren der Wahnsinn! Das kann man so stehen lassen! Ich danke euch für die vielen Hilfestellungen, Anregungen und den Spaß, den wir hier oben hatten. Ich bin unglaublich gerne zur Arbeit gekommen! Vielen Dank euch allen auch, dass ihr nie die Ausdauer und Geduld verloren habt, wenn ich wieder mal Kristalle in meinen Schlenks und NMR-Röhrchen zur Begutachtung vorbeigebracht habe, ihr wart mir eine riesen Hilfe, sowohl beim Aufsetzen als auch beim Lösen der Strukturen, nochmals vielen lieben Dank!

Weiterhin möchte ich mich allgemein beim dritten Stock bedanken, vielen Dank an den Ak Finze, besonderer Dank gilt dabei Shorty, Matze, Michl und Drisch.

Ein besonderer Dank geht natürlich an meinem Laborpartner und meiner Laborpartnerin aus Labor 321, Shorty und Ulli, es war eine wahnsinnig schöne Zeit mit euch beiden, die gemeinsame Zeit wird mir fehlen.

An dieser Stelle möchte ich auch den ehemaligen des Ak Radius danken, Dr. Flo, Dr. Schnurres, Dr. Awesome, Dr. Max und Dr. Zell, vielen Dank für die gemeinsame Zeit während meiner Bachelor-, Master- und Doktorarbeit. Ihr seid keine schlechten Vorbilder gewesen ☺ Ein großer Dank geht hierbei an Dr. Flo, danke für die vielen Hilfestellungen in word, endnote und deine unermüdliche Geduld mir Sachen zu erklären.

Acknowledgment

Vielen Dank natürlich auch an meine Bachelor- und Vertiefungspraktikanten Matthias Ferger, Kilian Reus, Alexander Okorn, Roman Ickert und Natalie Schäfer für die zahlreichen Ergebnisse.

Ein großer Dank geht an die NMR-Abteilung, Herr Dr. Rüdiger Bertermann und Frau Marie-Luise Schäfer, vielen Dank für die vielen NMR- und die schnellen Festkörper Messungen. Ich habe es nie bereut bei euch unten geklopft zu haben und ich bin gerne zum Lachen in den Keller gekommen!

Vielen Dank an Frau Lieselotte Michels und Frau Sabine Timmroth für die Anfertigung zahlreicher Elementaranalysen.

Bedanken möchte ich mich ebenfalls bei den wohl wichtigsten Frauen in diesem Institut, Ellen Klaus, Patricia Schmidt und Bianca Putz sowie Conny Walter, vielen Dank für die immer offenen Ohren und natürlich die Erledigung aller Verwaltungsangelegenheiten.

Weiterhin möchte ich den beiden Glasbläsern der Chemie bedanken, Berthold Fertig und Jonathan Landeck. Es war immer wieder schön bei euch und vielen Dank, dass man auch mal über andere Dinge reden konnte. Vielen Dank natürlich für die schnellen Reparaturen meiner Glasgeräte.

Des Weiteren möchte ich mich bei dem gesamten Team der Werkstatt (Alois Ruf, Wolfgang Obert, Manfred Reinhardt, Michael Ramold und den 4 mal die 4 Jungs) und Herrn Alfred Schertzer für die Behebung aller technischen Probleme bedanken.

Ein großer Dank geht an die Donnerstag-Mensa Gruppe, die über die Zeit leider immer kleiner wurde. Vielen Dank an Nicola, Dr. Nagel, Drisch, Dr. Fabian, Sarah, Fede und Dr. Lisa. Es hat wirklich riesen Spaß gemacht mit euch allen studiert und promoviert zu haben. An dieser Stelle möchte ich mich auch bei Dr. Julia Gmeiner und Dr. Do für die gemeinsame Bachelor-/Masterzeit an der Uni Würzburg bedanken.

Ganz besonders möchte ich mich bei Nicola bedanken, ich hätte nie gedacht, dass ein Schimpfwort zu einer so besonderen Freundschaft führen kann. Wir sind jetzt seit über 8 Jahren befreundet, das muss echte Liebe sein. :-*

Mama Heidi, Papa, Isabell, Florentina und Adrian, ich danke euch für die letzten 28 Jahre! Ihr seid wohl die beste Familie, die man sich vorstellen kann. Vielen Dank für die Unterstützung während der Schulzeit, Studium und meiner Promotion. Es war bestimmt nicht immer einfach mit mir, aber ihr könnt euch gar nicht vorstellen wie sehr ich euch brauche und liebe.

Oma Lieselotte und Oma Cäcilie, ihr beiden seid die besten. Ich hab euch so lieb!

Ich hätte mir nie vorstellen können, dass die Wahl meiner Bachelorarbeit mich zur Liebe meines Lebens führen wird. Max, du bist der tollste Mensch, den ich kenne und vielen Dank, das du hast mich zu deiner Ehefrau gemacht hast. Ich danke dir für die Unterstützung in all den Jahren und vor allem während der Schreibung dieser Arbeit. Ich liebe dich und freue mich jetzt schon auf klein Romeo Rock Würtemberger!

10. AFFIDAVIT

I hereby confirm that my thesis entitled “Anionic and Neutral Lewis-Base Adducts of Diboron(4) Compounds” is the result of my own work. I did not receive any help or support from commercial consultants. All sources and / or materials applied are listed and specified in the thesis.

Furthermore, I confirm that this thesis has not yet been submitted as part of another examination process neither in identical nor in similar form.

Würzburg, 30th of May 2016

Signature

11. EIDESSTAATLICHE ERKLÄRUNG

Hiermit erkläre ich an Eides statt, die Dissertation “Anionic and Neutral Lewis-Base Adducts of Diboron(4) Compounds” eigenständig, d.h. insbesondere selbstständig und ohne Hilfe eines kommerziellen Promotionsberaters angefertigt und keinen anderen als die von mir angegebenen Quellen und Hilfsmittel verwendet zu haben.

Ich erkläre außerdem, dass die Dissertation weder in gleicher noch in ähnlicher Form bereits in einem anderen Prüfungsverfahren vorgelegen hat.

Würzburg, 30. Mai 2016

Unterschrift

12. PUBLICATIONS

12.1. List of publications

The publication listed below is partly reproduced in this dissertation. The table itemizes to what extent the different sections of the paper have been reused at which position in this work. For the figures it is noted in the respective captions whether it is a reproduction or an adaption from the corresponding publication.

Publication	Chapter
S. Pietsch , E. C. Neeve, D. C. Apperley, R. Bertermann, F. Mo, D. Qiu, M. S. Cheung, L. Dang, J. Wang, U. Radius, Z. Lin, C. Kleeberg, T. B. Marder, <i>Chem. Eur. J.</i> 2015 , <i>21</i> , 7082-7098.	1.2.2.1.
	1.2.3.1.
	1.2.3.3.
S. Pietsch , U. Paul, I. A. Cade, M. J. Ingleson, U. Radius, T. B. Marder, <i>Chem. Eur. J.</i> 2015 , <i>21</i> , 9018-9021.	2.2.1.1.
	2.2.1.4.
	2.2.2.1.
	2.2.2.2.
S. Würtemberger-Pietsch , U. Radius, Todd B. Marder, <i>Dalton Trans.</i> 2016 , <i>45</i> , 5880-5895.	2.2.2.3.
	2.1.

2012:

D. Schmidt, J. H. J. Berthel, S. Pietsch, U. Radius, *Angew. Chem.* **2012**, *124*, 9011-9015; *Angew. Chem. Int. Ed.* **2012**, *51*, 8881-8885.

2015:

S. Pietsch, E. C. Neeve, D. C. Apperley, R. Bertermann, F. Mo, D. Qiu, M. S. Cheung, L. Dang, J. Wang, U. Radius, Z. Lin, C. Kleeberg, T. B. Marder, *Chem. Eur. J.* **2015**, *21*, 7082-7098.

S. Pietsch, U. Paul, I. A. Cade, M. J. Ingleson, U. Radius, T. B. Marder, *Chem. Eur. J.* **2015**, *21*, 9018-9021.

2016:

S. Würtemberger-Pietsch, U. Radius, T. B. Marder, *Dalton Trans.* **2016**, *45*, 5880-5895.